Chapter 8: Water cycle changes

Coordinating Lead Authors:
Hervé Douville (France), Krishnan Raghavan (India), James Renwick (New Zealand)

Lead Authors:
Richard Allan (UK), Paola A. Arias (Colombia), Mathew Barlow (USA), Ruth CerezoMota (Mexico), Annalisa Cherchi (Italy), ThianY. Gan (Canada), Joelle Gergis (Australia), Dabang Jiang (China), Asif Khan (Pakistan), Mohamed Meddi (Algeria), Wilfried Pokam Mba (Cameroon), Daniel Rosenfeld (Israel), Jessica Tierney (USA), Olga Zolina (Russia)

Review Editors:
Pascale Braconnot (France), AronaDiedhiou (Ivory Coast/Senegal)

Chapter Scientist(s):
Sabin ThazhePurayil (India)

Contributing Authors:
Gabriel Abramowitz (Australia), Robert Allen (USA), Kevin Anchukaitis(USA), Richard Betts (UK), Olivier Boucher(France), Michael Byrne (UK), Céline Bonfils(USA), Michael Bosilovich(USA), Josephine Brown (Australia), Michael Byrne (UK), Robin Chadwick (UK), Benjamin Cook (USA), Alejandro Di Luca (Australia), Petra Doell (Germany), Paul Durack (USA), Hayley Fowler (UK), Alexander Gershunov (USA), Jim Kossin (USA), Eric Maloney (USA), Vimal Mishra (India), Aida Diongue Niang (Senegal), Angeline Pendergrass (USA), Stephan Pfahl (Switzerland), Catherine Prigent (France), Catherine Rio (France), Benjamin Sanderson (France), Sergio Vicente-Serrano (Spain), Shoichi Shige (Japan), Vijay Singh (USA), Abigail Swann (USA), Richard Taylor (UK), Michael Wehner (USA), Laura Wilcox (UK)

Date of Draft: 29 April 2019

Note: TSU Compiled Version

Executive Summary

This chapter covers changes in the water cycle, beginning with the theoretical underpinning of why changes in the water cycle are expected as the climate system warms. The chapter assesses observed changes in the water cycle and their potential attribution, future projections and related key uncertainties associated with water cycle changes, and the potential for abrupt change. It concludes with a summary of key knowledge gaps. The chapter takes a large-scale and process-oriented approach, discussing both global-scale change and critical regional-scale features of the water cycle, such as monsoon circulations and mid-latitude storm tracks.

Expected changes in the water cycle based on physical understanding

On-going modification of Earth's energy budget by radiative forcing is *virtually certain* to drive pervasive and substantial changes in the global water cycle. Global mean evaporation and precipitation are *very likely* to increase as the planet continues to warm. Expected increases of around 2-3% per °C of global surface warming are currently offset by rapid atmospheric adjustments to radiative forcings but these counteracting effects will diminish in importance in the future (*high confidence*). Precipitation response to warming over land will belower in magnitude and less certain than over the ocean due to complex adjustments and feedbacks (*medium confidence*). {8.2.1}

Average increases in low-level water vapour with warming of around 6-7% per ºC are expected to drive an amplification of wet extremes when and where they occur (*high confidence* based on multiple lines of observational and numerical evidence). The precise increase in precipitation intensity is expected to deviate significantly from the water vapour response due to less well understood cloud microphysical and dynamical processes and large-scale changes in atmospheric circulation patterns. An overall increased severity of flooding in response to more intense wet extremes (from sub-daily up to seasonal time-scales) is expected at the global scale (*high confidence*).

Observed changes in the water cycle

It is *very likely* that human activities have affected the global water cycle since preindustrial times (*high confidence*). Anthropogenic influences, including greenhouse gas emissions, aerosol emissions, and land use change, have contributed to observed decreases in glaciers (*virtually certain*), increases in atmospheric moisture (*virtually certain*), global-scale changes in surface salinity and E-P over the oceans (*high confidence*), latitudinal and seasonal changes in precipitation over land (*high confidence*), regional-scale changes in river discharge due to earlier snowmelt, changes in precipitation and/or evapotranspiration, or growing water withdrawals (*medium confidence*), mid-latitude land surface drying (*medium confidence*), and intensification of precipitation extremes in many regions with available hourly to daily intensity records (*high confidence*), and severe drought events in some regions (*high confidence*). There are some regions and water cycle variables for which the anthropogenic aerosol forcings offset the response to anthropogenic emissions of greenhouse gases (*medium to high confidence*) {8.3.1}

It is *very likely* that Northern Hemispheric anthropogenic aerosol have induced a weakening of the regional boreal monsoons (eg., South Asia, East Asia and West Africa) by offsetting the GHG forcing during the 2nd half of the 20th century (*high confidence*). Recent changes in the regional monsoon precipitation have*very likely*been constrained by a tug-of-war between GHG and anthropogenic aerosol forcing (*medium to high confidence*).

Projected changes in the water cycle

Based on physical understanding, paleoclimate studies, and numerical simulations from global climate models, the on-going modification of Earth's energy budget by anthropogenic processes is *extremely likely* to drive pervasive and substantial changes in the global water cycle.

Global mean evaporation and precipitation are *very likely* to increase as the planet continues to warm. Robust increases in **atmospheric water vapour** in response to warming are *virtually certain* based upon multiple lines of observational evidence and simulations (*high confidence*). This increase in water vapour is expected to drive an **amplification of wet extremes** when and where they occur (*high confidence* based on multiple lines of observational and numerical evidence). Greater warming over land than ocean is expected to drive a decline in near-surface relative humidity and a drying over land (*medium to high confidence*). {8.2.1}

Substantial regional changes in the water cycle are projectedas a result of shifts in global atmospheric circulation patterns but there is *low confidence* in the exact manifestation of these shifts in many regions. However, subtropical expansion, poleward shifts in storm tracks, and a contraction and movement in the tropical rainy belt, based on energy and water budget constraints, are *likely* to dominate increases and decreases in fresh water availability in many regions (*medium confidence*). {8.2.1, 8.2.2}

Land use changes due to human activities are additionally expected to affect the water cycle in some regions through water resource management (extraction, irrigation) or through deforestation and its influence on the regional energy budget and atmospheric circulation (*high confidence*) {8.2.2}

It is *very likely* that the water cycle changes caused by human activities will intensify in the future {8.4.1.1}, even if their geographical pattern and magnitude still remain uncertain {8.4.1.1, 8.4.1.2.1}, based on physical understanding, multiple model simulations, and large ensembles of model simulations (multiple lines of evidence). The pattern of the forced hydrological response will remain relatively robust across the twenty-first century whatever the mitigation policy (*medium confidence*). There is *medium to high confidence* that the magnitude of water cycle changes, especially over land, will not necessarily remain proportional to global warming due to potential nonlinearities in both atmospheric dynamics and land surface processes.

Without strong and rapid mitigation initiatives, climate change will manifest in all components and features of the global water cycle, including a retreat of the mid-latitude seasonal snow cover {8.4.1.2.3, 8.4.1.6.2} and of the mid-altitude glaciers (*high confidence*) {8.4.1.6.1}, an expansion of arid areas towards the midlatitudes (*medium to high confidence*) {8.4.2.1.2, 8.4.2.7}, a global increase in the spatio-temporal variability of monthly to seasonal precipitation (*high confidence*) {8.4.1.2.1}, a global increase in the frequency/intensity of extreme hourly to daily precipitation (*high confidence*) {8.4.1.2.1}, and regional increases in drought severity (*high confidence*) with consequences for the management of water resources. {8.4.2.7}

Uncertainties in water cycle projections

Structural biases in models, internal variability, and non-linear responses continue to be the main source of uncertainties in future projections of water cycle changes (*high confidence*). **Emission scenarios or global mean temperature targets** do not represent the main source of uncertainty for most projected water cycle changes at the regional scale (*high confidence*) {8.5.1}. **Model uncertainties** (e.g. poorly-resolved processes, aerosol effects, surface feedbacks) are still the main obstacle that precludes a more confident assessment of long-term water cycle changes for most variables, seasons and regions (*high confidence*). More observations (e.g., longer records, improved spatial coverage, original field campaigns, new in situ and satellite instruments) are needed for model development and evaluation, as well as for constraining the projected water cycle changes. {8.5.1}

Internal variability also represents a major source of uncertainty for near-term water cycle projections (*high confidence*). This is particularly true for regional summer monsoons, winter mid-latitude storm tracks and related water cycle changes (*medium confidence*). The relative contribution of internal variability is less prominent in the high latitudes due to a stronger thermodynamic signal (*high confidence*), as well as in the subtropics and semi-arid areas due to a lower precipitation variability (*high confidence*).

Potential **non-linearities** in climate system response also challenge confident assessment of future water cycle changes (*medium confidence*). Non-linearities can arise from various sources such as changes in large-scale dynamics (e.g., northern mid-latitude storm tracks), potential thresholds in thermodynamic (e.g., moist convection) or biophysical (plant evapotranspiration) processes, or the influence of physical limitations (e.g., snow and soil moisture reservoirs) on surface runoff and river discharge. Such non-linearities are difficult to isolate from the strong internal variability, but may enhance regional water cycle changes compared to the widely-used pattern scaling technique for some variables, regions and seasons (*medium confidence*) {8.5.3} Continued model development, comparison with paleoclimate records, and improved observational records and systems can considerably reduce uncertainties and result in better characterization of internal variability and complex non-linearities (*high confidence*).

Potential for abrupt change

The non-linear sensitivity of hydrologic systems necessitates the consideration of low probability, high impact changes. Overall, there is evidence of abrupt change in some model projections, but models tend to disagree about the magnitude, speed, and timing of such changes. There is *low confidence* that abrupt changes in aridification and rainfall will occur by 2100 and *medium confidence* in changes by 2300, although the possibility of abrupt events cannot be ruled out. {8.6}

The paleoclimate record demonstrates that a **collapse in Atlantic Meridional Overturning Circulation** can cause abrupt and large-magnitude shifts in the water cycle (*high confidence*). Some model projections suggest that if AMOC collapses in future, a similar response in the water cycle will occur, although the pattern of change is compounded with the effects of higher atmospheric CO_2. It is *unlikely* that an AMOC-driven abrupt change in the water cycle will occur by 2100, but *about as likely as not* (*low confidence*) that such a change could occur by 2300, if emissions are not curtailed. {8.6.1}

Observations and model simulations suggest that there are strongly positive **land surface feedbacks** in the Earth system that cause abrupt changes in the water cycle, including changes in plant cover, dust, and snowpack. Such changes can facilitate rapid onset of drought, increased rainfall, and water availability on a regional basis. Continued deforestation of the Amazon rainforest, combined with climate change, raises the probability that this ecosystem will cross a tipping point into a dry state. Assuming continued levels of deforestation and greenhouse emissions, it is *about as likely as not* (*medium confidence*) that such a change will occur by 2100. {8.6.2}

It is *very likely* that abrupt water cycle changes will occur if **radiation management techniques** are implemented rapidly or terminated abruptly. The impact of radiation management is *likely* heterogeneous and will impact different regions in diverse and potentially disruptive ways.

8.1 Introduction

8.1.1 Overview of the global water cycle and water resource vulnerability

8.1.1.1 Importance of water for human societies and ecosystems

Water is vital to all life on Earth. Since approximately 70% of the Earth is covered by water, it is often referred to as the 'Blue Planet'. However, the distribution of water availability seen in Figure 1 shows that saline ocean water accounts for around 96% of total water availability, with freshwater only representing 1.8% of all water on Earth (Durack, 2015). Of this, ice caps, glaciers and snow pack make up 96.9% of freshwater resources, with a further 1.4% accounted for by deep groundwater. The remaining 1.7% of freshwater is considered easily accessible and available for essential ecosystem functioning and human society's water resource needs. This very small fraction of freshwater represents a total volume of about 210 thousand km^3, mostly contained in lakes, rivers, wetlands and soils (Oki and Kanae, 2006). Although this amount is theoretically enough to meet global water demands, there are large geographical and seasonal differences that greatly influence the availability of freshwater to meet specific regional needs.

Despite its scarcity, freshwater is recognized as being the most essential natural resource on the planet. It supports a range of human activities from the availability of domestic drinking water and irrigated agricultural crops, through to industrial processes including the generation of hydroelectricity and the cooling of thermoelectric power plants (Bates et al., 2008; Schewe et al., 2014). These activities rely on sufficient quantities of freshwater that can be drawn from rivers, lakes, groundwater stores, and in some cases, desalinated sea water (Schewe et al., 2014).

Water scarcity occurs when there are insufficient freshwater resources to meet water demands that adversely affects society and ecosystem functioning. As such, water availability is a major constraint on our society's ability to meet the future food and energy needs of a growing human population (D'Odorico et al., 2018). Water plays a key role in the production of energy, including hydroelectricity, bioenergy, and the extraction of unconventional fossil fuels. These dependencies have resulted in increasing competition for water between the food and energy sectors. This 'food-energy-water nexus' is further compounded by increasing globalization, which can transfer large-scale water demands to other regions of the world, raising serious concerns about local food and water security of regions that are highly dependent on the export of agricultural products (D'Odorico et al., 2018).

The impacts of climate change on society are primarily experienced through changes to the global water cycle (Jiménez Cisneros et al., 2014). Changes in the quantity, seasonality and availability of water due to climate change have long been recognized by the IPCC and development organizations as severely impairing the food security and economic prosperity of many countries, particularly in the arid and semi-arid areas of the world including Asia, Africa and Australia (Bates et al., 2008; Mekonnen and Hoekstra, 2016; Schewe et al., 2014). Having too much or too little water will increase the risk of flooding and drought, as precipitation intensity and variability increases in a warming climate(Hoegh-Guldberg et al., 2019; Stocker et al., 2013). Water scarcity is not only driven by physical processes, but is also influenced by insufficient investment in water management infrastructure and technology. Consequently, there is *high confidence* that anthropogenic climate change will make water management even more difficult during the 21st century.

Climate change poses a threat to water security as changes in precipitation influence other climate variables like surface and subsurface runoff and river flows, which are critical to the water, food and energy security of many regions (Jiménez Cisneros et al., 2014; Mekonnen and Hoekstra, 2016; Oki and Kanae, 2006; Schewe et al., 2014). Non-climatic drivers such as population increase, economic development, urbanization, and land use further challenge the sustainability of resources by decreasing water supply or increasing demand (Jiménez Cisneros et al., 2014). Future population increases are expected to increase pressure on global water resources that are already exhibiting changes related to observed warming of the climate system since the mid-20th century (Hoegh-Guldberg et al., 2019; IPCC, 2013a).

Working Group II of IPCC AR5 reported that approximately 80% of the world's population already suffers from serious water security threats (Jiménez Cisneros et al., 2014). Climate change is projected to reduce renewable surface water and groundwater resources significantly in most dry subtropical regions of the world, intensifying competition between agriculture, ecosystems, human settlements and industry for water resources (Jiménez Cisneros et al., 2014).

The AR5 also noted that freshwater-related threats from climate change increase significantly with increasing greenhouse gas (GHG) concentrations (Jiménez Cisneros et al., 2014). This conclusion has since been strengthened, with the IPCC Special Report on Global Warming of 1.5 °C (SR1.5) finding that reducing global warming from 2°C to 1.5°C reduces the proportion of the world population exposed to a climate change-induced increases in water stress by up to 50% (*medium confidence*) (SR1.5 3.4.2)(Hoegh-Guldberg et al., 2019; Masson-Delmotte et al., 2018).

Research since AR5 has found that around four billion people live under conditions of severe freshwater scarcity for at least one month of the year, with half a billion people in the world facing severe water scarcity all year round (Mekonnen and Hoekstra, 2016). Motivated by the vulnerability of the planet's freshwater resources to continued climate change, and their potential to seriously impact human societies and ecosystems (Hoegh-Guldberg et al., 2019; Masson-Delmotte et al., 2018), this chapter evaluates advances in the theoretical, observational and model based understanding of the global water cycle made since the IPCC's Fifth Assessment Report (AR5) (IPCC, 2013a).

8.1.1.2 Overview of the global water cycle

The global water cycle describes the continuous, naturally occurring movement of water through the climate system from its liquid, solid and gaseous forms into reservoirs of the ocean, atmosphere, cryosphere and land surface (Stocker et al., 2013). In the atmosphere, water primarily occurs as a gas (water vapour), but it is also present as ice and liquid water within clouds where it substantially affects Earth's energy balance. The ocean is mostly comprised of liquid water across much of the globe, but includes sections partly covered by ice in Polar Regions. Liquid freshwater on land forms surface water flows (lakes, rivers), soil moisture and groundwater stores (Stocker et al., 2013). Solid terrestrial water occurs as ice sheets, glaciers, snow and ice on the surface and permafrost (Stocker et al., 2013). Water that falls as snow in winter provides soil moisture in springtime and river flow in summer that are essential for human activities and ecosystem functioning.

The planet's water cycle primarily involves the evaporation and precipitation of moisture at the Earth's surface including evapotranspiration associated with biological processes. Water that falls on land as precipitation, supplying soil moisture and river flows, was once evaporated from the ocean or sublimated from ice-covered regions before being transported through the atmosphere as water vapour (Gimeno et al., 2010; van der Ent and Savenije, 2013). In addition, transpiration from vegetation contributes to atmospheric water vapour, especially in tropical regions (Bonan, 2016). The latent heat realised by condensation of atmospheric water vapour is critical to driving the circulation of the atmosphere on scales ranging from individual thunderstorm cells to the global circulation of the atmosphere (Stocker et al., 2013).

When assessing changes to the global water cycle, it is important to consider not only terrestrial freshwater components of the systems, but also the vast reservoir of salt water stored in the world's ocean (Figure 1). Movement of freshwater between the atmosphere and ocean influences ocean salinity, which is an important driver of the density and circulation of the ocean (Stocker et al., 2013). Together the atmospheric and oceanic components of the climate system modulate global and regional aspects of the water cycle.

[START FIGURE 8.1 HERE]

Figure 8.1: Components of the global water cycle. The ocean is the Earth's primary water reservoir (96.2%), with remaining water stored as ice (2.2%) or on land (1.6%). Approximately 86% of surface water fluxes

occurring over the ocean, with the remaining 14% generated over land. Reservoirs represented by solid boxes: 103 km3, fluxes represented by arrows: Sverdrups (106 m3 s–1). Source: Durack (2015).

[END FIGURE 8.1 HERE]

[START FIGURE 8.2 HERE]

Figure 8.2: Distribution of the Earth's water (hydrosphere). The global ocean is the primary water reservoir and the ultimate source of all terrestrial water (A, Left). Ice caps, glaciers and permanent snow comprise the largest freshwater stores (B, top right), and seasonal ice, snow and permafrost along with freshwater lakes comprise the largest surface and other fresh water storages that are available for human use (C, bottom left). Reproduced and updated from Shiklomanov and Sokolov (1985); Charette and Smith (2010); and Gleeson et al., (2015).

[END FIGURE 8.2 HERE]

8.1.2 Summary of observed and projected water cycle changes from AR5

This Sixth Assessment Report is the first IPCC assessment to include a chapter specifically developed to an integrated assessment of the global water cycle. This section summarises observed and projected water cycle changes reported across nine of the fourteen chapters prepared for the IPCC's Fifth Assessment Report (AR5) (IPCC, 2013a).

8.1.2.1 Summary of observed water cycle and circulation changes

The AR5 concluded it was *likely* that anthropogenic influence has affected the water cycle since 1960s (IPCC, 2013b). Detectable human influence on changes to the water cyclewere found in atmospheric moisture content (*medium confidence*), global-scale changes of precipitation over land (*medium confidence*), intensification of heavy precipitation events over land regions where sufficient data networks exist (*medium confidence*), and *very likely* changes to ocean salinity through its connection with evaporation and precipitation patterns (Stocker et al., 2013).

The AR5 concluded it is *likely* there has been an overall increase in precipitation averaged over the land areas of the mid-latitudes of the Northern Hemisphere (*medium confidence* since 1901, but *high confidence* after 1951). In particular, attribution studies showed a detectable anthropogenic influence on globally averaged precipitation over land and Arctic precipitation (Stocker et al., 2013). The AR5 also reported that it is *very likely* that global surface air specific humidity increased since the 1970s. There was *low confidence* in the observations of global-scale cloud variability and trends, *medium confidence* in reductions of pan-evaporation related to changes in wind speed, humidity and solar radiation, and *medium confidence* in the increases of global evapotranspiration between the 1980s and 1990s, as well as in the decreases detected after 1998, mainly due to reductions of soil moisture. Regarding streamflow and runoff, the AR5 identified *low confidence* on the increasing trends of global river discharge during the 20th century (Stocker et al., 2013).

In terms of water cycle extremes, the AR5 concluded that it is *likely* that the number of heavy precipitation events over land had increased in more regions than it had decreased, with highest confidence reported for North America and Europe where there have been likely increases in either the frequency or intensity of heavy precipitation with some seasonal and/or regional variation (Hartmann et al., 2013a). In land regions where observational coverage was sufficient for assessment, it was reported that there was *medium confidence* that anthropogenic forcing contributed to a global-scale intensification of heavy precipitation over the second half of the 20th century (Bindoff et al., 2013a).

Paleoclimate evidence of past floods evaluated in the AR5 concluded that there is *high confidence* that floods larger than those recorded since the 20th century have occurred during the past five centuries in northern and central Europe, the western Mediterranean region and eastern Asia (Masson-Delmotte et al., 2013). They report *medium confidence* in evidence from the Near East, India and central North America that large modern flood events are comparable or surpass the magnitude and/or frequency of historical floods (Masson-Delmotte et al., 2013).

Considering trends related to rainfall deficits, the AR5 concluded that there is *low confidence* in any global-scale observed trend in drought or dryness (lack of rainfall) since the mid-20th century (Hartmann et al., 2013a). The report cited issues related to the lack of direct observations, methodological uncertainties and high regional variability on decadal timescales. For example, changes in the frequency and intensity of drought *likely* increased in the Mediterranean and West Africa, while they *likely* decreased in central North America and north-western Australia since 1950 (Hartmann et al., 2013a). These factors resulted in *low confidence* in the attribution of changes in global drought since the mid-20th century due to human influences (Bindoff et al., 2013a).

There was *high confidence* in the paleoclimate evidence of past droughts that showed greater magnitudes and longer durations than those observed since the beginning of the 20th century in many regions over the last millennium (Masson-Delmotte et al., 2013). The AR5 reported *medium confidence* that more 'megadroughts' spanning several decades occurred in monsoon Asia, and that wetter conditions prevailed in arid Central Asia and the South American monsoon region during the Little Ice Age (1450 to 1850) compared to the warmer Medieval Climate Anomaly (950 to 1250) (Masson-Delmotte et al., 2013).

While the AR5 ascribed *low confidence* in long-term (centennial) changes in tropical cyclone activity globally, in some regions like the North Atlantic it was deemed *virtually certain* that the frequency and intensity of the strongest tropical cyclones have increased since the 1970s (Hartmann et al., 2013a). There was however *low confidence* in the attribution of changes in tropical cyclone activity to human influence due to insufficient observational evidence, lack of physical understanding of the links between anthropogenic drivers of climate and tropical cyclone activity, and the low agreement between studies as to the relative importance of internal variability, and anthropogenic and natural forcings(Bindoff et al., 2013a). There was *low confidence* in any large-scale trends in storminess or storminess proxies over the last century due to inconsistencies between studies or lack of long-term data available from some locations, especially in the Southern Hemisphere (Hartmann et al., 2013a). These issues also accounted for *low confidence* in any discernible trends in small-scale severe weather events including hail or thunderstorms (Hartmann et al., 2013a).

Assessment of changes in atmospheric circulation presented in the AR5 concluded that it is *likely* that the widening of the tropical belt, a poleward shift of storm tracks and jet streams, and a contraction of the northern polar vortex, have all moved poleward since the 1970s (Hartmann et al., 2013a). There was more confidence in evidence compiled for the Northern Hemisphere due to the availability of more observations. However, the report also concluded it *likely* that the Southern Annular Mode (SAM) has tended towards its positive phase since the 1950s (Hartmann et al., 2013a). Paleoclimate evidence assessed in AR5 provided *medium confidence* that the trend towards the positive phase of the SAM observed since 1950 was anomalous in the context of the past 500 years (Masson-Delmotte et al., 2013).

Robust conclusions about long-term changes in atmospheric circulation are hampered by the presence of large interannual to decadal variability in instrumental observations. Nevertheless, an evaluation of instrumental observations provided *high confidence* in the increase in the northern mid-latitude westerly winds and the North Atlantic Oscillation (NAO) index from the 1950s to the 1990s (Delworth et al., 2016; Douville et al., 2018) and the weakening of the Pacific Walker circulation from the late 19th century to the 1990s (Hartmann et al., 2013a). Paleoclimate evidence also provided *high confidence* in the conclusion that decadal and multi-decadal changes in the winter NAO observed since the 20th century are not unprecedented in the context of the past 500 years (Masson-Delmotte et al., 2013). There is *low confidence* in long-term changes in other aspects of global circulation features such as the behaviour of surface winds over land, the East Asian summer monsoon circulation, the tropical cold-point tropopause temperature and the strength of the Brewer Dobson circulation due to limited observations and/or theoretical understanding (Hartmann et al., 2013a).

Detection and attribution studies showed that it is *likely* that human influence has altered sea level pressure patterns globally, which has implications for circulation changes influencing the global water cycle (Bindoff et al., 2013a). The AR5 reported *medium confidence* that stratospheric ozone depletion has contributed to the observed poleward shift of the southern Hadley Cell border during austral summer, but large uncertainties in the magnitude of this poleward shift were noted. They concluded that it is *likely* that stratospheric ozone depletion contributed to the positive trend in the Southern Annular Mode seen in austral summer since the mid- 20th century, corresponding to sea level pressure reductions over the high latitudes and increases in subtropical locations. There is *medium confidence* that greenhouse gases (GHGs) also influenced observed trends in the southern Hadley Cell border and the Southern Annular Mode during the austral summer (Bindoff et al., 2013a).

As outlined in Section 8.1.1.2, it is important to consider both terrestrial freshwater and oceanic components when discussing changes in the global water cycle. Assessment of ocean salinity and freshwater content changes in the AR5 concluded that it is *very likely* that the mean geographical contrasts between high and low sea surface salinity regions had increased since the 1950s (Rhein et al., 2013). That is, saline surface waters in the evaporation-dominated sub-tropical oceans have become more saline, while relatively fresh surface waters in rainfall-dominated tropical and polar regions have become fresher since the mid-20th century (Rhein et al., 2013). For example, there was *high confidence* in the conclusion that the Atlantic has become saltier and the Pacific and Southern oceans have freshened. Similar spatial patterns of the salinity trends, mean salinity and the mean distribution of evaporation–precipitation (E – P) were reported, providing*medium confidence* that the pattern of E–P over the oceans has been amplified since the 1950s (Rhein et al., 2013). These changes in water mass properties are likely to be reflected in long-term observed trends in surface ocean warming and changes in E–P since the 1950s, as well as inter-annual to multi-decadal variability behaviour of climate modes that influence many aspects of the global water cycle(Rhein et al., 2013). Overall, the AR5 presented robust evidence from regional and global surface and subsurface salinity studies that displayed patterns consistent with theoretical understanding of human caused changes in the water cycle and ocean circulation, resulting in the conclusion that it is very likely that anthropogenic forcings have contributed to surface and subsurface ocean salinity changes since the 1960s (Bindoff et al., 2013).

8.1.2.2 Summary of projected water cycle changes

Projections for the water cycle in the AR5 were considered primarily in terms of precipitation, surface evaporation, water vapour, snowpack, and runoff. In the IPCC context, sea ice, glaciers, and permafrost are collectively considered as the cryosphere.

At the global scale, several factors were identified as important in understanding projected water cycle changes. At the most basic level, the upper limit on atmospheric moisture increases with temperature (7.6.1, 12.4.5.5)(Boucher et al., 2013; Collins et al., 2013b). The ‘wet-get-wetter, dry-get-drier’ paradigm, where precipitation was projected to generally increase in regions where precipitation is already abundant and decrease in regions that are already arid, was interpreted as resulting from changes in water vapour with little change in the atmospheric circulation, although mitigated somewhat by the anticipated slowdown of the atmospheric circulation and by gains from local surface evaporation (7.6.1, 12.4.5.2)(Boucher et al., 2013; Collins et al., 2013b).

The role of the non-uniform nature of surface warming in generating regional circulation shifts was identified as an important factor in affecting regional precipitation trends (7.6.1, 12.4.5.2)(Boucher et al., 2013; Collins et al., 2013b). The widening of the Hadley Cell is a robust feature of projections (12.4.2.2), with an associated decrease in precipitation on the poleward flanks of the associated subtropical dry zones

(12.4.5.2)(Collins et al., 2013b). Identified limitations in AR5 water cycle projections including limited understanding of soil moisture–precipitation feedbacks (7.6.1) and lack of spatial resolution of tropical cyclones (12.4.4)(Boucher et al., 2013; Collins et al., 2013b). Uncertainties at the global scale in the projections are due to variations in internal natural variability, model response, forcings pathways (12.4.1.2), and limited global coverage in observations (12.4.5.2)(Collins et al., 2013b).

Globally-averaged precipitation was projected to increase with temperature increases, with *virtual certainty*(12ES, 12.4.1.1), although there are expected to be large spatial and seasonal differences (12.4.5.2), and increased temporal variability (12.4.5.5)(Collins et al., 2013b). Regionally, precipitation in some areas of the tropics and polar regions could increase by more than 50% for high end scenarios, while precipitation in large areas of the subtropics could decrease by 30% or more (FAQ 12.2, Fig. 12.22)(Collins et al., 2013b). In terms of seasonal differences, winter precipitation in northern Asia could increase by more than 50% while the local summer precipitation remains largely unchanged (FAQ 12.2, Fig. 12.22).

For most of the globe, the contrast of annual mean precipitation between dry and wet regions and between dry and wet seasons ("wet-get-wetter and dry-get-drier") was projected to increase over most of the globe with *high confidence*(12ES, 12.4.5.2)(Collins et al., 2013b). Globally, the frequency of intense precipitation events was projected to increase while the frequency of all precipitation events was projected to decrease, leading to the contradictory-seeming projection of a simultaneous increase in both droughts and floods (FAQ 12.2, 12.4.5.5)(Collins et al., 2013b).

Global monsoon rainfall and area were projected to increase, although with some areas receiving less rainfall due to weakening tropical wind circulations (FAQ 12.2, 14.2.1)(Christensen et al., 2013; Collins et al., 2013b). Monsoon onset dates were assessed as *likely* to be early or change little and monsoon retreat dates were assessed as *likely* to be delayed, with the net result of an expected lengthening of the monsoon season (FAQ 12.2, 14.2.1).

Regionally, decreased precipitation was assessed as *likely* for the Mediterranean region, the Caribbean and Central America, the southwestern United States, and South Africa under the RCP8.5 scenario (12ES, Fig. 12.22), and was projected with *medium confidence* to be larger than natural variability by 2100 in some seasons (12ES, Box 12.1)(Collins et al., 2013b). Regional trends in monsoon rainfall amounts and timing were assessed as uncertain in many areas (FAQ 12.2, 14.2.1)(Christensen et al., 2013; Collins et al., 2013b).

Surface evaporation change was projected to be positive over most of the ocean and to generally follow the pattern of precipitation change over land (12ES, 12.4.5.4)(Collins et al., 2013b). Near-surface relative humidity reductions over many land areas were projected to be *likely*, with *medium confidence* (12.4.5.1). General decreases in soil moisture in present-day dry regions were considered *likely*, and projected with *medium confidence* under the RCP8.5 scenario (12.4.5.3). Soil moisture drying in the Mediterranean, southwest USA and southern African regions was considered *likely*, with *high confidence* by the end of this century under the RCP8.5 scenario (12.4.5.3). No increases of soil moisture were assessed with confidence. Projections for annual runoff included both decreases and increases. By the end of the 21st century under the RCP8.5 scenario, decreases were assessed as *likely* in parts of southern Europe, the Middle East, and southern Africa; and increases as *likely* in the high northern latitudes (12.4.5.4). For snow cover, decreases over the Northern Hemisphere were assessed as *very likely* (12.4.6.2). As temperatures increase, snow accumulation will begin later in the year and melt will occur earlier, with related changes in snowmelt-driven river flows (FAQ 12.2, 12.4.6.2)(Collins et al., 2013b).

In terms of the potential for abrupt change of components of the water cycle, long-term droughts and monsoonal circulation were identified as potentially undergoing rapid changes, but the assessment was made with *low confidence*(Table 12.4, 12.5.5.8.1, 12.5.5.8.2)(Collins et al., 2013b).

8.1.3 Summary of water cycle changes from special reports

8.1.3.1 Key findings of SR1.5

Here we focus on key findings related to the physical response of the water cycle, mainly assessed in Chapter 3 on the impacts of 1.5°C global warming on natural and human systems. Given the expected sensitivity of the global water cycle to global warming (cf. section 8.2), the SR1.5 provided an update of the observed increase in Global Mean Surface Air Temperate (GMST) (0.87°C ±0.12°C) for the decade 2006-2015 compared to the 1850-1900 reference period (SR1.5 SPM A.1.1). The report also states that most of the recent additional global warming was human-induced (Masson-Delmotte et al., 2018). This suggests that water cycle changes dominated by thermodynamic processes may be more easily detected than in the AR5 and, by extension may also be attributed to human activities (cf. section 8.3). While past GHG emissions alone are unlikely to raise GMST to 1.5°C above preindustrial levels (SR1.5 SPM A.2), the SR1.5 report emphasized that limiting global warming to 1.5 or even 2°C will need drastic mitigation policies, some of which rely on water availability (e.g., bio-energy with carbon capture and storage, and afforestation). The reader is referred to SR1.5 and AR6 WGIII for further details on this important issue.

The focus here is on the hydrological impacts of an additional 0.5°C of global warming when comparing 1.5°C versus 2°C global warming targets. The general conclusion of SR1.5 is that each half degree of additional warming makes a difference on the climate response although this difference can be hardly discernible at the regional scale for most water cycle variables given their large natural variability. A key finding is that "*limiting global warming to 1.5°C compared to 2°C would approximately halve the proportion of the world population expected to suffer water scarcity, although there is considerable variability between regions"* (*medium confidence*) (SR1.5 SPM B.5.4)

Looking at hydrological extremes, the SR1.5 report suggests a low signal-to-noise ratio of related changes in high mitigation scenarios and weak evidence for non-linearities, at least within the limited (1.5-2°C) range of global warming considered by the report. For instance, the assessment of projected changes in 5-day maximum precipitation revealed that the ensemble-mean response of model simulations per degree of global warming is generally independent of the considered emission scenario (Hoegh-Guldberg et al., 2019) (Chapter 3, SR1.5 IPCC, 2018). There is, however, *low confidence* in projected changes in heavy precipitation at +1.5°C versus +2°C at the regional scale (except in the high latitudes or at high altitude where there is *medium confidence*). The main conclusion is that heavy precipitation shows a global tendency to increase more at +2°C versus +1.5°C.

The SR1.5 also assessed recent studies which evaluated differences in drought and dryness occurrence at +1.5°C and +2°C global warming for various indices such as P-E (Greve et al., 2018), soil moisture anomalies (Lehner et al., 2017a), consecutive dry days (Schleussner et al., 2016), Palmer-Drought Severity Index (Lehner et al., 2017a), or annual mean runoff (Schleussner et al., 2016). These analyses are generally consistent, again suggesting stronger impacts at +2°C versus +1.5°C for most indices.

An assessment of P-E (Greve et al., 2018), which assumes a linear scaling with global warming, suggests that a 1.5°C target substantially reduces the risk of experiencing extreme changes in regional water availability. Scenario uncertainty is however lower than model uncertainty and less than uncertainty due to internal variability for all considered regions. Comparing the annual mean PDSI response in a set of simulations with the Community Earth System Model, Lehner et al. (2017) found an enhanced risk of drought in the Mediterranean and central Europe at +2°C versus +1.5°C, but such an increase was detected in only a few areas.

Also assessed in SR1.5 Chapter 3 is an analysis based on bias-corrected climate simulations and off-line global hydrological models (Döll et al., 2018). They analysed seven freshwater-related hazard indicators, identifying for all but one indicator that areas with significantly wetter or drier conditions (relative to 2006–2015) are smaller in the +1.5°C than in the +2°C world. Differences between hydrological hazards at the two global warming levels are however significant over less than 12% of global land area (Döll et al., 2018).

In summary, the SR1.5 report supports the AR5 key findings about the projected increase in the hydrological contrasts between dry and wet regions and seasons, and in the occurrence of related extremes. The report emphasized the need for both mitigation and adaptation policies relevant for water resource management. They also support the AR5 assessment that emission scenarios are not so far the main source of uncertainty for hydrological projections at continental to regional scales, especially compared to the role of inter-model spread and internal climate variability (cf. section 8.5).

8.1.3.2 Key findings of SROCC

The Special Report on the Ocean and Cryosphere in a changing Climate (SROCC), finalized in September 2019, provides a comprehensive assessment of recent and projected changes in snow and ice over land, which represent a key component of the water cycle in high-altitude and high-latitudes areas.

Since the early 20th century, high mountain regions have experienced significant warming. This has resulted in less snowpack (Marty et al., 2017b) especially at or below the mean snowline elevation, and most glaciers of high mountain regions have been retreating and losing mass in recent decades (Kraaijenbrink et al., 2017), with the largest retreat observed in the southern Andes, the low latitudes and central Europe (>900 kg $m^2yr^{-1).}$ Glacier shrinkage and snow cover changes have led to changes in streamflow in many mountain regions during recent decades (Milner et al., 2017). Permafrost in the European Alps, Scandinavia, and the Tibetan Plateau has also undergone recent warming, degradation and ground-ice loss (Lu et al., 2017). Beyond that, cryospheric changes include more and larger glacier lakes, reduced mountain slope stability, more wet snow avalanches, increased biodiversity in terrestrial and freshwater ecosystems, uneven impacts in agriculture, hydropower, tourism and recreation activities, and water cycle, but long-term adaptation responses remains uneven and limited.

With glaciers and polar ice sheets as the dominant sources of sea level rise (SLR) (Chen et al., 2013), and also contributions from ground water depletion (Konikow, 2011), global mean sea level (GMSL) is rising at an accelerated rate, and is expected to continue rising. SLR at the end of the 21st century will be strongly dependent on the projected global emission scenarios (Slangen et al., 2016). Under high emissions scenarios such as RCP8.5, Antarctica will likely contribute significantly to SLR by the end of the century (DeConto and Pollard, 2016) but processes controlling the timing of future ice-shelf collapse and a possible Marine Ice Cliff Instability (MICI) make Antarctica’s contribution to future SLR highly uncertain. Under projected GMSL rise, historically rare extreme sea level (ESL) events will become common by 2100 under all RCPs, which would lead to severe flooding in the absence of strong adaptation. Non-climatic anthropogenic drivers have played a dominant role in increasing coastal communities’ exposure and vulnerability to SLR (Nicholls and Cazenave, 2010) and ESL events and will continue to have a significant impact in the future. Coastal communities are implementing a variety of protective measures in response to coastal risk compounded by SLR, which could have crucial synergistic, complementary, or antagonistic consequences.

Climate change is increasingly exacerbating extremes and abrupt or irreversible changes in the ocean and cryosphere, causing multiple hazards, increasing the vulnerability of human and natural systems and exposure to compound risk and cascading impacts (Lee et al., 2015). Elevated sea surface temperatures and sea level have impacted observed tropical and extratropical cyclones and contributed to extreme sea level events including storm surges (Muis et al., 2016). Marine heatwaves (MHWs) have very likely doubled in frequency since early 1980s with one quarter of the worlds’ oceans experiencing either the longest or most intense events on record in 2015 and 2016 (Frölicher et al., 2018). About 90% of the observed MHWs have an anthropogenic component and they will get worse under future global warming, pushing marine organisms, fisheries and ecosystems beyond the limits of their resilience. Extreme El Niño and La Niña events are likely to occur more frequently in the future (Cai et al., 2014). The equatorial Pacific trade wind system has experienced extreme variability in recent decades and suppressed the rate of global warming (Kosaka and Xie, 2013).

The Atlantic Meridional Overturning Circulation (AMOC) will very likely weaken over the 21st century under all RCP scenarios (Caesar et al., 2018a). A substantially weakened AMOC would lead to widespread impacts on surface climate, affecting natural and human systems. Expected impacts are: more winter storms in Europe, a reduction in Sahel rainfall; a decrease in the Asian summer monsoon; fewer tropical cyclones over the North Atlantic; and an increase in regional sea-level around the Atlantic. A new tipping element, the Subpolar Gyre System (SPG) in the North Atlantic, identified in some climate models, involves an abrupt cooling of the North Atlantic on a shorter, decadal time scale (Hermanson et al., 2014). The special report also examines sustainable and resilient risk management strategies to mitigate future impacts of extremes and abrupt changes.

8.1.3.3 Key findings of SRCCL

The Special Report on climate change, desertification, land degradation, sustainable management, food security, and greenhouse gas fluxes in terrestrial ecosystems (SRCCL) has clear connections with the water cycle. Yet, it only provides a brief assessment on hydrological changes due to climate change. The focus is mostly on land use which is currently the largest source of anthropogenic greenhouse gas emissions after industry (Arneth et al., 2017; Guillaume et al., 2016).

Biophysical effects and changes in net CO_2 emissions from land influence weather and climate variability, including changes to surface evapotranspiration and the land surface water budget. Land surface processes modulate the likelihood, intensity and duration of many extreme events including heat waves, droughts and heavy precipitation. There is robust evidence and higher agreement that historical changes in land caused significant changes in regional mean annual and seasonal surface air temperature. Amplification and dampening of warming due to land feedbacks will differ by region and season, and will depend on the concurrent changes in hydrological cycles. Desertification exacerbates climate change through feedbacks involving vegetation cover greenhouse gases and mineral dust aerosol.

As a result of the warming climate, tropical and sub-tropical regions will see the emergence of distinct climates that are beyond the envelope of current natural variability (Maule et al., 2017) and hot, arid climates are projected to expand. Moreover, increasing number, frequency and intensity of extreme climatic events may increase the vulnerability of dryland to desertification. Many land-based systems will be exposed to disturbances beyond the range of current natural variability, which will alter the structure, composition and functioning of those systems (Gauthier et al., 2015; Intergovernmental Panel on Climate Change, 2014). Changes in spatial and temporal rainfall distribution and intensification of rainfall events increase the risk likelihood and consequences of land degradation. Conversely, land degradation drives climate change through emission of greenhouse gases and deteriorating sinks of atmospheric greenhouse gases. Despite advances in our understanding of land-climate feedback, major uncertainty still remains (Berg et al., 2017a).

Current food production systems contribute to climate change, accounting for around 40% of total human emissions of GHGs and are already affected by climate change and related impacts. Mitigation and adaptation measures such as peri-urban agricultural practices may contribute to improve food security. As the food-energy-water nexus is very complex, the SRCCL unfortunately did not assess the vulnerability of the global food system to projected changes in the water cycle.

8.1.4 Chapter motivations, framing and preview

8.1.4.1 New challenges and opportunities

The AR5 WG1 was a major step forward in the understanding of the human influence on the Earth's water cycle, yet global and regional projections of water resources remain very uncertain for a range of reasons including modelling uncertainty and the much larger influence of internal variability compared to projections of temperature. Global warming targets are mostly assessed in terms of regional temperatures, snow cover and sea-ice retreat, or global sea level rise. Although policy-relevant, these climate indices may not adequately take into account more complex interactions of the climate system that are relevant for evaluating regional climate change and the impacts related to natural ecosystems and human societies. Since the AR5, longer and more homogeneous observational and reanalysis datasets have been produced. Similarly, there has been development of new paleoclimate reconstructions of aspects of the water cycle, particularly from the Southern Hemisphere, that were not available for assessment during the AR5.

There have also been advances in understanding and tools to model clouds, atmospheric circulation, precipitation, surface fluxes, vegetation, floodplains, ground waters and other processes. Improvements in instrumental observations also mean that climate models can now be evaluated more thoroughly and global projections can be potentially better physically constrained. Ongoing research activities on climate model initialization and near-term climate predictions, together with emergent constraints on late twenty-first century climate projections are aimed at narrowing the range of plausible water cycle changes. Advances in observations, models, and detection and attribution tools also provide potential observational constraints on global climate change projections that are now emerging in the instrumental record.

This chapter represents a new opportunity to have a focussed assessment of water cycle changes (WCC) and to consider climate change from the perspective of its impact on water resources. Although highly policy-relevant, the use of climate sensitivity (defined as the response of global and annual mean temperature to increasing CO_2 concentrations) has resulted in a temperature-focused perspective in previous assessment reports. This chapter highlights the complexity and potential vulnerability of the water cycle response to multiple anthropogenic drivers, including not only emissions of greenhouse gases and aerosols, but also land and water management and the plausible deployment of 'geoengineering techniques' such as solar radiation modification. Here we also reconsider former paradigms (e.g., 'dry-get-drier and wet-get-wetter') and evaluate whether such notions are appropriate for adequately representing the complex spatio-temporal variability of the global water cycle and its multi-scale response to anthropogenic forcings. Compared to AR5, more emphasis is placed on nonlinear atmospheric and land surface processes and on 'low probability, high impact' climate trajectories, including the potential for abrupt changes in the water cycle.

8.1.4.2 Conceptual framework

In line with the scope of the AR6 WG1 report, Chapter 8 provides a process-oriented assessment of past, recent and projected water cycle changes. State-of-the-art observations, models, diagnostic and statistical tools are used for this purpose. The chapter assesses the fast atmospheric adjustments caused by changes in anthropogenic radiative forcings, slower water cycle responses resulting from increasing surface temperatures, and cloud-aerosol processes affecting the water cycle. Whenever possible, formal detection and attribution studies are scrutinized to assess human influences on observed trends and variability in different components of the global water cycle. Particular attention will be paid to forcings and feedbacks in the physical components of the water cycle, including land surface processes where human activities have both direct (land use change, irrigation) and indirect (climate mediated and biophysical) effects. Beyond the expected changes in atmospheric water content, large-scale atmospheric circulation and regional phenomena (e.g. monsoons, storm tracks), changes in surface fluxes and water reservoirs are also evaluated in both observations and models. Changes in seasonality and variability are also considered. While the most robust water cycle changes are emphasized, the multiple limitations to the reliability of global and regional hydrological projections is also assessed, as well as the likelihood of abrupt and/or irreversible changes.

Although the water cycle now appears as a unified chapter, it remains a cross-cutting theme within and beyond AR6 WG1. Within WG1, water cycle changes have clear links with both global (chapters 2 to 4) and regional (chapters 10 to 12) climates, but is also relevant to many other climate processes, such as the energy budget (chapter 7), the carbon cycle (chapter 5) and ocean or cryosphere processes (chapter 9). For the sake of brevity and consistency, particular attention has been paid to the coordination with Chapter 11 on weather and climate extreme events. Chapter 8 focuses on processes and changes in mean state, variability and seasonality. Chapter 11 pays greater attention to changes in the frequency and intensity of extreme (including water-related) events. Although there are expected overlaps, reading both chapters 8 and 11 is highly recommended to obtain a comprehensive assessment of recent and future water cycle changes and of their driving mechanisms. Beyond WGI, water is also a key priority for adaptation (WGII) and mitigation (WGIII) policies.

Demand for freshwater resources will continue to increase due to a growing world population, enhanced development of agriculture, industry and tourism in many countries, and even possibly due to some mitigation strategies such as bio-energy with carbon capture and storage (BECCS) or afforestation. Although these non-climate factors are mainly assessed in WGII, here they are briefly discussed thereby recognising that they may exacerbate water scarcity issues caused by continued climate change. The adverse impact of human activities is not confined to water quantity and its spatio-temporal distribution, but also increasingly affects water quality, where and when water temperature increases and/or water flow decreases due to climate change. Despite their importance, these topics are not covered by Chapter 8; instead the reader is referred to Chapter 4 of WGII for more details on the impacts of climate change on broader issues of water resource management.

8.1.4.3 Chapter overview

Chapter 8 is based on the evaluation of multiple lines of evidence, including theory, observations, and model simulations. Unlike previous assessment reports, we begin with theoretical arguments that link externally-forced perturbations of the Earth energy budget to physically-understood changes in the global water cycle. This approach highlights the fact that available observations are neither the sole nor the most reliable evidence for predicting near-term to long-term regional WCCs. Most water cycle variables show a strong spatio-temporal variability and are strongly influenced by internal climate variability. Their sensitivity to anthropogenic climate change has not necessarily emerged in the instrumental record. WCC are the results of multiple forcings, adjustments, feedbacks and scale interactions. Their projection cannot be based on empirical tools, but rely on state-of-the-art numerical climate models. Observations are mostly useful to support or falsify the climate change theory and projections. In line with this guiding principle, chapter 8 puts a particular emphasis on detection-attribution studies and on the possibility to use observations for constraining future projections.

Section 8.2 begins by assessing theoretical and paleoclimate evidence for expected changes in the global water cycle. Beyond the Clausius-Clapeyron relationship and the expected increase in atmospheric humidity, energy budget constraints on circulation and precipitation changes are also discussed. Physical expectations for regional responses are assessed, including the role of surface processes and of aerosols. Paleoclimate reconstructions are also used to illustrate the water cycle’s sensitivity to perturbations of the Earth radiative budget.

In section 8.3, the causes of observed water cycle changes are assessed both in terms of attribution (to human influence versus other sources) and mechanisms (dynamical, thermo-dynamical and biophysical). Beyond changes in atmospheric water content and precipitation assessed in Chapter 3, the focus is also on land surface evapotranspiration and runoff, as well as on soil moisture and freshwater reservoirs. Observed variations in large-scale phenomena (e.g., tropical overturning circulations, monsoons, mid-latitude storm tracks and stationary waves) and regional variability (e.g., relevant teleconnections, wet extremes, aridity and large-scale droughts) are also assessed.

Section 8.4 explores the same variables and phenomena but focuses on projected changes and on the most robust (i.e., physically understood and not heavily model-dependent) mechanisms. Changes are assessed in both CMIP5 and CMIP6 models, and using multiple greenhouse gas concentration scenarios. However, for the sake of simplicity, we show projected changes per degree (Celsius) of global warming, thereby assuming the validity of the widely used pattern-scaling technique.

Section 8.5 quantifies the main sources of uncertainties that still limit confidence in global and regional projections, namely modelling uncertainty and internal climate variability. The possibility of narrowing such uncertainties either using higher-resolution models or constraining the current-generation models with available observations is also briefly discussed (see also Chapters 4 and 10 for more details). The potential limitations of the pattern-scaling approach are assessed, with a particular emphasis on nonlinear processes and path-dependent water cycle responses. The hydrological consequences of unpredictable major volcanic eruptions and of deliberate solar radiation modification are also discussed.

Section 8.6 focuses on abrupt changes and tipping points in the water cycle. In this report, the term abrupt refers to non-linear changes that occur much faster than the rate of change of external forcing, typically on the order of several decades. A tipping point occurs when a critical threshold is breached that causes global or regional climate to change from one stable state to another. These events include the possible shutdown of the Atlantic meridional overturning circulation (AMOC), modified land surface feedbacks, changes in atmospheric dust loadings, and anthropogenic radiation management. Low-probability but high-impact water cycle changes are considered to help inform mitigation and adaptation policies and are also explored in terms of an abrupt termination of solar radiation modification although such scenarios remain hypothetical.

Finally, section 8.7 provides a brief synthesis of the main knowledge gaps that still preclude a more confident assessment of water cycle changes. Three FAQs are also addressed to highlight the multiple drivers of water cycle changes at the regional scale, and the potentially dominant adverse effect of global warming in low mitigation scenarios, which could lead to a global increase in the occurrence and intensity of both floods and droughts across and beyond the 21st century.

8.2 Why should we expect water cycle changes?

The tight coupling between Earth's energy budget and the water cycle forms a robust physical basis for expecting substantial changes as the climate warms in response to radiative forcings, including elevated greenhouse gases and aerosol emissions. Large changes in the water cycle are also expected from anthropogenic modification of Earth's energy balance (Allen and Ingram, 2002) (7.6), and direct alteration of regional water resources (Alter et al., 2015; Asoka et al., 2017; Li et al., 2018b).Evidence from paleoclimate and historical observations that climate changes in the past produced profound alterations in the water cycle with implications for societies and civilizations (Buckley et al., 2010; Haug et al., 2003; Pederson et al., 2014). Societies experience impacts through localized changes in water availability that are controlled by large-scale atmospheric circulation as well as smaller-scale physical processes. Many of these processes have physically intuitive mechanisms, even though complex and non-linear interactions challenge the detection and attribution of changes. This section assesses advances in physical understanding of the global to regional drivers of water cycle changes that underpin and strengthen our interpretation of past and future changes in the global water cycle.

8.2.1 Expected global to regional-scale responses of the water cycle

At the global-scale, the strength of the hydrological cycle is determined by well-understood physical processes. However, atmospheric circulation controls the distribution of precipitation and water availability across the planet, and has a more complex connection to climate change. Prior to AR5, it was well established based on robust physics, observations and detailed modelling that changes in water vapour are tightly constrained by thermodynamics. While global precipitation is determined by the Earth's energy balance, regional changes are dominated by the transport of water vapour and dynamical processes. These contrasting drivers of precipitation at local and global scales mean that characteristics of central importance to the water cycle, such as precipitation intensity, duration and intermittence, are expected to alter as the climate changes (Trenberth et al., 2003). Research since AR5 has further strengthened this expectation (Döll et al., 2018).

8.2.1.1 Energy budget constraints on global precipitation

Since the AR5 there has been a refinement of understanding of how radiative forcings affect global precipitation and evaporation change through their influence on the atmospheric and surface energy budgets (Fläschner et al., 2016; Myhre et al., 2018; O'Gorman et al., 2012; Samset et al., 2016; Siler et al., 2018b). Global precipitation is tightly linked to the atmospheric energy budget, whereby the latent heat released through precipitation is balanced by the net atmospheric longwave radiative cooling minus the heating from absorbed sunlight and sensible heat flux from the surface (Figure 8.3)(Allen and Ingram, 2002; O'Gorman et al., 2012; Pendergrass and Hartmann, 2014a). Complementary energetic arguments also apply to surface evaporation (Roderick et al., 2014; Siler et al., 2018b). While global average quantities are not directly related to local-scale impacts, they are valuable in developing physical understanding, important in building confidence in attribution of past changes and projecting future responses.

[START FIGURE 8.3 HERE]

Figure 8.3: **(TO BE ADAPTED/SIMPLIFIED)** Schematic diagram of the energy fluxes and fast and slow precipitation change (ΔP) processes. (left) At the TOA, in the atmosphere, and at the surface, the energy budget is nearly in balance on a global scale. Changes in the atmospheric radiative cooling ΔQ can be caused by changes in absorption of shortwave radiation (SW) or changes in absorption/emission of longwave radiation (LW) or both. Here, LH = LΔP is the latent heat and SH is the sensible heat. (left center) An external driver of climate change alters the radiative fluxes at the top of the atmosphere and this may alter the atmospheric absorption. (right center) The instantaneous change through radiation may further alter the atmospheric temperature, water vapor, and clouds, through rapid adjustments. These rapid adjustments may lead to decreases or increases in clouds and water vapor, and they can vary through the atmosphere. The instantaneous radiative perturbation and rapid adjustments change precipitation on a fast time scale (from days to a few years). (right) Climate feedback processes through changes in the surface temperature further alter the atmospheric absorption, which occurs on a long time scale (decades). Net radiative fluxes at the TOA are given as F, water vapor as WV, temperature as T, and latent heat of vaporization as L. In the left center and right panels, the blue curve indicates the unperturbed state, the orange curve represents the rapid adjustments, and the red curve represents the effects of both fast and slow adjustments. **https://journals.ametsoc.org/doi/10.1175/BAMS-D-16-0019.1#**

[END FIGURE 8.3 HERE]

8.2.1.1.1 Global hydrological sensitivity

Global precipitation response to warming was estimated as 1-3% per ºC in AR5, which included fast adjustments that scale with atmospheric forcing and slow temperature-driven responses to radiative forcings(Andrews et al., 2010; Bala et al., 2010; Cao et al., 2015; Kvalevåg et al., 2013; Lambert and Faull, 2007; Samset et al., 2016). In terms of fast adjustments, there is *high confidence*, based on robust physics and idealised modelling experiments since AR5 (Fläschner et al., 2016; Samset et al., 2016), that global mean precipitation increases at 2.1-3.3 % per ºC of global mean warming, termed **hydrological sensitivity (η)** (Figure 8.4).

The fast response is caused by near-instantaneous changes in the atmospheric energy budget and atmospheric properties (e.g. temperature, clouds and water vapour) in direct response to the radiative effects of a forcing agent (Sherwood et al., 2015). A further relatively fast response involves the land-surface temperature which responds more rapidly to radiative forcing than the ocean (Cao et al., 2015; Dong et al., 2014) and operates mostly at the regional scale (Chadwick et al., 2017). On the other hand, the slower temperature-dependent precipitation response (hydrological sensitivity) is driven by the increased atmospheric radiative cooling rate of a warming atmosphere. Larger net radiative cooling rates are primarily balanced by increased latent heating through precipitation, although changes in sensible heat also play a role (Myhre et al., 2018; O'Gorman et al., 2012).

Since AR5, the dual fast adjustment and slow response framework has been verified across a range of global climate models, and the global precipitation responses to different forcing agents are physically well understood (Fläschner et al., 2016; MacIntosh et al., 2016; Myhre et al., 2017; Samset et al., 2016). This has been extended to include energy budget constraints on surface evaporation (Richter and Xie, 2008; Siler et al., 2018b), which is important since it strengthens the link between energy budget and thermodynamic drivers of the global water cycle (Section 8.2.1.2). Idealised modelling experiments highlight the pivotal role of surface evaporation in setting the amount of tropospheric warming and enhanced radiative cooling rates that determines hydrological sensitivity (Webb et al., 2018). Further confidence in the coupled processes involved are provided by simple models representing the energy budget and thermodynamic constraints that limit global evaporation to around 1.5% per °C(Siler et al., 2018b).

The precise value of η is also determined by climate feedbacks (O'Gorman et al., 2012) and may be overestimated (*low confidence*). This is based upon evaluation of simulated low-altitude cloud responses (Watanabe et al., 2018) which are known to be linked with hydrological sensitivity through the influence on temperature lapse rate responses that determine estimated inversion strength (Webb et al., 2018). DeAngelis et al. (2015)showed the sensitivity of shortwave absorption to atmospheric water vapourmay drive a significant portion of the remaininguncertainty in the hydrologicalsensitivity, however Richardson et al. (in press) note that longwave feedbacks may also make a significant contribution. Observational estimates of η (2.83 ± 0.92 % per ºC) inferred from interannual variability (Allan et al., 2014) are unlikely to be representative of longer term responses due to amplifying feedbacks associated with ENSO-related changes in cloud (Stephens et al., 2018).

[START FIGURE 8.4 HERE]

Figure 8.4: Precipitation change with surface temperature change for abrupt4xCO2 experiment with the IPSL-CM5A LR model. The hydrological sensitivity parameter η is the slope of the global-mean precipitation response with respect to surface temperature change when explicitly taking into account the rapid "adjustment" of precipitation due to forcing agents. The apparent hydrological sensitivity parameter η_a is given by the slope of global time-mean responses without accounting for rapid precipitation adjustments. The equilibrium precipitation change due to a quadrupling of CO2 is denoted as equilibrium hydrological sensitivity at 4 × CO2 (EHS4×). Small circles signify annual global means, and large circles the endpoint and equilibrium mean. [Fläschner et al (2016) J. Climhttps://journals.ametsoc.org/doi/10.1175/JCLI-D-15-0351.1 – to updated with CMIP6 data]

[END FIGURE 8.4 HERE]

The actual rate of global precipitation change per ºC of global surface warming, known as **apparent hydrological sensitivity (η_a)**, is substantially reduced by the direct influence of radiative forcing agents on the atmospheric energy balance. Rapid atmospheric adjustments involving precipitation are primarily caused by greenhouse gases and absorbing aerosols. The precise magnitude of the response depends on forcing type and characteristics, and is understood with *medium confidence* based on idealised simulations (Fläschner et al., 2016; Samset et al., 2016). A range of fast precipitation adjustments to carbon dioxide between models are attributed to the response of vegetation leading to a repartitioning of surface latent and sensible heat fluxes (DeAngelis et al., 2016). The range obtained from simulations of the last glacial maximum and pre-industrial period ($\eta_{a=}$1.80–2.89%) is larger than for a 4xCO2 experiment ($\eta_{a=}$1.37–2.43%) in which larger CO_2 forcing suppresses precipitation response due to fast adjustments, although vegetation and land surface changes are expected to play a role and energetic limitation on evaporation is smaller in the colder state (Li et al., 2013b).

Since the AR5, it has been confirmed that climate drivers that primarily influence the surface energy budget (such as solar forcing and sulphate aerosol) have larger η_a than drivers that primarily modulate aspects of the atmospheric energy budget such as GHGs and absorbing aerosol (Liu et al., 2018a; Samset et al., 2016). Thus, global precipitation appears more sensitive to radiative forcing from sulphate aerosols (2.8±0.4 % per ºC, $\eta_{a\sim}\eta$) than GHGs (1.4±0.3 % per ºC, $\eta_{a<}\eta$) while the response to Black Carbon aerosol can be negative(-3.5±3.0 % per ºC,$\eta_{a<<}\eta$) due to strong atmospheric solar absorption (Samset et al., 2016). Responses in precipitation extremes (8.2.2.1.2) can be several times more sensitive to changes in aerosols than GHGs (Lin et al., 2018a). In four different climate models, the response to a complete removal of anthropogenic aerosol emissions was an increase in global mean precipitation of between 2 and 4.6% (Samset et al., 2016) and heavy precipitation intensity increased by 3.1-5.3% over land, mainly attributed to the removal of sulphate aerosol as opposed to other aerosol species. The vertical profile of black carbon and ozone influences the magnitude of the fast global precipitation response yet is more difficult to observe and simulate (Allen and Landuyt, 2014; MacIntosh et al., 2016; Stjern et al., 2017).

Global precipitation decreases due to the cooling effects of anthropogenic aerosol and rapid adjustments to GHGs and absorbing aerosol have masked increases relating to warming from GHGs. The warming influence of continued rises in CO_2 concentration, combined with declining aerosol cooling, are expected to increase the importance of the slow temperature-related effects on the energy budget relative to the more rapid direct radiative forcing effects as transient climate change progresses (Myhre et al., 2018; Salzmann, 2016; Shine et al., 2015). Modest multi-decadal trends in global precipitation responses observed in the satellite era (Section 8.3) are therefore expected, however observational uncertainty precludes confirmation of the energetic constraints.

In summary, it is *virtually certain* that global precipitation and evaporation will increase in response to future warming (8.4.1.3). Nevertheless, current changes (8.3.1) are offset by rapid adjustments to radiative forcings, the magnitude of which are known to *medium confidence* based upon a range of responses in climate models.

8.2.1.1.2 Regional precipitation responses to radiative forcing

Since AR5 there has been more focus on how fast and slow precipitation responses manifest on regional scales (Hodnebrog et al., 2016; Li and Ting, 2017; Richardson et al., 2016, 2018b, Samset et al., 2016, 2017; Tian et al., 2017). Atmospheric circulation changes (Section 8.2.1.3) generally dominate the spatial pattern of fast precipitation adjustments to different forcing agents in the tropics (Bony et al., 2013; He and Soden, 2015a; Richardson et al., 2016; Tian et al., 2017).

Radiative forcings with heterogeneous spatial patterns such as ozone and aerosol (including cloud interactions) are expected to drive substantial responses in regional atmospheric circulation through uneven heating and cooling effects (AR5). On regional scales, changes in energy transport are associated with regional precipitation responses. Idealised modelling also shows that responses are region-specific with larger η_a when sulphate aerosol is increased over Europe compared with Asia (Liu et al., 2018b). However, Asian sulphates were found to be more effective per unit forcing in driving local precipitation changes than European sulphates are for Europe.

Carbon dioxide is thought to drive large-scale fast circulation changes in the tropics through two main processes. Reduced longwave radiative cooling to space in regions of descent drives a general slowdown of circulation (Bony et al., 2013; Merlis, 2015; Richardson et al., 2016). Additionally, greater downwelling longwave radiation at the surface rapidly warms the land surface, which initially destabilizes the troposphere and strengthens vertical motion and precipitation over land in the short term (Chadwick et al., 2014; Richardson et al., 2016, 2018a).

The land-sea contrast in fast precipitation changes is evident across different forcing agents and leads to similar spatial patterns for greenhouse gases, solar forcing and absorbing aerosols (Samset et al., 2016). While fast precipitation adjustments to CO_2 have been counteracted by anthropogenic sulphate aerosol increases, this compensation is expected to diminish as aerosol forcing declines (Richardson et al., 2018a). Hydrological sensitivity is suppressed over land (0-2 % per ºC) relative to the global mean, in particular across low latitudes and for black carbon aerosol radiative forcing (Richardson et al., 2018a; Samset et al., 2017). Expected stronger warming over land means ocean air masses are unable to supply sufficient moisture to maintain relative humidity leading to a drying influence that is further amplified by land surface feedbacks (8.2.1.2). A weaker expected hydrological response over land is important for aridity changes (8.2.2.2.6), while also presenting a challenge for attribution of continental precipitation changes (3.3.2.1) to different climate forcings(Samset et al., 2017).

In summary it is *virtually certain* that large but variable regional responses in precipitation are expected to arise from atmospheric circulation changes driven by radiative forcing. This is explained by altered vertical and horizontal heating or cooling of the atmosphere that is particularly strong for spatially variable aerosol forcings while evolution of SST and changes in land-ocean thermal contrasts play a role on longer time-scales. It is *very likely* that a smaller precipitation response to warming over land than ocean is driven by a continental drying response to increasing land-ocean thermal contrast and land surface feedbacks.

8.2.1.2 Thermodynamic constraints on large-scale water cycle changes

The Clausius Clapeyron equation is a strong constraint on atmospheric water vapour which is *virtually certain* to increase globally with continued warming. The magnitude of changes are known to *high confidence* based on detailed modelling and observations (AR5; section 7.2.4) with expected increases in specific humidity near to the surface of around 6-7% per ^{o}C. This expectation is valid at continental to global scales, corroborated with observational evidence (Section 8.3) and explained by small changes in relative humidity that are expected to decline only slightly over land (Byrne and O'Gorman, 2018). Deviations from a similar thermodynamic response of integrated water vapour to surface warming are identified in idealised modelling experiments that show contrasting fast adjustments to drivers, varying from 6.4±0.9%/K for sulphate aerosol to 9.8±2%/K for black carbon (Hodnebrog et al. in review). Prevalent increases in atmospheric water vapour drive powerful amplifying climate feedbacks (7.4.2.2), intensify atmospheric moisture transport and associated heavy precipitation events (8.2.2.1.2), and increase the atmospheric absorption of sunlight and emission of infrared radiation to the surface with consequences for global-scale evaporation and precipitation responses (8.2.1.1).

Advances have been made in understanding ocean evaporation responses in terms of the thermodynamics of a water-saturated surface (Yang and Roderick, 2019). Warming leads to an increase in the ratio of latent to sensible heat fluxes due to an increase in the surface-air moisture gradient (required by the Clausius–Clapeyron equation), and a corresponding decrease in the surface-air temperature gradient (required by energy conservation). Applying this framework to 4xCO_2 climate model experiments predicts increases in evaporation with warming of around 1% per ^{o}C at low latitudes up to 5% per ^{o}C at high latitudes (Siler et al., 2018b). These changes are initially offset by rapid adjustments to CO_2 increases and resulting ocean heat uptake leading to a negative net available energy for evaporation.

Since the AR5 it has been further demonstrated that the Budyko framework, which links evapotranspiration to energy and water supply, is useful for identifying physically consistent surface hydrology parameters and in interpreting expected water cycle responses at the land surface (Greve et al., 2014; Roderick et al., 2014). For high precipitation regions suppression of evaporation below its upper potential is energy-limited while for low precipitation regions, evapotranspiration is limited by the availability of surface and ground water. Applying this framework demonstrates that changes in E-P over land are dominated by precipitation (Roderick et al., 2014). Precipitation changes are strongly determined by changes in atmospheric circulation but are also determined by increased moisture fluxes and further modified by land-ocean gradients in surface air temperature and humidity (Byrne and O'Gorman, 2015, 2016).

Prior to the AR5, increased atmospheric moisture with warming was established as a well-understood driver of contrasting regional responses in the water cycle. This is because resulting increases in atmospheric moisture transport are expected to amplify existing precipitation minus evaporation (P-E) patterns (Held and Soden, 2006b). Positive P-E determines fresh water flux from the atmosphere to the surface and negative P-E signifies a net flux of fresh water into the atmosphere with atmospheric moisture balance achieved primarily by horizontal moisture transport from net evaporative ocean regions into wet convergence zones. Over the land surface, P-E is balanced by runoff and storage while P-E influences salinity over the ocean. This provides a basic framework to interpret observed and simulated responses (8.3-8.4).

There is *high confidence* (based on thermodynamics, detailed modelling and observations) that amplification of P-E patterns are expected to apply over the oceans with an associated “fresh get fresher, salty get saltier” signature in ocean salinity (Durack, 2015; Roderick et al., 2014). This amplification is moderated by proportionally larger increases in E over the sub-tropical oceans and weakening of the tropical circulation (Section 8.2.1.3) (Chadwick et al., 2013; Siler et al., 2018b), an expectation corroborated by observed changes (Skliris et al., 2016). Atmospheric and ocean circulation changes are expected to further dampen the P-E amplification. However, ocean stratification due to heating of the upper layers through radiative forcing has been identified as a mechanism for amplifying the salinity patterns beyond the responses we expect to be driven by water cycle changes alone (Zika et al., 2018).

Since the AR5 numerous studies have confirmed that amplification of P-E patterns cannot be simply interpreted as a “wet gets wetter, dry gets drier” response (Byrne and O’Gorman, 2015; Chadwick et al., 2013; Greve et al., 2014; Roderick et al., 2014; Scheff and Frierson, 2015). Ocean regions experiencing increasing E-P cannot meaningfully be described as “dry” (Roderick et al., 2014), and over land P-E is not a good proxy for “dryness” or aridity that is better represented by potential evaporation determined primarily by net radiation (Greve and Seneviratne, 2015; Roderick et al., 2014; Scheff and Frierson, 2015). Amplified P-E patterns result from increased moisture transport from the divergent to the convergent portions of the atmospheric circulation. These are not geographically fixed and their movement further complicates regional interpretation. Although convergent parts of the atmospheric circulation are expected to become wetter (in terms of increasing P-E) and net evaporative regions drier (increasing E-P) the location of these regions will alter. Spatial shifts in atmospheric circulation are therefore expected to modify and even dominate these thermodynamic responses locally (Section 8.4). Paleoclimate evidence confirms that during the Last Glacial Maximum (21,000 years ago), global-scale changes in the zonal mean are roughly in agreement with thermodynamic scaling (Li et al., 2013b), but dynamical changes induce strong zonal asymmetries and regional deviations (Bhattacharya et al., 2017b; Boos, 2012; DiNezio and Tierney, 2013; Scheff et al., 2017) such that patterns in P-E are not well described by thermodynamic expectations.

Further refinement in understanding P-E responses over land have followed the AR5. Land P-E is generally positive and balanced by runoff over multi-annual time-scales, assuming minimal storage changes. As a result, the “wet gets wetter, dry gets drier” scaling suggests that P-E over land will become more positive (i.e. wetter) with warming (Byrne and O’Gorman, 2015; Greve et al., 2014; Roderick et al., 2014). However, climate models predict both positive and negative P-E responses in different land regions which do not conform to the “wet gets wetter, dry gets drier” scaling (Figure 8.5). Spatial gradients in temperature and relative humidity and their changes as land warms more than oceans have been identified as driving continental drying over some regions, causing many continents to deviate strongly from the simple “wet gets wetter, dry gets drier” scaling (Byrne and O’Gorman, 2015). This drying is partly explained by reductions in relative humidity (Byrne and O’Gorman, 2016; Lambert et al., 2017) that is further amplified by vegetation responses (8.2.2.2.2) (Berg et al., 2016; Byrne and O’Gorman, 2016). Furthermore, P-E may be negative in the tropical dry season where ground water storage becomes depleted so contrasting seasonal water cycle responses are also expected (Chou et al., 2013a; Kumar et al., 2015). Idealized modelling further shows that continental drying driven by increased land-sea thermal contrast can worsen aerosol pollution due to reduced cloud and precipitation (Allen et al., 2019).

[START FIGURE 8.5 HERE]

Figure 8.5: Multimodel-mean changes in zonal-mean P − E over (a) oceans and (b) land. Black lines show the simulated changes. Red dashed lines show a simple scaling in which P-E scales with the Clausius Clapeyron equation while the solid red line shows an extended scaling accounting for changes in relative humidity and spatial gradients in temperature and moisture and more realistically captures subtropical decline in P-E over land depicted by coupled climate models. The effect of land-ocean warming contrasts (c-d) can further drive continental drying through altered moisture fluxes driven by (c) asymmetric warming and (b) enhanced land warming. The heavy black arrows represent the modified moisture flux G in the base climate and the curves are idealized profiles of surface air temperature change verses

longitude. [Figure 3 and 8 from Byrne and O'Gorman (2015) J. Climhttps://journals.ametsoc.org/doi/full/10.1175/JCLI-D-15-0369.1 to be updated with CMIP6]

[END FIGURE 8.5 HERE]

To summarise, increased moisture transport from evaporative oceans to wet parts of the atmospheric circulation will drive amplified P-E and salinity patterns over the ocean (*high confidence*) while variable regional changes are expected over land. Based on the improved understanding of thermodynamic drivers since the AR5, there is *medium confidence* based upon multiple lines of evidence (Chadwick et al., 2016a; Chou et al., 2013b; Dong et al., 2018a; Kao et al., 2017; Lin et al., 2018b; Liu and Allan, 2013a; Polson and Hegerl, 2017) that the contrast between wet and dry meteorological regimes, seasons and events will increase in a warming climate.

8.2.1.3 Expected response in large-scale atmospheric circulation patterns

Changes in characteristics of the large-scale atmospheric circulation dominate responses in the hydrological cycle in some regions, affecting the availability of fresh water and the occurrence of climate extremes. Large-scale responses in atmospheric circulation identified in the AR5 are a weakening and broadening of tropical circulation with poleward movement of tropical dry zones and mid-latitude jets. Robust changes in atmospheric circulation are linked with rapid adjustments to radiative forcing and its spatial pattern as well as the resulting slower climate response involving changes in temperature and moisture gradients (Bony et al., 2013; Ma et al., 2018a). In this section, emphasis is placed on advances in knowledge of robust large-scale responses in the water cycle expected from physically well-understood drivers.

As recognised in the AR5, a long-term weakening of the tropical atmospheric overturning circulation is expected as climate warms in response to elevated CO_2. A reduced vertical mass flux (representing atmospheric overturning circulation) is required to reconcile low-level water vapour increases (around 6-7% per ºC) with smaller precipitation responses (about 1-3% per ºC), a consequence of thermodynamic and energy budget constraints (Section 8.2.1.1-8.2.1.2). The slowdown can occur in both the Hadley and Walker circulations, but in most climate models occurs preferentially in the Walker circulation (Vecchi and Soden, 2007). The balance between radiative cooling and adiabatic heating of the subsiding sub-tropical air is an important mechanism explaining tropical circulation weakening (Held and Soden, 2006b). Reduced radiative cooling is achieved through fast adjustments to increasing radiative forcing and slower responses to reduced temperature lapse rate (Cherchi et al., 2011; Plesca et al., 2018; Shaw and Tan, 2018; Xia and Huang, 2017).

Since the AR5, idealized modelling studies have further demonstrated a direct link between CO_2 increases and atmospheric circulation response, with the subtropical descent regimes playing a dominant role (Cherchi et al., 2011; Plesca et al., 2018; Shaw and Tan, 2018; Xia and Huang, 2017). An estimated 3-4% slowdown of the large-scale tropical circulation in response to quadrupling of CO_2 is dominated by reduced tropospheric radiative cooling in sub-tropical ocean subsidence regions. Subsequent surface warming contributes up to a 12% slowdown in circulation, driven by enhancement of atmospheric static stability through thermodynamic decreases in temperature lapse rate (Plesca et al., 2018). The pattern of SST response and land-ocean warming contrasts affect details of the atmospheric circulation response (He and Soden, 2015a) and resultant regional water cycle changes.

Since the driving mechanisms for Walker circulation weakening differ to those involved in determining ENSO variability, an El Niño pattern of regional hydrological cycle extremes is not expected, although internal variability is capable of generating temporary strengthening over decadal time-scales (L'Heureux et al., 2013a; Sohn et al., 2013b). Instead a weaker Walker circulation is expected to drive strongly asymmetric changes in P-E over the tropical Pacific with substantial associated regional changes in the water cycle and has also been linked to reduced tropical cyclone translation speed (Kossin, 2018), implying an expected increase in extreme precipitation (Section 8.2.2.2.5).

For the Last Glacial Maximum, model simulations suggest a stronger Pacific Walker circulation in response to a cooler climate (consistent with an expected weakening in a warmer climate), but a weaker Indian Walker circulation in response to the exposure of the Sunda and Sahul shelves due to lowered sea level (DiNezio et al., 2011). The latter effect is detectable in proxies for hydroclimate, and salinity, and sea-surface temperature, confirming a strong response of the water cycle to Walker perturbation (DiNezio et al., 2018; DiNezio and Tierney, 2013). A more direct analogue for future warming is found in the mid-Pliocene period (3 million years ago), the last time the Earth experienced comparable CO_2 levels. Sea-surface temperature reconstructions show a weakening of the Pacific zonal gradient and a pattern of warmth consistent with weaker Walker cycle response (Tierney et al., in review), supporting an expected future weakening.

The Intertropical Convergence Zone (ITCZ) is a key component of the tropical circulation. Its regional position, width and strength determine the location and seasonality of the tropical rainy belt with associated consequences for societies. The mean location of the ITCZ north of the equator is explained by northward heat transport by the ocean (Figure 8.6) that introduces a hemispheric energy budget imbalance (Frierson et al., 2013; Marshall et al., 2014). Changes in meridional overturning ocean circulation or other mechanisms that alter the hemispheric atmospheric energy imbalance are therefore expected to influence the position of the tropical rainy belt and regional water cycle. Paleoclimate data suggests that the position of the ITCZ has shifted in the past by 1 degree of latitude or less, due to energy constraints (McGee et al., 2014a). Paleoclimate data and modelling experiments further indicate the possibility for rapid shifts in the ITCZ and regional monsoons in response to changes in ocean circulation related to AMOC (6.2.1).

[START FIGURE 8.6 HERE]

Figure 8.6: Schematic of the role of the oceanic overturning circulation in forcing the Northern Hemisphere maximum of tropical precipitation. Heat is released from the ocean to the atmosphere in the Northern Hemisphere owing to cross-equatorial ocean heat transport (7.2). The atmosphere responds through eddy energy transports in the extratropics and a cross-equatorial Hadley circulation, which fluxes energy from the Northern Hemisphere to the Southern Hemisphere. The moisture transport by the Hadley circulation is in the opposite direction as the energy transport, so tropical precipitation moves northwards. SP, South Pole; NP, North Pole; cross-EQ, cross-equatorial; q, moisture transport; F, energy transport. [From Frierson et al (2013) Nature Geosci. https://www.nature.com/articles/ngeo1987 (Figure 3)]

[END FIGURE 8.6 HERE]

Since the AR5, research has established the importance of cross-equatorial energy transports in determining the mean position, width and strength of the ITCZ, and systematic biases in climate modelsimulations of the ITCZ(Adam et al., 2016; Boos and Korty, 2016; Byrne et al., 2018; Frierson et al., 2013; Loeb et al., 2016; Stephens et al., 2015b), particularly related to projected changes (8.4). Weakening of the average ITCZ circulation with warming (Byrne et al., 2018) results from a complex interplay between strengthened upward motion in the ITCZ core and weakened updrafts at the edges of the ITCZ (Lau and Kim, 2015). This leads to a drying tendency on the equatorward edges of the ITCZ (Byrne and Schneider, 2016b) and a moistening tendency in the ITCZ core. Stronger ascent in the ITCZ core amplifies the “wet get wetter” response while reduced moisture inflow near the ITCZ edges reduces the “wet gets wetter” response relative to the 7% per ºC rate of precipitation increase with warming predicted by basic thermodynamics.

Although a dynamical understanding of changes in ITCZ width and strength currently lags understanding of the controls on ITCZ position, energetic and dynamic theories are being developed (Byrne and Schneider, 2016b; Dixit et al., 2018; Harrop and Hartmann, 2016; Popp and Silvers, 2017). In particular, the importance of radiative forcing (Allen et al., 2015; Chung and Soden, 2017; Dong and Sutton, 2015a), feedbacks involving clouds (Su et al., 2017, 2019; Talib et al., 2018a) and vertical energy stratification (Byrne and Schneider, 2016a; Popp and Silvers, 2017) have been identified (8.3-8.4). Since the AR5, modelsimulationssuggest that orbital variations produce an expansion or contraction in the global zonal mean

ITCZ rather than shifts which are regionally dependent (Singarayer et al., 2017).

Monsoon systems form an integral component of the tropical rainy belt and affect billions of people through the supply of fresh water for agriculture. However, determining the drivers of wet and dry extremes yet are not simply related to the causes of ITCZ shifts. Monsoons are traditionally interpreted as driven by the seasonal heating of tropical land regions and the resulting atmospheric circulation response to contrasting temperature between land and the cooler ocean involving energy and moisture balance (Cherchi et al., 2011; Levermann et al., 2009). It was recognised in the AR5 that thermodynamic increases in moisture transport are expected to increase monsoon strength and area that is offset by a weakening tropical circulation.

Since the AR5 it has been further recognised that monsoon systems are sensitive to spatially varying radiative forcing relating to anthropogenic aerosol (Allen et al., 2015; Hwang et al., 2013b; Li et al., 2016b) and greenhouse gases (Dong and Sutton, 2015a) with changes in SST patterns resulting from radiative forcing (Guo et al., 2016b) that alter cross equatorial energy transports and land-ocean temperature contrasts playing a strong role (Section 8.3-8.4). Microphysical effects of aerosol on clouds, and local-scale processes and feedbacks, are also expected to influence monsoon rainfall characteristics (Section 8.2.2). Improved understanding of zonal asymmetries in the circulation, land/ocean differences in surface fluxes, and the character of convective systems have been identified since the AR5 as fundamental in reconciling disagreement between paleo and modern observations, physical theory and numerical simulations (Biasutti et al., 2018); Seth et al 2018 – submitted).

The poleward margin of the monsoons is limited by both orography as well as “ventilation” by cold, dry mid-latitude air (Chou and Neelin, 2003). Paleoclimate data and modelling experiments from the Last Glacial Maximum suggest that increased ventilation, as a result of the presence of the Laurentide ice sheet, substantially weakened the North American monsoon system (*medium confidence*), highlighting the importance of this mechanism in regulating regional monsoon strength (Bhattacharya et al., 2017b, 2018). In a warming world, mid-latitude ventilation might be expected to decrease, and increased moisture enhances convective instability; both factors would contribute to a stronger and more latitudinally expansive monsoon (Su and Neelin, 2005). On the other hand, higher temperatures raise the threshold for convection (“upped-ante mechanism”), limiting monsoon intensification (*low confidence*)(Chou et al., 2009; Chou and Neelin, 2004).

It is *likely* that amplified warming in the Arctic will influence the regional water cycle in mid-latitude regions through changes in atmospheric circulation, however the precise response is not yet well understood (8.3.2.6). For example, a plausible link between Arctic amplification and the jet stream with increased persistence of wet and dry climate events over northern mid-latitudes (Francis and Vavrus, 2012) was refuted on methodological grounds (Barnes, 2013a). An expected response based on simple physical grounds is unclear due to the large number of competing physical processes (Barnes and Polvani, 2013; Cohen et al., 2014; Hoskins and Woollings, 2015; Woollings et al., 2018a). A weaker jet stream associated with Arctic amplification was linked to reduced precipitation in middle latitudes based on paleoclimate data sampling the early Holocene (Routson et al., 2019). However, increased moisture and its transport and convergence within extra-tropical cyclones is expected to increase rainfall totals within wet events, leading to an increased likelihood of severe flooding when these extremes occur (Section 8.2.2.2.5, 11.5).

In summary, changes in the regional hydrological cycle across most regions are expected due to altered atmospheric wind patterns that are caused by the direct response to radiative forcing and the slower evolving response of surface temperature patterns (*high confidence*). A slowing of the tropical circulation and expansion of the subtropics is *very likely* based on simple and idealised modelling. A reduced thermal gradient between the Arctic and lower latitudes is expected to alter atmospheric circulation but the expected response is understood with *medium to low confidence* and increases in moisture transport between mid-latitudes and the Arctic are expected despite a reduced jet stream strength (*medium confidence*).

8.2.2 Physical expectations from local-scale processes affecting the water cycle

Processes operating at local scales are capable of influencing substantial modifications in the regional water cycle above those expected from large-scale influences with consequences for impacts globally. This section assesses the development of understanding since the AR5 in processes affecting the atmosphere, surface and subsurface including cryosphere and biosphere interactions.

8.2.2.1 Atmospheric processes

8.2.2.1.1 Aerosol effects on cloud systems

Aerosol emissions into the troposphere are expected to influence individual cloud systems and exert local and regional effects on precipitation amounts and intensities. These processes can influence the overall precipitation amount at a global scale if they alter the energy budget (Section 8.2.1.2). Based on the evaluation provide in the AR5 (7.6.4), it was unclear whether changes in aerosol-cloud interactions relating to aerosol-cloud condensation nuclei substantially affect the evolution of precipitating systems.

Microphysical processes occurring in clouds that affect precipitation are linked with the number of cloud condensation nuclei (CCN) into clouds. CCN consist of aerosols and cloud droplets nucleating on pre-existing aerosols particles. A lack of CCN leads to the formation of clouds with small concentrations of large cloud droplets that leads to fast formation of rain even from shallow clouds. This does not necessarily increase overall rainfall amount, as the fast coalescence leads to less condensation and less water available for precipitation (Fan et al., 2018a; Koren et al., 2014). Less condensation also means decreased latent heat release which decreases convection and decreases precipitation. Addition of even the smallest (e.g., 10 nm) ultrafine aerosol particles to such clouds can invigorate them substantially (Fan et al., 2018a; Khain et al., 2012).

Cloud drop coalescence rate increases with the 5th power of droplet mean radius (Freud and Rosenfeld, 2012). Since cloud drops mostly form at cloud base and grow as they rise, clouds forming in more polluted air masses (hence with more small drops) need to grow deeper to initiate rain (Braga et al., 2017; Freud and Rosenfeld, 2012; Konwar et al., 2012). Such aerosol-related processes often compensate or buffer each other (Stevens and Feingold, 2009). Therefore, despite the potentially large impacts, the net outcome of aerosol microphysical effects on precipitation has generally *low confidence*, especially when evaluated with respect to the background of high natural variability in precipitation.

8.2.2.1.2 Processes determining precipitation intensity

Precipitation changes are determined by the energy budget at large scales and by the moisture budget at smaller time and space scales and these contrasting constraints imply both a change in the mean and a shift in intensity distribution (Pendergrass, 2018; Pendergrass and Hartmann, 2014b). Building on the AR5, there is *high confidence* that extreme precipitation events will become more severe as the planet continues to warm (11.4) based on robust physics, extensive modelling and increasing observational corroboration (Fischer and Knutti, 2016). Expected increases in low-level moisture of around 6-7% per ºC (8.2.1.2) provide a robust baseline expectation for a similar rate of intensification in extreme precipitation. However this thermodynamic scaling is modified by microphysical and dynamical responses (Figure 8.7a; Box 11.2) that are less well understood (O'Gorman, 2015; Pendergrass et al., 2016; Pfahl et al., 2017).

[START FIGURE 8.7 HERE]

Figure 8.7: (a) Fractional changes relative to the 20th century (multi-model median, see (O'Gorman and Schneider, 2009) in the 99.9th percentile of daily precipitation (blue), zonally averaged atmospheric water vapor content (green), saturation water vapor content of the troposphere (black dotted), a simple scalingsaccounting for thermodynamic and dynamic changes (red dashed) and a thermodynamic-only

scaling (black dashed). Water vapour increases slighty less than expected from thermodynamics due to reduced relative humidity, particularly in the subtropics, while increases are larger than at surface levels as saturation specific humidity increases at a greater rate with temperature for higher, colder regions of the atmosphere. The precipitation scaling is closely related to but slightly less than thermodynamic changes near the surface due to dynamical changes (b) Observed scaling of the 90th, 99th and 99.9th percentile of hourly rainfall with daily mean surface temperature for the Netherlands (grey shading denotes the 98% uncertainty range) with the super-Clausius Clapeyron (14%/K) and Clausius Clapeyron (7%/K) scalings denoted. [Or use Figure 2 from O'Gorman 2015 Curr. Clim. Change. Rep. (Can this be updated to CMIP6?) http://link.springer.com/article/10.1007%2Fs40641-015-0009-3 and Lenderink et al. (2011) HESS https://www.hydrol-earth-syst-sci.net/15/3033/2011/ (Fig. 1)]

[END FIGURE 8.7 HERE]

Since the AR5 there has been further evidence for the intensification of heavy precipitation (Fischer and Knutti, 2016; Neelin et al., 2017; O'Gorman, 2015) particularly in mid-high latitudes (O'Gorman and Schneider, 2009). Globally, heavy snowfall events are not expected to decrease significantly with warming since they tend to occur close to freezing point, which will migrate poleward and may become more common in some cold climates (O'Gorman, 2014a). The amount and intensity of rainfall within extratropical storms is expected to increase with atmospheric moisture. This is particularly evident for atmospheric river events, which are long, narrow bands of intense horizontal moisture transport, within the warm sector of extra tropical cyclones (Dacre et al., 2015). Assuming minor changes in dynamical characteristics, it is expected with *high confidence* that atmospheric river events will intensify, primarily due to increases in atmospheric moisture (Espinoza et al., 2018b; Lavers et al., 2013; Ramos et al., 2016), although changes in atmospheric circulation are likely to dominate responses regionally (8.2.1.3). Idealised modelling experiments indicates that a weaker latitudinal temperature gradient is capable of increasing the duration of intense precipitation (Dwyer and O'Gorman, 2017).

Thermodynamic intensification of rainfall from tropical cyclones is potentially amplified by a reduced system speed linked to weakening tropical circulation (Kossin, 2018), as a consequence of the energetic and thermodynamic constrains on tropical precipitation (Chadwick et al., 2013). Increases in aerosols were found to enlarge tropical cyclone rainfall area and amount in the western North Pacific (Zhao et al., 2018a). Sensitivity experiments indicate that the most intense rainfall within tropical cyclone increases with warming above the Clausius Clapeyron rate (Phibbs and Toumi, 2016). Regional changes in land-ocean temperature gradients (Section 8.2.1.3) are also expected to influence intense precipitation, explaining the observed intensification of storms over the Sahel (Taylor et al., 2017a). Surface feedbacks are also expected to modify regional responses (Berg et al., 2016), for example, in active to break phase transition over India (Karmakar et al., 2017; Roxy et al., 2017).

For many regions the expected response of heavy precipitation is highly space and time-scale dependent (Pendergrass, 2018). Since the AR5, there have been advances in understanding the expected changes in intense rainfall at the sub-daily time-scale based on idealised and high resolution model experiments as well as assessments of observations (Westra et al., 2014). The intensity of convective storms is related to Convective Available Potential Energy (CAPE) which is expected to increase thermodynamically with warming (Romps, 2016). Sub-daily rainfall extremes are likely to intensify in regions and seasons without limitations on moisture supply (Prein et al., 2017)(Chan et al., submitted). Latent heat release, increased vertical velocities and subsequent lateral moisture convergence through the cloud base are shown to play a key role in the intensification of hourly and sub-hourly precipitation intensities, with the increasing height of the tropopause with warming allowing the establishment of larger systems (Lenderink et al., 2017). Intensification can exceed thermodynamic expectations since additional latent heating may invigorate individual storms (Berg et al., 2013; Molnar et al., 2015; Nie et al., 2018; Prein et al., 2017; Scoccimarro et al., 2015; Zhang et al., 2018f). This is corroborated by observed scalings (Figure 8.7b) up to 3 times the rate expected from the Clausius Clapeyron equation for some locations (Guerreiro et al., 2018a; Lenderink et al., 2017). Ship-based observations show increases in 99th percentile hourly rainfall extremes (above 8.5 %/ºC) with no reduction in duration at higher temperatures (Burdanowitz et al., 2019). A fixed threshold temperature above which precipitation extremes diminish, proposed at the time of AR5, is not supported by recent modelling work (Neelin et al., 2017).

Enhanced latent heating within storms can also suppress convection at larger-scales due to atmospheric stabilization as demonstrated with idealised and large ensemble modelling studies (Chan et al., 2018; Loriaux et al., 2017; Nie et al., 2018; Tandon et al., 2018). Large eddy simulations demonstrate that stability controls precipitation intensity, moisture convergence controls area fraction and relative humidity increases intensity while slightly decreasing area fraction (Loriaux et al., 2017). Stability is also influenced by the direct radiative heating effect of higher CO_2 concentration (Baker et al., 2018) as well as the effects of aerosol on the atmospheric energy budget and cloud development (8.2.2.1.2). Increased radiative forcing from declining aerosol is expected to intensify precipitation (Lin et al., 2018a), although the effects of different radiative forcings are difficult to separate from natural variability (Sillmann et al., 2017). Since the AR5, new modelling evidence shows increases in convective precipitation extremes may be limited by microphysical processes involving droplet/ice fall speeds (Sandvik et al., 2018; Singh and O'Gorman, 2014). Idealised modelling indicates that instantaneous precipitation extremes are more sensitive to microphysical processes while daily extremes are determined more by the degree of convective aggregation (Bao and Sherwood, 2019).

In summary, there is *high confidence* that the precipitation intensity distribution is expected to change in a warming climate. It is *virtually certain,* based on robust physics that heavy precipitation events, that in regions where intense precipitation events do occur, they will become more severe. There is *medium confidence* that the frequency of very wet events will increase in most regions since this depends on less certain changes in large-scale atmospheric circulation patterns and evolving dynamical and microphysical characteristics within storms.

8.2.2.2 Land surface processes, feedbacks and phenomena

Surface processes are expected to substantially modify influences from the large-scale atmospheric responses to warming through feedbacks and human influences through land use changes (SRCCL 2.6). The impacts of water cycle change are profoundly and primarily experienced across the land surface, while cryosphere and biosphere interactions are expected to play an important role regionally.

8.2.2.2.1 Cryosphere processes

The frozen component of the water cycle (consisting of ice sheets and shelves, sea-ice, river and lake ice, snow cover, permafrost, subsurface glacier and snowpack) is tightly coupled to the surface energy balance, which controls water exchanges with the atmosphere, the land surface and sub-surface and the oceans. Declining ice sheet mass, glacier extent and northern hemisphere sea ice and snow cover was reported in the AR5 with continued reduction in the stores of frozen water as an expected consequence of a warming climate (9.3-9.5). Changes and feedbacks involving the cryosphere operate on a range of time-scales that impact the regional water cycle through changes in surface evaporation, seasonal river flow and lakes.

Climate-related reductions in snow and freshwater ice, as well as changes to permafrost on Arctic land affect hydrology and vegetation, thereby decreasing water and food security. Increased evaporation from warmer lakes can be exacerbated by the loss of lake ice, driving increased fresh water loss through evaporation (Sharma et al., 2019; Wang et al., 2018c). Permafrost degradation is expected to reduce soil ice and the extent of thermokarst lake coverage (SRCCL 3.4.1.2). Soils (including permafrost) are expected to warm more slowly than the near-surface atmosphere due to thermal damping by soil heat capacity. This causes a delay between current climate change and permafrost degradation (SR1.5 3.6.3.3) that depends on sensitivity to surface snow cover. Increased spring rainfall is now known to accelerate thawing of permafrost through heat advection by infiltration leading to increased methane emissions (Neumann et al., 2019), further amplifying carbon cycle feedback (5.4.7).

A decline in mountain snowpack, glacier melt, and increases in snow melt will alter the amount and timing of seasonal runoff in mountain regions (SRCCL 2.3.1.1). This includes an earlier and more extensive winter and spring snowmelt (Zeng et al., 2018a) with decline in summer and autumn runoff in snow dominated river basins of mid-high latitudes of the Northern Hemisphere (Kerkhoven and Gan, 2011; Rhoades et al., 2018). Reduced snowfall during a shorter snow season may be offset by increased snowfall relating to thermodynamic increases in atmospheric moisture (Wu et al., 2018a). An expected decline in snowfall globally is likely to be less pronounced for the coldest regions where increases in snowfall can be expected during seasons in which temperatures stay below freezing (Turner et al., 2019).

Increased glacier melt and precipitation are expected to contribute to increasing lake levels in the inner Tibetan Plateau (Lei et al., 2017). Glacier mass balance over New Zealand is impacted by atmospheric rivers and other high moisture transport events, with the likelihood of extreme ablation or snowfall events dependent on air temperature (Little et al., 2019). Intrusions of warm, moist air, including atmospheric rivers and associated rainfall play a role throughout the year in Greenland melt events (Mattingly et al., 2018; Oltmanns et al., 2018). Substantial moisture transport events have been linked to melting of ice as a result of sensible heating from the warm air and increased infrared radiation from atmospheric water vapour and low-altitude clouds (Stuecker et al., 2018). Reduced sea ice drives increased evaporation locally (Bintanja and Selten, 2014; Laîné et al., 2014). Resulting changes in energy and moisture budgets and Arctic amplification of warming are expected to drive changes in atmospheric circulation (Section 8.2.1.3). However, the diversity of mechanisms involved in these processes preclude the identification of a simple expected response in the northern mid-latitude water cycle in response to circulation changes resulting from melting sea ice (Barnes, 2013a; Cohen et al., 2014; Henderson et al., 2018a; Tang et al., 2014; Woollings et al., 2018a).

In summary, it is *virtually certain* that a warming atmosphere, ocean and land surface will cause a loss of frozen water stores, except in areas where temperatures remain well below freezing. There is *medium confidence* that warm, moist atmospheric flows and associated precipitation play an important role in the melt of ice sheets and glaciers in some regions. There is *low confidence* in the processes determining regional water cycle changes linked to atmospheric circulation response to declining Arctic ice coverage.

8.2.2.2.2 Vegetation influences on water cycle changes

Vegetation provides a crucial interface between sub-surface water storage and exchange with the atmosphere through evapotranspiration, as well as contributing feedbacks through the surface energy balance. Multiple compensating factors contribute to the net effect of the land surface response coupling with hydrology. Plant stomata tend to close in response to higher CO_2 which reduces water fluxes, while higher CO_2 may also boost carbon uptake and plant growth of leaf area thereby increasing water fluxes to the atmosphere. Plants are additionally limited by the supply of water from the subsurface, as well as subject to the demand for water by the atmosphere which increases as temperatures rise (Scheff and Frierson, 2014).

Demand of water from the land surface by the atmosphere is frequently quantified as the potential evapotranspiration (PET). Physically-derived PET has been found to rise substantially with increasing temperature (Milly and Dunne, 2016; Scheff and Frierson, 2014) yet the actual evapotranspiration fluxes derived from climate models do not show the same spatial patterns or ubiquitous increase with rising temperatures as seen in observation(Swann et al., 2016). This is explained primarily by stomatal closure, which has been found to more than compensate for any increase in water flux due to additional leaf growth under high CO_2 conditions (Swann et al., 2016). The result is that hydrological metrics based on PET tend to show drying across much of the land surface while metrics that use climate model calculated evapotranspiration accounting for plant responses to rising CO_2 show less drying overall, and with a different spatial pattern (Lemordant et al., 2018; Swann, 2018; Swann et al., 2016).

SRCCL concluded there is *high confidence* that increasing atmospheric CO_2 could potentially enhance photosynthesis and water use efficiency of individual leaves, resulting in increased rates of plant growth and carbon sequestration (Jones et al., 2013b; Swann et al., 2016). Plant stomata closure in response to higher

CO_2 levels is expected to further reduce evaporation from vegetated surfaces, amplifying regional drying (Bonfils et al., 2017; Lemordant et al., 2018; Mankin et al., 2018; Milly and Dunne, 2016; Peters et al., 2018a), contributing to decreasing relative humidity over land. The decrease in water flux and subsequent reductions in humidity are not necessarily coupled with drier soils within the rooting zone (Berg et al., 2017a; Berg and Sheffield, 2018b). Also, reduced evapotranspiration and precipitation can be counteracted in some regions as increased plant growth in direct response to elevated CO_2 concentrations and since associated enhanced efficiency of plant water use enables greater tolerance to aridity (Bonfils et al., 2017; Lemordant et al., 2018; Mankin et al., 2018; Milly and Dunne, 2016; Peters et al., 2018a; Yang et al., 2018d).

The CO2 physiological response is expected to contribute to precipitation decline in the sub-tropics (He and Soden, 2017b) and over tropical land can lead to decline in areas with substantial precipitation recycling and enhancement in regions with significant moisture input (Kooperman et al., 2018a). Even with physiologically driven declines in precipitation there may be increasing runoff responses to rainfall, particularly extremes (Kooperman et al., 2018b; Lemordant et al., 2018). Defoliation has also been identified as a short-term driver of the regional hydrological cycle with enhanced runoff following a tropical cyclone (Miller et al., 2019).

In summary, vegetation responses to higher CO2 levels are expected to amplify drying tendencies over land through reduced evapotranspiration which contributes to decreased precipitation regionally though maintaining soil moisture in the rooting zone (medium confidence). Drying is expected to be offset regionally through increased growth as plants respond directly to increased CO2 levels and toleration of drier climates improves. As a result, vegetation feedbacks to regional climate change will complicate local water cycle responses.

8.2.2.2.3 Soil and sub-surface hydrology

In the upper-most soil layers, soil moisture supplies plants and crops with water while providing an interface between the ground and atmosphere through evapotranspiration. Groundwater changes are driven by processes that alter the balance between recharge and discharge which include natural variability in atmospheric circulation, direct human effects such as abstraction for irrigation as well as human caused climate change (Rodell et al., 2018). In some regions, groundwater use can lead to depletion while a warming climate adds further pressure on water resources and increases human water demands (SR1.5; 3.4.2.3). Sea level rise will also contaminate coastal sub-surface fresh water with salt. The control of soil moisture on evapotranspiration determines feedbacks onto surface climate which display a diversity across simulations (Berg and Sheffield, 2018b). This coupling depends on soil regime and affects local temperature responses to climate change (Schwingshackl et al., 2018).

As detailed in the AR5, decreases in soil moisture over many subtropical land regions are an expected response to a warming climate. This is influenced by thermodynamically driven increases in atmospheric demand for water vapour, a broadening of the tropical belt with poleward migration of the sub-tropical dry zones and an increasing land-ocean temperature contrast that drives declining relative humidity (8.2.1). Regional changes in soil moisture are determined by atmospheric circulation variability, including responses to radiative forcing and subsequent changes in SST patterns. Additionally, feedbacks with the atmosphere and physiological responses of vegetation are also important.

Since the AR5, there has been progress in understanding the processes determining recharge and discharge and the response timescales of groundwater. The SRCCL notes that an increasing intensity of rainfall leads to decreased partitioning between water storage in the soil (green water) and runoff and reservoir inflow increases (blue water) (Eekhout et al., 2018). Satellite data has identified that surface soil moisture retains a median 14% of precipitation falling on land after three days (McColl et al., 2017). Precipitation of varying intensities has been linked with groundwater recharge over regions of India (Asoka et al., 2018). Seasonal groundwater recharge is observed to respond linearly to rainfall above a threshold of 140-250 mm/year in a humid region and varies substantially (from 4-40% of annual rainfall) depending on geological environment

(Boukari et al., 2018). Combining groundwater models with hydrologic data sets, the time-scales over which groundwater equilibrates to recharge responses to climate change are ~100 years for nearly half of the active groundwater flows globally and longer still over the most sensitive, arid regions (Cuthbert et al., 2019), which is important for determining adaptation strategies. Soil moisture-determined aridity increases are nevertheless found to be less marked than atmospheric indicators due to increased water use efficiency by plants (Section 8.2.2.2.2) in response to higher CO_2 levels (Bonfils et al., 2017). Increased soil moisture variability is also found to suppress the uptake of CO_2 by the land based on Earth system climate simulations (Green et al., 2018).

Spatial variability in soil moisture is known to influence the timing and location of convective rainfall through altering the partitioning between latent and sensible heating. This has been demonstrated for the Sahel using satellite data and is not well represented by simulations that lack the spatial resolution (Moon et al., 2019; Taylor et al., 2013a) and a consistent but weaker signal is also detected over Europe (Taylor, 2015). Soil moisture-atmospheric coupling is known to influence characteristics of heatwaves in addition to the development of convection (Gevaert et al., 2018; Taylor et al., 2013a; Vogel et al., 2017). Antecedent soil moisture conditions are also an important modulator of flooding (8.2.2.2.5).

In summary, a warming climate combined with direct human demand for ground water are expected to deplete ground water resources in some regions (*high confidence*). More intense, less frequent rainfall decreases the efficiency of recharge from rainfall (*medium confidence*), however recharge characteristics depend on the geological environment and soil characteristics and involve complex land surface feedbacks involving vegetation and responses to intense convective precipitation.

8.2.2.2.4 Surface water and hydrology

Changes in surface water and runoff depend on the balance between P-E and infiltration while variability is further impacted by changes in frozen stores of water. Regionally variable changes in P-E (8.2.1.2) modulated by complex land-surface responses involving vegetation (8.2.2.2.2) mean there is *low confidence* in a simple surface hydrological response to climate change. Local hydrological response is complicated by direct human impact on river and lake systems through resource management and use of water (8.2.2.2.7). The direct impact of aerosol pollution induced surface solar dimming can increase river flow by reducing surface evaporation (Gedney et al., 2014b). However, it is *likely* that increases in the amount of rainfall during wet events (8.2.2.1.2; 11.4.1) will drive subsequent increases in runoff although the response timescale depends on catchment characteristics including precursor conditions. This response is expected to be reduced by declining soil moisture due to climate change and water abstraction but increased by more intense less frequent precipitation (8.2.2.2.3).

As known in the AR5 and SROCC, thermodynamic increases in atmospheric moisture transport into the Arctic with warming (8.2.1.2) are expected to amplify river discharge through increased precipitation (Zhang et al., 2013b). Under a warmer climate, the winter snowpack of snow-dominated river basins is expected to decrease, while the onset of spring snowmelt will occur earlier with more spring snowmelt but likely at the expense of summer, autumn and the overall annual streamflow. Based on sensitivity analysis of 96 Canadian catchments, stream flow at high latitudes is expected to increase in response to climate change This relates to increased precipitation and melting of snowpack or glaciers with evapotranspiration also playing a role, but these changes can be overwhelmed by direct human impact (Tan and Gan, 2015).

Under warmer water temperatures, the summer stratified season is expected to become longer, which has significant ecological impact for freshwater lakes. For example, for many aquatic ecosystems that depend on the freshwater ice cover, e.g., plankton will be more resilient when protected by ice cover; cold water fish species could be forced to compete with warm water species migrating north with rising temperatures. With greater lake stratification, mixing is reduced (Woolway and Merchant, 2019) and oxygen can become depleted in the productive lower levels, leading to "dead zones". Warming of river and lake water also adversely impact ecosystems (Hannah and Garner, 2015) while sea level rise can contaminate coastal fresh water reserves with salt.

8.2.2.2.5 Expected drivers of flooding

Here we consider drivers of river flooding (fluvial) as well as flash (or pluvial) flooding that can also result from rapid rates of river rise as well as the emergence of temporary water bodies, including in heavily managed urban environments. Both types of flooding are strongly influenced by land surface characteristics.

Expected increases in the intensity of wet events (8.2.2.1.2; 11.4.1) will increase the severity of any associated flooding. However, the response of flooding to changing rainfall characteristics are complex and depend upon time and space scale, the nature of the land surface (including river catchment or urban environment) and precursor conditions. The likelihood of flooding is modulated by antecedent soil moisture (McColl et al., 2017; Woldemeskel and Sharma, 2016), the response of which to climate change is regionally dependent (8.2.2.2.3). Floods at the monthly scale are not well correlated with precipitation when reanalyses are used to drive a global-scale hydrological model (Emerton et al., 2017; Stephens et al., 2015a).

Increased severity of flooding on larger, more slowly-responding rivers is expected as precipitation increases during persistent wet events over a season. This can occur in mid-latitudes where blocking patterns continually steer extra tropical cyclones across large river catchments with groundwater flooding also playing a role (Muchan et al., 2015). Catastrophic floods recorded across Europe have been linked with the NAO (Zanardo et al., 2019) while flooding from an alpine lake was attributed to multiple precipitation events linked to atmospheric blocking (Lenggenhager et al., 2018a). Increased atmospheric moisture will amplify the severity of these events when they occur yet drivers of change in the occurrence of blocking patterns, stationary waves and jet stream position are not well understood (8.2.1.3).

Research since the AR5 has confirmed links between flooding and atmospheric rivers(Froidevaux and Martius, 2016; Paltan et al., 2017; Waliser and Guan, 2017). These events depend upon the intensity of moisture transport by the atmosphere, which is expected to increase with warming (8.2.1.2). This expectation is complicated by potential changes in the dynamics of storm systems including position of storm tracks and how they interact with topography as well as local-scale dynamical processes and pre-cursor conditions of the river catchments. A changing occurrence of rain on snow and snow melt events will also affect seasonal characteristics of flooding (Musselman et al., 2018), although the expected response will be regionally specific (11.5).

Increased seasonality in lower latitudes with more intense wet seasons (Chou et al., 2013a; Liu and Allan, 2013a) is expected to alter seasonal flood characteristics with decreases in precursor soil moisture after more intense dry seasons offsetting increased rainfall in the wet season (8.2.1.2). Flooding related to tropical cyclones is expected to become more severe as increased moisture and slower system speed (Kossin, 2018) drives greater totals of rainfall (8.2.1.2, 8.2.2.1.1). This will be exacerbated by increased severity of coastal inundation linked to sea level rise (4.3.2.2; 9.6.4) as well as a less certain influence from the strengthening of the most powerful tropical cyclones.

Compared with multiple-day events, larger potential increases in precipitation have been identified in short-duration (sub-daily) events with changes of up to three times the Clausius Clapeyron rate identified in some locations (Guerreiro et al., 2018a; Lenderink et al., 2017). Therefore an increased severity and frequency of flash flooding may be particularly acute (Chan et al., 2016b; Sandvik et al., 2018) as increases in convective available potential energy and moisture convergence intensify convective storms (8.2.2.1.2). More intense, less frequent storms are also expected to favour runoff and flash flooding rather than recharge (Eekhout et al., 2018; Yin et al., 2018).

Expected drivers of flooding are dependent on direct human intervention (8.2.2.2.7) such as the management of river catchments as well as mismanagement leading to infrastructure failure (e.g. reservoirs) or detrimental changes in the catchment drainage properties or stability of the land (e.g. mudslides). Flood risk can also be indirectly affected by human activities. Serious flooding over China has been linked to heating by atmospheric aerosol in polluted basins that suppresses convection locally and allows moisture to be instead transported into mountainous regions where intense rainfall can occur (Fan et al., 2015).

In summary, there is *very likely* that increases in precipitation intensity and amount during wet events will drive more severe flooding in locations where it occurs. However, there is *low confidence* in how local drivers will change in flood risk frequency which is strongly dependent upon complex catchment characteristics, antecedent conditions and how atmospheric circulation systems respond to climate change, which is less certain than thermodynamic drivers (11.5).

8.2.2.2.6 Expected drivers of drought and aridification

A *drought* is a transient moisture deficit relative to some climatological baseline (Cook et al., 2018; Wilhite, 2000; Wilhite and Glantz, 1985). Most droughts begin as persistent precipitation deficits (*meteorological drought*) that propagate over time into soil moisture (*agricultural drought*) and runoff, streamflow, or reservoir storage (*hydrological drought*). While traditionally viewed as “slow moving" disasters that typically take weeks or months to develop, rapidly evolving and often unpredictable *flash droughts* can also occur (Otkin et al., 2016, 2018). Droughts may persist for months or even decades, be highly localized or cover thousands of square kilometres, arise through different climate system dynamics (e.g., internal atmospheric variability, ocean teleconnections), and be amplified or ameliorated by a variety of physical and biological processes. As such, drought events occupy a unique space within the framework of extreme climate and weather events, possessing no singular definition or unifying underlying theory.

While the role of precipitation in droughts is obvious, other processes may also be important, especially in the case of agricultural and hydrological droughts. High temperatures and low humidity increase evaporative demand in the atmosphere, amplifying surface drying by increasing moisture losses from evapotranspiration (*high confidence*) (Dai et al., 2018). Vegetation, however, modulates these exchanges of moisture and energy. Depending on how they ultimately respond to climate change and increased atmospheric carbon dioxide concentrations, plants may either amplify (Ukkola et al., 2016) or ameliorate (Swann et al., 2016) warming impacts on drought at the surface. Therefore there is *low confidence* in drought predictions in regions where vegetation is changing rapidly. In snow-dominated regions, high temperatures increase the fraction of precipitation falling as rain instead of snow, increase sublimation losses from the surface snowpack, and advance the timing of spring snowmelt (*high confidence*). All these factors can result in lower than normal snowpack levels (a snow drought), even if total precipitation is at or above normal for the cold season (Harpold et al., 2017).

While human interactions with drought were previously treated as a fourth category (socioeconomic), the capacity for human activities and decision-making to amplify or ameliorate drought events and their impacts is now being increasingly recognized (AghaKouchak et al., 2015; Van Loon et al., 2016). Societies have developed a variety of strategies to manipulate the hydrologic cycle to increase resiliency in the face of water scarcity, including irrigation, creation of artificial reservoirs, and groundwater pumping. While potentially buffering water resource capacity, in some cases these manipulations may unexpectedly increase vulnerability (*medium confidence*). For example, while increased irrigation efficiency may ensure more water is available to crops, the corresponding reduction in runoff and subsurface recharge may exacerbate hydrologic drought deficits (Grafton et al., 2018). Furthermore, while building dams and increasing surface reservoir capacity can boost water resources, they may actually increase drought vulnerability if demands rise to take advantage of the increased supply or if over-reliance on these surface reservoirs is encouraged (Di Baldassarre et al., 2018).

[Figure 8.8 HERE]

Figure 8.8: Definitions of drought and the role of precipitation, temperature, soil and groundwater storage, and anthropogenic influences. From Cook, Mankin&Anchukaitis, 2018.

[Figure 8.8 HERE]

8.2.2.2.7 Direct anthropogenic influence on the regional water cycle

Human activities influence the regional water cycle directly through modifying and exploiting stores and flows from rivers, lakes and ground water and by altering land cover characteristics, thus altering surface energy and water balances through changes in permeability, surface albedo, evapotranspiration, surface roughness and leaf area. Since AR5, modelling evidence has demonstrated that large-scale irrigation is capable of altering rainfall through changes in the surface energy balance (Alter et al., 2015) leading to regional as well as remote effects. For example, irrigation in the Mississippi basin was found to increase precipitation in arid regions to the west but decrease precipitation in wet regions to the east while also delaying the onset of the Indian monsoon by 6 days due to a reduction in the land-sea temperature contrast (De Vrese et al., 2016) and irrigation in Asia was linked to increased precipitation in Africa due to strengthened atmospheric moisture advection (Guimberteau et al., 2012).

The SRCCL presented evidence that abstraction of water from the ground or river systems and intensive irrigation increases evapotranspiration and atmospheric water vapour locally. Although irrigation can explain declining groundwater storage over north-western India, precipitation variability was found to dominate in other regions of the subcontinent (Asoka et al., 2017). Depletion and contamination of groundwater through human activities has also been identified over north America (Ferguson et al., 2018). Large-scale extraction of water from rivers can reduce flows and decrease the level and area of inland seas – for example, both the Aral Sea and Dead Sea are shrinking. Between 1985 and 2015, approximately 139,000 km^2 of inland water areas have become land, while creation of dams has converted approximately 95,000 km^2 of land to water, particularly in the Amazon and Tibetan Plateau (Donchyts et al., 2016).

Altered thermodynamic and aerodynamic properties of the land surface through urbanisation is able to affect precipitation systems through altered stability and turbulence (Jiang et al., 2016b; Pathirana et al., 2014; Sarangi et al., 2018) that are further perturbed through the link between aerosol pollution and cloud microphysics (Schmid and Niyogi, 2017)(Section 8.2.2.1). Urbanisation also tends to decrease permeability of the surface, leading to increased surface runoff (Chen et al., 2017a). Large-scale infrastructure, such as the construction and operation of hydropower plants, dikes and weirs, also alter surface energy and moisture exchanges, potentially influencing the regional water cycle. Over the Sahel, for example, a modelling study found large-scale solar and wind farms could double precipitation but only when dynamic vegetation responses are included (Li et al., 2018d).

Changes in land use from forest to agriculture can exert profound regional effects on the hydrological cycle through reducing evapotranspiration and moisture recycling as well as altering the surface energy balance. This can drive remote effects: higher surface albedo of agricultural land has been linked with a weakening of the south Asian monsoon through supressed low-level temperature and reduced evapotranspiration (Singh et al., 2019b). As noted in SR1.5, deforestation can initiate additional pronounced forest dieback through reinforcing feedbacks if a threshold point is passed (Section 8.6), estimated as around 40% forest clearance for the Amazon (Nobre et al., 2016). Modelling studies simulate total tropical deforestation to cause large reductions in precipitation, but smaller reductions are seen with more realistic scenarios of more limited deforestation, and small-scale deforestation may actually increase precipitation (Lawrence and Vandecar, 2015). Substantial forest and grassland fires are also capable of modifying hydrological response at the watershed scale. The SR1.5 further reports limited evidence that increases in global runoff resulting from deforestation are counterbalanced by decreases resulting from irrigation.

In summary, there is *high confidence* that direct alteration of the land surface by human activities and abstraction of water for irrigation will drive local, regional and remote responses in the water cycle based on robust mechanisms supported by detailed modelling and observations. There is *high confidence* that depletion and contamination of surface and groundwater will affect some regions.

8.3 How is the water cycle changing and why?

This section uses observational and model-based datasets to assess water cycle changes including stores of water as well as fluxes and interchanges between them. Changes in seasonal to annual means, variability and wet and dry extremes are assessed across the atmosphere, oceans, land-surface and sub-surface and the cryosphere. Interpretation based on physical expectations and simple to complex simulations of the historical and paleo record enables attribution between human activities and natural causes and helps to build confidence in the capability to project future changes.

8.3.1 Observed water cycle changes based on multiple datasets

Observed changes in the water cycle can be forced naturally and by human activities. Early 20th century warming (1890-1940) was associated with events of particular hydrological significance: Indian monsoon failures in the 1900s, the North American dust bowl drought in the 1930s, and the World War II-period drought in Australia between 1937 and 1945 (Hegerl et al., 2018). Attribution studies estimate that about half of the global warming from 1901 to 1950 resulted from a combination of increasing greenhouse gases and natural forcing, offset to some extent by aerosols, with a large contribution from natural variability (Hegerl et al., 2018).

8.3.1.1 Closing the observed global water budget

Quantification of the global water budget is essential for making reliable assessments of changes in all the elements of the global water cycle. This requires quantifying the budget terms and estimating the uncertainties and errors through the use of advanced observing systems and modelling approaches (Brown and Kummerow, 2014; Hegerl et al., 2015). Currently, regional annual water budgets can be closed to a residual uncertainty of 10% while monthly residuals are over 20% and largest in cold seasons based on multiple observations for 2000-2010 (Rodell et al., 2015). Atmospheric reanalyses are not designed to close the water and energy budget so residuals in global P-E (up to 0.35 mm/day in magnitude) highlight this uncertainty and gaps in current understanding (Fig 8.9). Inclusion of mass constraints in the data assimilation process maintains the global water vapour mass (eg., MERRA-2) (Takacs et al., 2016) although the regional analysis correction from observations is non-negligible (Bosilovich et al., 2017).

[START FIGURE 8.9 HERE]

Figure 8.9: Intercomparison of global (P-E) from various reanalyses over the satellite data period (monthly means, with a 12 month running mean). Updated from (Bosilovich et al., 2017). CFSR, ERA-I, JRA-55, MERRA and MERRA-2 are satellite data reanalyses, ERA20C and 20CRv3 use reduced observing systems. ERA20CM and M2AMIP are atmospheric model ensemble simulations.

[END FIGURE 8.9 HERE]

8.3.1.1.1 P-E and salinity over oceans

The flux of fresh water between the ocean and atmosphere is determined by P-E, which influences ocean surface salinity. Directly measuring ocean P-E is challenging and generally relies on indirect reanalysis estimates (Fig 8.10a). Significant variations among the different reanalysis are partly linked to observing system changes.

[START FIGURE 8.10 HERE]

Figure 8.10: As in Fig.8.10, except for P-E over (a) Global oceans (b) Global land

[END FIGURE 8.10 HERE]

8.3.1.1.2 P-E over land

Continental P-E estimated from reanalyses (Fig.8.10b) and land-surface models (Fig.8.11) driven by meteorological data (Kumar et al., 2018; Liu et al., 2011) do not agree in terms of mean P-E, while there is agreement among methods in representing interannual variability with reanalyses data showing larger trends (Robertson et al., 2014). Trends in P-E during the last 30 years based on land models are not statistically significant. Observations and models show evidence of increasing (decreasing) P-E in the wet (dry) parts of the tropical circulation or season, respectively since 1979 (Chou et al., 2013a; Fu and Feng, 2014; Liu and Allan, 2013b).

The hydrological response to P-E over land corresponds to runoff to the oceans (minus storage).Dai (2016) found that 55 of 200 of the largest river basins showed statistically significant trends in streamflow and continental runoff during 1948-2012, with an even distribution of increasing and decreasing trends that are consistent withprecipitation trends. Global land runoff and precipitation variations correlate significantly to ENSO (Schubert et al., 2016).

[START FIGURE 8.11 HERE]

Figure 8.11: P-E land surface anomalies (base climate 1990-2010) from land surface models for the area between 60N and 60S (including 3 month running mean). Updated from Robertson et al., (2016). Units are kg m^{-2}.

[END FIGURE 8.11 HERE]

8.3.1.1.3 Transport of water vapour

Water vapour transports are expected to increase in proportion with the amount of atmospheric water although atmospheric circulation changes can dominate responses regionally (8.2.2.1). Water vapour transport (convergence) estimates from observations have significant uncertainties even in regions of high quality radiosonde data(Yarosh et al., 1999). Hence many studies use reanalyses for water transport estimates. Dufour et al., (2016) found reanalysis moisture transport into the Arctic region consistent with radiosondes, but reanalyses generally exhibit larger transports. In using evaporation and precipitation terms from land and ocean, and including atmospheric moisture transport (Trenberth et al., 2011) the influence of the observational analysis is shown as a residual difference among the budget terms (Fig 8.12).

Combining knowledge of reanalysis water budgets with statistical techniques, Robertson et al., (2016) demonstrated consistency between atmospheric moisture convergence and observationally-driven land model estimates of E-P, largely confirmingthat global E-P over land is changing slowly. Increases with warming in low-level (800-1000 hPa) moisture convergence into the tropical wet regime with a smaller outflow in the mid-troposphere (400-800 hPa) was detected in one reanalysis (Allan et al., 2014), broadly consistent with physical expectations and a high resolution simulation. Since AR5, capability to track moisture through stable isotope analysis has improved understanding of regional transports, source regions and atmospheric transports (Agudelo et al., 2018; Arias et al., 2015b; Drumond et al., 2014; Durán-Quesada et al., 2017; Gomez-Hernandez et al., 2013; Hoyos et al., 2018; Hu and Dominguez, 2015; Martinez and Dominguez, 2014; Ordoñez et al., 2019; Salih et al., 2015; Van Der Ent et al., 2014; Vázquez et al., 2018; Wang-Erlandsson et al., 2014) .

[START FIGURE 8.12 HERE]

Figure 8.12: Water cycle fluxes and reservoirs originally published by (Trenberth et al., 2011) and a placeholder for an updated analysis of the reanalysis data.

[END FIGURE 8.12 HERE]

8.3.1.2 Atmospheric moisture

AR5 presented evidence of increases in global near-surface and tropospheric specific humidity since the 1970s but with *medium confidence* of abatement in near-surface moistening trends over land associated with reduced relative humidity since around 2000.

Robust signals of widespread increases in atmospheric water vapour have been presented based on in situ, satellite and reanalysis data (Blunden and Arndt, 2017) and are consistent with expectations from the Clausius-Clapeyron equation (Allan et al., 2014). Continued moistening over the oceans is consistent with thermodynamic increases in saturation vapour pressure with warming for low-level or near-surface water vapour (Allan et al., 2014; Byrne and O'Gorman, 2018). However, declining near-surface relative humidity over land remains evident in surface observations (Willett et al., 2014). This is consistent with a faster rate of warming over land than ocean (Byrne and O'Gorman, 2018) although this is based on a relatively short observational record. CMIP5 simulations appear unable to capture the observed variability in relative humidity even when observed SSTs are prescribed (Dunn et al., 2017), which implies potential deficiencies in water cycle projections but this result is questionable based upon considerable uncertainty related to homogenization of the data (Willett et al., 2014).

Increases in near-surface atmospheric moisture are widespread across northern continents but not detected for SH land; the largest magnitude increases affect warm, low-latitude regions including the Caribbean, West Africa, India and the maritime continent but also regions experiencing declining relative humidity such as the Mediterranean (Willett et al., 2014). Satellite data imply substantial increases in upper tropospheric humidity since 1979 (Blunden and Arndt, 2017). Increasing moisture in mid- and upper-tropospheric levels contributes to a powerful amplifying climate feedback (AR5) while larger water vapour amounts at low altitudes increases the supply of moisture for precipitation events (Roderick et al., 2019). Consistent with AR5, it is *very likely* that water vapour has increased globally and throughout the troposphere since the 1970s while there is *medium confidence* that relative humidity has decreased over many land regions meaning that atmospheric moisture content is increasing but continental air is becoming less saturated.

8.3.1.3 Precipitation

Since AR5 there have been updates of several major satellite, surface, reanalysis and merged data sets of precipitation. The magnitude of global mean precipitation is likely to be underestimated based on observational analysis of the atmospheric energy budget (Chapter 7).

8.3.1.3.1 Global precipitation

AR5 reported a *likely* increase in NH land precipitation, particularly after 1951 but with contrasting regional trends that depend upon time period. Improved assessments of precipitation changes at global and regional scales have been achieved since AR5. Total global precipitation since 1979, across several datasets, does not reveal consistent significant positive trends (Adler et al., 2017; Allan et al., 2014; Liu and Allan, 2013b; Nguyen et al., 2017), consistent with physical expectations (8.2.1.1) combined with observational uncertainty. Accounting for internal variability and volcanic eruptions, a small global increase in precipitation with warming is identified (0.5 % per °C), primarily attributed to changes over the oceans (Adler et al., 2017). Zonal mean precipitation trends are generally within the range simulated by CMIP5 models (Marvel et al., 2017) with largest increases in the ITCZ (up to ~2%/decade).

The latest merged satellite data available since 1979 (GPCP) displays a very narrow increase in precipitation along the Pacific ITCZ with decreases either side extending into the eastern Pacific and onto land (Adler et al., 2017), consistent with the "wet areas getting wetter, dry areas getting drier (WWDD)" paradigm. Byrne et al., (2018) also showed a narrowing and strengthening of rainfall in the ITCZ for 1979-2017 in both Atlantic and Pacific basins, but little change in ITCZ location. Tan et al., (2015) suggested that a narrowing and strengthening of rainfall of the Pacific ITCZ is linked to changes in frequency of well-organized mesoscale convective systems. Large discrepancies between different satellite observing systems reduce the confidence in the details of regional changes in precipitation and its type (Henderson et al., 2018b).

Over global land, observed trends since 1950 are generally smaller and less significant than CMIP5 simulations (Liu and Allan, 2013b) but trends are consistently more positive in the satellite era (since 1979). Observed decreases in precipitation over land since 1979 have been identified in the dry part of the tropical atmospheric circulation or dry season (Chou et al., 2013c; Fu and Feng, 2014; Liu and Allan, 2013b). An absence of wet/wetter, dry/drier signals over land is seen when considering historical observations of precipitation (Greve et al., 2014; Murray-Tortarolo et al., 2017). A reason for this contradiction is that local precipitation is dependent on the location of the wet portion of the atmospheric circulation that moves between regions depending on internal climate fluctuations and responses to the complex time-evolving mix of radiative forcings over the historical period. If the large-scale atmospheric circulation shifts in location, the region experiencing the wettest part of the circulation can only change to a drier part of the circulation (wet gets drier). Accounting for the influence of circulation changes leads to clearer and more contrasting signals of precipitation (Liu and Allan, 2013b; Polson and Hegerl, 2017; Zhou and Lau, 2017) yet contradicting the simple expectation for positive P-E to become increasingly positive over all land regions (8.2.1.2).

8.3.1.3.2 Regional precipitation

Large-scale patterns of regional precipitation changes include the drying of the North American continent, with strongest trends in precipitation totals over the Great Plains and the southwestern US, plus precipitation increase over Europe and most of Eurasia with the strongest trends over Eastern Europe (Nguyen et al., 2017). Significant changes in precipitation totals were found over the desert regions of northern and southern Africa. There are significant differences in the magnitude and sign of precipitation trends, both globally and regionally, among multiple reanalyses datasets (Bosilovich, 2013; Bosilovich et al., 2017).

Rain gauge-based trend estimates are subject to uncertainties associated with inhomogeneous sampling and data completeness as noted in AR5. For relatively well-sampled areas (such as the US), station records demonstrate a trend pattern which is qualitatively consistent with most reanalyses (drying Central and southwestern US and increase of precipitation total in the northeastern US), but with weaker trends than in reanalyses (Cui et al., 2017). Precipitation trends since 1979 over Europe derived from station data do not demonstrate any regular pattern, with differences in the trend values among different datasets (Zolina et al., 2014). There is consistency in trend estimates (1998-2015) over mainland China between several satellite-based products and station data with primarily increasing precipitation total in autumn and winter and decreasing summer precipitation (Chen and Gao, 2018). This suggests a decreasing intensity of Asian monsoon precipitation, in contradiction with conclusions from other studies (Deng et al., 2018; Lin et al., 2014). Further details of observed changes in the regional monsoon systems are presented in (8.3.2.4).

Over longer periods, multi-decadal trends (1930-2004) derived from CRU station collection (Kumar et al., 2013) (Fig.8.13)show the strongest increase in precipitation totals in the western and northwestern US, La Plata river basin and northern Australia (up to 0.7 mm/day per decade) with trends in Northern and Eastern Europe being about 0.3 mm/day per decade. A robust pattern of decreasing total precipitation is observed over tropical rain bands with the strongest upward trends over equatorial Africa of up to 0.4-0.5 mm/day per decade. This is qualitatively consistent with the WWDD pattern in precipitation trends for the last 80 years.

[START FIGURE 8.13 HERE]

Figure 8.13: Linear trends in annual precipitation, using CRU precipitation data, 1930-2004. From(Kumar et al., 2013).

[END FIGURE 8.13 HERE]

Regional trends in precipitation over South America are variable. For example, central Chile has experienced a precipitation decline since 1970 that has been attributed largely to the PDO, although at least 25% of the decline could not be explained without considering anthropogenic influence (Boisier et al., 2016). There is evidence for declining precipitation trends in the South American Altiplano during the past 50 years both from observational data and tree ring reconstructions (Morales et al., 2012). GPCC precipitation data for the period 1902-2005 indicate positive trends over southeastern South America and negative trends over the southern Andes, with at least a partial contribution from anthropogenic forcing (Vera and Diaz, 2015).

Rain gauge observations in the Brazilian Legal Amazon for 1973-2013 indicate that the annual and seasonal precipitation trends over the Amazon basin are insignificant; although some stations showed significant increase in the annual and wet season precipitation and few showed decrease in dry season precipitation (Almeida et al., 2017). Based on multiple observational datasets for 1990-2010, other studies suggest an increase of total annual precipitation due to increased wet season rainfall in the northwestern, northern, and central parts of the Amazon basin, although small decreases during the dry season have been detected (Gloor et al., 2015).

In summary, there is *medium/high confidence*in the increase of mean precipitation over mid- and sub-polar latitudes of both hemispheres after 1930. For the post-1979 period, there is a *high confidence* of decreasing total precipitation over the US and most parts of the North America and a *medium confidence* on increasing of precipitation total over central-eastern Europe.

8.3.1.3.3 Seasonality

Increases in seasonality are expected from the wet-get-wetter response to warming but local changes can be dominated by shifts in atmospheric circulation (8.2.1.3). Decreasing precipitation trends in warm climate regions and increasing trends in arid and polar climate regions in one dataset for 1983-2016 (Nguyen et al., 2017)contradict the wet-get-wetter response. A decreasing annual cycle amplitude in the tropical rain band and increasing amplitude of annual cycle in the subtropics and mid-latitudes were identified since 1979 in two merged satellite products (Marvel et al., 2017). Reduced seasonality at a global scale was also identified since 1950 (Murray-Tortarolo et al., 2017) although this is in contrast with the more recent period since 1979 where a wetter wet season dominated changes (Chou et al., 2013c). Analysis of wet and dry parts of the tropical atmospheric circulation show wet regimes becoming wetter and dry regimes getting drier since 1979 in a range of observations and CMIP5 simulations over the ocean with less consistency for the observations over land regions (Liu and Allan, 2013b). There is *medium confidence* that the magnitude of the annual cycle of precipitation has increased since 1979 due to anthropogenic forcing.

8.3.1.3.4 Precipitation intensities and extremes

Estimates of precipitation extremes and alternative statistics show a general increase in the intensity of heavy precipitation in most areas. For the period from 1901, station data and most reanalyses indicate increasing trends in the number of days with heavy rainfall, as well as the intensity of precipitation from most wet days (Donat et al., 2016a)(Fig.8.14). Statistically significant upward trends in annual maximum precipitation have been observed at more than two thirds of locations globally, with robust tendencies over the US, Europe and South Africa, (Westra et al., 2013). Changes in precipitation extremes over Europe show an increase of the duration of wet periods in northern Europe and an opposite tendency in the Southern Europe, which results in an increase of precipitation falling during continuous periods (Serra et al., 2014; Zolina et al., 2013). More discussions of precipitation extremes are presented in Chapter 11.

[START FIGURE 8.14 HERE]

Figure 8.14: Regional and global changes in heavy precipitation days (R10mm). From (Donat et al., 2016a).

[END FIGURE 8.14 HERE]

Observational detection of precipitation extremes is confounded by spatial heterogeneity and sensitivity to shifts in atmospheric circulation (Barbero et al., 2017; Wasko et al., 2016a) but signal-to-noise ratio is improved by analysing intensity distributions independent of region (Allan et al., 2014; Pendergrass and Hartmann, 2014b). Increases in precipitation extremes with warming are generally consistent with Clausius Clapeyron (CC) scaling but within the range of natural variability for daily extremes while hourly extremes are found to increase around double this rate, outside the range of natural variability (Guerreiro et al., 2018b). Donat et al. (2016) identify more extreme rainfall in wet and dry regions (see Section 8.2.1.2) defined based on a 1950-1980 reference although this time period contains unusually large aerosol forcing relative to greenhouse gas forcing and changes in spatial pattern of wet/dry regions may be important (Sippel et al., 2017). Modelling studies find that increased precipitation extremes are strongest in wet regions and seasons with agreement depending on the physics shared across models (Bador et al., 2018). Consistent with preliminary findings in AR5, there is observational evidence that climate models may underestimate precipitation responses but the signal is not robust (Borodina et al., 2017),possible associated with changing meteorological regimes(Berg and Haerter, 2013), and/or spatial shifts in atmospheric circulation patterns (Blenkinsop et al., 2015; Chan et al., 2016a; Vittal et al., 2016; Wang et al., 2017a).

Fujibe (2013)analysed precipitation data from Japanese 92 rain-gauge stations covering1951–2010 and showed that the rate of change in saturation vapour pressure following the CC relation roughly holds for multi-decadal changes in extreme 10-minute and hourly precipitation. Based on 874 long-term time series from 1975 onwards,Groisman et al. (2016)found that the frequency of freezing rain events increased moderately over the North American Arctic, in European Russia and western Siberia (by about 1 day yr^{-1}), and increased substantially over Norway, especially the Norwegian Arctic. Over southern Eurasia and the US opposite trends (decrease) in the frequency of freezing rain was found.

Observations during 1966-2016 over northern Eurasia show increases in the contribution of heavy convective showers to total precipitation by 1-2% on average (with local trends of up to 5%) for all seasons except for winter (Chernokulsky et al., 2019). Increases in convective precipitation intensity as a response to warming above thermodynamic expectation have been identified, particularly on sub-daily time-scales, using a range of modelling and observational data (Ali and Mishra, 2018; Bao et al., 2017; Berg et al., 2013; Giorgi et al., 2016; Guerreiro et al., 2018b; Kendon et al., 2014; Pfahl et al., 2017). Spatio-temporal responses are likely to be manifest as modification in convective organisation (Bhattacharya et al., 2017a; Chan et al., 2016a; Lochbihler et al., 2017; Loriaux et al., 2017; Moseley et al., 2016; Pendergrass et al., 2016; Tan et al., 2015; Tandon et al., 2018; Wasko et al., 2016b). An apparent decline in precipitation extremes at high temperature in the present day climate (Chan et al., 2016b) is likely to be affected by regional dynamical changes and does not imply a potential upper limit for future precipitation extremes (Ali and Mishra, 2018; Wang et al., 2017a). Regional changes in land-ocean temperature gradients (Section 8.2.1.1.2) are also expected to impact intense precipitation; intense heating of the Sahara by rising greenhouse gases (Dong and Sutton, 2015a) has been attributed in increasing latitudinal temperature gradients leading to intensifying storms in the Sahel based on observational evidence (Taylor et al., 2017b).

The radiative effects of absorbing aerosols increase both instability and convective inhibition thereby suppressing low rain intensities and promoting high rain intensities from local convective systems (Wang et al., 2013e). Such trends were found in India (Krishnan et al., 2016; Roxy et al., 2017) and over eastern China with the latter having associations with increasing amounts of aerosols (Day et al., 2018; Guo et al., 2017; Qian et al., 2009; Xu et al., 2017a). Factors relating this trend to increasing aerosols in Eastern China are: (a) the suppression of low rain intensities and increase of high rain intensities, and (b) having a maximum occurrence of the local convective storms in modest level of aerosol concentrations, with very high aerosol concentrations acting the suppress convection, in agreement with the expectation for such a maximum based on both radiative and microphysical effects of aerosols on clouds and precipitation (Koren et al., 2008; Rosenfeld et al., 2008b; Yang et al., 2013). Precipitation suppression through aerosol microphysical effects is also seen in South America and the southeast Atlantic, associated with local biomass burning (Andreae et al., 2004; Costantino and Bréon, 2010), and in industrial regions in Australia (Heinzeller et al., 2016; Hewson et al., 2013).

In summary, it is *very likely* that precipitation extremes are increasing over most part of the global land.

8.3.1.4 Land-surface evapotranspiration

Evapotranspiration (ET) is an important component of the water cycle, and is composed of two sub-processes: evaporation from soil and vegetation surfaces and transpiration, the exchange of moisture between the plant and atmosphere through plant stomata. Modelled ET is usually estimated by applying an empirical soil moisture stress on potential ET as estimated from the surface energy budget. According to AR5 and in contradiction of the AR4, there is only *medium confidence* that pan evaporation (a controversial estimate of potential ET) declined in most continental areas over recent decades, related to observed changes in wind speed, solar radiation and humidity. On a global scale, there is in contrast medium confidence that land-surface ET increased from the early 1980s to the late 1990s. After 1998, a lack of moisture availability in SH land areas, particularly decreasing soil moisture, has presumably acted as a constraint to further increase of global ET (Hartmann et al., 2013b; Jung et al., 2010).

Although many in-situ techniques exist for ET measurements at the local to regional scale, direct measurements at global scale is still not feasible (Zeng et al., 2018c) (Fig.8.15). Observation-driven reconstructions of global land ET data show a positive trend of global terrestrial evaporation over the past three decades (Jung et al., 2010; Miralles et al., 2016; Zeng et al., 2014, 2018b, Zhang et al., 2015a, 2016d). However, the rate of increase varies among datasets, ranging from 0.42 to 2.16 trillion tonnes/year/decade, with an ensemble mean terrestrial average rate of 7.65 mm/yr/decade (Zeng et al., 2018b). Uncertainties in the amplitude of ET trend arise from different assumptions among the reconstruction techniques (Miralles et al., 2016), while incorrect estimation of the contribution of canopy transpiration to total ET is the main factor of spread in simulated ET (Lian et al., 2018; Zeng and Cai, 2016).

The lack of global ET increase recorded from 1998 to 2008 and reported in AR5 was shown to be an episodic phenomenon associated to ENSO variability (Zhang et al., 2015a). Using remote sensing based global land ET estimates, they found a recovery growth of global ET from 2008 onward, thereby further supporting that the recent apparent pause in global ET increase was due to internal variability rather than to anthropogenic forcings (*medium confidence*).

There has been so far only one attempt to formally attribute reconstructed ET changes at the global scale (Douville et al., 2012a). The study used four ET reconstructions and a set of ensemble historical simulations with one global coupled climate model to demonstrate that the latitudinal and decadal differentiation of recent ET variations could not be understood without invoking anthropogenic radiative forcing. In the mid-latitudes, the emerging picture of enhanced ET confirmed the end of the "dimming decades" and highlighted the possible threat posed by enhanced GHG concentration and related global warming to ET and freshwater resources.

[START FIGURE 8.15 HERE]

Figure 8.15: Linear trends in total annual terrestrial evapotranspiration. From (Zeng et al., 2018a).

[END FIGURE 8.15 HERE]

Regionally, large spatial heterogeneities have been observed in trends of land ET. Using MODIS data, (Li et al., 2016a) found that ET increases faster in the NH than in the SH. Positive trends of land ET were recorded over several regions as Europe, North America, India, Amazon basin (Zhang et al., 2016b), China (Li et al., 2018), Congo forest, southern Africa (Zeng et al., 2018a) and eastern north America (Zhang et al., 2016b). Intensification of vegetation greening was the main driver of positive trend ET trend over these regions, with other land regions experiencing negative trends during the recent decades. Negative ET trends found over Middle East, Western United States, Northern China and South-eastern Asia are driven by reduction in soil evaporation (Zhang et al., 2016b; Mao et al., 2015a).

Since AR5, the predominant contribution of transpiration to terrestrial ET has been established (Good et al., 2015; Jasechko et al., 2013). Using satellite and ecosystem models, Zhu et al., (2016) found a positive trend in leaf area index (LAI) during recent decades thereby supporting the Earth's greening hypothesis. This contributes to growth of interest on the potential contribution of the Earth's greening to the observed positive trend of evapotranspiration these last decades (Zhang et al., 2015a; Zeng et al., 2018a)). At the global scale, while increased precipitation and temperature-induced climate change accounts for 46% of the increasing trend in terrestrial ET, 52% of this increased trend is driven by enhance vegetation greening in recent decades. The predominating influence of changed precipitation in the trend of ET (found by Mao et al., (2015a) may result from poor integration of the effects of positive trends in vegetation greening in their study.

In summary, there is *low confidence* in the interpretation of recent changes in global and regional ET changes given the lack of direct measurements, the large uncertainties in global ET reconstructions, and the lack of formal detection-attribution studies accounting for the biophysical effects (stomatal closure, greening) on plant's transpiration. Yet, there is *high confidence* that the impact of increasing atmospheric concentration of GHG has been partly obscured by confounding factors such as internal climate variability, regional dimming effects due to anthropogenic aerosols, and increasing water use efficiency due to a stomatal closure effect, so that linear trends in regional ET do not necessarily provide a best estimate of the ET response to global warming and should not be used to extrapolate future changes in land-surface ET.

8.3.1.5 Runoff and streamflow

According to AR5, there is *low confidence*in trends in global runoff during the 20th century, since annual mean streamflow observations have been impacted by direct human influences and show either positive or negative (significant or insignificant) trends at the basin scale (Hartmann et al., 2013b). In regions with snowfall (except very cold regions), global warming has led to changes in the seasonality of streamflow, with earlier spring maxima, increased winter flows and smaller snowmelt floods (*high agreement, robust evidence*). Where streamflow is low in the summer, decrease in snow (or glacier) storage has exacerbated summer low dryness (Jiménez Cisneros et al., 2014). Observed changes of other streamflow characteristics, e.g. annual means, low and high flows, often follow changes in precipitation but attribution to climate change is often very difficult due to confounding factors (e.g., land use change, human water use and reservoir management) (Jiménez Cisneros et al., 2014). Also, there is no scientific consensus on whether the direct CO_2 effects on plants already have a significant influence on runoff at the global scale (Gerten et al., 2014).

A strong and significant decrease of mean annual streamflow is observed during 1956-2005 in the Mediterranean region of Europe, generally along with a weak increase in northern Europe, whereas there is little change in transitional central Europe. It is likely this pattern was caused by anthropogenic greenhouse gas emissions as climate models simulate this pattern only if human emissions are accounted for, although the models significantly underestimate the response (Gudmundsson et al., 2017). Attempts at attribution have been made at the global scale(Alkama et al., 2013) and some studies suggest a significant influence of anthropogenic aerosols in the northern extra-tropics (e.g., Gedney et al., 2014). Globally, increasing trends (between 1951 and 2010) of in-situ measured low flow are in most cases associated with increasing high flows (Gudmundsson et al., 2019).

The occurrence of river floods with a return period of 30 years was observed to have significantly increased between the two periods 1980-1994 and 1995-2009 in Europe and the United States but not in Australia and Brazil (Berghuijs et al., 2017). While the investigated 1744 small (1-10,000 km^2) catchments are near-natural, the observation period is too short to attribute the observed changes to climate change; they could be just due to climate variability. According to an ensemble study with 21 climate model-GHM model combinations, the historical global warming of 1°C until today has already doubled the global land area that is annually affected by floods with return period of 100 years (occurrence frequency under pre-industrial conditions,Lange et al. (2019); submitted).

8.3.1.6 Soil moisture

Observed changes in SM were not assessed thoroughly in AR5, largely because of the scarcity of ground-based data and the lack of global datasets with a sufficient time period. Since AR5, several satellite products and land-surface reanalyses have been used to document recent changes in surface or total SM at the global scale. Despite their limited coverage, in situ measurements remain critical to assess regional changes, to calibrate and reduce signal uncertainties in satellite retrievals, and to evaluate and compare SM from land-surface models (LSM). Global land-surface and climate models are also increasingly useful for reconstructing, detecting and attributing recent changes in SM.

Various agencies provide continuous near-surface (typically 0-10 cm) SM measurements from different microwave remote sensing platforms. Recent attempts have been made to combine different products such as SMAP, ASCAT and AMSR2 (Kim et al., 2018) or former passive microwave datasets with active datasets in the framework of the European Space Agency (ESA) Climate Change Initiative (CCI) project (Dorigo et al., 2015). The added value of blended products has been emphasized by global-scale evaluation studies (Chen et al., 2018a; Kim et al., 2018). Despite data gaps, the ESA CCI product spans the 1979-2015 period, thereby allowing an analysis of interannual variations and trends (Dorigo et al., 2017). Although the data quality is not homogeneous over time (Su et al., 2016), contrasting regional trends have been documented (*high confidence*), which are more or less consistent with those derived from in situ measurements and alternative global datasets (Jia et al., 2018; Liu et al., 2019; Zhang et al., 2019a).

A strong limitation of microwave remote sensing is that it can only retrieve topsoil estimates. Other satellite products such as the Gravity Recovery and Climate Experiment (GRACE) (Famiglietti et al., 2015) may be useful for this purpose, but they operate at coarse space and time resolutions and they only measure total terrestrial water storage (TWS) variations, from which groundwater, root-zone and surface SM contributions must be estimated. Preliminary attempts have been made to attribute the recent trends in TWS to warming-induced variations in precipitation patterns and ice-sheet and glaciers loss, to internal climate variability or to water withdrawn (Fasullo et al., 2016; Rodell et al., 2018). These have been unsuccessful to date, because of the brevity of the records. LSM and data assimilation techniques therefore remain the main source of global information about root-zone and total SM. Several global reanalyses (e.g., GLDAS, MERRA-Land2, ERA-Interim/Land, CFSR or GLEAM) have been widely used over recent years. They are based on offline land-surface simulations driven by bias-corrected meteorological reanalyses. Their evaluation against in situ SM measurements (e.g., International Soil Moisture Network) or global satellite products (e.g., ESA CCI) suggests a reasonable ability to capture the high-frequency variability of SM (Balsamo et al., 2015). Low-frequency SM variability is less reliable (e.g., Liu et al., 2019 - submitted) given the lack of homogenised meteorological forcings(Hegerl et al., 2015) and land-atmosphere coupling (Berg and Sheffield, 2018a).

Despite their inherent limitations (see section 8.5.1), global climate models also provide valuable datasets for interpreting historical changes in SM. Mueller and Zhang(2016) used a combination of offline SM reconstructions and CMIP5 historical simulations to attribute the late 20th century warm season SM decrease found in NH dry regions to anthropogenic forcings. Douville and Plazzotta (2017) found a significant summertime drying in the northern mid-latitudes after 1979, attributable to anthropogenic greenhouse gas forcing.Gu et al. (2019) used an independent SM reconstruction (the GLDAS land-surface reanalysis) and a formal optimal fingerprint D&A technique to further demonstrate that the drying trends found in GLDAS are mainly due to anthropogenic GHG forcing. Marvel et al. (2019) identified externally-forced spatial patterns of semi-global summertime surface and root-zone SM changes in CMIP5 models. They reflect a northern mid-latitude drying in response to GHG forcing, and concluded trends over 1981-2017 are too large to be caused by internal noise variability alone. These fingerprints, however, are not detectable in the MERRA2 and GLEAM reanalyses over this period. Despite the variable skill of CMIP5 models to capture the main features of near-surface or total SM (Lauer et al., 2017; Vilasa et al., 2017; Yuan and Quiring, 2017), there are therefore multiple lines of evidence that human activities have contributed to enhance the dry or warm season aridity in subtropical and mid-latitude regions, at least since the middle of the 20th century (*high confidence*). Such results will need to be confirmed by further D&A studies using multiple aridity indicators (Cook et al., 2018) and the outputs of the CMIP6 global climate models (Gillett et al., 2016).

8.3.1.7 Freshwater reservoirs

8.3.1.7.1 Glaciers

Glaciers are losing mass globally due to the impact of global warming (Marzeion et al., 2018). Glaciers have been retreating worldwide, contributing significantly to sea-level rise (SLR) over the 20th century (about 40%) and will continue to contribute during the 21st century (Gardner et al., 2013). Between 1941 and 2004, the Muir Glacier on Glacier Bay in Alaska retreated more than 12 km and thinned by more than 800 m (Fig 8.16). For glaciers in the southern Coast Mountains of British Columbia, glacier recession was the greatest between 1920s and 1950s, with typical frontal retreat rates of 30 m a^{-1}(Koch et al., 2009). In central Asia, glacier recession varies from about 8 to 40% in surface area over the last 40-50 years (Kutuzov and Shahgedanova, 2009). In Himalaya, the amount of glacial ice loss observed and estimated in the last four decades was 443±136 Gt out of 3600-4400 Gt of glacial ice stored (about 13% of volume loss) in the Indian Himalaya (Kulkarni and Karyakarte, 2014). In the Southern Hemisphere, glaciers have similarly retreated, such as in New Zealand where Hoelzle et al. (2007) estimated a volume loss of about 60% from 1850 to 1970s. In the Amundsen Sea Embayment of West Antarctica, from 1992 to 2017, the Thwaites Glacier showed a complex pattern of retreat and ice thinning, with sectors retreating at 0.8 km/year and ice melting at 200 m/year, to retreat at 0.3 km/year with ice melting 10 times slower (Milillo et al., 2019).

[START FIGURE 8.16 HERE]

Figure 8.16: The Muir Glacier, Alaska photographed in August 1941 (a) by William O Field and in August 2004 from the same vantage point (b) by Bruce F. Molnia of U.S. Geological Survey (taken from Barry and Gan, 2011).

[END FIGURE 8.16 HERE]

8.3.1.7.2 Seasonal snow

Since AR5, a decreasing trend in snowfall has been detected in the NH (Rupp et al., 2013). Despite theory suggesting that warming would result in an increase in the intensity of extreme snowfall events (O'Gorman, 2014b), observed changes show decreases in extreme snowfall (Kunkel et al., 2016). Snowfall has likely decreased in the NH, but *confidence* is *medium*. Documentation is not available for the SH.

Under a warmer climate, the fraction of precipitation falling as snow has decreased significantly in recent years, with significant socio-economic consequences as more than $1/6^{th}$ of the world's population depend on meltwater for their water supply. Climate warming has been the dominant factor in the observed decrease in winter snow cover extent (SCE) and earlier spring ablation over North America (Dyer and Mote, 2006), and air temperature anomalies over NH mid-latitude land areas explaining about 50% of the observed variability in SCE (Brown and Robinson, 2011). Changes in annual flood occurrences also point towards a shift from snowmelt-dominated to rainfall-dominated flow regimes in some regions with consistent changes towards earlier timing of the flood peak.

Numerous observations have shown that NH spring SCE has been decreasing rapidly over recent decades, mostly in areas where SCE are closely linked to temperature variability, e.g., March–April SCE is decreasing at 3.4%±1.1% decade^{-1} (1979–2005) (Brown and Robinson, 2011; Hernández-Henríquez et al., 2015).Wu et al. (2018)found slower snowmelt rates over the entire NH during 1980–2017, with higher ablation rates in locations with deep snow water equivalent (SWE), but due to the reduction of SWE in deep snowpack regions, moderate and high snow ablation rates showed a decreasing trend. Kapnick and Hall (2012) detected significant loss of spring mountain snowpack in western US over past several decades. For Canada, there has been extensive decreasing snow depths and snow cover duration and extent since the mid-1970s, with the largest declines in western Canada and proportionally greater changes later in winter and spring (DeBeer et al., 2016). Berghuijs et al. (2014) show that in USA, catchmentswith a higher fraction of precipitationfalling as snow tends to have highermeanstreamflow, whichislikely to decrease in catchmentsthatexperiencesignificantreductions in the fraction of precipitationfalling as snowbecause of a warmerclimate.

Most studies show negative trends in snow depth and snow duration over past decades in the mountain cryosphere of Europe (Beniston et al., 2018), with less pronounced changes at high elevations (Terzago et al., 2013). Spring SWE shows a decreasing trend in Alps (Marty et al., 2017a). However, there were positive trends of maximum snow depth and SWE in higher and colder parts of the Fennoscandian Mountains although it turns out to be negative trends in recent years (Kivinen and Rasmus, 2015). Matti et al. (2017) show that the flood seasonality for snowmelt-dominated Scandinavian catchments have changed over the Twentieth century with statistically significant decreasing (increasing) trends in summer (winter and spring) maximum and mean daily flows in some catchments.

8.3.1.7.3 Wetlands and lakes

Continental surface water comprises a large diversity of spatial structures from very small rivers to extended floodplains and a large range of temporal behaviours from permanent lakes, to seasonal wetlands, to dramatic flash floods. They affect the climate through their impact on carbon and methane global budget (e.g. Saunois et al. 2016) and on the global surface heat fluxes, with coupled weather and climate effects (e.g., Zhan et al., 2019), but are also affected by human activities and by climate change.

IPCC AR5 did not specifically report on the surface water extent and dynamics. Only floods were considered, with low confidence in the observed changes.

Inventories of surface waters are produced at national or regional levels, but are not systematic, but consolidation efforts are undertaken at the global scale (Ramsar Convention on Wetlands, 2018). Satellite-derived global datasets have emerged, some providing temporal dynamics. Optical imagery provides high spatial resolution (down to 30m), long time-series (30 years with Landsat images), but fail to distinguish water under vegetation canopy or clouds and are thus limited to the detection of open water bodies (Donchyts et al., 2016; Pekel et al., 2016). Merging multiple satellite sensors makes it possible to detect surface water even under vegetation and clouds, over long time series (25 years) but with low spatial resolution (Prigent et al., 2016). High spatial resolution estimates of surface waters are produced by combing these low resolution estimates with topography information in a downscaling strategy (Aires et al., 2017; Fluet-Chouinard et al., 2015). Inter-comparison studies tend to reconcile the different estimates (Aires et al., 2018; Davidson et al., 2018). A broad literature is dedicated to the analysis of surface water extent and dynamics at local scale, some of them providing information on the changes in surface extent and dynamics.

Most recent multi-satellite estimates produce and estimated surface water of ~12.106-14.106 km^2 (including permanent and transitory surfaces, e.g., Aires et al., 2018; Davidson et al., 2018) in reasonable agreement with inventories (Davidson et al., 2018). These estimates are much higher than the ones provided by optical imageries that are limited to un-vegetated open water surfaces (~3.106 km^2).

Inventories show a strong decrease in natural surface water of ~0.8% per year in total from 1970 to the present (Ramsar Convention on Wetlands, 2018), however the Ramsar sites are not evenly distributed (limited coverage for instance in South America and Russia). These findings cannot be compared to the results from optical satellite imagery, most wetlands being partly covered by vegetation. Multi-satellite estimates capture the full surface water areas: they show a strong inter-annual variability in the extent over the last 25 years, and no clear long term trend is observed, despite a small decrease in global surface water extent up to 2006, especially in the Tropics lately compensated by a small increase (Prigent et al., to be submitted). As a consequence, due to the lack of agreement in the observational evidences at global scale, only *low confidence* is attributed to the decline of the natural surface water extent over the last years, as derived from the inventories.

Total man-made water surfaces represent ~10% of the total continental water surfaces (Ramsar Convention on Wetlands, 2018) and essentially comprise reservoirs and rice paddies. High resolution optical imagery over the last 30 years(Donchyts et al., 2016; Pekel et al., 2016) show that large areas of permanent open surface water have disappeared but that new permanent open water surfaces have formed, with a net increase of ~1. 105 km^2, in addition to changes in the temporal behaviour of some water bodies from permanent to transitory or vice versa. The permanent surface water increase is essentially attributed to the construction of man-made reservoirs. Surfaces of rice paddies are also increasing, especially in South East Asia (Davidson et al., 2018). It can be stated with *high confidence* that the man-made surface water extent is increasing.

For flood studies and prediction, mapping systems have been set up (Alfieri et al., 2014; Policelli et al., 2017) along with model developments (Hirabayashi et al. 2013; Sampson et al., 2015). It has not been possible to provide clear evidence of global changes in flood characteristics yet. For instance in Europe (Kundzewicz et al. 2017), despite some increase in the number of severe floods but that could be related to natural strong year to year variability.

8.3.1.7.4 Groundwater

Observed water cycle changes affecting groundwater include the intensification of precipitation and changes in meltwater regimes from glaciers and seasonal snow packs that influence the magnitude and timing of groundwater recharge.

Attribution of observed changes in groundwater volume (storage), whether it is at localized scales from piezometry (Kolusu et al., 2019; Taylor et al., 2013b) or at regional scales (> 100 000 km^2) estimated from GRACE satellite measurements (Rodell et al., 2018)(Fig.8.17), is complicated by non-climate influences on terrestrial water budgets that include land-use change (Favreau et al., 2009) and human withdrawals (Doell et al., 2014; Famiglietti, 2014; IPCC AR5 WGI Chapter). As the world's largest distributed store of freshwater (Taylor et al., 2013b), groundwater withdrawals supply substantial proportions of the estimated water used for domestic (36%), agricultural (42%) and industrial (27%) purposes globally (Döll et al., 2012). Groundwater is therefore well intertwined with hydrological systems influenced by human activity.

Regionally, groundwater depletion associated with a large groundwater footprint (Gleeson et al., 2012) was observed in the US High Plains, California's Central Valley (Scanlon et al., 2012), northwest India (Asoka et al., 2017; Rodell et al., 2009), Upper Ganges in India (MacDonald et al., 2016), North China Plain (Feng et al., 2013), and north-central Middle East (Tigris-Euphrates-Western Iran region) (Voss et al., 2013). Global groundwater depletion from 2000 to 2010 has increased from 240 km^3 to 292 km^3, which is mainly attributed to the rise in depletion rates in India (23%), USA (31%), and China (102%) (Dalin et al., 2017). GRACE satellite-based observations showed a loss of 109 km^3 of groundwater in northwest India between August 2002 and October 2008 with a rate of 4 ± 1 cm yr^{-1} (Rodell et al., 2009). Moreover, Wada et al. (2010) estimated that global groundwater depletion has more than doubled from 126 ± 32 (1960) to 283 ± 40 km^3 yr^{-1} (2000). Groundwater depletion in north China was estimated to 8.3 ± 1.1 km^3 yr^{-1} (2.2 ± 0.3 cm yr^{-1}) for 2003-2010, consistent with ground monitoring well observations (Feng et al., 2013).Voss et al.

(2013)showedthat the Middle East regionlostgroundwater volume of 91.3 ± 10.9 km^3 (17.3 ± 2.1 mm yr^{-1}) during 2003-2009. Asoka et al. (2017) showed contrasting trends in groundwater in north (declining at 2 cm yr^{-1}) and south India (increasing at 1-2 cm yr^{-1}) and explained it as anthropogenic pumping and precipitation variability linked to Indian Ocean SST variability.

Since the AR5 in 2013 and a global review of groundwater and climate change by Taylor et al. (2013b), evidence from piezometric observations of an association between heavy or statistically extreme precipitation and groundwater recharge has continued to grow, especially in tropical (Asoka et al., 2018; Kotchoni et al., 2019) and sub-tropical regions (Meixner et al., 2016a). Döll and Fiedler (2008) reported groundwater recharge of 12666 km^3 yr^{-1} (32% of total renewable water) during 1961-1990. Wada et al. (2010) found groundwater recharge of 15200 km^3 yr^{-1} during the period of 1960-2000. Scanlon et al. (2012) showed high recharge in northern High Plains (HP) while lower recharge in central and southern HP, resulting in localized depletion of fossil groundwater about 330 km^3 from 1950 to 2007. Relating long-term records of stable-isotope ratios of O and H in tropical precipitation at 15 sites across the tropics to those in local groundwater, Jasechko and Taylor, (2015) reveal that groundwater recharge in the tropics is near-uniformly biased to intensive monthly rainfall, commonly exceeding the ~70th intensity decile. Consequently, the intensification of precipitation (i.e. fewer low and medium intensity rain events, more very heavy rain events) resulting from radiative forcing is expected to enhance groundwater recharge. As noted in IPCC AR5 WG II Chapter 3 (section 3.2.5), rapid deterioration of groundwater quality, particularly from contamination by pathogenic microorganisms, has been observed in response to heavy rain events and linked to human activity and local land-use practices. The vulnerability of groundwater traced by these observations, reflects the preferential pathways bypassing soil matrices by which recharge often occurs (Beven and Germann, 2013).

Climate variability and drought affect groundwater depletion mainly due to higher groundwater abstraction. For instance, the depletion rate in Central Valley aquifer from 2006 to 2010 is estimated around 6–8 km^3 yr^{-1} using GRACE data (Scanlon et al., 2012). Asoka et al. (2018)reportedthat the decline in low-intensityprecipitationresults in reducedgroundwater recharge during the monsoonseason in major parts of India.

Changes in meltwater regimes from glaciers and seasonal snow packs tend to reduce the seasonal duration and magnitude of recharge (Tague and Grant, 2009). Aquifers in mountain valleys show shifts in the timing and magnitude of: (1) peak groundwater levels due to an earlier spring melt (2) low groundwater levels associated with longer and lower baseflow periods (Allen et al., 2010).The effects of receding alpine glaciers on groundwater systems are not well understood but long-term loss of glacial storage is estimated to reduce summer baseflow (Gremaud et al., 2009). In permafrost regions, coupling between surface-water and groundwater systems may be particularly enhanced by warming. In areas of seasonal or perennial ground frost, increased recharge is expected despite decrease of absolute snow volume (Okkonen and Kløve, 2011).

Coastal aquifers form the interface between the oceanic and terrestrial hydrological systems. Global SLR serves to induce fresh–saline-water interfaces to move inland. The extent of seawater intrusion into coastal aquifers depends on a variety of factors including coastal topography, recharge, and groundwater abstraction from coastal aquifers. Analytical models suggest that the impact of SLR on seawater intrusion is negligible compared to that of groundwater abstraction (Ferguson and Gleeson, 2012). Coastal aquifers under very low hydraulic gradients, such as the Asian mega-deltas, are theoretically sensitive to SLR but, in practice, are expected to be more severely affected in coming decades by saltwater inundation from storm surges than SLR.

[START FIGURE 8.17 HERE]

Figure 8.17: Trends in TWS (in centimetres per year) obtained on the basis of GRACE observations from April 2002 to March 2016. The cause of the trend in each outlined study region is briefly explained and colour-coded by category. The trend map was smoothed with a 150-km-radius Gaussian filter for the purpose of

visualization; however, all calculations were performed at the native 3° resolution of the data product. Figure from Rodell et al. (2018).

[END FIGURE 8.17 HERE]

8.3.2 Observed variations in large-scale phenomena and regional variability

8.3.2.1 ITCZ and tropical rainbelts

The intertropical convergence zone (ITCZ) is a predominantly east-west strip of heavy rainfall circling the globe at low latitudes. The ITCZ and its migrations largely determine the characteristics of regional water cycles in tropical regions. The majority of the ITCZ lies over oceans, where in situ rainfall measurements are sparse. As a result, observational analyses of the ITCZ are derived largely from satellite-based remote sensing of cloud reflectivity (Waliser et al., 1993), outgoing longwave radiation (Bain et al., 2011) and precipitation (Lau and Wu, 2007). As the satellite period has lengthened, observations have increasingly been used to assess trends in the ITCZ. Lau and Wu, (2007) examined tropical rainfall trends between 1979 and 2003 and found increases in the frequency of heavy events, with this positive trend being most pronounced in the core of the ITCZ. Studies analysing similar periods have found consistent trends, with precipitation increases in the core of the Pacific ITCZ and decreases on the ITCZ margins (Adler et al., 2008; Gu et al., 2016). In general, observational evidence supports a decrease in ITCZ width with cloud feedbacks playing a role (Su et al., 2017) and manifesting as more organised convection in the ITCZ core and less in the periphery (Tan et al., 2015). The observed changes are affected by internal variability and local feedbacks, for example relating to cloud (Talib et al., 2018b), and simulated decreases in width are smaller (Byrne et al., 2018) and mainly determined by a northward shift in the southern extent (Byrne and Schneider, 2016b).

Analysing atmospheric reanalyses, Wodzicki and Rapp(2016) used a series of dynamic and thermodynamic masks to identify the ITCZ and evaluate trends in its characteristics over a 35-year timeseries. Consistent with Zhou et al.(2011), Wodzicki and Rapp (2016) found significant narrowing and strengthening of the Pacific ITCZ over recent decades but no change in the ITCZ location. An updated 39-year time series spanning 1979–2017 was used to assess ITCZ trends in both the Atlantic and Pacific basins (Byrne et al., 2018). This study found substantial ITCZ narrowing and strengthening of precipitation in the cores of the Atlantic and Pacific ITCZs, but no significant changes in ITCZ locations. These observed ITCZ trends are qualitatively similar to the projected narrowing and strengthening of the ITCZ over the 21st century (Byrne and Schneider, 2016b; Lau and Kim, 2015) (see also Section 4.2.1.1).

The ITCZ trends derived from satellites, precipitation measurements and reanalysis data are supported by ocean surface-salinity observations. Long-term salinity observations show an overall strengthening of the tropical hydrological cycle (Durack, 2015) together with a freshening in the cores of the Atlantic and Pacific ITCZs and increased salinity on the ITCZ margins (Durack et al., 2012a; Durack and Wijffels, 2010; Skliris et al., 2014; Terray et al., 2012).

Rainfall reconstructions based on carbon isotope analysis of speleothems from Belize suggest the southward displacement of the tropical rainbelt has occurred since 1850, which coincides with increasing NH anthropogenic aerosol emissions and tropical rainfall reductions during the entire twentieth century (Ridley et al., 2015). NH station data indicate that decreasing precipitation trends during 1950s-1980s have since recovered, and these changes are attributable to anthropogenic aerosol emissions from North America and Europe, which peaked during the late-1970s and declined thereafter following improved air quality regulations causing dimming (brightening) through reduced (increased) surface solar radiation(Wild, 2012) (Fig.8.18).

[START FIGURE 8.18 HERE]

Figure 8.18: Global dimming and brightening, from (Wild, 2012).

[END FIGURE 8.18 HERE]

Although there have been no significant shifts in the locations of the Pacific and Atlantic ITCZs over recent decades, rain-gauge data show a southward migration of the rainbelt over land during the 20th century (Hwang et al., 2013b; Rotstayn and Lohmann, 2002), which is thought to be associated with large emissions of scattering sulphate aerosols in the NH, though it is unclear why similar southward shifts are not observed over oceans (e.g., Byrne et al., 2018). Model simulations link the southward shift of rainbelts to anthropogenic sulphate aerosol cooling of the NH (Ackerley et al., 2011a; Biasutti and Giannini, 2006a; Chiang et al., 2013; Hwang et al., 2013a). This is consistent with energetic constraints, which shows tropical precipitation shifts are anti-correlated with cross-equatorial energy transports (Frierson and Hwang, 2012).

Dimming over the NH causes a relative cooling of the NH compared to the SH, which induces an anomalous Hadley circulation with anomalous southward moisture flow and southward shift of the tropical rainbelt. This likely explains the severe drought in the Sahel that peaked in the mid-1980s (Rotstayn and Lohmann, 2002; Undorf et al., 2018b) and the southward shift of the NH tropical edge from the 1950s to the 1980s (Allen et al., 2014; Brönnimann et al., 2015). The impact of aerosols and volcanic activity on the position of the ITCZ has been investigated for instance in (Chang et al., 2011; Chung and Soden, 2017; Colose et al., 2016; Friedman et al., 2013). The change in ITCZ position is however difficult to characterize in observations. Yet, a forced behavior of the ITCZ can have important regional impacts (Fig 8.19).

[START FIGURE 8.19 HERE]

Potential figure for D&A of ITCZ shift in the SOD

Figure 8.19: Placeholder for Bonfils et al. 2019 - Formal pattern-based D&A for meridional shift in the ITCZ

[END FIGURE 8.19 HERE

In summary, a range of studies and independent datasets demonstrate that the ITCZ over the oceans has been narrowing and strengthening in recent decades (*moderate confidence*). However, there has been little investigation of the physical processes causing these observed ITCZ changes. Further work is required to understand the contrasting trends in ITCZ location over land and ocean, and also to estimate and understand trends in ITCZ width and strength over land regions where the impacts of changing rainfall patterns are most critical.

8.3.2.2 Hadley circulation and subtropical belt

Precipitation distribution over the tropics and monsoon-dominated regions is closely tied to large-scale Walker and Hadley-type overturning circulations. A robust technique to partition the 3-dimensional tropical overturning circulation into the Walker (zonal) and Hadley (meridional) components through a decomposition of the vertical mass-flux has been proposed by Schwendike et al., (2014). This technique also provides a more precise basis to quantify the Walker and Hadley circulations on regional / local scales. An analysis and documentation of long-term trends in the local Hadley and Walker circulations from 1979 to 2009 by Schwendike et al. (2015), using multiple reanalysis datasets, indicates a southward shift of the local Hadley circulation over Africa, the Maritime Continent and the western and central Pacific by about 1 degree of latitude, which is consistent with the observed southward shift of the ITCZ and tropical rainfall belt (Greve et al., 2014).

A poleward shift in the Hadley Cell is dominated by responses of the sub-tropical subsiding branch of the atmospheric circulation to CO_2 increases. Since AR5, this has been linked with strengthening and an upward shift of the subtropical jet (Chemke and Polvani, 2019; Shaw and Tan, 2018) although changes in the equator to pole temperature gradient also play a role. Poleward expansion of the tropical belt strongly contributes to subtropical precipitation decline (Cai et al., 2012; Nguyen et al., 2018a; Scheff and Frierson, 2012) and this expectation has been corroborated since AR5 (He and Soden, 2017a; Tang et al., 2018). A poleward shift in the subtropics and storm tracks have been explained by amplified Arctic surface warming using a simple diffusive moist static energy transport model (Siler et al., 2018a). Responses are modified by patterns of ocean heat uptake and local feedbacks including cloud cover (Li et al., 2018e). Based upon detailed modelling, much of this response is related to rapid circulation adjustments to CO_2 forcing rather than the warming response (Ceppi et al., 2018) while anthropogenic aerosol and ozone changes are also known to play a role (Allen et al., 2012).

Observational evidence supports simulated expansion of subtropical dry zones, and increasing height of the highest cloud tops (Norris et al., 2016) while associated precipitation decline is found to be dominated by direct circulation response to radiative forcing (He and Soden, 2017a), particularly for the Mediterranean (Tang et al., 2018). Simulated strengthening of subtropical high pressure primarily during April-June in the NH has been linked to the seasonal delay of monsoon rains (Song et al., 2018) while sub-tropical changes at upper levels can conversely influence tropical regions through western disturbances (Madhura et al., 2014).

Multiple observational evidences indicate that in most seasons the Hadley cell expanded in both hemispheres, but its intensity remained almost unchanged (Nguyen et al., 2013). A poleward shift in the subtropical highs of both hemispheres has been identified, consistently with the observed poleward expansion of the Hadley circulation and widening of the tropical belt (Lucas and Nguyen, 2015; Nguyen et al., 2013; Vizy and Cook, 2016). Although the rate of widening has been disputed (Davis and Rosenlof, 2012), with published estimates ranging up to 3° latitude per decade, recent analyses suggest a more modest rate of widening (~0.5° latitude per decade) (Staten et al., 2018). Since the late 1970s, the WNPSH has extended westward, resulting in a monsoon rain band shift over China with excessive rainfall along the middle and lower reaches of the Yangtze River valley along ~ 30° N over eastern China, and deficient rainfall in north China (Hu, 2003; Yu and Zhou, 2007); and northern parts of South Asia (Preethi et al., 2017). In the last 30 years, the precipitation variability over the eastern USA increased because of changes in the intensity and position of the western ridge of the North Atlantic subtropical high (Diem, 2013; Li et al., 2011b). In the SH the expansion has been associated with both the intensification and poleward shift of the subtropical high pressure belt, with consequences on precipitation over Africa, Australia and South America (Nguyen et al., 2015). Part of the recent expansion (last 30 years) of the Hadley cell has been driven by a swing from warm to cold phase of the IPO (Meehl et al., 2016), but other factors also contributed, especially external anthropogenic forcing (Lucas et al., 2012; Nguyen et al., 2015).

8.3.2.3 Walker circulation

There is consistent evidence from multiple observational datasets and reanalyses that the Pacific Walker circulation has strengthened since the 1980s (de Boisséson et al., 2014; Ma and Zhou, 2016; Merrifield, 2011; Sohn and Park, 2010). The sign of Walker circulation trends over longer periods (50-100 year) is inconclusive due to sparse observations and large decadal variability, with apparently inconsistent evidence from different observational datasets and studies. Analyses of sea-level pressure (SLP) observations have found either weakening (Tokinaga et al., 2012) or strengthening (L'Heureux et al., 2013b) Walker circulation trends since the 1950s and a weakening trend (Power and Kociuba, 2011; Vecchi et al., 2006) over the 20th century, though SLP observations before the 1950s may be unsuitable for trend analysis (L'Heureux et al., 2013b). Cloud observations suggest a weakening Walker circulation over both the 50 (Tokinaga et al., 2012) and 100 year (Bellomo and Clement, 2015) periods. Centennial SST trends may be consistent with a neutral or strengthening trend in the Walker circulation, but with large observational uncertainty (Coats and Karnauskas, 2017). In addition, it has been reported that the Pacific Walker circulation shows a slight change (1-2%), whereas the local Walker circulationsover the Indian Ocean and

Atlantic show weakening (Schwendike et al., 2015).

The observed Walker circulation strengthening since the 1980s cannot be explained as an externally-forced signal (Kociuba and Power, 2015; Sohn et al., 2013b) and is only consistent with the most extreme trends simulated from the internal variability of models (Bordbar et al., 2017; Kociuba and Power, 2015). The associated relative cooling of the east and central equatorial Pacific over the same time period (Meng et al., 2011) was likely to be a major driver of the recent global warming hiatus period (Kosaka and Xie, 2013). Trends in Atlantic SSTs are likely to have been influential on the Pacific Walker circulation in recent decades (Kucharski et al., 2011; McGregor et al., 2014), and volcanic aerosol forcing could also have contributed (Takahashi and Watanabe, 2016).

In climate models, the forced signal of Walker circulation weakening can be explained by dry static stability increasing at a faster rate than atmospheric radiative cooling (Knutson and Manabe, 1995a) under GHG forcing, combined with a weakened Equatorial Pacific SST gradient in model simulations (Tokinaga et al., 2012; Xie et al., 2010). Ozone forcing could also have contributed to weakening of the Walker circulation between 1955-2005 (Polvani and Bellomo, 2019).

8.3.2.4 Monsoons

The distribution of monsoon precipitation over different regions of the globe is closely tied to the seasonal cycle of the movement of the ITCZ and the accompanying seasonal wind reversals (Zhisheng et al., 2015). The AR5 concluded that *"globally, the area encompassed by the monsoon systems will increase over the 21st century. While monsoon winds are likely to weaken, monsoon precipitation is likely to intensify due to increase in atmospheric moisture".* Since AR5 there have been improved assessments of precipitation changes associated with the global and regional monsoon systems.

8.3.2.4.1 Global monsoon

Multiple precipitation datasets indicate a long-term decreasing trend, together with significant decadal-scale variations, in the global monsoon precipitation during 1948-2003, primarily contributed by a weakening trend of the NH summer monsoon rainfall (Wang and Ding, 2006). More recent estimates indicate an increasing trend in global monsoon precipitation in the NH and a non-significant decreasing trend for the SH during post-1979 (Deng et al., 2018). The intensified global monsoon precipitation reported during the recent 2-3 decades has been linked to an upward trend in the NH summer precipitation over oceanic areas (Hsu et al., 2011; Wang et al., 2012; Zhou et al., 2008). The increase in atmospheric moisture associated with the warming of the atmosphere is one of the main drivers of that increase (Cherchi et al., 2011; Held and Soden, 2006b; Richter and Xie, 2008; Wentz et al., 2007). Enhancement of large-scale SST patterns with warmer SST in the NH as compared to the SH (Liu et al., 2009a) or enhanced east-west thermal contrast in the Pacific Ocean (Wang et al., 2012), are viewed as important drivers for intensification of the global monsoon precipitation. Furthermore, natural variability may also play a role in observed changes, for example through shifts of the AMO phase from negative to positive around the mid-1990s associated with an increase of rainfall over the global monsoon regions (Kamae et al., 2017; Lopez et al., 2016; Wang et al., 2013a). Likewise, an intensification of the NH summer monsoon rainfall during 1979-2011 is reported to have linkages to the cold phase of a mega ENSO (a leading mode of interannual-to-interdecadal variation of global SST) (Wang et al., 2012).

8.3.2.4.2 South Asian Monsoon (SASM)

The seasonal summer monsoon rains from June through September contributes to more than 75% of the annual rainfall for many countries in South and Southeast Asia. The AR5 concluded that there is *medium confidence* that overall precipitation associated with the Asian-Australian monsoon will increase but with a north–south asymmetry: Indian and East Asian monsoon precipitation is projected to increase, while projected changes in Australian summer monsoon precipitation are small.

Since AR5, several studies have documented long-term changes in SASM rainfall since the 1950s. Observed Indian summer monsoon precipitation is reported to have declined by about 7% since 1950, with an associated weakening of the large-scale monsoon circulation (Abish et al., 2013; Bollasina et al., 2011; Guhathakurta et al., 2017; Krishnan et al., 2013, 2016; Mishra et al., 2012; Roxy et al., 2015; Saha et al., 2014; Singh et al., 2014) and a significant increase in the the frequency and duration of monsoon breaks ('dry spells') during recent decades (Dash et al., 2009; Kumar et al., 2009; Singh et al., 2014; Turner and Hannachi, 2010). The landsurface hydro-climatic response to the declining monsoon rains is also evidenced as a decreasing trend of SM over India during the last few decades (Krishnan et al., 2016; Niranjan Kumar et al., 2013; Ramarao et al., 2015, 2018). Jin and Wang (2017) reported an apparent recovery of the Indian summer monsoon for a short period during 2003-2013, although this claim is contentious given that the region experienced four major monsoon droughts since 2003 with two consecutive droughts during 2014 and 2015, respectively (Mujumdar et al., 2017).

Large natural variability of the monsoon on multi-decadal time-scales, evident in precipitation reconstructions over the last two millennia, poses inherent challenges in detecting anthropogenic forced changes in the SASM precipitation (Sinha et al., 2015). While increasing concentrations of atmospheric GHGs have caused warming globally, there is growing evidence of the role of anthropogenic aerosols in altering regional monsoon precipitation. Using high-resolution model simulations, Krishnan et al. (2016) attributed the declining trend in the Indian summer monsoon precipitation since 1950 to the combined effects of anthropogenic aerosol forcing, land-use changes and rapid warming of the equatorial Indian Ocean. In particular, the observed decrease of SASM precipitation during the second half of the 20th century is largely related to the dominance of NH aerosol radiative effects in suppressing precipitation over the expected precipitation enhancement due to increased GHG (Bollasina et al., 2011; Krishnan et al., 2016; Lau and Kim, 2017; Lin et al., 2018; Sanap, 2015; Undorf et al., 2018b)(Fig.8.20).

While the aerosol surface negative radiative forcing over the northern Indian Ocean decreases the local SST, leading to a northward gradient of SST cooling (Krishnan et al., 2016; Patil et al., 2018), the oceanic response to a weakened monsoon cross-equatorial flow can accelerate SST warming in the central-eastern equatorial Indian Ocean, beyond the GHG-induced warming, and thereby amplify the northward gradient of SST cooling and further weaken the monsoon, in a positive feedback loop (Krishnan et al., 2006; Swapna et al., 2012). Land-cover changes due to replacement of natural forest vegetation by croplands also contributes to the SASM weakening through increase of planetary-albedo (Krishnan et al., 2016) and a decrease in ET and convection that reduces the amount of recycled moisture (Paul et al., 2016).

Remote aerosols may be just as important as regional emissions in influencing the Asian summer monsoon (Song et al., 2014; Wang et al., 2017e; Zhang et al., 2016b). Undorf et al., (2018a) found that weakening of the SASM was related to North American and European aerosols up until ~1975, after which the increase in regional emissions tend to dominate the weakening, especially during the early stages of the monsoon (Ganguly et al., 2012).This is also consistent with weakening of NH monsoon precipitation (Polson et al., 2014), likely related to evolution of the inter-hemispheric temperature gradient and tropical precipitation shift (Shindell et al., 2012), where the influence of remote aerosols often outweighs the local forcing.

[START FIGURE 8.20 HERE]

Figure 8.20: Excerpt from Fig. 1 of (Undorf et al., 2018b).

[END FIGURE 8.20 HERE]

Absorption of solar radiation by anthropogenic aerosols over South and East Asia warms the lower troposphere, suppresses surface heating and evaporation. This builds moist static energy in the troposphere along with larger convection inhibition (Wang et al., 2013e) (Fig.8.21). Release of instability, often triggered by topographical barriers, produces intense rainfall and flooding (Fan et al., 2015)(Guo et al., 2016a). The warming and enhanced convection near the Himalayanfoothillsinducesuplifting and mid-level convergence, which pulls air from the south and can alsoadvance the monsoononset(Lau, 2016; Lau and Kim, 2006). This paradigm is termed as the "Elevated Heat Pump" hypothesis (EHP). Continued pollution of anthropogenic aerosols after the monsoon onset can weaken the circulation by reducing the overall solar heating available for convection (Li et al., 2016b). The EHP can also modulate transitions between active and break cycles on intra-seasonal time-scales (Manoj et al., 2011).

[START FIGURE 8.21 HERE]

Figure 8.21: Redistribution of surface and low tropospheric heating due to aerosol absorption of solar radiation. The broken blue line represents the temperature in clean atmosphere. The solid blue line shows low level cooling and mid-level warming due to air pollution, which inhibits cloud formation, but increasing the conditional instability. This leads to suppression of small clouds and light precipitation while enhancing deep clouds with heavy precipitation. From (Wang et al., 2013e).

[END FIGURE 8.21 HERE]

Proxy reconstructions indicate weakening of the Asian summer monsoon, including the SASM, during cold epochs (*high confidence*), like the Last Glacial Maximum (LGM) and Younger Dryas (Chandana et al., 2018; Cheng et al., 2012; Dutt et al., 2015; Dykoski et al., 2005; Hong et al., 2018; Shakun et al., 2007; Zhang et al., 2018a). These changes in monsoon intensity are tightly linked (*medium confidence*) to changes in solar insolation and high-latitude climate (Araya-Melo et al., 2015; Battisti et al., 2014; Bosmans et al., 2018; Braconnot et al., 2008; Rachmayani et al., 2016; Zhang et al., 2018a).

8.3.2.4.3 East Asian Summer Monsoon (EASM)

CMIP5 models show robust changes in EASM precipitation due to increased atmospheric moisture content, whereas the dynamic effect from circulation changes show regional differences in rainfall change with large uncertainties(Zhou et al., 2017). Model-dependent uncertainties in the position and extension of circulation over the western North Pacific Ocean (WNP) can introduce large uncertainties in future precipitation over Japan which can offset the thermodynamic effect (“wet-get-wetter”) and possibly even cause a decrease of precipitation in the future (Ose, 2019).

Precipitation observations from China during 1951-2000 indicate a conspicuous trend of drying in the north and wetting in the southeast (Zhai et al., 2005), with associated weakening of the EASM low-level circulation and increased surface pressure over northeast China and southward shift of the jet stream (Song et al., 2014). The southward shift and enhancement of the jet stream (Li et al., 2010) explains the increase of rainfall especially from the Meiyu front (Day et al., 2018) at the expense of drying over northeast China. This was likely caused by aerosol-induced enhancement of thermal contrast that was incurred by both remote and local enhancement of aerosol emissions (Chen et al., 2018b; Undorf et al., 2018a).

GHG and anthropogenic aerosols are identified (*high confidence*) as drivers of the EASM precipitation change (Chen and Sun, 2017; Ma et al., 2017; Wang et al., 2013c; Xie et al., 2016; Zhang et al., 2017a). Increased precipitation in the southern region has been linked to increased moisture transport convergence by GHG forcing, whilst changes in anthropogenic aerosols weaken the EASM thus reducing precipitation in the northern regions (Tian et al., 2018a). Aerosol-induced cooling, associated atmospheric circulation changes and SST feedbacks can weaken the EASM and favour the dry-north and wet-south pattern of rainfall anomalies (Wang et al., 2013c; Song et al., 2014; Zhang et al., 2017b;Chen et al., 2018c). Natural variability and volcanic eruptions can further contribute to the weakened EASM (Hsu et al., 2014; Li et al., 2010; Qian and Zhou, 2014). Anthropogenic aerosol-induced cooling and anomalous high pressure over the East China Sea can also decrease winter precipitation over China by enhancing the offshore winter monsoon circulation (Bennartz et al., 2011; Wilcox et al., 2018).

The WNP monsoon is a sub-component of the EASM (Wang et al., 2001; Wang and LinHo, 2002) and exhibits pronounced interannual variability that impacts the North Pacific gyre oscillation (Zhang and Luo, 2016) and tropical cyclone activities over East Asia (Choi et al., 2016b). The interannual variability of the WNP monsoon has increased in the last decades and shows close links to the central Pacific ENSO (Lee et al., 2014), whereas it was less variable and stronger during the beginning of the 20th century (Vega et al., 2018).

Representation of "warm type" heavy rainfall in climate models seems crucial for assessment of changes in the EASM rainfall. Sohn et al., (2013a) showed that the majority of summer rainfall over the Korean peninsula is ''warm type'' with TRMM PR echo-top heights lower than 8 km, in contrast to the prevailing view that heavy rainfall results from cumulonimbus with a considerable vertical extent of radar echo ("cold type"). Moreover, Sohn et al., (2013a)suggested that the concept of ''warm type'' heavy rainfall is consistent with the medium depth convection observed by radar under humid environments near the East Asian monsoon front in previous studies. Orographic heavy rainfall in East Asia is also "warm type" with low TRMM PR echo-top heights (Shige et al., 2013; Taniguchi et al., 2013).

Pliocene reconstructions indicate stronger intensity of the EASM with a more northerly penetration of the monsoon rainbelt, supporting the projection that EASM rainbelt shifts northward in a warmer world (Yang et al., 2018b). EASM variability has been related to AMOC dynamics, especially during the last glacial period (Sun et al., 2012). But whether the relationship is negative or positive remains controversial (Cheung et al., 2018; Kang et al., 2018; Sun et al., 2012; Zhang and Delworth, 2005).

8.3.2.4.4 West African Monsoon (WAM)

There is *very high* confidence that West African Monsoon (WAM) region experienced the wettest decade in the twentieth century during the 1950s and early 1960s, followed abruptly by unprecedented rainfall deficits from the late 1960s to the mid-1990s; particularly in the semi-arid Sahel zone with a mean decrease of annual cumulative rainfall of about 36% compared to (1931-1960) (Ali and Lebel, 2009; Descroix et al., 2015; Nicholson, 2013). The long decline in annual rainfall is related to a decrease in the number of rain events (Balme et al., 2006; Barbé and Lebel, 1997), with contributions from decreases in large convective events in the core of the rainy season (Bell et al., 2006) that modulate interannual variability (Lebel et al., 2003; Nicholson, 2000; Panthou et al., 2018). There is *medium confidence* that the decrease in annual mean precipitation is due to the decrease in the number of rainy days (Bodian et al., 2016; Frappart et al., 2009).

Reduced Sahel rainfall has been linked with southward ITCZ shifts associated with cooling of the northern hemisphere by anthropogenic aerosol including indirect effects on cloud (Allen et al., 2015; Chung and Soden, 2017; Dong et al., 2014; Hwang et al., 2013b) and volcanic aerosol preferentially affecting the northern extratropics(Haywood et al., 2013). SST patterns (Rodríguez-Fonseca et al., 2015a) and the distribution of clouds (Potter et al., 2017; Stephens et al., 2015b) also play a role while greenhouse gas forcing combined with water vapour feedback is expected to strengthen the Sahara heat low and drive a northward shift in the West African monsoon system (Allen et al., 2015; Dong and Sutton, 2015a; Dunning et al., 2018; Evan et al., 2015).

Wetter conditions of the WAM prevailed from the mid-to-late 1990's, but with less spatial coherence and temporal persistence; with *medium confidence*intheGuinean coastal region and *high confidence*in the Sahel (Ali and Lebel, 2009; Bodian et al., 2016; Descroix et al., 2015; Nicholson, 2005; Sanogo et al., 2015a).In the Sahel region, the recovery is reflected in the increase in the number of heavy and extreme events, compared to the drought period but without exceeding the values noted during the wet period (Descroix et al., 2013, 2015, Panthou et al., 2014, 2018; Sanogo et al., 2015b). The Sahel rainfall recovery is also characterized by high interannual variability (Descroix et al., 2018; Zhang et al., 2017c); associated with SST variations in the Tropical Atlantic, Pacific and Mediterranean Sea (Ackerley et al., 2011b; Giannini, 2003; Rodríguez-Fonseca et al., 2015a). There is *highconfidence* that extreme intense events are more frequent in the Sahel since the beginning of the twenty-first century (Giannini et al., 2013; Panthou et al., 2014, 2018; Sanogo et al., 2015b; Taylor et al., 2017b).

Taylor et al., (2017b) argued that the intensification of mesoscale convective systems, responsible for extreme rains, is favoured by meridional temperature gradient induced by the warming of the Sahara desert at a pace that is 2–4 times greater than that of the tropical-mean temperature (Cook et al., 2015c; Vizy et al., 2017). Periods of monsoon-breaks and the persistence of low rainfall events are still prominent, particularly after the onset, thus exposing West Africa simultaneously to the risks of dry spells (Zhang et al., 2017b) and also extreme localized rains and floods in cities and rural areas (Engel et al., 2017; Lafore et al., 2017). Occurrence of extreme events is compounded by landuse and landcover changes to increased runoff (Bamba et al., 2015; Descroix et al., 2018). Summer (July through September) rains over parts of Ethiopia and South Sudan, which have linkages to the WAM, have also significantly decreased during the post-1960s (Nicholson, 2017).

Sahel drought [1968-1995/1998] was *likely* related to anthropogenic emissions of sulphate aerosols in the Atlantic sector, which cause an inter-hemispheric pattern of SST anomalies (Ackerley et al., 2011b; Baines et al., 2007; Biasutti and Giannini, 2006b; Hwang et al., 2013b). High-resolution climate model experiments demonstrate that in addition to aerosol forcing, the rapid warming of the equatorial Indian Ocean during post-1950s and land-atmosphere interactive feedbacks have led to prolonged deficits in the WAM rainfall (Krishnan et al., 2016) (Fig.8.22). The recent recovery has been attributed to prevailing positive SST anomalies in the tropical North Atlantic potentially associated with a positive phase of the Atlantic multidecadal oscillation (Diatta and Fink, 2014; Rodríguez-Fonseca et al., 2015b). The Sahel rainfall recovery has also been attributed to higher levels of GHG in the atmosphere and increase in atmospheric temperature (Dong and Sutton, 2015b).

[START FIGURE 8.22 HERE]

Figure 8.22: Attributing the monsoonweakening to anthropogeninfluence Map showing the difference in June–September mean precipitation (mm day^{-1}) and 850 hPa winds (vectors; ms^{-1}) between the HIST1 and HISTNAT1 simulations for the period (1951–2005). *Grey dots* correspond to mean precipitation differences (HIST1 minus HISTNAT1) which exceed 95 % confidence level based on a two-tailed student's t-test Krishnan et al., (2016).

[END FIGURE 8.22 HERE]

8.3.2.4.5 North American Monsoon System (NAMS)

AR5 concluded *low confidence* in the projected precipitation changes associated to the North American monsoon system (NAMS) but *medium confidence* that the NAMS will trigger and persist later in the annual cycle. However, recent rainfall-based studies suggest more frequent occurrence of earlier retreats of the NAMS since 1979 (Arias et al., 2012, 2015a), in association with the positive phase of AMO and westward expansion of the North Atlantic Subtropical High (Li et al., 2011b, 2012b).

Trends of June–to-September precipitation during 1948-2010 show significant increases over New Mexico and the core NAMS region, and significant precipitation decreases over southwestern Mexico (Hoell et al., 2016). Daily precipitation data during 1910-2010 shows an increase in the number of precipitation events across the northern Chihuahuan Desert despite a decrease in their magnitude, and an increase in the length of extreme dry and wet periods (Petrie et al., 2014). Precipitation from multiple reanalyses show that increases in the NAMS rainfall have contributed to the increasing trend of global monsoon precipitation (Lin et al., 2014). Other studies suggest a strengthening of the NAMS anticyclone since the mid-1970s, with a more frequent northward location (Diem et al., 2013). Therefore there is *low confidence* in detection of any anthropogenic-driven trend in the NAMS.

Precipitation reconstructions from tree-rings in the NAMS region indicate that decadal droughts of the last five centuries were characterized by winter precipitation deficits and concurrent failures of summer monsoon, and that these droughts were more severe and persistent than any of the instrumental period (*high confidence*) (Griffin et al., 2013). Tree-rings also indicate the presence of prolonged megadroughts (droughts lasting two decades or more) throughout the last millennium in the NAMS region that were more severe than 20th and 21st century events (*high confidence*) (Cook et al., 2004, 2010a, 2015b). Model simulations demonstrate that forced changes in solar and volcanic activity do not consistently produce megadroughts, thus these events were *likely* forced by internal climate variability (*medium confidence*) (Coats et al., 2016; Cook et al., 2016b). Likewise, (Jones et al., 2015)find no evidence of solar forcing of the NAMS in a finely-resolvedlacustrinesedimentary record.

On longer timescales, the strength of NAMS has varied as a function of glacial boundary conditions and seasonal changes in insolation. During the Last Glacial Maximum (21,000 yr ago), the NAMS was substantially weaker due to ventilation of the system by cold, dry mid-latitude air associated with the Laurentide Ice Sheet (Bhattacharya et al., 2017b, 2018) . The NAMS strengthened up until the mid-Holocene period, in response to ice sheet retreat and rising summer insolation, but did not likely exceed the strength of the modern system (*low confidence*) (Bhattacharya et al., 2018; Metcalfe et al., 2015). PMIP3°MIP5 simulations suggest reduced winter atmospheric moisture transport from the southwest into the northern NAMS region during the mid-Holocene (Hermann et al., 2018).

8.3.2.4.6 South American Monsoon System (SAMS)

AR5 concluded there is *high confidence* in the expansion of SAMS monsoon area and *low confidence* in the projected changes in SAMS precipitation.

Since AR5, several observational studies identified delayed onsets of the SAMS after 1978 related to longer dry seasons in the southern Amazon (Arias et al., 2015a; Debortoli et al., 2015; Fu et al., 2013; Seth et al., 2010; Yin et al., 2014b). In contrast, other studies find earlier SAMS onsets during 1971-2010 (Jones and Carvalho, 2013). Total rainfall reductions are observed in the southern Amazon during September-October-November after 1978 (Bonini et al., 2014; Debortoli et al., 2015, 2016; Espinoza et al., 2018a; Fu et al., 2013) whereas increases are observed in the northern Amazon in March-April-May after 1998 (Espinoza et al., 2018a).

Analyses of regional rain-gauge data show positive trends in the occurrences of heavy and extreme precipitation in southern and southeastern Brazil after 1950 (Marengo et al., 2013b; Pinto et al., 2013; Skansi et al., 2013). By contrast, drier conditions have been reported over central and northeastern Brazil since the mid-1990's (Marengo et al., 2018), with a severe drought affecting the region between 2012 and 2015 (Marengo et al., 2013a, 2017). In Bolivia, increases in precipitation were observed during 1965 -1984, while reductions have occurred afterward (Seiler et al., 2013). The Peruvian Amazon does not reveal significant changes in mean rainfall during 1965–2007, although significant interannual variability of precipitation has been observed (Lavado et al., 2013). Other studies indicate a strengthening of the hydrological cycle over the Amazon basin, with more severe flooding since late-1990s (Espinoza and Marengo, 2015; Gloor et al., 2013), which has been linked to a strengthening of the Walker circulation due to strong tropical Atlantic warming and tropical Pacific cooling (Barichivich et al., 2018).

In addition, increases in the frequency of wet days are observed after 1995 over the northern part of the western Amazon (Marañon basin), in association with changes in Pacific SSTs and the Walker cell; whereas the frequency of dry days has increased over the central and southern part of this region (Bolivia, Perú and southern Brazilian Amazon) after 1986 due to a warming of the tropical North Atlantic and enhanced subsidence of the southern branch of the Hadley cell over the region (Espinoza et al., 2016, 2018a).

On longer time-scales, paleoclimate evidence suggests a stronger SAMS during the LIA (Apaéstegui et al., 2014; Ledru et al., 2013; Novello et al., 2016; Vuille et al., 2012; Wortham et al., 2017) in comparison to warmer epochs such as the Medieval Climate Anomaly (Rojas et al., 2016) or the current warming period (Díaz and Vera, 2018), according to GCMs simulations through the last millennium provided by PMIP3/CMIP5 (Schmidt et al., 2011, 2012). Other PMIP3/CMIP5 simulations indicate a weaker SAMS during the mid-Holocene (6k yr ago) in comparison to current conditions (Prado et al., 2013a), favouring savannah/grassland-like vegetation (Smith and Mayle, 2018) and in agreement with climate reconstructions from different proxies (Prado et al., 2013b). Furthermore, during the mid-Holocene, the SAMS appears to be weaker than that during the LGM according to climate reconstructions (Novello et al., 2017).

Isotope records from caves in the central Peruvian Andes show that the late Holocene was characterized by two periods of significant decline in SAMS intensity even when insolation is reaching a local maximum and the monsoon would be expected to intensify, which in part could be due to a reduction in the zonal SST gradient of the Pacific Ocean, favouring El Niño-like conditions (Kanner et al., 2013). However, other studies suggest increased SAMS precipitation during the Late Holocene, in association with the expansion of tropical forest (Smith and Mayle, 2018). Also, model simulations of the LGM show precipitation decline over the Amazon in comparison to present-day simulations in association with delayed monsoon onset and reduced atmospheric moisture transport from the Atlantic (Cook and Vizy, 2006).

8.3.2.4.7 Australian and Maritime Continent Monsoon (AUSMCM)

The Maritime Continent experiences the influence of both the Asian and the Australian monsoons, with rainfall peaking during boreal winter/austral summer. Seasonal asymmetries occur across the region, and land-ocean interactions and topographic forcing of rainfall play an important role (Chang et al., 2005; Robertson et al., 2011). There have been observed reductions in land rainfall and marine cloudiness over the Maritime Continent and weakening of surface moisture flux convergence in the period 1950-1999 (Tokinaga et al., 2012; Yoden et al., 2017). These trends are indicative of a slowdown of the Walker Circulation, with positive sea level pressure trends over the Maritime Continent and negative trends over the central equatorial Pacific (Tokinaga et al., 2012). However, Hassim and Timbal (2019) identify a trend of increasing annual rainfall over large areas of the Maritime Continent in the period from 1981-2014. Given the large variability in Maritime Continent rainfall on interannual time scales, the choice of time period may influence the calculated rainfall trend (e.g. Hassim and Timbal, 2019).

Rainfall data during (1951-2007) shows reductions in daily rainfall extremes over the Maritime Continent, in contrast to the rest of Southeast Asia (Villafuerte and Matsumoto, 2015). Rainfall extremes in Indonesia (from weather station data for 1983-2012) were found to increase in austral summer (Supari et al., 2018).

The Australian monsoon is characterized by the seasonal reversal of prevailing easterly winds to westerly winds and the onset of periods of active convection and heavy rainfall. The timing of monsoon onset and retreat varies over northern Australia, with the peak of the wet season occurring around December to March (Zhang and Moise, 2016).

There has been an observed increased in rainfall over northern Australia over the past 50 years, with most of the increase occurring in the north-west (Dey et al., 2018; Rotstayn and co-authors, 2007; Smith, 2004; Taschetto and England, 2009) and decreases observed in the north-east (Li et al., 2012a). Research continues to investigate the cause of the observed Australian monsoon rainfall trends, with some studies suggesting changes are due to natural climate variability and processes (e.g. Berry et al., 2011; Cai et al., 2011; Catto et al., 2012; Clark et al., 2018; Shi et al., 2008; Taschetto and England, 2009) and others finding a possible contribution from anthropogenic aerosols (e.g. Dey et al., 2018; Rotstayn et al., 2012; Rotstayn and co-authors, 2007).

Since the early 1990s the biennial monsoon transitions associated with the Tropical Biennial Oscillation (TBO) have shifted from involving the Indian–Australian summer monsoons to involving the WNP–Australian summer monsoons, and tropical Atlantic SST anomalies have become an important part of the monsoon–ocean interactions associated with the TBO (Wang and Yu, 2018).

On longer time scales, paleoclimate studies indicate that the intensity of the Australian-Maritime Continent monsoon varies in response to changes in external factors such as insolation, sea level and the intensity of the East Asian winter monsoon outflow (e.g. Ayliffe et al., 2013; Denniston et al., 2013; Griffiths et al., 2009; Mohtadi et al., 2011). Paleoclimate reconstructions and modelling indicate that the Indo-Australian monsoon may vary in or out of phase with the East Asian monsoon, depending on whether there is a meridional displacement or expansion of the tropical rainfall belt (Denniston et al., 2016).

In summary, there is *high confidence* that anthropogenic forcing has *very likely* influenced precipitation changes of the global and regional monsoons since the latter half of the 20th century. While recognizing that natural forcing of the climate system can also alter the global and regional monsoon precipitation patterns on decadal and longer scales, further work is needed to unravel the role of climate change on the monsoon water cycle.

[START FIGURE 8.23 HERE]

Figure 8.23: Placeholder for D & A of changes in the global and regional monsoon precipitation based on CMIP6

[END FIGURE 8.23 HERE]

8.3.2.5 Stationary waves

Stationary waves occur in the atmospheric circulation through interaction of major topographic features with the prevailing westerly wind circulation in mid-latitudes. There is a prominent zonal wave number two pattern (two high pressure and two low pressure centres) in the NH wintertime circulation, associated with the two main continental regions and the effects of the Rocky Mountains and Tibetan Plateau. NH planetary waves are responsible for a significant fraction of poleward energy and moisture transport in the winter and spring months.

In the SH, planetary waves are less prominent, mostly present near the Antarctic coast. In the mid-latitudes, a range of large-scale waves are present but none are truly stationary. As a result, planetary waves play a minor role in poleward energy and moisture transports in the SH.

Changing planetary wave activity is assessed as it is affected by the warming Arctic and reduced north-south temperature gradient. The AR5 did not explicitly consider planetary wave activity, but noted changes in related circulation features such as an increase in frequency and eastward shift in North Atlantic blocking anticyclones (AR5 WG1, Section 2.7.6.2). The SROCC noted recent instances of persistent amplified planetary waves in the NH mid-latitudes (SROCC, Box 3.1) but concluded that understanding of systematic effects upon planetary waves and other circulation features is still developing.

Since AR5, there has been considerable work on linkages between Arctic warming and the mid-latitude circulation. A review by Overland et al. (2015) concluded that mechanisms remain uncertain as there are many dynamical processes involved, and considerable internal variability masks any signals in the observation record. There is weak evidence that stationary wave amplitude has increased over the north Atlantic region (Overland et al., 2015), possibly as a result of weakening of the north Atlantic storm track and transfer of energy to the mean flow and stationary waves (Wang et al., 2017b). The limited amount of research on SH stationary waves suggests there may have been an eastward shift in stationary wave phase, with little change in amplitude (Wang et al., 2013b), suggesting little change in poleward moisture fluxes.

In summary, there is limited evidence and *low confidence* in strengthened stationary wave activity over the north Atlantic, associated with increased poleward moisture fluxes east of North America. There appears to be *low confidence* in and little evidence for changes in SH stationary wave activity.

8.3.2.6 Storm-tracks

Since AR5 there has been considerable progress in quantifying the uncertainties in storm-track activity using multiple reanalysis products and different methodologies. The Intercomparison of Mid-Latitude Storm Diagnostics project (Neu et al., 2013) demonstrated consistent upward trend in the total number of boreal-winter cyclones over the NH (about 3-4% per decade) during 1989-2010, implied by primarily moderately deep and shallow cyclones; while the number of deep cyclones (< 980 hPa) showed a consistent decrease (about 10-12% per decade). Trend estimates of the total number of cyclones over the NH during 1979-2010 reveal a large spread across the reanalysis products (Tilinina et al., 2013; Wang et al., 2016b)(Fig. 8.24). Grieger et al., (2018) found growing number of cyclones over sub-Antarctic region (south of 60°S) in the austral-summer during 1979-2010, while statistically significant trends were absent during the austral-winter, with winter cyclone count being twice as large compared to summer. All the reanalysis datasets demonstrated upward trends in the number of moderately deep and shallow cyclones (7 to 11% per decade for both winter and summer) with decreasing number of deep cyclones especially evident for the period 1989-2010 (Fig.8.24).

[START FIGURE 8.24 HERE]

Figure 8.24: Left - time series of (a) the total annual number of cyclones over the NH and (b),(c) the number of very deep (<960 hPa) cyclones over the North Atlantic and North Pacific, respectively. Thin lines correspond to interannual values and thick lines show 5-yr running means. Right - changes in the number of cyclones of different intensities during the 32-yr period (1979–2010) for (a) DJF and (b) JJA in different reanalyses (Tilinina et al., 2013).

[END FIGURE 8.24 HERE]

Changes in the number of deep storms over the North Atlantic and North Pacific exhibit strong seasonal differences, as well as decadal-scale variability (Chang et al., 2016; Colle et al., 2015; Matthews et al., 2016). There are considerable uncertainties with regard to changes in the Arctic cyclone activity (Koyama et al., 2017; Tilinina et al., 2013). In general, analysis of storm-track activity for longer periods suffers from uncertainties associated with changing data assimilation and observations before and during satellite era resulting in large variations across assessments of storm-track changes (Chang and Yau, 2016; Turner et al., 2013; Wang et al., 2016b). Additionally, strong inhomogeneities and discontinuities in centennial reanalysis data products affect accurate assessment of long-term signals in cyclone activity (Varino et al., 2019; Wang et al., 2013d). For selected regions additional regional constraints provide somewhat more robust centennial-scale estimates – e.g., changes in the number of low pressure systems over the Australian east coast during 1911-1960(Pepler et al., 2017).

Poleward deflection of mostly oceanic storm trajectories in NH winter during 1979-2010 was reported in both the North Atlantic and North Pacific byTilinina et al. (2013). They noted a storm-track shift by about 5-8^{o} latitude over the 32-yr period. Over the Pacific this signal was found by (Wang et al., 2017a). This large-scale tendency has regional variations. Wise and Dannenberg (2017) reported a tendency for a southward shift in the east Pacific storm-track from the 1950s to mid-1980s followed by northward deflection in the later decades. Over centennial time-scales, Gan and Wu, (2014) reported intensification of cyclone activity in the poleward and downstream regions of the North Pacific and North Atlantic upper troposphere using 20CR reanalysis. Poleward deflection of the SH storm-tracks austral-summer was revealed by Wang et al., (2016c).

Cyclone deepening, which is implicitly connected to cyclone intensity and propagation velocities, is an important cyclone life-cycle characteristic. Allen et al., (2010) noted no significant changes in the number of rapidly intensifying (deepening higher than 24 hPa per 24 hours) cyclones over the NH during 1979-2008, however they found a significant increase in the number of these systems over the SH. Tilinina et al., (2013) noted significant increases in the number of rapidly intensifying cyclone over North Atlantic during 1979-2010 based on five reanalysis datasets.

In summary, it is *more likely than unlikely* that winter cyclone activity has intensified over the NH starting from 1979 and it is *likely* that it has weakened in boreal-summer during the same period. Over the SH it is likely that cyclone activity intensified during austral-summer with no significant changes in austral-winter. There is *medium confidence* that boreal-winter storm-tracks during the last decades experienced poleward shifts over the NH oceans.

8.3.2.7 Atmospheric Blocking

Atmospheric blocking refers to persistent, quasi-stationary weather patterns characterized by a high-pressure (anticyclonic) anomaly that interrupts the westerly flow in the mid-latitudes. By redirecting the pathways of mid-latitude cyclones, blocking can affect the water cycle and lead to negative precipitation anomalies in the region of the blocking anticyclone and positive anomalies in the surrounding areas (Sousa et al., 2017). In this way, blocking can also be associated with extreme events such as heavy precipitation (Lenggenhager et al., 2018b) and drought (Schubert et al., 2014).

Currently, no consensus exists on observed trends in blocking during the recent decades. On the one hand, Horton et al. (2015) identified increasing trends in anticyclonic circulation regimes based on geopotential height fields in the mid troposphere (which might, however, be partly related to the tropospheric warming itself and thus not represent real changes in the statistics of weather) (Horton et al., 2015; Woollings et al., 2018b). Also, a weakening of the zonal wind, eddy kinetic energy and amplitude of Rossby waves in summer (Coumou et al., 2015a) as well as an increased waviness of the jet stream associated with Arctic warming (Francis and Vavrus, 2015) have been identified, which may be linked to an increase in blocking frequencies. On the other hand, it has been shown that observed trends in blocking are sensitive the choice of the blocking index, and that there is a huge natural variability that complicates the detection of forced trends (Barnes et al., 2014; Woollings et al., 2018b), compromising the robustness of observed changes in blocking.

8.3.2.8 Atmospheric rivers

Atmospheric rivers (ARs) are thin bands of intense moisture transport, which tend to be associated with warm cores of extratropical cyclones (AMS Glossary). ARs accomplish much of the moisture transport from the tropics to the mid and high latitudes (Zhu and Newell, 1998). Although ephemeral, these “rivers in the sky” transport instantaneously more water than the largest surface rivers on Earth (Ralph et al., 2004). Original studies of ARs were based on satellite-derived integrated water vapor data (IWV, e.g. Neiman et al., (2008). Modern AR definitions typically involve integrated vapour transport (IVT) – a product of vertically integrated specific humidity and wind. ARs play key roles in the hydroclimate of west coasts of extratropical continents and islands (e.g., Kingston and McMecking, 2015) as well as Polar Regions (Gorodetskaya and co-authors, 2014)(Gorodetskaya and co-authors, 2014; Komatsu et al., 2018). In California, for example, they produce roughly half of total annual precipitation (Gershunov et al. 2017). They can produce extreme orographic precipitation and flooding, particularly when strong ARs encounter topography oriented perpendicular to their IVT vectors (e.g., Ralph and Dettinger, 2011). This largely explains the regional foci of much AR research – from Greenland to Antarctica (Gorodetskaya and co-authors, 2014)(Gorodetskaya and co-authors, 2014) and mountainous west coasts in between. ARs can be both beneficial and hazardous depending on their strength (Ralph et al., 2004) and orientation relative to regional topography (Guirguis et al., 2018). Much of the literature on ARs focuses on their meteorological characteristics and predictability as well as regional hydrological impacts (Guan et al., 2018; Konrad and Dettinger, 2017). Their economic consequences are also beginning to be assessed(Corringham et al., 2018).

Limited literature exists on decadal variability and trends in ARs, mainly because the available historical data sources are too short to resolve inter-decadal timescales. The vertically resolved humidity and wind data required to compute IVT are available from reanalysis products and are mostly confined to the satellite era spanning four decades. The longest study of AR activity to date(Gershunov et al., 2017) demonstrated strong evidence of natural interannual and inter-decadal variability as well as a hint at an observed anthropogenic trend in the activity of ARs land-falling upon the North American west coast. This trend emerged in a coupled statistical analysis of Pacific SST and IVT at the North American west coast, whereby SST warming in the far-western Tropical Pacific was associated with somewhat enhanced AR-related IVT, as well as total seasonal IVT, along the west coast of Canada and United States (Fig 8.25). Importantly, spurious causes due to possible biases in the long-term reanalysis product (Kalnay et al., 1996) used by Gershunov et al., (2017), to assess AR activity were examined and eliminated, and land-falling AR activity was validated against an independent observed long-term daily precipitation data. In subsequent work (Ralph et al., 2018), spatial resolution of the available reanalyses products was shown not to be a significant issue in their portrayal of land-falling ARs. Although real, this trend is revealed only via a sophisticated coupled analysis of SST and IVT. It is not yet detectable in IVT data alone, along the North American west coast.

[START FIGURE 8.25 HERE]

Figure 8.25: Excerpts from Gershunov et al. 2017 (Panels e-h of Figure 3 (top) and e-h of Figure S10 (bottom) in). Results of directional Canonical Correlation Analysis (CCA) applied to Pacific SST and AR IVT landfalling upon the North American West Coast during January – March. Second leading canonical correlates (time series, panel a) and their associated spatial patterns expressed as correlations between the time series and their respective fields of variables: SST (b) during the January – March, JFM, season and seasonally summed AR-associated IVT (c). Correlations between the IVT time series (a, blue bars) and AR-associated precipitation (d). The bottom row shows the second leading coupled mode (e-h) of an analogous CCA applied to Pacific SST and TOTAL IVT while the bottom row shows the third leading mode (i-l). The analysis was done on AR-related vector IVT confined to the coastal zone grid cells and expressed as correlations with the entire domain of AR-related IVT, both u and v components (arrows) and magnitude (colors), while the coastal grids that comprised the analysis domain are marked with thick arrows (c, g, k). Maximum possible arrow length is sqrt(2), shown to the right of the color scale, corresponding to unit (r=1) u and v components. AR-associated JFM precipitation (PRCP) correlated with the corresponding modal IVT time series shown in panels (d, h, l). Note that PRCP data span a shorter period (1950-2013) compared to SST and IVT data (1948-2017). The least squares-fitted trends on panel (e) are significant with p-values < 0.0005.

[END FIGURE 8.25 HERE]

8.3.2.9 Modes of variability and related teleconnections

Modes of variability influence climatic variations on different time-scales and the associated teleconnections have implications for water cycle changes (WCC). Chapters 2, 3 and 4 list and assess the main modes of variability as observed, as reproduced in models in terms of anthropogenic influence and as projected in future scenarios, respectively. Here those modes of variability, plus others such as the MJO which are relevant to the WCC will be assessed in terms of their impacts on the water cycle.

8.3.2.9.1 El Nino Southern Oscillation – ENSO

ENSO affects precipitation and evaporation dynamics on the largest portion of land in both the hemispheres, while most other teleconnections have their impacts over relatively confined areas (Martens et al., 2018).

ENSO has a large control on terrestrial evaporation over Australia, southern Africa and eastern South America (Miralles et al., 2014). ENSO causes synchronous hydroclimate fluctuations (*medium confidence*) in south eastern Australia and South Africa (Gergis and Henley, 2017). Over the past 200 years concurrent dry (wet) periods in south eastern Australia, South Africa and southern South America are known to have associations with El Niño (La Niña) and the negative (positive) phases of the Southern Annular Mode (SAM) (Abram et al., 2014; Fogt et al., 2011; Gergis and Henley, 2017). The observed increasing trend of precipitation in Curitiba (Brazil) during 1889-2013 is closely linked to ENSO (mostly springtime) and to the Atlantic Multidecadal Oscillation (AMO) (mostly summertime), with impacts from other sources including the South Atlantic Convergence Zone (SACZ) and SAMS (Pedron et al., 2017). Wintertime precipitation deficits over the southern US are closely linked to La Nina episodes (Mo and Schemm, 2008; Ropelewski and Halpert, 1989; Schubert et al., 2016; Seager and Hoerling, 2014). Multi-year La Niña episodes are associated with strengthening of atmospheric circulation anomalies which zonally elongate over the North Pacific in the second winter. The associated precipitation deficits over the US remain large, while the region of reduced precipitation shifts northeastward(Okumura et al., 2017). El Niño (La Niña) summers are generally associated with below (above) average rainfall in southern Africa (Reason et al., 2000). The relationship is modulated by the Botswana High and may affect precipitation variability as well as extreme events (Driver and Reason, 2017).

El Niño affects precipitation over East Asia and favours a tripolar structure of precipitation response with positive anomalies in northeast and southeast Asia, and negative anomalies in northern/central China (Wen et al., 2018). El Nino conditions favour enhancement of summer precipitation over southeastern China through anomalous onshore moisture fluxes (Yang et al., 2018c), and rainy winters over Central Asia through transport of water vapour fluxes generated from the Indian and north Atlantic oceans by enhanced westerlies to Central Asia (Chen et al., 2018c). The influence of ENSO on the Indian summer monsoon has been known since the beginning of the 19th century (Walker, 1925). Although ENSO variance has increased since the 1980s (Cobb et al., 2013; Li et al., 2011a), the connection between the ISM and ENSO has apparently weakened during the recent decades (Kumar et al., 2006). The influence of tropical Atlantic SST on the ISM rainfall has been identified (*medium confidence*) as one of the plausible reasons for the weakening of the ENSO-ISM connection (Barimalala et al., 2012; Kucharski and Joshi, 2017; Pottapinjara et al., 2014, 2016; Yadav, 2017). The ISM exhibits significant correlation with the south equatorial Atlantic SSTs, particularly in the absence of the ENSO signal (Cash et al., 2013; Cherchi et al., 2018b; Kucharski et al., 2009). In short, interactions between the Atlantic and the Pacific Oceans have become more important to the dynamics of the tropospheric biennial oscillation (TBO) in recent decades and their influence on the Indian and West North Pacific monsoons (Wang and Yu, 2018). Precipitation variability over the region of the Middle East is also linked to ENSO. During El Niño years, moisture transport from the Red and Arabian Seas toward the Arabian Gulf is stronger and covers the entire region. On the other hand, during La Niña and neutral years, much of the transport is directed toward the northern Gulf (Sandeep and Ajayamohan, 2018).

ENSO diversity may have different effects on precipitation and streamflow (Liang et al., 2016). The dry-north and wet-south pattern in western US more likely occurred during central Pacific (CP) El Niño, while much of the western US is wet during eastern Pacific (EP) El Niño (Weng et al., 2009). Winter droughts over most parts of the US (except southwest), during post-1990s have closer links to CP El Nino rather than the EP El Nino (Yu and Zou, 2013). While ENSO conditions favor enhanced summer precipitation in southeastern China, CP El Nino events induce anomalous anticyclone and dry conditions over southeastern China and northwestern Pacific (Yang et al., 2018c).

Interannual variations in terrestrial water storage (TWS) are strongly correlated with ENSO over much of the globe, with strongest correlation found in the tropical and subtropical regions, including Amazon, Orinoco and La Plata basin(Ni et al., 2018). The connection between ENSO and TWS has been studied in specific regions, like Blue Nile river basin (Abtew et al., 2009), Colorado river basin (Hurkmans et al., 2009), Amazon (Chen et al., 2010a), Yangtze River basin (Zhang et al., 2015b). Rivers of North Patagonia have large interannual variability with the El Nino signal accounting for wet conditions, balanced by a decadal signal from the SAM (Rivera et al., 2018). Anomalous precipitation and streamflow variations in specific regions like northwestern and southern US, northeastern and southeastern South America, northeastern and southern Africa, southwestern Europe and central-south Russia have strong linkages to ENSO, with lagged streamflow responses to variations in snowmelt, soil moisture and/or cumulative hydrological processes (Lee et al., 2018b).

Anomalous warming in the central Pacific favours increased frequency of Atlantic hurricanes with higher likelihood of landfall along the Gulf of Mexico and Central America (Kim et al., 2009) The frequency of tropical cyclones (TC) over the western North Pacific is significantly higher during CP El Nino compared to EP El Nino (Chen and Tam, 2010).. Over the South China Sea, the displacement of the west Pacific subtropical high (WPSH) during the EP El Nino is favorable for typhoons to make landfall in China (Wang and Wang, 2013; Xu and Huang, 2015). Most climate models face serious challenges in capturing the differences in TC activity between different flavors of ENSO (Han et al., 2016).

Global warming can potentially slowthe tropical Walker circulation, weaken equatorial Pacific Ocean currents and increase the frequency of extreme El Niño events (Cai et al., 2015c). Additionally, enhancement of negative surface radiative forcing due to increased aerosol optical depths from forest fires over the equatorial West Pacific and Marine Continent during El Niño events can further weaken the Walker circulation through a positive feedback mechanism (Xu and Yu, 2018). While the observed Walker circulation actually strengthened during the recent two decades, fingerprinting the global-warming induced changes on WCC remains a challenging issue especially given the large uncertainties among climate models in representing ENSO characteristics and associated shifts in tropical precipitation (Cai et al., 2015c; Todd Alexander, 2018).

8.3.2.9.2 Indian Ocean Dipole (IOD)

AR5 concluded that the IOD is likely to remain active, affecting climate extreme in Australia, Indonesia and east Africa. Over Australia and east equatorial Indian Ocean the precipitation increases due to GHG and the decrease due to aerosols oppose each other(Salzmann, 2016). GHG increases result in a positive IOD-like pattern, while aerosols induce a basin-wide cooling, slowing down the effect of GHG (Dong and Zhou, 2014). A negative IOD-like SST anomaly pattern is produced only when the direct aerosol effect is considered (Dey et al., 2019). Over southeast Australia, a positive IOD contributes to drought conditions (*high confidence*) (Cai et al., 2009b; Ummenhofer et al., 2009a), increasing the fuel load into summer thus exacerbating bushfires (Cai et al., 2009a), with consequences also on yield production (Yuan and Yamagata, 2015). Over northern and eastern Australia major ENSO and IOD events affected the main river basins with increased rainfall trends during 1981-2014 (Ashok et al., 2003; Forootan et al., 2016; Gong et al., 2019; Risbey et al., 2009; Ummenhofer et al., 2009a).

Over Indonesia, positive IOD is linked with drought conditions (*high confidence*) that, if persisting for more than one season, may increase the risk of damaging forest fires (Field et al., 2009; Saji and Yamagata, 2003; Wooster et al., 2012). The combined effect of positive (negative) IOD event and a following El Nino (La Nina) is more effective in inducing significant decrease (increase) of rainfall over Indonesia (As-syakur et al., 2014; Nur'utami and Hidayat, 2016; Pan et al., 2018). Similarly, over Ganges and Brahmaputra river basins, major droughts (floods) occurred during El Nino (La Nina) and co-occurrences of El Nino (La Nina) and positive (negative) IOD (Pervez and Henebry, 2015). Over Korea, the IOD is identified as a driver for precipitation variability in September and November (Lee et al., 2019). Over equatorial East Africa IOD, independently from ENSO, affects the short rain season (*medium confidence*) exacerbating flooding and inundations (Behera et al., 2005; Conway et al., 2005; Ummenhofer et al., 2009b), with dramatic consequences for infectious disease (Hashizume et al., 2012).

The IOBW is forced by ENSO, and the literature separating the two effects is rare. Over South America, IOD and IOBW are both linked to precipitation, with the latter responsible of increased rainfall in the LPB and decreased precipitation in the northern regions of the continent. IOBW can also modulates the persistence of dry conditions over northeastern South America during austral autumn (Taschetto and Ambrizzi, 2012). Since AR5, IOD teleconnections extending farther have been identified to the Middle East (Chandran et al., 2016), to the Yangtze river (Xiao et al., 2015), where in summer and autumn positive IOD events tend to increase the precipitation in the southeastern and central part of the basin, and to the southern Africa extreme wet seasons (Hoell and Cheng, 2018).

8.3.2.9.3 Northern and Southern Annular Modes (including North Atlantic, Arctic and Antarctic Oscillations)

The linkages of NAM with weather and extreme in the northern extra-tropics are still unclear and controversial, in models and observations (Overland et al., 2016; Screen et al., 2018; Vihma, 2014). Precipitation trends in Europe are linked with the phases of the NAO (Comas-Bru and McDermott, 2014; Moore et al., 2013). Over the Mediterranean its multi-decadal variations are responsible (*low confidence*) of the drying during the last three decades (Kelley et al., 2012). Over Southern Europe and Mediterranean countries, reduction of precipitation in winter are well correlated with the NAO phase (Corona et al., 2018; Kalimeris et al., 2017). Over Portugal, the impact of NAO alone is clear since lower (higher) groundwater levels occur during years of positive (negative) NAO phases (Neves et al., 2019). Over Turkey and northern Iran, negative NAO and AO extreme phases could affect the hydrological drought stronger but in a shorter period, while positive NAO and AO phases could affect them for a longer period (Vazifehkhah and Kahya, 2018).

The NAO may affect also remote regions: over Northern China and Yangtze River valley its positive phase seems to induce more rainfall in the region through circumglobal teleconnections in the mid-latitudes (Jin and Guan, 2017). Its summer manifestation is significantly correlated with the variations of East China summer rainfall, with the thermal forcing of the Tibetan Plateau providing an intermediate bridge effect in this Eurasian teleconnection (Wang et al., 2018d). From the Southern Hemisphere, SAM in May can trigger a south Indian Ocean dipole SSTA favouring more or less precipitation over the Indian sub-continent and adjacent areas (Dou et al., 2017). In the same month, it is inversely related to the South China Sea subsequent summer monsoon (Liu et al., 2018c).

Instrumental and paleoclimate proxy records indicate the influence of SAM is modulated by regional effects (Dätwyler et al., 2018). Some key-regions where the teleconnections are mostly stationary over the instrumental period are identified over South America, Tasmania and New Zealand (Dätwyler et al., 2018). Interannual to centennial-scale rainfall anomalies and fire activity in southwest Tasmania and southern South America are significantly correlated with shifts in the southern westerly winds associated with the SAM (Fletcher et al., 2018). A positive SAM is associated with an expanded hemispheric Hadley cell over Australia during spring/summer but not in winter (Kang and Polvani, 2011; Nguyen et al., 2018b), because of the presence of the strong winter subtropical jet (Hendon et al., 2014). Other studies attributes the seasonality of the linkage to La Nina (Lim and Hendon, 2015; Nguyen et al., 2018b; Seager et al., 2003). SAM positive polarity enhances precipitation over West Antarctica, in concomitance with PSA patterns (Marshall et al., 2017). Over New Zealand large-scale SLP and zonal wind patterns associated with SAM phases modulate regional river flow (Li and McGregor, 2017).

Over South America, the positive phase of the SAM is associated with dry conditions (Holz et al., 2017) due to reduced frontal and orographic precipitation (Garreaud, 2007), and weakening of moisture convergence (Garreaud et al., 2009; Silvestri, 2003). Robust drying trend over Chile in the period 1960-2016 is consistent with the positive SAM-like changes in the southern hemisphere circulation (Boisier et al., 2018). Extended drought in Chile has clear impacts on vegetation and watersheds (Garreaud et al., 2017), the biogeochemistry of coastal water (Aguirre et al., 2018; León-Muñoz et al., 2018), and the intensity of forest fires (Urrutia-Jalabert et al., 2018). The rivers of central Patagonia show a relevant contribution from PDO and SAM toward dry conditions (Rivera et al., 2018). During the El Nino 2015-2016 the influence on the austral summer circulation anomalies over extratropical and polar regions of the Southern Hemisphere was altered by the strong SAM positive phase, with unusual regional impacts like negative precipitation anomalies in southeastern South America, ever recorded for previous strong El Nino events (Vera and Osman, 2018). SAM and its interplay with other large-scale modes of climate variability, like ENSO and the Southern Indian Ocean Dipole, are responsible of fluctuations of rainfall in Southern Africa (Nash, 2017).

The positive positive trend of AAO in summer in the last decades has been linked with the gradual decrease in water vapor over Antarctica (Oshima and Yamazaki, 2017).

8.3.2.9.4 Madden-Julian Oscillation (MJO)

The MJO produces eastward-propagating wind and precipitation anomalies on 30-60 day timescales in the tropical Indo-Pacific warm pool (Madden and Julian, 1994). It is clearly linked with enhanced rainfall in western North America, northeast Brazil, southeast Africa and Indonesia during boreal winter and central America/Mexico and south East Asia during boreal summer. It is recognized as a tropical phenomenon but with clear impacts elsewhere, and it is one of the modes of variability the current climate models have the least skill in reproducing (Christensen et al., 2013). Since AR5, studies on connections to other parts of the tropics and higher latitudes with impact on extreme weather, such as tropical cyclones and atmospheric rivers, continued (Guan et al., 2012; Maloney and Hartmann, 2000; Mundhenk et al., 2018). Over the last century as climate has warmed the strength of the MJO and number of events has increased (*medium confidence*), although substantial caveats and some conflicting evidence temper the robustness of this conclusion (Maloney et al., 2019a).

A reconstruction of the MJO for the whole 20th Century based on tropical surface pressure from a reanalysis suggests a 13% increase of MJO amplitude per century (Oliver and Thompson, 2012). A seasonal cycle in MJO amplitude trends over the last few decades has been noted with amplitude increases preferentially occurring during boreal summer (Tao et al., 2015). Certain MJO phases may have also become more frequent with possible rectification onto higher latitude temperatures through teleconnections (Yoo et al., 2011). However, the advent of satellite measurements in the 1970s has produced increasingly better reanalysis products, which might explain part of the perceived MJO activity change after the 1970s (Pohl and Matthews, 2007). One model study using unforced millennial simulations suggests that internal variability could be responsible for up to half of MJO amplitude changes during the last half of the 20th Century (Schubert et al., 2013a). Results from multi-model comparisons and other model studies indicate that changes in MJO precipitation amplitude are extremely sensitive to the pattern of SST warming (Arnold et al., 2015; Maloney and Xie, 2013; Takahashi et al., 2011). Hence, failure to account for tropical SST pattern changes makes it difficult to extrapolate the observational record of MJO activity change using Indo-Pacific warm pool SSTs alone.

The MJO has substantial influence on precipitation anomalies over South America (Alvarez et al., 2017; Paegle et al., 2000), specifically over the SACZ region (Carvalho et al., 2004; De Souza and Ambrizzi, 2006) all-year round but with less influence during austral winter. Over South America in the 30-90-day band between October and April the leading OLR patter is a dipole with centres of action in the SACZ and in the SESA. Enhanced (inhibited) convection over SESA (SACZ) occurs during MJO progression from the eastern Indian Ocean to the western Pacific (Maritime Continent sector). While enhanced (inhibited) convection over SACZ (SESA) are observed when the MJO active phase locates between the western Pacific and the western Indian Ocean (Alvarez et al., 2017). Over the Southern Hemisphere, where the tropical cyclones season coincide with the strongest MJO activity (boreal winter and spring), the MJO itself is identified as the main source of predictability for tropical storm activity (Nakazawa, 1986), and in some locations the modulation of tropical cyclone numbers is largely driven by the phase of the MJO (Maloney and Hartmann, 2000). Sub-seasonal to seasonal prediction (S2S) models display some skill to predict the MJO up to about three weeks on average (Vitart and Robertson, 2018) and improved convective parameterization in the ECMWF model physics (Vitart, 2014) helps to increase the limit of predictability up to beyond four weeks. Still S2S models do not fully exploit the predictability associated with the MJO in the northern extra-tropics, particularly over Europe (Vitart, 2017).

8.3.2.10 Wet extremes

8.3.2.10.1 Tropical cyclones

Tropical cyclones (TCs) typically cause extreme local rainfall and flooding but are also an important contributor to regional fresh water resources. There is *medium confidence* that there is a detectable signal of anthropogenic influence on global near-surface water vapour increases (Bindoff et al., 2013b), which is expected to increase TC rainfall. There is *medium confidence* that anthropogenic forcing has contributed to observed extreme rainfall events over the United States (Easterling et al., 2017) and other regions with sufficient data coverage (Bindoff et al., 2013b), and TCs contribute to these events (Kunkel et al., 2012). There has been increased frequency of TC heavy-rainfall events over the coterminous U.S. since the late 19th century that is greater than what would be expected solely from changes in U.S. landfall frequency, suggesting that TCs have become more likely to cause heavy-rainfall events (Kunkel et al., 2010). There is evidence for an anthropogenic contribution to the extreme rainfall of Hurricane Harvey (2017) (Emanuel, 2017; Risser and Wehner, 2017; Trenberth et al., 2018; Van Oldenborgh et al., 2017; Wang et al., 2018b).

Local TC rainfall totals depend on TC rain-rate and translation speed (the speed of TC movement along the storm track) with slow TCs such as Hurricane Harvey (2017) providing a clear example of the effect of slow translation speed on local rainfall accumulation. In addition to evidence that rain-rates have increased, there is evidence that TC translation speed has slowed globally (Kossin, 2018) and may be linked to anthropogenic forcing (Gutmann et al., 2018). This evidence is limited however, and *confidence* is presently *low* that there is a detectable change in TC translation speed (Knutson et al., 2019; Kossin, 2019; Lanzante et al., 2018; Moon et al., 2019). In general, despite growing evidence that measures of TC rainfall indicate increases, confidence remains *low* that a global anthropogenically forced trend in TC precipitation has been detected (Knutson et al., 2019), due, in part, to limitations in the data records (e.g., Lau and Zhou, 2012).

There is observational evidence (Rosenfeld et al., 2011, 2012; Zhao et al., 2018a), supported by simulations (Khain et al., 2010; Qu et al., 2017; Wang et al., 2014), that ingestion of aerosols into tropical cyclones can invigorate the peripheral rain bands and increase the overall area and precipitation of the storm. This occurs on expense of the air converging to the eyewall, thus may decreasing the storm's maximum wind speed by up to one class in the Saffir-Simpson scale.

From direct observations there is a poleward migration of tropical cyclones lifetime maximum intensity for the period from 1981 to 2016 in the NH of 0.1° latitude decade^{-1} and in the SH of 0.45° latitude decade^{-1} in hemispheric averages (Studholme and Gulev, 2018).

8.3.2.10.2 Extratropical storms

SREX asserted that “it is *likely* that there has been a poleward shift in the main NH and SH extratropical storm-tracks during the last 50 years” (Seneviratne et al., 2012) although they assigned*low confidence* to these changes “due to inconsistencies between studies or lack of long-term data in some parts of the world (particularly in the SH)”. Inconsistencies within reanalyses remain as most current reanalyses products were already available at the time of SREX and AR5 (except for the ERA20C reanalysis). The major source of inconsistencies when performing trend analysis in extratropical cyclones (ETC) characteristics derived using reanalyse is related with changes in the type and/or amount of observed data assimilated by the reanalysis systems (Chang and Yau, 2016; Tilinina et al., 2013; Wang et al., 2016b). Wang et al. (2016) showed that differences in the number and intensity of ETCs among reanalyses are much larger before 1979 when satellite data starts to be assimilated mostly over the SH. They also show a significant and consistent increase in the total number of strong ETCs over both hemispheres. Chang and Yau (2016) compared MSLP trends in the two century-long reanalyses (ERA20C and 20CR) and concluded that trends in Pacific and Atlantic basin wide storm track activity prior to the 1950s are unlikely to be reliable due to changes in the density of surface observations. Krueger et al. (2013) also showed inconsistencies between the variability and long-term trends as estimated using the 20CR reanalysis and century-long pressure observations over a densely monitored marine area in the North Atlantic.Over the NH, Wang et al. (2016) reported that most reanalyses agree on an increase in the density of ETCs including the most strong ETCs although reanalyses showed little agreement about their intensity changes after 1979. During the boreal summer, however, Chang et al. (2016) showed a weakening of the ETC activity and a decrease in the number of strong ETCs over the whole

NH and over North America based on ERA-Interim and other reanalysis datasets.

Over the SH, Wang et al. (2016) reported non-significant trends in the density of ETCs after 1979 although most reanalyses agree on a positive trend of the density of deeper cyclones both over land and over the ocean. Overall trends in the number of ETCs might not be a useful quantity as seasonal and spatial variation has been shown to be important. Specifically, the most robust change in the SH storm-tracks has been observed during austral summer and is related with the poleward shift in the storm-tracks. The summer shift has been found in several atmospheric fields including the number of ETCs (Grise et al., 2014) and the associated frontal activity (Solman and Orlanski, 2014, 2016).

The representation of ETCs is resolution-dependent in both climate models and reanalyses and any changes must be assessed with caution (Chapter 3). In particular, CMIP5 models show a systematic underestimation of the intensity of ETCs (Zappa et al., 2013), a feature that is partially related with their relatively coarse resolution but also possibly with other deficiencies such as an excess of dissipation (Chang et al., 2013). The best representation of ETCs and their intensity on the North Atlantic are provided by CMIP5 models with relatively high horizontal resolution (Zappa et al., 2013). Using a single high-resolution climate model, Hawcroft et al. (2016) showed that the simulated precipitation associated with ETCs was on average well simulated but the models produced too much precipitation when considering the strongest ECTs compared to observed estimations.

The summertime observed poleward shift of the SH storm-tracks appears to be driven by both increases of greenhouse gases and ozone depletion although mainly dominated by the later (Gerber and Son, 2014; Gonzalez et al., 2014; Grise et al., 2014; Lee and Feldstein, 2013; Orlanski, 2013). Orlanski (2013) used reanalysis and model simulations to show that the positive trend in equatorial near-surface temperature associated with increasing GHGs and the negative trend in near-150-hPa temperature at high latitudes of the SH associated with stratospheric ozone depletion both contributed to recent circulation changes in the SH. Based on CMIP3, CMIP5 and the CCMVal2 multi-model ensembles, Gerber and Son (2014) estimated that about 75% of the total shift in the austral summer SH storm-tracks was associated with ozone depletion.

Confidence in most past changes in the frequency and intensity of ETC is *low* due to inhomogeneities in the data and inconsistencies between studies. *Medium confidence* might be associated.

8.3.2.11 Aridity and Drought

AR5 concluded that "there is low confidence in attributing changes in drought over global land areas since the mid-20th century to human influence owing to observational uncertainties and difficulties in distinguishing decadal-scale variability in drought from long-term trends" (Bindoff et al., 2013b). The science of detection and attribution has progressed considerably since then, especially in the area of extreme event attribution (Easterling et al., 2016; Stott et al., 2016; Trenberth et al., 2015). Attribution efforts have further benefited from the increased use of paleoclimate information (either from empirical reconstructions or simulations), which provides an important constraint on natural variability that is insufficiently sampled in the relatively short observational record (Cook et al., 2018; Kageyama et al., 2018). With these advancements, there is now medium to high confidence in attribution of recent drought trends and events to a human influence for many (but not all) regions.

At the global scale, a human influence on precipitation has been detected in changes to the annual cycle(Marvel et al., 2017) and inter-annual variability (Tapiador et al., 2016) (*high confidence*). Attributing regional precipitation trends to climate change, however, remains difficult due to the noisy nature of precipitation variability and the typically lower quality of available precipitation records. In the Mediterranean, previous work (Hoerling et al., 2012) demonstrating a strong and significant role for anthropogenic climate change in twentieth-century precipitation declines has been largely reaffirmed. Climate change has significantly increased meteorological drought risk in the Mediterranean (Gudmundsson and Seneviratne, 2016), and contributed directly to some of the worst recent drought events in the region. (Kelley et al., 2015) concluded that climate change caused a three-fold increase in the likelihood of the

2007—2010 meteorological drought in the eastern Mediterranean that preceded the ongoing Syrian conflict. Paleoclimate evidence additionally indicates that this period of drought was likely the driest of the last 900 years (Cook et al., 2016a).

In all, these studies indicate *high confidence* in a human influence on precipitation changes in the Mediterranean, a signal that is also beginning to emerge in other Mediterranean-climate regions (*medium confidence*). This includes the West Cape region of South Africa, where human influences increased the likelihood of the 2015—2017 drought by a factor of three (Otto et al., 2018), and southwest and southern Australia, where precipitation declines have been largely attributed to anthropogenic changes in greenhouse gases and ozone (Delworth and Zeng, 2014). For most other regions, however, precipitation deficits during recent droughts are largely indistinguishable from natural variability (*low confidence*). This includes events in California (Berg and Hall, 2015; Seager et al., 2015), the southwestern United States (Lehner et al., 2018), Central Europe (Hauser et al., 2017), South America (Martins et al., 2018), and Africa (Philip et al., 2018; Uhe et al., 2018). Over Eastern Africa droughts have become longer and more intense in recent decades, continuing across rainy seasons (Hoell et al., 2017a; Nicholson, 2017), and this trend appears to be unusual in the context of the last 1500 years (Tierney et al., 2015). This may be a signature of anthropogenic forcing (*low confidence*) but cannot as yet be distinguished from natural variability (Hoell et al., 2017a; Philip et al., 2018). Over central equatorial Africa long-term drought may result from tropical Indo-Pacific SST variations associated with the enhanced and westward extended tropical Walker circulation (Hua et al., 2018). Over India, the intensity and areal extent of monsoon droughts have significantly risen during the post-1950s (Niranjan Kumar et al., 2013). This enhanced propensity of monsoon droughts has been attributed to the declining trend of monsoon rains in response to the combined influence of anthropogenic aerosol forcing, land-use changes and rapid warming of the equatorial Indian Ocean SST (Krishnan et al., 2016).

Over western North America, snow water equivalent has declined by 15-20% since the mid-twentieth century (Mote et al., 2018; Pierce et al., 2008). The decline is directly attributable to anthropogenic warming (Mote et al., 2018) (*high confidence*) and represents a volume of water comparable to the largest surface reservoir in the western US (Lake Mead) (Mote et al., 2018). Anthropogenic warming also contributed to recent snow droughts in the Pacific Northwest and California (*high confidence*). Spring snow water equivalent across the Sierra Nevada Mountains reached a record low in surface and satellite observations in 2015 (Margulis et al., 2016; Mote et al., 2016) and was possibly the lowest of the last five hundred years in a tree-ring based paleoclimate reconstruction (Belmecheri et al., 2016). Over the longer California drought (2011-2015) anthropogenic warming alone reduced the overall snowpack levels in the Sierras by 25% (Berg and Hall, 2017). The Pacific Northwest also experienced an intense snow drought in 2015, despite near-normal levels of total cold season precipitation (Marlier et al., 2017; Mote et al., 2016). As with California, anthropogenic warming contributed significantly to the exceptionally low snowpack in this region (Mote et al., 2016). Changes in atmospheric circulation, combined with increased greenhouse gases have combined to cause a steep hydroclimate trends within the context of the last several centuries (Lehner et al., 2017b, 2018; Williams et al., 2015).

Anthropogenic warming is also amplifying surface (soil moisture and runoff) droughts in western North America and elsewhere by increasing evaporative demand and losses to the atmosphere (*medium confidence*) (Cook et al., 2014; Griffin and Anchukaitis, 2014; Hessl et al., 2018; Overpeck, 2013; Weiss et al., 2009). Confidence in these cases is somewhat muted compared to other drought indicators (e.g., the impact of warming on snow) because few long-term soil moisture and runoff datasets are available and there are also substantial extant uncertainties in important underlying processes (e.g., vegetation responses to changes in climate and atmospheric carbon dioxide concentrations). For the California drought in 2012-2014, (Williams et al., 2015) concluded that anthropogenic warming accounted for 8-27% of the resulting soil moisture deficit. This was supported by (Griffin and Anchukaitis, 2014), who used paleoclimate reconstructions to demonstrate that soil moisture anomalies during this drought were the driest of the last 1200 years and also substantially more severe than would have been predicted from precipitation alone. (Robeson, 2015) used extreme value analysis to estimate the California drought was a 1-in-10,000 year event. Evidence for human signals in evapotranspiration and drought is also found for the Colorado River Basin. The most recent drought in the basin (2000-2012) had streamflow deficits similar in magnitude to two mid-twentieth century droughts (1950-1956, 1959-1969) (Woodhouse et al., 2016). Precipitation was much higher (near normal) during the most recent drought compared to the earlier events, suggesting that higher temperatures associated with long-term warming trends are responsible for most of the drying (Woodhouse et al., 2016). This most recent event is part of a long-term decline in streamflow across the Colorado River Basin, with up to 30-50% of this multi-decadal decline attributed to anthropogenic warming impacts on snow and evapotranspiration (McCabe et al., 2017; Udall and Overpeck, 2017; Xiao et al., 2018). (Hessl et al., 2018) also found evidence that higher temperatures exacerbated drought conditions in central Asia in the early 21st century.

[START BOX 8.1 HERE]

BOX 8.1: Example of water cycle change (Capetown, Central Chile, Jordan river – drying of Mediterranean climates (Ch2?), Sahel drought & recovery, Mexico City (aerosol pollution, land use)

[END BOX 8.1 HERE]

8.4 What are the projected water cycle changes?

We consider water cycle projections from different perspectives: changes on each of the components of the water cycle in section 4.1; and global-scale and regional phenomena in section (including seasonality, variability, and extremes in section 4.2. This assessment is still mainly based on CMIP5 models and may need major updates after the FOD.

8.4.1 Projected water cycle changes

Most projected water cycle changes are not expected to be uniform in space and are superimposed on substantial day-to-day and year-to-year natural fluctuations in weather and climate. Regional projections are therefore challenging. However a number of physically understood responses operating at larger scales (see Section 2) are important in guiding decision making that anticipates, prepares for, and responds to water cycle changes.

8.4.1.1 Global water cycle intensity

There are a range of interpretations for global water cycle "intensity," from definitions based on precipitation increases per degree of warming , to broader joint considerations of water vapour and its transport, precipitation and evaporation rates (e.g., Durack et al., 2012b)

In AR5, globally-averaged precipitation was projected to increase with temperature increases, with *virtual certainty* (AR5 12ES, 12.4.1.1). Surface evaporation change was projected to be positive over most of the ocean and to generally follow the pattern of precipitation change over land (AR5 12ES, 12.4.5.4). Note that there are expected to be large spatial differences (AR5 12.4.5.2) and so the global mean will not be representative of all areas; indeed, some areas may be expected to experience substantial depletion of water and water movement, and some stores of water may disappear entirely (AR5 FAQ 12.2). Research since AR5 has reinforced these conclusions.

[START FIGURE 8.26 HERE]

Figure 8.26: AR5 Fig. 11.13 CMIP5 multi-model projections of changes in annual and zonal mean (a) precipitation (%) and (b) precipitation minus evaporation (mm day^{-1}) for the period 2016–2035 relative to 1986–2005 under RCP4.5. The light blue denotes the 5 to 95% range, the dark blue the 17 to 83% range of model spread. The grey indicates the 1s range of natural variability derived from the pre-industrial control runs. **Need an updated AR6 version of this figure.**

[END FIGURE 8.26 HERE]

[Assuming CMIP6 looks as expected]. Based on this body of evidence, global water cycle intensity considered in terms of global mean precipitation and evaporation increases is *virtually certain* to increase. Water cycle intensity increase in terms of evaporation over the oceans is *very likely* and, in terms of water vapour transport, is *likely*. As in AR5, we emphasize that changes in the water cycle over land (Samset et al., 2017) and for individual regions may be very different from the global mean, thereby suggesting that global water cycle intensity is not necessarily a policy-relevant metric.

8.4.1.2 Atmospheric moisture

The atmosphere is the smallest global water reservoir in the climate system with a mean residence time of about a week. As such and given the constant relative humidity hypothesis discussed in section 8.2 and verified in section 8.3, water vapour changes arguably exhibit the most striking response to global warming (cf. Chapter 4). The current generation of global climate models project a steady increase in global mean column integrated water vapour (*high confidence*) which is consistent with the Clausius-Clapeyron relationship (Held and Soden, 2006) where every degree Celsius of warming is associated with a 6-7% increase in near-surface atmospheric water content. Since precipitable water is dominated by water vapour which is a primary GHG in the atmosphere, such an increase sustains a positive feedback on anthropogenic global warming (*high confidence*) although this is determined primarily by mid to upper tropospheric water vapour changes (Soden et al., 2005). In contrast, the response of water condensates (cloud) is much more spatially heterogeneous, microphysically complex, and model-dependent so that the projected cloud feedbacks remain a key uncertainty for constraining climate sensitivity (cf. Chapter 7).

Climate models project a contrasting response of near-surface relative humidity, with a slight and possibly overestimated increase over the oceans (*medium confidence*) versus a robust and substantial decrease over land (*high confidence*) (Fig. 8.27; (Byrne and O'Gorman, 2016; Zhang et al., 2018). . This is expected from the larger warming over land than ocean combined with responses and feedbacks involving vegetation (Section 2). Regional changes in near-surface humidity over land are dominated by thermodynamic processes and are primarily controlled by the non-homogeneous warming of sea surface temperature (Chadwick et al., 2016), amplified by land-atmosphere feedbacks such as soil moisture and plant stomatal changes (see section 8.2.1.2) (Berg et al., 2016). Global climate models tend to warm (and dry) more near the land surface in future projections where evapotranspiration is more soil-moisture limited in the present-day climate (Berg and Sheffield, 2018).

[START FIGURE 8.27 HERE]

Figure 8.27: Changes in surface-air relative humidity from (Byrne and O'Gorman, 2016). To be updated or duplicated with CMIP6 model outputs when available. [To be updated or duplicated with CMIP6 model outputs when available. Could be also (rather) shown in subsection 4.2 or 4.3]

[END FIGURE 8.27 HERE]

8.4.1.3 Precipitation

8.4.1.3.1 Global and regional precipitation

Global mean precipitation shows a systematic increase in climate projections (Fig. 8.28) of X+-X %/K across models and scenario (*effective hydrological sensitivity*)[TO BE COMPLETED WITH CMIP6]. There is a relatively robust pattern of global precipitation response across different GHG forcing scenarios and across the twenty-first century (Tebaldi and Arblaster, 2014). Responses are well understood based on energy budget constraints that include rapid adjustments to each radiative forcing agent (8.2.1.1). The CMIP5 multi-model mean projections can be effectively reconstructed using simple models that represent the temperature-dependent response (hydrological sensitivity) and the more rapid adjustments to radiative forcings(Thorpe and Andrews, 2014), as discussed in section 8.2. Contrasting regional and seasonal responses are explained by regional thermodynamic drivers relating to increased water vapour transport and substantial shifts in atmospheric circulation. Such circulation changes reconcile the relatively large water vapour increases with the smaller global precipitation increase with warming that lead to a slowdown in tropical circulation (Section 8.2.1).

[START FIGURE 8.28 HERE]

Figure 8.28: Hydrological sensitivity in CMIP5 from (Fläschner et al., 2016).

[END FIGURE 8.28 HERE]

Both theory (Held and Soden, 2006a) and models (Vecchi et al., 2006) suggest a slowdown of the tropical circulation and an increasing lifetime of water molecules in the tropical atmosphere, as precipitation frequency is not projected to increase at the global scale (Trenberth, 2011). An implication is that the distribution of precipitation intensities will experiene change significantly (Trenberth et al., 2003; Trenberth, 2011), with fewer but potentially stronger events (*high confidence,* cf. section 4.3.3). The projected increase in precipitable water is expected to lead to an increase in the highest possible precipitation intensities and in the frequency of extreme precipitation events, regardless of how annual mean precipitation may change (O'Gorman, 2015; O'Gorman and Schneider, 2009). An increase in the number of dry days is also projected in several regions of the world, which can dominate the annual precipitation change at least in the subtropics ((Polade e atl., 2014). Most climate models however simulate too frequent and too light precipitation events (Section 8.5), resulting in a water recycling that is too large (Trenberth, 2011). Improving the spatio-temporal distribution of precipitation intensities in global climate models is therefore needed to reduce uncertainties in the projected water cycle changes.

In a high emissions scenario, about half the tropical circulation slowdown and a large fraction of the regional precipitation change projected by the end of the twenty-first century has been attributed to this effect (Bony et al., 2013). Despite uncertainty in the location of future rainfall shifts, climate models consistently project that large rainfall changes will occur for a considerable proportion of tropical land during the twenty-first century (Chadwick et al., 2016b).

Despite this, a robust shortening of the rainy season is projected for tropical Africa and northeast Brazil. For example, West Africa is projected to experience a rainy season shortening of about 7 days with 1.5°C warming (Fahad et al., 2018). A delay in the wet season over West Africa and the Sahel (Lee and Wang, 2014)by 5-10 days under RCP8.5 is attributed to a strengthening of the Sahara heat low (Dunning et al., 2018). Outside the tropics, fast atmospheric adjustment drives a poleward shift of the mid-latitude storm tracks and precipitation maxima (Ceppi et al., 2018).

RCPs anticipate a decrease in anthropogenic aerosol emissions, by as much as 80% by 2100 (Moss et al., 2010). As discussed in Section 8.3.3.1, aerosols decrease global mean precipitation, and have likely offset the expected increase due to GHGs. Thus, future decreases in aerosols would help unmask GHG effects, leading to further intensification of the water cycle (Richardson et al., 2018a; Rotstayn et al., 2013; Salzmann, 2016; Samset et al., 2018; Westervelt et al., 2018; Wu et al., 2013) A drier Mediterranean region is expected due to the effect of increasing well-mixed GHGs in the atmosphere, but the pace of change in global BC emission may largely modify the drying rate in the short term (Tang et al., 2018).

Using the fast and slow precipitation response framework, Richardson et al., (2018) used a simple model to emulate global land (and sea) precipitation responses. During the 20th century, the effect of rising surface temperature on land-mean precipitation has largely been masked by sulphate (and volcanic) aerosol. However, as sulphate forcing declines through the 21st century, and GHG concentrations and global mean surface temperatures continue to rise, land-mean precipitation will increase more rapidly. On this basis, precipitation changes are *likely* to become clearly observable by middle of the century.

Other modelling studies also show that future aerosol reductions will lead to an increase global mean precipitation, particularly in East and South Asia (Levy et al., 2013b)(Dwyer & O'Gorman, 2017; Westerveltet al., 2015). Westervelt et al. (2018) explored SO_2 and carbonaceous aerosol emission reductions within six world regions and found that global and regional precipitation generally increases, particularly in response to European and US SO_2 reductions. The increase in precipitation due to aerosol reductions may even be comparable to that due to continued, moderate GHGs increases (Rotstayn et al., 2013). CMIP5 models with a larger aerosol forcing project larger increases in future precipitation as aerosol loading decrease, suggesting that uncertainty in future precipitation projections is related to uncertainty in aerosol ERF.

Considering annual means, the interannual variability of precipitation increases in CMIP5 projections over the majority of land areas, except for some small regions. In April-September, variability is largely dominated by an increase, except over areas of the Northern Hemisphere high latitudes and some areas around major mountain systems. During October to March, variability increase is more widespread, but areas of decreased variability are more extended over northern Eurasia, northern North America and some equatorial African regions (Giorgi et al., 2018; Pendergrass, 2018; Sanderson et al., 2017).

8.4.1.3.2 Seasonality

In AR5 (12.4.5.2), there was *high confidence* in long-term projections of increased seasonality of precipitation. Increases in seasonality are expected from the wet-get-wetter in response to warming (wet seasons get wetter). When wetter seasons have larger increases in precipitation than drier seasons, then the magnitude of their difference increases. Work since AR5 has continued to reinforce increases in projected seasonality of precipitation in many regions, quantified by the concentration of precipitation over the annual cycle and the number of dry months (Pascale et al., 2016). Confidence remains *high* in increasing seasonality of precipitation.

The Mediterranean climate with dry summers and wet winters is projected to shift northward and eastward in CMIP5 climate scenarios with the equatorward margins replaced by arid climate type (Alessandri et al., 2015a). These changes appear less robust over California in winter: the CMIP5 disagreement in the projections over the region reflects a precarious balance between the subtropical highs expanding from the south and the Aleutian low extending southeastward(Choi et al., 2016; Polade et al., 2017).

Over southwestern Australia, decreases in future winter, spring and annual rainfall are projected with *high confidence:* by 2030, winter rainfall may change by −15 to + 5%, and by 2090, these ranges are around -30 to − 5% under RCP4.5 and − 45 to − 5% under RCP8.5 (Hope et al., 2015). Despite these projected decreases, the intensity of heavy rainfall events across southwestern Australia is likely to increase (Hallett et al., 2018) and forecast changes in the temporal pattern of storms will intensify runoff profiles (Min et al., 2011; Wasko and Sharma, 2015). Very large fluctuations in summer rainfall intensity are projected (Andrys et al., 2017) reflecting a progressive southward shift of winter storm systems (Hope et al., 2015), with potentially dramatic consequences in estuarine hydrology (Hallett et al., 2018).

Central Asia is projected to experience warmer and wetter winters at both 1.5° and 2°C warming, likely associated with an increase in snow depth in the northeastern regions (Li et al., 2019).

[Further discussion of other regions could be guided by key changes in CMIP6 map.]

[START FIGURE 8.29 HERE]

Figure 8.29: Rate of change of moisture mean and variability with temperature from (Pendergrass et al., 2017). To be updated with CMIP6 model outputs (using another colour) when available.

[END FIGURE 8.29 HERE]

8.4.1.3.3 Precipitation types: convective, non-convective and snowfall

AR5 did not address the decomposition of precipitation into convective and non-convective components which are expected to respond differently to climate change (8.2.2.1.2). Since AR5, studies have begun to document a shift from large-scale toward convective precipitation in model projections. there is a fundamental discrepancy between convective precipitation in high-resolution observations (Houze, 1997) and precipitation produced by convective parameterizations in climate models. In models, convective precipitation depends on model resolution nd is generally not well-resolved. However, evidence from theory and idealized model simulations has been accumulating to reinforce climate model projections of increasing convective precipitation. In particular, CAPE (closely related to the available energy for formation of convective systems) is projected to increase with warming (Romps, 2016; Seeley and Romps, 2015)s. Regionally, most documentation has focused on the US (Diffenbaugh et al., 2013). Changes in convective precipitation and associated severe weather would be impactful. Confidence in these projections is *moderate*.

Many regions of the world rely on snowfall for water resources. AR5 (12.4.5.2/12.4.6.2) identified that snowfall would increase in Northern Hemisphere high latitude cold regions due to an increase in total precipitation amount, and decrease in warmer regions due to a decreased number of freezing days. The fraction of precipitation falling as snow and the duration of snow cover were projected to decrease. Since AR5, it has been theorized that heavy snow events are strongest around freezing, and so warming would result in an increase in the intensity of extreme snowfall events for regions where snowfall occurs significantly below 0^{o}C while decreases in heavy snow events are likely in milder regions (O’Gorman, 2014). There are only a small number of studies evaluating the implications of this mechanism in specific regions. A study for the northeastern US indicates smaller reductions for major snowfall events against the broader decline in snowfall expected from thermodynamic effects (Zarzycki, 2018). Another shows that Arctic snowfall is projected to decrease as rainfall makes up more of the precipitation (Bintanja and Andry, 2017). Confidence in a projected shift from snowfall toward rainfall is *high*, though the impacts for specific regions are uncertain and need further documentation.

8.4.1.4 Land surface evapotranspiration

In AR5, annual surface evapotranspiration was projected to change over land following a similar pattern to precipitation as global mean temperatures rises. Since AR5, there is a growing body of evidence that projected changes in precipitation are not necessarily the main driver of the long-term evolution of evapotranspiration and freshwater resources over land (Laîné et al, 2014; Pan et al., 2015; Ukkola et al., 2016). At the global scale, the projected increase in potential evapotranspiration is a major constraint on actual evapotranspiration. At the regional scale, growing water demand due to both the direct (increasing water withdrawals and consumption) and, mostly, indirect (increasing atmospheric water demand due to climate change) human influence may also represent a major threat for water availability.

Atmospheric water demand is usually defined as the evapotranspiration rate from a well-watered land surface, referred to as potential evapotranspiration (PET), and computed from climate or meteorological data using empirical equations (Scheff and Frierson, 2014). PET is therefore a supply-independent measure of the evaporative demand and cannot be easily measured given the fundamental coupling of the land-atmosphere system. Looking at a high-emissions scenario in a set of CMIP5 models, (Scheff and Frierson, 2014) found a robust increase in global mean PET over land (*high confidence*), which is dominated by the direct effect of constant-relative humidity warming (5-6% per °Cof local warming during the warm season where the evaporative demand is the strongest), but can be further enhanced by the projected decrease in near-surface relative humidity (Byrne and O'Gorman, 2016).

Not surprisingly, the same generation of global climate models project an increase (*medium confidence*) in the actual annual and global mean evapotranspiration (ET) over land (Laîné et al., 2014). Over most of the tropical, subtropical and mid-latitude regions, the direct contribution from surface temperature increase and the related decrease in near surface relative humidity are found to dominate this projected increase. Regional changes in ET are not only governed by changes in precipitation, but are also influenced by changes in soil moisture and vegetation, which modulate the direct effects of increased surface air temperature and of generally reduced surface air relative humidity over land.

Moreover, the usual perspective of hydrological changes dominated by precipitation and PET has been challenged by a number of studies suggesting a strong CO_2 effect on the vegetation physiology (Lemordant et al., 2018; Milly and Dunne, 2016). Plant transpiration accounts for a large fraction of total land evapotranspiration, and is expected to decrease in response to rising CO_2 concentrations through a stomatal regulation.

There is however only *low confidence* in the global importance of this biophysical effect given the variety of species, the opposite effects of the associated increase in canopy temperature and of CO_2 fertilization, the possible long term adjustment of the vegetation physiology to enhanced CO_2 conditions, and, the simple parameterizations accounting for these complex physiological processes in global climate models (Franks et al., 2017). The important role of the CO_2 physiological effect on the projected evapotranspiration has been emphasized in an idealized climate change experiment where the gradual CO_2 increase (1% per year) is seen by the atmosphere and/or the vegetation physiology (Lemordant et al., 2018). There is increasing observational evidence supporting the relevance of the stomatal closure effect and an increase in the vegetation water use efficiency (WUE) at the continental scale (Huang et al., 2015).

While this recent increase seems to be underestimated by state-of-the-art climate models (Peters et al., 2018b), the long-term vegetation response (including mortality) is still not clear, as well as the magnitude of its effect on the projected global evapotranspiration given the potential counteracting influence of enhanced vegetation density at least over recent decades (Alessandri et al., 2015; Zeng, Peng, & Piao, 2018; Zhang et al., 2015).

In summary, there are still substantial uncertainties in the projected response of land surface ET, both at the global and regional scales. While ET is projected to decrease by the end of the 21st century in most areas where annual mean precipitation is also projected to decrease (*medium confidence*), precipitation has not been the only driver of recent ET changes and so may the case across the 21st century given the projected increase in PET, the direct human influence on the land surface water budget (see section 8.2.2.2.5) and the complex and model-dependent vegetation response to global warming and enhanced atmospheric CO_2 concentration (see section 8.2.2.2.3).

[START FIGURE 8.30 HERE]

Figure 8.30: CMIP6 global map of change in ET.

[END FIGURE 8.30 HERE]

8.4.1.5 Surface runoff and streamflow

The AR5 showed that average annual runoff is projected to increase at high latitudes and in the wet tropics, and to decrease in most dry subtropical regions. For some regions there is very considerable uncertainty in the magnitude and direction of change. Both the patterns of change and the uncertainty are largely driven by projected changes in precipitation, particularly across south Asia (Jiménez Cisneros et al., 2014). Based on multiple GCMs, fractional change in projected runoff per fractional change of projected precipitation of 194 large river basins generally ranges between 1.0 and 3.0 (mostly between 1.4 and 2.6) (Jiménez Cisneros et al., 2014). It is uncertain how vegetation responses to future increases in CO_2 and climate change will modulate the impacts of climate change on runoff (Gerten etal., 2014). The response is found to somewhat non-linear (Zhang et al.,, 2018) and partly disconnected from changes in surface aridity possibly due to a stronger runoff sensitivity to changes in precipitation than in evapotranspiration (Yang et al., 2018).

New evidence shows that global-scale mean annual runoff increases with mean global temperature rise (Zhang et al., 2018; Zhang and Tang, 2014), but is highly heterogeneous regionally (Chen et al., 2017; Yang et al., 2017). For example it increases in most parts of the northern high latitudes and Asia, but also in eastern Africa, and decreases in the Mediterranean region, southern Africa, Australia and in parts of western Africa, as well as in Central and South America (Greve et al., 2018).The 90th percentile of the multi-model output indicates an increase of runoff with global warming everywhere, while the 10th percentile indicates a decrease everywhere except in the Arctic (Greve et al., 2018).

Mean annual streamflow changes more strongly as global warming increases, mostly over the very high northern latitudes as well as the Mediterranean, India and the Congo basins (Döll et al., 2018). Projected changes in the phase of high-latitude or high-altitude precipitation (Lutz et al., 2014) as well as a partial thawing of the boreal permafrost (Alkama et al., 2013) could also contribute to increase global runoff without any substantial change in annual mean precipitation and evapotranspiration (*medium confidence*). Increased streamflow variability is projected in some parts of the globe (Betts et al., 2018)(Döll et al., 2018). For a 4°C global warming, half of the land area is projected to be exposed to increased high flows (average increase 25%), while about 60% may be exposed to decreased low flows (average decrease 50%). Average changes are only half as large as those associated with a 2°C global warming (Asadieh and Krakauer, 2017).

Some regions may first experience an increase of high extremes before the drying trend under further global warming results in decreased extreme high flows. According to an ensemble study with 21 combinations of global climate and global hydrological models, the global land area that is annually affected by floods that occurred with return period of 100 years under pre-industrial condition is projected to be 1.5, 2 and almost 3 times as large as under current conditions in case of a 2 °C, 3 C and 4 °C global warming (Lange et al. 2019 ;submitted).

[START FIGURE 8.31 HERE]

Figure 8.31: Relative changes in global mean runoff from (Zhang et al., 2018e). To be updated or duplicated with CMIP6 model outputs when available. Also add relative changes in precipitation and evapotranspiration? [**T**o be updated or duplicated with CMIP6 model outputs when available. Also add relative changes in precipitation and evapotranspiration? (Hervé)]

[END FIGURE 8.31 HERE]

8.4.1.6 Soil moisture

Global projections of soil moisture (SM) are the result of highly uncertain (section 8.5) and contrasting changes in the various components of the land surface water budget. The main AR5 outcome was that "regional to global-scale projected decreases in SM are *likely* in presently dry regions and are projected with *medium confidence* by the end of the 21st century". Prominent areas of decreasing SM included the Mediterranean, southwest USA and southern African regions, in line with projected surface warming (thermodynamic effect) and changes in Hadley Circulation (dynamic effect). Post-AR5 studies strengthen this key finding and further document regional changes in SM and related feedbacks.

The focus here is on long-term drying rather than on drought events (cf. section 8.4.2.6 and Chapter 11) which represent transient departures from the local climatological SM. As expected from the expansion of the Hadley circulation and the decrease in land surface relative humidity (cf. section 8.2), the AR5 conclusion about a widespread projected decrease in annual mean SM was further supported by recent studies (Berg et al., 2017b; Cook et al., 2018). Such a drying is more pronounced for low-mitigation scenarios and is projected not only in semi-arid areas but also over a large fraction of the European continent (Ruosteenoja et al., 2018). In contrast, even the sign of future SM changes remains model-dependent over the northern midlatitudes (Douville and Plazzotta, 2017) or West Africa (Berg et al., 2017a) in summer.

Focusing on the multi-model ensemble mean (Fig. 8.33), the geographical pattern of SM change reveals (…) [update with CMIP6] decreasing SM in the subtropics and semi-arid areas (*high confidence*), and enhanced seasonality in most tropical and mid-latitude regions (*medium confidence*). Soil moisture in the top soil layer shows a more widespread drying than total SM (Cook et al., 2018). This is related to a greater sensitivity of the upper soil layer to increasing evaporative demand, the buffering effect of contrasting seasonal precipitation anomalies (Berg et al., 2017b) and less responsive groundwater systems (Cuthbert et al., 2019) on deep SM, and the physiological CO_2 effect on plant transpiration (Betts et al., 2007). The latter effect is represented by poorly constrained stomatal conductance parametrizations in most climate models (Franks et al., 2017). Land surface processes represent a major source of modelling uncertainty and there is only *medium confidence* in the projected total SM change.

Over the Tibetan Plateau, a persistently decreasing soil moisture trend is projected in CMIP5, associated mostly with projected increasing potential evapotranspiration. Such drying may lead to potential water deficiency for Asian rivers, (Zhang et al., 2019b).

Narrowing such uncertainties remains a priority not only for impact studies but also for constraining regional climate change. SM represents a key land surface feedback which has been explored in dedicated atmosphere-only experiments (Seneviratne et al., 2013). Strong and consistent effects have been found in both hemispheres on temperature (drier is warmer, *high confidence*) and precipitation (positive feedback, low confidence), although the sign of the soil moisture-precipitation feedback is both model- (Berg et al., 2017a) and scale-dependent (Taylor et al., 2013a). The SM feedback also plays a key role in shaping the future distribution of daily maximum temperatures and related changes in hot extremes (Douville et al., 2016; Seneviratne et al., 2013; Vogel et al., 2017) (*high confidence*). Such results will need to be revisited by dedicated experiments based on the new-generation Earth System Models (Van Den Hurk et al., 2016), possibly including an improved dynamics of plant-available water compared to the CMIP5 generation (e.g., Huang et al., 2016).

[START FIGURE 8.32 HERE]

Figure 8.32: CMIP6 global map of change in soil moisture.

[END FIGURE 8.32 HERE]

8.4.1.7 Freshwater reservoirs

8.4.1.7.1 Glaciers

Mountain glaciers are sensitive indicators of global climate change and have been retreating worldwide, with significant contributions to SLR, and a potential threat to water supplies. However, projections of glacier mass losses involve large uncertainties because of such things as widely differing spatial scales, limitations of surface mass balance glaciation models, effects of complex terrain characteristics and local climate.

According to the Hindu Kush Himalaya Assessment report (Wester et al., 2019), two thirds of glaciers in the Himalayas, the world's "Third Pole", that feed 10 of the world's most important river systems and are critical water sources for nearly two billion people, could melt by 2100 if global emissions are not sharply reduced. Even if the goal of limiting global warming to 1.5ºC is achieved, one third of the glaciers would disappear by 2100.

(Huss and Hock, 2018) computed global glacier runoff and glacier-volume changes for 56 large-scale glacierized drainage basins selected from North and South America, Europe and Asia. Based on three RCP emission scenarios and 14 GCMs, between 2010 and 2100 the total glacier volume in all the investigated basins wasprojected to decrease by 43 ± 14% (RCP2.6), 58 ± 13% (RCP4.5) and 74 ± 11% (RCP8.5). They found the maximum or 'peak water' has already been reached in 45% of the basins (in 2017), and thereafter the annual runoff was expected to decline. In the remaining basins, the modelled annual glacier runoff continued to rise until a maximum is reached, which tends to occur later in basins with larger glaciers and higher ice-cover fractions. By 2100 one-third of them may experience runoff decreases greater than 10% due to glacier mass loss in at least one month of the melt season, with the largest reductions in central Asia and the Andes.

Such results are supported by Radić et al. (2014) who found a reduction incurrent global glacier volume by 29-41% depending on scenario, with glaciers in the North American and Russian Arctic, and those peripheral to the major ice sheets as the largest contributors. Moreover, (Clark et al., 2015) reported that by 2100, the volume of glacier ice in western Canada could shrink by 70 ± 10% relative to 2005. Few glaciers would remain in Interior and Rockies regions, but maritime glaciers in northwestern British Columbia will remain in a diminished state.

Over the past decade, ice loss from the Greenland Ice Sheet (GIS) increased due to both increased surface melting and the acceleration of ice flow and subsequent thinning of fast-flowing marine terminating outlet glaciers (Nick et al., 2013).

8.4.1.7.2 Wetlands and lakes

8.4.1.7.3 Groundwater (vimal and taylor)

Assessments of the projected impacts of water cycle changes on groundwater commonly rely on the application of climate projections to hydrological models. At local scales, differences in climate projections, algorithms to compute evapotranspiration, and model structures typically hinder comparative analyse (Todd et al., 2010). At global scales, groundwater is inadequately represented in Land-Surface Models (LSMs) that are embedded in GCMs and ESMs. Estimates of groundwater recharge derived from these global-scale models remain largely untested due to an absence of accessible observational records. GRACE satellite measurements of changes in total water storage (ΔTWS) provide a potential criterion to test output from global-scale models; evidence from a global-scale comparison of ΔTWS estimated by GLDAS LSMs (Rodell et al., 2004) and GRACE indicates that LSMs systematically underestimate water storage changes (Scanlon et al., 2018).

Global-scale analyses of groundwater recharge under climate change reported in IPCC AR5 revealed that substantial changes are projected in dryland environments such as the Sahel, Middle East and northern China (P. Döll and Fiedler, 2008; Portmann et al., 2013) projected to reduce renewable groundwater resources significantly in most dry subtropical regions. Recent research challenges this conclusion as it shows: (1) focused recharge (section 3.1.7.4) is often the dominant pathway in dryland environments but is largely excluded from consideration in global-scale models; and (2) recharge in sub-tropical drylands depends disproportionately on heavy rainfall events associated with large-scale controls on climate variability (e.g. El Niño, La Niña) that are inadequately represented in climate projections (Cuthbert et al., 2019; Kolusu et al., 2019).

Recent, regional-scale analyses of the impact of water cycle changes on groundwater recharge (e.g. (Meixner et al., 2016a; Shrestha et al., 2018; Tillman et al., 2017) reveal a series of consistent outcomes: (1) changing seasonality in recharge with increases during wet, winter periods and declines during dry summer periods; and (2) changing spatial distribution in recharge with rises in more humid regions and declines in more arid locations; these trends were generally amplified under a higher greenhouse-gas emission trajectory (i.e. Representative Concentration Pathway 8.5 versus 4.5). Uncertainty in projections of groundwater under climate change were found to be substantially influenced by conceptual and numerical models employed to estimate recharge ((Hartmann et al., 2017; Meixner et al., 2016b). Current research on estimating water cycles change on groundwater is thus focused on improved numerical representation of groundwater systems as a precursor to improved projections of these impacts (Bierkens et al., 2015; Doll et al., 2016).

Changing groundwater storage will be affected by the expansion of irrigated area, which directly affects groundwater abstraction. Irrigation demand will generate more recharge from surface water irrigation depending upon the emission scenarios and precipitation changes. However, groundwater recharge may not always rise as increases in evapotranspiration will offset the water surplus. Using econometric models, Zaveri et al. (2016) reported an increase in irrigated area in the dry season (±50% uncertainty) than the wet season (±15% uncertainty) by 2050. They found that projected increases in precipitation may not reduce water stress due to the expansion of irrigated areas in India. Therefore, the projected increase in precipitation alone cannot ensure increase in groundwater storage under a warming climate, as more unsustainable groundwater will be abstracted to meet the needs of the growing population. (Crosbie et al., 2013)reported a reduction in groundwater recharge in parts of Australia under a warming climate. Wada and Bierkens (2014) estimated abstraction of non-renewable groundwater to be 450 $km^3\ yr^{-1}$ by 2050, which may be an underestimation as the rise in irrigated area was not considered in their analysis, and argue that an improvement in irrigation efficiency may compensate the future increase in irrigated water.

8.4.2 Projected changes in large scale phenomena and regional variability

Here, we begin with changes at the largest scales, from the tropical overturning circulations and monsoons (8.4.2.1); the extra-tropics (8.4.2.3); to modes of variability and teleconnections (8.4.2.3), and wet extremes and their impacts on the water cycle (8.4.2.5).

8.4.2.1 Tropical overturning circulation (including ITCZ and subtropics)

8.4.2.1.1 ITCZ and tropical belts

Future projections show no consistent movement of the zonal mean ITCZ (Byrne et al., 2018; Donohoe et al., 2013; Donohoe and Voigt, 2017). ITCZ position is strongly connected to cross- equatorial energy transport (Bischoff and Schneider, 2014; Kang et al., 2008), which also shows no consistent change in future projections (Donohoe et al., 2013). The zonal mean ITCZ is projected to narrow in future (Byrne and Schneider, 2016; Su et al., 2017), but the total area of tropical ascent is not projected to change (Chadwick et al., 2013; Muller and O'Gorman, 2011)(Johnson and Xie, 2010).

Regional shifts in tropical convergence zones are much larger than their zonal mean, dominate regional changes in precipitation (Chadwick et al., 2013; Muller and O'Gorman, 2011; Seager et al., 2010), and are often very uncertain across models (Kent et al, 2015; Oueslati et al., 2016). Over the tropical oceans, rain-band shifts are strongly coupled to SST pattern change (Xie et al., 2010; Huang et al, 2013), whereas over tropical land influences include remote SST increases (Giannini, 2010), the direct CO_2 effect (Biasutti, 2013a) and the plant physiological effect (Chadwick et al., 2017; Kooperman et al., 2018).Future warming pattern responses to greenhouse gas forcing indicate a regional northward ITCZ shift and increased Sahel precipitation (Dong and Sutton, 2015) with later wet season cessation over northern Africa (Dunning et al., 2018).

As known at the time of AR5, the tropical circulation is consistently projected to weaken (Byrne et al., 2018; Vecchi and Soden, 2007), in line with theoretical expectations (8.2.1.3). A weakening is required to reconcile thermodynamic increases in low level water vapour (6-7%/K) with smaller increases in precipitation (1-3%/K) that are influenced by rapid adjustments to radiative forcings as well as slow responses to warming (Bony et al., 2013; Chadwick et al., 2013; Ma et al., 2018a) . Since AR5, additional drivers of weakening have been identified, including increased depth of convection under warming (O'Gorman and Singh, 2013), SST warming patterns (He and Soden, 2015a) and the direct CO_2 radiative effect (Bony et al., 2013; Merlis, 2015) . However Allen and Ajoku (2016) show that 21st century aerosol reductions will reinforce GHG-induced poleward expansion of the NH tropical belt through this century.

CMIP3 and CMIP5 coupled models project unambiguous intensification of the subtropical highs in both hemispheres because of enhanced diabatic heating over the continents and cooling over the oceans, favouring a stronger near-surface anticyclonic circulation (Li et al, 2012), together with a positive feedback with the marine boundary layer clouds mostly over the southern Atlantic and Pacific subtropical oceans (Li et al., 2013). Subtropical highs over the North Pacific, South Atlantic, and southern Indian Ocean are projected to weaken, while those over North Atlantic and South Pacific are projected to intensify, though there is uncertainty for the latter (He and Soden, 2017). Compensating signals from direct carbon dioxide radiative forcing effects and sea surface temperature increases resulting from the radiative forcings and ensuing feedbacks modulate the climate change response. Coupled ocean-atmosphere processes, low frequency variability, sensitivity to climate forcing as well as inter-relationships among different climate phenomena and their variability are mostly responsible of deficiencies in the representation of the subtropical highs, as evidenced from multi-model comparisons (Cherchi et al., 2018a).

8.4.2.1.2 Hadley Circulation

Models project a stronger and more consistent weakening of the northern hemisphere winter Hadley cell than the southern hemisphere winter cell (Seo et al., 2014). The weakening is related to the meridional temperature gradient, static stability, and tropopause height (D'Agostino et al., 2017; Seo et al., 2014). SST pattern change acts to reduce the magnitude of Hadley cell weakening (Gastineau et al., 2009; Ma et al., 2012). There is considerable zonal structure in Hadley circulation strength changes, associated with cloud-circulation interactions (Su et al., 2014). The expansion of the Hadley cell and northeastward shift of the northern hemisphere storm tracks are associated with distinct drying in the southern semi-arid part of the Mediterranean and slight wetting tendencies in the northern wet part in 21st century projections (Barcikowska et al., 2018).

A consistent poleward expansion of the edges of the Hadley cells is projected (Kang and Lu, 2012), particularly in the southern hemisphere, which appears to be consistent with observed trends (Grise et al., 2019). The main driver of future expansion appears to be greenhouse gas forcing (Grise et al., 2019), with uncertainty in magnitude due to internal variability (Kang et al., 2013). Explanations include increased dry static stability (Lu et al., 2007 ; Frierson et al., 2007), increased tropopause height (Chen and Held, 2007; Chen et al., 2008), stratospheric influences (Kidston et al., 2015) and radiative effects of clouds and water vapour (Shaw and Voigt, 2016). Hadley cell expansion could be associated with the decreases in precipitation projected in many subtropical regions (Shaw and Voigt, 2016), but more recent work suggests that these reductions are mainly due to the direct radiative effect of CO_2 forcing (He and Soden, 2015b), land-sea contrasts in the response to forcing (Shaw and Voigt, 2016) and SST pattern change (Sniderman et al., 2019). The response would be expected to drive the Mediterranean climate, characterized by dry summers and wet winters, towards more arid conditions (Alessandri et al., 2015b), although is complicated over California by a precarious balance between the subtropical high expanding from the south and the Aleutian low extending southeastward(Choi et al., 2016a; Polade et al., 2017) .

8.4.2.2 Walker circulation

The Walker circulation is projected to weaken more consistently and profoundly than the Hadley circulation (Vecchi and Soden, 2007)and to shift eastwards in the Pacific (Bayr et al., 2014). The fundamental weakening can be explained as a result of heating from dry static stability increasing faster than net atmospheric radiative cooling (Knutson and Manabe, 1995; Ma et al., 2012), while the greater magnitude of weakening compared to the Hadley circulation is associated with a reduction of zonal SST gradients (Gastineau et al., 2009; Ma and Xie, 2013), and changing land-sea temperature contrasts (Zhang & Li, 2017). However, it is uncertain whether projected changes in equatorial SST gradients are consistent with observed trends (Coats and Karnauskas, 2017), and one CMIP5 model that projects a strengthened future Walker circulation may be more consistent with observations than other models (Kohyama et al., 2017). Rain-band shifts in model projections are more pronounced in the zonal than the meridional direction (Wills et al., 2016a), associated with changes in the Walker circulation.

[START FIGURE 8.33 HERE]

Figure 8.33: CMIP5 multi-model ensemble average percent change in (a) annual mean precipitation; (b) precipitation intensity during precipitating days. Stippling indicates areas where at least 70% of the models agree on the sign of the change.[Fig. 3 from (Polade et al., 2014)]

[END FIGURE 8.33 HERE]

8.4.2.3 Monsoons (including onset and breaks)

A projected intensification of global monsoons was explained in AR5 by thermodynamic increases in moisture convergence that is reduced by weakening tropical circulation (8.2.1.3). Since AR5, CMIP3 and CMIP5 agree in projecting intensification of global monsoon precipitation in the 21st century, as well as an increase of its area and intensity, while the monsoon circulation weakens (Kitoh et al., 2013). Global monsoon precipitation is projected to increase by less than 10% for RCP4.5 and more than 15% for RCP8.5 (Hsu et al., 2013; Kitoh et al., 2013), with eastern and northern hemisphere monsoons producing more precipitation than the western and southern hemisphere ones (Lee and Wang, 2014). Enhanced moisture convergence and evaporation are the main contributors to the increase in global monsoon precipitation (Hsu et al., 2013; Kitoh et al., 2013).

Global monsoon area is projected to increase by 3-6% from the late 20th century to the end of the 21st century under RCP4.5 and by about 9% under RCP8.5 for CMIP5 models (Hsu et al., 2013; Kitoh et al., 2013)(Lee and Wang, 2014). For intermediate scenarios the simulated monsoon domain tends to increase over oceanic monsoon regions, with apparently no change over land except for a westward movement over the Asian continent (Lee and Wang, 2014). Under RCP8.5 the monsoon domain is projected to expand mainly over the central-to-eastern Tropical Pacific, thesouthern Indian Ocean and eastern Asia (Kitoh et al., 2013). The expansion of the global monsoon domain in future projections may be attributed to both an increased annual range of precipitation under global warming ((Chou and Lan, 2012) and a stronger summer-to-annual rainfall ratio (Hsu et al., 2012; Lee and Wang, 2014). Global warming may induce a wetter summer over the GM regions, and enhance the contrast between rainy and dry seasons, especially in the southern hemisphere (Hsu, 2016)(Chou et al., 2013a; Liu and Allan, 2013c).

Precipitation extremes in all regional monsoons are projected to increase at a much greater rate than the global monsoon precipitation (Kitoh et al., 2013), with indices of extreme dry events projected to increase within the global monsoon area (Turner and Annamalai, 2012). Although the frequency of precipitation events would decrease in a future warmer climate, the precipitation intensity of individual events could be greater (Kitoh et al., 2013). CMIP5 models project that monsoon retreat dates will delay, while onset dates will either advance or show no change, resulting in lengthening of the monsoon season (Kitoh et al., 2013). Year-to-year standard deviation of global monsoon precipitation is projected to intensify, suggesting that more extreme monsoon years may occur in the future (Turner and Annamalai, 2012). [To be updated with

CMIP6 results]

[START FIGURE 8.34 HERE]

Figure 8.34: Fig3 and Fig 10 from (Kitoh et al., 2013)

[END FIGURE 8.34 HERE]

8.4.2.3.1 North American Monsoon (NAM)

Analysis of CMIP5 models suggested little change in the overall amount of warm season North American monsoon (NAM) precipitation in response to rising greenhouse gases, but a shift in the timing of peak monsoon rain from June-July to September-October (Cook et al., 2013). However, CMIP5 models were generally too coarse resolution to simulate the Gulf of California and the moisture surges associated with the NAM system (Pascale et al., 2017). Higher resolution modelling experiments with bias or flux corrections have much better representation of NAM dynamics, but yield varied responses, with predictions of a weaker monsoon system (Pascale et al., 2017) and stronger monsoon system depending Pascale et al., (2017) and stronger monsoon system (Meyer and Jin, 2017) depending on the model used. The number of gulf surge events appears unchanged under a doubling of CO_2, although daily surge-related precipitation events are still predicted to increase. Given inter-model disagreement, there is *low confidence* in projections of North American Monsoon activity.

8.4.2.3.2 West African Monsoon System

The AR5 suggested a small delay in the West African monsoon with intensification late in the season. Later wet seasons with more intense rainfall have been confirmed more recently and attributed to intensification of the Sahara heat low (Dunning et al., 2018). CMIP3 and CMIP5 models agree in projecting overall a wetter West African monsoon (WAM) (Biasutti, 2013b), with a statistically significant increase (decrease) of rainfall in central-eastern (western) Sahel (Akinsanola and Zhou, 2018)). Projected changes in the annual cycle are indicative of a longer monsoon season (Akinsanola and Zhou, 2018; John et al., 2014). A higher-precipitation future outcome for the WAM is sensitive to the convection parameterization used (Hill et al., 2017), but is consistent with past understanding of the role of external forcing (Chang and Yau, 2016).

Precipitation over Eastern Equatorial Africa is projected to increase because moisture convergence over the adjacent Congo Basin and Maritime Continent centres of convection weakens, thus weakening near-surface winds that consequently increase moisture advection from the Congo basin centre toward the east African margin (Giannini et al., 2018). This projection is not consistent with the recent decreasing trend observed (Hoell et al., 2017) which could be explained by internal variability. Uncertainty in projected seasonal mean East Africa short rains is primarily due to uncertainties in the regional response to SST warming and a small direct CO_2 impact, while for East Africa long rains the uncertain atmospheric response to SST pattern change is less important, and some key regional uncertainties are primarily located beyond Africa (Rowell and Chadwick, 2018). More rainfall in the short rains relating to a later end and an earlier end to the long rains are projected when accounting for the onset and cessation dates.

Southern Africa is characterized by a local summer wet season, a pronounced rainfall gradient from the dry southwest to the humid north and northeast, and a peak wet season rainfall maximum extending from the continent into the adjacent southwest Indian Ocean (Lazenby et al., 2016). In austral spring and summer, CMIP5 precipitation projections show a wetting/drying dipole across the continent and Indian Ocean (Lazenby et al., 2018). Over land, the drying in spring is larger than in summer, thus delaying the onset of the wet season over southern Africa (Lazenby et al., 2018). CMIP5 projections of rainfall to 2050 over South Africa mostly agree on slight decreasing trends, except for the eastern coastal plain, the slope in past observations is close to the models projections, when averaged over most of South Africa (Knight and Rogerson, 2019). Projections over southern Africa for the 21st century show less seasonal rainfall, characterized regionally by a later onset and/or a shorter wet season with an earlier end to the wet season (Dunning et al., 2018). A later monsoon onset is projected with *high confidence* in the Sahel in few studies using CMIP5 and regional models and a late cessation with *medium confidence* suggesting a shift in the annual cycle as a regional manifestation of a global response (Biasutti, 2013a).

8.4.2.3.3 Southern Asia (SAS)

Over the Asian monsoon domain, projected changes in extreme precipitation indices are larger than over other monsoon domains, indicating the strong sensitivity of Asian monsoon to global warming (Cherchi et al., 2011; Kitoh et al., 2013).

A significantly slower rate of increase of precipitation as compared to the rate of increase of moisture content in response to global warming can weaken the large-scale tropical and monsoon circulations due to increased dry static-stability of the atmosphere (Douville et al., 2012b; Held and Soden, 2006a; Krishnan et al., 2013; Sugi and Yoshimura, 2004; Vecchi and Soden, 2007). Future projections of the South Asian monsoon towards the end of the 21st century, based on a very high resolution (grid size ~ 20 km) global climate model, indicate that a slowdown of the summer monsoon Hadley overturning circulation and the associated cross-equatorial monsoon winds can weaken the orographically forced ascent of moist winds over the narrow Western Ghats (WG) escarpment along the west coast of India leading to a possible decrease of orographic precipitation over the WG (Krishnan et al., 2013; Rajendran et al.,, 2012).While CMIP5 models mostly indicate likely increases in South Asian monsoon precipitation in the future, one high-resolution model projection indicates a likely decrease of monsoon precipitation during the 21st century following the RCP4.5 scenario(Krishnan et al., 2016).

Over South Asia the moisture-bearing monsoon low level jet is projected to shift northward (Sandeep and Ajayamohan, 2015). High resolution models projections indicate that the genesis distribution of monsoon low pressure systems weakens and shifts poleward, implying an increased frequency of extreme precipitation events over northern India (Sandeep et al., 2018). CMIP5 models project increased short intense active days and decreased long active days with no significant change in the number of break spells for India (Sudeepkumar et al, 2018).

8.4.2.3.4 East Asian Summer (EAS)

Interhemispheric mass exchange acts as a bridge connecting Southern Hemisphere circulation with the East Asian Summer Monsoon (EASM) rainfall. Its decrease as projected in CMIP5 RCP8.5 scenarios implies that EASM will be less affected by the Southern Hemisphere circulation in a future warmer climate (Yu et al., 2018). Multi-model ensemble pattern regression analysis applied to CMIP5 projections indicate that the EASM will weaken with decreased precipitation over the Meiyu belt and increased precipitation over the high latitudes of East Asia and central China. The changes in early summer are attributed to a southward retreat of the western North Pacific subtropical high and a southward shift of the East Asian subtropical jet.

8.4.2.3.5 South America Monsoon System (SAMS)

The South American monsoon system (SAMS) is projected to be wetter and longer in a warmer world (Jones and Carvalho, 2013), but with diminished early season precipitation and enhanced late season precipitation (de Carvalho and Cavalcanti, 2016).

8.4.2.3.6 Australian-Maritime Continent (AUSMC) jo brown

Current generation global climate models have limited ability to capture the spatial and temporal features of the Maritime Continent monsoon due to their coarse resolution (e.g. Jourdain et al., 2013). Based on CMIP5 simulations, most of the Maritime Continent has projected increases in boreal winter (DJF) rainfall (Siew et al., 2014), with greater increases and higher model agreement over land [see Figure 8.35]. In boreal summer (JJA), the northern and eastern part of the Maritime Continent has projected increases in rainfall, while there are projected decreases over Java, Sulawesi and southern parts of Borneo and Sumatra [see Figure 8.35]. [Expand and update for CMIP6]

Projections of future changes in mean Australian monsoon rainfall based on CMIP5 [and CMIP6?] models are uncertain; with some models projecting increases and others projecting decreases for the range of emissions scenarios. Models which perform better in simulating present day regional climate project little change or an increase in Australian monsoon rainfall (Brown et al., 2016; Jourdain et al., 2013). Rainfall changes are correlated with the extent of warming in the western tropical Pacific (Brown et al., 2016) and decomposition of projected rainfall changes indicates that the largest source of model uncertainty is due to shifts in the spatial pattern of convection (Brown et al., 2016; Chadwick et al., 2013).

The role of anthropogenic aerosol forcing in future projections of the Australian monsoon has been investigated for CMIP5 models (Dey et al., 2019);. Decreases in anthropogenic aerosol concentrations over the 21st century are expected to produce relatively greater warming in the Northern Hemisphere than Southern Hemisphere, favouring a northward shift of tropical precipitation (e.g. (Rotstayn et al., 2015).

Projected changes in rainfall variability and extremes for the Australian monsoon are more robust. Rainfall variability in the Australian monsoon domain increases on time scales from daily to decadal in CMIP5 models (Josephine et al.,, 2017), indicating either more intense wet days or more dry days or both. There is also a projected increase in the intensity of extreme rainfall but a reduction in the frequency of heavy rainfall days for the Australian monsoon (Dey et al., 2019). This is consistent with Smith et al. (submitted), who found an increase in Australian monsoon active phase or "burst" rainfall intensity but reduction in the number of burst days and events.

Changes in the onset and duration of the Australian monsoon have also been identified in model projections. (Zhang et al., 2013) examined changes in Australian monsoon onset and duration in CMIP3 models and found model agreement over a delay in onset and shortened duration to the north of Australia, but less agreement over the interior of the continent. An updated study of CMIP5 models found similar mean changes with delayed onset and shortened duration, but substantial model disagreement (Zhang et al., 2016). [Update for CMIP6].

[START FIGURE 8.35 HERE]

Figure 8.35: Fig 5 from (Kitoh et al., 2013) – probably better for a box dedicated to Monsoons ("How will monsoons change in a changing climate?" or something similar)

[END FIGURE 8.35 HERE]

8.4.2.4 Extratropics (including stationary waves, stormtracks and blocking)

8.4.2.4.1 Stationary waves

Both idealized modelling (Wills and Schneider, 2016) and analysis of CMIP5 model output (Wills et al., 2016a) suggest that the stationary wave response to warmer can regionally outweigh the general expectation of wet-gets-wetter, dry-gets-drier. However, there do appear to be characteristic biases in model representations of intermediate-scale stationary waves (Simpson et al., 2016) and modelled stationary wave responses are known to be sensitive to the parameterization of orographic drag (Pithan et al., 2016; van Niekerk et al., 2017), so the stationary wave projections must be viewed with some caution.

8.4.2.4.2 Storm-tracks

In the AR5, the SH storm track was deemed *likely* to shift poleward, the North Pacific storm track *more likely than not* to shift poleward, and the North Atlantic storm track *unlikely* to have a simple poleward shift.

There was *low confidence* in regional storm track changes and the associated surface climate impacts, although a weakening of the Mediterranean storm track was a robust response of the models. Although thermodynamic effects were considered to be the most important factor in overall projections of increased mid-latitude precipitation, the general poleward shift and increased intensity in storm tracks may play a role. [Have to also update this when chapter 4 text is available, to make sure it is consistent.]

In AR5, several factors were identified as relevant to the uncertainty of the projections, including horizontal resolution, resolution of the stratosphere, and how changes in the Atlantic meridional overturning circulation (AMOC) were simulated. Some important competing factors were also identified. Increased moisture availability may increase the maximum intensity of individual storms while reducing the overall frequency as poleward energy transport becomes more efficient. Contrasting temperature trends in the upper and lower troposphere have opposing influences on storm track shifts. Coupling with the large-scale circulation and the remote influence of tropical SSTs are important to the storm tracks, and influence individual model projections.

Since AR5, these themes have been further examined, largely reinforcing the initial assessments.

The role of temperature trends in influencing storm tracks has been further explored, both in terms of upper tropospheric tropical warming (Zappa and Shepherd 2017) and lower tropospheric Arctic amplification (Wang et al., 2017), including the direct role of Arctic sea ice loss (G. et al., 2018), and the competition between the influences(Shaw et al., 2016). [May need to link to cross-chapter box on Arctic Amplification.] The remote and local SST influence has been further examined by (Ciasto et al., 2016), who further confirmed sensitivity of the storm tracks to the SST trends generated by the models and suggested that the primary greenhouse gas influence on storm track changes was indirect, acting through the greenhouse gas influence on SSTs. The importance of the stratospheric polar vortex in storm track changes has received more attention (Zappa and Shepherd, 2017) and the anticipated recovery of the ozone layer further complicates the role of the stratosphere(Shaw et al., 2016). Atmospheric rivers, which are associated with extratropical cyclones, have been the focus of considerable research, especially with regards to extreme precipitation; this is discussed in section 8.4.2.6.4.

In terms of projections, the decreases in cyclone occurrence over the Mediterranean was robust in a higher resolution model (Raible et al., 2018).

A review of model realization of extratropical cyclones concluded that important biases remain in cyclone locations, intensities, cloud features, and precipitation (Catto, 2016). While front frequency is well represented, frontal precipitation frequency is too high and the intensity is too low(Catto et al., 2015). Some of the bias in storm tracks appears to be related to limitations in model realization of blocking (Zappa et al. 2014).

Simulation of storm tracks and their associated precipitation generally improve with increasing resolution beyond that used in most current climate models (Barcikowska et al., 2018; Jung et al., 2006; Michaelis et al., 2017), and higher resolution results in more sensitivity to warming (Willison et al.,, 2015).

The projected changes in storm tracks and the associated mechanisms have several important implications for water cycle projections. Where the storm tracks are robustly projected to shift (Southern Hemisphere, North Pacific) or weaken (Mediterranean), understanding the physical causes of the related changes in precipitation helps increase confidence in the projections. Understanding the competing influences provides context for why other regions don’t exhibit a consistent signal and cautions against regional projections based on individual models. However, model bias and the need for relatively high resolution to reproduce the relevant dynamics is an important overall limit on confidence in current projections. While the projected changes in storm tracks have implications for the water cycle beyond precipitation, these have not yet been explicitly examined.

8.4.2.4.3 Blocking

Simulated future changes in blocking are regionally variable, but for most regions a decrease in blocking frequencies is projected (Masato et al., 2013; Matsueda and Endo, 2017; Parsons et al., 2016; Woollings et al., 2018a). However, the magnitude and sign of these projected changes depend on the choice of the blocking index and vary among models. Furthermore, the robustness of the projected changes is compromised by the fact that most climate model have (mostly negative) biases in the representation of blocking for present-day conditions, although there are some improvements in more recent model versions (Davini and D'Andrea, 2016), and that no complete theory is available of blocking dynamics and its sensitivity to external forcing (Woollings et al., 2018a). For instance, the increase of latent heat release in clouds in a warming climate may have systematic effects on blocking (Pfahl et al., 2015), which have not yet been systematically explored.

Nevertheless, future changes in blocking occurrence may have important consequences for the hydrological cycle, in a similar manner as future changes in stationary waves (Simpson et al., 2016; Wills et al., 2016b): zonal shifts of the stationary troughs and ridges lead to accompanying shifts in E-P patterns, since excess precipitation typically occurs on the western flank of anticyclonic anomalies, where poleward moisture fluxes prevail.

8.4.2.5 Modes of variability and related teleconnections

In AR5, the primary relevance of climate modes for the water cycle was through ENSO, which was assessed with *high confidence* to remain the dominant mode of interannual variability, with an increased influence on rainfall variability due to changes in moisture availability. There was *medium confidence* that ENSO teleconnections would shift eastward over the North Pacific and North America. (AR5 14.4.4). For the NAO, its internal variability is sufficiently large that it was considered *very likely* to differ between individual climate model projections. The positive SAM trend was considered *likely* to weaken with ozone recovery. For the both the NAO and SAM there was *medium confidence* that projected changes were sensitive to poorly-represented boundary processes. There was *low confidence* in the projections of other modes. (14.5.3)

Since AR5, research has continued on ENSO and the other modes of variability. Changes in ENSO teleconnections under global warming may be expected in case of changes in the mean state of the tropical Pacific, but also elsewhere, and in case of changes in ENSO properties (Cai et al., 2015a; Dommenget and Yu, 2017). A warmer world may intensify the nonlinear tropical precipitation response to ENSO events, thus adding more complexity to its teleconnections (Power et al., 2013). CMIP3 and CMIP5 models strongly disagree on future changes in ENSO properties (Cai et al., 2015b; Collins et al., 2010; Ham and Kug, 2016; Meehl et al., 2007; Zheng et al., 2016), but weakly agree in projecting faster warming in the eastern tropical Pacific rather than in the western tropical Pacific (Yeh et al., 2018). This change suggested the possibility of "El Nino-like" conditions in the tropical Pacific mean state (Vecchi & Soden, 2007; Cherchi 2008) . The most likely response is an amplification and eastern shift of the ENSO influence on precipitation (Bonfils et al., 2015; Müller and Roeckner, 2008; Power et al., 2013).

Under RCP8.5, the frequency of ENSO events is likely to increase, mostly in the second half of the century (Cai et al., 2014, 2015b). CMIP5 models that are realistic in reproducing ISM rainfall reveal a strengthening ISM-ENSO relationship in RCP8.5 projections, though the response is not robust for different flavours of ENSO (Roy et al., 2019). However, ENSO variability is sufficiently large that more than 30 simulations of the same model are necessary to robustly estimate it, and attribution of anthropogenic forcing to ENSO changes in the near future will likely not be possible (Maher et al., 2018). In CESM-LE, to detect a significant change in ENSO amplitude under future warming, a relatively large number (~15) of ensemble members is needed to suppress interference of internal variability (Zheng et al., 2018). While ENSO-rainfall teleconnections are well established, the link with flood hazard is found to be more complex when combining reanalyses with global hydrological models (Emerton et al., 2017).

An analysis of seven models showed increases in the boreal winter NAO, consistent with higher precipitation in northern Europe and lower precipitation in southern Europe in the RCP8.5 scenario (Tsanis and Tapoglou, 2019). CMIP3 models projected a strengthening NAM/NAO in winter, while CMIP5 projections show considerable inter-model differences (Cattiaux and Cassou, 2013). Large-ensembles analyses show how the NAO imparts substantial uncertainty to future changes in regional climate over coming decades, more than 85% for increased precipitation over northern Europe and western Russia as well as over most of eastern North America. Similar results are found for drying over northwestern Africa and regions adjacent to the Mediterranean Sea (Deser et al., 2017).

Future changes in the PDO and its teleconnections to the water cycle are very uncertain, as studies have come to opposite conclusions: that the PDO and its teleconnections will strengthen (Fuentes-Franco et al., 2016) and that they will weaken (Xu and Hu, 2018).

In austral summer, rainfall over the Southern Hemisphere subtropics is projected to increase because of a robust positive trend projected for the SAM (Lim et al., 2016).

A positive IOD in boreal fall is linked with precipitation reductions (increases) over eastern Indian Ocean and Australia (eastern Africa). In future projections, the changes in these teleconnections is strictly linked to the models' performance in representing the amplitude of the IOD and its teleconnections in the present climate, where both CMIP3 and CMIP5 models tend to have an IOD with amplitude far greater than observed (Weller and Cai, 2013). Response of IOD to global warming is largely uncertain: in a large ensemble (CESM-LE) the inter-member uncertainty of IOD amplitude change is 50% of the intermodal uncertainty in a set of CMIP5 models, evidencing the important role of internal variability in IOD future projections (Hui and Zheng, 2018).

Individual model studies generally project increases of MJO precipitation amplitude in a warmer climate, with increases of up to 14% per °C of warming (Adames et al., 2017b; Arnold et al., 2015; Arnold et al., 2013; Caballero and Huber, 2013; Carlson and Caballero, 2016; Haertel, 2018; Liu and Allan, 2013; Maloney and Xie, 2013; Pritchard and Yang, 2016; Schubert et al, 2013; Subramanian et al., 2014; Wolding et al., 2017). Different ways to define the MJO generally make quantitative comparisons of changes in MJO precipitation amplitude across studies difficult. A more direct comparison of precipitation amplitude changes in a warmer climate come from multi-models studies. CMIP5 models with good historical MJO behavior indicate a spread in Indo-Pacific warm pool MJO precipitation amplitude change of -4% to +8% per °C in the RCP8.5 scenario relative to the end of the 20th Century (Bui and Maloney, 2018; Maloney et al, 2019).

MJO precipitation amplitude changes are highly sensitive to the pattern of SST change, with El Niño-like warming patterns favouring increased MJO precipitation amplitude (Takahashi et al., 2011), also confirmed by aqua-planet studies (Maloney and Xie, 2013). For models with MJO precipitation amplitude increasing with warming, an increase in the lower tropospheric vertical moisture gradient, that supports stronger vertical moisture advection per unit diabatic heating, is considered as a leading factor for such amplitude increases (Adames et al., 2017b, 2017a; Arnold et al., 2015; Wolding et al., 2017). Most models also project that MJO activity will penetrate farther east into the central and east Pacific with warming given the tendency for model to produce an El Niño-like warming pattern (Adames et al., 2017a; Subramanian et al., 2014). MJO convective variability may increase in a warming climate, but its role in bridging weather and climate in the extra-tropics may not (Wolding et al., 2017).

The primary implications for water cycle projections from climate modes is the likelihood that ENSO's influence on precipitation will strengthen and shift eastward. Internal variability associated with most modes (ENSO, NAO, IOD) results in considerable uncertainty in precipitation projections in regions influenced by their teleconnections.

8.4.2.6 *Wet extremes (including floods, atmospheric rivers)*

8.4.2.6.1 Tropical cyclones

The atmospheric environment during future El Niño events seems to be conducive for more storm events (Chand et al., 2017). However model projections do not show significant increase in the interannual occurrence of tropical cyclones by the end of the twenty first century around North Pacific tropical islands (Widlansky et al., 2019). In IPCC AR5 the consensus projection was for decreases in TC numbers, increases in frequency of high-intensity events and increase in TC rainfall amount. But these projections have been identified as largely uncertain with even high resolution simulations struggling to adequately capture tropical cyclone intensity (Roberts et al., 2015; Strachan et al., 2013), and are dependent on the different TC detection methods are used (Walsh et al., 2016).

8.4.2.6.2 Extratropical cyclones

In AR5, extratropical storms were expected to decrease in the Northern Hemisphere (12.4.4.3), but unlikely by more than a few percent (Chapter 14). Meanwhile, precipitation associated with extratropical storms was projected to increase (14.6.2.1). Thermodynamic factors, particularly the projected increase in moisture, would be expected to increase precipitation associated with extratropical storms. Meanwhile, latent heating is what drives extratropical storms, so it is plausible that changes in precipitation and its associated latent heating could affect extratropical storm intensity and thus precipitation. Evidence has continued to accrue that precipitation associated with individual extratropical storms is projected to increase, following thermodynamic drivers with negligible dynamic change (Yettella and Kay, 2017). Comparisons with observational analogues of climate change also support the projected increase in thermodynamic precipitation increase with little dynamic response for precipitation associated with extratropical storms (Li et al., 2014)). Confidence in projected increases in precipitation associated with extratropical storms in most regions is high. At the same time, some regions continue to be projected to experience decreases in precipitation associated with extratropical cyclones due to local changes in their track and intensity (Simpson et al., 2016; Wodzicki & Rapp, 2016; Zappa et al., 2015).

8.4.2.6.3 Flooding

8.4.2.6.4 Atmospheric rivers

Lavers et al.(2015)indicate that integrated vapour transport under RCP 8.5 and 4.5 could increase and this thermodynamic response (O'Gorman, 2015) could affect mostly the mid-latitudes where orographic precipitation is important. This might increase the intensity of heavy precipitation events on the west coast of the US (Lavers et al., 2015; Ralph and Dettinger, 2011; Warner and Mass, 2017) and in Europe (Lavers et al., 2015; Ralph et al., 2016; Ramos et al., 2016), where all models analysed agree (*very likely; high confidence*) under both scenarios, except over the Iberian Peninsula (Ramos et al., 2016) (*likely, low confidence).*

In a warming world, thermodynamics ensure that atmospheric rivers (ARs) will be wetter and therefore more spatially extensive, i.e. wider and longer. This fact is clearly borne out in several regional (Gao & others, 2015; Gershunov et al., 2019; Hagos et al., 2016; Payne & Magnusdottir, 2015; Ralph & Dettinger, 2011; Warner et al., 2015) and one global study (Espinoza et al., 2018) of AR activity in CMIP5 model projections. All these authors identify increasing AR activity under future warming due to thermodynamic moistening. Hints at possible regional changes due to dynamical factors are mostly second-order and largely uncertain (Gao and others, 2015; Payne and Magnusdottir, 2015). There is unsurprisingly *strong agreement* that as ARs become wetter, they will become broader, longer, stronger, and longer-lasting. This follows directly from the definition of ARs as IVT surpassing a threshold first and foremost, with geometric constraints sometimes also imposed, which are all more likely satisfied by wetter ARs. (Espinoza et al., 2018b), however, also suggest that, the frequency of ARs will decrease somewhat globally. This is not necessarily the case regionally, though, as, for example, more ARs are projected to landfall at the North American West

Coast (e.g. (Gershunov et al., 2019), although larger increases are projected for other AR variables, e.g. peak intensity and duration. These increasing trends in regional AR activity in CMIP5 projections clearly begin to emerge only in the early 21st century – just about now. Most GCMs do not show significant trends during the historical period (Gershunov et al., 2019). Moreover, validating GCMs for their ability to realistically simulate landfalling AR behavior and their contribution to regional total precipitation and using only the most realistic models was shown to significantly constrain CMIP5 multi-model projection uncertainty. (Gershunov et al., 2019) show that ARs are projected to become progressively stronger contributors to the regional hydroclimate of Western North America.

Given the predominantly direct thermodynamic causes of change, similar conclusions may be warranted for other regions where ARs have been historically important. Particularly, in Mediterranean climate regimes, where precipitation is mainly confined to the cold season and precipitation frequency is clearly projected to decrease (Polade et al., 2017), contribution of ARs to the annual total may be expected to grow disproportionately. In California, for example, decreases in precipitation frequency are projected due to fewer non-AR storms, while ARs are almost entirely responsible for the projected increase in heavy and extreme precipitation events. Importantly, year-to-year precipitation amounts become more variable/volatile because of this decrease in the sample size of storms but a stronger dependence on extremes (Polade et al., 2014), particularly due to ARs(Gershunov et al., 2019) . In California, where major topography is oriented perpendicular to the prevailing direction of IVT due to land-falling ARs, this projected enhancement of heavy and extreme precipitation appears to be accentuated (Gershunov et al., 2019; Polade et al., 2014). Understanding the mechanistic causes of projected regional precipitation regime change provides a nuanced knowledge of future changes in regional hydroclimates. In the case of ARs, confidence in such trends and their impacts can be relatively high.

[START FIGURE 8.36 HERE]

Figure 8.36: From (Gershunov et al., 2019).Annual average maximum IVT for AR events landfalling upon the West Coast of North America [20-60N] in historical (1951-2005, left) and projected (2006-2100, right) epochs. Real-5 GCMs are plotted in thin colored lines, while other GCMs are outlined in gray. Thick curves represent the ensemble averages of the Real-5 GCMs (red), the other 11 GCMs (green), and the full ensemble of 16 GCMs (blue). The thick black curve shows the observed (SIO-R1) variability.

[END FIGURE 8.36 HERE]

8.4.2.7 Aridity and droughts

Climate change projections of drought are complex, with the magnitude, robustness, and even sign of responses changing depending on the region, season, and even variable being considered. This complexity precludes broad statements or generalizations regarding climate change and drought, and instead requires a more nuanced consideration of the full hydrologic cycle response. Encouragingly, the mechanisms within the model projections that underlie shifts in drought severity and risk are broadly congruent with both basic theory (*subsection 8.2.2.2.7*) and observations (*subsection 3.2.6*), providing some confidence in our mechanistic understanding.

Consistent with the highly robust nature of warming in the projections, warming induced increases in vapour pressure deficit and evaporative demand are widespread, robust, and consistent across regions, seasons, and models (Figure 8.37) (*virtually certain*). Conversely, precipitation responses are much more uncertain, with the most robust ensemble responses occurring in specific regions and seasons. Indeed, while the expected zonally symmetric “wet-get-wetter/dry-get-drier” patterns emerging from thermodynamic and dynamic considerations (Held and Soden, 2006b) (*Section 8.2*) appear robust over the oceans, precipitation responses over land often diverge widely from this narrative (Greve et al., 2014). Broadly, the most robust and significant increases in precipitation occur during the boreal cold season at high northern latitudes (*very* *likely*) and over major monsoon regions (e.g., India, Southeast Asia, etc.) during summer (*very likely*).

Robust precipitation declines over land are much more localized. This includes the Mediterranean and other 'Mediterranean-climate' regions (e.g. southwest Australia, the Western Cape of South Africa), as well as Southern Africa, Mexico, and the Central United States and Pacific Northwest (*very likely*). Beyond changes in total precipitation, snowfall and surface snowpack levels also change significantly in the projections. At high latitudes and elevations that remain below the 0˚C isotherm even in a warmer climate, snowfall increases during the cold season (*virtually certain*). This isotherm does, however, migrate poleward (and upward in elevation) with warming, resulting in significant declines in the fraction of total precipitation falling as snow at low elevations and across the mid-latitudes (*virtually certain*). Over most regions, spring snowpack levels also decline with warming (*virtually certain*), a result of both an advancement in timing of the snowmelt season and increased losses from sublimation.

Surface drought indicators (e.g., soil moisture and runoff) are sensitive to changes in supply (precipitation) and demand (evapotranspiration), and this is reflected in their patterns of response. Robust soil moisture declines occur across Western North America, Mexico and Central America, Europe and the Mediterranean, Southern Africa, and Southwest Australia (*likely to very likely*). While much of this drying overlaps with regions experiencing significant and robust precipitation declines (e.g., the Mediterranean), drying also occurs over areas where precipitation responses to warming are much more ambiguous (e.g., the Central Plains)(Phillips et al., 2019). In regions such as the Mediterranean and western North America, aridification trends take future soil moisture conditions outside the range observed and reconstructed values spanning the last millennium (Cook et al., 2014; Otto-Bliesner et al., 2016), while in regions where precipitation is projected to increase future soil moisture trajectories are more uncertain (Hessl et al., 2018) (Fig.8.38). Increased evaporative losses are clearly implicated in this enhanced drying (Dai et al., 2018), though broadly speaking near surface soil moisture appears to be more sensitive to warming induced evaporative drying than soil moisture deeper in the soil column (Berg et al., 2017). These differences likely reflect carry-over of moisture from previous seasons deeper in the soil column and the potentially higher sensitivity of these deeper pools to vegetation processes (Berg et al., 2017b). Some studies, however, suggest this pattern of amplified surface soil moisture drying and diminished responses deeper in the soil column are not universal (Cook et al., 2015; Mankin et al., 2017). For many regions, runoff increases during the cold season and declines during the warming season (*likely*), a shift in timing mediated by changes in seasonal precipitation, snowfall and snowmelt, and evaporative losses from the surface.

Soil moisture and runoff changes with climate are clearly the most relevant for impacts to people and ecosystems, but model responses of these variables are extremely sensitive to vegetation processes that are highly uncertain and poorly constrained. Almost universally, models project increases in two factors that have opposite effects on surface water availability: plant water use efficiency (WUE) and leaf area index (LAI). Increases in WUE (a consequence of rising atmospheric CO_2) are expected to ameliorate evaporative drying because carbon assimilation rates can be maintained or increased with no associated increase in water use (Swann et al., 2016). Conversely, increases in LAI (reflecting larger overall carbon gains with rising atmospheric CO_2) increase the total evaporative surface area and total plant water use, increasing evaporative losses in a warmer world (Mankin et al., 2017, 2018). The empirical evidence on which process will be more important in a warmer, higher CO_2 world is mixed (De Kauwe et al., 2013; Lu et al., 2016; Trancoso et al., 2017; Ukkola et al., 2016), though in the models the latter appears to dominate, helping drive regional reductions in soil moisture and streamflow with warming (Dai et al., 2018; Mankin et al., 2018). Increasing confidence in these projections, however, will require improved understanding of these critical underlying processes.

[START FIGURE 8.37 HERE]

Figure 8.37: End-of-century changes in hydroclimate variables from 17 models in the CMIP5 archive (2070-2099 minus 1976-2005) in (a) water-year (WY; October--September in the Northern Hemisphere and July-June in the Southern Hemisphere) precipitation (P), (b) WY precipitation minus evapotranspiration (P-E), (c)

summer (June-July-August in the Northern Hemisphere; December-January-February in the Southern Hemisphere) leaf area index (LAI), (d) annual plant water use efficiency (WUE), (e) WY transpiration, (f) summer total runoff, (g) summer near surface soil moisture (~0.1m), (h) summer full-column soil moisture (note depth varies by model), (i) summer vapor pressure deficit (VPD) all in percent (%). In all panels, drying tendencies are indicated in brown, wetting tendencies in blue (note the reverse color scales in (e) and (i)). Ensemble agreement is based on a pooled model-year K-S test (95%), with the additional requirement that at least two-thirds of models agree with the direction of ensemble mean change. Hatched areas are insignificant. From (Cook et al., 2018).

[END FIGURE 8.37 HERE]

[START FIGURE 8.38 HERE]

Figure 8.38: Past-to-future drought variability in paleoclimate reconstructions and models for regions of (a,b) the Mediterranean (10W-45E, 30N-47N); (c,d) western North America (124W--117W, 32N-38N), and (e,f) central Asia (99E-107E, 47N-49N). Long tree-ring reconstructed Palmer Drought Severity Index (PDSI) series (black line) for the (a) Mediterranean (Cook et al., 2015b, 2016a), (b) California and Nevada (Cook et al., 2010b; Griffin and Anchukaitis, 2014) and (c) Mongolia (Hessl et al., 2018; Pederson et al., 2014) plotted in comparison to the past-to-future fully-forced simulations from the NCAR CESM Last Millennium (red line) (Otto-Bliesner et al., 2016) for the same region. The pink envelope represents the range of historical and future PDSI simulations from CMIP5 for the same regions (Cook et al., 2014) (b,d,f: The distribution of annual PDSI values from the paleoclimate and historical period (850 to 2005 CE) and future (2006 to 2100 CE) from the long past-to-future CESM simulations.

[END FIGURE 8.38 HERE]

8.5 What are the limits for projecting water cycle changes?

Projected water cycle changes are generally much more uncertain than projected changes in near-surface temperature. Here the main sources of uncertainties in climate projections are assessed following three main aspects. At first, anthropogenic climate change has no observational analogue, which makes model verification particularly difficultand modelling uncertainty a fundamental feature of climate projections (section 8.5.1). Also, internal decadal climate variability is large, partly unpredictable, and therefore represents an irreducible uncertainty, especially for near-term climate projections (section 8.5.2). At last, projected water cycle changes are also conditional on human behaviour (e.g., mitigation of GHG emissions, geoengineering) and on random natural radiative forcing such as major volcanic eruptions (section 8.5.3).

8.5.1 Modelling uncertainties of relevance for the water cycle

Uncertainties in projected water cycle changes are not dominated by the assumed range of plausible emissions of greenhouse gases across the 21st century (*high confidence*), but by model deficiencies and their difficulty to agree on the hydrological response to a given emission scenario (Giuntoli et al., 2015, 2018; Hawkins and Sutton, 2011) (FIG. 8.39). Modelling uncertainties are usually classified in two categories: structural and parametric. Here the focus is mainly on structural uncertainties related to poorly constrained processes and to limited model resolution, but parametric uncertainties and model tuning will be also briefly discussed (cf. Chapter 1 for more details).

[START FIGURE 8.39HERE]

Figure 8.39: Fraction of total variance in decadal mean precipitation projections explained by internal variability (orange), model uncertainty (blue) and scenario uncertainty (green), for (a) global, annual mean, (b) Sahel JJA mean, (c) European DJF mean, and (d) South East Asian JJA mean. All calculations are based on

CMIP3 models and SRES scenarios (*Hawkins and Sutton*, *2011*). Partly replicated with CMIP5 models and RCP scenarios (Fig. 11.8 dealing with both T and P) in AR5 WGI. To be replicated with CMIP6 models and SSP scenarios.

[END FIGURE 8.39HERE]

8.5.1.1 Poorly constrained key processes

Model development and evaluation has continued since the AR5, with a particular emphasis on the representation of new model components such as interactive chemistry, aerosols and biogeochemical cycles. The new-generation of global climate and Earth system models however still suffers from a number of deficiencies rooted in our limited knowledge of the fundamental processes and in the need to account empirically for fine-scale processes through so-called sub-grid parametrizations. This longstanding issue is here illustrated by a brief assessment of the inherent model limitations and the recent advances in three specific areas: atmospheric convection, cloud-aerosol interactions and land surface processes.

8.5.1.1.1 Atmospheric convection

Atmospheric convection and associated precipitation is fundamental to the Earth's climate and water cycle, through its influence on atmospheric momentum, heat, and moisture budgets. Given the limited computing resources, the current-generation global climate models cannot account explicitly for small-scale cloud processes and hence represent shallow and deep convection by sub-grid-scale parametrizations (Arakawa and Schubert, 1974). AR5 reported that such parametrizations are particularly important for the simulation of regional precipitation, especially in the tropics where the former generation global climate models still showed substantial systematic errors such as a double-ITCZ syndrome (Oueslati and Bellon, 2015; Xiang et al., 2017) or too light and too frequent precipitation events (Sun et al., 2015; Trenberth et al., 2017). Most CMIP5 models underestimate the rainfall from organized convection, which provide half of the total observed precipitation in the tropics (Tan et al., 2018). They also have difficulties to adequately simulate the diurnal cycle of precipitation over land (Couvreux et al., 2015), the rainfall intensity distribution associated with monsoon regimes (Roehrig et al., 2013), or the precipitation variability from intra-seasonal to multi-decadal time scales (Ault et al., 2012; Klingaman et al., 2015).

When comparing state-of-the-art climate models with observations, uncertainties have been documented also in the observational datasets, over the South Asian monsoon region for example (Collins et al., 2013a; Lin and Huybers, 2019; Shige et al., 2017; Singh et al., 2019a). In fact, the rainfall at 0.05° resolution from the TRMM Precipitation Radar (PR) indicates rainfall maximal on the upslope of the Western Ghats (Shige et al., 2017), which is in contrast to the offshore locations of the rainfall maxima identified from infrared radiometers (IR). Although the absolute precipitation amounts estimated from TRMM PR are lower than rain-gauge observations over the Western Ghats (Shige et al., 2015), a nearly homogenous dataset of rainfall over land and ocean from the TRMM PR preserve spatial variation, providing the opportunity to evaluate models. Historical simulations capturing the decreasing trend of the Indian summer monsoon precipitation after the1950s (Krishnan et al., 2016) appear to resolve the spatial pattern of rainfall as seen in the rainfall climatology from the TRMM PR.

Since AR5, further developments have been made for improving the representation of convective clouds and related precipitation in global climate models. The multi-scale aspect of convection makes it particularly challenging to represent in general circulation models. Processes to parameterize include vertical transport associated with dry, shallow and deep convective regimes, vertical velocities, microphysical processes, precipitation efficiency, mesoscale organization and cloud cover. The importance of representing convection/aerosols interactions is still debated (Varble, 2018), as well as the sensitivity of convection to changes in aerosol concentrations (Fan et al., 2018a). A cloud regime-based study highlights an apparent disconnection between cloud and precipitation processes in global climate models (Tan et al., 2018), suggesting that a good representation of clouds does not lead to systematic or appreciable improvement in simulated precipitation (*low confidence*). The recent and robust finding that climatological precipitation patterns, including the double ITCZ syndrome, simulated with and without parameterized convection schemes are relatively similar, despite the strong impact of convective parameterizations on daily precipitation extremes (Maher et al., 2018b), strengthened the idea that the uncertainties in convection represented in models is large.

Many biases related to the representation of convection still exist in state-of-the-art general circulation models. CMIP6 models show for instance difficulties to adequately simulate the vertical profile of the apparent heat source and moisture sink derived from field campaign measurements (Abdel-Lathif et al., 2018). (…). Yet, significant advances have been obtained such as the alleviation of the double ITCZ problem in the CESM model (Qin and Lin, 2018), thereby highlighting the relevance of subtropical low clouds and of air-sea interactions in the tropics. TO BE EXPANDED BASED ON CMIP6 MODEL DESCRIPTION AND EVALUATION

Convection also contributes to the vertical transport of heat, moisture, momentum, trace species and aerosols, with a direct impact on atmospheric thermodynamical properties and large-scale circulation. The underestimation of the vertical transport by shallow convection may be partly responsible for the systematic warm SST bias over the eastern part of tropical ocean (Hourdin et al., 2015), with potential implications for the tropical overturning circulations. The representation of the transition from shallow to deep convection is also challenging, due in particular to the difficulty of representing mixing between convective updrafts and their environment. Large eddy simulations (LES) results suggest that it is not possible to find a formulation valid for both shallow and deep convection (Del Genio and Wu, 2010; Zhang et al., 2016a). This is key for the representation of the diurnal cycle of precipitation, but also of the suppressed phase of the MJO in the tropics (Del Genio et al., 2012), for example.

Since AR5, spatial aggregation of tropical convection has also received a growing attention in both observations (Holloway et al., 2017) and models (Muller and Bony, 2015; Wing et al., 2017). Yet, only a few convective parameterizations represent some aspects of convective systems organized at the mesoscale (e.g., Hourdin et al., 2013). This is related to the complexity of related mechanisms: interactions of convection with planetary waves, wind shear, gravity waves; cold pools and mesoscale circulations within anvil clouds or below, which depending on the horizontal resolution, may be partially resolved by the model. Cloud Resolving Models (CRMs, cf. subsection 8.5.1.2.2) therefore represent the main tool for a better understanding and parametrization of mesoscale convective systems. An explicit simulation of clouds is still not feasible at the global scale, even if CRMs are increasingly used over large domains (Guichard and Couvreux, 2017; Leutwyler et al., 2017). Such studies highlight an improved simulation of the summer convection over land and of the precipitation diurnal cycle (*high confidence*), but may also reveal significant deficiencies such as contrasted performances between region with and without strong orographic forcing. Machine learning may represent a more efficient way to parameterize moist convection after training the model with a conventional or a super parametrization (Gentine et al., 2018; O'Gorman and Dwyer, 2018). While such methods show promising results, they have not been used in CMIP6 models and they need to be trained with a warmer climate to be usable in climate projections. There is therefore *medium to high confidence* that the response of moist convection will remain a key uncertainty in global climate projections as long as CRMs cannot be integrated globally and in multiple realizations of both recent and future climates.

8.5.1.1.2 Aerosol microphysical effects on clouds and precipitation

The large uncertainty in aerosol cloud-mediated radiative forcing stems from incomplete knowledge of adjustment processes of clouds to aerosol primary effects as cloud condensation nuclei (CCN). The adjustment occurs mainly as a dynamic response to the impacts of CCN on cloud drop size and number concentrations on precipitation-forming processes (Camponogara et al., 2018; Goren and Rosenfeld, 2014; Koren et al., 2014; Rosenfeld et al., 2008a).

Validation of model simulations of cloud-aerosol interactions must rely on observational comparisons of cloud and aerosol properties, which are practical over large areas only from satellite measurements. De facto, there is a lack of observational constraints on aerosol-cloud interactions (ACI) at the regime where the sensitivity is greatest (Levy et al., 2013b; Rosenfeld et al., 2014; Shinozuka et al., 2015). This leads to large uncertainties in the quantification of ACI by both observations and simulations. An assessment of this limitation shows that direct comparisons of AOD with cloud properties should lead to a large underestimation of the effective radiative forcing due to cloud-aerosol interactions (Ma et al., 2018b).

Uncertainties are large for deep clouds, as their processes are much more complex and include also the impacts of aerosols on ice precipitation processes. Recent work has shown large effects of aerosols on invigorating (Fan et al., 2018b; Koren et al., 2014; Rosenfeld et al., 2008a) and electrifying (Thornton et al., 2017) deep tropical convective clouds. These processes are not yet fully implemented in cloud parameterization of climate models. Specifically, the potential major role of ultrafine aerosol particles in this process (Fan et al., 2018b) is not yet accounted for in cloud parameterization. Observational studies comparing aerosols to cloud properties are also lacking due to the limitations of satellite retrieval of CCN. Moreover, satellite retrievals of ultrafine aerosol particles based on their optical signals are inherently impossible. A possible way forward is offered by using satellite-retrieved cloud composition and updrafts for retrieving CCN (Rosenfeld et al., 2016), and possibly ultrafine aerosol particles in the future.

These uncertainties affect precipitation directly by the aerosol effects on precipitation-forming processes, and indirectly by changing latent heating and radiation, which in turn can affect atmospheric circulation systems and the resultant changes in precipitation. In summary, there is still *low confidence* in the attribution of these effects on future precipitation changes. Future aerosol emissions are also uncertain (Riahi et al., 2017), and this contributes substantially to uncertainty in multi-decadal-scale projections of water cycle changes. Black carbon stands out as a component that may cause significant model diversity in predicted precipitation change (Bond et al., 2013). Processes linked to atmospheric absorption are less consistently modeled than those linked to top-of-atmosphere radiative forcing (Samset et al., 2016).

Aerosols and GHGs may yield similar, but opposite regional patterns of precipitation change, due to atmosphere-ocean feedbacks (Xie et al., 2013). The similarity in GHG and aerosol climate responses, including precipitation, also exists in fixed SST simulations due to fixed land-sea contrasts (Persad et al., 2018). This makes detection of anthropogenic effects on the hydrological cycle more difficult.

The simulated response to anthropogenic aerosol may be influenced by the experimental design. Studies of the Asian monsoon have shown that feedbacks to the aerosol-induced SST changes are important to the final response (Dong et al., 2019; Tian et al., 2018b), which may limit the utility of atmosphere-only experiments. The summer monsoon response to aerosol more generally has been shown to be sensitive to both local and remote changes in aerosol emissions (Dong et al., 2014, 2016; Song et al., 2014; Wang et al., 2017d), which may lead studies with regional models to underestimate the role of aerosol. However, such studies have shown the microphysical effects of aerosol on convective clouds to be important in monsoon changes (Wu et al., 2013), which will not properly be represented by GCMs at their current resolutions.

Attribution of precipitation changes to anthropogenic aerosol is currently limited by model biases (Wilcox et al., 2015; Zhang et al., 2017a). Many models have a poor representations of regional water cycles (Kusunoki and Arakawa, 2015; Sperber et al., 2013). However, often they are able to capture circulation changes, which may be used as a proxy for precipitation changes (Song et al., 2014; Wilcox et al., 2015; Zhang et al., 2017a).

8.5.1.1.3 Land surface processes

Land surface processes determine the partitioning of net surface radiation into sensible and latent heat fluxes, the partitioning of precipitation into evapotranspiration and runoff, and the lower temperature and humidity boundary conditions to the atmosphere. Since AR5, researchers have examined the improvement of existing and the inclusion of new processes in land surface models (LSMs): soil freezing and permafrost (Chadburn et al., 2015; Gao et al., 2019; Vergnes et al., 2014; Yang et al., 2018a), soil and snowhydrology(Brunke et al., 2016; Decharme et al., 2016), glaciers (Shannon et al., 2019), surface waters and rivers (Decharme et al., 2012), as well as vegetation (Bartlett and Verseghy, 2015; Betts et al., 2015; Knauer et al., 2015; Tang et al., 2015) and the representation of hydraulic gradients throughout the soil-plant-atmosphere continuum (Bonan et al., 2014).

Several areas of process representation appear to have an agreed focus across different research centres internationally. These include anthropogenic water management at the global scale, which is recognized as critical for the closure of regional surface water budgets (Pokhrel et al., 2016, 2017; Veldkamp et al., 2018). Improving groundwater representation as part of extraction at larger scales (Collins, 2017; Leng et al., 2014; Pokhrel et al., 2015; Vergnes et al., 2014), and improved representation of inland water bodies (Gu et al., 2015; Verseghy and MacKay, 2017) is also part of this broader effort. There has also been a drive to improve the representation of land surface heterogeneity and its effects. This has been in the form of improved vegetation stand, disturbance and fire dynamics (Fisher et al., 2018; Haverd et al., 2018; Li et al., 2013a; Yue et al., 2018; Zou et al., 2019) and better representation of urban surfaces (Best and Grimmond, 2015; Lipson et al., 2018), particularly in modelling systems with higher resolutions and driven by increasing awareness of the local to regional effects of urban landscapes. The representation of a realistic vegetation cover has also been reported to have significant effects in the simulation and prediction of temperature and precipitation at multiple time-scales (Alessandri et al., 2017). Large effects have been shown over middle-to-high latitudes due to the shadowing/masking of snow surfaces by boreal forests (Bartlett and Verseghy, 2015; Loranty et al., 2014; Qiu et al., 2016; Thackeray et al., 2015; Thackeray and Fletcher, 2016a; Wang et al., 2016a). This is particularly relevant for the spring season, when variations in surface albedo feedback are correlated to subsequent summer drying in both models (Hall et al., 2008) and satellite observations (Chen et al., 2017c).

Besides LSMs, global hydrological models (GHMs) have been further developed for offline simulations of the hydrological impacts of both climate change and water management (Döll et al., 2016, 2018; Jiménez Cisneros et al., 2014; Pokhrel et al., 2016; Schewe et al., 2014). GHMs can equal or outweigh the contribution of global climate models to uncertainties in hydrological projections at the regional scale (Giuntoli et al., 2015). A good performance of hydrological models in historical simulations is necessary but not sufficient to increase the confidence in water cycle projections (Krysanova et al., 2018). Projected daily river discharge may be highly scenario-dependent, but climate model uncertainty is generally much larger, specifically in periods of the year and regions where precipitation dominates the river flow regime (Hattermann et al., 2018). Uncertainties related to the land surface hydrology dominate in seasons and regions where snow, soil freezing and evapotranspiration may influence substantially the river regime (Hattermann et al., 2018; Pechlivanidis et al., 2017; Samaniego et al., 2017).

Biophysical vegetation processes are still not accounted for in many GHMs, which may lead to inaccurate projections of terrestrial runoff and water resources. Yet, hydrological models that do simulate these effects still disagree among each other and do not necessarily support the added value of a more sophisticated representation of vegetation processes given the other multiple sources of modelling uncertainties (Döll et al., 2016). Significant improvements to the modelling of vegetation are required to address the role of land-surface feedbacks properly within LSMs (Prentice et al., 2015). Since AR5, more dynamic global vegetation models (DGVMs) have been introduced in a number of ESMs. Yet, they probably need to be further constrained by observations (Cantú et al., 2018; Franks et al., 2018; Medlyn et al., 2015; Prentice et al., 2015) in order to provide valuable information on potential vegetation feedbacks. Plant's migration and mortality are often ignored or poorly represented in the current-generation climate and Earth system models (Fisher et al., 2018). Plant's physiological response to the atmospheric CO2 increase is generally accounted for, but using models of stomatal conductance that are characterized by a single critical parameter representing intrinsic water-use efficiency (Franks et al., 2017, 2018). Ball-Berry type parametrizations are shared by many models, suggesting a lack of structural diversity and caution about the apparent consensus of the photosynthesis response to increasing CO2, even if contrasted behaviors may favor dry conditions (Huang et al., 2016; Knauer et al., 2015). Model evaluation against *in situ* measurements suggest that most CMIP5 ESMs underestimate the water use efficiency at many sites and, thereby, overestimate the ratio of evapotranspiration to precipitation (Li et al., 2018).

Such a deficiency may also alter the soil moisture – evapotranspiration coupling, which is primarily controlled by the soil moisture climatology. Many land areas exhibit a dry bias and a too strong control of soil moisture on evapotranspiration, with potential implications for the projected land surface warming (Berg and Sheffield, 2018b). Since AR5, there is increasing recognition of the need to better understand and quantify the role of land-atmosphere coupling (Berg et al., 2016; Santanello et al., 2018). This has led to the use of field campaign data (Dirmeyer et al., 2018; Phillips et al., 2017; Song et al., 2016) and remotely sensed information (Ferguson and Wood, 2011; Roundy and Santanello, 2017) specifically tailored to evaluating coupling in modelling systems, as well development of coupling diagnostics and testing approaches (Dirmeyer and Halder, 2017; Tawfik et al., 2015a, 2015b), and led to the creation of LS3MIP (van den Hurk et al, 2016) to examine this issue in more detail as part of CMIP6. In addition, the land surface modelling community will have to face new challenges in representing terrestrial ecosystems within the next generation Earth system models, such as accounting for mortality, increased disturbances from wild fires, insects and extreme events, addition of an interactive nitrogen cycle, or the impact of increased levels of tropospheric ozone (Bonan and Doney, 2018).

In summary, there is are multiple lines of evidence and there is therefore *high confidence* that land surface processes remain a key source of modelling uncertainty, both in global climate models and global hydrological models. Despite their higher resolution (cf. next subsection), regional climate and hydrological models may suffer from similar deficiencies given the small-scale nature of most land surface processes and the need to parametrize them even in higher-resolution models. Yet, topography plays a key role in triggering precipitation and runoff and should be considered in sub-grid land surface parametrizations in order to avoid major hydrological biases in global models.

8.5.1.2 Added value of increased model resolution

Beyond the structural modelling uncertainties discussed in section 8.5.1.1, the influence of horizontal resolution in all ESM components is also a longstanding issue which has received an increasing attention over recent years. The lack of resolution is generally assumed as one of the key factors that hamper the credibility of global climate projections. Various numerical solutions have been proposed such as a uniform or regional increase in the resolution of global climate models or the use of regional climate models (RCMs) driven by lower resolution global models at their lateral boundary conditions. Statistical downscaling tools are also widely used to generate the fine-scale regional climate information necessary for impact and adaptation studies. These tools are assessed in Chapter 10 and will not be here discussed although they represent another significant source of uncertainty for regional climate information.

8.5.1.2.1 High-resolution global climate models

Since AR5, a growing number studies suggest the benefit of increasing the atmospheric horizontal resolution for simulating many features of the global water cycle. High resolution is obviously important for simulating the regional water cycle in areas with steep or complex orography (Vanniere et al., 2018). Yet, the added value of higher resolution global climate models is not ubiquitous and needs a careful assessment. Several AGCM studies suggest a better simulation of the precipitation climatology (Demory et al., 2014), as well as a better frequency distribution of daily precipitation intensities (Zhang et al., 2016c) including extremes (Jacob et al., 2014; Westra et al., 2014). Some inconsistencies however appear among models such as the simulation of extreme wet conditions over the tropical oceans (Zhang et al., 2016c) or the ratio of land versus ocean precipitation (Demory et al., 2014; Huang et al., 2018a). Part of the improvement in the simulated precipitation statistics is related to a better simulation of the frequency and/or mean intensity of tropical (Roberts et al., 2015; Walsh et al., 2015) and extratropical (Hawcroft et al., 2016; Zappa et al., 2014b) cyclones. Increased atmospheric resolution is also important for simulating Euro-Atlantic blockings or projecting the seasonality and intraseasonal variability of monsoon rainfall (Chen et al., 2018; Zhang et al., 2018a). Variable resolution based on grid stretching may also represent a cheaper and valuable alternative to a uniform increase in horizontal resolution for the simulation of regional phenomena like monsoons (Krishnan et al., 2016; Sabin et al, 2013) or tropical cyclones over specific tropical ocean basins (Chauvin et al., 2017; Harris et al., 2016).

There are however many cases where higher spatial resolution does not lead to a systematic improvement of the simulation of the present-day water cycle. For instance, higher horizontal resolution does not make a major difference in summer mean precipitation errors among CMIP5 models (Huang et al., 2018a; cf Fig.8.40). Differences between the two categories of models are however visible in terms of ratio of stratiform and convective precipitation, with low resolution models having more convective precipitation. A more coordinated and systematic evaluation of high-resolution global simulations at climate timescales, with resolutions of at least 50 km in the atmosphere and 0.25° in the ocean, is part of the HighResMIP initiative (Haarsma et al., 2016). Preliminary results suggest that… (TO BE CONTINUED ONCE AVAILABLE). Yet, Roberts et al. (2018) argue that the next breakthrough in global climate modelling will be only reached at atmospheric resolution finer than 1 km, close to resolving the large boundary layer eddies (*medium confidence*).

[START FIGURE 8.40 HERE]

Figure 8.40: The 27-year mean precipitation in the high-resolution multi-model ensemble (HMME) (a), low-resolution multi-model ensemble (LMME) (b), and the differences between HMME and LMME (c), LMME and GPCP (d, f) and HMME and LMME (e, g). (unit: mm/day). The d, e, f, and g indicate the differences over continent and ocean, respectively. Calculations are based on the outputs of the top-six and bottom-six horizontal resolution models among 23 CMIP5 models (*Huang et al., 2018*). All model outputs as well as the GPCP observed climatology have been regridded onto a common 128xG4 regular grid. Similar maps to be replicated with CMIP6 models, paying attention to focus on pairs of simulations differing only by their resolution (in order to avoid mixing structural uncertainties with the influence of model resolution), and possibly distinguishing a third category of 'very-high' resolution models from HighResMIP. Stippling should be added to highlight statistical significance.

[END FIGURE 8.40 HERE]

8.5.1.2.2 Regional Climate Models and Cloud Resolving Models

Regional Climate Models (RCMs) are limited-area models with representations of climate processes comparable to those in the atmospheric and land surface components of the General Circulation Models but at higher resolution (usually in the order of 10 to 50 km). RCMs are used to dynamically downscale global model simulations to a particular region. AR5 reported that RCMs may add values both in regions with variable topography and for small-scale phenomena such as coastal breezes, cyclones, convective storms, orographic precipitation or the shadowing effect of topographic barriers on downwind precipitation. It was however recognized that RCMs inherit biases from the driving global models. Therefore, while there is *high confidence* in their added value for the simulation of present-day climate, at least when they are driven by lateral boundary conditions derived from atmospheric reanalyses, this does not necessarily mean that they provide more credible projections of future climate. Beyond uncertainties in the driving GCMs, one concern is about the potential lack of physical consistency between the GCM and RCM, which may lead to spurious mass, momentum and energy fluxes across the lateral boundaries.

Since AR5, there has been an ongoing debate on how to define the added value of RCMs (Benestad, 2016; Di Luca et al., 2015), as well as growing evidence that the potential for more credible projections of regional climate may be achieved under specific circumstances. In the last decade, the application of RCMs has largely increased mainly due to international inter-comparison models experiments such as CLARIS (Sánchez et al., 2015), NARCCAP (Mearns et al., 2013) and CORDEX(Giorgi et al., 2009; Gutowski et al., 2016). Many studies have focused on climatological precipitation, showing with *high confidence* an added value for monthly to seasonal accumulation and its spatial distribution (Carril et al., 2018; Dosio et al., 2015; Giorgi et al., 2016). RCMs are also useful tools for assessing the impact of land and water management, especially irrigation and urbanization, on both temperature and precipitation over the contiguous regions.

Yet, the regional climate modelling community is presently wrestling with question about where dynamical downscaling is heading in the future (Benestad, 2016), as global climate and Earth system models are moving to higher spatial resolution (Haarsma et al., 2016; Roberts et al., 2018). If that is the case, CRMs may become the next standard for regional climate modelling, with the potential for better understanding and projecting changes in extreme precipitation (Chan et al., 2016b, 2018; Fosser et al., 2017; Kendon et al., 2017; Moseley et al., 2016; Westra et al., 2014), improved simulation of land-atmosphere coupling (Hohenegger and Stevens, 2018; Hsu et al., 2017; Moon et al., 2019; Taylor et al., 2013), or fine-scale projections of climate change in megacities (Best and Grimmond, 2015; Sarangi et al., 2018).

8.5.1.2.3 High-resolution land surface hydrology

High resolution in the land surface component is also important for simulating many features of both present-day and future terrestrial water cycles (especially in complex topography areas), as well as the hydrological response to recent and future changes in land use (Lawrence et al., 2016). Yet, in practice, most climate models use the same horizontal resolution in their atmosphere and land surface components, so that their water cycle biases and sensitivity may be dominated by the atmosphere (Döll et al., 2016). A low-resolution topography is a major obstacle for the simulation of runoff, river streamflow, floodplains and, thereby, of the whole water budget at the basin scale. This problem can be mitigated by the use of land surface parametrizations accounting for the effect of sub-grid topography on the land surface hydrology (Decharme and Douville, 2007).

The benefits of increasing the horizontal resolution might be easier to detect in offline rather than online land surface simulations (Döll et al., 2016). Offline high-resolution global or regional hydrological models, either derived from the land surface component of global climate models or developed for this purpose, are routinely used to monitor water resources but also to produce global projections driven by bias-corrected atmospheric forcings(Davie et al., 2013; Huang et al., 2017, 2018b). Bias correction techniques however rely on debatable assumptions and therefore represent an additional source of uncertainty in off-line hydrological projections (Hagemann et al., 2011). Offline land surface projections may also suffer from the lack of land-atmosphere coupling (Berg et al., 2016; Berg and Sheffield, 2018a). Moreover, the development and calibration of hyper-resolution hydrological models raise a number of issues given the lack of reliable subsurface information (Bierkens et al., 2015b).

To sum up, the ultimate objective to provide locally relevant information on projected hydrological impacts of climate change is therefore not only hampered by uncertainties in both global and regional projections, but also by epistemic uncertainties and the lack of global high-resolution data (e.g., soil and vegetation properties, groundwater reservoirs and their connections, land and water management) for developing reliable hydrological models. There is therefore only *low to medium confidence* that higher resolution models necessarily lead to more reliable hydrological projections despite the obvious benefit of a better resolved topography. Beyond the lack of subsurface information, the structural model uncertainties discussed in 8.5.1.1 will always remain a major obstacle that is not totally overcome by regional climate and impact models given the need to drive them at their boundary conditions.

8.5.1.3 Limitations of model benchmarking, tuning and weighting

8.5.1.3.1 Model benchmarking and tuning

The increasing complexity of ESMs has triggered efforts to assess model fidelity through objective and rigorous comparisons with multiple observational datasets. The overall performance of global climate and Earth system models is evaluated in Chapter 3. The focus here is on the benchmarking and tuning of the land surface models (LSMs), although the tuning of global climate models and the use of perturbed parameter (or perturbed physics) ensembles will be also briefly discussed. The nature of LSM evaluation is becoming more and more sophisticated. The land surface modelling community is increasingly aware of the benefits of defining model performance expectations *a priori* (before the simulations begin) when determining model performance (Abramowitz et al., 2008; Haughton et al., 2018), a process that is often referred to as model 'benchmarking' as opposed to model evaluation (Abramowitz, 2012; Best et al., 2015; Clark et al., 2015).

Model complexity has raised a suite of difficult epistemological issues for the land surface modelling community that are not yet entirely resolved. This stems from the very different role that LSMs play in coupled climate prediction to other climate model components, such atmospheric or ocean models. The land surface is highly heterogeneous, involves many more processes, and the nature of coupling between these processes is not always entirely clear. The treatment of a significant number of processes is therefore necessarily empirical, at almost any spatial and temporal scale, so that while most LSMs have no explicit length scale, it is often implicit in the nature of process representation. This includes processes such as photosynthesis (Jefferson et al., 2017), respiration (Lombardozzi et al., 2015) and evapotranspiration (Ershadi et al., 2014, 2015).

Another difficulty arises in the prescription of model parameter values at global and regional scales. Most state of the art LSMs contain 30+ parameters describing soil and vegetation properties. While many of these are potentially observable at ecosystem scales, their prescription at much larger scales generally requires aggregating parameter values into discrete clusters of vegetation and soil 'types'. The value for each parameter for one of these types needs to be calibrated for each LSM, which may be done at local scales using flux tower data (Raoult et al., 2016) or global scales using gridded forcing data and gridded observationally-based evaluation products (Yang et al., 2016). In both cases, ascertaining the nature of uncertainty arising from this procedure is very difficult, given the generally unquantified uncertainties in gridded LSM forcing data, gridded evaluation data, and parameter variability within a given vegetation or soil type. Note that the calibration of parameters in this 'offline' mode is simply about determining default parameter values for global gridded simulations, and is an entirely separate process to tuning LSMs with the coupled model environment.

Calibration or tuning is an essential aspect of hydrological modelling. The growing physical basis of global-scale or basin-scale distributed hydrological models has not reduced the need for model calibration or parameter optimization (Li et al., 2018a; Sood and Smakhtin, 2015). Calibration is a demonstration that the model is able to capture the observed behavior of the hydrological system, for instance the discharge at various gauging stations along the river. Generally, it requires a manual or automatic adjustment of the most empirical parameters. Tuning techniques are often based on systematic parameter perturbations within a plausible range (while other parameters are held constant) until the simulation matches the observed records. While such a strategy can be quite efficient, especially at the basin scale, it may also lead to over-confident hydrological projections due to a lack of observational constraints on the multiple model parameters (Xu et al., 2017b).

These multiple difficulties collectively highlight a tension in the land surface modelling community in terms of the cost of the addition of new processes. On one hand, adding new processes that are clearly important in the natural system should improve our ability to represent interactions that may play a key role in the hydrological effects of climatic change. On the other hand, they increase the degrees of freedom in a model and may lack the observational constraint to adequately parameterize them (Ginzburg and Jensen, 2004). The addition of more processes may also decrease our ability to evaluate individual process representations in isolation, since they are increasingly dependent on more process interactions, leading to what Lenhard and Winsberg (2010) have termed 'confirmation holism'. This becomes increasingly problematic where processes are poorly observationally constrained at the intended scale of the model's application. The growing realization of these issues has led to the development of community-based model evaluation and benchmarking environments, such as ILAMB (Collier et al., 2018), ESMvalTool(Eyring et al., 2016), LVT (Kumar et al., 2012) and PALS (Abramowitz, 2012). Despite these advances, putting meaningful uncertainty bounds on projections based on LSM uncertainty at global and regional scales is still not possible with any degree of confidence. The range of simulation outcomes from different models, different parameter values and sets of assumptions can be explored, but this remains a proxy for true, observationally-based uncertainty quantification.

Tuning of global climate models has also received an increasing attention over recent years (Hourdin et al., 2017; Mauritsen et al., 2012; Schmidt et al., 2017). While the main objective is the simulation of a stable and realistic global mean energy budget when the model is forced with fixed preindustrial radiative forcings, more subtle tuning strategies may be implemented to improve the cloud and precipitation climatology (Schmidt et al., 2017; Yang et al., 2013; Zhao et al., 2018b). A perturbed physics ensemble (PPE) approach can be also used to assess the most sensitive parameters, for instance in the deep convection scheme of the Community Earth System Model (Bernstein and Neelin, 2016). The main uncertainty arises from the determination of the turbulent entrainment parameter. The mean tropical precipitation differences between two sets of plausible parameters may be as large as the difference between future and present-day precipitation in a low-mitigation scenario (cf. Fig.8.41). The non-linear precipitation behavior emphasizes the need to reduce the range of possible values for constraining the simulated hydrological sensitivity.

In summary, there is multiple evidence and *high confidence* that the current benchmarking and tuning of both land surface and climate models do not strongly constrain their hydrological response to anthropogenic forcing. The inter-model spread in global and regional hydrological projections is not only due to structural model uncertainties, but also to our limited ability to define accurate values for poorly constrained model parameters.

[START FIGURE 8.41 HERE]

Figure 8.41: (a) Precipitation (mm/d) change for 2081–2100 relative to the 1986–2005 base period under the RCP8.5 global warming scenario for CESM1 standard values for JJA. Differences in projected JJA precipitation change (mm/d) under global warming (2081–2100 relative to the 1986–2005 base period) for simulations done with different parameter values. Differences are across the feasible range for four parameters in the deep convection scheme: (b) entrainment; (c) deep convective adjustment time; (d) downdraft fraction; (e) evaporation efficiency. Stippled areas pass a t test at the 95% level (Bernstein and Neelin, 2016).

[END FIGURE 8.41 HERE]

8.5.1.3.2 Model selection and weighting

Beyond the long-term improvement and tuning of global climate and Earth system models, recent years have seen a growing interest in a 'top-down' approach consisting in using observations and emergent constraints to narrow the range of plausible climate changes projected by the current-generation models (cf. cross-chapter box 4.X). Only few emergent constraints have been applied so far to projected water cycle changes. Such studies have been more or less successful at constraining the increase in global mean (Deangelis et al., 2015), tropical mean (Ham et al., 2018) or Indian summer monsoon (Li et al., 2017) precipitation, the sensitivity of extreme precipitation (Borodina et al., 2017), the regional patterns of future runoff changes (Yang et al., 2017), or the drying of the northern mid-latitude continents in summer (Douville and Plazzotta, 2017). Some studies emphasize an underestimation of projected water cycle changes (*medium confidence*), including the increase of extreme precipitation (Borodina et al., 2017), the magnitude of mid-latitude drying (Douville and Plazzotta, 2017), or the decrease in Amazonian runoff (Yang et al., 2017). If further supported by CMIP6 results, such results would represent a major concern for adaptation strategies.

Model weighting is motivated by model performance but also by the fact that many global climate and Earth system models share similar individual components or similar parametrizations so that CMIP simulations cannot be considered as fully independent realizations of present-day and future climates. Model similarities diagnosed *a priori* (e.g., Boé, 2018) and *a posteriori*(Herger et al., 2018; Knutti et al., 2017; Sanderson et al., 2017) both suggest a strong model interdependency, not only from one model generation to the next but also within the same generation of models. This raises a number of issues about the best use of climate information based on multi-model ensembles and about the 'one-model-one-vote' approach adopted so far by the IPCC. Moreover, both model performance and model interdependency metrics should be used with great caution given the large internal variability of most water cycle variables at the regional scale (cf. section 8.5.3).

Beyond model weighting, there are other research avenues for narrowing model uncertainty. A first one is through the use of bias-corrected rather than raw model outputs. Model errors in both present and future hydrological variables can be reduced by focusing on hydrological phenomena or events (Polson and Hegerl, 2017; Weller et al., 2017) rather than on geographical patterns, but also by morphing model outputs onto observations using non-local bias correction techniques (Levy et al., 2013a). Bias corrections can be also used for climate impact studies, like agriculture production changes in future projections (Prasanna, 2018). Such calibration techniques are more widely used based on regional climate models, hence more details are given in Chapter 10. A second original method is based on the 'storyline' whereby no a priori probability is used and emphasis is rather put on understanding the main drivers and their plausibility (Shepherd et al., 2018). Beyond its physical basis, such an approach allows the use of regional climate projections or regional climate models in a conditioned manner, as well as emphasis on low-probability but high-impact water cycle changes. A telling illustration of this strategy (cf. Fig.8.42) is the assessment of winter Mediterranean precipitation changes projected by CMIP5 models conditional to the response of the stratospheric polar vortex and to tropical upper troposphere warming (Zappa and Shepherd, 2017b).

In summary, cherry picking a few models, focusing on the multi-model ensemble mean, or using only raw model outputs may lead to overconfident and misleading regional hydrology information for adaptation planning. Water cycle projections are generally biased and inherently probabilistic and should be dealt with accordingly. Great attention should be paid to low probability but physically plausible high impact scenarios (Sutton, 2018). While recent progress has been made to characterize uncertainties throughout the modeling process and to reduce uncertainties through the use of performance metrics as emergent constraints (Clark et al., 2016), model weighting is still limited by the small number of independent models and emergent constraints paradoxically need poor models to pop up from an ensemble of opportunity. A growing number of studies advocate for the end of "model democracy" (Knutti et al., 2017; Sanderson et al., 2017). Yet, it might be wise to check first that the proposed emergent constraints still apply to CMIP6 models, to develop alternative observational constraints based on detection-attribution when feasible, and to better understand the processes at work in the most sensitive models before excluding them because they are outliers or they align on a poorly constrained regression line.

[START FIGURE 8.42 HERE]

Figure 8.42: Cold season Mediterranean precipitation response per degree of global warming (mm day-1 K-1) according to (a),(b),(d),(e) four plausible storylines of climate change that are conditioned on the tropical amplification and stratospheric vortex responses. The storylines have been selected to be of particular relevance for Mediterranean precipitation change. The storylines in (a) and (b) are characterized by a stronger stratospheric vortex, while those in (d) and (e) have a weaker vortex; also, the storylines in (b) and (e) are characterized by higher tropical amplification of global warming, while those in (a) and (d) have lower tropical amplification. (c) The multimodel mean response scaled by global warming. (Fig. 8 from Zappa and Shepperd, 2017) [Check whether it is not used in Chapter 10 and could be updated with CMIP6 models]

[END FIGURE 8.42 HERE]

8.5.2 Internal climate variability

Beyond modelling uncertainties, internal climate variability also represents a major source of uncertainty for projected water cycle changes, especially for near-term projections and at the regional scale (Fatichi et al., 2016; Hawkins and Sutton, 2011; Kent et al., 2015; Thompson et al., 2015). The emphasis here is first on quantifying the terrestrial water cycle internal variability using multiple evidence such as paleo reconstructions, preindustrial simulations or large Initial Condition Ensembles (ICE) (Sect 8.5.2.1). Then key drivers of multi-decadal variability in the Pacific and Atlantic Oceans, as well as the related implications for the predictability of near-term water cycle changes, are specifically assessed as they show significant but model-dependent teleconnections with regional hydrological fingerprints over land (Sect 8.5.2.2).

8.5.2.1 Quantification of water cycle internal variability

The dominance of internal climate variability represents an enormous challenge in the projection and assessment of anthropogenically caused changes in precipitation, because of the weak signal to noise ratio (Deser et al., 2012; Sarojini et al., 2016; Shepherd, 2014; Xie et al., 2015). For example, internal atmospheric variability needs to be taken into account to explain the recent tropical belt poleward expansion of comparable magnitude in both hemispheres (Grise et al., 2019). It may also impede the detection of the anthropogenic climate change signal until the middle to late century in many regions of the world for mean and extreme precipitation (Martel et al, 2018).

The relatively short length of the instrumental record limits our ability to quantify the magnitude of internal climate variability in the water cycle, particularly over long timescales (decadal and beyond). However, paleoclimate archives (tree rings, corals, lake and ocean sediments) provide extended reconstructions of key water cycle parameters and large-scale circulation features, like ENSO, that strongly influence regional rainfall teleconnections. Comparisons between model output and paleoclimate proxy records can be used assess confidence in decadal-scale projections of water cycle changes from models, and to validate the magnitude and physical drivers of internal variability. Numerous studies comparing paleoclimate records of hydroclimate to model output have indicated that CMIP5 models underestimated or inconsistently simulated variability at decadal and longer timescale, and therefore may be missing important processes in the climate system (Ault et al., 2012, 2013; Bunde et al., 2013; Cheung et al., 2017; Franke et al., 2013; Hope et al., 2017; Kravtsov, 2017).

However, recent work suggests that CMIP5 models can in fact reproduce internal variability at decadal and longer variability, including the severity, persistence, and spatial extent of megadroughts (Coats et al., 2015; PAGES Hydro2K Consortium, 2017; Stevenson et al., 2015). The discrepancy is attributed to the fact that the earlier assessments were based on incompatible proxy-model comparisons and failed to account for signal reddening by proxy archives (Dee et al., 2017; PAGES Hydro2K Consortium, 2017). Implementation of proxy system models, i.e., functions that transform model variables into proxy units, has reduced model-proxy disagreement, although some differences in the magnitude of internal variability may remain, particularly at centennial timescales (Dee et al., 2017; Parsons et al., 2017). Incorporation of the core PMIP simulations into the framework of CMIP has allowed for cross-time period analyses of past, present and future climate states and variability. For example, the amplification of the Northern Hemisphere monsoons is a robust features of CMIP5 models in RCP scenarios, but models persistently underestimate the magnitude of regional precipitation changes over Africa and Asia during the mid-Holocene, for example, suggesting that future projections could be similarly affected (Harrison et al., 2015). It is unclear whether remaining discrepancies represent limitations of the climate models or limitations of the proxy system models.

The mechanisms driving internal variability in the water cycle in climate models may vary between models, and also be different from those in nature. For example, tropical Pacific SSTs, in particular anomalies associated with El Niño and La Niña, are known from observations to influence drought in the Southwest USA (Seager et al., 2005; Trenberth et al., 1998). While some models reproduce a relationship between drought in the Southwest USA and tropical Pacific SSTs, others do not, and instead associate drought with atmospheric variability (Coats et al., 2015, 2016; Parsons et al., 2018; Stevenson et al., 2015). In the western Pacific, CMIP5–PMIP3 last millennium simulations reproduce the observed negative correlation between eastern Australian rainfall and the NINO3.4 SSTs with varying skill, and also display periods when the ENSO teleconnection weakens substantially for several decades (Brown et al., 2016). Although an increase in eastern Australian rainfall was simulated by the majority of climate models during the period following the major volcanic eruptions, the lack of significant correlations indicate that rainfall variability in this region is primarily driven by internal variability inherent to each model, rather than by external forcing (Brown et al., 2016).

Differences in simulated internal variability have been found to be responsible for the inter-model spread in terms of shifts in subtropical dry zones for a given shift in the Hadley cell (Seviour et al., 2018). Such differences are related to the simulated mean state. Indices of precipitation extremes tested in three different CMIP5 scenarios reflect the dominant role of internal variability even at the end of the twenty-first century (Aerenson et al., 2018). However, for precipitation internal climate variability remains lower than inter-model spread for all projections time horizons and spatial resolutions (Kumar and Ganguly, 2018).Using ensembles of atmosphere-only simulations driven by observed or reconstructed SST, it is possible to disentangle the models' ability to capture the circulation and/or precipitation variability observed over the historical period (Deng et al., 2018; Douville et al., 2018; Zhou et al., 2016). Such AGCM-based attribution methods have debated limitations and may lead to erroneous attribution conclusions in some regions for local circulation and mean and extreme precipitation (Dong et al., 2017). Other methods to measure the portion of precipitation variability linked with internal dynamics include the partitioning into dynamical versus thermodynamical components or the analysis of variance. For example, the former applied to European rainfall variability indicated that in winter a substantial fraction is accounted for by circulation variability (Fereday et al., 2018). Similarly, the latter applied to DJF extreme precipitation in US west coast indicate that 80% of variability is due to internal atmospheric dynamics, while the remaining 20% can be attributed to SST forcing (Dong et al., 2018b).

Anyway the most powerful instrument to document and measure the magnitude of internal variability in both recent and future climates is the use of large ICE. Results from these ensembles indicate, for example, that the internal variability of the NAO imparts substantial uncertainty to future changes in European regional climate over the coming decades (Deser et al., 2017; cf. Fig.8.43). Also, results from CanESM2 (Sigmond and Fyfe, 2016) and CESM1 (Kay et al., 2015) large ensembles for the period 1950-2100 indicate that natural climate variability can impede the detection of the anthropogenic climate change signal until the middle to late century in many parts of the world for both mean and extreme precipitation (Martel et al., 2018). Large ICE ensembles (e.g. CESM and FLOR) have been also used to identify the "time of emergence", i.e. the time when the anthropogenic change is outside the range expected from internal variability only. Within the next several decades anthropogenic shifts will exceed the bounds of natural variability over most of the planet, under medium-high emissions scenarios (Zhang and Delworth, 2018). Compared to 1950-1999, by 2000-2009 simulated anthropogenic shifts in precipitation mean state were already distinguishable over 36-41% of the globe (high latitudes, eastern subtropical oceans and the tropics).

[START FIGURE 8.43 HERE]

Figure 8.43: Impact of the NAO on future 30-year climate trends (2016–2045). (e) Regressions of winter SLP and precipitation trends upon the normalized leading PC of winter SLP trends in the CESM1 Large Ensemble, multiplied by two to correspond to a two standard deviation anomaly of the PC; (f) CESM1 ensemble-mean winter SLP and precipitation trends; (g) f − e; (h) f + e. Precipitation in color shading (mm/day per 30 years) and SLP in contours (interval = 1 hPa per 30 years with negative values dashed) (*Deser et al. 2017*). Possibly duplicated using other large Initial Condition Ensembles

[END FIGURE 8.43 HERE]

In summary, research to date suggests that state-of-the-art climate models reproduce the magnitude and character of internal water cycle reasonably well (*medium confidence*), but that the mechanisms causing such variability are still model-dependent, and thus not always mechanistically plausible. This has implications for estimating the future risk of persistent intervals of drought and aridity that influence locations including southwest USA, eastern Australia, southern Africa, the Mediterranean, and the Amazon basin (Ault et al., 2014; Cook et al., 2018).

8.5.2.2 Key drivers and implications for near-term water cycle projections

8.5.2.2.1 Multi-decadal key drivers

Since AR5, growing attention has been paid to the main modes of low-frequency climate variability, which may represent a potential source of predictability for near-term climate change. AMO, PDO, ENSO, and PNA all have significant influence on precipitation and groundwater fluctuations across a north-south gradient of the west coast of the U.S., but the low frequency climate modes (like AMO and PDO) have a greater influence on hydrologic patterns than the high frequency ones (Velasco et al., 2017a). Climate variability has important implications for recharge rates and changes in groundwater storage (Fleming and Quilty, 2006; Gurdak et al., 2007; Hanson et al., 2006; Kuss and Gurdak, 2014). However, the same teleconnection patterns that exist in surface hydrologic processes are not necessarily the same as those preserved in subsurface processes that affect groundwater storage, because the vadose zone has a partial control on the degree of damping of surface variable fluxes and how each of the climate variability modes is expressed in groundwater fluctuations (Velasco et al., 2017b).

The warm (cold) phase of the PDO is associated with deficit (excess) rainfall over India: the PDO extends its influence to the tropical Pacific, modifying the relationship between monsoon rainfall and ENSO (Krishnamurthy and Krishnamurthy, 2014; Krishnan and Sugi, 2003). Observed summertime drying trend over Northern Central India is related to the observed positive trend of the PDO index, but as the trend is not reproduced by CMIP5 models and as the spread within models is very large, internal variability is suggested to play an important role in explaining it (Salzmann and Cherian, 2015). Approximately 70% of the drying trend in North China during 1960-1990 originates from the multi-decadal variability related to the PDO phase changes, including influence from a weakening of the East Asian summer monsoon (Qian and Zhou, 2014). Improved simulation of the present-day response of atmospheric circulation to SSTAs could be effective in lowering the uncertainty in global modes', including ENSO, amplitude change under global warming (Ying et al., 2019). The quantification of the canonical influence of ENSO on North American climate is subject to considerable uncertainty due to aliasing of unrelated climate variability (Deser et al., 2018; Sun et al., 2018). Natural SST variability associated with ENSO/PDO is mostly responsible of the recent tropical widening, particularly in the Northern Hemisphere (Allen et al., 2017; Mantsis et al., 2017).

The Atlantic Multidecadal Variability (AMV or AMO) modulates the influence of ENSO on the South China Sea summer rainfall as well as its relationship with the subsequent ENSO development: the negative correlation between the decaying phase ENSO and the South China Sea summer rainfall is significant (non-significant) during negative (positive) phases of the AMO (Fan et al., 2018c). Multiple lines of investigations (including observations, theoretical models and Rossby wave tracing analysis) suggest that the Atlantic multi-decadal variability can be identified as a driver of the decadal-scale variations of the Siberian warm season precipitation, with anomalous southerly winds bringing moisture northward to Siberia, and the precipitation there increasing correspondingly (Sun et al 2015). The AMO also triggers multi-decadal variations in precipitation and reflects onto multi-decadal variability in river flows over France (*medium to high confidence*), mostly in spring and summer (Boé and Habets, 2014; Giuntoli et al., 2013). These variations are reflected also in other hydrological variables, like evapotranspiration, snow cover and soil moisture (Bonnet et al., 2017). These variations in river flows may have practical implications in hydropower production, for example. Considering the nature of these large-scale variations related to the AMV, internal variability may have an important role in the evolution of river flows in coming decades, potentially limiting, reversing or seriously aggravating the long-term impacts of anthropogenic climate change.

The AMV has played an important role in recent trends in tropical precipitation (Kamae et al., 2017) and can substantially modulate the global monsoon system (Wang et al., 2017c, 2018a; Zhisheng et al., 2015), in terms of mean precipitation, total precipitation, and monsoon area (Monerie et al., 2019a). During positive AMO phase, ITCZ is shifted northward leading to increased precipitation in the Northern Hemisphere, also found in observations modulated by the Pacific Ocean (Wang et al., 2013a), and decreased precipitation in the Southern Hemisphere (Monerie et al., 2019b). The northward shift of the Atlantic ITCZ warms the upper troposphere over the North American continent, reducing vertical motion and providing mean drying in the region as well as reduced precipitation variability (Lee et al., 2018a). During boreal summer, it modifies the Walker circulation with an anomalous rising branch over the North Atlantic and an anomalous sinking branch over the Pacific (Lee et al., 2018a; Ruprich-Robert et al., 2017). The effects of these changes in the Walker circulation are precipitation anomalies over the whole tropical belt, strengthening monsoon activities over Asia and Africa, and weakening those over South America and Australia (Monerie et al., 2019b). Over the Sahel, the precipitation signal is dominated directly by the AMO in the west (O'Reilly et al., 2017), while in the east the warm AMO phase influence is modulated by warm SST anomalies over the Mediterranean (Gaetani et al., 2010; Park et al., 2016). The majority of CMIP5 models fail to capture the relationship between AMO and Sahel precipitation on decadal time scales, primarily because the distribution of North Atlantic SST associated with the AMO is not correctly represented in the tropics (Martin et al., 2014). Relatively high predictability of the AMV impacts over the Mediterranean basin, central Asia and the Americas (from us to north of South America) during boreal summer, but in boreal winter the signal to noise ratio shows only weak predictability over land (Ruprich-Robert et al., 2017; Yamamoto and Palter, 2016).

The internal component of the AMV is small in CMIP5 models compared to observations. One of the causes could rely on internal ocean dynamics that depends on the ability of the models to resolve the Gulf Stream front and ocean eddies, precluded by the coarse resolution of CMIP5 models (Siqueira and Kirtman, 2016). Indeed, considerable uncertainties remain in estimating the internal component of the observed AMV (Peings et al., 2016) . External forcings have a dominant role in driving the observed AMO (Murphy et al., 2017), including solar and volcanic forcing since at least 1775AD (Knudsen et al., 2014; Otterå et al., 2010; Otto-Bliesner et al., 2016). Increases in AMO variability is linked to overall cooling, but it may also reflect the influence of volcanic forcing on the AMO (Stevenson et al., 2018). Availability of centennial climate simulations evidences that stochastic fluctuations may as well explain longer time-scale relationship, like for the decadal ENSO-ISM connection (Cash et al., 2017; DelSole and Shukla, 2012; Gershunov et al., 2001; Yun and Timmermann, 2018), not requiring low-frequency modulation caused by other climate modes, like AMV (Chen et al., 2010b; Kucharski et al., 2009), or global warming effects (Azad and Rajeevan, 2016; Wang et al., 2015), or shifts in ENSO's centers(Fan et al., 2017; Kumar et al., 2006).

To sum up, there are therefore multiple lines of evidence, both from observations and models that the water cycle is not only influenced by anthropogenic forcings but it also responds to multiple modes of internal climate variability at the regional scale. The statistical properties of these modes and the related teleconnections are not accurately simulated in most global climate models. There is therefore only *low confidence* in their projected changes. There is however *high confidence* that these modes will not disappear with global warming and will remain a large source of uncertainty for predicting near-term climate change.

8.5.2.2.2 Predictability of near-term water cycle changes

Adapting water resource management in the face of climate change would greatly benefit from the prediction of land surface hydrology at the decadal timescale. Climate predictions differ from climate projections by constraining the initial state of the slow components of the climate system (i.e. the ocean, the cryosphere and the terrestrial hydrology) with observations. Anthropogenic and natural radiative forcing (e.g., solar cycles, major volcanic eruptions) and low-frequency modes of internal climate variability (e.g., AMV and IPV) suggest a possible predictability of near-term climate in addition to the projected response to the anthropogenic forcing. This relatively recent field of research activity, identified as near-term climate predictions (NTCP), aims to bridge the gap between initialized predictions (from weather to seasonal timescales) and uninitialized climate change projections, and are of potential utility and benefit for decision-makers in many sectors of the economy, including those concerned with adaptation and resilience to climate variability and change (Kushnir et al., 2019).

In AR5 (Chapter 11), a systematic comparison of initialized predictions versus non-initialized projections highlighted an added value of constraining the initial ocean state with available observations for near-term temperature changes. In contrast, although near-term predictions of precipitation over some land areas also exhibited positive skill, it was mostly due to the specified radiative forcing (*high confidence*) with almost no added value of initialization (*low confidence*). Since AR5, more studies have been devoted to understanding the potential or effective water cycle predictability related to the ocean multi-decadal variability. Decadal hindcast experiments based on large ensembles with the CESM global climate model highlight increasing skill scores in annual mean precipitation 3-7 year ahead, at least over Sahel and Europe (Yeager et al., 2018). To be continued WITH CMIP6 DCPP RESULTS

The additional skill associated with the initialization of the cryosphere and the land surface has received so far less attention. There is however observational evidence that oceanic decadal variations can propagate into the atmosphere and, thereby, accumulate into terrestrial land surface reservoirs (e.g., Bonnet et al., 2017) and vegetation (e.g., Zeng et al., 1999). This land surface memory may also contribute to the decadal predictability of the terrestrial component of the water cycle, but remains difficult to assess given the lack of long and/or reliable enough observational records. It has been primarily explored under idealized experimental settings (e.g., the so-called "perfect-model" approach). A preliminary assessment of the impact of vegetation initialization suggest that this additional degree of freedom generates as much noise as signal and does not translate into improved skill (Weiss et al., 2014).

Decadal hydrological predictability has been also investigated through offline land surface hindcast experiments, driven by observed atmospheric forcing and/or perfect initial conditions(Yuan and Zhu, 2018). The selected land surface model (CLM4.5) includes 15 soil layers from the surface down to 42 m and shows a significant (i.e., longer than 6 years) memory for terrestrial water storage over 11% of global land areas. The perfect model approach suggests skilful predictions over 31%, 43%, and 59% of global land areas for terrestrial water storage, deep soil moisture, and groundwater, respectively. Yet, a real-world assessment is hampered by the lack of observations and will be only feasible when multi-decadal records of satellite estimates of terrestrial water storage, snow mass or soil moisture become available.

In summary, the chaotic nature of the climate system imposes stringent limits on the extent to which skilful decadal predictions of water cycle statistics may be made (*high confidence*). Dynamical decadal predictions of precipitation and land surface hydrology remain so far mostly an unfulfilled promise (Cox and Stephenson, 2007). Statistical hindcasts may suggest higher scores (e.g., Årthun et al., 2017), but maybe overconfident given the limited observational record. Decadal predictions of global mean temperature are more skilful but, unlike long-term climate sensitivity, do not scale on regional water cycle variations and have therefore no practical relevance for water management. Water cycle predictions for the forthcoming decade should be considered with *low confidence* in most land areas. Adaptive decision-making should focus on both the human-induced water cycle response (and related uncertainties) and on the magnitude of the irreducible internal multi-decadal variability, which may offset or amplify the forced near-term response. Any action aimed at increasing the resilience of human societies to natural hydroclimate hazards may be also beneficial to climate change adaptation since projected water cycle changes suggest an enhanced seasonal to interannual variability over most land areas (cf. section 8.4).

8.5.3 Non-linear behaviour across emissions scenarios

Scenario uncertainty has been discussed in section 8.4 (and in Chapter 4). The focus here is on potential limitations to the validity of the widely used "pattern-scaling" technique (Tebaldi and Arblaster, 2014) due to non-linear changes in the water cycle across different emissions scenarios. The path-dependence of projected water cycle changes in high-mitigation scenarios will be also briefly discussed.

8.5.3.1 Non-linearities in atmospheric responses and feedbacks

AR5 concluded that mean precipitation change can be represented, to some extent, by linear pattern scaling techniques which represent change in precipitation as a linear function of global temperature change (Osborn et al., 2016; Tebaldi and Arblaster, 2014). AR5 however noted a number of caveats to the standard approach (Santer and Wigley, 1990). Even in a system governed by linear processes, pattern-scaling assumptions can fail because the different forcing time response of different parts of the Earth system cause evolving spatial warming patterns in response to a forcing step function (Good et al., 2016a) (*high confidence*). This occurs primarily because different feedbacks occur at different timescales (Andrews et al., 2015; Armour et al., 2013) which in turn implies that the atmospheric circulation and water cycle is dependent both on the level and the rate of change of global warming (Ceppi et al., 2018; McInerney and Moyer, 2012).

AR5 also noted that different atmospheric forcing agents vary in their influence on surface and atmospheric column energetic balance per unit surface warming, and thus have very different effects on global and regional precipitation (Hegerl et al., 1997; Polson et al., 2014), hence the amount of precipitation change per unit global temperature change differs between scenarios (Shiogama et al., 2010). Extreme precipitation, however, is considered to be mostly a function of atmospheric moistening – which scales with surface temperature (Chou et al., 2012; Trenberth, 1999), hence the relationship between extreme precipitation and temperature is found to hold more constant between scenarios (Pendergrass et al., 2015). Examined regionally, scenario dependencies in model experiments have been found to be more prevalent over the oceans, where the changes in shortwave partitioning resulted in a change in evaporative flux, but less over land (Ishizaki et al., 2013).

However, there is recent evidence that there may be nonlinearities in the response of the hydrological cycle to magnitude and interaction of different types of forcing. Results from specific models suggest that both globally and regionally, nonlinearities arise because water cycle responses to forcing vary as a function of state and forcing type (Good et al., 2012; Schaller et al., 2013). Precipitation changes in certain models following a doubling step change in carbon dioxide from pre-industrial levels are not consistent with the response to the step from doubling to quadrupling, despite a similar change in radiative forcing (Good et al., 2016b).

These nonlinearities have been proposed to arise for number of reasons. Some radiative feedbacks, such as the ice-albedo feedback are state dependent causing evolving patterns and amplitude of net warming (Caballero and Huber, 2013). Loss of sea-ice may result in a direct increase in evaporation and Arctic precipitation (Bintanja and Selten, 2014) and a potential nonlinear response of northern hemisphere atmospheric circulation and storm characteristics at high latitudes by modifying the stability of the Arctic polar vortex (Peings and Magnusdottir, 2014; Semenov and Latif, 2015), but limited observations make such mechanisms difficult to validate (Barnes, 2013b; Screen and Simmonds, 2013). Beyond sea-ice, the response of North Atlantic SST may also represent a significant source of nonlinearity in the atmospheric response. For example, the Atlantic meridional overturning circulation (AMOC) is expected to weaken under warming (Caesar et al., 2018b) although at a highly model-dependent rate (Kageyama et al., 2013; Stouffer et al., 2006). Models in general exhibit cooling and drying over the North Atlantic and a southward shift of the ITCZ in response to a weakened AMOC which can potentially impact precipitation over Central and South America, Africa and south east Asia, but the precipitation responses are highly model-dependent (Jackson et al., 2015; Kageyama et al., 2013; Michael and Richard, 2002; Stouffer et al., 2006). A weakening AMOC may also influence the modes of atmospheric variability (Timmermann et al., 2007; Wen et al., 2011) which modulate rainfall patterns (Chen and Tung, 2018; Parsons et al., 2014) (*low confidence*). The weakening of the AMOC itself is also thought to be enhanced by the freshwater flux from increased Arctic precipitation under warming (Bintanja and Selten, 2014; Holland et al., 2006), presenting the possibility of a coupled feedback between AMOC and Arctic precipitation.

Nonlinearities can also be rooted in the atmospheric processes. The response of convective precipitation may exhibit nonlinearities because it is itself modulated by both dynamics and atmospheric water content, each responding independently to warming (Chadwick and Good, 2013). An example of this type of process was evident in a single model study (Neupane and Cook, 2013) where low levels of Atlantic warming resulted in increased low level moisture producing an increase in convectively driven Sahel precipitation, whereas at larger levels of warming, precipitation decreased with a shift in the dominant prevailing wind direction. It has been also suggested that the Indian Summer Monsoon may exhibit a moisture-advection feedback which allows multiple stable states as boundary conditions change, raising the potential of a “dry” monsoon mode in which summer precipitation is greatly reduced (*low confidence*) (Zickfeld et al., 2005). Specific model studies have found that forced responses of the East Asian Summer Monsoon to land use and aerosol forcing may interact nonlinearly, because surface energy balance perturbations (albedo, heat capacity, evaporative flux) associated with urbanization are modulated by the incoming shortwave flux (Deng and Xu, 2016).

However, there is *low confidence* in the nonlinear responses to single or multiple forcings because a suitable multi-model ensemble of relevant experiments has not to date been available, so that inference is often made from a single model. The "nonlinmip" project (Good et al., 2016a) is designed to address this knowledge gap, detailing a set of perturbations to the standard CO_2 quadrupling step-change experiment used to derive climate sensitivity, assessing non-linearities in response using CO_2 doubling or halving experiments and comparing results with linearly scaled CMIP6 CO_2 quadrupling responses (FIG.8.44). While it has been demonstrated that the errors introduced by representing annual mean precipitation change as a function of global mean temperature are less than the inter-model disagreement in precipitation change (Tebaldi and Arblaster, 2014), there have been efforts to address these scenario dependencies with additional terms to represent the land-sea temperature offset to transient and equilibrium response (Herger et al., 2015), by representing non-greenhouse gas forcing components (Frieler et al., 2012; Kravitz et al., 2017) or more complex response functions (Good et al., 2015) which have been found to provide some improvements in performance (*high confidence*).

[START FIGURE 8.44 HERE]

Figure 8.44: Ensemble mean precipitation differences (in mm per day) between the second 2K minus the first 2K global warming under RCP8.5 mitigation conditions. Calculations are based on a subset of 25 CMIP5 models (*Good et al., 2016*). Could be duplicated with CMIP6 models under the same mitigation scenario or using the abrupt2xCO2 and abrupt4xCO2 simulations, and possibly showing not only precipitation but also evapotranspiration and runoff (or even soil moisture).

[END FIGURE 8.44 HERE]

8.5.3.2 Non-linearities in land surface responses and feedbacks

Land surface responses and feedbacks also represent a potential source of non-linearity for the water cycle response, at least at regional scale. The forced response of soil moisture and freshwater resources does not only depend on precipitation, but also on land surface evapotranspiration (Laîné et al., 2014), snowmelt (Thackeray et al., 2016), and runoff (Zhang et al., 2018e) which are all non-linear processes.

Land surface evapotranspiration (ET) is the sum of bare ground evaporation and vegetation evapotranspiration. Bare ground evaporation is usually estimated as a non-linear function of surface soil moisture (Jefferson and Maxwell, 2015). Plant's transpiration requires more complex formulations with non-linear dependencies on multiple environmental factors including root-zone soil moisture and atmospheric CO2 concentration (Franks et al., 2017). Depending on regions and seasons, evapotranspiration is either energy-limited or soil-moisture limited. Non-linearities may be particularly strong in transitional regimes where and when soil moisture limitation plays a major role (Berg and Sheffield, 2018b).

Snowmelt is a non-linear process. Global warming may lead to a non-linear snowpack response, with increasing specific humidity and snowfall as long as surface temperature remains under 0°C but increasing snowmelt as soon as it exceeds this threshold. This may contribute to some geographical and seasonal contrasts in the observed and projected retreat of the northern hemisphere snow cover (Thackeray et al., 2016) and of the mountain glaciers (Kraaijenbrink et al., 2017; Shannon et al., 2019). Glaciers act as natural freshwater reservoirs by storing water in the cold season and releasing it during warmer periods. This is vital for seasonal water supply in large river systems, especially in South America and South Asia. Beyond the temperature melting point, the limited volume of the snow pack and of the mountain glaciers represents a potential tipping point for freshwater resources once snow and ice have totally disappeared (see Section 6 for more details). Glacier runoff changes simulated on large-scale drainage basins to 2100 indicate that annual mean runoff may increase until a maximum is reached, beyond which runoff steadily declines thereby highlighting a highly nonlinear response (Huss and Hock, 2018).

Land surface runoff is the sum of surface runoff and subsurface drainage. Non-linear snow and ice processes may be reflected in the total runoff response, especially in the springtime discharge of snow-influenced watersheds. The permafrost thawing is another mechanism which can trigger a non-linear hydrological response (Walvoord and Kurylyk, 2016). Subsurface drainage is controlled by the vertical profile of soil moisture and is thus potentially influenced by non-linearities in the evapotranspiration response. Surface runoff is also a non-linear process which occurs when precipitation intensity exceeds the infiltration capacity. The runoff response to global warming may be highly non-linear where and when surface runoff represents a significant fraction of total runoff.

Non-linearities tend to vanish when averaged in space and time. Yet, major turning points were found in the projected annual mean runoff response to global warming, even over large river basins such as Amazon, Yangtze or Amu-Darya (Zhang et al., 2018; cf. Fig. 8.45). One implication is that long-term changes in runoff cannot be extrapolated from recent or even near-term trends. The main non-linearities are found in subtropical river basins and cannot be entirely explained by precipitation changes. Even the global and annual mean change in continental runoff is only approximately linear and accelerates at increasing global mean temperature (*medium confidence*). Finally, the response of terrestrial water reservoirs (lakes, rivers, wetlands, groundwaters) may be also affected by a direct and abrupt human influence (e.g., dams, irrigation) and is potentially sensitive to topographic thresholds such as river depth for the occurrence and magnitude of seasonal floodplains (Decharme et al., 2012).

To sum up, many non-linear effects may challenge the validity of the pattern-scaling technique for projecting water cycle changes at the regional scale (*medium confidence*). Such nonlinearities are also evidenced in water scarcity projections, suggesting a stronger sensitivity to the first 2°C increase in global mean surface temperature compared to the next one (Gosling and Arnell, 2016). They probably deserve further attention and decision-making on acceptable global warming targets should include a more detailed assessment of water cycle changes, not just precipitation.

[START FIGURE 8.45 HERE]

Figure 8.45: Relative changes (%) in basin-averaged annual mean runoff estimated as the multi-model ensemble mean averaged across a subset of CMIP5 models and across all RCPs over two representative river basins: Amazon (top panel) and Yangtze (bottom penel) rivers. The dashed line indicates the critical global mean temperature (GMT) warming at which a turning point is identified in the projected runoff. BFTD indicates the magnitude of trend before TP; AFTD indicates the magnitude of trend after TP; OTD indicates the magnitude of overall trend. The shaded area indicates the interquartile range of the ensemble values across all RCPs. Only the warming levels with more than 10 models available are shown for each RCP scenario. To be replaced or duplicated with CMIP6 models/scenarios. [RCP2.6 : Blue, RCP4.5 : Green, RCP6.0 : Yellow, RCP8.5 : Red, All RCPs : Black]

[END FIGURE 8.45 HERE]

8.5.3.3 Volcanoes, SRM and high mitigation scenarios

Despite their limited relative contribution to the total uncertainty of projected water cycle changes at the regional scale, mitigation scenarios remain essential when it comes to avoiding the most adverse hydrological impacts of global warming, such as the rising risks of droughts and heavy precipitation at the global scale (Pfahl et al., 2017; Greve et al., 2018; Park et al., 2018). Yet, a weak signal-to-noise ratio challenges the identification of potential non-linearities related to the implementation of high-mitigation scenarios or of plausible geo-engineering techniques (see Chapter 4 for more details on Solar Radiation

Management). Moreover, natural radiative forcings (e.g., major volcanic eruptions) can also represent a transient source on non-linear behaviour in the forced water cycle response, regardless the non-linear feedbacks discussed in sections 8.5.3.1 and 8.5.3.2.

Global mean precipitation significantly reduces after large volcanic eruptions (*high confidence*, Gu and Adler, 2011; Iles et al., 2013; Robock and Liu, 1994; Schneider et al., 2009; Trenberth and Dai, 2007), with the largest decrease in wet tropical regions (Iles and Hegerl, 2014). Global precipitation changes have larger sensitivity to temperature changes due to volcanic forcing (3.3 %K-1) rather than to GHG forcing (1.5 %K-1) (Iles et al., 2013). This stronger hydrological sensitivity (*medium confidence*) arises due to differing magnitudes of the fast response to GHG and sulfate aerosol forcing, despite consistent slow responses to these forcings(Richardson et al., 2018a) and may be explained by a stronger solar irradiance change in the wet tropics compared to a uniform relative decrease in solar radiation (Liu et al., 2018a). Major volcanic eruptions usually weaken the Intertropical Convergence Zone and reduce global (Liu et al., 2016) as well as summer monsoon (Zambri et al., 2017) precipitation, specifically in monsoon-fed regions like South Asian and African tropical rain-belt for the weakening and equatorward displacement of the Hadley cell (Dogar, 2018). Monsoon precipitation in one hemisphere can however be enhanced by the remote volcanic forcing occurring in the other hemisphere (*medium confidence*), and equatorial eruptions have weaker effects in weakening off-equatorial monsoon circulation than subtropical or extra-tropical volcanoes do (Liu et al., 2016).

The response of the poleward jet shift to volcanic eruptions is highly uncertain in both hemispheres (Barnes et al., 2016; Driscoll et al., 2012; Marshall et al., 2009; McGraw et al., 2016; Roscoe and Haigh, 2007), indicative of the role of internal variability (DallaSanta et al., 2019). Data for six major eruptions in the last century corroborated by CMIP5 historical experiments indicate that volcanic eruptions cause a detectable decrease in streamflow in northern South America, central Africa, high-latitude Asia and in wet tropical-subtropical regions, and a detectable increase in southwestern North America and southern South America (Iles and Hegerl, 2015). This signature seems to emerge from the direct radiative impact of volcanic eruptions, leading to a global cooling of the surface ocean (Swingedouw et al., 2017). A more thorough assessment of the water cycle response to volcanic forcing will be soon possible with CMIP6 models (Zanchettin et al., 2016), but volcanic eruptions will always be an irreducible source of uncertainty in near-term climate projections since they cannot be predicted in advance. Random eruptions have not been considered in CMIP5 and CMIP6 global projections. From a risk assessment perspective, it is a reasonable assumption as long as volcanic aerosols compete with anthropogenic GHG forcings. A possible exception is the occurrence of regional drought which may be enhanced by both volcanic (Gao and Gao, 2017; Liu et al., 2016; Zambri et al., 2017) and GHG (e.g., Cook et al., 2018)forcings (*medium confidence*).

Volcanic eruptions are sometimes considered as a natural analogue for understanding and constraining the climate response to solar radiation management (SRM) techniques (Plazzotta et al., 2018). Solar geoengineering consists of a deliberate reduction in the amount of solar radiation retained by the Earth and are aimed at mitigating global warming rather than or in addition to atmospheric CO2 emissions (cf. Chapter 4). Global climate models are ultimately the only way to assess the efficacy of SRM techniques and their potential side-effects on the global water cycle. Different methods of SRM have been modelled to have different impacts on global and regional precipitation (Dagon and Schrag, 2016; Jackson et al., 2016; Kristjánsson et al., 2015; Niemeier et al., 2013). There is *low confidence* in the spatial distribution of changes in precipitation minus evaporation, at least in the tropics (Smyth et al., 2017). A non-linear behavior of the water cycle response has been noticed in some models, partly due to vegetation-climate interactions (Dagon and Schrag, 2016). Extreme precipitation events and dry day frequency would also likely be impacted by SRM (*low confidence*), though the impacts may be again sensitive to the method of implementation (Aswathy et al., 2015). Further details on the climate response to SRM and the related hydrological impacts are discussed in Chapter 4 (cf. cross-chapter box 4.X). Also, Section 8.6.3 provides an assessment of the implications of SRM in the framework of abrupt climate changes.

Even without SRM, high-mitigation scenarios aimed at reducing drastically the anthropogenic GHG emissions may lead to non-linearities in the global water cycle response. Although there is found to be a robust relationship between cumulative emissions of carbon dioxide and global mean surface temperature, precipitation is likely to continue to evolve after the cessation of emissions as a function of the direct radiative effect of CO2 (Zickfeld et al., 2012) which may cause a temporary increase in precipitation in the case of a period of negative emissions where the surface temperature lags the CO2 concentration (*medium confidence*). Such effects are more pronounced in "ramp-up/ramp-down" experiments conducted in some specific models, where CO2 forcing is linearly increased and then decreased. The multi-century timescales associated with ocean heat content (Solomon et al., 2009) implies persistence or growth of ocean temperature anomalies after the point at which concentrations are reduced, which when combined with a reduced direct radiative effect of CO2 is likely to produce a temporary acceleration of the global hydrological cycle during a period of concentration reduction (Wu et al., 2010). Although it has been demonstrated that the relationship between global mean temperatures and cumulative emissions in Earth System Models is relatively robust up to forcing levels which would be expected in a fossil-fuel intensive future (Leduc et al., 2015; Zickfeld et al., 2016), the scaling of precipitation with cumulative emissions over land shows inconsistent behaviour among models due to differences in surface hydrological and vegetation response to warming (Liddicoat et al., 2016; Zickfeld et al., 2012).

8.6 What is the potential for abrupt change?

In this report, *abrupt climate change* is defined as a severe shift in the global or regional climate that occurs faster than the rate of change of the forcing (see Chapter 1 and Glossary). Often, abrupt change arises from positive feedbacks in the climate system that cause the current state to become unstable. This class of abrupt change is called a "tipping point" (Lenton et al., 2008); i.e., a threshold that separates stable climate states. When tipping points are crossed, rapid change occurs until the system reaches a new steady state. The water cycle has several attributes with potential to produce abrupt change. Non-linear interactions between the ocean, atmosphere, vegetation cover and dust emissions can result in rapid shifts between wet and dry states. Albedo feedbacks can cause snowpack to abruptly decline, affecting regional water availability. Cessation of anthropogenic radiation management could also result in abrupt changes. We review these types of abrupt shifts below and assess the likelihood that they will occur by 2100 and/or 2300.

8.6.1 Abrupt water cycle responses to shifts in ocean circulation and sea ice

8.6.1.1 Response to a collapse of Atlantic Meridional Overturning Circulation

Multiple lines of evidence, including both paleoclimate reconstructions and simulations, suggest that a severe weakening or collapse of Atlantic Meridional Overturning Circulation (AMOC, see Glossary) causes rapid cooling in the Northern Hemisphere and abrupt and profound changes in the global hydrological cycle (Broccoli et al., 2006; Chiang and Bitz, 2005; Chiang and Friedman, 2012; Renssen et al., 2018). Deep water formation in the North Atlantic is dependent on a delicate balance of heat and salt fluxes; disruption in either of these factors due to melting ice sheets, a change in precipitation and evaporation, or ocean circulation can force AMOC to cross a tipping point (Lenton et al., 2008). During the last glacial transition, one such slowdown in AMOC – during the Younger Dryas event (12,800—11,600 years ago) – caused worldwide changes in precipitation patterns. These included a southwards migration of the tropical ITCZ (McGee et al., 2014b; Mohtadi et al., 2016; Peterson et al., 2000; Reimi and Marcantonio, 2016; Schneider et al., 2014; Wang et al., 2017c) and systematic weakening of the African and Asian monsoons (Cheng et al., 2016; Kathayat et al., 2016; Otto-Bliesner et al., 2014; Stager et al., 2011; Tierney et al., 2008; Wurtzel et al., 2018). Conversely, the Southern Hemisphere monsoon systems intensified (Ayliffe et al., 2013; Cruz et al., 2005; Stríkis et al., 2015). Drying occurred in Mesoamerica (Lachniet et al., 2013) while the North American monsoon system was largely unaffected (Bhattacharya et al., 2018). The mid-latitude region in North America was wetter (Grimm et al., 2006; Polyak et al., 2004; Voelker et al., 2015; Wagner et al., 2010), while Europe wasdrier(Genty et al., 2006; Rach et al., 2017). Overall, the global-scale hydroclimatic response to the Younger Dryas disruption in AMOC can be understood as an asymmetric response to changes in cross-equatorial heat transport (Chiang and Friedman, 2012; Kang et al., 2008). Climate model simulations are able to reproduce the large-scale features of the event (Liu et al., 2009b) (Figure 8.46).

These patterns of past change are relevant for future projections because climate models uniformly project that the AMOC will weaken substantially in response to greenhouse gas emissions (Bakker et al., 2016; Drijfhout et al., 2015; Golledge et al., 2019; Reintges et al., 2017; Weaver et al., 2012). Some observations and historical paleoclimate evidence suggest that an unusual slowdown in AMOC may already be happening (Caesar et al., 2018a; Rahmstorf et al., 2015; Thornalley et al., 2018) although formal attribution of this recent slowdown is stymied by the short length of in situ measurements and substantial multidecadal variability (Smeed et al., 2018). AR5 determined that it was *very likely* that AMOC would weaken over the 21st century, but *very unlikely* that AMOC would completely collapse. In this report, the likelihood of AMOC weakening is still considered to be *very likely* (see Chapter 9) and the likelihood of AMOC collapse by 2100 is considered *unlikely* (see Chapter 9). This slight change in confidence is due to new evidence suggesting that AMOC was too stable in CMIP5 simulations, and that collapse is possible under high-emissions scenarios, if meltwater from the Greenland ice sheet is included and if the projections are extended to 2300 (Bakker et al., 2016; Liu et al., 2017; Sgubin et al., 2017).

[START FIGURE 8.46 HERE]

Figure 8.46: (a) Model simulation of precipitation response to the Younger Dryas event, relative to the preceding warm Bølling-Allerød period (base colors, from the TraCE paleoclimate simulation of (Liu et al., 2009b)), with paleoclimate proxy evidence superimposed on top (dots, see Technical Annex II). (b) Model simulation of precipitation response to an abrupt collapse in AMOC under a doubling of CO_2 (after (Liu et al., 2017)). Regions with rainfall rates below 20 mm/year are masked.

[END FIGURE 8.46 HERE]

The response of precipitation to hypothetical AMOC collapse under elevated greenhouse gases (Liu et al., 2017) mimics the paleoclimate response during the Younger Dryas, with some important differences due to effects of increased CO_2 on global precipitation patterns (Figure 8.6). As with the paleoclimate events, AMOC collapse results in cooling in the Northern Hemisphere and a southward shift in the ITCZ that is most pronounced in the tropical Atlantic (Figure 8.6.1b). This could cause drying in the Sahel region (Defrance et al., 2017) as well as Mesoamerica and northern Amazonia (Chen et al., 2018e; Parsons et al., 2014). AMOC collapse also causes the Indian and Asian monsoon systems to weaken (Liu et al., 2017)(Figure 6.1) counteracting the strengthening expected in response to elevated greenhouse gases (see Section 8.4). Europe is projected to experience moderate drying in response to AMOC collapse (Jackson et al., 2015).

Although AMOC is bi-stable, such that rapid (decadal or less) changes are theoretically possible (Rahmstorf, 1995; Stommel, 1961) in model simulations AMOC shutdown occurs more gradually across a time period of about 50-100 years (Bakker et al., 2016; Golledge et al., 2019; Liu et al., 2017; Rind et al., 2018). Abrupt melting events from the Greenland ice sheet, however, could produce a faster change, e.g. on the order of a decade (Defrance et al., 2017). The atmosphere responds very quickly to the change in heat transport associated with AMOC weakening (Chiang and Friedman, 2012), so abrupt collapse in AMOC would translate to abrupt changes in the water cycle. By the definition in this report, AMOC collapse is irreversible because the recovery timescale is longer than the timescale associated with the collapse. However, model projections run out to over 1,000 years in the future suggest that AMOC shutdown and associated water cycle responses can eventually reverse and could do so abruptly. Global warming slowly heats the deep ocean until the stratification in the North Atlantic is destabilized, at which point AMOC restarts, aided by positive feedbacks in heat and salt transports (Rind et al., 2018). This behavior is analogous to the rapid AMOC recoveries during the last deglaciation (McManus et al., 2004).

Given large inter-model uncertainties regarding collapse, and uncertain estimates of Greenland ice sheet melting, it is *unlikely* that an AMOC-driven abrupt change in the water cycle will occur by 2100, but *about* *as likely as not* (*low confidence*) that such a change could occur by 2300 under a high-emissions greenhouse gas scenario. If AMOC collapse does occur, it is *very likely* (*high confidence*) that there would be large regional impacts on the water cycle.

8.6.1.2 Response to sea ice retreat

The rapid loss of summer sea ice in the Arctic was identified as an abrupt change in the AR5, the SR15 and the SROCC. The severity of the loss of sea ice extent and volume is however scenario-dependent. A global warming of 2°C would result in much more frequent ice-free Arctic summers than would be likely to occur in a 1.5°C warmer world (SR15, section 3.3.8, AR6 Chapter 9.3). The SR15 gave *medium confidence* of at least one sea ice-free Arctic summer after about 10 years of stabilized warming at 2°C, while about 100 years are required at 1.5°C.

Around the Antarctic, there is considerable regional interannual variability and the magnitude of overall trends is small in comparison (Jones et al., 2016) and not statistically significant (AR6 Chapter 9.3). There is currently *low confidence* in Antarctic sea ice projections (SR15, Section 3.3.8, AR6 Chapter 9.3). At both poles, there is *high confidence* that sea ice recovery would occur relatively rapidly if global temperatures were decreased (e.g., by deployment of large-scale negative-emissions technology), thus sea ice retreat is considered a reversible abrupt change.

Abrupt sea ice retreat affects the water cycle by modifying surface moisture fluxes in polar regions and altering meridional temperature gradients and thus mid-latitude circulation. Specific impacts on storm tracks and moisture fluxes are still contentious (Overland et al., 2015). The SROCC assesses that there is *low confidence* associated with the effects of Arctic sea ice loss on mid-latitude storm behaviour.

There is evidence from the paleoclimate record that abrupt loss of Arctic sea ice causes rapid temperature change over Greenland, and associated changes in regional precipitation (Sime et al., 2019). Recent work on summertime effects, when Arctic sea ice loss is more marked, suggest that rapid loss of sea ice is associated with increased mid-latitude drying. A reduced meridional temperature gradient is associated with weaker westerly jet streams, lower baroclinicity and weaker storm tracks in the mid-latitudes, leading to reduced poleward moisture fluxes and precipitation on the poleward side of the storm track. At the same time, wave amplitude increases in a weaker background flow, associated with longer-lived anticyclonic conditions and increased surface evaporation and heating over land (Coumou et al., 2018). Both effects are associated with drying in mid-latitude regions of the Northern Hemisphere in summer. However, there is *low confidence* that rapid loss of Arctic sea ice leads to mid-latitude drying as there are many uncertainties and large natural variability in the chain of dynamical responses and effects. There is also considerable disagreement between model simulations of these effects (Deser et al., 2015; J.Vavrus, 2018).

8.6.2 Abrupt water cycle responses to changes in the land surface

Changes in the terrestrial land surface – including vegetation cover, the cryosphere (snow and ice), and dust emissions – can all trigger abrupt changes in the water cycle. Plants regulate the exchange of water and energy between the terrestrial land surface and the atmosphere by shifting the balance between latent and sensible heat flux, modifying near surface humidity, and altering albedo (Swann, 2018) (see Section 8.2). Sudden shifts in plant functions, types, or biomes can thus trigger positive vegetation-atmosphere feedbacks that have the potential to cause abrupt changes in the regional water cycle. Elevated greenhouse gas emissions are *very likely* to cause regional declines in snowpack due to increased temperatures (see Chapter 9). When snowpack levels dip below a certain level, non-linear reduction in streamflow or groundwater availability may occur. Finally, dust emissions, that arise from either climatic or land use changes, affect the radiation budget and can regionally exacerbate hydroclimatic extremes. Below, we assess the likelihood of abrupt changes in the water cycle for several regions where vegetation-precipitation feedbacks are relatively well studied (the Amazon and the Sahel). We then focus on snowpack projections in key regions, and whether tipping points in water availability are projected, and we discuss observed and projected impact of dust on abrupt change.

8.6.2.1 Amazon deforestation and drying

Rapid alterations in forest cover, due to climate-induced changes in water availability and/or anthropogenic factors, have the potential to result in large regional changes in the water cycle. The Amazon forest is a potential hotspot for abrupt change because its vulnerability to both deforestation and drought is projected to increase by 2100. Observational analyses indicate a strengthening of the Amazonian dry season during the last three decades (Arias et al., 2015a; Debortoli et al., 2015; Fu et al., 2013).This trend is projected to continue towards the end of the 21st century in response to elevated greenhouse gases (Boisier et al., 2015). [*insert statement here about CMIP6 vs. CMIP5 results]*. At the same time, the Amazon basin is likely to continue to experience deforestation; a worst-case scenario has projected a 47% loss by 2050 (Soares-Filho et al., 2006).

Recent work suggests that anthropogenic deforestation, acting in combination with climate change, could result in an abrupt shift in the water cycle in Amazon basin, with large consequences for regional hydrology and water availability (e.g., Salazar et al. 2018). Anthropogenic deforestation in the Amazon reduces evapotranspiration and increases albedo (Davidson et al., 2012; Spracklen et al., 2012), raising the possibility of catastrophic fires (Brando et al., 2014). Both of these factors can push the rainforest ecosystem across a tipping point, beyond which there is rapid land surface degradation, a sharp reduction in moisture recycling, and therefore a shift towards a drier climate (Zemp et al., 2017). Regional climate model experiments confirm that increased deforestation leads to a drier climate, although not all models show a true tipping point, at least under present-day climatic conditions (Lejeune et al., 2015; Spracklen and Garcia-Carreras, 2015). When climate change and deforestation are combined, the theoretical possibility of abrupt change increases. Tree cover modeling suggests that there are two stable states for the Amazon – a forest state and a savanna state (Staal et al., 2015). A moderate decline in precipitation (20%) combined with simultaneous deforestation (ca. 30%) is sufficient to push the system across the threshold and cause an abrupt shift to a savanna state through due to the combined impact of drought and deforestation on fire intensity (Staal et al., 2015).

The Amazon forest plays an active role in driving atmospheric moisture transport and the generation of precipitation in the region, as transpiration provides latent heat that feeds the development of precipitation (Agudelo et al., 2018; Drumond et al., 2014; Makarieva et al., 2013; Molina et al., 2019; Wright et al., 2017; Yin et al., 2014a). Boers et al., (2017 proposed that this aspect of forest-water cycle interaction may also lead to a tipping point in response to deforestation. They find that once Amazon deforestation is extensive enough to reduce transpiration, and thus atmospheric moisture, beyond the point where there is no enough latent heat released to maintain water vapor transport from the Atlantic Ocean, a rapid shift to dry climate state occurs.

In AR5, some simulations using a coupled climate-carbon cycle model exhibited an abrupt dieback of the Amazon forest in future climate scenarios (Cox et al., 2004; Malhi et al., 2008; Oyama and Nobre, 2003). However, subsequent work demonstrated that abrupt Amazon dieback does not occur consistently across, or even within, Earth system models (Boulton et al., 2017; Lambert et al., 2013). The occurrence of dieback is highly dependent on both how dry the simulated climate is in the present day (Malhi et al., 2009) as well as the representation of forest structure and competitive dynamics (Levine et al., 2016). Models with a low diversity of plant characteristics and types have a higher propensity for abrupt change (Sakschewski et al., 2016). Furthermore, abrupt shifts and ecosystem disruptions could occur on the sub-regional level (Pires and Costa, 2013), and therefore would necessitate much higher-resolution modeling studies. Since AR5, interactive terrestrial ecosystems have been added to most Earth System models, including simultaneous dynamic representations of terrestrial carbon cycling, plant growth, and stomatal conductance (Bonan and Doney, 2018). Despite these improvements in land surface simulation, CMIP6 projections of abrupt changes in the Amazon continue to be highly dependent on model biases in precipitation and the simulation of the land surface, meaning that the timing, and probability, of an abrupt shift remains difficult to ascertain.

[NOTE: *placeholder pending CMIP6 results*]. Therefore, while there is a strong theoretical expectation that Amazon drying and deforestation can cause a rapid change in the regional water cycle, it is *about as likely as not* that such a change will occur by 2100.

8.6.2.2 Greening of the Sahara and the Sahel

Greening of the Sahara and Sahel regions in North Africa has long been considered a source of abrupt precipitation change. Although the high surface albedo of the desert stabilizes the energy balance of the system (Charney, 1975), greening can induce strong, positive feedbacks between the land surface and precipitation that can shift the region into a "Green Sahara" state. The fact that the transition phase between a Desert Sahara and Green Sahara is not theoretically stable (Brovkin et al., 1998) creates a tipping point and allows for the possibility of an abrupt shift between dry and wet climate regimes. Paleoclimate reconstructions provide evidence of past "Green Sahara" states (deMenocal and Tierney, 2012), under which rainfall rates increased by an order of magnitude (Tierney et al., 2017), leading to a vegetated landscape (Jolly et al., 1998) with large lake basins (Drake and Bristow, 2006; Gasse, 2000). The "Green Saharas" of the past occurred periodically for at least the last 9 million years (deMenocal, 1995) with the most recent one occurring 11,000—5,000 years ago. The underlying driver of the Green Sahara is the 10,000-year periodic increase in summer insolation associated with the orbital precession cycle (Kutzbach, 1981) of about 20 W m^{-2} (deMenocal and Tierney, 2012). In this sense, the past Green Saharas are not direct analogs for a response to greenhouse gas emissions, as they were forced by seasonal changes in shortwave radiation. However, the dynamics of past Green Saharas, and the speed of the transitions between Desert Saharas and Green Saharas, are potentially relevant for future projections.

The paleoclimate record suggests that transitions between Desert and Green Sahara are always faster than the underlying forcing, in agreement with theoretical considerations (*high confidence*) (deMenocal et al., 2000; Kröpelin et al., 2008; Shanahan et al., 2015; Tierney et al., 2017; Tierney and deMenocal, 2013). This meets the definition of abrupt change in this report, but the exact speed of the transition is unclear because sedimentary records cannot typically resolve change on these timescales (Tierney and deMenocal, 2013). The paleoclimate record also suggests that the timing and speed of the transition is spatially heterogeneous (*high confidence*). At some locations, the termination of the last Green Sahara at around 5,000 years ago occurred within centuries or less (deMenocal et al., 2000; Tierney et al., 2017; Tierney and deMenocal, 2013) but in others it appears to be more gradual (Kröpelin et al., 2008). This last transition was also time-transgressive, with northern Saharan locations transitioning to Desert Sahara thousands of years before more equatorial locations (Shanahan et al., 2015; Tierney et al., 2017). These observations are consistent with theoretical studies suggesting that spatial heterogeneity and diversity in ecosystems can mitigate the probability of catastrophic change (Claussen et al., 2013; Van Nes and Scheffer, 2005). Conversely, low ecosystem diversity can produce local or regional "hot spots" of abrupt change such as those seen in some paleoclimate records (Bathiany et al., 2013).

CMIP5 models**,** some of which include dynamic vegetation schemes, cannot simulate the magnitude, nor the spatial extent, of greening and precipitation change associated with the last Green Sahara under standard mid-Holocene (6 ka) boundary conditions (*high confidence*) (Harrison et al., 2014; Tierney et al., 2017), suggesting that the strength of the feedbacks between vegetation and the water cycle in the models is too weak (Hopcroft et al., 2017). *[Insert statement here about the performance of CMIP6 models for 6 ka]*. To date, climate models only reproduce Green Sahara conditions if they are given prescribed changes in the land surface, such as changes in surface albedo, soil moisture, vegetation cover and/or dust emissions (Bartlein et al., 2011; Claussen et al., 1999; Levis et al., 2004; Pausata et al., 2016; Peyron et al., 2006; Skinner and Poulsen, 2016; Tierney et al., 2017).

Some climate model simulations suggest that under future high-emissions scenarios, CO_2 forcing causes rapid greening in the Sahel and Sahara regions, analogous to the Green Saharas of the past, albeit in response to longwave rather shortwave forcing (Claussen et al., 2003; Drijfhout et al., 2015). In the RCP8.5 simulation of BNU-ESM, the change is abrupt – the percentage of bare soil drops from 45% to 15%, and percentage of tree cover rises from 50% to 75%, within 10 years (2050-2060) (Drijfhout et al., 2015). However, other modelling results suggest that this may be a short-lived response to CO_2 fertilization, and that in the longer term, declining precipitation in the Sahara and Sahel leads to aridification and reduced land cover (Bathiany et al., 2014).

[START FIGURE 8.47 HERE]

[*Add in any relevant results from CMIP6 future scenarios*]

Figure 8.47: Examples of abrupt changes in plant cover, precipitation, aridification in future model projection scenarios from CMIP6 [*TBD, if these occur*]

[END FIGURE 8.47 HERE]

Given outstanding uncertainties in how well the current generation of climate models capture land-surface feedbacks in the Sahel and Sahara, there is *low confidence* that an abrupt change in the water cycle will occur in these regions before 2100 or 2300. However, both the paleoclimate record and individual modelling results suggest that the possibility of abrupt change cannot be ruled out.

8.6.2.3 Tipping points in snowpack and snow water equivalent

Climate change has already caused large declines in snowpack extent and snow water equivalent in many regions of the world, and these declines are projected to continue. As snow cover decreases, local albedo decreases, which results in an increase in the amount of solar energy absorbed at the surface and the potential for nonlinear feedback. This snow-albedo feedback does not appear to be a key factor globally but can be important regionally (Thackeray and Fletcher, 2016b).

In terms of the potential for future abrupt changes, analysis of CMIP5 projections by (Drijfhout et al., 2015) identified the Tibetan plateau as a region where some models project large and rapid changes in snow volume for the higher emission scenarios – locally, up to an eightfold decrease in less than 20 years. While the specific parameterizations and resolution of these models may partly account for the abrupt shift, the changes appear to be due to a physically-reasonable regime-change to a negative annual snow mass flux balance. These temperature-related changes are potentially complicated by carbon soot emissions, which, while resident in the atmosphere, can reduce the incoming solar radiation and so oppose the melting effects of temperature, or, when deposited on the snow, can dramatically reduce albedo and so enhance the melting effects of temperature (e.g., (Ramanathan and Carmichael, 2008). [*Note: further assessment regarding the probability of abrupt changes in snow and/or SWE await CMIP6 results*].

[START FIGURE 8.48 HERE]

[*up on availability from CMIP6 results*].

Figure 8.48: Abrupt snowpack/SWE changes for select regions (Sierra Nevada, Andes, Himalaya?) for the CMIP6 high-emissions scenario [*TBD, if these occur*].

[END FIGURE 8.48 HERE]

8.6.2.4 Amplification of drought by dust

Mineral dust aerosols in the climate system originate from both semi-permanent and transient sources (Ginoux et al., 2012; Prospero et al., 2002). The former are typically dried lake beds in arid regions where significant alluvial sediments have accumulated over time, while the latter are often associated with natural (e.g., droughts, wildfires) and anthropogenic (e.g. land use change, desertification) disturbances. Modern-day dust emissions are dominated by natural (75%) sources (Ginoux et al., 2012), with human emissions estimated to contribute 10—60% of the global atmospheric dust load (Webb and Pierre, 2018). Paleoclimate records, however, suggest that human factors (land use change and landscape disturbance) may have doubled global dust emissions since 1750 CE (Hooper and Marx, 2018).

Dust aerosols influence the climate system and hydrologic cycle through both direct impacts on radiation (absorbing and scattering longwave and shortwave) and via indirect effects on cloud and precipitation processes (Choobari et al., 2014; Schepanski, 2018). Broadly speaking, dust aerosols suppress precipitation by reducing droplet size and increasing cloud lifetimes (Rosenfeld et al., 2002) and by reducing humidity and energy availability and increasing stability in the atmosphere (Cook et al., 2013; Huang et al., 2014).There is therefore strong potential for dust feedbacks to contribute to abrupt changes in the water cycle, especially in semi-arid regions where wind erosion is highly sensitive to vegetation cover and drought variability (Yu et al., 2015). One such event occurred over the Central United States during the 1930s: the Dust Bowl drought, an iconic event characterized by widespread land degradation and historically unprecedented levels of dust storm activity (Hansen and Libecap, 2004; Lee and Gill, 2015). While initialized by modest ocean forcing, modeling work indicates that the dust storms that occurred amplified the drought by further suppressing precipitation over much of the region during the warm season (Cook et al., 2009). Similar evidence for the amplifying effect of dust on drought in this region has also been found for the Medieval-era megadroughts, multi-decadal long droughts that are difficult to attribute solely to ocean-atmosphere variability (Cook and Seager, 2013). As noted above, there is increasing evidence that dust aerosol feedbacks (along with vegetation and other land surface feedbacks) are a necessary component to explain the relatively abrupt transitions into and out of the Green Sahara period during the mid-Holocene (Pausata et al., 2016; Tierney et al., 2017).

The importance of dust aerosol feedbacks in future abrupt climate events, like droughts or rapid aridification, is unclear. In part, this is because the response of dust aerosol emissions and loading levels in the atmosphere to climate change is highly uncertain (Tegen and Schepanski, 2018; Webb and Pierre, 2018). This difficulty in predicting future dust responses is rooted in the fact that emissions depend on both changes to the land surface (e.g., land use/land cover change, desertification, ecological responses to climate change) and the state of the atmosphere (Tegen and Schepanski, 2018). There is some evidence that global dust aerosol concentrations in the future will increase as a consequence of decreased precipitation over land (Tegen and Schepanski, 2018), but such a broad generalization can obscure potentially important regional responses. For example, amplified warming over North Africa may weaken winds over the region, decreasing emissions from some of the most important global sources of dust (Cook and Vizy, 2015). There is thus *low confidence* in any conclusions regarding the role of dust in abrupt climate change events over the next century.

8.6.3 Abrupt water cycle responses to initiation or termination of radiation management

Radiation management (RM) techniques seek to reduce the impacts of climate change by either reflecting a small fraction of incoming solar radiation (solar radiation management; SRM) or increasing the amount of heat lost to space (longwave radiation management; LRM). A variety of methods have been proposed, including injection of aerosols or their precursors into the stratosphere, cloud brightening, and cirrus cloud thinning (see Table XX in Chapter 4). Since SRM alters the planetary energy balance, changes in the hydrological cycle are expected (see Section 8.2). These changes can be abrupt if the initial magnitude of RM is large (rather than gradually increased). Since AR5, a larger diversity of RM techniques has been tested with climate model simulations, with an increasing focus on consequences for regional water availability. SRM techniques (sulfate injection, surface albedo modification, cloud brightening) are very likely to reduce global mean precipitation (high confidence) relative to future CO_2 emissions scenarios (Bala et al., 2008; Crook et al., 2015; Ferraro et al., 2014; Jones et al., 2013a; Tilmes et al., 2013).

In contrast, cirrus cloud thinning, a LRM technique, results in increased global precipitation because it causes enhanced cooling in the troposphere (*high confidence*) (Crook et al., 2015; Jackson et al., 2016; Kristjánsson et al., 2015). Under abrupt RM implementation, hydrological shifts are rapid, occurring within the first decade (Crook et al., 2015). On a regional and seasonal level, the response of the water cycle varies widely and is also dependent on which RM technique is used. Broadly speaking, the largest changes occur in the tropics. Artificial enhancement of albedo in desert regions causes a southwards shift in the Hadley cell and ITCZ and extreme drying in the northern tropics (Crook et al., 2015). Stratospheric sulfate injection weakens the African and Asian summer monsoons but also shifts the Hadley cell northwards (especially over the ocean) and causes drying in the Amazon (Crook et al., 2015; Dagon and Schrag, 2016; Robock et al., 2008). Changes in evapotranspiration lead to strong regional non-linearities, producing large deficits or surpluses in soil moisture and runoff in different regions and seasons (Dagon and Schrag, 2016). Crucially, such non-linearities mean that RM-induced changes in the water cycle cannot directly compensate for changes caused by elevated CO_2 (*medium confidence*) (Crook et al., 2015; Dagon and Schrag, 2016, 2019).

Rapid changes in the hydrological cycle are also expected if SRM is terminated abruptly, either purposefully or because of technical failure or political disagreement. We reiterate the AR5 conclusion that, if RM "were terminated for any reason, there is high confidence that surface temperatures would increase rapidly (within a decade or two) to values consistent with the GHG forcing." The additional global warming due to RM termination would very likely cause a rapid increase in global mean precipitation (*high confidence*) (Jones et al., 2013). Heterogenous regional and seasonal changes are also expected, but are model-dependent (Jones et al., 2013a) thus there is *low confidence* in regional-level projections for the effects of RM termination. As with RM initiation, the impact of RM termination is expected to be method-dependent.

Although the magnitude of hydrological disruption for both initiation and termination of RM will depend on the strength and duration of the RM implementation and on the underlying mitigation scenario (Ekholm and Korhonen, 2016; Irvine et al., 2019), it is very likely that abrupt water cycle changes will occur if strong RM is abruptly initiated or halted, especially in tropical regions. More details on the potential side-effects of RM can be found in Chapter 4.

8.7 Key knowledge gaps

- Most observational time series of water cycle components are short, and some components are poorly observed (e.g. groundwater, streamflow, snow cover). Development of pre-instrumental data, via data rescue and interpretation of paleoclimate proxies, is a priority. Our knowledge of how the water cycle responded in past high CO_2 climates remains limited; improved reconstructions from warm times during the Cenozoic Era, for example, would provide guidance on what to expect in the future.

- The lack of homogeneous long-term records and reanalyses and the poorly-understood but strong internal variability of most hydrological variables make the detection of observed water cycle changes difficult at the regional scale. Development of longer observational time series, improved simulation of internal modes, and the creation of large ensembles of simulations will aid in the detection of forced trends.

- While global-scale responses to future emissions are qualitatively robust, regional-scale projections vary widely due in part to poor representation in models of precipitation-forming processes and the effects of aerosols on them, land surface feedbacks, and other boundary layer processes. Efforts to develop high-resolution "cloud-resolving climate models" will likely improve model representation. Observing campaigns combined with laboratory-scale and theory-based research are needed to improve our understanding of cloud-aerosol effects and important surface feedbacks.

- Anthropogenic aerosol radiative forcing has a strong influence on the water cycle which can occur far away from the emission sources. Therefore, its magnitude and time variations remain very uncertain and are a major obstacle for the attribution of hydrological changes across the 20th and their projection through the 21st century.

- Water cycle responses tend to be non-linear, such that pattern-scaling does not always encompass the possible range of future changes, especially as the magnitude of climate change increases.

- The potential for abrupt changes in the water cycle remains a major threat for global and regional freshwater resources, but is difficult to project or predict with certainty.

Frequently Asked Questions

FAQ 8.1: How does climate and land use change alter the water cycle?

Components of the surface energy balance and surface water balance are altered with land use change. In particular, land use changes lead to changes of precipitation, evapotranspiration, infiltration, and groundwater recharge, modifying the water cycle and freshwater availability.

Land use changes induce alterations in the water cycle. For example, when changing the surface from any type of vegetation cover to an urban cover, also changes the *surfacealbedo* (i.e., the property of the surface, or any object, to reflect solar radiation). By changing the amount of reflected solar radiation, we alter the *surface energy balance* (i.e., the difference between incoming radiation and outgoing radiation). Hence if the capacity of the surface to reflect solar incoming radiation decreases, the energy balance becomes positive, warming the surface. Changes in surface cover also induce modifications in soil infiltration, altering the *surface water balance* (i.e., the difference between precipitation and the total amount of evaporation, ground storage and surface runoff). When soil losses its capacity to infiltrate water, more precipitation can become in runoff. This implies that the water that would normally contribute to groundwater recharge will now overflow, enhancing the probability of flash floodings.

Changes in soil moisture content can also modify the surface thermal contrast. Water retained in the porous of the soil layers allows for heat to be stored during the day, which is gradually released during the night, inducing warming. Whereas if soil moisture is lower than normal or null then the heat stored will be less and it will also be released much quicker. This alters the energy budget, as the *sensible heat* (i.e. a conductive flux of heat) and *latent heat* (i.e. turbulent flux associated with a phase change of water: evaporation or condensation) changes. Warming induces evaporation and therefore cooling of the surface. By cooling down the surface, there is a stabilization of the *surface boundary layer*. This stabilization prevents deep convective activity, altering the occurrence of precipitation, which may, in turn, modify the water surface balance, reducing precipitation.

There is another factor to be considered in land use change: it increases the amount of aerosols in the atmosphere. *Aerosols* play a rather complex role in weather and climate, but regarding water cycle, they have at least three important effects. First, aerosols modulate the rate of conversion of cloud water to precipitation; since aerosols serve as *condensation nuclei* on which water molecules can adhere and grow until reaching a weight large enough to precipitate, then aerosols can modify the water balance. Second, aerosols have a cooling effect by scattering and absorbing solar radiation. Third, aerosols can modify cloud optical properties, altering the surface energy balance.

Even when land use change implies shifting from one vegetation cover to another (for example, deforestation for agricultural uses), surface albedo is altered as each type of vegetation has a different albedo, modifying the surface energy balance. But not only surface albedo varies with vegetation changes. The water balance gets also modify as vegetation also play an important role by transpiration and capturing CO_2 (stomatal reaction). Recent studies over extensive irrigation areas exhibit a reduction on the surface temperature.

Due to the complexity of the interactions between the different land surface processes, there are large uncertainties when determining the net effect of land use change on the water cycle; however, there is abundant evidence that shows that land use change can alter both the surface energy and water balance, ultimately endangering the availability of freshwater.

FAQ 8.2: Should we expect more severe floods from climate change, and why?

Flooding presents a hazard when it affects human activities and infrastructure. A warming climate will increase the amount and intensity of rainfall during wet events that is expected to contribute to an increased severity of flooding. However, the link between rainfall and flooding is not simple and so while the largest flooding events can be expected to worsen, flood occurrence may decrease in some regions.

Flooding describes a temporary accumulation of water on the land surface that may result from rivers overtopping their banks or a more local build-up where the influx of water exceeds outflow. This natural and important part of the water cycle causes harm where it affects human activities and infrastructure. As climate changes, the location, occurrence and severity of flooding are likely to alter. Sea level rise due to expanding of the ocean and melting of ice sheets as climate warms worsens coastal flood risk and this can combine with flooding from heavy rainfall.

Flooding is usually caused by a rapid influx of water supplied by heavy and often sustained rainfall events that are expected to become more severe in a warming climate. As the air near Earth's surface warms it carries around 7% more water in its gas phase (vapour) for each ºC rise in temperature on average. This extra moisture is drawn in to weather systems, fueling heavier rainfall. Rainfall intensity can be further amplified by extra heat released through condensing of water vapour into droplets thus energizing storm systems. On the other hand, this energy release and also the effects of pollution can inhibit uplift required for cloud development over larger time and space scales. This means that the character of precipitation is expected to alter as the climate warms. More intense but less frequent downpours can cause less of the rainfall to be soaked up by the ground and more to runoff into lakes, rivers and hollows. Changing wind patterns and the pathway that storms usually travel are a less well understood aspect of climate change and also vary a lot from one year to the next. This makes it difficult to observe that heavy rainfall events are increasing over many regions. An intensification of heavy rainfall in the future is simulated for most places though. It is therefore very likely that when and where extremely wet events or seasons occur, the rainfall amount will be greater, potentially contributing to more serious flooding.

The link between heavy rainfall and flooding is, however, not simple. Heavier rainfall does not always lead to greater flooding but depends upon the type of river catchment or surface landscape, how extensive, long lasting and intense the rainfall event is and also how wet the ground is before the rainfall event. Some regions may experience a drying in the soil, particularly in sub-tropical climates, which could make floods from a rainfall event less likely as the ground can potentially soak up more of the rain. Earlier spring snowmelt and associated flood events are likely in a warmer climate while in some regions reduced winter snow cover can decrease the chance of flooding associated with rain combined with rapid snowmelt. Observations of how high river flows have changed remain inconclusive yet flooding is projected to double in frequency over 40% of the globe by 2050, with the largest increases expected in Asia with decreases also projected in many regions. Future flood risk is also affected by changes in the management of the land and river systems and the location of where people live and work. Accounting for these many factors, there is an overall expectation that when weather patterns cause flood events, these will become more severe as the climate warms yet some regions will experience decreased flooding.

FAQ 8.3: What causes droughts, and will climate change make them worse?

Droughts are initially caused by a lack of precipitation, but then propagate to other parts of the water cycle (soils, rivers, and reservoirs). They can also be influenced by factors like temperatures, vegetation, and human management responses. In a warmer world, droughts will get worse in some regions and seasons, particularly in the arid subtropics. Other places may receive more precipitation, reducing the risk of drought.

A drought is broadly defined as drier than normal conditions; that is, a moisture deficit relative to the average water availability at a given location. Since they are locally defined, a drought in a wet place (like Brazil) will not have the same amount of water loss as a drought in a drier region (like Israel). Droughts are divided into different categories based on where in the water cycle the moisture deficit occurs: meteorological drought (precipitation), agricultural drought (soil moisture), and hydrological drought (runoff, streamflow, and reservoir storage) (see FAQ 8.3, Figure 1) Special categories of drought also exist. For example, a snow drought occurs when snowpack levels over the winter are below average, leading to abnormally low streamflow in the spring. And while many drought events develop slowly over months or years, some events, called flash droughts, can intensify over the course of days or weeks. One such event occurred in 2012 in the US Midwest and had a severe impact on agricultural production, with losses exceeding $30 billion dollars. Droughts typically only become a concern when they adversely affect people (reducing water available for municipal and industrial needs) and/or ecosystems (inhibiting growth of crops and natural vegetation). When a drought lasts for a very long time (more than two decades) it is sometimes called a megadrought. The opposite of a drought – a period of wetter than normal conditions – is called a pluvial.

[START FAQ 8.3, FIGURE 1 HERE]

FAQ 8.3, Figure 1: Clip-art style illustration of types of droughts.

[END FAQ 8.3, FIGURE 1 HERE]

Most droughts begin when precipitation is below normal for an extended period of time (meteorological drought). This typically occurs when high pressure in the atmosphere sets up over a region, inhibiting clouds and local precipitation and deflecting away storms. The lack of rainfall then propagates across the water cycle to create agricultural drought in soils and hydrological drought in waterways. Other processes act to amplify or ameliorate droughts. For example, if temperatures are abnormally high, evaporation increases, drying out soils and streams beyond what would have occurred just from the lack of precipitation. Vegetation can play a critical role because it modulates many important hydrologic processes (soil water, evapotranspiration, runoff). Human modifications also determine how severe a drought is. For example, irrigating croplands can reduce the impact of a drought; conversely, depletion of groundwater in aquifers can make a drought worse.

The impact of climate change on drought will vary across regions and seasons. Across the subtropics (e.g., the Mediterranean, southern North America, Central America, southern Africa, and southern Australia), precipitation is expected to decline as the world warms, increasing drought risk throughout the year. Some studies suggest that the risk of megadroughts in western North America will increase substantially. Warming will decrease snowpack, amplifying drought in regions where snowmelt is an important water resource (e.g. the western United States, and parts of south Asia and South America). Higher temperatures lead to increased evaporation, resulting in soil drying and agricultural drought, even in regions where large changes in precipitation are not expected (e.g., the central United States, and central and northern Europe). If emissions are not curtailed, about a third of global land areas are projected to suffer from at least moderate drought by 2100. On the other hand, some areas and seasons may experience increases in precipitation as a result of climate change (such as the humid mid- to high-latitudes, and the summer monsoon regions) which will decrease drought risk. FAQ 8.3, Figure 2 illustrates the projected effect of climate change on drought in different places.

[START FAQ 8.3, FIGURE 2 HERE]

FAQ 8.3, Figure 2: Global map with regions expected to experience more or less drought labeled in brown (more) and blue-green (less) (use colors from precipitation diverging palette). Recommend contour-hugging shading; mock up below is just for the general idea. Would need to ensure accuracy w/r/t both CMIP5 and CMIP6 results.

[END FAQ 8.3, FIGURE 2 HERE]

References

Abdel-Lathif, A. Y., Roehrig, R., Beau, I., and Douville, H. (2018). Single-Column Modeling of Convection During the CINDY2011/DYNAMO Field Campaign With the CNRM Climate Model Version 6. *J. Adv. Model. Earth Syst.* 10, 578–602. doi:10.1002/2017MS001077.

Abish, B., Joseph, P. V., and Johannessen, O. M. (2013). Weakening trend of the tropical easterly jet stream of the boreal summer monsoon season 1950-2009. *J. Clim.* 26, 9408–9414. doi:10.1175/JCLI-D-13-00440.1.

Abram, N. J., Mulvaney, R., Vimeux, F., Phipps, S. J., Turner, J., and England, M. H. (2014). Evolution of the Southern Annular Mode during the past millennium. *Nat. Clim. Chang.* 4, 564–569. doi:10.1038/nclimate2235.

Abramowitz, G. (2012). Towards a public, standardized, diagnostic benchmarking system for land surface models. *Geosci. Model Dev.* 5, 819–827. doi:http://dx.doi.org/10.5194/gmd-5-819-2012.

Abramowitz, G., Leuning, R., Clark, M., and Pitman, A. (2008). Evaluating the Performance of Land Surface Models. *J. Clim.* 21, 5468. Available at: https://doi.org/10.1175/2008JCLI2378.1.

Abtew, W., Melesse, A. M., and Dessalegne, T. (2009). El Niño Southern Oscillation link to the Blue Nile River Basin hydrology. *Hydrol. Process.*, n/a-n/a. doi:10.1002/hyp.7367.

Ackerley, D., Booth, B. B. B., Knight, S. H. E., Highwood, E. J., Frame, D. J., Allen, M. R., et al. (2011a). Sensitivity of Twentieth-Century Sahel Rainfall to Sulfate Aerosol and CO_2 Forcing. *J. Clim.* 24, 4999–5014. doi:10.1175/JCLI-D-11-00019.1.

Ackerley, D., Booth, B. B. B., Knight, S. H. E., Highwood, E. J., Frame, D. J., Allen, M. R., et al. (2011b). Sensitivity of Twentieth-Century Sahel rainfall to sulfate aerosol and CO2 forcing. *J. Clim.* 24, 4999–5014. doi:10.1175/JCLI-D-11-00019.1.

Adam, O., Schneider, T., Brient, F., and Bischoff, T. (2016). Relation of the double-ITCZ bias to the atmospheric energy budget in climate models. *Geophys. Res. Lett.* 43, 7670–7677. doi:10.1002/2016GL069465.

Adames, Á. F., Kim, D., Sobel, A. H., Del Genio, A., and Wu, J. (2017a). Changes in the structure and propagation of the MJO with increasing CO 2. *J. Adv. Model. Earth Syst.* 9, 1251–1268. doi:10.1002/2017MS000913.

Adames, Á. F., Kim, D., Sobel, A. H., Del Genio, A., and Wu, J. (2017b). Characterization of Moist Processes Associated With Changes in the Propagation of the MJO With Increasing CO 2. *J. Adv. Model. Earth Syst.* 9, 2946–2967. doi:10.1002/2017MS001040.

Adler, R. F., Gu, G., Sapiano, M., Wang, J.-J., and Huffman, G. J. (2017). Global Precipitation: Means, Variations and Trends During the Satellite Era (1979-2014). *Surv. Geophys.* 38, 679–699. doi:10.1007/s10712-017-9416-4.

Adler, R. F., Gu, G., Wang, J.-J., Huffman, G. J., Curtis, S., and Bolvin, D. (2008). Relationships between global precipitation and surface temperature on interannual and longer timescales (1979–2006). *J. Geophys. Res.* 113, D22104. doi:10.1029/2008JD010536.

Aerenson, T., Tebaldi, C., Sanderson, B., and Lamarque, J.-F. (2018). Changes in a suite of indicators of extreme temperature and precipitation under 1.5 and 2 degrees warming. *Environ. Res. Lett.* 13, 035009. doi:10.1088/1748-9326/aaafd6.

AghaKouchak, A., Feldman, D., Hoerling, M., Huxman, T., and Lund, J. (2015). Water and climate: Recognize anthropogenic drought. *Nat. News* 524, 409.

Agudelo, J., Arias, P. A., Vieira, S. C., and Martínez, J. A. (2018). Influence of longer dry seasons in the Southern Amazon on patterns of water vapor transport over northern South America and the Caribbean. *Clim. Dyn.* 0, 1–19. doi:10.1007/s00382-018-4285-1.

Aguirre, C., García-Loyola, S., Testa, G., Silva, D., and Farias, L. (2018). Insight into anthropogenic forcing on coastal upwelling off south-central Chile. *Elem Sci Anth* 6, 59. doi:10.1525/elementa.314.

Aires, F., Miolane, L., Prigent, C., Pham, B., Fluet-Chouinard, E., Lehner, B., et al. (2017). A global dynamic long-term inundation extent dataset at high spatial resolution derived through downscaling of satellite observations. Journal of Hydrometeorology. 18, 1305–1325.

Aires, F., Prigent, C., Fluet-Chouinard, E., Yamazaki, D., Papa, F., and Lehner, B. (2018). Comparison of visible and multi-satellite global inundation datasets at high-spatial resolution. Remote sensing of environment. 216, 427–441.

Akinsanola, A. A., and Zhou, W. (2018). Ensemble-based CMIP5 simulations of West African summer monsoon rainfall: current climate and future changes. *Theor. Appl. Climatol.* doi:10.1007/s00704-018-2516-3.

Alessandri, A., Catalano, F., De Felice, M., Van Den Hurk, B., Doblas Reyes, F., Boussetta, S., et al. (2017). Multi-scale enhancement of climate prediction over land by increasing the model sensitivity to vegetation variability in EC-Earth. *Clim. Dyn.* doi:10.1007/s00382-016-3372-4.

Alessandri, A., De Felice, M., Zeng, N., Mariotti, A., Pan, Y., Cherchi, A., et al. (2015a). Robust assessment of the expansion and retreat of Mediterranean climate in the 21 st century. *Sci. Rep.* 4, 7211. doi:10.1038/srep07211.

Alessandri, A., De Felice, M., Zeng, N., Mariotti, A., Pan, Y., Cherchi, A., et al. (2015b). Robust assessment of the expansion and retreat of Mediterranean climate in the 21stcentury. *Sci. Rep.* 4, 7211. doi:10.1038/srep07211.

Alfieri, L., Salamon, P., Bianchi, A., Neal, J., Bates, P., and Feyen, L. (2014). Advances in pan-European flood hazard mapping. Hydrol. *Process*, 28, 4067–4077.
Ali, A., and Lebel, T. (2009). The Sahelian standardized rainfall index revisited. *Int. J. Climatol.* 29, 1705–1714. doi:10.1002/joc.1832.
Ali, H., and Mishra, V. (2018). Increase in Subdaily Precipitation Extremes in India Under 1.5 and 2.0 °C Warming Worlds. *Geophys. Res. Lett.* 45, 6972–6982. doi:10.1029/2018GL078689.
Alkama, R., Marchand, L., Ribes, A., and Decharme, B. (2013). Detection of global runoff changes: Results from observations and CMIP5 experiments. *Hydrol. Earth Syst. Sci.* 17, 2967–2979. doi:10.5194/hess-17-2967-2013.
Allan, R. P., Liu, C., Zahn, M., Lavers, D. A., Koukouvagias, E., and Bodas-Salcedo, A. (2014). Physically Consistent Responses of the Global Atmospheric Hydrological Cycle in Models and Observations. *Surv. Geophys.* 35, 533–552. doi:10.1007/s10712-012-9213-z.
Allen, D. M., Whitfield, P. H., and Werner, A. (2010). Groundwater level responses in temperate mountainous terrain: Regime classification, and linkages to climate and streamflow. *Hydrol. Process.* 24, 3392–3412.
Allen, M. R., and Ingram, W. J. (2002). Constraints on future changes in climate and the hydrologic cycle. *Nature* 419, 224–232. doi:10.1038/nature01092.
Allen, R. J., and Ajoku, O. (2016). Future aerosol reductions and widening of the northern tropical belt. *J. Geophys. Res. Atmos.* 121, 6765–6786. doi:10.1002/2016JD024803.
Allen, R. J., Evan, A. T., and Booth, B. B. B. (2015). Interhemispheric aerosol radiative forcing and tropical precipitation shifts during the late Twentieth Century. *J. Clim.* 28, 8219–8246. doi:10.1175/JCLI-D-15-0148.1.
Allen, R. J., Hassan, T., Randles, C. A., and Su, H. (2019). Enhanced land–sea warming contrast elevates aerosol pollution in a warmer world. *Nat. Clim. Chang.* 9, 300–305. doi:10.1038/s41558-019-0401-4.
Allen, R. J., Kovilakam, M., Allen, R. J., and Kovilakam, M. (2017). The Role of Natural Climate Variability in Recent Tropical Expansion. *J. Clim.* 30, 6329–6350. doi:10.1175/JCLI-D-16-0735.1.
Allen, R. J., and Landuyt, W. (2014). The vertical distribution of black carbon in CMIP5 models: Comparison to observations and the importance of convective transport. *J. Geophys. Res.* 119, 4808–4835. doi:10.1002/2014JD021595.
Allen, R. J., Norris, J. R., and Kovilakam, M. (2014). Influence of anthropogenic aerosols and the Pacific Decadal Oscillation on tropical belt width. *Nat. Geosci.* 7, 270–274. doi:10.1038/ngeo2091.
Allen, R. J., Sherwood, S. C., Norris, J. R., and Zender, C. S. (2012). Recent Northern Hemisphere tropical expansion primarily driven by black carbon and tropospheric ozone. *Nature* 485, 350–354. doi:10.1038/nature11097.
Almeida, A. C. ., Oliveira-Júnior, J. F., Delgado, R. C., Cubob, P., and Ramos, M. C. (2017). Spatiotemporal rainfall and temperature trends throughout the Brazilian Legal Amazon, 1973–2013. *Int. J. Climatol.* 37, 2013–2026.
Alter, R. E., Im, E. S., and Eltahir, E. A. B. (2015). Rainfall consistently enhanced around the Gezira Scheme in East Africa due to irrigation. *Nat. Geosci.* 8, 763–767. doi:10.1038/ngeo2514.
Alvarez, M., Vera, C., and Kiladis, G. (2017). MJO Modulating the Activity of the Leading Mode of Intraseasonal Variability in South America. *Atmosphere (Basel).* 8, 232. doi:10.3390/atmos8120232.
Andreae, M. O., Rosenfeld, D., Artaxo, P., Costa, A. A., Frank, G. P., Longo, K. M., et al. (2004). Smoking rain clouds over the Amazon. *Science (80-.).* 303, 1337–1342.
Andrews, T., Forster, P. M., Boucher, O., Bellouin, N., and Jones, A. (2010). Precipitation, radiative forcing and global temperature change. *Geophys. Res. Lett.* 37, n/a--n/a. doi:10.1029/2010GL043991.
Andrews, T., Gregory, J. M., and Webb, M. J. (2015). The dependence of radiative forcing and feedback on evolving patterns of surface temperature change in climate models. *J. Clim.* 28, 1630–1648. doi:10.1175/JCLI-D-14-00545.1.
Andrys, J., Kala, J., and Lyons, T. J. (2017). Regional climate projections of mean and extreme climate for the southwest of Western Australia (1970–1999 compared to 2030–2059). *Clim. Dyn.* 48, 1723–1747. doi:10.1007/s00382-016-3169-5.
Apaéstegui, J., Cruz, F. W., Sifeddine, A., Vuille, M., Espinoza, J. C., Guyot, J. L., et al. (2014). Hydroclimate variability of the northwestern Amazon Basin near the Andean foothills of Peru related to the South American Monsoon System during the last 1600 years. *Clim. Past* 10, 1967–1981. doi:10.5194/cp-10-1967-2014.
Arakawa, A., and Schubert, W. H. (1974). Interaction of a cumulus cloud ensemble with the large-scale environment, {P}art {I}. *J. Atmos. Sci* 31, 674–701.
Araya-Melo, P. A., Crucifix, M., and Bounceur, N. (2015). Global sensitivity analysis of the Indian monsoon during the Pleistocene. *Clim. Past* 11, 45–61. doi:10.5194/cp-11-45-2015.
Arias, P. A., Fu, R., and Mo, K. (2012). Decadal Variation of Rainfall Seasonality in the North American Monsoon Region and Its Potential Causes. *J. Clim.* 25, 4258–4274. doi:DOI: 10.1175/JCLI-D-11-00140.1.
Arias, P. A., Fu, R., Vera, C., and Rojas, M. (2015a). A correlated shortening of the North and South American monsoon seasons in the past few decades. *Clim. Dyn.* 45, 3183–3203. doi:DOI: 10.1007/s00382-015-2533-1.
Arias, P. A., Martínez, J. A., and Vieira, S. C. (2015b). Moisture sources to the 2010–2012 anomalous wet season in northern South America. *Clim. Dyn.* 45, 2861–2884. doi:10.1007/s00382-015-2511-7.

Armour, K. C., Bitz, C. M., and Roe, G. H. (2013). Time-Varying Climate Sensitivity from Regional Feedbacks. *J. Clim.* 26, 4518–4534. doi:10.1175/JCLI-D-12-00544.1.
Arneth, A., Sitch, S., Pongratz, J., Stocker, B. D., Ciais, P., Poulter, B., et al. (2017). Historical carbon dioxide emissions caused by land-use changes are possibly larger than assumed. *Nat. Geosci.* 10, 79. Available at: https://doi.org/10.1038/ngeo2882.
Arnold, N. P., Branson, M., Kuang, Z., Randall, D. A., and Tziperman, E. (2015). MJO Intensification with Warming in the Superparameterized CESM. *J. Clim.* 28, 2706–2724. doi:10.1175/JCLI-D-14-00494.1.
Arnold, N. P., Kuang, Z., and Tziperman, E. (2013). Enhanced MJO-like Variability at High SST. *J. Clim.* 26, 988–1001. doi:10.1175/JCLI-D-12-00272.1.
Årthun, M., Eldevik, T., Viste, E., Drange, H., Furevik, T., Johnson, H. L., et al. (2017). Skillful prediction of northern climate provided by the ocean. *Nat. Commun.* 8, 15875. doi:10.1038/ncomms15875.
As-syakur, A. R., Adnyana, I. W. S., Mahendra, M. S., Arthana, I. W., Merit, I. N., Kasa, I. W., et al. (2014). Observation of spatial patterns on the rainfall response to ENSO and IOD over Indonesia using TRMM Multisatellite Precipitation Analysis (TMPA). *Int. J. Climatol.* 34, 3825–3839. doi:10.1002/joc.3939.
Asadieh, B., and Krakauer, N. Y. (2017). Global change in streamflow extremes under climate change over the 21st century. *Hydrol. Earth Syst. Sci.* doi:10.5194/hess-21-5863-2017.
Ashok, K., Guan, Z., and Yamagata, T. (2003). A Look at the Relationship between the ENSO and the Indian Ocean Dipole. *J. Meteorol. Soc. Japan* 81, 41–56. doi:10.2151/jmsj.81.41.
Asoka, A., Gleeson, T., Wada, Y., and Mishra, V. (2017). Relative contribution of monsoon precipitation and pumping to changes in groundwater storage in India. *Nat. Geosci.* doi:10.1038/ngeo2869.
Asoka, A., Wada, Y., Fishman, R., and Mishra, V. (2018). Strong Linkage Between Precipitation Intensity and Monsoon Season Groundwater Recharge in India. *Geophys. Res. Lett.* 45, 5536–5544. doi:10.1029/2018GL078466.
Aswathy, V. N., Boucher, O., Quaas, M., Niemeier, U., Muri, H., Mülmenstädt, J., et al. (2015). Climate extremes in multi-model simulations of stratospheric aerosol and marine cloud brightening climate engineering. *Atmos. Chem. Phys.* 15, 9593–9610. doi:10.5194/acp-15-9593-2015.
Ault, T. R., Cole, J. E., Overpeck, J. T., Pederson, G. T., George, S. S., Otto-Bliesner, B., et al. (2013). The Continuum of hydroclimate variability in Western North America during the last millennium. *J. Clim.* doi:10.1175/JCLI-D-11-00732.1.
Ault, T. R., Cole, J. E., Overpeck, J. T., Pederson, G. T., and Meko, D. M. (2014). Assessing the Risk of Persistent Drought Using Climate Model Simulations and Paleoclimate Data. *J. Clim.* 27, 7529–7549. doi:10.1175/JCLI-D-12-00282.1.
Ault, T. R., Cole, J. E., and St. George, S. (2012). The amplitude of decadal to multidecadal variability in precipitation simulated by state-of-the-art climate models. *Geophys. Res. Lett.* doi:10.1029/2012GL053424.
Ayliffe, L. K., Gagan, M. K., Zhao, J., Drysdale, R. N., Hellstrom, J. C., Hantoro, W. S., et al. (2013). Rapid interhemispheric climate links via the Australasian monsoon during the last deglaciation. *Nat. Commun.* 4, 2908. Available at: https://doi.org/10.1038/ncomms3908.
Azad, S., and Rajeevan, M. (2016). Possible shift in the ENSO-Indian monsoon rainfall relationship under future global warming. *Sci. Rep.* 6, 20145. doi:10.1038/srep20145.
Bador, M., Donat, M. G., Geoffroy, O., and Alexander, L. V. (2018). Assessing the Robustness of Future Extreme Precipitation Intensification in the CMIP5 Ensemble. *J. Clim.* 31, 6505–6525. doi:10.1175/JCLI-D-17-0683.1.
Bain, C. L., De Paz, J., Kramer, J., Magnusdottir, G., Smyth, P., Stern, H., et al. (2011). Detecting the ITCZ in Instantaneous Satellite Data using Spatiotemporal Statistical Modeling: ITCZ Climatology in the East Pacific. *J. Clim.* 24, 216–230. doi:10.1175/2010JCLI3716.1.
Baines, P. G., Folland, C. K., Baines, P. G., and Folland, C. K. (2007). Evidence for a Rapid Global Climate Shift across the Late 1960s. *J. Clim.* 20, 2721–2744. doi:10.1175/JCLI4177.1.
Baker, H. S., Millar, R. J., Karoly, D. J., Beyerle, U., Benoit, P., Mitchell, D., et al. (2018). Higher CO 2 concentrations increase extreme event risk in a 1 . 5 ◦ C world. *Nat. Clim. Chang.* 8, 267–283. doi:10.1038/s41558-018-0190-1.
Bakker, P., Schmittner, A., Lenaerts, J. T. M., Abe-Ouchi, A., Bi, D., van den Broeke, M. R., et al. (2016). Fate of the Atlantic Meridional Overturning Circulation: Strong decline under continued warming and Greenland melting. *Geophys. Res. Lett.* doi:10.1002/2016GL070457.
Bala, G., Caldeira, K., and Nemani, R. (2010). Fast versus slow response in climate change: implications for the global hydrological cycle. *Clim. Dyn.* 35, 423–434. doi:10.1007/s00382-009-0583-y.
Bala, G., Duffy, P. B., and Taylor, K. E. (2008). Impact of geoengineering schemes on the global hydrological cycle. *Proc. Natl. Acad. Sci.* doi:10.1073/pnas.0711648105.
BALME, M., LEBEL, T., and AMANI, A. (2006). Années sèches et années humides au Sahel: *quo vadimus?Hydrol. Sci. J.* 51, 254–271. doi:10.1623/hysj.51.2.254.
Balsamo, G., Albergel, C., Beljaars, A., Boussetta, S., Brun, E., Cloke, H., et al. (2015). ERA-Interim/Land: A global land surface reanalysis data set. *Hydrol. Earth Syst. Sci.* 19, 389–407. doi:10.5194/hess-19-389-2015.

Bamba, A., Dieppois, B., Konaré, A., Pellarin, T., Balogun, A., Dessay, N., et al. (2015). Changes in Vegetation and Rainfall over West Africa during the Last Three Decades (1981-2010). *Atmos. Clim. Sci.* 05, 367–379. doi:10.4236/acs.2015.54028.

Bao, J., and Sherwood, S. C. (2019). The Role of Convective Self-Aggregation in Extreme Instantaneous Versus Daily Precipitation. *J. Adv. Model. Earth Syst.* doi:10.1029/2018MS001503.

Bao, J., Sherwood, S. C., Alexander, L. V., and Evans, J. P. (2017). Future increases in extreme precipitation exceed observed scaling rates. *Nat. Clim. Chang.* 7, 128–132. doi:10.1038/nclimate3201.

Barbé, L. Le, and Lebel, T. (1997). Rainfall climatology of the HAPEX-Sahel region during the years 1950–1990. *J. Hydrol.* 188–189, 43–73. doi:10.1016/S0022-1694(96)03154-X.

Barbero, R., Fowler, H. J., Lenderink, G., and Blenkinsop, S. (2017). Is the intensification of precipitation extremes with global warming better detected at hourly than daily resolutions? *Geophys. Res. Lett.* 44, 974–983. doi:10.1002/2016GL071917.

Barcikowska, M. J., Weaver, S. J., Feser, F., Russo, S., Schenk, F., Stone, D. A., et al. (2018). Euro-Atlantic winter storminess and precipitation extremes under 1.5 °C vs. 2 °C warming scenarios. *Earth Syst. Dyn.* 9, 679–699. doi:10.5194/esd-9-679-2018.

Barichivich, J., Gloor, E., Peylin, P., Brienen, R. J. W., Schöngart, J., Espinoza, J. C., et al. (2018). Recent intensification of Amazon flooding extremes driven by strengthened Walker circulation. *Sci. Adv.* 4, eaat8785. doi:10.1126/sciadv.aat8785.

Barimalala, R., Bracco, A., and Kucharski, F. (2012). The representation of the South Tropical Atlantic teleconnection to the Indian Ocean in the AR4 coupled models. *Clim. Dyn.* 38, 1147–1166. doi:10.1007/s00382-011-1082-5.

Barnes, E. A. (2013a). Revisiting the evidence linking Arctic amplification to extreme weather in midlatitudes. *Geophys. Res. Lett.* 40, 4734–4739. doi:10.1002/grl.50880.

Barnes, E. A. (2013b). Revisiting the evidence linking Arctic amplification to extreme weather in midlatitudes. *Geophys. Res. Lett.* 40, 4734–4739. doi:10.1002/grl.50880.

Barnes, E. A., Dunn-Sigouin, E., Masato, G., and Woollings, T. (2014). Exploring recent trends in Northern Hemisphere blocking. *Geophys. Res. Lett.* 41, 638–644. Available at: https://doi.org/10.1002/2013GL058745.

Barnes, E. A., and Polvani, L. (2013). Response of the midlatitude jets, and of their variability, to increased greenhouse gases in the CMIP5 models. *J. Clim.* 26, 7117–7135. doi:10.1175/JCLI-D-12-00536.1.

Barnes, E. A., Solomon, S., and Polvani, L. M. (2016). Robust Wind and Precipitation Responses to the Mount Pinatubo Eruption, as Simulated in the CMIP5 Models. *J. Clim.* 29, 4763–4778. doi:10.1175/JCLI-D-15-0658.1.

Bartlein, P. J., Harrison, S. P., Brewer, S., Connor, S., Davis, B. A. S., Gajewski, K., et al. (2011). Pollen-based continental climate reconstructions at 6 and 21 ka: a global synthesis. *Clim. Dyn.* 37, 775–802.

Bartlett, P. A., and Verseghy, D. L. (2015). Modified treatment of intercepted snow improves the simulated forest albedo in the Canadian Land Surface Scheme. *Hydrol. Process.* 29, 3208–3226. doi:10.1002/hyp.10431.

Bates, B. C., Kundzewicz, Z. W., Wu, S., and Palutikof, J. (2008). *Climate Change and Water. Technical Paper of the Intergovernmental Panel on Climate Change*. Geneva: Intergovernmental Panel on Climate Change.

Bathiany, S., Claussen, M., and Brovkin, V. (2014). CO2-induced sahel greening in three CMIP5 earth system models. *J. Clim.* doi:10.1175/JCLI-D-13-00528.1.

Bathiany, S., Claussen, M., and Fraedrich, K. (2013). Detecting hotspots of atmosphere–vegetation interaction via slowing down – Part 2: Application to a global climate model. *Earth Syst. Dyn.* 4, 79–93. doi:10.5194/esd-4-79-2013.

Battisti, D. S., Ding, Q., and Roe, G. H. (2014). Coherent pan-Asian climatic and isotopic response to orbital forcing of tropical insolation. *J. Geophys. Res. Atmos.* 119, 11,997-12,020. doi:10.1002/2014JD021960.

Bayr, T., Dommenget, D., Martin, T., and Power, S. B. (2014). The eastward shift of the Walker Circulation in response to global warming and its relationship to ENSO variability. *Clim. Dyn.* doi:10.1007/s00382-014-2091-y.

Behera, S. K., Luo, J.-J., Masson, S., Delecluse, P., Gualdi, S., Navarra, A., et al. (2005). Paramount Impact of the Indian Ocean Dipole on the East African Short Rains: A CGCM Study. *J. Clim.* 18, 4514–4530. doi:10.1175/JCLI3541.1.

Bell, M. A., Lamb, P. J., Bell, M. A., and Lamb, P. J. (2006). Integration of Weather System Variability to Multidecadal Regional Climate Change: The West African Sudan–Sahel Zone, 1951–98. *J. Clim.* 19, 5343–5365. doi:10.1175/JCLI4020.1.

Bellomo, K., and Clement, A. C. (2015). Evidence for weakening of the Walker circulation from cloud observations. *Geophys. Res* 42, 7758–7766. Available at: https://doi.org/10.1002/2015GL065463.

Belmecheri, S., Babst, F., Wahl, E. R., Stahle, D. W., and Trouet, V. (2016). Multi-century evaluation of Sierra Nevada snowpack. *Nat. Clim. Chang.* doi:10.1038/nclimate2809.

Benestad, R. (2016). *Downscaling Climate Information*. doi:10.1093/acrefore/9780190228620.013.27.

Beniston, M., Farinotti, D., Stoffel, M., Andreassen, L. M., Coppola, E., Eckert, N., et al. (2018). The European mountain cryosphere: a review of its current state, trends, and future challenges. *Cryosph.* 12, 759–794. doi:10.5194/tc-12-759-2018.

Bennartz, R., Fan, J., Rausch, J., Leung, L. R., and Heidinger, A. K. (2011). Pollution from China increases cloud droplet number, suppresses rain over the East China Sea. *Geophys. Res. Lett* 38, 9704. doi:10.1029/2011GL047235.
Berg, A., Findell, K., Lintner, B., Giannini, A., Seneviratne, S. I., Van Den Hurk, B., et al. (2016). Land-atmosphere feedbacks amplify aridity increase over land under global warming. *Nat. Clim. Chang.* 6, 869–874. doi:10.1038/nclimate3029.
Berg, A., Lintner, B. R., Findell, K., and Giannini, A. (2017a). Uncertain soil moisture feedbacks in model projections of Sahel precipitation. *Geophys. Res. Lett.* 44, 6124–6133. doi:10.1002/2017GL073851.
Berg, A., and Sheffield, J. (2018a). Climate Change and Drought: the Soil Moisture Perspective. *Curr. Clim. Chang. Reports*. doi:10.1007/s40641-018-0095-0.
Berg, A., and Sheffield, J. (2018b). Soil moisture-evapotranspiration coupling in CMIP5 models: Relationship with simulated climate and projections. *J. Clim.* 31, 4865–4878. doi:10.1175/JCLI-D-17-0757.1.
Berg, A., Sheffield, J., and Milly, P. C. D. (2017b). Divergent surface and total soil moisture projections under global warming. *Geophys. Res. Lett.* 44, 236–244. doi:10.1002/2016GL071921.
Berg, N., and Hall, A. (2015). Increased interannual precipitation extremes over California under climate change. *J. Clim.* doi:10.1175/JCLI-D-14-00624.1.
Berg, N., and Hall, A. (2017). Anthropogenic warming impacts on California snowpack during drought. *Geophys. Res. Lett.* doi:10.1002/2016GL072104.
Berg, P., and Haerter, J. O. (2013). Unexpected increase in precipitation intensity with temperature - A result of mixing of precipitation types? *Atmos. Res.* 119, 56–61. doi:10.1016/j.atmosres.2011.05.012.
Berg, P., Moseley, C., and Haerter, J. O. (2013). Strong increase in convective precipitation in response to higher temperatures. *Nat. Geosci.* 6, 181–185. doi:10.1038/ngeo1731.
Berghuijs, W. R., Aalbers, E. E., Larsen, J. R., Trancoso, R., and Woods, R. A. (2017). Recent changes in extreme floods across multiple continents. *Environ. Res* 12, 11.
Berghuijs, W. R., Woods, R. A., and Hrachowitz, M. (2014). A precipitation shift from snow towards rain leads to a decrease in streamflow. *Nat. Clim. Chang.* 4, 583–586. doi:10.1038/nclimate2246.
Bernstein, D. N., and Neelin, J. D. (2016). Identifying sensitive ranges in global warming precipitation change dependence on convective parameters. *Geophys. Res. Lett.* 43, 5841–5850. doi:10.1002/2016GL069022.
Berry, G., Reeder, M. J., and Jakob, C. (2011). Physical mechanisms regulating summertime rainfall over northwestern Australia. *J. Clim.* 24, 3705–3717. doi:10.1175/2011JCLI3943.1.
Best, M. J., Abramowitz, G., Johnson, H. R., Pitman, A. J., Balsamo, G., Boone, A., et al. (2015). The Plumbing of Land Surface Models: Benchmarking Model Performance. *J. Hydrometeorol.* 16, 1425–1442. doi:10.1175/JHM-D-14-0158.1.
Best, M. J., and Grimmond, C. S. B. (2015). Key conclusions of the first international urban land surface model comparison project. *Bull. Am. Meteorol. Soc.* 96, 805–819.
Betts, R. A., Alfieri, L., Bradshaw, C., Caesar, J., Feyen, L., Friedlingstein, P., et al. (2018). Changes in climate extremes, fresh water availability and vulnerability to food insecurity projected at 1.5°C and 2°C global warming with a higher-resolution global climate model. *Philos. Trans. R. Soc. A Math. Phys. Eng. Sci.* doi:10.1098/rsta.2016.0452.
Betts, R. A., Boucher, O., Collins, M., Cox, P. M., Falloon, P. D., Gedney, N., et al. (2007). Projected increase in continental runoff due to plant responses to increasing carbon dioxide. *Nature* 448, 1037–1041. doi:10.1038/nature06045.
Betts, R. A., Golding, N., Gonzalez, P., Gornall, J., Kahana, R., Kay, G., et al. (2015). Climate and land use change impacts on global terrestrial ecosystems and river flows in the HadGEM2-ES Earth system model using the representative concentration pathways. *Biogeosciences* 12, 1317–1338. doi:10.5194/bg-12-1317-2015.
Beven, K., and Germann, P. (2013). Macropores and water flow in soils revisited. *Water Resour. Res.* 49, 3071–3092.
Bhattacharya, R., Bordoni, S., and Teixeira, J. (2017a). Tropical precipitation extremes: Response to SST-induced warming in aquaplanet simulations. *Geophys. Res. Lett.* 44, 3374–3383. doi:10.1002/2017GL073121.
Bhattacharya, T., Tierney, J. E., Addison, J. A., and Murray, J. W. (2018). Ice-sheet modulation of deglacial North American monsoon intensification. *Nat. Geosci.* doi:10.1038/s41561-018-0220-7.
Bhattacharya, T., Tierney, J. E., and DiNezio, P. (2017b). Glacial reduction of the North American Monsoon via surface cooling and atmospheric ventilation. *Geophys. Res. Lett.* doi:10.1002/2017GL073632.
Biasutti, M. (2013a). Forced Sahel rainfall trends in the CMIP5 archive. *J. Geophys. Res. Atmos.* doi:10.1002/jgrd.50206.
Biasutti, M. (2013b). Forced Sahel rainfall trends in the CMIP5 archive. *J. Geophys. Res. Atmos.* 118, 1613–1623. doi:10.1002/jgrd.50206.
Biasutti, M., and Giannini, A. (2006a). Robust Sahel drying in response to late 20th century forcings. *Geophys. Res. Lett.* 33, L11706. doi:10.1029/2006GL026067.
Biasutti, M., and Giannini, A. (2006b). Robust Sahel drying in response to late 20th century forcings. *Geophys. Res.*

Lett. 33.
Biasutti, M., Voigt, A., Boos, W. R., Braconnot, P., Hargreaves, J. C., Harrison, S. P., et al. (2018). Global energetics and local physics as drivers of past, present and future monsoons. *Nat. Geosci.* 11, 392–400. doi:10.1038/s41561-018-0137-1.
Bierkens, M. F. P., Bell, V. A., Burek, P., Chaney, N., Condon, L. E., David, C. H., et al. (2015a). Hyper-resolution global hydrological modelling: What is next?: "Everywhere and locally relevant" M. F. P. Bierkens et al. Invited Commentary. *Hydrol. Process.* 29, 310–320. doi:10.1002/hyp.10391.
Bierkens, M. F. P., Bell, V. A., Burek, P., Chaney, N., Condon, L. E., David, C. H., et al. (2015b). Hyper-resolution global hydrological modelling: What is next?: "Everywhere and locally relevant" M. F. P. Bierkens et al. Invited Commentary. *Hydrol. Process.* 29, 310–320. doi:10.1002/hyp.10391.
Bindoff, N. L., Stott, P. A., AchutaRao, K. M., Allen, M. R., Gillett, N., Gutzler, D., et al. (2013a). "Detection and Attribution of Climate Change: from Global to Regional," in *Climate Change 2013: The Physical Science Basis. Contribution of Working Group I to the Fifth Assessment Report of the Intergovernmental Panel on Climate Change*, eds. T. F. Stocker, D. Qin, G.-K. Plattner, M. Tignor, S. K. Allen, J. Boschung, et al. (Cambridge, United Kingdom and New York, NY, USA: Cambridge University Press), 867–952. doi:10.1017/CBO9781107415324.022.
Bindoff, N. L., Stott, P. A., AchutaRao, K. M., Allen, M. R., Gillett, N., Gutzler, D., et al. (2013b). "Detection and Attribution of Climate Change: from Global to Regional," in *Climate Change 2013: The Physical Science Basis. Contribution of Working Group I to the Fifth Assessment Report of the Intergovernmental Panel on Climate Change*, eds. T. F. Stocker, D. Qin, G.-K. Plattner, M. Tignor, S. K. Allen, J. Boschung, et al. (Cambridge, United Kingdom and New York, NY, USA: Cambridge University Press), 867–952. doi:10.1017/CBO9781107415324.022.
Bintanja, R., and Andry, O. (2017). Towards a rain-dominated Arctic. *Nat. Clim. Chang.* doi:10.1038/nclimate3240.
Bintanja, R., and Selten, F. M. (2014). Future increases in Arctic precipitation linked to local evaporation and sea-ice retreat. *Nature* 509, 479–482. doi:10.1038/nature13259.
Bischoff, T., and Schneider, T. (2014). Energetic constraints on the position of the intertropical convergence zone. *J. Clim.* doi:10.1175/JCLI-D-13-00650.1.
Blenkinsop, S., Chan, S. C., Kendon, E. J., Roberts, N. M., and Fowler, H. J. (2015). Temperature influences on intense UK hourly precipitation and dependency on large-scale circulation. *Environ. Res. Lett.* 10, 54021. doi:10.1088/1748-9326/10/5/054021.
Blunden, J., and Arndt, D. S. (2017). State of the Climate in 2016. *Bull. Am. Meteorol. Soc.* 98, Si--S280. doi:10.1175/2017bamsstateoftheclimate.1.
Bodian, A., Ndiaye, O., and Dacosta, H. (2016). Evolution des caractéristiques des pluies journalières dans le bassin versant du fleuve Sénégal: Aavant et après rupture. *Hydrol. Sci. J.*, 1–9. doi:10.1080/02626667.2014.950584.
Boé, J. (2018). Interdependency in Multimodel Climate Projections: Component Replication and Result Similarity. *Geophys. Res. Lett.* 45, 2771–2779. doi:10.1002/2017GL076829.
Boé, J., and Habets, F. (2014). Multi-decadal river flow variations in France. *Hydrol. Earth Syst. Sci.* 18, 691–708. doi:10.5194/hess-18-691-2014.
Boers, N., Marwan, N., Barbosa, H. M. J., and Kurths, J. (2017). A deforestation-induced tipping point for the South American monsoon system. *Sci. Rep.* 7, 1–9. doi:10.1038/srep41489.
Boisier, J. P., Alvarez-Garretón, C., Cordero, R. R., Damiani, A., Gallardo, L., Garreaud, R. D., et al. (2018). Anthropogenic drying in central-southern Chile evidenced by long-term observations and climate model simulations. *Elem Sci Anth* 6, 74. doi:10.1525/elementa.328.
Boisier, J. P., Ciais, P., Ducharne, A., and Guimberteau, M. (2015). Projected strengthening of Amazonian dry season by constrained climate model simulations. *Nat. Clim. Chang.* 5, 656–660. doi:10.1038/nclimate2658.
Boisier, J. P., Rondanelli, R., Garreaud, R., and Muñoz, F. (2016). Anthropogenic and natural contributions to the Southeast Pacific precipitation decline and recent megadrought in central Chile. *J. Geophys. Res.* 43, 413–421.
Bollasina, M. A., Ming, Y., and Ramaswamy, V. (2011). Anthropogenic aerosols and the weakening of the south asian summer monsoon. *Science (80-.).* 334, 502–505. doi:10.1126/science.1204994.
Bonan, G. B. (2016). Forests, Climate, and Public Policy: A 500-Year Interdisciplinary Odyssey. *Annu. Rev. Ecol. Evol. Syst.* 47, 97–121. Available at: https://www.annualreviews.org/doi/full/10.1146/annurev-ecolsys-121415-032359#_i12.
Bonan, G. B., and Doney, S. C. (2018). Climate, ecosystems, and planetary futures: The challenge to predict life in Earth system models. *Science (80-.).* 359, eaam8328.
Bonan, G. B., Williams, M., Fisher, R. A., and Oleson, K. W. (2014). Modeling stomatal conductance in the earth system: Linking leaf water-use efficiency and water transport along the soil-plant-atmosphere continuum. *Geosci. Model Dev.* 7, 2193–2222. doi:10.5194/gmd-7-2193-2014.
Bond, T. C., Doherty, S. J., Fahey, D. W., Forster, P. M., Berntsen, T., DeAngelo, B. J., et al. (2013). Bounding the role of black carbon in the climate system: A scientific assessment. *J. Geophys. Res. Atmos.* 118, 5380–5552.

doi:10.1002/jgrd.50171.
Bonfils, C., Anderson, G., Santer, B. D., Phillips, T. J., Taylor, K. E., Cuntz, M., et al. (2017). Competing influences of anthropogenic warming, ENSO, and plant physiology on future terrestrial aridity. *J. Clim.* 30, 6883–6904. doi:10.1175/JCLI-D-17-0005.1.
Bonfils, C. J. W., Santer, B. D., Phillips, T. J., Marvel, K., Leung, L. R., Doutriaux, C., et al. (2015). Relative Contributions of Mean-State Shifts and ENSO-Driven Variability to Precipitation Changes in a Warming Climate*. *J. Clim.* 28, 9997–10013. doi:10.1175/JCLI-D-15-0341.1.
Bonini, I., Rodrigues, C., Dallacort, R., Hur, B. E. N., Junior, M., Antônio, M., et al. (2014). Rainfall and deforesetation in the municipality of Colider, Southern Amazon. *Rev. Bras. Meteorol.* 29, 483–493.
Bonnet, R., Boé, J., Dayon, G., and Martin, E. (2017). Twentieth-Century Hydrometeorological Reconstructions to Study the Multidecadal Variations of the Water Cycle Over France. *Water Resour. Res.* 53, 8366–8382. doi:10.1002/2017WR020596.
Bony, S., Bellon, G., Klocke, D., Sherwood, S., Fermepin, S., and Denvil, S. (2013). Robust direct effect of carbon dioxide on tropical circulation and regional precipitation. *Nat. Geosci.* 6, 447–451. doi:10.1038/ngeo1799.
Boos, W. R. (2012). Thermodynamic scaling of the hydrological cycle of the last glacial maximum. *J. Clim.* doi:10.1175/JCLI-D-11-00010.1.
Boos, W. R., and Korty, R. L. (2016). Regional energy budget control of the intertropical convergence zone and application to mid-Holocene rainfall. *Nat. Geosci.* 9, 892–897. doi:10.1038/ngeo2833.
Bordbar, M. H., Martin, T., Latif, M., and Park, W. (2017). Role of internal variability in recent decadal to multidecadal tropical Pacific climate changes. *Geophys. Res* 44, 4246–4255. Available at: https://doi.org/10.1002/2016GL072355.
Borodina, A., Fischer, E. M., and Knutti, R. (2017). Models are likely to underestimate increase in heavy rainfall in the extratropical regions with high rainfall intensity. *Geophys. Res. Lett.* 44, 7401–7409. doi:10.1002/2017GL074530.
Bosilovich, M. G. (2013). Regional climate and variability of NASA MERRA and recent reanalyses: U.S. summertime precipitation and temperature. *J. Appl. Meteorol. Climatol.* doi:10.1175/JAMC-D-12-0291.1.
Bosilovich, M. G., Robertson, F. R., Takacs, L., Molod, A., and Mocko, D. (2017). Atmospheric water balance and variability in the MERRA-2 reanalysis. *J. Clim.* doi:10.1175/JCLI-D-16-0338.1.
Bosmans, J. H. C., Erb, M. P., Dolan, A. M., Drijfhout, S. S., Tuenter, E., Hilgen, F. J., et al. (2018). Response of the Asian summer monsoons to idealized precession and obliquity forcing in a set of GCMs. *Quat. Sci. Rev.* 188, 121–135. doi:10.1016/j.quascirev.2018.03.025.
Boucher, O., Randall, D., Artaxo, P., Bretherton, C., Feingold, G., Forster, P., et al. (2013). Clouds and Aerosols. *Clim. Chang. 2013 - Phys. Sci. Basis*, 571–658. doi:10.1017/CBO9781107415324.016.
Boukari, M., Kotchoni, D. O. V., Adjomayi, P., Taylor, R. G., Lawson, F. M. A., and Vouillamoz, J.-M. (2018). Relationships between rainfall and groundwater recharge in seasonally humid Benin: a comparative analysis of long-term hydrographs in sedimentary and crystalline aquifersLes relations entre les précipitations et la recharge des eaux souterraines dans le c. *Hydrogeol. J.* 27, 447–457. doi:10.1007/s10040-018-1806-2.
Boulton, C. A., Booth, B. B. B., and Good, P. (2017). Exploring uncertainty of Amazon dieback in a perturbed parameter Earth system ensemble. *Glob. Chang. Biol.* 23, 5032–5044. doi:10.1111/gcb.13733.
Braconnot, P., Marzin, C., Grégoire, L., Mosquet, E., and Marti, O. (2008). Monsoon response to changes in Earth's orbital parameters: comparisons between simulations of the Eemian and of the Holocene. *Clim. Past* 4, 281–294. doi:10.5194/cp-4-281-2008.
Braga, R. C., Rosenfeld, D., Weigel, R., Jurkat, T., Andreae, M. O., Wendisch, M., et al. (2017). Further evidence for CCN aerosol concentrations determining the height of warm rain and ice initiation in convective clouds over the Amazon basin. *Atmos. Chem. Phys.* 17, 14433–14456.
Brando, P. M., Balch, J. K., Nepstad, D. C., Morton, D. C., Putz, F. E., Coe, M. T., et al. (2014). Abrupt increases in Amazonian tree mortality due to drought{\textendash}fire interactions. *Proc. Natl. Acad. Sci.* doi:10.1073/pnas.1305499111.
Broccoli, A. J., Dahl, K. A., and Stouffer, R. J. (2006). Response of the ITCZ to Northern Hemisphere cooling - Broccoli - 2006 - Geophysical Research Letters - Wiley Online Library. *Geophys. Res. Lett.*
Brönnimann, S., Fischer, A. M., Rozanov, E., Poli, P., Compo, G. P., and Sardeshmukh, P. D. (2015). Southward shift of the northern tropical belt from 1945 to 1980. *Nat. Geosci.* 8, 969–974. doi:10.1038/ngeo2568.
Brovkin, V., Claussen, M., Petoukhov, V., and Ganopolski, A. (1998). On the stability of the atmosphere-vegetation system in the Sahara/Sahel region. *J. Geophys. Res. Atmos.* 103, 31613–31624.
Brown, J. R., Hope, P., Gergis, J., and Henley, B. J. (2016). ENSO teleconnections with Australian rainfall in coupled model simulations of the last millennium. *Clim. Dyn.* 47, 79–93. doi:10.1007/s00382-015-2824-6.
Brown, J. R., Moise, A. F., and Colman, R. A. (2017). Projected increases in daily to decadal variability of Asian-Australian monsoon rainfall. *Geophys. Res. Lett.* 44, 5683–5690. doi:10.1002/2017GL073217.
Brown, P. J., and Kummerow, C. D. (2014). An assessment of atmospheric water budget components over tropical

oceans. *J. Clim.* 27, 2054–2071. doi:10.1175/JCLI-D-13-00385.1.
Brown, R. D., and Robinson, D. A. (2011). Northern Hemisphere spring snow cover variability and change over 1922–2010 including an assessment of uncertainty. *Cryosph.* 5, 219–229. doi:10.5194/tc-5-219-2011.
Brunke, M. A., Broxton, P., Pelletier, J., Gochis, D., Hazenberg, P., Lawrence, D. M., et al. (2016). Implementing and evaluating variable soil thickness in the Community Land Model, version 4.5 (CLM4.5). *J. Clim.* 29, 3441–3461. doi:10.1175/JCLI-D-15-0307.1.
Buckley, B. M., Anchukaitis, K. J., Penny, D., Fletcher, R., Cook, E. R., Sano, M., et al. (2010). Climate as a contributing factor in the demise of Angkor, Cambodia. *Proc. Natl. Acad. Sci.* doi:10.1073/pnas.0910827107.
Bui, H. X., and Maloney, E. D. (2018). Changes in Madden-Julian Oscillation Precipitation and Wind Variance Under Global Warming. *Geophys. Res. Lett.* 45, 7148–7155. doi:10.1029/2018GL078504.
Bunde, A., Büntgen, U., Ludescher, J., Luterbacher, J., and von Storch, H. (2013). Is there memory in precipitation? *Nat. Clim. Chang.* doi:10.1038/nclimate1830.
Burdanowitz, J., Buehler, S. A., Bakan, S., and Klepp, C. (2019). On the sensitivity of oceanic precipitation to sea surface temperature. *Atmos. Chem. Phys. Discuss.*, 1–21. doi:10.5194/acp-2019-136.
Byrne, M. P., and O'Gorman, P. A. (2015). The response of precipitation minus evapotranspiration to climate warming: Why the "Wet-get-wetter, dry-get-drier" scaling does not hold over land. *J. Clim.* 28, 8078–8092. doi:10.1175/JCLI-D-15-0369.1.
Byrne, M. P., and O'Gorman, P. A. (2016). Understanding decreases in land relative humidity with global warming: Conceptual model and GCM simulations. *J. Clim.* 29, 9045–9061. doi:10.1175/JCLI-D-16-0351.1.
Byrne, M. P., and O'Gorman, P. A. (2018). Trends in continental temperature and humidity directly linked to ocean warming. *Proc. Natl. Acad. Sci.* 115, 4863–4868. doi:10.1073/pnas.1722312115.
Byrne, M. P., Pendergrass, A. G., and Rapp, A. D. (2018). Response of the Intertropical Convergence Zone to Climate Change : Location , Width and Strength Precipitation climatology. *Curr. Clim. Chang. Reports*. doi:10.1007/s40641-018-0110-5.
Byrne, M. P., and Schneider, T. (2016a). Energetic constraints on the width of the intertropical convergence zone. *J. Clim.* doi:10.1175/JCLI-D-15-0767.1.
Byrne, M. P., and Schneider, T. (2016b). Narrowing of the ITCZ in a warming climate: Physical mechanisms. *Geophys. Res. Lett.* 43, 11,350-11,357. doi:10.1002/2016GL070396.
Caballero, R., and Huber, M. (2013). State-dependent climate sensitivity in past warm climates and its implications for future climate projections. *Proc. Natl. Acad. Sci.* doi:10.1073/pnas.1303365110.
Caesar, L., Rahmstorf, S., Robinson, A., Feulner, G., and Saba, V. (2018a). Observed fingerprint of a weakening Atlantic Ocean overturning circulation. *Nature*. doi:10.1038/s41586-018-0006-5.
Caesar, L., Rahmstorf, S., Robinson, A., Feulner, G., and Saba, V. (2018b). Observed fingerprint of a weakening Atlantic Ocean overturning circulation. *Nature* 556, 191–196. doi:10.1038/s41586-018-0006-5.
Cai, W., Borlace, S., Lengaigne, M., van Rensch, P., Collins, M., Vecchi, G., et al. (2014). Increasing frequency of extreme El Niño events due to greenhouse warming. *Nat. Clim. Chang.* 4, 111–116. doi:10.1038/nclimate2100.
Cai, W., Cowan, T., and Raupach, M. (2009a). Positive Indian Ocean Dipole events precondition southeast Australia bushfires. *Geophys. Res. Lett.* 36, L19710. doi:10.1029/2009GL039902.
Cai, W., Cowan, T., and Sullivan, A. (2009b). Recent unprecedented skewness towards positive Indian Ocean Dipole occurrences and its impact on Australian rainfall. *Geophys. Res. Lett.* 36, L11705. doi:10.1029/2009GL037604.
Cai, W., Cowan, T., Sullivan, A., Ribbe, J., and Shi, G. (2011). Are anthropogenic aerosols responsible for the northwest Australia summer rainfall increase? A CMIP perspective and implications,. *J. Clim.* 3, 2556–2564. doi:10.1175/2010JCLI3832.1.
Cai, W., Cowan, T., and Thatcher, M. (2012). Rainfall reductions over Southern Hemisphere semi-arid regions: the role of subtropical dry zone expansion. *Sci. Rep.* 2, 702. doi:10.1038/srep00702.
Cai, W., Santoso, A., Wang, G., Yeh, S.-W., An, S.-I., Cobb, K. M., et al. (2015a). ENSO and greenhouse warming. *Nat. Clim. Chang.* 5, 849–859. doi:10.1038/nclimate2743.
Cai, W., Santoso, A., Wang, G., Yeh, S.-W., An, S.-I., Cobb, K. M., et al. (2015b). ENSO and greenhouse warming. *Nat. Clim. Chang.* 5, 849–859. doi:10.1038/nclimate2743.
Cai, W., Santoso, A., Wang, G., Yeh, S., An, S., Cobb, K. M., et al. (2015c). ENSO and greenhouse warming. *Nat. Publ. Gr.* 5, 849–859. doi:10.1038/nclimate2743.
Camponogara, G., Faus da Silva Dias, M. A., and Carrió, G. G. (2018). Biomass burning CCN enhance the dynamics of a mesoscale convective system over the La Plata Basin: a numerical approach. *Atmos. Chem. Phys.* 18, 2081–2096. doi:10.5194/acp-18-2081-2018.
Cantú, A. G., Frieler, K., Reyer, C. P. O., Ciais, P., Chang, J., Ito, A., et al. (2018). Evaluating changes of biomass in global vegetation models: the role of turnover fluctuations and ENSO events. *Environ. Res. Lett.* 13, 075002. doi:10.1088/1748-9326/aac63c.
Cao, L., Bala, G., Zheng, M., and Caldeira, K. (2015). Fast and slow climate responses to CO2 and solar forcing: A linear multivariate regression model characterizing transient climate change. *J. Geophys. Res. Atmos.* 120,

12037–12053. doi:10.1002/2014JD022994.Received.

Carlson, H., and Caballero, R. (2016). Enhanced MJO and transition to superrotation in warm climates. *J. Adv. Model. Earth Syst.* 8, 304–318. doi:10.1002/2015MS000615.

Carril, A. F., Menéndez, C. G., Zaninelli, P. G., Li, L. Z. X., and Falco, M. (2018). Assessment of CORDEX simulations over South America: added value on seasonal climatology and resolution considerations. *Clim. Dyn.* doi:10.1007/s00382-018-4412-z.

Carvalho, L. M. V., Jones, C., and Liebmann, B. (2004). The South Atlantic Convergence Zone: Intensity, Form, Persistence, and Relationships with Intraseasonal to Interannual Activity and Extreme Rainfall. *J. Clim.* 17, 88–108. doi:10.1175/1520-0442(2004)017<0088:TSACZI>2.0.CO;2.

Cash, B. A., Barimalala, R., Kinter, J. L., Altshuler, E. L., Fennessy, M. J., Manganello, J. V., et al. (2017). Sampling variability and the changing ENSO–monsoon relationship. *Clim. Dyn.* 48, 4071–4079. doi:10.1007/s00382-016-3320-3.

Cash, B. A., Rodó, X., Ballester, J., Bouma, M. J., Baeza, A., Dhiman, R., et al. (2013). Malaria epidemics and the influence of the tropical South Atlantic on the Indian monsoon. *Nat. Clim. Chang.* 3, 502–507. doi:10.1038/nclimate1834.

Cattiaux, J., and Cassou, C. (2013). Opposite CMIP3/CMIP5 trends in the wintertime Northern Annular Mode explained by combined local sea ice and remote tropical influences. *Geophys. Res. Lett.* 40, 3682–3687. doi:10.1002/grl.50643.

Catto, J., Jakob, C., and Nicholls, N. (2012). The influence of changes in synoptic regimes on north Australian wet season rainfall trends. *J. Geophys. Res.* 117. doi:10.1029/2012JD017472.

Catto, J. L. (2016). Extratropical cyclone classification and its use in climate studies. *Rev. Geophys.* 54, 486–520. doi:10.1002/2016RG000519.

Catto, J. L., Jakob, C., and Nicholls, N. (2015). Can the CMIP5 models represent winter frontal precipitation? *Geophys. Res. Lett.* 42, 8596–8604. doi:10.1002/2015GL066015.

Ceppi, P., Zappa, G., Shepherd, T. G., and Gregory, J. M. (2018). Fast and slow components of the extratropical atmospheric circulation response to CO2forcing. *J. Clim.* 31, 1091–1105. doi:10.1175/JCLI-D-17-0323.1.

Chadburn, S., Burke, E., Essery, R., Boike, J., Langer, M., Heikenfeld, M., et al. (2015). An improved representation of physical permafrost dynamics in the JULES land-surface model. *Geosci. Model Dev.* 8, 1493–1508. doi:10.5194/gmd-8-1493-2015.

Chadwick, R., Boutle, I., and Martin, G. (2013). Spatial patterns of precipitation change in CMIP5: Why the rich do not get richer in the tropics. *J. Clim.* 26, 3803–3822. doi:10.1175/JCLI-D-12-00543.1.

Chadwick, R., Douville, H., and Skinner, C. B. (2017). Timeslice experiments for understanding regional climate projections: applications to the tropical hydrological cycle and European winter circulation. *Clim. Dyn.* 49, 3011–3029. doi:10.1007/s00382-016-3488-6.

Chadwick, R., and Good, P. (2013). Understanding nonlinear tropical precipitation responses to CO2 forcing. *Geophys. Res. Lett.* doi:10.1002/grl.50932.

Chadwick, R., Good, P., Andrews, T., and Martin, G. (2014). Surface warming patterns drive tropical rainfall pattern responses to CO_2 forcing on all timescales. *Geophys. Res. Lett.* 41, 610–615. doi:10.1002/2013GL058504.

Chadwick, R., Good, P., Martin, G., and Rowell, D. P. (2016a). Large rainfall changes consistently projected over substantial areas of tropical land. *Nat. Clim. Chang.* 6, 177–181. doi:10.1038/nclimate2805.

Chadwick, R., Good, P., and Willett, K. (2016b). A simple moisture advection model of specific humidity change over land in response to SST warming. *J. Clim.* 29, 7613–7632. doi:10.1175/JCLI-D-16-0241.1.

Chan, S. C., Kendon, E. J., Roberts, N., Blenkinsop, S., and Fowler, H. J. (2018). Large-Scale Predictors for Extreme Hourly Precipitation Events in Convection-Permitting Climate Simulations. *J. Clim.* 31, 2115–2131. doi:10.1175/JCLI-D-17-0404.1.

Chan, S. C., Kendon, E. J., Roberts, N. M., Fowler, H. J., and Blenkinsop, S. (2016a). Downturn in scaling of UK extreme rainfall with temperature for future hottest days. *Nat. Geosci.* 9, 24–28. doi:10.1038/ngeo2596.

Chan, S. C., Kendon, E. J., Roberts, N. M., Fowler, H. J., and Blenkinsop, S. (2016b). The characteristics of summer sub-hourly rainfall over the southern UK in a high-resolution convective permitting model. *Environ. Res. Lett.* 11, 94024. doi:10.1088/1748-9326/11/9/094024.

Chand, S. S., Tory, K. J., Ye, H., and Walsh, K. J. E. (2017). Projected increase in El Niño-driven tropical cyclone frequency in the Pacific. *Nat. Clim. Chang.* 7, 123–127. doi:10.1038/nclimate3181.

Chandana, K.R., Banerji U.S., B. R. (2018). Review on Indian summer monsoon (ISM) reconstructions since LGM from Northern Indian Ocean. *Earth Sci. India* 11.

Chandran, A., Basha, G., and Ouarda, T. B. M. J. (2016). Influence of climate oscillations on temperature and precipitation over the United Arab Emirates. *Int. J. Climatol.* 36, 225–235. doi:10.1002/joc.4339.

Chang, C.-Y., Chiang, J. C. H., Wehner, M. F., Friedman, A. R., and Ruedy, R. (2011). Sulfate Aerosol Control of Tropical Atlantic Climate over the Twentieth Century. *J. Clim.* 24, 2540–2555. doi:10.1175/2010JCLI4065.1.

Chang, C. -p., Wang, Z., McBride, J., and Liu, C. -h. (2005). Annual cycle of southeast Asia-Maritime Continent

rainfall and the asymmetric monsoon transition, J. *Climate* 18, 287–301.
Chang, E. K. M., Guo, Y., Xia, X., and Zheng, M. (2013). Storm-track activity in IPCC AR4/CMIP3 model simulations. *J. Clim.* 26, 246–260. doi:10.1175/JCLI-D-11-00707.1.
Chang, E. K. M., Ma, C. G., Zheng, C., and Yau, A. M. W. (2016). Observed and projected decrease in Northern Hemisphere extratropical cyclone activity in summer and its impacts on maximum temperature. *Geophys. Res. Lett.* doi:10.1002/2016GL068172.
Chang, E. K. M., and Yau, A. M. W. (2016). Northern Hemisphere winter storm track trends since 1959 derived from multiple reanalysis datasets. *Clim. Dyn.* 47, 1435–1454. doi:10.1007/s00382-015-2911-8.
Charette, M. A., and Smith, W. H. F. (2010). The Volume of Earth's Ocean. *Oceanography* 23, 112–114. doi:doi: 10.5670/oceanog.2010.51.
Charney, J. G. (1975). Dynamics of deserts and drought in the Sahel. *Q. J. R. Meteorol. Soc.* 101, 193–202.
Chauvin, F., Douville, H., and Ribes, A. (2017). Atlantic tropical cyclones water budget in observations and CNRM - CM5 model. *Clim. Dyn.* 49, 4009–4021. doi:10.1007/s00382-017-3559-3.
Chemke, R., and Polvani, L. M. (2019). Exploiting the abrupt 4 × CO 2 scenario to elucidate tropical expansion mechanisms. *J. Clim.* 32, 859–875. doi:10.1175/JCLI-D-18-0330.1.
Chen, F., Crow, W. T., Bindlish, R., Colliander, A., Burgin, M. S., Asanuma, J., et al. (2018a). Global-scale evaluation of SMAP, SMOS and ASCAT soil moisture products using triple collocation. *Remote Sens. Environ.* 214, 1–13. doi:10.1016/j.rse.2018.05.008.
Chen, F., and Gao, Y. (2018). Evaluation of precipitation trends from high-resolution satellite precipitation products over Mainland China. *Clim. Dyn.* doi:10.1007/s00382-018-4080-z.
Chen, G., and Held, I. M. (2007). Phase speed spectra and the recent poleward shift of Southern Hemisphere surface westerlies. *Geophys. Res. Lett.* doi:10.1029/2007GL031200.
Chen, G., Lu, J., and Frierson, D. M. W. (2008). Phase speed spectra and the latitude of surface westerlies: Interannual variability and global warming trend. *J. Clim.* doi:10.1175/2008JCLI2306.1.
Chen, G., and Tam, C.-Y. (2010). Different impacts of two kinds of Pacific Ocean warming on tropical cyclone frequency over the western North Pacific. *Geophys. Res. Lett.* 37, n/a-n/a. doi:10.1029/2009GL041708.
Chen, G., Wang, W. C., and Chen, J. P. (2018b). Circulation responses to regional aerosol climate forcing in summer over East Asia. *Clim. Dyn.* 51, 3973–3984. doi:10.1007/s00382-018-4267-3.
Chen, H., and Sun, J. (2017). Anthropogenic warming has caused hot droughts more frequently in China. *J. Hydrol.* 544, 306–318. doi:10.1016/j.jhydrol.2016.11.044.
Chen, J. L., Wilson, C. R., and Tapley, B. D. (2013). Contribution of ice sheet and mountain glacier melt to recent sea level rise. *Nat. Geosci.* 6, 549. Available at: https://doi.org/10.1038/ngeo1829.
Chen, J. L., Wilson, C. R., Tapley, B. D., Longuevergne, L., Yang, Z. L., and Scanlon, B. R. (2010a). Recent La Plata basin drought conditions observed by satellite gravimetry. *J. Geophys. Res.* 115, D22108. doi:10.1029/2010JD014689.
Chen, J., Theller, L., Gitau, M. W., Engel, B. A., and Harbor, J. M. (2017a). Urbanization impacts on surface runoff of the contiguous United States. *J. Environ. Manage.* 187, 470–481. doi:10.1016/j.jenvman.2016.11.017.
Chen, Q., Koren, I., Altaratz, O., Heiblum, R. H., Dagan, G., and Pinto, L. (2017b). How do changes in warm-phase microphysics affect deep convective clouds? *Atmos. Chem. Phys.* 17, 9585–9598. doi:10.5194/acp-17-9585-2017.
Chen, W., Dong, B., and Lu, R. (2010b). Impact of the Atlantic Ocean on the multidecadal fluctuation of El Niño–Southern Oscillation–South Asian monsoon relationship in a coupled general circulation model. *J. Geophys. Res.* 115, D17109. doi:10.1029/2009JD013596.
Chen, X., Liang, S., and Cao, Y. (2017c). Sensitivity of Summer Drying to Spring Snow-Albedo Feedback Throughout the Northern Hemisphere From Satellite Observations. *IEEE Geosci. Remote Sens. Lett.* 14, 2345–2349. doi:10.1109/LGRS.2017.2764543.
Chen, X., and Tung, K. K. (2018). Global surface warming enhanced by weak Atlantic overturning circulation. *Nature*. doi:10.1038/s41586-018-0320-y.
Chen, X., Wang, S., Hu, Z., Zhou, Q., and Hu, Q. (2018c). Spatiotemporal characteristics of seasonal precipitation and their relationships with ENSO in Central Asia during 1901–2013. *J. Geogr. Sci.* 28, 1341–1368. doi:10.1007/s11442-018-1529-2.
Chen, Y., Langenbrunner, B., and Randerson, J. T. (2018d). Future drying in Central America and northern SouthAmerica linked with Atlantic meridional overturning circulation. *Geophys. Res. Lett.* doi:10.1029/2018GL077953.
Chen, Y., Langenbrunner, B., and Randerson, J. T. (2018e). Future drying in Central America and northern SouthAmerica linked with Atlantic meridional overturning circulation. *Geophys. Res. Lett.* doi:10.1029/2018GL077953.
Cheng, H., Edwards, R. L., Sinha, A., Spötl, C., Yi, L., Chen, S., et al. (2016). The Asian monsoon over the past 640,000 years and ice age terminations. *Nature*. doi:10.1038/nature18591.
Cheng, H., Sinha, A., Wang, X., Cruz, F. W., and Edwards, R. L. (2012). The Global Paleomonsoon as seen through

speleothem records from Asia and the Americas. *Clim. Dyn.* 39, 1045–1062. doi:10.1007/s00382-012-1363-7.
Cherchi, A., Alessandri, A., Masina, S., and Navarra, A. (2011). Effects of increased CO2 levels on monsoons. *Clim. Dyn.* 37, 83–101. doi:10.1007/s00382-010-0801-7.
Cherchi, A., Ambrizzi, T., Behera, S., Freitas, A. C. V., Morioka, Y., and Zhou, T. (2018a). The Response of Subtropical Highs to Climate Change. *Curr. Clim. Chang. Reports*, 1–12. doi:10.1007/s40641-018-0114-1.
Cherchi, A., Kucharski, F., and Colleoni, F. (2018b). Remote SST forcing on Indian summer monsoon extreme years in AGCM experiments. *Int. J. Climatol.* 38, e160–e177. doi:10.1002/joc.5360.
Cherchi, A., and Navarra, A. (2013). Influence of ENSO and of the Indian Ocean Dipole on the Indian summer monsoon variability. *Clim. Dyn.* 41, 81–103. doi:10.1007/s00382-012-1602-y.
Chernokulsky, A., Kozlov, F., Zolina, O., Bulygina, O. N., Mokhov, I., and Semenov, V. (2019). Observed changes in convective and stratiform precipitation over Northern Eurasia during the last decades. *Environ. Res. Lett.*
Cheung, A. H., Mann, M. E., Steinman, B. A., Frankcombe, L. M., England, M. H., and Miller, S. K. (2017). Comparison of Low-Frequency Internal Climate Variability in CMIP5 Models and Observations. *J. Clim.* 30, 4763–4776. doi:10.1175/JCLI-D-16-0712.1.
Cheung, R. C. W., Yasuhara, M., Mamo, B., Katsuki, K., Seto, K., Takata, H., et al. (2018). Decadal- to Centennial-Scale East Asian Summer Monsoon Variability Over the Past Millennium: An Oceanic Perspective. *Geophys. Res. Lett.* 45, 7711–7718. doi:10.1029/2018GL077978.
Chiang, J. C. H., and Bitz, C. M. (2005). Influence of high latitude ice cover on the marine Intertropical Convergence Zone. *Clim. Dyn.* doi:10.1007/s00382-005-0040-5.
Chiang, J. C. H., and Friedman, A. R. (2012). Extratropical Cooling, Interhemispheric Thermal Gradients, and Tropical Climate Change. *Annu. Rev. Earth Planet. Sci.* doi:10.1146/annurev-earth-042711-105545.
Chiang, J., Chang, C., and Wehner, M. (2013). Long-Term Behavior of the Atlantic Interhemispheric SST Gradient in the CMIP5 Historical Simulations. *J. Clim.* 26, 8628–8640. doi:10.1175/JCLI-D-12-00487.1.
Choi, J., Lu, J., Son, S.-W., Frierson, D. M. W., and Yoon, J.-H. (2016a). Uncertainty in future projections of the North Pacific subtropical high and its implication for California winter precipitation change. *J. Geophys. Res. Atmos.* 121, 795–806. doi:10.1002/2015JD023858.
Choi, K.-S., Cha, Y., Kim, H.-D., and Kang, S.-D. (2016b). Possible influence of western North Pacific monsoon on TC activity in mid-latitudes of East Asia. *Clim. Dyn.* 46, 1–13. doi:10.1007/s00382-015-2562-9.
Choobari, O. A., Zawar-Reza, P., and Sturman, A. (2014). The global distribution of mineral dust and its impacts on the climate system: A review. *Atmos. Res.* doi:10.1016/j.atmosres.2013.11.007.
Chou, C., and Chen, C. A. (2010). Depth of convection and the weakening of tropical circulation in Global Warming. *J. Clim.* doi:10.1175/2010JCLI3383.1.
Chou, C., Chen, C. A., Tan, P. H., and Chen, K. T. (2012). Mechanisms for global warming impacts on precipitation frequency and intensity. *J. Clim.* doi:10.1175/JCLI-D-11-00239.1.
Chou, C., Chiang, J. C. H., Lan, C. W., Chung, C. H., Liao, Y. C., and Lee, C. J. (2013a). Increase in the range between wet and dry season precipitation. *Nat. Geosci.* 6, 263–267. doi:10.1038/ngeo1744.
Chou, C., Chiang, J. C. H., Lan, C. W., Chung, C. H., Liao, Y. C., and Lee, C. J. (2013b). Increase in the range between wet and dry season precipitation. *Nat. Geosci.* 6, 263–267. doi:10.1038/ngeo1744.
Chou, C., Chiang, J. C. H., Lan, C. W., Chung, C. H., Liao, Y. C., and Lee, C. J. (2013c). Increase in the range between wet and dry season precipitation. *Nat. Geosci.* 6, 263–267. doi:10.1038/ngeo1744.
Chou, C., and Lan, C.-W. (2012). Changes in the Annual Range of Precipitation under Global Warming. *J. Clim.* 25, 222–235. doi:10.1175/JCLI-D-11-00097.1.
Chou, C., and Neelin, J. D. (2003). Mechanisms limiting the northward extent of the northern summer monsoons over North America, Asia, and Africa. *J. Clim.* doi:10.1175/1520-0442(2003)016<0406:MLTNEO>2.0.CO;2.
Chou, C., and Neelin, J. D. (2004). Mechanisms of global warming impacts on regional tropical precipitation. *J. Clim.* doi:10.1175/1520-0442(2004)017<2688:MOGWIO>2.0.CO;2.
Chou, C., Neelin, J. D., Chen, C. A., and Tu, J. Y. (2009). Evaluating the "rich-get-richer" mechanism in tropical precipitation change under global warming. *J. Clim.* doi:10.1175/2008JCLI2471.1.
Christensen, J. H., Krishna Kumar, K., Aldrian, E., An, S.-I., Cavalcanti, I. F. A., de Castro, M., et al. (2013). "Climate Phenomena and their Relevance for Future Regional Climate Change," in *Climate Change 2013: The Physical Science Basis. Contribution of Working Group I to the Fifth Assessment Report of the Intergovernmental Panel on Climate Change*, eds. T. F. Stocker, D. Qin, G.-K. Plattner, M. Tignor, S. K. Allen, J. Boschung, et al. (Cambridge, United Kingdom and New York, NY, USA: Cambridge University Press), 1217–1308. doi:10.1017/CBO9781107415324.028.
Chung, E. S., and Soden, B. J. (2017). Hemispheric climate shifts driven by anthropogenic aerosol-cloud interactions. *Nat. Geosci.* 10, 566–571. doi:10.1038/NGEO2988.
Ciasto, L. M., Li, C., Wettstein, J. J., and Kvamstø, N. G. (2016). North Atlantic Storm-Track Sensitivity to Projected Sea Surface Temperature: Local versus Remote Influences. *J. Clim.* 29, 6973–6991. doi:10.1175/JCLI-D-15-0860.1.

Clark, M. P., Fan, Y., Lawrence, D. M., Adam, J. C., Bolster, D., Gochis, D. J., et al. (2015). Improving the representation of hydrologic processes in Earth System Models. *Water Resour. Res.* 51, 5929–5956. doi:10.1002/2015WR017096.
Clark, M. P., Wilby, R. L., Gutmann, E. D., Vano, J. A., Gangopadhyay, S., Wood, A. W., et al. (2016). Characterizing Uncertainty of the Hydrologic Impacts of Climate Change. *Curr. Clim. Chang. Reports* 2, 55–64. doi:10.1007/s40641-016-0034-x.
Clark, S., Reeder, M. J., and Jakob, C. (2018). *Rainfall regimes over northwestern Australia*. Quarterly Journal of the Royal Meteorological Society doi:10.1002/qj.3217.
Claussen, M., Bathiany, S., Brovkin, V., and Kleinen, T. (2013). Simulated climate-vegetation interaction in semi-arid regions affected by plant diversity. *Nat. Geosci.* 6, 954–958. doi:10.1038/ngeo1962.
Claussen, M., Brovkin, V., Ganopolski, A., Kubatzki, C., and Petoukhov, V. (2003). Climate change in northern Africa: The past is not the future. *Clim. Change* 57, 99–118. doi:10.1023/A:1022115604225.
Claussen, M., Kubatzki, C., Brovkin, V., Ganopolski, A., Hoelzmann, P., and Pachur, H.-J. (1999). Simulation of an abrupt change in Saharan vegetation in the Mid-Holocene. *Geophys. Res. Lett.* 26, 2037–2040.
Coats, S., and Karnauskas, K. B. (2017). Are Simulated and Observed Twentieth Century Tropical Pacific Sea Surface Temperature Trends Significant Relative to Internal Variability? *Geophys. Res. Lett.* doi:10.1002/2017GL074622.
Coats, S., Smerdon, J. E., Cook, B. I., and Seager, R. (2015). Are Simulated Megadroughts in the North American Southwest Forced? *J. Clim.* 28, 124–142. doi:10.1175/JCLI-D-14-00071.1.
Coats, S., Smerdon, J. E., Cook, B. I., Seager, R., Cook, E. R., and Anchukaitis, K. J. (2016). Internal ocean-atmosphere variability drives megadroughts in Western North America. *Geophys. Res. Lett.* 43, 9886–9894. doi:10.1002/2016GL070105.
Cobb, K. M., Westphal, N., Sayani, H. R., Watson, J. T., Di Lorenzo, E., Cheng, H., et al. (2013). Highly Variable El Nino-Southern Oscillation Throughout the Holocene. *Science (80-.).* 339, 67–70. doi:10.1126/science.1228246.
Cohen, J., Screen, J. A., Furtado, J. C., Barlow, M., Whittleston, D., Coumou, D., et al. (2014). Recent Arctic amplification and extreme mid-latitude weather. *Nat. Geosci.* 7, 627–637. doi:10.1038/ngeo2234.
Colle, B. A., Booth, J. F., and Chang, E. K. M. (2015). A Review of Historical and Future Changes of Extratropical Cyclones and Associated Impacts Along the US East Coast. Curr. Clim. Change Rep. 1, 13–17.
Collier, N., Hoffman, F. M., Lawrence, D. M., Keppel-Aleks, G., Koven, C. D., Riley, W. J., et al. (2018). The International Land Model Benchmarking (ILAMB) System: Design, Theory, and Implementation. *J. Adv. Model. Earth Syst.*, 2731–2754. doi:10.1029/2018MS001354.
Collins, M., Achutarao, K., Ashok, K., Bhandari, S., Mitra, A. K., Prakash, S., et al. (2013a). Observational challenges in evaluating climate models. *Nat. Clim. Chang.* 3, 940–941. Available at: https://doi.org/10.1038/nclimate2012.
Collins, M., An, S.-I., Cai, W., Ganachaud, A., Guilyardi, E., Jin, F.-F., et al. (2010). The impact of global warming on the tropical Pacific Ocean and El Niño. *Nat. Geosci.* 3, 391–397. doi:10.1038/ngeo868.
Collins, M., Knutti, R., Arblaster, J., Dufresne, J.-L., Fichefet, T., Friedlingstein, P., et al. (2013b). "Long-term Climate Change: Projections, Commitments and Irreversibility," in *Climate Change 2013: The Physical Science Basis. Contribution of Working Group I to the Fifth Assessment Report of the Intergovernmental Panel on Climate Change*, eds. T. F. Stocker, D. Qin, G.-K. Plattner, M. Tignor, S. K. Allen, J. Boschung, et al. (Cambridge, United Kingdom and New York, NY, USA: Cambridge University Press), 1029–1136. doi:10.1017/CBO9781107415324.024.
Collins, S. (2017). Incorporating groundwater flow in land surface models: literature review and recommendations for further work. *Br. Geol. Surv. Open Report, OR/* 68, 23.
Colose, C., LeGrande, A., and Vuille, M. (2016). Hemispherically asymmetric volcanic forcing of tropical hydroclimate during the last millennium. *Earth Syst. Dyn.* 7, 681–696. doi:10.5194/esd-7-681-2016.
Comas-Bru, L., and McDermott, F. (2014). Impacts of the EA and SCA patterns on the European twentieth century NAO-winter climate relationship. *Q. J. R. Meteorol. Soc.* 140, 354–363. doi:10.1002/qj.2158.
Conway, D., Allison, E., Felstead, R., and Goulden, M. (2005). Rainfall variability in East Africa: implications for natural resources management and livelihoods. *Philos. Trans. R. Soc. A Math. Phys. Eng. Sci.* 363, 49–54. doi:10.1098/rsta.2004.1475.
Cook, B. I., Anchukaitis, K. J., Touchan, R., Meko, D. M., and Cook, E. R. (2016a). Spatiotemporal drought variability in the mediterranean over the last 900 years. *J. Geophys. Res.* doi:10.1002/2015JD023929.
Cook, B. I., Ault, T. R., and Smerdon, J. E. (2015a). Unprecedented 21st century drought risk in the American Southwest and Central Plains. *Sci. Adv.* 1, e1400082.
Cook, B. I., Cook, E. R., Smerdon, J. E., Seager, R., Williams, A. P., Coats, S., et al. (2016b). North American megadroughts in the Common Era: reconstructions and simulations. *Wiley Interdiscip. Rev. Clim. Chang.* 7, 411–432. doi:10.1002/wcc.394.
Cook, B. I., Mankin, J. S., and Anchukaitis, K. J. (2018). Climate Change and Drought: From Past to Future. *Curr. Clim. Chang. Reports* 4, 164–179. doi:10.1007/s40641-018-0093-2.
Cook, B. I., Miller, R. L., and Seager, R. (2009). Amplification of the North American "Dust Bowl" drought through

human-induced land degradation. *Proc. Natl. Acad. Sci.* doi:10.1073/pnas.0810200106.
Cook, B. I., and Seager, R. (2013). The response of the North American Monsoon to increased greenhouse gas forcing. *J. Geophys. Res. Atmos.* 118, 1690–1699. doi:10.1002/jgrd.50111.
Cook, B. I., Seager, R., Miller, R. L., and Mason, J. A. (2013). Intensification of north american megadroughts through surface and dust aerosol forcing. *J. Clim.* doi:10.1175/JCLI-D-12-00022.1.
Cook, B. I., Smerdon, J. E., Seager, R., and Coats, S. (2014). Global warming and 21stcentury drying. *Clim. Dyn.* 43, 2607–2627. doi:10.1007/s00382-014-2075-y.
Cook, E. R., Anchukaitis, K. J., Buckley, B. M., D'Arrigo, R. D., Jacoby, G. C., and Wright, W. E. (2010a). Asian monsoon failure and megadrought during the last millennium. *Science (80-.).* doi:10.1126/science.1185188.
Cook, E. R., Seager, R., Heim, R. R., Vose, R. S., Herweijer, C., and Woodhouse, C. (2010b). Megadroughts in North America: Placing IPCC projections of hydroclimatic change in a long-term palaeoclimate context. *J. Quat. Sci.* doi:10.1002/jqs.1303.
Cook, E. R., Seager, R., Kushnir, Y., Briffa, K. R., Büntgen, U., Frank, D., et al. (2015b). Old World megadroughts and pluvials during the Common Era. *Sci. Adv.* doi:10.1126/sciadv.1500561.
Cook, E. R., Woodhouse, C. A., Eakin, C. M., Meko, D. H., and Stahle, D. W. (2004). Long-term aridity changes in the western United States. *Science (80-.).* doi:10.1126/science.1102586.
Cook, K. H., and Vizy, E. K. (2006). South American climate during the Last Glacial Maximum: Delayed onset of the South American monsoon. *J. Geophys. Res. Atmos.* 111, 1–21. doi:10.1029/2005JD005980.
Cook, K. H., and Vizy, E. K. (2015). Detection and analysis of an amplified warming of the Sahara Desert. *J. Clim.* doi:10.1175/JCLI-D-14-00230.1.
Cook, K. H., Vizy, E. K., Cook, K. H., and Vizy, E. K. (2015c). Detection and Analysis of an Amplified Warming of the Sahara Desert. *J. Clim.* 28, 6560–6580. doi:10.1175/JCLI-D-14-00230.1.
Corona, R., Montaldo, N., and Albertson, J. D. (2018). On the Role of NAO-Driven Interannual Variability in Rainfall Seasonality on Water Resources and Hydrologic Design in a Typical Mediterranean Basin. *J. Hydrometeorol.* 19, 485–498. doi:10.1175/JHM-D-17-0078.1.
Corringham, W., Richard, C., and Daniel, C. (2018). *Wildfires, Floods, and Climate Variability*. UC San Diego Dissertation: Floods Available at: https://escholarship.org/uc/ucsd_etd.
Costantino, L., and Bréon, F.-M. (2010). Analysis of aerosol-cloud interaction from multi-sensor satellite observations. *Geophys. Res. Lett.* 37, n/a-n/a. doi:10.1029/2009GL041828.
Coumou, D., Di Capua, G., Vavrus, S., Wang, L., and Wang, S. (2018). The influence of Arctic amplification on mid-latitude summer circulation. *Nat. Commun.* 9, 2959. doi:10.1038/s41467-018-05256-8.
Coumou, D., Lehmann, J., and Beckmann, J. (2015a). The weakening summer circulation in the Northern Hemisphere mid-latitudes. *Science (80-.).* 348, 324–327.
Coumou, D., Lehmann, J., and Beckmann, J. (2015b). The weakening summer circulation in the Northern Hemisphere mid-latitudes. *Science (80-.).* 348, 324–327. doi:10.1126/science.1261768.
Couvreux, F., Roehrig, R., Rio, C., Lefebvre, M.-P., Caian, M., Komori, T., et al. (2015). Representation of daytime moist convection over the semi-arid Tropics by parametrizations used in climate and meteorological models. *Q. J. R. Meteorol. Soc.* 141, 2220–2236. doi:10.1002/qj.2517.
Cox, P. M., Betts, R. A., Collins, M., Harris, P. P., Huntingford, C., and Jones, C. D. (2004). Amazonian forest dieback under climate-carbon cycle projections for the 21st century. *Theor. Appl. Climatol.* doi:10.1007/s00704-004-0049-4.
Cox, P., and Stephenson, D. (2007). CLIMATE CHANGE: A Changing Climate for Prediction. *Science (80-.).* 317, 207–208. doi:10.1126/science.1145956.
Crook, J. A., Jackson, L. S., Osprey, S. M., and Forster, P. M. (2015). A comparison of temperature and precipitation responses to different earth radiation management geoengineering schemes. *J. Geophys. Res.* doi:10.1002/2015JD023269.
Crosbie, R. S., Pickett, T., Mpelasoka, F. S., Hodgson, G., Charles, S. P., and Barron, O. V. (2013). An assessment of the climate change impacts on groundwater recharge at a continental scale using a probabilistic approach with an ensemble of GCMs. *Clim. Change* 117, 41–53. doi:10.1007/s10584-012-0558-6.
Cruz, F. W., Burns, S. J., Karmann, I., Sharp, W. D., Vuille, M., Cardoso, A. O., et al. (2005). Insolation-driven changes in atmospheric circulation over the past 116,000 years in subtropical Brazil. *Nature*. doi:10.1038/nature03365.
Cui, W., Dong, X., Xi, B., and Kennedy, A. (2017). Evaluation of Reanalyzed Precipitation Variability and Trends Using the Gridded Gauge-Based Analysis over the CONUS. *J. Hydrometeorol.* doi:10.1175/JHM-D-17-0029.1.
Cuthbert, M. O., Gleeson, T., Moosdorf, N., Befus, K. M., Schneider, A., Hartmann, J., et al. (2019). Global patterns and dynamics of climate–groundwater interactions. *Nat. Clim. Chang.* doi:10.1038/s41558-018-0386-4.
D'Agostino, R., Lionello, P., Adam, O., and Schneider, T. (2017). Factors controlling Hadley circulation changes from the Last Glacial Maximum to the end of the 21st century. *Geophys. Res. Lett.* doi:10.1002/2017GL074533.
D'Odorico, P., Davis, K. F., Rosa, L., Carr, J. A., Chiarelli, D., Dell'Angelo, J., et al. (2018). The Global Food-Energy-

Water Nexus. *Rev. Geophys.*, 1–76. doi:10.1029/2017RG000591.
Dacre, H. F., Clark, P. A., Martinez-Alvarado, O., Stringer, M. A., and Lavers, D. A. (2015). How Do Atmospheric Rivers Form? *Bull. Am. Meteorol. Soc.* 96, 1243–1255. doi:10.1175/bams-d-14-00031.1.
Dagon, K., and Schrag, D. P. (2016). Exploring the effects of solar radiation management on water cycling in a coupled land-atmosphere model. *J. Clim.* 29, 2635–2650. doi:10.1175/JCLI-D-15-0472.1.
Dagon, K., and Schrag, D. P. (2019). Quantifying the effects of solar geoengineering on vegetation. *Clim. Change*. doi:10.1007/s10584-019-02387-9.
Dai, A. (2016). Historical and future changes in streamflow and continental runoff: {A} review. *Terr. Water Cycle Clim. Chang. Nat. Human-Induced Impacts, Geophys. Monogr* 221, 17–37.
Dai, A., Zhao, T., and Chen, J. (2018). Climate Change and Drought: a Precipitation and Evaporation Perspective. *Curr. Clim. Chang. reports* 4, 301–312.
Dalin, C., Wada, Y., Kastner, T., and Puma, M. J. (2017). Groundwater depletion embedded in international food trade. *Nature* 543, 700–704. doi:10.1038/nature21403.
DallaSanta, K., Gerber, E. P., and Toohey, M. (2019). The Circulation Response to Volcanic Eruptions: The Key Roles of Stratospheric Warming and Eddy Interactions. *J. Clim.* 32, 1101–1120. doi:10.1175/JCLI-D-18-0099.1.
Dash, S. K., Kulkarni, M. A., Mohanty, U. C., and Prasad, K. (2009). Changes in the characteristics of rain events in India. *J. Geophys. Res. Atmos.* 114. doi:10.1029/2008JD010572.
Dätwyler, C., Neukom, R., Abram, N. J., Gallant, A. J. E., Grosjean, M., Jacques-Coper, M., et al. (2018). Teleconnection stationarity, variability and trends of the Southern Annular Mode (SAM) during the last millennium. *Clim. Dyn.* 51, 2321–2339. doi:10.1007/s00382-017-4015-0.
Davidson, E. A., de Araujo, A. C., Artaxo, P., Balch, J. K., Brown, I. F., Bustamante, M. M. C., et al. (2012). The Amazon basin in transition. *Nature* 481, 321–328. doi:DOI 10.1038/nature10717.
Davidson, N. C., Fluet-Chouinard, E., and Finlayson, C. M. (2018). Global extent and distribution of wetlands: trends and issues. Marine and Freshwater Research. 69, 620–627.
Davie, J. C. S., Falloon, P. D., Kahana, R., Dankers, R., Betts, R., Portmann, F. T., et al. (2013). Comparing projections of future changes in runoff from hydrological and biome models in ISI-MIP. *Earth Syst. Dyn.* 4, 359–374. doi:10.5194/esd-4-359-2013.
Davini, P., and D'Andrea, F. (2016). Northern Hemisphere atmospheric blocking representation in global climate models: Twenty years of improvements? *J. Clim.* 29, 8823–8840. doi:10.1175/JCLI-D-16-0242.1.
Davis, S. M., and Rosenlof, K. H. (2012). A multidiagnostic intercomparison of tropical-width time series using reanalyses and satellite observations. *J. Clim.* 25, 1061–1078.
Day, J. A., Fung, I., and Liu, W. (2018). Changing character of rainfall in eastern China, 1951-2007. *Proc. Natl. Acad. Sci. U. S. A.* 115, 2016–2021. doi:10.1073/pnas.1715386115.
de Boisséson, E., Balmaseda, M. A., Abdalla, S., K"allén, E., and Janssen, P. A. E. M. (2014). How robust is the recent strengthening of the tropical Pacific trade winds? *Geophys. Res* 41, 4398–4405. doi:10.1002/2014GL060257.
de Carvalho, L. M. V., and Cavalcanti, I. F. A. (2016). "The South American Monsoon System (SAMS)," in *The monsoons and climate change: Observations and modeling*, 121–148. doi:10.1007/978-3-319-21650-8_6.
De Kauwe, M. G., Medlyn, B. E., Zaehle, S., Walker, A. P., Dietze, M. C., Hickler, T., et al. (2013). Forest water use and water use efficiency at elevated CO2: A model-data intercomparison at two contrasting temperate forest FACE sites. *Glob. Chang. Biol.* doi:10.1111/gcb.12164.
De Souza, E. B., and Ambrizzi, T. (2006). Modulation of the intraseasonal rainfall over tropical Brazil by the Madden–Julian oscillation. *Int. J. Climatol.* 26, 1759–1776. doi:10.1002/joc.1331.
De Vrese, P., Hagemann, S., and Claussen, M. (2016). Asian irrigation, African rain: Remote impacts of irrigation. *Geophys. Res. Lett.* 43, 3737–3745. doi:10.1002/2016GL068146.
DeAngelis, A. M., Qu, X., and Hall, A. (2016). Importance of vegetation processes for model spread in the fast precipitation response to CO2forcing. *Geophys. Res. Lett.* 43, 12,550-12,559. doi:10.1002/2016GL071392.
Deangelis, A. M., Qu, X., Zelinka, M. D., and Hall, A. (2015). An observational radiative constraint on hydrologic cycle intensification. *Nature* 528, 249–253. doi:10.1038/nature15770.
DeBeer, C. M., Wheater, H. S., Carey, S. K., and Chun, K. P. (2016). Recent climatic, cryospheric, and hydrological changes over the interior of western Canada: a review and synthesis. *Hydrol. Earth Syst. Sci.* 20, 1573–1598. doi:10.5194/hess-20-1573-2016.
Debortoli, N., Dubreuil, V., Fanatsu, B., Delahaye, F., de Oliveira Henke, C., Rodrigues-Filho, S., et al. (2015). Rainfall Patterns in the Southern Amazon: a chronological perspective (1970-2010). *Clim. Change* 130, 1573–1480. doi:DOI: 10.1007/s10584-015-1415-1.
Debortoli, N. S., Dubreuil, V., Hirota, M., Filho, S. R., Lindoso, D. P., and Nabucet, J. (2016). Detecting deforestation impacts in Southern Amazonia rainfall using rain gauges. *Int. J. Climatol.* 37, 2889–2900. doi:10.1002/joc.4886.
Decharme, B., Alkama, R., Papa, F., Faroux, S., Douville, H., and Prigent, C. (2012). Global off-line evaluation of the ISBA-TRIP flood model. *Clim. Dyn.* 38, 1389–1412. doi:10.1007/s00382-011-1054-9.
Decharme, B., Brun, E., Boone, A., Delire, C., Le Moigne, P., and Morin, S. (2016). Impacts of snow and organic soils

parameterization on northern Eurasian soil temperature profiles simulated by the ISBA land surface model. *Cryosphere* 10, 853–877. doi:10.5194/tc-10-853-2016.
Decharme, B., and Douville, H. (2007). Global validation of the ISBA sub-grid hydrology. *Clim. Dyn.* 29, 21–37. doi:10.1007/s00382-006-0216-7.
DeConto, R. M., and Pollard, D. (2016). Contribution of Antarctica to past and future sea-level rise. *Nature* 531, 591. Available at: https://doi.org/10.1038/nature17145.
Dee, S. G., Parsons, L. A., Loope, G. R., Overpeck, J. T., Ault, T. R., and Emile-Geay, J. (2017). Improved spectral comparisons of paleoclimate models and observations via proxy system modeling: Implications for multi-decadal variability. *Earth Planet. Sci. Lett.* doi:10.1016/j.epsl.2017.07.036.
Defrance, D., Ramstein, G., Charbit, S., Vrac, M., Famien, A. M., Sultan, B., et al. (2017). Consequences of rapid ice sheet melting on the Sahelian population vulnerability. *Proc. Natl. Acad. Sci.* doi:10.1073/pnas.1619358114.
Del Genio, A. D., Chen, Y., Kim, D., and Yao, M. S. (2012). The mjo transition from shallow to deep convection in cloudsat/calipso data and giss gcm simulations. *J. Clim.* 25, 3755–3770.
Del Genio, A. D., and Wu, J. (2010). The role of entrainment in the diurnal cycle of continental convection. *J. Clim.* 23, 2722–2738.
DelSole, T., and Shukla, J. (2012). Climate models produce skillful predictions of Indian summer monsoon rainfall. *Geophys. Res. Lett.* 39, n/a-n/a. doi:10.1029/2012GL051279.
Delworth, T. L., and Zeng, F. (2014). Regional rainfall decline in Australia attributed to anthropogenic greenhouse gases and ozone levels. *Nat. Geosci.* doi:10.1038/ngeo2201.
Delworth, T. L., Zeng, F., Vecchi, G. A., Yang, X., Zhang, L., and Zhang, R. (2016). The North Atlantic Oscillation as a driver of rapid climate change in the Northern Hemisphere. 9, 509–513. doi:10.1038/NGEO2738.
deMenocal, P. B. (1995). Plio-Pleistocene African climate. *Science (80-.).* 270, 53–59.
deMenocal, P. B., Ortiz, J., Guilderson, T., Adkins, J. F., Sarnthein, M., Baker, L., et al. (2000). Abrupt onset and termination of the African Humid Period: rapid climate responses to gradual insolation forcing. *Quat. Sci. Rev.* 19, 347–361.
deMenocal, P. B., and Tierney, J. E. (2012). Green Sahara: African humid periods paced by Earth's orbital changes. *Nat. Educ. Knowl.* 3, 12.
Demory, M. E., Vidale, P. L., Roberts, M. J., Berrisford, P., Strachan, J., Schiemann, R., et al. (2014). The role of horizontal resolution in simulating drivers of the global hydrological cycle. *Clim. Dyn.* 42, 2201–2225. doi:10.1007/s00382-013-1924-4.
Deng, J., and Xu, H. (2016). Nonlinear effect on the East Asian summer monsoon due to two coexisting anthropogenic forcing factors in eastern China: an AGCM study. *Clim. Dyn.* 46, 3767–3784. doi:10.1007/s00382-015-2803-y.
Deng, K., Yang, S., Ting, M., Tan, Y., and He, S. (2018). Global Monsoon Precipitation: Trends, Leading Modes, and Associated Drought and Heat Wave in the Northern Hemisphere. *J. Clim.* 31, 6947–6966. doi:10.1175/JCLI-D-17-0569.1.
Denniston, R. F., Ummenhofer, C. C., Wanamaker, A. D., Lachniet, M. S., Villarini, G., Asmerom, Y., et al. (2016). Expansion and contraction of the Indo-Pacific tropical rain belt over the last three millennia. *Sci. Rep.* 6, 34485. doi:10.1038/srep34485.
Denniston, R. F., Wyrwoll, K. -h., Polyak, V. J., Brown, J. R., Asmerom, Y., Jr, A. D. W., et al. (2013). A Stalagmite record of Holocene Indonesian-Australian summer monsoon variability from the Australian tropics. *Quat. Sci. Rev.* 78, 155–168.
Descroix, L., Diongue Niang, A., Dacosta, H., Panthou, G., Quantin, G., Diedhiou, A., et al. (2013). ÉVOLUTION DES PLUIES DE CUMUL ÉLEVÉ ET RECRUDESCENCE DES CRUES DEPUIS 1951 DANS LE BASSIN DU NIGER MOYEN (SAHEL). Available at: http://lodel.irevues.inist.fr/climatologie/docannexe/file/78/37_descroix.pdf [Accessed March 27, 2019].
Descroix, L., Diongue Niang, A., Panthou, G., Bodian, A., Sane, Y., Dacosta, H., et al. (2015). ÉVOLUTION RÉCENTE DE LA PLUVIOMÉTRIE EN AFRIQUE DE L'OUEST À TRAVERS DEUX RÉGIONS : LA SÉNÉGAMBIE ET LE BASSIN DU NIGER MOYEN. Available at: http://lodel.irevues.inist.fr/climatologie/docannexe/file/1105/descroix_et_al_climatologie_2015_pages_25_a_43.pdf [Accessed March 27, 2019].
Descroix, L., Guichard, F., Grippa, M., Lambert, L., Panthou, G., Mahé, G., et al. (2018). Evolution of Surface Hydrology in the Sahelo-Sudanian Strip: An Updated Review. *Water* 10, 748. doi:10.3390/w10060748.
Deser, C., Hurrell, J. W., and Phillips, A. S. (2017). The role of the North Atlantic Oscillation in European climate projections. *Clim. Dyn.* 49, 3141–3157. doi:10.1007/s00382-016-3502-z.
Deser, C., Phillips, A., Bourdette, V., and Teng, H. (2012). Uncertainty in climate change projections: the role of internal variability. *Clim. Dyn.* 38, 527–546. doi:10.1007/s00382-010-0977-x.
Deser, C., Simpson, I. R., Phillips, A. S., and McKinnon, K. A. (2018). How Well Do We Know ENSO's Climate Impacts over North America, and How Do We Evaluate Models Accordingly? *J. Clim.* 31, 4991–5014. doi:10.1175/JCLI-D-17-0783.1.

Deser, C., Tomas, R. A., and Sun, L. (2015). The Role of Ocean–Atmosphere Coupling in the Zonal-Mean Atmospheric Response to Arctic Sea Ice Loss. *J. Clim.* 28, 2168–2186. doi:10.1175/JCLI-D-14-00325.1.
Dey, R., Lewis, S. C., and Abram, N. J. (2019). Investigating observed northwest Australian rainfall trends in Coupled Model Intercomparison Project phase 5 detection and attribution experiments. *Int. J. Climatol.* 39, 112–127. doi:10.1002/joc.5788.
Dey, R., Lewis, S. C., and N. J., A. (2018). Investigating observed northwest Australian rainfall trends in Coupled Model Intercomparison Project phase 5 detection and attribution experiments. *Int. J. Climatol.* 10, 1–16.
Di Baldassarre, G., Wanders, N., AghaKouchak, A., Kuil, L., Rangecroft, S., Veldkamp, T. I. E., et al. (2018). Water shortages worsened by reservoir effects. *Nat. Sustain.* 1, 617–622.
Di Luca, A., de Elía, R., and Laprise, R. (2015). Challenges in the Quest for Added Value of Regional Climate Dynamical Downscaling. *Curr. Clim. Chang. Reports* 1, 10–21. doi:10.1007/s40641-015-0003-9.
Diatta, S., and Fink, A. H. (2014). Statistical relationship between remote climate indices and West African monsoon variability. *Int. J. Climatol.* 34, 3348–3367. doi:10.1002/joc.3912.
Díaz, L. B., and Vera, C. S. (2018). South American precipitation changes simulated by PMIP3/CMIP5 models during the Little Ice Age and the recent global warming period. *Int. J. Climatol.* 38, 2638–2650. doi:10.1002/joc.5449.
Diem, J. E. (2013). Influences of the Bermuda High and atmospheric moistening on changes in summer rainfall in the Atlanta, Georgia region, USA. *Int. J. Climatol.* 33, 160–172. doi:10.1002/joc.3421.
Diem, J. E., Brown, D. P., and McCann, J. (2013). Multi-decadal changes in the North American monsoon anticyclone. *Int. J. Climatol.* 33, 2274–2279.
Diffenbaugh, N. S., Scherer, M., and Trapp, R. J. (2013). Robust increases in severe thunderstorm environments in response to greenhouse forcing. *Proc. Natl. Acad. Sci.* doi:10.1073/pnas.1307758110.
DiNezio, P. N., Clement, A., Vecchi, G. A., Soden, B., Broccoli, A. J., Otto-Bliesner, B. L., et al. (2011). The response of the Walker circulation to Last Glacial Maximum forcing: Implications for detection in proxies. *Paleoceanography* 26. doi:10.1029/2010PA002083.
DiNezio, P. N., and Tierney, J. E. (2013). The effect of sea level on glacial Indo-Pacific climate. *Nat. Geosci.* 6, 485–491. doi:10.1038/ngeo1823.
DiNezio, P. N., Tierney, J. E., Otto-Bliesner, B. L., Timmermann, A., Bhattacharya, T., Rosenbloom, N., et al. (2018). Glacial changes in tropical climate amplified by the Indian Ocean. *Sci. Adv.* 4, eaat9658.
Dirmeyer, P. A., Chen, L., Wu, J., Shin, C., Huang, B., Cash, B. A., et al. (2018). Verification of Land–Atmosphere Coupling in Forecast Models, Reanalyses, and Land Surface Models Using Flux Site Observations. *J. Hydrometeorol.* 19, 375. Available at: https://doi.org/10.1175/JHM-D-17-0152.1.
Dirmeyer, P. A., and Halder, S. (2017). Application of the Land–Atmosphere Coupling Paradigm to the Operational Coupled Forecast System, Version 2 (CFSv2). *J. Hydrometeorol.* 18, 85. Available at: https://doi.org/10.1175/JHM-D-16-0064.1.
Dixit, V., Geoffroy, O., and Sherwood, S. C. (2018). Control of ITCZ Width by Low-Level Radiative Heating From Upper-Level Clouds in Aquaplanet Simulations. *Geophys Res Lett* 10, 5788–5797. doi:10.1029/2018GL078292.
Doell, P., Schmied, H. M., Schuh, C., Portmann, F. T., and Eicker, A. (2014). Global-scale assessment of groundwater depletion and related groundwater abstractions: Combining hydrological modeling with information from well observations and GRACE satellites. *Water Resour. Res.* 50, 5698–5720.
Dogar, M. M. (2018). Impact of Tropical Volcanic Eruptions on Hadley Circulation Using a High-Resolution AGCM. *Curr. Sci.* 114, 1284. doi:10.18520/cs/v114/i06/1284-1294.
Döll, P., Douville, H., Güntner, A., Müller Schmied, H., and Wada, Y. (2016). Modelling Freshwater Resources at the Global Scale: Challenges and Prospects. *Surv. Geophys.* 37, 195–221. doi:10.1007/s10712-015-9343-1.
Doll, P., Douville, H., Guntner, A., Schmied, H. M., and Wada, Y. (2016). Modelling Freshwater Resources at the Global Scale: Challenges and Prospects. *Surv. Geophys.* 37, 195–221. doi:10.1007/s10712-015-9343-1.
Döll, P., and Fiedler, K. (2008). Global-scale modeling of groundwater recharge. *Hydrol. Earth Syst. Sci.* 12, 863–885. doi:10.5194/hess-12-863-2008.
Döll, P., Hoffmann-Dobrev, H., Portmann, F. T., Siebert, S., Eicker, A., Rodell, M., et al. (2012). Impact of water withdrawals from groundwater and surface water on continental water storage variations. *J. Geodyn.* 59, 143–156.
Döll, P., Trautmann, T., Gerten, D., Schmied, H. M., Ostberg, S., Fahad, S., et al. (2018). Risks for the global freshwater system at 1.5°C and 2°C global warming. *Environ. Res. Lett.* Volume 13, 15.
Dommenget, D., and Yu, Y. (2017). The effects of remote SST forcings on ENSO dynamics, variability and diversity. *Clim. Dyn.* 49, 2605–2624. doi:10.1007/s00382-016-3472-1.
Donat, M. G., Alexander, L. V., Herold, N., and Dittus, A. J. (2016a). Temperature and precipitation extremes in century-long gridded observations, reanalyses, and atmospheric model simulations. *J. Geophys. Res.* doi:10.1002/2016JD025480.
Donat, M. G., Lowry, A. L., Alexander, L. V., O'Gorman, P. A., and Maher, N. (2016b). More extreme precipitation in the world's dry and wet regions. *Nat. Clim. Chang.* 6, 508–513. doi:10.1038/nclimate2941.
Donchyts, G., Baart, F., Winsemius, H., Gorelick, N., Kwadijk, J., and Van De Giesen, N. (2016). Earth's surface water

change over the past 30 years. Nature Climate Change. 6, 810.

Dong, B., and Sutton, R. (2015a). Dominant role of greenhouse-gas forcing in the recovery of Sahel rainfall. *Nat. Clim. Chang.* 5, 757–760. doi:10.1038/nclimate2664.

Dong, B., and Sutton, R. (2015b). Dominant role of greenhouse-gas forcing in the recovery of Sahel rainfall. *Nat. Clim. Chang.* 5, 757–760. doi:10.1038/nclimate2664.

Dong, B., Sutton, R. T., Highwood, E. J., and Wilcox, L. J. (2016). Preferred response of the East Asian summer monsoon to local and non-local anthropogenic sulphur dioxide emissions. *Clim. Dyn.* 46, 1733–1751.

Dong, B., Sutton, R. T., Highwood, E., and Wilcox, L. (2014). The impacts of European and Asian anthropogenic sulfur dioxide emissions on Sahel rainfall. *J. Clim.* 27, 7000–7017. doi:10.1175/JCLI-D-13-00769.1.

Dong, B., Sutton, R. T., Shaffrey, L., and Klingaman, N. P. (2017). Attribution of Forced Decadal Climate Change in Coupled and Uncoupled Ocean–Atmosphere Model Experiments. *J. Clim.* 30, 6203–6223. doi:10.1175/JCLI-D-16-0578.1.

Dong, B., Wilcox, L. J., Highwood, E. J., and Sutton, R. T. (2019). Impacts of recent decadal changes in Asian aerosols on the East Asian summer monsoon: roles of aerosol–radiation and aerosol–cloud interactions. *Clim. Dyn.* doi:10.1007/s00382-019-04698-0.

Dong, L., Leung, L. R., Song, F., and Lu, J. (2018a). Roles of SST versus Internal Atmospheric Variability in Winter Extreme Precipitation Variability along the U.S. West Coast. *J. Clim.* 31, 8039–8058. doi:10.1175/JCLI-D-18-0062.1.

Dong, L., Leung, L. R., Song, F., and Lu, J. (2018b). Roles of SST versus Internal Atmospheric Variability in Winter Extreme Precipitation Variability along the U.S. West Coast. *J. Clim.* 31, 8039–8058. doi:10.1175/JCLI-D-18-0062.1.

Dong, L., and Zhou, T. (2014). The Indian Ocean Sea Surface Temperature Warming Simulated by CMIP5 Models during the Twentieth Century: Competing Forcing Roles of GHGs and Anthropogenic Aerosols. *J. Clim.* 27, 3348–3362. doi:10.1175/JCLI-D-13-00396.1.

Donohoe, A., Marshall, J., Ferreira, D., and Mcgee, D. (2013). The relationship between ITCZ location and cross-equatorial atmospheric heat transport: From the seasonal cycle to the last glacial maximum. *J. Clim.* doi:10.1175/JCLI-D-12-00467.1.

Donohoe, A., and Voigt, A. (2017). "Why Future Shifts in Tropical Precipitation Will Likely Be Small," in doi:10.1002/9781119068020.ch8.

Dorigo, W. A., Gruber, A., De Jeu, R. A. M., Wagner, W., Stacke, T., Loew, A., et al. (2015). Evaluation of the ESA CCI soil moisture product using ground-based observations. *Remote Sens. Environ.* 162, 380–395. doi:10.1016/j.rse.2014.07.023.

Dorigo, W., Wagner, W., Albergel, C., Albrecht, F., Balsamo, G., Brocca, L., et al. (2017). ESA CCI Soil Moisture for improved Earth system understanding: State-of-the art and future directions. *Remote Sens. Environ.* 203, 185–215. doi:10.1016/j.rse.2017.07.001.

Dosio, A., Panitz, H. J., Schubert-Frisius, M., and Lüthi, D. (2015). Dynamical downscaling of CMIP5 global circulation models over CORDEX-Africa with COSMO-CLM: evaluation over the present climate and analysis of the added value. *Clim. Dyn.* doi:10.1007/s00382-014-2262-x.

Dou, J., Wu, Z., and Zhou, Y. (2017). Potential impact of the May Southern Hemisphere annular mode on the Indian summer monsoon rainfall. *Clim. Dyn.* 49, 1257–1269. doi:10.1007/s00382-016-3380-4.

Douville, H., Colin, J., Krug, E., Cattiaux, J., and Thao, S. (2016). Midlatitude daily summer temperatures reshaped by soil moisture under climate change. *Geophys. Res. Lett.* 43, 812–818. doi:10.1002/2015GL066222.

Douville, H., Decharme, B., Ribes, A., Alkama, R., and Sheffield, J. (2012a). *Anthropogenic influence on multi-decadal changes in reconstructed global evapotranspiration*. Nature Climate Change doi:10.1038/NCLIMATE1632.

Douville, H., and Plazzotta, M. (2017). Midlatitude Summer Drying: An Underestimated Threat in CMIP5 Models? *Geophys. Res. Lett.* 44, 9967–9975. doi:10.1002/2017GL075353.

Douville, H., Ribes, A., Decharme, B., Alkama, R., Sheffield, J., Ribes, A., et al. (2012b). *Anthropogenic influence on multidecadal changes in reconstructed global evapotranspiration*. Nature Climate Change doi:10.1038/NCLIMATE1632.

Douville, H., Ribes, A., and Tyteca, S. (2018). Breakdown of NAO reproducibility into internal versus externally-forced components: a two-tier pilot study. *Clim. Dyn.* 0, 1–20. doi:10.1007/s00382-018-4141-3.

Drake, N., and Bristow, C. (2006). Shorelines in the Sahara: Geomorphological evidence for an enhanced monsoon from palaeolake Megachad. *Holocene* 16, 901–911. doi:10.1191/0959683606hol981rr.

Drijfhout, S., Bathiany, S., Beaulieu, C., Brovkin, V., Claussen, M., Huntingford, C., et al. (2015). Catalogue of abrupt shifts in Intergovernmental Panel on Climate Change climate models. *Proc. Natl. Acad. Sci.* 112, E5777–E5786. doi:10.1073/pnas.1511451112.

Driscoll, S., Bozzo, A., Gray, L. J., Robock, A., and Stenchikov, G. (2012). Coupled Model Intercomparison Project 5 (CMIP5) simulations of climate following volcanic eruptions. *J. Geophys. Res. Atmos.* 117, n/a-n/a. doi:10.1029/2012JD017607.

Driver, P., and Reason, C. J. C. (2017). Variability in the Botswana High and its relationships with rainfall and temperature characteristics over southern Africa. *Int. J. Climatol.* 37, 570–581. doi:10.1002/joc.5022.
Drumond, A., Marengo, J., Ambrizzi, T., Nieto, R., Moreira, L., and Gimeno, L. (2014). The role of the Amazon Basin moisture in the atmospheric branch of the hydrological cycle: A Lagrangian analysis. *Hydrol. Earth Syst. Sci.* 18, 2577–2598. doi:10.5194/hess-18-2577-2014.
Dufour, A., Zolina, O., and Gulev, S. K. (2016). Atmospheric Moisture Transport to the Arctic: Assessment of Reanalyses and Analysis of Transport Components. *J. Clim.* 29, 5061–5081. doi:10.1175/JCLI-D-15-0559.1.
Dunn, R. J. H., Willett, K. M., Ciavarella, A., and Stott, P. A. (2017). Comparison of land surface humidity between observations and CMIP5 models. *Earth Syst. Dyn.* 8, 719–747. doi:10.5194/esd-8-719-2017.
Dunning, C. M., Black, E., and Allan, R. P. (2018). Later wet seasons with more intense rainfall over Africa under future climate change. *J. Clim.*, JCLI-D-18-0102.1. doi:10.1175/JCLI-D-18-0102.1.
Durack, P. (2015). Ocean Salinity and the Global Water Cycle. *Oceanography* 28, 20–31. doi:10.5670/oceanog.2015.03.
Durack, P. J., and Wijffels, S. E. (2010). Fifty-Year Trends in Global Ocean Salinities and Their Relationship to Broad-Scale Warming. *J. Clim.* 23, 4342–4362. doi:10.1175/2010JCLI3377.1.
Durack, P. J., Wijffels, S. E., and Matear, R. J. (2012a). During 1950 to 2000. *Science (80-.).* 336, 455–458. doi:10.1126/science.1212222.
Durack, P. J., Wijffels, S. E., and Matear, R. J. (2012b). Ocean salinities reveal strong global water cycle intensification during 1950 to 2000. *Science* 336, 455–8. doi:10.1126/science.1212222.
Durán-Quesada, A. M., Gimeno, L., and Amador, J. (2017). Role of moisture transport for Central American precipitation. *Earth Syst. Dyn.* 8, 147–161. doi:10.5194/esd-8-147-2017.
Dutt, S., Gupta, A. K., Clemens, S. C., Cheng, H., Singh, R. K., Kathayat, G., et al. (2015). Abrupt changes in Indian summer monsoon strength during 33,800 to 5500 years B.P. *Geophys. Res. Lett.* 42, 5526–5532. doi:10.1002/2015GL064015.
Dwyer, J. G., Biasutti, M., and Sobel, A. H. (2014). The Effect of Greenhouse Gas–Induced Changes in SST on the Annual Cycle of Zonal Mean Tropical Precipitation. *J. Clim.* 27, 4544–4565. doi:10.1175/JCLI-D-13-00216.1.
Dwyer, J. G., and O'Gorman, P. A. (2017). Changing duration and spatial extent of midlatitude precipitation extremes across different climates. *Geophys. Res. Lett.* 44, 5863–5871. doi:10.1002/2017GL072855.
Dyer, J. L., and Mote, T. L. (2006). Spatial variability and trends in observed snow depth over North America. *Geophys. Res. Lett.* 33, L16503. doi:10.1029/2006GL027258.
Dykoski, C., Edwards, R., Cheng, H., Yuan, D., Cai, Y., Zhang, M., et al. (2005). A high-resolution, absolute-dated Holocene and deglacial Asian monsoon record from Dongge Cave, China. *Earth Planet. Sci. Lett.* 233, 71–86. doi:10.1016/j.epsl.2005.01.036.
Easterling, D. R., Kunkel, K. E., Arnold, J. R., Knutson, T., LeGrande, A. N., Leung, L. R., et al. (2017). "Precipitation change in the United States," in *Climate Science Special Report: Fourth National Climate Assessment*, eds. V. I. [Wuebbles, D. W. F. D. J., K. A. Hibbard, D. J. Dokken, B. C. Stewart, and T. K. Maycock (Washington, DC, USA: U.S. Global Change Research Program), 207–230. doi:10.7930/J0H993CC.
Easterling, D. R., Kunkel, K. E., Wehner, M. F., and Sun, L. (2016). Detection and attribution of climate extremes in the observed record. *Weather Clim. Extrem.* doi:10.1016/j.wace.2016.01.001.
Eekhout, J. P. C., Hunink, J. E., Terink, W., and de Vente, J. (2018). Why increased extreme precipitation under climate change negatively affects water security. *Hydrol. Earth Syst. Sci.* 22, 5935–5946. doi:10.5194/hess-22-5935-2018.
Ekholm, T., and Korhonen, H. (2016). Climate change mitigation strategy under an uncertain Solar Radiation Management possibility. *Clim. Change* 139, 503–515. doi:10.1007/s10584-016-1828-5.
Emanuel, K. (2017). Assessing the present and future probability of Hurricane Harvey's rainfall. in *Proc. Nat* (114: Acad. Sci), 12681–12684.
Emerton, R., Cloke, H. L., Stephens, E. M., Zsoter, E., Woolnough, S. J., and Pappenberger, F. (2017). Complex picture for likelihood of ENSO-driven flood hazard. *Nat. Commun.*8, 14796. doi:10.1038/ncomms14796.
Engel, T., Fink, A. H., Knippertz, P., Pante, G., Bliefernicht, J., Engel, T., et al. (2017). Extreme Precipitation in the West African Cities of Dakar and Ouagadougou: Atmospheric Dynamics and Implications for Flood Risk Assessments. *J. Hydrometeorol.* 18, 2937–2957. doi:10.1175/JHM-D-16-0218.1.
Ershadi, A., McCabe, M., Evans, J., Chaney, N., and Wood, E. (2014). Multi-site evaluation of terrestrial evaporation models using FLUXNET data. *Agric. For. Meteorol.* 187, 46. doi:10.1016/j.agrformet.2013.11.008.
Ershadi, A., McCabe, M., Evans, J., and Wood, E. (2015). Impact of model structure and parameterization on Penman-Monteith type evaporation models. *J. Hydrol.* 525, 521. doi:10.1016/j.jhydrol.2015.04.008.
Espinoza, J. C., and Marengo, J. A. (2015). Extreme seasonal droughts and floods in Amazonia: causes, trends and impacts. *Int. J. Climatol.* 36, 1033–1050.
Espinoza, J. C., Ronchail, J., Marengo, J. A., and Segura, H. (2018a). Contrasting North–South changes in Amazon wet-day and dry-day frequency and related atmospheric features (1981–2017). *Clim. Dyn.*, 1–22.

doi:https://doi.org/10.1007/s00382-018-4462-2.
Espinoza, J. C., Segura, H., Ronchail, J., Drapeau, G., and Gutierrez-Cori, O. (2016). Evolution of wet-day and dry-day frequency in the western Amazon basin: Relationship with atmospheric circulation and impacts on vegetation. *Water Resour. Res.* 52, 8546–8560. doi:10.1002/2016WR019305.
Espinoza, V., Waliser, D. E., Guan, B., Lavers, D. A., and Ralph, F. M. (2018b). Global Analysis of Climate Change Projection Effects on Atmospheric Rivers. *Geophys. Res. Lett.* 45, 4299–4308. doi:10.1029/2017GL076968.
Evan, A. T., Flamant, C., Lavaysse, C., Kocha, C., and Saci, A. (2015). Water vapor-forced greenhouse warming over the Sahara desert and the recent recovery from the Sahelian drought. *J. Clim.* 28, 108–123. doi:10.1175/JCLI-D-14-00039.1.
Eyring, V., Righi, M., Lauer, A., Evaldsson, M., Wenzel, S., Jones, C., et al. (2016). ESMValTool (v1.0)-a community diagnostic and performance metrics tool for routine evaluation of Earth system models in CMIP. *Geosci. Model Dev.* 9, 1747–1802. doi:10.5194/gmd-9-1747-2016.
Fahad Saeed and Ingo Bethke and Erich Fischer and Stephanie Legutke and Hideo Shiogama and Dáithí A Stone and Carl-Friedrich Schleussner (2018). Robust changes in tropical rainy season length at 1.5 °C and 2 °C. *Environ. Res. Lett.* 13, 64024. Available at: http://stacks.iop.org/1748-9326/13/i=6/a=064024.
Famiglietti, J., Cazenave, A., Eicker, A., Reager, J., Rodell, M., and Velicogna, I. (2015). Satellites provide the big picture. *Science (80-.).* 349, 684–685.
Famiglietti, J. S. (2014). The global groundwater crisis. *Nat. Clim. Chang.* 4, 945–948.
Fan, F., Dong, X., Fang, X., Xue, F., Zheng, F., and Zhu, J. (2017). Revisiting the relationship between the South Asian summer monsoon drought and El Niño warming pattern. *Atmos. Sci. Lett.* 18, 175–182. doi:10.1002/asl.740.
Fan, J., Rosenfeld, D., Yang, Y., Zhao, C., Ruby Leung, L., and Li, Z. (2015). Substantial contribution of anthropogenic air pollution to catastrophic floods in Southwest China. *Geophys. Res. Lett.* 42, 6066–6075. doi:10.1002/2015GL064479.
Fan, J., Rosenfeld, D., Zhang, Y., Giangrande, S. E., Li, Z., Machado, L. A. T., et al. (2018a). Substantial convection and precipitation enhancements by ultrafine aerosol particles. *Science (80-.).* 359, 411–418. doi:10.1126/science.aan8461.
Fan, J., Rosenfeld, D., Zhang, Y., Giangrande, S. E., Li, Z., Machado, L. A. T., et al. (2018b). Substantial convection and precipitation enhancements by ultrafine aerosol particles. *Science (80-.).* 359. doi:10.1126/science.aan8461.
Fan, Y., Fan, K., Xu, Z., and Li, S. (2018c). ENSO–South China Sea summer monsoon interaction modulated by the Atlantic Multidecadal Oscillation. *J. Clim.*, JCLI-D-17-0448.1. doi:10.1175/JCLI-D-17-0448.1.
Fasullo, J., Lawrence, D., and Swenson, S. (2016). *Are GRACE-era Terrestrial Water Trends Driven by Anthropogenic Climate Change?*. Advances in Meteorology.
Fatichi, S., Ivanov, V. Y., Paschalis, A., Peleg, N., Molnar, P., Rimkus, S., et al. (2016). Uncertainty partition challenges the predictability of vital details of climate change. *Earth's Futur.* 4, 240–251. doi:10.1002/2015EF000336.
Favreau, G., Cappelaere, B., Massuel, S., Leblanc, M., Boucher, M., Boulain, N., et al. (2009). Land clearing, climate variability, and water resources increase in semiarid southwest Niger: A review. *Water Resour. Res.* 45.
Feng, W., Zhong, M., Lemoine, J.-M., Biancale, R., Hsu, H.-T., and Xia, J. (2013). Evaluation of groundwater depletion in North China using the Gravity Recovery and Climate Experiment (GRACE) data and ground-based measurements. *Water Resour. Res.* 49, 2110–2118. doi:10.1002/wrcr.20192.
Fereday, D., Chadwick, R., Knight, J., and Scaife, A. A. (2018). Atmospheric Dynamics is the Largest Source of Uncertainty in Future Winter European Rainfall. *J. Clim.* 31, 963–977. doi:10.1175/JCLI-D-17-0048.1.
Ferguson, C. R., and Wood, E. F. (2011). Observed land-Atmosphere coupling from satellite remote sensing and reanalysis. *J. Hydrometeorol.* 12, 1221. doi:10.1175/2011JHM1380.1.
Ferguson, G., and Gleeson, T. (2012). Vulnerability of coastal aquifers to groundwater use and climate change. *Nat. Clim. Chang.* 2, 342–345.
Ferguson, G., McIntosh, J. C., Perrone, D., and Jasechko, S. (2018). Competition for shrinking window of low salinity groundwater. *Environ. Res. Lett.* 13, 114013. doi:10.1088/1748-9326/aae6d8.
Ferraro, A. J., Highwood, E. J., and Charlton-Perez, A. J. (2014). Weakened tropical circulation and reduced precipitation in response to geoengineering. *Environ. Res. Lett.* doi:10.1088/1748-9326/9/1/014001.
Field, R. D., van der Werf, G. R., and Shen, S. S. P. (2009). Human amplification of drought-induced biomass burning in Indonesia since 1960. *Nat. Geosci.* 2, 185–188. doi:10.1038/ngeo443.
Fischer, E. M., and Knutti, R. (2016). Observed heavy precipitation increase confirms theory and early models. *Nat. Clim. Chang.* 6, 986–991. doi:10.1038/nclimate3110.
Fisher, R. A., Koven, C. D., Anderegg, W. R. L., Christoffersen, B. O., Dietze, M. C., Farrior, C. E., et al. (2018). Vegetation demographics in Earth System Models: A review of progress and priorities. *Glob. Chang. Biol.* 24, 35–54. doi:10.1111/gcb.13910.
Fläschner, D., Mauritsen, T., and Stevens, B. (2016). Understanding the intermodel spread in global-mean hydrological sensitivity. *J. Clim.* 29, 801–817. doi:10.1175/JCLI-D-15-0351.1.

Fleming, S. W., and Quilty, E. J. (2006). Aquifer Responses to El Niño-Southern Oscillation, Southwest British Columbia. *Ground Water* 44, 595–599. doi:10.1111/j.1745-6584.2006.00187.x.
Fletcher, M.-S., Benson, A., Bowman, D. M. J. S., Gadd, P. S., Heijnis, H., Mariani, M., et al. (2018). Centennial-scale trends in the Southern Annular Mode revealed by hemisphere-wide fire and hydroclimatic trends over the past 2400 years. *Geology* 46, 363–366. doi:10.1130/G39661.1.
Fluet-Chouinard, E., Lehner, B., Rebelo, L. M., Papa, F., and Hamilton, S. K. (2015). Development of a global inundation map at high spatial resolution from topographic downscaling of coarse-scale remote sensing data. Remote Sensing of Environment. 158, 348–361.
Fogt, R. L., Bromwich, D. H., and Hines, K. M. (2011). Understanding the SAM influence on the South Pacific ENSO teleconnection. *Clim. Dyn.* 36, 1555–1576. doi:10.1007/s00382-010-0905-0.
Forootan, E., Khandu, Awange, J. L., Schumacher, M., Anyah, R. O., van Dijk, A. I. J. M., et al. (2016). Quantifying the impacts of ENSO and IOD on rain gauge and remotely sensed precipitation products over Australia. *Remote Sens. Environ.* 172, 50–66. doi:10.1016/j.rse.2015.10.027.
Fosser, G., Khodayar, S., and Berg, P. (2017). Climate change in the next 30 years: What can a convection-permitting model tell us that we did not already know? *Clim. Dyn.* 48, 1987–2003. doi:10.1007/s00382-016-3186-4.
Francis, J. A., and Vavrus, S. J. (2012). Evidence linking Arctic amplification to extreme weather in mid-latitudes. *Geophys. Res. Lett.* 39, n/a--n/a. doi:10.1029/2012gl051000.
Francis, J. A., and Vavrus, S. J. (2015). Evidence for a wavier jet stream in response to rapid Arctic warming. *Env. Res. Lett.* 10, 14005. Available at: https://doi.org/10.1088/1748-9326/10/1/014005.
Franke, J., Frank, D., Raible, C. C., Esper, J., and Brönnimann, S. (2013). Spectral biases in tree-ring climate proxies. *Nat. Clim. Chang.* doi:10.1038/nclimate1816.
Franks, P. J., Berry, J. A., Lombardozzi, D. L., and Bonan, G. B. (2017). Stomatal Function across Temporal and Spatial Scales: Deep-Time Trends, Land-Atmosphere Coupling and Global Models. *Plant Physiol.* 174, 583–602. doi:10.1104/pp.17.00287.
Franks, P. J., Bonan, G. B., Berry, J. A., Lombardozzi, D. L., Holbrook, N. M., Herold, N., et al. (2018). Comparing optimal and empirical stomatal conductance models for application in Earth system models. *Glob. Chang. Biol.* 24, 5708–5723. doi:10.1111/gcb.14445.
Frappart, F., Hiernaux, P., Guichard, F., Mougin, E., Arjounin, M., Lavenu, F., et al. (2009). Rainfall regime across the Sahel band in the Gourma region, Mali. *J. Hydrol.* 375, 128–142. doi:10.1016/J.JHYDROL.2009.03.007.
Freud, E., and Rosenfeld, D. (2012). Linear relation between convective cloud drop number concentration and depth for rain initiation. *J. Geophys. Res. Atmos.* 117.
Friedman, A. R., Hwang, Y.-T., Chiang, J. C. H., and Frierson, D. M. W. (2013). Interhemispheric temperature asymmetry over the twentieth century and in future projections. *J. Clim.* 26, 5419–5433.
Frieler, K., Meinshausen, M., Mengel, M., Braun, N., and Hare, W. (2012). A scaling approach to probabilistic assessment of regional climate change. *J. Clim.* 25, 3117–3144. doi:10.1175/JCLI-D-11-00199.1.
Frierson, D. M. W., and Hwang, Y.-T. (2012). Extratropical influence on ITCZ shifts in slab ocean simulations of global warming. *J. Clim.* 25, 720–733.
Frierson, D. M. W., Hwang, Y. T., Fučkar, N. S., Seager, R., Kang, S. M., Donohoe, A., et al. (2013). Contribution of ocean overturning circulation to tropical rainfall peak in the Northern Hemisphere. *Nat. Geosci.* 6, 940–944. doi:10.1038/ngeo1987.
Froidevaux, P., and Martius, O. (2016). Exceptional integrated vapour transport toward orography: an important precursor to severe floods in Switzerland. *Q. J. R. Meteorol. Soc.* 142, 1997–2012. doi:10.1002/qj.2793.
Frölicher, T. L., Fischer, E. M., and Gruber, N. (2018). Marine heatwaves under global warming. *Nature* 560, 360–364. doi:10.1038/s41586-018-0383-9.
Fu, Q., and Feng, S. (2014). Responses of terrestrial aridity to global warming. *J. Geophys. Res.* 119, 7863–7875. doi:10.1002/2014JD021608.
Fu, R., Yin, L., Li, W., Arias, P. A., Dickinson, R. E., Huang, L., et al. (2013). Increased dry season length over southern Amazonia in recent decades and its implication for future climate projection. *Proc. Nat. Acad. Sci.* 110, 18110–18115. doi:doi:10.1073/pnas.1302584110.
Fuentes-Franco, R., Giorgi, F., Coppola, E., and Kucharski, F. (2016). The role of ENSO and PDO in variability of winter precipitation over North America from twenty first century CMIP5 projections. *Clim. Dyn.* 46, 3259–3277. doi:10.1007/s00382-015-2767-y.
Fujibe, F. (2013). Clausius-Clapeyron-like relationship in multidecadal changes of extreme short-term precipitation and temperature in Japan. *Atmos. Sci. Lett.* 14, 3.
G., Z., F., P., and G., S. T. (2018). Multimodel Evidence for an Atmospheric Circulation Response to Arctic Sea Ice Loss in the CMIP5 Future Projections. *Geophys. Res. Lett.* 45, 1011–1019. doi:10.1002/2017GL076096.
Gaetani, M., Fontaine, B., Roucou, P., and Baldi, M. (2010). Influence of the Mediterranean Sea on the West African monsoon: Intraseasonal variability in numerical simulations. *J. Geophys. Res. Atmos.* 115. doi:10.1029/2010JD014436.

Gan, B., and Wu, L. (2014). Centennial trends in Northern Hemisphere winter storm tracks over the twentieth century. *Q. J. R Meteorol. Soc.* 140, 1945–1957. doi:10.1002/qj.2263.
Ganguly, D., Rasch, P. J., Wang, H., Yoon, J.-H., Ganguly, D., Rasch, P. J., et al. (2012). Fast and slow responses of the South Asian monsoon system to anthropogenic aerosols. *Geophys. Res. Lett.* 39. doi:10.1029/2012GL053043.
Gao, J., Xie, Z., Wang, A., Liu, S., Zeng, Y., Liu, B., et al. (2019). *A New Frozen Soil Parameterization including Frost and Thaw Fronts in the Community Land Model*. doi:10.1029/2018MS001399.
Gao, Y., and Gao, C. (2017). European hydroclimate response to volcanic eruptions over the past nine centuries. *Int. J. Climatol.* 37, 4146–4157. doi:10.1002/joc.5054.
Gao, Y., and others (2015). Dynamical and thermodynamical modulations on future changes of landfalling atmospheric rivers over western North America. *Geophys. Res. Lett.* 42, 7179–7186.
Gardner, A. S., Moholdt, G., Cogley, J. G., Wouters, B., Arendt, A. A., Wahr, J., et al. (2013). A reconciled estimate of glacier contributions to sea level rise: 2003 to 2009. *Science (80-.).* 340, 852–857. doi:10.1126/science.1234532.
Garreaud, R. (2007). Precipitation and Circulation Covariability in the Extratropics. *J. Clim.* 20, 4789–4797. doi:10.1175/JCLI4257.1.
Garreaud, R. D., Alvarez-Garreton, C., Barichivich, J., Boisier, J. P., Christie, D., Galleguillos, M., et al. (2017). The 2010–2015 megadrought in central Chile: impacts on regional hydroclimate and vegetation. *Hydrol. Earth Syst. Sci.* 21, 6307–6327. doi:10.5194/hess-21-6307-2017.
Garreaud, R. D., Vuille, M., Compagnucci, R., and Marengo, J. (2009). Present-day South American climate. *Palaeogeogr. Palaeoclimatol. Palaeoecol.* 281, 180–195. doi:10.1016/j.palaeo.2007.10.032.
Gasse, F. (2000). Hydrological changes in the African tropics since the Last Glacial Maximum. *Quat. Sci. Rev.* 19, 189–211.
Gastineau, G., Li, L., and Le Treut, H. (2009). The Hadley and Walker circulation changes in global warming conditions described by idealized atmospheric simulations. *J. Clim.* doi:10.1175/2009JCLI2794.1.
Gauthier, S., Bernier, P., Kuuluvainen, T., Shvidenko, A. Z., and Schepaschenko, D. G. (2015). Boreal forest health and global change. *Science (80-.).* 349, 819 LP-822. doi:10.1126/science.aaa9092.
Gedney, N., Huntingford, C., Weedon, G. P., Bellouin, N., Boucher, O., and Cox, P. M. (2014a). *Detection of aerosol effects on historical Northern Hemisphere river flow*. Nature Geoscience doi:10.1038/NGEO2263.
Gedney, N., Huntingford, C., Weedon, G. P., Bellouin, N., Boucher, O., and Cox, P. M. (2014b). *Detection of solar dimming and brightening effects on Northern Hemisphere river flow*. Nature Geoscience doi:10.1038/ngeo2263.
Gentine, P., Pritchard, M., Rasp, S., Reinaudi, G., and Yacalis, G. (2018). Could Machine Learning Break the Convection Parameterization Deadlock? *Geophys. Res. Lett.* 45, 5742–5751. doi:10.1029/2018GL078202.
Genty, D., Blamart, D., Ghaleb, B., Plagnes, V., Causse, C., Bakalowicz, M., et al. (2006). Timing and dynamics of the last deglaciation from European and North African δ13C stalagmite profiles-comparison with Chinese and South Hemisphere stalagmites. *Quat. Sci. Rev.* doi:10.1016/j.quascirev.2006.01.030.
Gerber, E. P., and Son, S. W. (2014). Quantifying the summertime response of the Austral jet stream and hadley cell to stratospheric ozone and greenhouse gases. *J. Clim.* 27, 5538–5559. doi:10.1175/JCLI-D-13-00539.1.
Gergis, J., and Henley, B. J. (2017). Southern Hemisphere rainfall variability over the past 200 years. *Clim. Dyn.* 48, 2087–2105. doi:10.1007/s00382-016-3191-7.
Gershunov, A., Schneider, N., and Barnett, T. (2001). Low-Frequency Modulation of the ENSO–Indian Monsoon Rainfall Relationship: Signal or Noise? *J. Clim.* 14, 2486–2492. doi:10.1175/1520-0442(2001)014<2486:LFMOTE>2.0.CO;2.
Gershunov, A., Shulgina, T. M., Clemesha, R. E. S., Guirguis, K., Pierce, D. W., Dettinger, M. D., et al. (2019). "Precipitation regime change in Western North America: The role of Atmospheric Rivers," in *Nature Communications* (submitted).
Gershunov, A., Shulgina, T., Ralph, F. M., Lavers, D. A., and Rutz, J. J. (2017). Assessing the climate-scale variability of atmospheric rivers affecting western North America. *Geophys. Res. Lett.* 44, 7900–7908.
Gerten, D., Betts, R., and D"oll, P. (2014). "Cross-chapter box on the active role of vegetation in altering water flows under climate change," in *Climate Change 2014: Impacts*, eds. Adaptation, V. P. A. Global, D. J. D. K. J. M. M. D. M. T. E. B. M. C. K. L. E. Y. O. E. R. C. G. B. G. E. S. K. A. N. L. S. M. P. R. M. S. A. C. of W. G. I. to the F. A. R. of the I. P. of Working Group Ii to the Fifth Assessment Report of the Intergovernmental Panel on Climate Change [Field Sectoral Aspects. Contribution of Working Group Ii to the Fifth Assessment Report of the Intergovernmental Panel on Climate Change [Field C. B. V. R, and L. L. White (Cambridge, United Kingdom and New York, NY, USA: Cambridge University Press), 157–161.
Gevaert, A. I., Miralles, D. G., de Jeu, R. A. M., Schellekens, J., and Dolman, A. J. (2018). Soil Moisture-Temperature Coupling in a Set of Land Surface Models. *J. Geophys. Res. Atmos.* 123, 1481–1498. doi:10.1002/2017JD027346.
Giannini, A. (2010). Mechanisms of climate change in the semiarid African Sahel: The local view. *J. Clim.* doi:10.1175/2009JCLI3123.1.
Giannini, A. . S. R. C. P. (2003). Oceanic Forcing of Sahel Rainfall on Interannual to Interdecadal Time Scales. *Science (80-.).* 302, 1027–1030. doi:10.1126/science.1089357.

Giannini, A., Lyon, B., Seager, R., and Vigaud, N. (2018). Dynamical and Thermodynamic Elements of Modeled Climate Change at the East African Margin of Convection. *Geophys. Res. Lett.* 45, 992–1000. doi:10.1002/2017GL075486.
Giannini, A., Salack, S., Lodoun, T., Ali, A., Gaye, A. T., and Ndiaye, O. (2013). A unifying view of climate change in the Sahel linking intra-seasonal, interannual and longer time scales. *Environ. Res. Lett.* 8, 024010. doi:10.1088/1748-9326/8/2/024010.
Gillett, N. P., Shiogama, H., Funke, B., Hegerl, G., Knutti, R., Matthes, K., et al. (2016). Detection and Attribution Model Intercomparison Project (DAMIP). *Geosci. Model Dev. Discuss.*, 1–19. doi:10.5194/gmd-2016-74.
Gimeno, L., Drumond, A., Nieto, R., Trigo, R. M., and Stohl, A. (2010). On the origin of continental precipitation. *Geophys. Res. Lett.* 37. doi:10.1029/2010GL043712.
Ginoux, P., Prospero, J. M., Gill, T. E., Hsu, N. C., and Zhao, M. (2012). Global-scale attribution of anthropogenic and natural dust sources and their emission rates based on MODIS Deep Blue aerosol products. *Rev. Geophys.* doi:10.1029/2012RG000388.
Ginzburg, L. R., and Jensen, C. X. J. (2004). Rules of thumb for judging ecological theories. *Trends Ecol. Evol.* 19, 121.
Giorgi, F., Jones, C., Asrar, G. R., and others (2009). Addressing climate information needs at the regional level: the CORDEX framework. *World Meteorol. Organ. Bull.* 58, 175.
Giorgi, F., Raffaele, F., and Coppola, E. (2018). The response of precipitation characteristics to global warming from global and regional climate projections. *Earth Syst. Dyn. Discuss.* 10, 1–41. doi:10.5194/esd-2018-64.
Giorgi, F., Torma, C., Coppola, E., Ban, N., Schär, C., and Somot, S. (2016). Enhanced summer convective rainfall at Alpine high elevations in response to climate warming. *Nat. Geosci.* 9, 584–589. doi:10.1038/ngeo2761.
Giuntoli, I., Renard, B., Vidal, J.-P., and Bard, A. (2013). Low flows in France and their relationship to large-scale climate indices. *J. Hydrol.* 482, 105–118. doi:10.1016/j.jhydrol.2012.12.038.
Giuntoli, I., Vidal, J.-P., Prudhomme, C., and Hannah, D. M. (2015). Future hydrological extremes: the uncertainty from multiple global climate and global hydrological models. *Earth Syst. Dyn.* 6, 267–285. doi:10.5194/esd-6-267-2015.
Giuntoli, I., Villarini, G., Prudhomme, C., and Hannah, D. M. (2018). Uncertainties in projected runoff over the conterminous United States. *Clim. Change* 150, 149–162. doi:10.1007/s10584-018-2280-5.
Gleeson, T., Befus, K. M., Jasechko, S., Luijendijk, E., and Cardenas, M. B. (2015). The global volume and distribution of modern groundwater. *Nat. Geosci.* 9, 161. Available at: https://doi.org/10.1038/ngeo2590.
Gleeson, T., Wada, Y., Bierkens, M. F. P., and Van Beek, L. P. H. (2012). Water balance of global aquifers revealed by groundwater footprint. *Nature* 488, 197–200. doi:10.1038/nature11295.
Gloor, M., Barichivich, J., Ziv, G., Brienen, R., Schöngart, J., Peylin, P., et al. (2015). Recent Amazon climate as background for possible ongoing and future changes of Amazon humid forests. *Glob. Biochem. Cycles* 29, 1–16.
Gloor, M., Brienen, R. J. W., Galbraith, D., Feldpausch, T. R., Schöngart, J., Guyot, J.-L., et al. (2013). Intensification of the Amazon hydrological cycle over the last two decades. *Geophys. Res. Lett.* 40, 1729–1733. doi:10.1002/grl.50377.
Golledge, N. R., Keller, E. D., Gomez, N., Naughten, K. A., Bernales, J., Trusel, L. D., et al. (2019). Global environmental consequences of twenty-first-century ice-sheet melt. *Nature* 566, 65.
Gomez-Hernandez, M., Drumond, A., Gimeno, L., and Garcia-Herrera, R. (2013). Variability of moisture sources in the Mediterranean region during the period 1980-2000. *Water Resour. Res.* 49, 6781–6794. doi:10.1002/wrcr.20538.
Gong, H., Zhou, W., Chen, W., Wang, L., Leung, M. Y. -T., Cheung, P. K. -Y., et al. (2019). Modulation of the southern Indian Ocean dipole on the impact of El Niño–Southern Oscillation on Australian summer rainfall. *Int. J. Climatol.* 39, 2484–2490. doi:10.1002/joc.5941.
Gonzalez, P. L. M., Polvani, L. M., Seager, R., and Correa, G. J. P. (2014). Stratospheric ozone depletion: A key driver of recent precipitation trends in South Eastern South America. *Clim. Dyn.* 42, 1775–1792. doi:10.1007/s00382-013-1777-x.
Good, P., Andrews, T., Chadwick, R., Dufresne, J. L., Gregory, J. M., Lowe, J. A., et al. (2016a). NonlinMIP contribution to CMIP6: Model intercomparison project for non-linear mechanisms: Physical basis, experimental design and analysis principles (v1.0). *Geosci. Model Dev.* doi:10.5194/gmd-9-4019-2016.
Good, P., Booth, B. B. B., Chadwick, R., Hawkins, E., Jonko, A., and Lowe, J. A. (2016b). Large differences in regional precipitation change between a first and second 2 K of global warming. *Nat. Commun.* 7. doi:10.1038/ncomms13667.
Good, P., Ingram, W., Lambert, F. H., Lowe, J. A., Gregory, J. M., Webb, M. J., et al. (2012). A step-response approach for predicting and understanding non-linear precipitation changes. *Clim. Dyn.* doi:10.1007/s00382-012-1571-1.
Good, P., Lowe, J. A., Andrews, T., Wiltshire, A., Chadwick, R., Ridley, J. K., et al. (2015). Nonlinear regional warming with increasing CO2concentrations. *Nat. Clim. Chang.* 5, 138–142. doi:10.1038/nclimate2498.
Goren, T., and Rosenfeld, D. (2014). Decomposing aerosol cloud radiative effects into cloud cover, liquid water path and Twomey components in marine stratocumulus. *Atmos. Res.* 138, 378–393.

doi:10.1016/J.ATMOSRES.2013.12.008.
Gorodetskaya, I. V, and co-authors (2014). The role of atmospheric rivers in anomalous snow accumulation in East Antarctica. *Geophys. Res. Lett.* 41, 6199–6206.
Gosling, S. N., and Arnell, N. W. (2016). A global assessment of the impact of climate change on water scarcity. *Clim. Change* 134, 371–385. doi:10.1007/s10584-013-0853-x.
Grafton, R. Q., Williams, J., Perry, C. J., Molle, F., Ringler, C., Steduto, P., et al. (2018). The paradox of irrigation efficiency. *Science (80-.).* 361, 748–750.
Green, J. K., Seneviratne, S. I., Berg, A. M., Findell, K. L., Lawrence, D. M., and Gentine, P. (2018). Large influence of soil moisture variability on long-term terrestrial carbon uptake. *Nature* Accepted, 476–479. doi:10.1038/s41586-018-0848-x.
Gremaud, V., Goldscheider, N., Savoy, L., Favre, G., and Masson, H. (2009). Geological structure, recharge processes and underground drainage of a glacierised karst aquifer system, Tsanfleuron-Sanetsch, Swiss Alps. *Hydrogeol. J.* 17, 1833–1848.
Greve, P., Gudmundsson, L., and Seneviratne, S. I. (2018). Regional scaling of annual mean precipitation and water availability with global temperature change. *Earth Syst. Dyn.* 9, 227–240. doi:10.5194/esd-9-227-2018.
Greve, P., Orlowsky, B., Mueller, B., Sheffield, J., Reichstein, M., and Seneviratne, S. I. (2014). Global assessment of trends in wetting and drying over land. *Nat. Geosci.* 7, 716–721. doi:10.1038/NGEO2247.
Greve, P., and Seneviratne, S. I. (2015). Assessment of future changes in water availability and aridity. *Geophys. Res. Lett.* 42, 5493–5499. doi:10.1002/2015GL064127.Received.
Grieger, J., Leckebusch, G. C., Raible, C. C., Rudeva, I., and Simmonds, I. (2018). Subantarctic cyclones identified by 14 tracking methods, and their role for moisture transports into the continent. *Tellus, Ser. A Dyn. Meteorol. Oceanogr.* 70, 1. doi:10.1080/16000870.2018.1454808.
Griffin, D., and Anchukaitis, K. J. (2014). How unusual is the 2012-2014 California drought? *Geophys. Res. Lett.* doi:10.1002/2014GL062433.
Griffin, D., Woodhouse, C. A., Meko, D. M., Stahle, D. W., Faulstich, H. L., Carrillo, C., et al. (2013). North American monsoon precipitation reconstructed from tree-ring latewood. *Geophys. Res. Lett.* 40, 954–958. doi:10.1002/grl.50184.
Griffiths, M. L., Drysdale, R. N., Gagan, M. K., Zhao, J. -x., Ayliffe, L. K., Hellstrom, J. C., et al. (2009). Increasing Australian–Indonesian monsoon rainfall linked to early Holocene sea-level rise. *Nat. Geosci.* 2, 636. Available at: https://doi.org/10.1038/ngeo605.
Grimm, E. C., Watts, W. A., Jacobson, G. L., Hansen, B. C. S., Almquist, H. R., and Dieffenbacher-Krall, A. C. (2006). Evidence for warm wet Heinrich events in Florida. *Quat. Sci. Rev.* doi:10.1016/j.quascirev.2006.04.008.
Grise, K. M., Davis, S. M., Simpson, I. R., Waugh, D. W., Fu, Q., Allen, R. J., et al. (2019). Recent Tropical Expansion: Natural Variability or Forced Response? *J. Clim.* 32, 1551–1571. doi:10.1175/JCLI-D-18-0444.1.
Grise, K. M., Son, S. W., Correa, G. J. P., and Polvani, L. M. (2014). The response of extratropical cyclones in the Southern Hemisphere to stratospheric ozone depletion in the 20th century. *Atmos. Sci. Lett.* 15, 29–36. doi:10.1002/asl2.458.
Groisman, P. Y., Bulygina, O. N., Yin, X., Vose, R. S., Gulev, S. K., Hanssen-Bauer, I., et al. (2016). Recent changes in the frequency of freezing precipitation in North America and Northern Eurasia. *Environ. Res. Lett.* 11, 45007.
Gu, G., and Adler, R. F. (2011). Precipitation and Temperature Variations on the Interannual Time Scale: Assessing the Impact of ENSO and Volcanic Eruptions. *J. Clim.* 24, 2258–2270. doi:10.1175/2010JCLI3727.1.
Gu, G., Adler, R. F., and Huffman, G. J. (2016). Long-term changes/trends in surface temperature and precipitation during the satellite era (1979–2012). *Clim. Dyn.* 46, 1091–1105. doi:10.1007/s00382-015-2634-x.
Gu, H., Jin, J., Wu, Y., Ek, M. B., and Subin, Z. M. (2015). Calibration and validation of lake surface temperature simulations with the coupled WRF-lake model. *Clim. Change* 129, 471. Available at: https://doi.org/10.1007/s10584-013-0978-y.
Gu, X., Zhang, Q., Li, J., Singh, V. P., Liu, J., Sun, P., et al. (2019). Attribution of global soil moisture drying to human activities: a quantitative viewpoint. *Geophys. Res. Lett.* doi:10.1029/2018GL080768.
Guan, B., Waliser, D. E., Molotch, N. P., Fetzer, E. J., and Neiman, P. J. (2012). Does the Madden–Julian Oscillation Influence Wintertime Atmospheric Rivers and Snowpack in the Sierra Nevada? *Mon. Weather Rev.* 140, 325–342. doi:10.1175/MWR-D-11-00087.1.
Guan, B., Waliser, D. E., and Ralph, F. M. (2018). An intercomparison between reanalysis and dropsonde observations of the total water vapor transport in individual atmospheric rivers. *J. Hydrometeorol.* 19, 321–337.
Gudmundsson, L., Leonard, M., Do, H. X., Westra, S., and Seneviratne, S. I. (2019). Observed Trends in Global Indicators of Mean and Extreme Streamflow. *Geophys. Res. Lett.* 46, 756–766. doi:10.1029/2018GL079725.
Gudmundsson, L., and Seneviratne, S. I. (2016). Anthropogenic climate change affects meteorological drought risk in Europe. *Environ. Res. Lett.* doi:10.1088/1748-9326/11/4/044005.
Gudmundsson, L., Seneviratne, S. I., and Zhang, X. (2017). Anthropogenic climate change detected in European renewable freshwater resources. *Nat. Clim. Chang.* 7, 813–816.

Guerreiro, S. B., Fowler, H. J., Barbero, R., Westra, S., Lenderink, G., Blenkinsop, S., et al. (2018a). Detection of continental-scale intensification of hourly rainfall extremes. *Nat. Clim. Chang.* 8, 803–807. doi:10.1038/s41558-018-0245-3.
Guerreiro, S. B., Fowler, H. J., Barbero, R., Westra, S., Lenderink, G., Blenkinsop, S., et al. (2018b). Detection of continental-scale intensification of hourly rainfall extremes. *Nat. Clim. Chang.* 8, 803–807. doi:10.1038/s41558-018-0245-3.
Guhathakurta, P., Menon, P., Inkane, P. M., Krishnan, U., and Sable, S. T. (2017). Trends and variability of meteorological drought over the districts of India using standardized precipitation index. *J. Earth Syst. Sci.* 126, 1–18. doi:10.1007/s12040-017-0896-x.
Guichard, F., and Couvreux, F. (2017). A short review of numerical cloud-resolving models. *Tellus, Ser. A Dyn. Meteorol. Oceanogr.* 69, 1–36. doi:10.1080/16000870.2017.1373578.
Guillaume, T., Holtkamp, A. M., Damris, M., Brümmer, B., and Kuzyakov, Y. (2016). Soil degradation in oil palm and rubber plantations under land resource scarcity. *Agric. Ecosyst. Environ.* 232, 110–118. doi:https://doi.org/10.1016/j.agee.2016.07.002.
Guimberteau, M., Laval, K., Perrier, A., and Polcher, J. (2012). Global effect of irrigation and its impact on the onset of the Indian summer monsoon. *Clim. Dyn.* 39, 1329–1348. doi:10.1007/s00382-011-1252-5.
Guirguis, K., Gershunov, A., Shulgina, T., Clemesha, R. E. S., and Ralph, F. M. (2018). Atmospheric rivers impacting Northern California and their modulation by a variable climate. *Clim. Dyn.*, 1–15.
Guo, J., Deng, M., Lee, S. S., Wang, F., Li, Z., Zhai, P., et al. (2016a). Delaying precipitation and lightning by air pollution over the Pearl River Delta. Part I: Observational analyses. *J. Geophys. Res. Atmos.* 121, 6472–6488. doi:10.1002/2015JD023257.
Guo, J., Su, T., Li, Z., Miao, Y., Li, J., Liu, H., et al. (2017). Declining frequency of summertime local-scale precipitation over eastern China from 1970 to 2010 and its potential link to aerosols. *Geophys. Res. Lett.* 44, 5700–5708. doi:10.1002/2017GL073533.
Guo, L., Turner, A. G., and Highwood, E. J. (2016b). Local and remote impacts of aerosol species on indian summer monsoon rainfall in a GCM. *J. Clim.* 29, 6937–6955. doi:10.1175/JCLI-D-15-0728.1.
Gurdak, J. J., Hanson, R. T., McMahon, P. B., Bruce, B. W., McCray, J. E., Thyne, G. D., et al. (2007). Climate Variability Controls on Unsaturated Water and Chemical Movement, High Plains Aquifer, USA. *Vadose Zo. J.* 6, 533. doi:10.2136/vzj2006.0087.
Gutmann, E. D., Rasmussen, R. M., Liu, C., Ikeda, K., Bruyere, C. L., Done, J. M., et al. (2018). Changes in hurricanes from a 13-year convection-permitting pseudo-global warming simulation. *J. Clim.* 31, 3643–3657. Available at: https://doi.org/10.1175/JCLI-D-17-0391.1.
Gutowski, J. W., Giorgi, F., Timbal, B., Frigon, A., Jacob, D., Kang, H. S., et al. (2016). WCRP COordinated Regional Downscaling EXperiment (CORDEX): A diagnostic MIP for CMIP6. *Geosci. Model Dev.* 9, 4087–4095. doi:10.5194/gmd-9-4087-2016.
Haarsma, R. J., Roberts, M. J., Vidale, P. L., Catherine, A., Bellucci, A., Bao, Q., et al. (2016). High Resolution Model Intercomparison Project (HighResMIP v1.0) for CMIP6. *Geosci. Model Dev.* 9, 4185–4208. doi:10.5194/gmd-9-4185-2016.
Haertel, P. (2018). Sensitivity of the Madden Julian Oscillation to Ocean Warming in a Lagrangian Atmospheric Model. *Climate* 6, 45. doi:10.3390/cli6020045.
Hagos, S. M., Leung, L. R., Yoon, J. -h., Lu, J., and Gao, Y. A. (2016). projection of changes in landfalling atmospheric river frequency and extreme precipitation over western North America from the large ensemble CESM simulations. *Geophys. Res* 43, 1357–1363.
Hall, A., Qu, X., and Neelin, J. D. (2008). Improving predictions of summer climate change in the United States. *Geophys. Res. Lett.* 35, 1–5. doi:10.1029/2007GL032012.
Hallett, C. S., Hobday, A. J., Tweedley, J. R., Thompson, P. A., McMahon, K., and Valesini, F. J. (2018). Observed and predicted impacts of climate change on the estuaries of south-western Australia, a Mediterranean climate region. *Reg. Environ. Chang.* 18, 1357–1373. doi:10.1007/s10113-017-1264-8.
Ham, Y.-G., and Kug, J.-S. (2016). ENSO amplitude changes due to greenhouse warming in CMIP5: Role of mean tropical precipitation in the twentieth century. *Geophys. Res. Lett.* 43, 422–430. doi:10.1002/2015GL066864.
Ham, Y. G., Kug, J. S., Choi, J. Y., Jin, F. F., and Watanabe, M. (2018). Inverse relationship between present-day tropical precipitation and its sensitivity to greenhouse warming. *Nat. Clim. Chang.* 8, 64–69. doi:10.1038/s41558-017-0033-5.
Han, R., Wang, H., Hu, Z.-Z., Kumar, A., Li, W., Long, L. N., et al. (2016). An Assessment of Multimodel Simulations for the Variability of Western North Pacific Tropical Cyclones and Its Association with ENSO. *J. Clim.* 29, 6401–6423. doi:10.1175/JCLI-D-15-0720.1.
Hannah, D. M., and Garner, G. (2015). River water temperature in the United Kingdom: Changes over the 20th century and possible changes over the 21st century. *Prog. Phys. Geogr.* 39, 68–92. doi:10.1177/0309133314550669.
Hansen, Z. K., and Libecap, G. D. (2004). Small farms, externalities, and the Dust Bowl of the 1930s. *J. Polit.*

*Econ.*112, 665–694.
Hanson, R. T., Dettinger, M. D., and Newhouse, M. W. (2006). Relations between climatic variability and hydrologic time series from four alluvial basins across the southwestern United States. *Hydrogeol. J.* 14, 1122–1146. doi:10.1007/s10040-006-0067-7.
Harpold, A., Dettinger, M., and Rajagopal, S. (2017). Defining snow drought and why it matters. *Eos, Earth Sp. Sci. News* 98. doi:10.1029/2017EO068775.
Harris, L. M., Lin, S.-J., and Tu, C. (2016). High-Resolution Climate Simulations Using GFDL HiRAM with a Stretched Global Grid. *J. Clim.* 29, 4293–4314. doi:10.1175/JCLI-D-15-0389.1.
Harrison, S. P., Bartlein, P. J., Brewer, S., Prentice, I. C., Boyd, M., Hessler, I., et al. (2014). Climate model benchmarking with glacial and mid-Holocene climates. *Clim. Dyn.* 43, 671–688. doi:10.1007/s00382-013-1922-6.
Harrison, S. P., Bartlein, P. J., Izumi, K., Li, G., Annan, J., Hargreaves, J., et al. (2015). Evaluation of CMIP5 palaeo-simulations to improve climate projections. *Nat. Clim. Chang.* 5, 735–743.
Harrop, B. E., and Hartmann, D. L. (2016). The role of cloud radiative heating in determining the location of the ITCZ in aquaplanet simulations. *J. Clim.* doi:10.1175/JCLI-D-15-0521.1.
Hartmann, A., Gleeson, T., Wada, Y., and Wagener, T. (2017). Enhanced groundwater recharge rates and altered recharge sensitivity to climate variability through subsurface heterogeneity. *Proc. Natl. Acad. Sci.* doi:10.1073/pnas.1614941114.
Hartmann, D. L., Klein Tank, A. M. G., Rusticucci, M., Alexander, L. V, Brönnimann, S., Charabi, Y., et al. (2013a). “Observations: Atmosphere and Surface,” in *Climate Change 2013: The Physical Science Basis. Contribution of Working Group I to the Fifth Assessment Report of the Intergovernmental Panel on Climate Change*, eds. T. F. Stocker, D. Qin, G.-K. Plattner, M. Tignor, S. K. Allen, J. Boschung, et al. (Cambridge, United Kingdom and New York, NY, USA: Cambridge University Press), 159–254. doi:10.1017/CBO9781107415324.008.
Hartmann, D. L., Klein Tank, A. M. G., Rusticucci, M., Alexander, L. V, Brönnimann, S., Charabi, Y., et al. (2013b). “Observations: Atmosphere and Surface,” in *Climate Change 2013: The Physical Science Basis. Contribution of Working Group I to the Fifth Assessment Report of the Intergovernmental Panel on Climate Change*, eds. T. F. Stocker, D. Qin, G.-K. Plattner, M. Tignor, S. K. Allen, J. Boschung, et al. (Cambridge, United Kingdom and New York, NY, USA: Cambridge University Press), 159–254. doi:10.1017/CBO9781107415324.008.
Hashizume, M., Chaves, L. F., and Minakawa, N. (2012). Indian Ocean Dipole drives malaria resurgence in East African highlands. *Sci. Rep.* 2, 269. doi:10.1038/srep00269.
Hassim, M. E., and Timbal, B. (2019). Observed rainfall trends over Singapore and the Maritime Continent from the perspective of regional-scale weather regimes. J. *Appl. Meteor Clim. , ,* 58, 365–384. doi:10.1175/JAMC-D-18-0136.1.
Hattermann, F. F., Vetter, T., Breuer, L., Su, B., Daggupati, P., Donnelly, C., et al. (2018). Sources of uncertainty in hydrological climate impact assessment: a cross-scale study. *Environ. Res. Lett.* 13, 015006. doi:10.1088/1748-9326/aa9938.
Haug, G. H., Günther, D., Peterson, L. C., Sigman, D. M., Hughen, K. A., and Aeschlimann, B. (2003). Climate and the collapse of Maya civilization. *Science (80-.).* doi:10.1126/science.1080444.
Haughton, N., Abramowitz, G., and Pitman, A. J. (2018). On the predictability of land surface fluxes from meteorological variables. *Geosci. Model Dev.* 11, 195–212. Available at: https://doi.org/10.5194/gmd-11-195-2018.
Hauser, M., Gudmundsson, L., Orth, R., Jézéquel, A., Haustein, K., Vautard, R., et al. (2017). Methods and Model Dependency of Extreme Event Attribution: The 2015 European Drought. *Earth’s Futur.* doi:10.1002/2017EF000612.
Haverd, V., Smith, B., Nieradzik, L., Briggs, P. R., Woodgate, W., Trudinger, C. M., et al. (2018). A new version of the CABLE land surface model (Subversion revision r4601) incorporating land use and land cover change, woody vegetation demography, and a novel optimisation-based approach to plant coordination of photosynthesis. *Geosci. Model Dev.* 11, 2995–3026. Available at: https://doi.org/10.5194/gmd-11-2995-2018.
Hawcroft, M. K., Shaffrey, L. C., Hodges, K. I., and Dacre, H. F. (2016). Can climate models represent the precipitation associated with extratropical cyclones? *Clim. Dyn.* doi:10.1007/s00382-015-2863-z.
Hawkins, E., and Sutton, R. (2011). The potential to narrow uncertainty in projections of regional precipitation change. *Clim. Dyn.* 37, 407–418. doi:10.1007/s00382-010-0810-6.
Haywood, J. M., Jones, A., Bellouin, N., and Stephenson, D. (2013). Asymmetric forcing from stratospheric aerosols impacts Sahelian rainfall. *Nat. Clim. Chang.* 3, 660–665. doi:10.1038/nclimate1857.
He, J., and Soden, B. J. (2015a). Anthropogenic weakening of the tropical circulation: The relative roles of direct CO2 forcing and sea surface temperature change. *J. Clim.* 28, 8728–8742. doi:10.1175/JCLI-D-15-0205.1.
He, J., and Soden, B. J. (2015b). Anthropogenic weakening of the tropical circulation: The relative roles of direct CO2forcing and sea surface temperature change. *J. Clim.* doi:10.1175/JCLI-D-15-0205.1.
He, J., and Soden, B. J. (2017b). A re-examination of the projected subtropical precipitation decline. *Nat. Clim. Chang.* 7, 53–57. doi:10.1038/nclimate3157.

He, J., and Soden, B. J. (2017a). A re-examination of the projected subtropical precipitation decline. *Nat. Clim. Chang.* 7, 53–57. doi:10.1038/nclimate3157.
He, J., and Soden, B. J. (2017c). A re-examination of the projected subtropical precipitation decline. *Nat. Clim. Chang.* 7, 53–57. doi:10.1038/nclimate3157.
Hegerl, G. C., Black, E., Allan, R. P., Ingram, W. J., Polson, D., Trenberth, K. E., et al. (2015). Challenges in quantifying changes in the global water cycle. *Bull. Am. Meteorol. Soc.* 96. doi:10.1175/BAMS-D-13-00212.1.
Hegerl, G. C., Brönnimann, S., Schurer, A., and Cowan, T. (2018). The early 20th century warming: Anomalies, causes, and consequences. *Wiley Interdiscip. Rev. Clim. Chang.* 9, e522. doi:10.1002/wcc.522.
Hegerl, G. C., Hasselmann, K., Cubasch, U., Mitchell, J. F. B., Roeckner, E., Voss, R., et al. (1997). Multi-fingerprint detection and attribution analysis of greenhouse gas, greenhouse gas-plus-aerosol and solar forced climate change. *Clim. Dyn.* 13, 613–634. doi:10.1007/s003820050186.
Heinzeller, D., Junkermann, W., and Kunstmann, H. (2016). Anthropogenic Aerosol Emissions and Rainfall Decline in Southwestern Australia: Coincidence or Causality? *J. Clim.* 29, 8471–8493. doi:10.1175/JCLI-D-16-0082.1.
Held, I. M., and Soden, B. J. (2006a). Robust responses of the hydrologic cycle to global warming. *J. Clim.* 19, 5686–5699. doi:10.1175/JCLI3990.1.
Held, I. M., and Soden, B. J. (2006b). Robust responses of the hydrological cycle to global warming (vol 19, pg 5686, 2006). *J. Clim.* 19, 5686–5699. doi:10.1175/2010JCLI4045.1.
Henderson, G. R., Peings, Y., Furtado, J. C., and Kushner, P. J. (2018a). Snow–atmosphere coupling in the Northern Hemisphere. *Nat. Clim. Chang.* 8, 954–963. doi:10.1038/s41558-018-0295-6.
Henderson, G. R., Peings, Y., Furtado, J. C., and Kushner, P. J. (2018b). Snow–atmosphere coupling in the Northern Hemisphere. *Nat. Clim. Chang.* 8, 954–963. doi:10.1038/s41558-018-0295-6.
Hendon, H. H., Lim, E.-P., and Nguyen, H. (2014). Seasonal Variations of Subtropical Precipitation Associated with the Southern Annular Mode. *J. Clim.* 27, 3446–3460. doi:10.1175/JCLI-D-13-00550.1.
Herger, N., Abramowitz, G., Knutti, R., Angélil, O., Lehmann, K., and Sanderson, B. M. (2018). Selecting a climate model subset to optimise key ensemble properties. *Earth Syst. Dyn.* 9, 135–151. doi:10.5194/esd-9-135-2018.
Herger, N., Sanderson, B. M., and Knutti, R. (2015). Improved pattern scaling approaches for the use in climate impact studies Supplementary Information. *Geophys. Res. Lett.* 42, n/a-n/a. doi:10.1002/2015GL063569.
Hermann, N. W., Oster, J. L., and Ibarra, D. E. (2018). Spatial patterns and driving mechanisms of mid-Holocene hydroclimate in western North America. *J. Quat. Sci.* 33, 421–434. doi:10.1002/jqs.3023.
Hermanson, L., Eade, R., Robinson, N. H., Dunstone, N. J., Andrews, M. B., Knight, J. R., et al. (2014). Forecast cooling of the Atlantic subpolar gyre and associated impacts. *Geophys. Res. Lett.* 41, 5167–5174. doi:10.1002/2014GL060420.
Hernández-Henríquez, M. A., Déry, S. J., and Derksen, C. (2015). Polar amplification and elevation-dependence in trends of Northern Hemisphere snow cover extent, 1971–2014. *Environ. Res. Lett.* 10, 044010. doi:10.1088/1748-9326/10/4/044010.
Hessl, A. E., Anchukaitis, K. J., Jelsema, C., Cook, B., Byambasuren, O., Leland, C., et al. (2018). Past and future drought in Mongolia. *Sci. Adv.* 4, e1701832.
Hewson, M., McGowan, H., Phinn, S., Peckham, S., and Grell, G. (2013). Exploring aerosol effects on rainfall for Brisbane, Australia. *Climate* 1, 120–147.
Hill, S. A., Ming, Y., Held, I. M., and Zhao, M. (2017). A Moist Static Energy Budget–Based Analysis of the Sahel Rainfall Response to Uniform Oceanic Warming. *J. Clim.* 30, 5637–5660. doi:10.1175/JCLI-D-16-0785.1.
Hirabayashi, Y., Mahendran, R., Koirala, S., Konoshima, L., Yamazaki, D., and Watanabe, S. ... & Kanae, S. (2013). *Glob. flood risk under Clim. Chang.* 3, 9.
Hodnebrog, Ø., Myhre, G., Forster, P. M., Sillmann, J., and Samset, B. H. (2016). Local biomass burning is a dominant cause of the observed precipitation reduction in southern Africa. *Nat. Commun.* 7, 11236. doi:10.1038/ncomms11236.
Hoegh-Guldberg, O., Jacob, D., Taylor, M., Bindi, M., Brown, S., Camilloni, I., et al. (2019). "Impacts of 1.5ºC global warming on natural and human systems.," in *IPCC Special Report on the impacts of global warming of 1.5°C above pre-industrial levels and related global greenhouse gas emission pathways, in the context of strengthening the global response to the threat of climate change.*, eds. V. Masson-Delmotte, P. Zhai, H.-O. Pörtner, D. Roberts, J. Skea, P. R. Shukla, et al. (Cambridge, United Kingdom and New York, NY, USA: Cambridge University Press), 175–311. Available at: https://www.ipcc.ch/sr15/chapter/chapter-3/.
Hoell, A., and Cheng, L. (2018). Austral summer Southern Africa precipitation extremes forced by the El Niño-Southern oscillation and the subtropical Indian Ocean dipole. *Clim. Dyn.* 50, 3219–3236. doi:10.1007/s00382-017-3801-z.
Hoell, A., Funk, C., Barlow, M., and Shukla, S. (2016). "Recent and Possible Future Variations in the North American Monsoon," in *The Monsoons and Climate Change*, eds. L. M. V. de Carvalho and C. Jones (Springer), 149–162.
Hoell, A., Hoerling, M., Eischeid, J., Quan, X.-W., and Liebmann, B. (2017a). Reconciling Theories for Human and Natural Attribution of Recent East Africa Drying. *J. Clim.* 30, 1939–1957. doi:10.1175/JCLI-D-16-0558.1.

Hoell, A., Hoerling, M., Eischeid, J., Quan, X.-W., and Liebmann, B. (2017b). Reconciling Theories for Human and Natural Attribution of Recent East Africa Drying. *J. Clim.* 30, 1939–1957. doi:10.1175/JCLI-D-16-0558.1.

Hoelzle, M., Chinn, T., Stumm, D., Paul, F., Zemp, M., and Haeberli, W. (2007). The application of glacier inventory data for estimating past climate change effects on mountain glaciers: A comparison between the European Alps and the Southern Alps of New Zealand. *Glob. Planet. Change* 56, 69–82. doi:10.1016/j.gloplacha.2006.07.001.

Hoerling, M., Eischeid, J., Perlwitz, J., Quan, X., Zhang, T., and Pegion, P. (2012). On the increased frequency of mediterranean drought. *J. Clim.* doi:10.1175/JCLI-D-11-00296.1.

Hohenegger, C., and Stevens, B. (2018). The role of the permanent wilting point in controlling the spatial distribution of precipitation. *Proc. Natl. Acad. Sci.* 115, 5692–5697. doi:10.1073/pnas.1718842115.

Holland, M. M., Finnis, J., and Serreze, M. C. (2006). Simulated Arctic Ocean freshwater budgets in the twentieth and twenty-first centuries. *J. Clim.* 19, 6221–6242. doi:10.1175/JCLI3967.1.

Holloway, C. E., Wing, A. A., Bony, S., Muller, C., Masunaga, H., L'Ecuyer, T. S., et al. (2017). *Observing Convective Aggregation*. Springer Netherlands doi:10.1007/s10712-017-9419-1.

Holz, A., Paritsis, J., Mundo, I. A., Veblen, T. T., Kitzberger, T., Williamson, G. J., et al. (2017). Southern Annular Mode drives multicentury wildfire activity in southern South America. *Proc. Natl. Acad. Sci.* 114, 9552–9557. doi:10.1073/pnas.1705168114.

Hong, B., Uchida, M., Hong, Y., Peng, H., Kondo, M., and Ding, H. (2018). The respective characteristics of millennial-scale changes of the India summer monsoon in the Holocene and the Last Glacial. *Palaeogeogr. Palaeoclimatol. Palaeoecol.* 496, 155–165. doi:10.1016/j.palaeo.2018.01.033.

Hooper, J., and Marx, S. (2018). A global doubling of dust emissions during the Anthropocene? *Glob. Planet. Change*. doi:10.1016/j.gloplacha.2018.07.003.

Hopcroft, P. O., Valdes, P. J., Harper, A. B., and Beerling, D. J. (2017). Multi vegetation model evaluation of the Green Sahara climate regime. *Geophys. Res. Lett.* doi:10.1002/2017GL073740.

Hope, P., Grose, M., Timbal, B., Dowdy, A., Bhend, J., Katzfey, J., et al. (2015). Seasonal and regional signature of the projected southern Australian rainfall reduction. *Aust. Meteorol. Oceanogr. J.* 65, 54–71. doi:10.22499/2.6501.005.

Hope, P., Henley, B. J., Gergis, J., Brown, J., and Ye, H. (2017). Time-varying spectral characteristics of ENSO over the Last Millennium. *Clim. Dyn.* 49, 1705–1727. doi:10.1007/s00382-016-3393-z.

Horton, D. E., Johnson, N. C., Singh, D., Swain, D. L., Rajaratnam, B., and Diffenbaugh, N. S. (2015). Contribution of changes in atmospheric circulation patterns to extreme temperature trends. *Nature* 522, 465–469.

Hoskins, B., and Woollings, T. (2015). Persistent extratropical regimes and climate extremes. *Curr. Clim. Chang. Reports* 1, 115–124. doi:10.1007/s40641-015-0020-8.

Hourdin, F., Gəinusə-Bogdan, A., Braconnot, P., Dufresne, J. L., Traore, A. K., and Rio, C. (2015). Air moisture control on ocean surface temperature, hidden key to the warm bias enigma. *Geophys. Res. Lett.* 42, 10885–10893. doi:10.1002/2015GL066764.

Hourdin, F., Grandpeix, J. Y., Rio, C., Bony, S., Jam, A., Cheruy, F., et al. (2013). LMDZ5B: the atmospheric component of the IPSL climate model with revisited parameterizations for clouds and convection. *Clim Dyn* 40, 12–382.

Hourdin, F., Mauritsen, T., Gettelman, A., Golaz, J.-C., Balaji, V., Duan, Q., et al. (2017). The Art and Science of Climate Model Tuning. *Bull. Am. Meteorol. Soc.* 98, 589–602. doi:10.1175/BAMS-D-15-00135.1.

Houze, R. A. (1997). Stratiform Precipitation in Regions of Convection: A Meteorological Paradox? *Bull. Am. Meteorol. Soc.* doi:10.1175/1520-0477(1997)078<2179:SPIROC>2.0.CO;2.

Hoyos, I., Cañón-Barriga, J., Arenas-Suárez, T., Dominguez, F., and Rodríguez, B. A. (2018). Variability of regional atmospheric moisture over Northern South America: patterns and underlying phenomena. *Clim. Dyn.*, 1–19. doi:10.1007/s00382-018-4172-9.

Hsu, H.-H., Zhou, T., and Matsumoto, J. (2014). East Asian, Indochina and western North Pacific summer monsoon-an update. *Asia-Pacific J. Atmos. Sci.* 50, 45–68.

Hsu, H., Lo, M. H., Guillod, B. P., Miralles, D. G., and Kumar, S. (2017). Relation between precipitation location and antecedent/ subsequent soil moisture spatial patterns. *J. Geophys. Res.* 122, 6319–6328. doi:10.1002/2016JD026042.

Hsu, P.-C. (2016). "Global Monsoon in a Changing Climate," in, 7–24. doi:10.1007/978-3-319-21650-8_2.

Hsu, P., Li, T., Luo, J.-J., Murakami, H., Kitoh, A., and Zhao, M. (2012). Increase of global monsoon area and precipitation under global warming: A robust signal? *Geophys. Res. Lett.* 39, n/a-n/a. doi:10.1029/2012GL051037.

Hsu, P., Li, T., Murakami, H., and Kitoh, A. (2013). Future change of the global monsoon revealed from 19 CMIP5 models. *J. Geophys. Res. Atmos.* 118, 1247–1260. doi:10.1002/jgrd.50145.

Hsu, P., Li, T., and Wang, B. (2011). Trends in global monsoon area and precipitation over the past 30 years. *Geophys. Res. Lett.* 38, n/a-n/a. doi:10.1029/2011GL046893.

Hu, H., and Dominguez, F. (2015). Evaluation of Oceanic and Terrestrial Sources of Moisture for the North American

Monsoon Using Numerical Models and Precipitation Stable Isotopes. *J. Hydrometeorol.* 16, 19–35. doi:10.1175/jhm-d-14-0073.1.
Hu, Z.-Z. (2003). Long-term climate variations in China and global warming signals. *J. Geophys. Res.* 108, 4614. doi:10.1029/2003JD003651.
Hua, W., Zhou, L., Chen, H., Nicholson, S. E., Jiang, Y., and Raghavendra, A. (2018). Understanding the Central Equatorial African long-term drought using AMIP-type simulations. *Clim. Dyn.* 50, 1115–1128. doi:10.1007/s00382-017-3665-2.
Huang, D., Yan, P., Zhu, J., Zhang, Y., Kuang, X., and Cheng, J. (2018a). Uncertainty of global summer precipitation in the CMIP5 models: a comparison between high-resolution and low-resolution models. *Theor. Appl. Climatol.* 132, 55–69. doi:10.1007/s00704-017-2078-9.
Huang, J., Wang, T., Wang, W., Li, Z., and Yan, H. (2014). Climate effects of dust aerosols over east asian arid and semiarid regions. *J. Geophys. Res.* doi:10.1002/2014JD021796.
Huang, M., Piao, S., Sun, Y., Ciais, P., Cheng, L., Mao, J., et al. (2015). Change in terrestrial ecosystem water-use efficiency over the last three decades. *Glob. Chang. Biol.* 21, 2366–2378. doi:10.1111/gcb.12873.
Huang, S., Kumar, R., Flörke, M., Yang, T., Hundecha, Y., Kraft, P., et al. (2017). Evaluation of an ensemble of regional hydrological models in 12 large-scale river basins worldwide. *Clim. Change* 141, 381–397. doi:10.1007/s10584-016-1841-8.
Huang, S., Kumar, R., Rakovec, O., Aich, V., Wang, X., Samaniego, L., et al. (2018b). Multimodel assessment of flood characteristics in four large river basins at global warming of 1.5, 2.0 and 3.0 K above the pre-industrial level. *Environ. Res. Lett.* 13, 124005. doi:10.1088/1748-9326/aae94b.
Huang, Y., Gerber, S., Huang, T., and Lichstein, J. W. (2016). Evaluating the drought response of CMIP5 models using global gross primary productivity, leaf area, precipitation, and soil moisture data. *Global Biogeochem. Cycles* 30, 1827–1846. doi:10.1002/2016GB005480.
Hui, C., and Zheng, X.-T. (2018). Uncertainty in Indian Ocean Dipole response to global warming: the role of internal variability. *Clim. Dyn.* doi:10.1007/s00382-018-4098-2.
Hurkmans, R., Troch, P. A., Uijlenhoet, R., Torfs, P., and Durcik, M. (2009). Effects of Climate Variability on Water Storage in the Colorado River Basin. *J. Hydrometeorol.* 10, 1257–1270. doi:10.1175/2009JHM1133.1.
Huss, M., and Hock, R. (2018). Global-scale hydrological response to future glacier mass loss. *Nat. Clim. Chang.* 8, 135–140. doi:10.1038/s41558-017-0049-x.
Hwang, Y.-T. T., Frierson, D. M. W. W., and Kang, S. M. (2013a). Anthropogenic sulfate aerosol and the southward shift of tropical precipitation in the late 20th century. *Geophys. Res. Lett.* 40, 2845–2850. doi:10.1002/grl.50502.
Hwang, Y. T., Frierson, D. M. W., and Kang, S. M. (2013b). Anthropogenic sulfate aerosol and the southward shift of tropical precipitation in the late 20th century. *Geophys. Res. Lett.* 40, 2845–2850. doi:10.1002/grl.50502.
Iles, C. E., and Hegerl, G. C. (2014). The global precipitation response to volcanic eruptions in the CMIP5 models. *Environ. Res. Lett.* 9, 104012. doi:10.1088/1748-9326/9/10/104012.
Iles, C. E., and Hegerl, G. C. (2015). Systematic change in global patterns of streamflow following volcanic eruptions. *Nat. Geosci.* 8, 838–842. doi:10.1038/ngeo2545.
Iles, C. E., Hegerl, G. C., Schurer, A. P., and Zhang, X. (2013). The effect of volcanic eruptions on global precipitation. *J. Geophys. Res. Atmos.* 118, 8770–8786. doi:10.1002/jgrd.50678.
Intergovernmental Panel on Climate Change ed. (2014). “Terrestrial and Inland Water Systems,” in *Climate Change 2014 – Impacts, Adaptation and Vulnerability: Part A: Global and Sectoral Aspects: Working Group II Contribution to the IPCC Fifth Assessment Report: Volume 1: Global and Sectoral Aspects* (Cambridge: Cambridge University Press), 271–360. doi:DOI: 10.1017/CBO9781107415379.009.
IPCC (2013a). *Climate Change 2013: The Physical Science Basis. Contribution of Working Group I to the Fifth Assessment Report of the Intergovernmental Panel on Climate Change*. Cambridge, United Kingdom and New York, NY, USA: Cambridge University Press doi:10.1017/CBO9781107415324.
IPCC (2013b). “Summary for Policymakers,” in *Climate Change 2013: The Physical Science Basis. Contribution of Working Group I to the Fifth Assessment Report of the Intergovernmental Panel on Climate Change*, eds. T. F. Stocker, D. Qin, G.-K. Plattner, M. Tignor, S. K. Allen, J. Boschung, et al. (Cambridge, United Kingdom and New York, NY, USA: Cambridge University Press), 1–30. doi:10.1017/CBO9781107415324.004.
Irvine, P., Emanuel, K., He, J., Horowitz, L. W., Vecchi, G., and Keith, D. (2019). Halving warming with idealized solar geoengineering moderates key climate hazards. *Nat. Clim. Chang.* doi:10.1038/s41558-019-0398-8.
Ishizaki, Y., Shiogama, H., Emori, S., Yokohata, T., Nozawa, T., Takahashi, K., et al. (2013). Dependence of precipitation scaling patterns on emission scenarios for representative concentration pathways. *J. Clim.* doi:10.1175/JCLI-D-12-00540.1.
J.Vavrus, S. (2018). The Influence of Arctic Amplification on Mid-latitude Weather and Climate. *Curr. Clim. Chang. Reports* 4, 238–249.
Jackson, L. C., Kahana, R., Graham, T., Ringer, M. A., Woollings, T., Mecking, J. V., et al. (2015). Global and European climate impacts of a slowdown of the AMOC in a high resolution GCM. *Clim.*

*Dyn.*doi:10.1007/s00382-015-2540-2.
Jackson, L. S., Crook, J. A., and Forster, P. M. (2016). An intensified hydrological cycle in the simulation of geoengineering by cirrus cloud thinning using ice crystal fall speed changes. *J. Geophys. Res. Atmos.* 121, 6822–6840. doi:10.1002/2015JD024304.
Jacob, D., Petersen, J., Eggert, B., Alias, A., Christensen, O. B., Bouwer, L. M., et al. (2014). EURO-CORDEX: New high-resolution climate change projections for European impact research. *Reg. Environ. Chang.* 14, 563–578. doi:10.1007/s10113-013-0499-2.
Jasechko, S., Sharp, Z. D., Gibson, J. J., Birks, S. J., Yi, Y., and Fawcett, P. J. (2013). Terrestrial water fluxes dominated by transpiration. *Nature* 496, 347.
Jasechko, S., and Taylor, R. G. (2015). Intensive rainfall recharges tropical groundwaters. *Environ. Res. Lett.* 10, 5.
Jefferson, J. L., and Maxwell, R. M. (2015). Evaluation of simple to complex parameterizations of bare ground evaporation. *J. Adv. Model. Earth Syst.* 7, 1075–1092. doi:10.1002/2014MS000398.
Jefferson, J. L., Maxwell, R. M., and Constantine, P. G. (2017). Exploring the Sensitivity of Photosynthesis and Stomatal Resistance Parameters in a Land Surface Model. *J. Hydrometeorol.* 18, 897. Available at: https://doi.org/10.1175/JHM-D-16-0053.1.
Jia, B., Liu, J., Xie, Z., and Shi, C. (2018). Interannual Variations and Trends in Remotely Sensed and Modeled Soil Moisture in China. *J. Hydrometeorol.* 19, 831–847. doi:10.1175/JHM-D-18-0003.1.
Jiang, M., Li, Z., Wan, B., and Cribb, M. (2016a). Impact of aerosols on precipitation from deep convective clouds in eastern China. *J. Geophys. Res. Atmos.* 121, 9607–9620. doi:10.1002/2015JD024246.
Jiang, P., Wang, D., and Cao, Y. (2016b). Spatiotemporal characteristics of precipitation concentration and their possible links to urban extent in China. *Theor. Appl. Climatol.* 123, 757–768. doi:10.1007/s00704-015-1393-2.
Jiménez Cisneros, B. E., Oki, T., Arnell, N. W., Benito, G., Cogley, J. G., Döll, P., et al. (2014). "Freshwater resources," in *Climate Change 2014: Impacts, Adaptation, and Vulnerability. Part A: Global and Sectoral Aspects. Contribution of Working Group II to the Fifth Assessment Report of the Intergovernmental Panel of Climate Change*, eds. C. B. Field, V. R. Barros, D. J. Dokken, K. J. Mach, M. D. Mastrandrea, T. E. Bilir, et al. (Cambridge, United Kingdom and New York, NY, USA: Cambridge University Press), 229–269.
Jin, D., and Guan, Z. (2017). Summer Rainfall Seesaw between Hetao and the Middle and Lower Reaches of the Yangtze River and Its Relationship with the North Atlantic Oscillation. *J. Clim.* 30, 6629–6643. doi:10.1175/JCLI-D-16-0760.1.
Jin, Q., and Wang, C. (2017). A revival of Indian summer monsoon rainfall since 2002. *Nat. Clim. Chang.* 7, 587–594. doi:10.1038/nclimate3348.
Johnson, N. C., and Xie, S. P. (2010). Changes in the sea surface temperature threshold for tropical convection. *Nat. Geosci.* doi:10.1038/ngeo1008.
Jolly, D., Prentice, I. C., Bonnefille, R., Ballouche, A., Bengo, M., Brenac, P., et al. (1998). Biome reconstruction from pollen and plant macrofossil data for Africa and the Arabian peninsula at 0 and 6000 years. *J. Biogeogr.* 25, 1007–1027.
Jones, A., Haywood, J. M., Alterskjær, K., Boucher, O., Cole, J. N. S., Curry, C. L., et al. (2013a). The impact of abrupt suspension of solar radiation management (termination effect) in experiment G2 of the Geoengineering Model Intercomparison Project (GeoMIP). 118, 9743–9752. doi:10.1002/jgrd.50762.
Jones, C., and Carvalho, L. M. V. (2013). Climate Change in the South American Monsoon System: Present Climate and CMIP5 Projections. *J. Clim.* 26, 6660–6678. doi:10.1175/JCLI-D-12-00412.1.
Jones, C. D., Liddicoat, S. K., Meinshausen, M., Knutti, R., Anav, A., Arora, V. K., et al. (2013b). Uncertainties in CMIP5 Climate Projections due to Carbon Cycle Feedbacks. *J. Clim.* 27, 511–526. doi:10.1175/jcli-d-12-00579.1.
Jones, J. M., Gille, S. T., Goosse, H., Abram, N. J., Canziani, P. O., Charman, D. J., et al. (2016). Assessing recent trends in high-latitude Southern Hemisphere surface climate. *Nat. Clim. Chang.* 6, 917–926. doi:10.1038/nclimate3103.
Jones, M. D., Metcalfe, S. E., Davies, S. J., and Noren, A. (2015). Late Holocene climate reorganisation and the North American Monsoon. *Quat. Sci. Rev.* 124, 290–295. doi:10.1016/j.quascirev.2015.07.004.
Jourdain, N. C., Gupta, A. Sen, Taschetto, A. S., Ummenhofer, C. C., Moise, A. F., and Ashok, K. (2013). The Indo-Australian monsoon and its relationship to ENSO and IOD in reanalysis data and the CMIP3/CMIP5 simulations. *Clim. Dyn.* 41, 3073–3102. doi:10.1007/s00382-013-1676-1.
Jung, M., Reichstein, M., Ciais, P., Seneviratne, S. I., Sheffield, J., Goulden, M. L., et al. (2010). Recent decline in the global land evapotranspiration trend due to limited moisture supply. *Nature* 467, 951–954. doi:10.1038/nature09396.
Jung, T., Gulev, S. K., Rudeva, I., and Soloviov, V. (2006). Sensitivity of extratropical cyclone characteristics to horizontal resolution in the ECMWF model. *Q. J. R. Meteorol. Soc.* 132, 1839–1857. doi:10.1256/qj.05.212.
Kageyama, M., Braconnot, P., Harrison, S. P., Haywood, A. M., Jungclaus, J. H., Otto-Bliesner, B. L., et al. (2018). The PMIP4 contribution to CMIP6 - Part 1: Overview and over-arching analysis plan. *Geosci. Model*

*Dev.*doi:10.5194/gmd-11-1033-2018.
Kageyama, M., Merkel, U., Otto-Bliesner, B., Prange, M., Abe-Ouchi, A., Lohmann, G., et al. (2013). Climatic impacts of fresh water hosing under last glacial Maximum conditions: A multi-model study. *Clim. Past* 9, 935–953. doi:10.5194/cp-9-935-2013.
Kalimeris, A., Ranieri, E., Founda, D., and Norrant, C. (2017). Variability modes of precipitation along a Central Mediterranean area and their relations with ENSO, NAO, and other climatic patterns. *Atmos. Res.* 198, 56–80. doi:10.1016/j.atmosres.2017.07.031.
Kalnay, E., Kanamitsu, M., Kistler, R., Collins, W., Deaven, D., Gandin, L., et al. (1996). The NCEP/NCAR 40-year reanalysis project. *Bull. Am. Meteorol. Soc.* 77, 437–472.
Kamae, Y., Li, X., Xie, S.-P., and Ueda, H. (2017). Atlantic effects on recent decadal trends in global monsoon. *Clim. Dyn.* 49, 3443–3455. doi:10.1007/s00382-017-3522-3.
Kang, S. M., Deser, C., and Polvani, L. M. (2013). Uncertainty in climate change projections of the hadley circulation: The role of internal variability. *J. Clim.* doi:10.1175/JCLI-D-12-00788.1.
Kang, S. M., Held, I. M., Frierson, D. M. W., and Zhao, M. (2008). The response of the ITCZ to extratropical thermal forcing: Idealized slab-ocean experiments with a GCM. *J. Clim.* doi:10.1175/2007JCLI2146.1.
Kang, S. M., and Lu, J. (2012). Expansion of the Hadley cell under global warming: Winter versus summer. *J. Clim.* doi:10.1175/JCLI-D-12-00323.1.
Kang, S. M., and Polvani, L. M. (2011). The Interannual Relationship between the Latitude of the Eddy-Driven Jet and the Edge of the Hadley Cell. *J. Clim.* 24, 563–568. doi:10.1175/2010JCLI4077.1.
Kang, S., Wang, X., Roberts, H. M., Duller, G. A. T., Cheng, P., Lu, Y., et al. (2018). Late Holocene anti-phase change in the East Asian summer and winter monsoons. *Quat. Sci. Rev.* 188, 28–36. doi:10.1016/j.quascirev.2018.03.028.
Kanner, L. C., Burns, S. J., Cheng, H., Edwards, R. L., and Vuille, M. (2013). High-resolution variability of the South American summer monsoon over the last seven millennia: Insights from a speleothem record from the central Peruvian Andes. *Quat. Sci. Rev.* 75, 1–10. doi:10.1016/j.quascirev.2013.05.008.
Kao, A., Jiang, X., Li, L., Su, H., and Yung, Y. (2017). Precipitation, circulation, and cloud variability over the past two decades. *Earth Sp. Sci.* 4, 597–606. doi:10.1002/2017EA000319.
Kapnick, S., and Hall, A. (2012). Causes of recent changes in western North American snowpack. *Clim. Dyn.* 38, 1885–1899.
Karmakar, N., Chakraborty, A., and Nanjundiah, R. S. (2017). Increased sporadic extremes decrease the intraseasonal variability in the Indian summer monsoon rainfall. *Sci. Rep.* 7, 7824. doi:10.1038/s41598-017-07529-6.
Kathayat, G., Cheng, H., Sinha, A., Spötl, C., Edwards, R. L., Zhang, H., et al. (2016). Indian monsoon variability on millennial-orbital timescales. *Sci. Rep.* doi:10.1038/srep24374.
Kay, J. E., Deser, C., Phillips, A., Mai, A., Hannay, C., Strand, G., et al. (2015). The Community Earth System Model (CESM) Large Ensemble Project: A Community Resource for Studying Climate Change in the Presence of Internal Climate Variability. *Bull. Am. Meteorol. Soc.* 96, 1333–1349. doi:10.1175/BAMS-D-13-00255.1.
Kelley, C. P., Mohtadi, S., Cane, M. A., Seager, R., and Kushnir, Y. (2015). Climate change in the Fertile Crescent and implications of the recent Syrian drought. *Proc. Natl. Acad. Sci.* 112, 3241–3246.
Kelley, C., Ting, M., Seager, R., and Kushnir, Y. (2012). Mediterranean precipitation climatology, seasonal cycle, and trend as simulated by CMIP5. *Geophys. Res. Lett.* 39, n/a-n/a. doi:10.1029/2012GL053416.
Kendon, E. J., Ban, N., Roberts, N. M., Fowler, H. J., Roberts, M. J., Chan, S. C., et al. (2017). Do Convection-Permitting Regional Climate Models Improve Projections of Future Precipitation Change? *Bull. Am. Meteorol. Soc.* 98, 79–93. doi:10.1175/BAMS-D-15-0004.1.
Kendon, E. J., Roberts, N. M., Fowler, H. J., Roberts, M. J., Chan, S. C., and Senior, C. A. (2014). Heavier summer downpours with climate change revealed by weather forecast resolution model. *Nat. Clim. Chang.* 4, 570–576. doi:10.1038/nclimate2258.
Kent, C., Chadwick, R., and Rowell, D. P. (2015). Understanding Uncertainties in Future Projections of Seasonal Tropical Precipitation. *J. Clim.* 28, 4390–4413. doi:10.1175/JCLI-D-14-00613.1.
Kerkhoven, E., and Gan, T. Y. (2011). Differences and sensitivities in potential hydrologic impact of climate change to regional-scale Athabasca and Fraser River basins of the leeward and windward sides of the Canadian Rocky Mountains respectively. *Clim. Change*. doi:10.1007/s10584-010-9958-7.
Khain, A., Lynn, B., Atmospheric, J. D.-J. of the, and 2010, U. (2010). Aerosol effects on intensity of landfalling hurricanes as seen from simulations with the WRF model with spectral bin microphysics. *journals.ametsoc.org*.
Khain, A. P., Phillips, V., Benmoshe, N., and Pokrovsky, A. (2012). The role of small soluble aerosols in the microphysics of deep maritime clouds. *J. Atmos. Sci.* 69, 2787–2807.
Kidston, J., Scaife, A. A., Hardiman, S. C., Mitchell, D. M., Butchart, N., Baldwin, M. P., et al. (2015). Stratospheric influence on tropospheric jet streams, storm tracks and surface weather. *Nat. Geosci.* doi:10.1038/NGEO2424.
Kim, H.-M., Webster, P. J., and Curry, J. A. (2009). Impact of Shifting Patterns of Pacific Ocean Warming on North Atlantic Tropical Cyclones. *Science (80-.).* 325, 77–80. doi:10.1126/science.1174062.
Kim, H., Parinussa, R., Konings, A. G., Wagner, W., Cosh, M. H., Lakshmi, V., et al. (2018). Global-scale assessment

and combination of SMAP with ASCAT (active) and AMSR2 (passive) soil moisture products. *Remote Sens. Environ.* 204, 260–275. doi:10.1016/j.rse.2017.10.026.
Kingston, D. G., and McMecking, J. (2015). Precipitation delivery trajectories associated with extreme river flow for the Waitaki River, New Zealand. *Proc. Int. Assoc. Hydrol. Sci.* 369, 19–24.
Kitoh, A., Endo, H., Krishna Kumar, K., Cavalcanti, I. F. A., Goswami, P., and Zhou, T. (2013). Monsoons in a changing world: A regional perspective in a global context. *J. Geophys. Res. Atmos.* 118, 3053–3065. doi:10.1002/jgrd.50258.
Kivinen, S., and Rasmus, S. (2015). Observed cold season changes in a Fennoscandian fell area over the past three decades. *Ambio* 44, 214–225. doi:10.1007/s13280-014-0541-8.
Klingaman, N. P., Jiang, X., Xavier, P. K., Petch, J., Waliser, D., and Woolnough, S. J. (2015). Vertical structure and physical processes of the madden-julian oscillation: Synthesis and summary. *J. Geophys. Res. Atmos.* 120, 4671–4689.
Knauer, J., Werner, C., and Zaehle, S. (2015). Evaluating stomatal models and their atmospheric drought response in a land surface scheme: A multibiome analysis. *J. Geophys. Res. Biogeosciences* 120, 1894–1911. doi:10.1002/2015JG003114.
Knight, J., and Rogerson, C. M. eds. (2019). *The Geography of South Africa*. Cham: Springer International Publishing doi:10.1007/978-3-319-94974-1.
Knudsen, M. F., Jacobsen, B. H., Seidenkrantz, M.-S., and Olsen, J. (2014). Evidence for external forcing of the Atlantic Multidecadal Oscillation since termination of the Little Ice Age. *Nat. Commun.* 5, 3323. doi:10.1038/ncomms4323.
Knutson, T., Camargo, S. J., Chan, J. C. L., Emanuel, K., Ho, C. -h., Kossin, J., et al. (2019). Tropical cyclones and climate change assessment: Part I.
Knutson, T. R., and Manabe, S. (1995a). Time-mean response over the tropical Pacific to increase CO2 in a coupled ocean--atmosphere model. *J. Clim.* 8, 2181–2199.
Knutson, T. R., and Manabe, S. (1995b). Time-mean response over the tropical Pacific to increased CO2 in a coupled ocean-atmosphere model. *J. Clim.* 8, 2181–2199. doi:10.1175/1520-0442(1995)008<2181:TMROTT>2.0.CO;2.
Knutti, R., Sedláček, J., Sanderson, B. M., Lorenz, R., Fischer, E. M., and Eyring, V. (2017). A climate model projection weighting scheme accounting for performance and interdependence. *Geophys. Res. Lett.* 44, 1909–1918. doi:10.1002/2016GL072012.
Koch, J., Menounos, B., and Clague, J. J. (2009). Glacier change in Garibaldi Provincial Park, southern Coast Mountains, British Columbia, since the Little Ice Age. *Glob. Planet. Change* 66, 161–178. doi:10.1016/j.gloplacha.2008.11.006.
Kociuba, G., and Power, S. B. (2015). Inability of CMIP5 models to simulate recent strengthening of the Walker circulation: Implications for projections. *J. Clim.* 28, 20–35. doi:10.1175/JCLI-D-13-00752.1.
Kohyama, T., Hartmann, D. L., and Battisti, D. S. (2017). La Niña-like mean-state response to global warming and potential oceanic roles. *J. Clim.* doi:10.1175/JCLI-D-16-0441.1.
Kolusu, S. R., Shamsudduha, M., Todd, M. C., Taylor, R. G., Seddon, D., Kashaigili, J. J., et al. (2019). (in press). *El Ni{\ n}o event*, 2015–2016.
Komatsu, K. K., Alexeev, V. A., Repina, I. A., and Tachibana, Y. (2018). Poleward upgliding Siberian atmospheric rivers over sea ice heat up Arctic upper air. *Sci. Rep.* 8, 2872.
Konikow, L. F. (2011). Contribution of global groundwater depletion since 1900 to sea-level rise. *Geophys. Res. Lett.* 38. doi:10.1029/2011GL048604.
Konrad, C. P., and Dettinger, M. D. (2017). Flood runoff in relation to water vapor transport by atmospheric rivers over the western United States, 1949--2015. *Geophys. Res. Lett.* 44.
Konwar, M., Maheskumar, R. S., Kulkarni, J. R., Freud, E., Goswami, B. N., and Rosenfeld, D. (2012). Aerosol control on depth of warm rain in convective clouds. *J. Geophys. Res. Atmos.* 117.
Kooperman, G. J., Chen, Y., Hoffman, F. M., Koven, C. D., Lindsay, K., Pritchard, M. S., et al. (2018a). Forest response to rising CO2 drives zonally asymmetric rainfall change over tropical land. *Nat. Clim. Chang.* 8, 434–440. doi:10.1038/s41558-018-0144-7.
Kooperman, G. J., Fowler, M. D., Hoffman, F. M., Koven, C. D., Lindsay, K., Pritchard, M. S., et al. (2018b). Plant Physiological Responses to Rising CO 2 Modify Simulated Daily Runoff Intensity With Implications for Global-Scale Flood Risk Assessment. *Geophys. Res. Lett.* 45. doi:10.1029/2018GL079901.
Koren, I., Dagan, G., and Altaratz, O. (2014). From aerosol-limited to invigoration of warm convective clouds. *Science (80-.).* 344, 1143–1146.
Koren, I., Martins, J. V., Remer, L. A., and Afargan, H. (2008). Smoke invigoration versus inhibition of clouds over the Amazon. *Science* 321, 946–9. doi:10.1126/science.1159185.
Kosaka, Y., and Xie, S. P. (2013). Recent global-warming hiatus tied to equatorial Pacific surface cooling. *Nature* 501, 403–407. doi:10.1038/nature12534.
Kossin, J. P. (2018). A global slowdown of tropical-cyclone translation speed. *Nature* 558, 104–107.

doi:10.1038/s41586-018-0158-3.
Kossin, J. P. (2019). Matters Arising. *Nature*.
Kotchoni, V. D. O., Vouillamoz, J. -m., Lawson, F. M. A., Adjomayi, P., Boukari, M., and Taylor, R. G. (2019). Relationships between rainfall and groundwater recharge in seasonally humid Benin: a comparative analysis of long-term hydrographs in sedimentary and crystalline rock aquifers. *Hydrogeol. J.* 27, 447–457.
Koyama, T., Stroeve, J., Cassano, J., and Crawford, A. (2017). Sea Ice Loss and Arctic Cyclone Activity from 1979 to 2014. *J. Clim.* 30, 4735–4754. Available at: https://doi.org/10.1175/JCLI-D-16-0542.1.
Kraaijenbrink, P. D. A., Bierkens, M. F. P., Lutz, A. F., and Immerzeel, W. W. (2017). Impact of a global temperature rise of 1.5 degrees Celsius on Asia's glaciers. *Nature* 549, 257–260. doi:10.1038/nature23878.
Kravitz, B., Lynch, C., Hartin, C., and Bond-Lamberty, B. (2017). Exploring precipitation pattern scaling methodologies and robustness among CMIP5 models. *Geosci. Model Dev.* doi:10.5194/gmd-10-1889-2017.
Kravtsov, S. (2017). Pronounced differences between observed and CMIP5-simulated multidecadal climate variability in the twentieth century. *Geophys. Res. Lett.* 44, 5749–5757. doi:10.1002/2017GL074016.
Krishnamurthy, L., and Krishnamurthy, V. (2014). Influence of PDO on South Asian summer monsoon and monsoon–ENSO relation. *Clim. Dyn.* 42, 2397–2410. doi:10.1007/s00382-013-1856-z.
Krishnan, R., Ramesh, K. V., Samala, B. K., Meyers, G., Slingo, J. M., and Fennessy, M. J. (2006). Indian Ocean-monsoon coupled interactions and impending monsoon droughts. *Geophys. Res. Lett.* 33, L08711. doi:10.1029/2006GL025811.
Krishnan, R., Sabin, T. P., Ayantika, D. C., Kitoh, A., Sugi, M., Murakami, H., et al. (2013). Will the South Asian monsoon overturning circulation stabilize any further? *Clim. Dyn.* 40, 187–211. doi:10.1007/s00382-012-1317-0.
Krishnan, R., Sabin, T. P., Vellore, R., Mujumdar, M., Sanjay, J., Goswami, B. N., et al. (2016). Deciphering the desiccation trend of the South Asian monsoon hydroclimate in a warming world. *Clim. Dyn.* 47, 1007–1027. doi:10.1007/s00382-015-2886-5.
Krishnan, R., and Sugi, M. (2003). Pacific decadal oscillation and variability of the Indian summer monsoon rainfall. *Clim. Dyn.* 21. doi:10.1007/s00382-003-0330-8.
Kristjánsson, J. E., Muri, H., and Schmidt, H. (2015). The hydrological cycle response to cirrus cloud thinning. *Geophys. Res. Lett.* 42, 10,807-10,815. doi:10.1002/2015GL066795.
Kröpelin, S., Verschuren, D., Lézine, A. M., Eggermont, H., Cocquyt, C., Francus, P., et al. (2008). Climate-driven ecosystem succession in the Sahara: The past 6000 years. *Science (80-.).* 320, 765–768. doi:10.1126/science.1154913.
Krueger, O., Schenk, F., Feser, F., and Weisse, R. (2013). Inconsistencies between long-term trends in storminess derived from the 20CR reanalysis and observations. *J. Clim.* 26, 868–874. doi:10.1175/JCLI-D-12-00309.1.
Krysanova, V., Donnelly, C., Gelfan, A., Gerten, D., Arheimer, B., Hattermann, F., et al. (2018). How the performance of hydrological models relates to credibility of projections under climate change. *Hydrol. Sci. J.* 63, 696–720. doi:10.1080/02626667.2018.1446214.
Kucharski, F., Bracco, A., Yoo, J. H., Tompkins, A. M., Feudale, L., Ruti, P., et al. (2009). A Gill-Matsuno-type mechanism explains the tropical Atlantic influence on African and Indian monsoon rainfall. *Q. J. R. Meteorol. Soc.* 135, 569–579. doi:10.1002/qj.406.
Kucharski, F., and Joshi, M. K. (2017). Influence of tropical South Atlantic sea-surface temperatures on the Indian summer monsoon in CMIP5 models. *Q. J. R. Meteorol. Soc.* 143, 1351–1363. doi:10.1002/qj.3009.
Kucharski, F., Kang, I. -s., Farneti, R., and Feudale, L. (2011). Tropical Pacific response to 20th century Atlantic warming, Geophys. *Res* 38. doi:10.1029/2010GL046248.
Kulkarni, A., and Karyakarte, Y. (2014). Observed changes in Himalayan glaciers. *Curr. Sci.* 106, 237–244.
Kumar, D., and Ganguly, A. R. (2018). Intercomparison of model response and internal variability across climate model ensembles. *Clim. Dyn.* 51, 207–219. doi:10.1007/s00382-017-3914-4.
Kumar, K. K., Rajagopalan, B., Hoerling, M., Bates, G., and Cane, M. (2006). Unraveling the Mystery of Indian Monsoon Failure During El Nino. *Science (80-.).* 314, 115–119. doi:10.1126/science.1131152.
Kumar, M. R. R., Krishnan, R., Sankar, S., Unnikrishnan, A. S., and Pai, D. S. (2009). Increasing Trend of Break-Monsoon Conditions Over India - Role of Ocean-Atmosphere Processes in the Indian Ocean. *IEEE Geosci. Remote Sens. Lett.* 6, 332–336. doi:10.1109/LGRS.2009.2013366.
Kumar, S., Allan, R. P., Zwiers, F., Lawrence, D. M., and Dirmeyer, P. A. (2015). Revisiting trends in wetness and dryness in the presence of internal climate variability and water limitations over land. *Geophys. Res. Lett.* 42, 10867–10875. doi:10.1002/2015GL066858.
Kumar, S., Merwade, V., Kinter, J. L., and Niyogi, D. (2013). Evaluation of temperature and precipitation trends and long-term persistence in CMIP5 twentieth-century climate simulations. *J. Clim.* doi:10.1175/JCLI-D-12-00259.1.
Kumar, S. V, Jasinski, M., Mocko, D., Rodell, M., Borak, J., Li, B., et al. (2018). NCA-LDAS land analysis: Development and performance of a multisensor, multivariate land data assimilation system for the National Climate Assessment. *J. Hydrometeorol.*
Kumar, S. V, Peters-Lidard, C. D., Santanello, J., Harrison, K., Liu, Y., and Shaw, M. (2012). Land surface Verification

Toolkit (LVT) – a generalized framework for land surface model evaluation. *Geosci. Model Dev.* 5, 869–886. Available at: https://doi.org/10.5194/gmd-5-869-2012.
Kundzewicz, Z. W., Pińskwar, I., and Brakenridge, G. R. Changes in river flood hazard in Europe: A review. Hydrol. *Res* 2017.
Kunkel, K. E., Easterling, D. R., Kristovich, D. A., Gleason, B., Stoecker, L., and Smith, R. (2012). Meteorological causes of the secular variations in observed extreme precipitation events for the conterminous United States. *J. Hydrometeorol.* 13, 1131–1141. doi:10.1175/JHM-D-11-0108.1.
Kunkel, K. E., Easterling, D. R., Kristovich, D. A. R., Gleason, B., Stoecker, L., and Smith, R. (2010). Recent increases in {U}.S. heavy precipitation associated with tropical cyclones. *Geophys. Res* 37. doi:10.1029/2010GL045164.
Kunkel, K. E., Robinson, D. A., Champion, S., Yin, X., Estilow, T., and Frankson, R. M. (2016). Trends and Extremes in Northern Hemisphere Snow Characteristics. *Curr. Clim. Chang. Reports* 2, 65–73. doi:10.1007/s40641-016-0036-8.
Kushnir, Y., Scaife, A. A., Arritt, R., Balsamo, G., Boer, G., Doblas-Reyes, F., et al. (2019). Towards operational predictions of the near-term climate. *Nat. Clim. Chang.* 9, 94–101. doi:10.1038/s41558-018-0359-7.
Kuss, A. J. M., and Gurdak, J. J. (2014). Groundwater level response in U.S. principal aquifers to ENSO, NAO, PDO, and AMO. *J. Hydrol.* 519, 1939–1952. doi:10.1016/j.jhydrol.2014.09.069.
Kusunoki, S., and Arakawa, O. (2015). Are CMIP5 Models Better than CMIP3 Models in Simulating Precipitation over East Asia? *J. Clim.* 28, 5601–5621. doi:10.1175/JCLI-D-14-00585.1.
Kutuzov, S., and Shahgedanova, M. (2009). Glacier retreat and climatic variability in the eastern Terskey–Alatoo, inner Tien Shan between the middle of the 19th century and beginning of the 21st century. *Glob. Planet. Change* 69, 59–70. doi:10.1016/j.gloplacha.2009.07.001.
Kutzbach, J. E. (1981). Monsoon climate of the early Holocene: climate experiment with the Earth's orbital parameters for 9000 years ago. *Science (80-.).* 214, 59–61.
Kvalevåg, M. M., Samset, B. H., and Myhre, G. (2013). Hydrological sensitivity to greenhouse gases and aerosols in a global climate model. *Geophys. Res. Lett.* 40, 1432–1438. doi:10.1002/grl.50318.
L'Heureux, M. L., Lee, S., and Lyon, B. (2013a). Recent multidecadal strengthening of the Walker circulation across the tropical Pacific. *Nat. Clim. Chang.* 3, 571–576. doi:10.1038/nclimate1840.
L'Heureux, M. L., Lee, S., and Lyon, B. (2013b). Recent multidecadal strengthening of the Walker circulation across the tropical Pacific. *Nat. Clim. Chang.* 3, 571–576. doi:10.1038/nclimate1840.
Lachniet, M. S., Asmerom, Y., Bernal, J. P., Polyak, V. J., and Vazquez-Selem, L. (2013). Orbital pacing and ocean circulation-induced collapses of the Mesoamerican monsoon over the past 22,000 y. *Proc. Natl. Acad. Sci.* doi:10.1073/pnas.1222804110.
Lafore, J.-P., Beucher, F., Peyrillé, P., Diongue-Niang, A., Chapelon, N., Bouniol, D., et al. (2017). A multi-scale analysis of the extreme rain event of Ouagadougou in 2009. *Q. J. R. Meteorol. Soc.* 143, 3094–3109. doi:10.1002/qj.3165.
Laîné, A., Nakamura, H., Nishii, K., and Miyasaka, T. (2014). A diagnostic study of future evaporation changes projected in CMIP5 climate models. *Clim. Dyn.* 42, 2745–2761. doi:10.1007/s00382-014-2087-7.
Lambert, F. H., and Faull, N. E. (2007). Tropospheric adjustment: The response of two general circulation models to a change in insolation. *Geophys. Res. Lett.* 34, L03701. doi:10.1029/2006GL028124.
Lambert, F. H., Ferraro, A. J., and Chadwick, R. (2017). Land-ocean shifts in tropical precipitation linked to surface temperature and humidity change. *J. Clim.* 30, 4527–4545. doi:10.1175/JCLI-D-16-0649.1.
Lambert, F. H., Harris, G. R., Collins, M., Murphy, J. M., Sexton, D. M. H., and Booth, B. B. B. (2013). Interactions between perturbations to different Earth system components simulated by a fully-coupled climate model. *Clim. Dyn.* 41, 3055–3072. doi:10.1007/s00382-012-1618-3.
Lanzante, J. R., Dixon, K. W., Nath, M. J., Whitlock, C. E., and Adams-Smith, D. (2018). Some pitfalls in statistical downscaling of future climate. *Bull. Am. Meteorol. Soc.* 99, 791–803.
Lau, K.-M., and Kim, K.-M. (2006). Observational relationships between aerosol and Asian monsoon rainfall, and circulation. *Geophys. Res. Lett.* 33. doi:10.1029/2006GL027546.
Lau, K. M., and Wu, H. T. (2007). Detecting trends in tropical rainfall characteristic, 1979-2003. *Int. J. Climatol.* 27, 979–988. doi:10.1002/joc.1454.
Lau, W. K.-M., and Kim, K.-M. (2017). Competing influences of greenhouse warming and aerosols on Asian summer monsoon circulation and rainfall. *Asia-Pacific J. Atmos. Sci.* 53, 181–194. doi:10.1007/s13143-017-0033-4.
Lau, W. K. M. (2016). The aerosol-monsoon climate system of Asia: A new paradigm. *J. Meteorol. Res.* 30, 1–11. doi:10.1007/s13351-015-5999-1.
Lau, W. K. M., and Kim, K.-M. (2015). Robust Hadley Circulation changes and increasing global dryness due to CO2 warming from CMIP5 model projections. *Proc. Natl. Acad. Sci. U. S. A.* 112, 3630–5. doi:10.1073/pnas.1418682112.
Lau, W. K. M., Kim, K.-M., and Ruby Leung, L. (2017). Changing circulation structure and precipitation characteristics in Asian monsoon regions: greenhouse warming vs. aerosol effects. *Geosci. Lett.* 4, 28. doi:10.1186/s40562-017-

0094-3.

Lau, W. K. M., and Zhou, Y. P. (2012). Observed recent trends in tropical cyclone rainfall over the North Atlantic and North Pacific. *J. Geophys. Res* 117. doi:10.1029/2011JD016510.

Lauer, A., Eyring, V., Righi, M., Buchwitz, M., Defourny, P., Evaldsson, M., et al. (2017). Benchmarking CMIP5 models with a subset of ESA CCI Phase 2 data using the ESMValTool. *Remote Sens. Environ.* 203, 9–39. doi:10.1016/j.rse.2017.01.007.

Lavado, W. S., Labat, D., Ronchail, J., Espinoza, J. C., and Guyot, J. L. (2013). Trends in rainfall and temperature in the Peruvian Amazon-Andes basin over the last 40years (1965-2007). *Hydrol. Process.* 27, 2944–2957. doi:10.1002/hyp.9418.

Lavers, D. A., Allan, R. P., Villarini, G., Lloyd-Hughes, B., Brayshaw, D. J., and Wade, A. J. (2013). Future changes in atmospheric rivers and their implications for winter flooding in Britain. *Environ. Res. Lett.* 8. doi:10.1088/1748-9326/8/3/034010.

Lavers, D. A., Ralph, F. M., Waliser, D. E., Gershunov, A., and Dettinger, M. D. (2015). Climate change intensification of horizontal water vapor transport in CMIP5. *Geophys. Res. Lett.* 42, 5617–5625. doi:10.1002/2015GL064672.

Lawrence, D. M., Hurtt, G. C., Arneth, A., Brovkin, V., Calvin, K. V., Jones, A. D., et al. (2016). The Land Use Model Intercomparison Project (LUMIP) contribution to CMIP6: Rationale and experimental design. *Geosci. Model Dev.* 9, 2973–2998. doi:10.5194/gmd-9-2973-2016.

Lawrence, D., and Vandecar, K. (2015). Effects of tropical deforestation on climate and agriculture. *Nat. Clim. Chang.* 5, 27–36. doi:10.1038/nclimate2430.

Lazenby, M. J., Todd, M. C., Chadwick, R., and Wang, Y. (2018). Future Precipitation Projections over Central and Southern Africa and the Adjacent Indian Ocean: What Causes the Changes and the Uncertainty? *J. Clim.* 31, 4807–4826. doi:10.1175/JCLI-D-17-0311.1.

Lazenby, M., Todd, M., and Wang, Y. (2016). Climate model simulation of the South Indian Ocean Convergence Zone: mean state and variability. *Clim. Res.* 68, 59–71. doi:10.3354/cr01382.

Lebel, T., Diedhiou, A., and Laurent, H. (2003). Seasonal cycle and interannual variability of the Sahelian rainfall at hydrological scales. *J. Geophys. Res.* 108, 8389. doi:10.1029/2001JD001580.

Ledru, M.-P., Jomelli, V., Samaniego, P., Vuille, M., Hidalgo, S., Herrera, M., et al. (2013). The Medieval Climate Anomaly and the Little Ice Age in the eastern Ecuadorian Andes. *Clim. Past* 9, 307–321. doi:10.5194/cp-9-307-2013.

Leduc, M., Matthews, H. D., de El\'\ia, R., Leduc, M., Matthews, H. D., and El\'\ia, R. de (2015). *Quantifying the Limits of a Linear Temperature Response to Cumulative CO 2 Emissions*. J. Clim doi:10.1175/JCLI-D-14-00500.1.

Lee, D. E., Ting, M., Vigaud, N., Kushnir, Y., and Barnston, A. G. (2018a). Atlantic Multidecadal Variability as a Modulator of Precipitation Variability in the Southwest United States. *J. Clim.* 31, 5525–5542. doi:10.1175/JCLI-D-17-0372.1.

Lee, D., Ward, P. J., and Block, P. (2018b). Identification of symmetric and asymmetric responses in seasonal streamflow globally to ENSO phase. *Environ. Res. Lett.* 13, 044031. doi:10.1088/1748-9326/aab4ca.

Lee, E.-J., Ha, K.-J., and Jhun, J.-G. (2014). Interdecadal changes in interannual variability of the global monsoon precipitation and interrelationships among its subcomponents. *Clim. Dyn.* 42, 2585–2601. doi:10.1007/s00382-013-1762-4.

Lee, J.-Y., and Wang, B. (2014). Future change of global monsoon in the CMIP5. *Clim. Dyn.* 42, 101–119. doi:10.1007/s00382-012-1564-0.

Lee, J.-Y., and Wang, B. (2014). Future change of global monsoon in the CMIP5. *Clim. Dyn.* 42, 101–119. doi:10.1007/s00382-012-1564-0.

Lee, J. A., and Gill, T. E. (2015). Multiple causes of wind erosion in the Dust Bowl. *Aeolian Res.* doi:10.1016/j.aeolia.2015.09.002.

Lee, J. H., Ramirez, J. A., Kim, T. W., and Julien, P. Y. (2019). Variability, teleconnection, and predictability of Korean precipitation in relation to large scale climate indices. *J. Hydrol.* 568, 12–25. doi:10.1016/j.jhydrol.2018.08.034.

Lee, S.-K., Park, W., Baringer, M. O., Gordon, A. L., Huber, B., and Liu, Y. (2015). Pacific origin of the abrupt increase in Indian Ocean heat content during the warming hiatus. *Nat. Geosci.* 8, 445. Available at: https://doi.org/10.1038/ngeo2438.

Lee, S., and Feldstein, S. B. (2013). Detecting Ozone- and Greenhouse Gas–Driven Wind Trends with Observational Data. *Science (80-.).* 339, 563–567.

Lehner, F., Coats, S., Stocker, T. F., Pendergrass, A. G., Sanderson, B. M., Raible, C. C., et al. (2017a). Projected drought risk in 1.5°C and 2°C warmer climates. *Geophys. Res. Lett.* 44, 7419–7428. doi:10.1002/2017GL074117.

Lehner, F., Deser, C., Simpson, I. R., and Terray, L. (2018). Attributing the U.S. Southwest's Recent Shift Into Drier Conditions. *Geophys. Res. Lett.* doi:10.1029/2018GL078312.

Lehner, F., Wahl, E. R., Wood, A. W., Blatchford, D. B., and Llewellyn, D. (2017b). Assessing recent declines in Upper Rio Grande runoff efficiency from a paleoclimate perspective. *Geophys. Res. Lett.* 44, 4124–4133.

doi:10.1002/2017GL073253.
Lei, Y., Yao, T., Yang, K., Sheng, Y., Kleinherenbrink, M., Yi, S., et al. (2017). Lake seasonality across the Tibetan Plateau and their varying relationship with regional mass changes and local hydrology. *Geophys. Res. Lett.* 44, 892–900. doi:10.1002/2016GL072062.
Lejeune, Q., Davin, E. L., Guillod, B. P., and Seneviratne, S. I. (2015). Influence of Amazonian deforestation on the future evolution of regional surface fluxes, circulation, surface temperature and precipitation. *Clim. Dyn.* 44, 2769–2786. doi:10.1007/s00382-014-2203-8.
Lemordant, L., Gentine, P., Swann, A. S., Cook, B. I., and Scheff, J. (2018). Critical impact of vegetation physiology on the continental hydrologic cycle in response to increasing CO 2. *Proc. Natl. Acad. Sci.* 0, 201720712. doi:10.1073/pnas.1720712115.
Lenderink, G., Barbero, R., Loriaux, J. M., and Fowler, H. J. (2017). Super-Clausius-Clapeyron scaling of extreme hourly convective precipitation and its relation to large-scale atmospheric conditions. *J. Clim.* 30, 6037–6052. doi:10.1175/JCLI-D-16-0808.1.
Leng, G., Huang, M., Tang, Q., Gao, H., and Leung, L. (2014). Modeling the Effects of Groundwater-Fed Irrigation on Terrestrial Hydrology over the Conterminous United States. *J. Hydrometeorol.* 15, 13–49.
Lenggenhager, S., Croci-Maspoli, M., Brönnimann, S., and Martius, O. (2018a). On the dynamical coupling between atmospheric blocks and heavy precipitation events: A discussion of the southern Alpine flood in October 2000. *Q. J. R. Meteorol. Soc.* doi:10.1002/qj.3449.
Lenggenhager, S., Croci-Maspoli, M., Brönnimann, S., and Martius, O. (2018b). On the dynamical coupling between atmospheric blocks and heavy precipitation events: A discussion of the southern Alpine flood in October 2000. *Q. J. R. Meteorol. Soc.* doi:10.1002/qj.3449.
Lenhard, J., and Winsberg, E. (2010). Holism, entrenchment, and the future of climate model pluralism. *Stud. Hist. Philos. Sci.* 41, 253.
Lenton, T. M., Held, H., Kriegler, E., Hall, J. W., Lucht, W., Rahmstorf, S., et al. (2008). Tipping elements in the Earth's climate system. *Proc. Natl. Acad. Sci.* 105, 1786–1793.
León-Muñoz, J., Urbina, M. A., Garreaud, R., and Iriarte, J. L. (2018). Hydroclimatic conditions trigger record harmful algal bloom in western Patagonia (summer 2016). *Sci. Rep.* 8, 1330. doi:10.1038/s41598-018-19461-4.
Leutwyler, D., Lüthi, D., Ban, N., Fuhrer, O., and Schär, C. (2017). Evaluation of the convection-resolving climate modeling approach on continental scales. *J. Geophys. Res.* 122, 5237–5258. doi:10.1002/2016JD026013.
Levermann, A., Schewe, J., Petoukhov, V., and Held, H. (2009). Basic mechanism for abrupt monsoon transitions. *Proc. Natl. Acad. Sci.* 106, 20572–20577. doi:10.1073/pnas.0901414106.
Levine, N. M., Zhang, K., Longo, M., Baccini, A., Phillips, O. L., Lewis, S. L., et al. (2016). Ecosystem heterogeneity determines the ecological resilience of the Amazon to climate change. *Proc. Natl. Acad. Sci.* 113, 793–797. doi:10.1073/pnas.1511344112.
Levis, S., Bonan, G. B., and Bonfils, C. (2004). Soil feedback drives the mid-Holocene North African monsoon northward in fully coupled CCSM2 simulations with a dynamic vegetation model. *Clim. Dyn.* doi:10.1007/s00382-004-0477-y.
Levy, A. A. L., Ingram, W., Jenkinson, M., Huntingford, C., Lambert, F. H., and Allen, M. (2013a). Can correcting feature location in simulated mean climate improve agreement on projected changes? *Geophys. Res. Lett.* 40, 354–358. doi:10.1029/2012GL053964.
Levy, R. C., Mattoo, S., Munchak, L. A., Remer, L. A., Sayer, A. M., Patadia, F., et al. (2013b). The Collection 6 MODIS aerosol products over land and ocean. *Atmos. Meas. Tech.* 6, 2989–3034. doi:10.5194/amt-6-2989-2013.
Li, F., Levis, S., and Ward, D. S. (2013a). Quantifying the role of fire in the Earth system – Part 1: Improved global fire modeling in the Community Earth System Model (CESM1). *Biogeosciences* 10, 2293–2314. Available at: https://doi.org/10.5194/bg-10-2293-2013.
Li, G., Harrison, S. P., Bartlein, P. J., Izumi, K., and Colin Prentice, I. (2013b). Precipitation scaling with temperature in warm and cold climates: An analysis of CMIP5 simulations. *Geophys. Res. Lett.* 40, 4018–4024. doi:10.1002/grl.50730.
Li, G., Xie, S. P., Du, Y., and Luo, Y. (2016a). Effects of excessive equatorial cold tongue bias on the projections of tropical Pacific climate change. Part I: the warming pattern in CMIP5 multi-model ensemble. *Clim. Dyn.* doi:10.1007/s00382-016-3043-5.
Li, G., Xie, S. P., He, C., and Chen, Z. (2017). Western Pacific emergent constraint lowers projected increase in Indian summer monsoon rainfall. *Nat. Clim. Chang.* 7, 708–712. doi:10.1038/nclimate3387.
Li, H., Dai, A., Zhou, T., and Lu, J. (2010). Responses of East Asian summer monsoon to historical SST and atmospheric forcing during 1950–2000. *Clim. Dyn.* 34, 501–514. doi:10.1007/s00382-008-0482-7.
Li, J., Duan, Q., Wang, Y. P., Gong, W., Gan, Y., and Wang, C. (2018a). Parameter optimization for carbon and water fluxes in two global land surface models based on surrogate modelling. *Int. J. Climatol.* 38, e1016–e1031. doi:10.1002/joc.5428.
Li, J., Feng, J., and Li, Y. (2012a). A possible cause of decreasing summer rainfall in northeast Australia. *Int. J.*

Climatol. 32, 995–1005. doi:10.1002/joc.2328.
Li, J., Xie, S.-P., Cook, E. R., Chen, F., Shi, J., Zhang, D. D., et al. (2018b). Deciphering human contributions to Yellow River flow reductions and downstream drying using centuries-long tree ring records. *Geophys. Res. Lett.* doi:10.1029/2018GL081090.
Li, J., Xie, S.-P., Cook, E. R., Chen, F., Shi, J., Zhang, D. D., et al. (2018c). Deciphering human contributions to Yellow River flow reductions and downstream drying using centuries-long tree ring records. *Geophys. Res. Lett.* doi:10.1029/2018GL081090.
Li, J., Xie, S.-P., Cook, E. R., Huang, G., D'Arrigo, R., Liu, F., et al. (2011a). Interdecadal modulation of El Niño amplitude during the past millennium. *Nat. Clim. Chang.* 1, 114–118. doi:10.1038/nclimate1086.
Li, M., Woollings, T., Hodges, K., and Masato, G. (2014). Extratropical cyclones in a warmer, moister climate: A recent Atlantic analogue. *Geophys. Res. Lett.* doi:10.1002/2014GL062186.
Li, N., and McGregor, G. R. (2017). Linking interannual river flow river variability across New Zealand to the Southern Annular Mode, 1979-2011. *Hydrol. Process.* 31, 2261–2276. doi:10.1002/hyp.11184.
Li, W., Li, L., Fu, R., Deng, Y., and Wang, H. (2011b). Changes to the North Atlantic Subtropical High and Its Role in the Intensification of Summer Rainfall Variability in the Southeastern United States. *J. Clim.* 24, 1499–1506. doi:10.1175/2010JCLI3829.1.
Li, W., Li, L., Ting, M., Deng, Y., Kushnir, Y., Liu, Y., et al. (2013c). Intensification of the Southern Hemisphere summertime subtropical anticyclones in a warming climate. *Geophys. Res. Lett.* 40, 5959–5964. doi:10.1002/2013GL058124.
Li, W., Li, L., Ting, M., and Liu, Y. (2012b). Intensification of Northern Hemisphere subtropical highs in a warming climate. *Nat. Geosci.* 5, 830–834. doi:10.1038/ngeo1590.
Li, W., Li, L., Ting, M., and Liu, Y. (2012c). Intensification of Northern Hemisphere subtropical highs in a warming climate. *Nat. Geosci.* 5, 830–834. doi:10.1038/ngeo1590.
Li, X., and Ting, M. (2017). Understanding the Asian summer monsoon response to greenhouse warming: the relative roles of direct radiative forcing and sea surface temperature change. *Clim. Dyn.* 49, 2863–2880. doi:10.1007/s00382-016-3470-3.
Li, Y., Kalnay, E., Motesharrei, S., Rivas, J., Kucharski, F., Kirk-Davidoff, D., et al. (2018d). Climate Model Shows Large-Scale Wind and Solar Farms in the Sahara Increase Rain and Vegetation. *Science (80-.).* 361, 1019–1022. doi:10.1126/science.aar5629.
Li, Y., Tao, H., Su, B., Kundzewicz, Z. W., and Jiang, T. (2019). Impacts of 1.5 °C and 2 °C global warming on winter snow depth in Central Asia. *Sci. Total Environ.* 651, 2866–2873. doi:10.1016/j.scitotenv.2018.10.126.
Li, Y., Thompson, D. W. J., Bony, S., and Merlis, T. M. (2018e). Thermodynamic Control on the Poleward shift of the Extratropical Jet in Climate Change Simulations: The Role of Rising High Clouds and their Radiative Effects. *J. Clim.* 32, JCLI-D-18-0417.1. doi:10.1175/JCLI-D-18-0417.1.
Li, Z., Lau, W. K. M., Ramanathan, V., Wu, G., Ding, Y., Manoj, M. G., et al. (2016b). Aerosol and monsoon climate interactions over Asia. *Rev. Geophys.* 54, 866–929. doi:10.1002/2015RG000500.
Lian, X., Piao, S., Huntingford, C., Li, Y., Zeng, Z., Wang, X., et al. (2018). Partitioning global land evapotranspiration using CMIP5 models constrained by observations. *Nat. Clim. Chang.* 8, 640–646. doi:10.1038/s41558-018-0207-9.
Liang, Y.-C., Chou, C.-C., Yu, J.-Y., and Lo, M.-H. (2016). Mapping the locations of asymmetric and symmetric discharge responses in global rivers to the two types of El Niño. *Environ. Res. Lett.* 11, 044012. doi:10.1088/1748-9326/11/4/044012.
Liddicoat, S. K., Booth, B. B. B., and Joshi, M. M. (2016). An investigation into linearity with cumulative emissions of the climate and carbon cycle response in HadCM3LC. *Environ. Res. Lett.* 11. doi:10.1088/1748-9326/11/6/065003.
Lim, E.-P., and Hendon, H. H. (2015). Understanding and predicting the strong Southern Annular Mode and its impact on the record wet east Australian spring 2010. *Clim. Dyn.* 44, 2807–2824. doi:10.1007/s00382-014-2400-5.
Lim, E.-P., Hendon, H. H., Arblaster, J. M., Delage, F., Nguyen, H., Min, S.-K., et al. (2016). The impact of the Southern Annular Mode on future changes in Southern Hemisphere rainfall. *Geophys. Res. Lett.* 43, 7160–7167. doi:10.1002/2016GL069453.
Lin, L., Wang, Z., Xu, Y., Fu, Q., and Dong, W. (2018a). Larger Sensitivity of Precipitation Extremes to Aerosol Than Greenhouse Gas Forcing in CMIP5 Models. *J. Geophys. Res. Atmos.* 123, 8062–8073. doi:10.1029/2018JD028821.
Lin, L., Xu, Y., Wang, Z., Diao, C., Dong, W., and Xie, S.-P. (2018b). Changes in extreme rainfall over India and China attributed to regional aerosol-cloud interaction during the late 20th century rapid industrialization. *Geophys. Res. Lett.* doi:10.1029/2018GL078308.
Lin, M., and Huybers, P. (2019). If rain falls in India and no one reports it, are historical trends in monsoon extremes biased? *Geophys. Res. Lett.* 46. Available at: https://doi.org/10.1029/2018GL079709.
Lin, R., Zhou, T., and Qian, Y. (2014). Evaluation of global monsoon precipitation changes based on five reanalysis

datasets. *J. Clim.* 27, 1271–1289. doi:10.1175/JCLI-D-13-00215.1.
Lipson, M. J., Thatcher, M., Hart, M. A., and Pitman, A. (2018). A building energy demand and urban land surface model. *Q. J. R. Meteorol. Soc.* 144, 1572. Available at: https://doi.org/10.1002/qj.3317.
Little, K., Kingston, D. G., Cullen, N. J., and Gibson, P. B. (2019). The Role of Atmospheric Rivers for Extreme Ablation and Snowfall Events in the Southern Alps of New Zealand. *Geophys. Res. Lett.* doi:10.1029/2018GL081669.
Liu, C., and Allan, R. P. (2013a). Observed and simulated precipitation responses in wet and dry regions 1850-2100. *Environ. Res. Lett.* 8. doi:10.1088/1748-9326/8/3/034002.
Liu, C., and Allan, R. P. (2013b). Observed and simulated precipitation responses in wet and dry regions 1850-2100. *Environ. Res. Lett.* 8. doi:10.1088/1748-9326/8/3/034002.
Liu, C., and Allan, R. P. (2013c). Observed and simulated precipitation responses in wet and dry regions 1850-2100. *Environ. Res. Lett.* 8. doi:10.1088/1748-9326/8/3/034002.
Liu, F., Chai, J., Wang, B., Liu, J., Zhang, X., and Wang, Z. (2016). Global monsoon precipitation responses to large volcanic eruptions. *Sci. Rep.* 6, 24331. doi:10.1038/srep24331.
Liu, F., Zhao, T., Wang, B., Liu, J., and Luo, W. (2018a). Different Global Precipitation Responses to Solar, Volcanic, and Greenhouse Gas Forcings. *J. Geophys. Res. Atmos.* 123, 4060–4072. doi:10.1029/2017JD027391.
Liu, J., Wang, B., Ding, Q., Kuang, X., Soon, W., and Zorita, E. (2009a). Centennial Variations of the Global Monsoon Precipitation in the Last Millennium: Results from ECHO-G Model. *J. Clim.* 22, 2356–2371. doi:10.1175/2008JCLI2353.1.
Liu, L., Shawki, D., Voulgarakis, A., Kasoar, M., Samset, B. H., Myhre, G., et al. (2018b). A PDRMIP Multimodel study on the impacts of regional aerosol forcings on global and regional precipitation. *J. Clim.* 31, 4429–4447. doi:10.1175/JCLI-D-17-0439.1.
Liu, T., Li, J., Li, Y., Zhao, S., Zheng, F., Zheng, J., et al. (2018c). Influence of the May Southern annular mode on the South China Sea summer monsoon. *Clim. Dyn.* 51, 4095–4107. doi:10.1007/s00382-017-3753-3.
Liu, W., Xie, S. P., Liu, Z., and Zhu, J. (2017). Overlooked possibility of a collapsed atlantic meridional overturning circulation in warming climate. *Sci. Adv.* doi:10.1126/sciadv.1601666.
Liu, Y., Liu, Y., and Wang, W. (2019). Inter-comparison of satellite-retrieved and Global Land Data Assimilation System-simulated soil moisture datasets for global drought analysis. *Remote Sens. Environ.* 220, 1–18. doi:10.1016/j.rse.2018.10.026.
Liu, Y. Y., de Jeu, R. A. M., McCabe, M. F., Evans, J. P., and van Dijk, A. I. J. M. (2011). Global long-term passive microwave satellite-based retrievals of vegetation optical depth. *Geophys. Res. Lett.* 38.
Liu, Z., Otto-Bliesner, B. L., He, F., Brady, E. C., Tomas, R., Clark, P. U., et al. (2009b). Transient simulation of last deglaciation with a new mechanism for bolling-allerod warming. *Science (80-.).* doi:10.1126/science.1171041.
Lochbihler, K., Lenderink, G., and Siebesma, A. P. (2017). The spatial extent of rainfall events and its relation to precipitation scaling. *Geophys. Res. Lett.* 44, 8629–8636. doi:10.1002/2017GL074857.
Loeb, N. G., Wang, H., Cheng, A., Kato, S., Fasullo, J. T., Xu, K. M., et al. (2016). Observational constraints on atmospheric and oceanic cross-equatorial heat transports: revisiting the precipitation asymmetry problem in climate models. *Clim. Dyn.* 46, 3239–3257. doi:10.1007/s00382-015-2766-z.
Lombardozzi, D. L., Bonan, G. B., Smith, N. G., Dukes, J. S., and Fisher, R. A. (2015). Temperature acclimation of photosynthesis and respiration: A key uncertainty in the carbon cycle-climate feedback. *Geophys. Res. Lett.* 42, 8624. doi:10.1002/2015GL065934.
Lopez, H., Dong, S., Lee, S.-K., and Campos, E. (2016). Remote influence of Interdecadal Pacific Oscillation on the South Atlantic meridional overturning circulation variability. *Geophys. Res. Lett.* 43, 8250–8258. doi:10.1002/2016GL069067.
Loranty, M. M., Berner, L. T., Goetz, S. J., Jin, Y., and Randerson, J. T. (2014). Vegetation controls on northern high latitude snow-albedo feedback: Observations and CMIP5 model simulations. *Glob. Chang. Biol.* 20, 594–606. doi:10.1111/gcb.12391.
Loriaux, J. M., Lenderink, G., and Pier Siebesma, A. (2017). Large-scale controls on extreme precipitation. *J. Clim.* 30, 955–968. doi:10.1175/JCLI-D-16-0381.1.
Lu, J., Vecchi, G. A., and Reichler, T. (2007). Expansion of the Hadley cell under global warming. *Geophys. Res. Lett.* doi:10.1029/2006GL028443.
Lu, Q., Zhao, D., and Wu, S. (2017). Simulated responses of permafrost distribution to climate change on the Qinghai–Tibet Plateau. *Sci. Rep.* 7, 3845. doi:10.1038/s41598-017-04140-7.
Lu, X., Wang, L., and McCabe, M. F. (2016). Elevated CO2 as a driver of global dryland greening. *Sci. Rep.* doi:10.1038/srep20716.
Lucas, C., and Nguyen, H. (2015). Regional characteristics of tropical expansion and the role of climate variability. *J. Geophys. Res. Atmos.* 120, 6809–6824. doi:10.1002/2015JD023130.
Lucas, C., Nguyen, H., and Timbal, B. (2012). An observational analysis of Southern Hemisphere tropical expansion. *J. Geophys. Res. Atmos.* 117, n/a-n/a. doi:10.1029/2011JD017033.

Lutz, A. F., Immerzeel, W. W., Shrestha, A. B., and Bierkens, M. F. P. P. (2014). Consistent increase in High Asia's runoff due to increasing glacier melt and precipitation. *Nat. Clim. Chang.* 4, 587–592. doi:10.1038/nclimate2237.
Ma, J., Chadwick, R., Seo, K.-H., Dong, C., Huang, G., Foltz, G. R., et al. (2018a). Responses of the Tropical Atmospheric Circulation to Climate Change and Connection to the Hydrological Cycle. *Annu. Rev. Earth Planet. Sci.* 46, 549–580. doi:10.1146/annurev-earth-082517-010102.
Ma, J., and Xie, S. P. (2013). Regional Patterns of Sea Surface Temperature Change: A Source of Uncertainty in Future Projections of Precipitation and Atmospheric Circulation. *J. Clim.* doi:10.1175/JCLI-D-12-00283.1.
Ma, J., Xie, S. P., and Kosaka, Y. (2012). Mechanisms for tropical tropospheric circulation change in response to global warming. *J. Clim.* doi:10.1175/JCLI-D-11-00048.1.
Ma, P.-L., Rasch, P. J., Chepfer, H., Winker, D. M., and Ghan, S. J. (2018b). Observational constraint on cloud susceptibility weakened by aerosol retrieval limitations. *Nat. Commun.* 9, 2640. doi:10.1038/s41467-018-05028-4.
Ma, S., and Zhou, T. (2016). Robust Strengthening and Westward Shift of the Tropical Pacific Walker Circulation during 1979--2012: A Comparison of 7 Sets of Reanalysis Data and 26 CMIP5 Models, J. *Climate* 29, 3097–3118.
Ma, S., Zhou, T., Stone, D. A., Polson, D., Dai, A., Stott, P. A., et al. (2017). Detectable Anthropogenic Shift toward Heavy Precipitation over Eastern China. *J. Clim.* 30, 1381–1396. doi:10.1175/JCLI-D-16-0311.1.
MacDonald, A. M., Bonsor, H. C., Ahmed, K. M., Burgess, W. G., Basharat, M., Calow, R. C., et al. (2016). Groundwater quality and depletion in the Indo-Gangetic Basin mapped from in situ observations. *Nat. Geosci.* 9, 762–766. doi:10.1038/ngeo2791.
MacIntosh, C. R., Allan, R. P., Baker, L. H., Bellouin, N., Collins, W., Mousavi, Z., et al. (2016). Contrasting fast precipitation responses to tropospheric and stratospheric ozone forcing. *Geophys. Res. Lett.* 43, 1263–1271. doi:10.1002/2015GL067231.
Madden, R. A., and Julian, P. R. (1994). Observations of the 40–50-Day Tropical Oscillation—A Review. *Mon. Weather Rev.* 122, 814–837. doi:10.1175/1520-0493(1994)122<0814:OOTDTO>2.0.CO;2.
Madhura, R. K., Krishnan, R., Revadekar, J. V., Mujumdar, M., and Goswami, B. N. (2014). Changes in western disturbances over the Western Himalayas in a warming environment. *Clim. Dyn.* 44, 1157–1168. doi:10.1007/s00382-014-2166-9.
Maher, N., Matei, D., Milinski, S., and Marotzke, J. (2018a). ENSO Change in Climate Projections: Forced Response or Internal Variability? *Geophys. Res. Lett.* 45, 11,390-11,398. doi:10.1029/2018GL079764.
Maher, P., Vallis, G. K., Sherwood, S. C., Webb, M. J., and Sansom, P. G. (2018b). The Impact of Parameterized Convection on Climatological Precipitation in Atmospheric Global Climate Models. *Geophys. Res. Lett.* 45, 3728–3736. doi:10.1002/2017GL076826.
Makarieva, A. M., Gorshkov, V. G., and Li, B. L. (2013). Revisiting forest impact on atmospheric water vapor transport and precipitation. *Theor. Appl. Climatol.* 111, 79–96. doi:10.1007/s00704-012-0643-9.
Malhi, Y., Aragão, L. E. O. C., Galbraith, D., Huntingford, C., Fisher, R., Zelazowski, P., et al. (2009). Exploring the likelihood and mechanism of a climate-change-induced dieback of the Amazon rainforest. *Proc. Natl. Acad. Sci.* 106, 20610.
Malhi, Y., Roberts, J. T., Betts, R. A., Killeen, T. J., Li, W., and Nobre, C. A. (2008). Climate change, deforestation, and the fate of the Amazon. *Science (80-.).* doi:10.1126/science.1146961.
Maloney, E. D., Adames, Á. F., and Bui, H. X. (2019a). Madden–Julian oscillation changes under anthropogenic warming. *Nat. Clim. Chang.* 9, 26–33. doi:10.1038/s41558-018-0331-6.
Maloney, E. D., Adames, Á. F., and Bui, H. X. (2019b). Madden–Julian oscillation changes under anthropogenic warming. *Nat. Clim. Chang.* 9, 26–33. doi:10.1038/s41558-018-0331-6.
Maloney, E. D., and Hartmann, D. L. (2000). Modulation of Eastern North Pacific Hurricanes by the Madden–Julian Oscillation. *J. Clim.* 13, 1451–1460. doi:10.1175/1520-0442(2000)013<1451:MOENPH>2.0.CO;2.
Maloney, E. D., and Xie, S.-P. (2013). Sensitivity of tropical intraseasonal variability to the pattern of climate warming. *J. Adv. Model. Earth Syst.* 5, 32–47. doi:10.1029/2012MS000171.
Mankin, J. S., Seager, R., Smerdon, J. E., Cook, B. I., Williams, A. P., and Horton, R. M. (2018). Blue Water Trade-Offs With Vegetation in a CO2-Enriched Climate. *Geophys. Res. Lett.* 45, 3115–3125. doi:10.1002/2018GL077051.
Mankin, J. S., Smerdon, J. E., Cook, B. I., Williams, A. P., and Seager, R. (2017). The Curious Case of Projected Twenty-First-Century Drying but Greening in the American West. *J. Clim.* 30, 8689–8710. doi:10.1175/JCLI-D-17-0213.1.
Manoj, M. G., Devara, P. C. S., Safai, P. D., and Goswami, B. N. (2011). Absorbing aerosols facilitate transition of Indian monsoon breaks to active spells. *Clim. Dyn.* 37, 2181–2198. doi:10.1007/s00382-010-0971-3.
Mantsis, D. F., Sherwood, S., Allen, R., and Shi, L. (2017). Natural variations of tropical width and recent trends. *Geophys. Res. Lett.* 44, 3825–3832. doi:10.1002/2016GL072097.
Marengo, J. A., Alves, L. M., Alvala, R. C. S., Cunha, A. P., Brito, S., and Moraes, O. L. L. (2018). Climatic

characteristics of the 2010-2016 drought in the semiarid northeast Brazil region. *An. Acad. Bras. Cienc.* 90, 1973–1985. doi:10.1590/0001-3765201720170206.
Marengo, J. A., Alves, L. M., Soares, W. R., Rodriguez, D. A., Riveros, M. P., and Pabló, A. D. (2013a). Two Contrasting Severe Seasonal Extremes in Tropical South America in 2012: Flood in Amazonia and Drought in Northeast Brazil. *J. Clim.* 26, 9137–9154. doi:10.1175/jcli-d-12-00642.1.
Marengo, J. A., Torres, R. R., and Alves, L. M. (2017). Drought in Northeast Brazil—past, present, and future. *Theor. Appl. Climatol.* 129, 1189–1200. doi:10.1007/s00704-016-1840-8.
Marengo, J. A., Valverde, M. C., and Obregon, G. O. (2013b). Observed and projected changes in rainfall extremes in the Metropolitan Area of São Paulo. *Clim. Res.* 57, 61–72. doi:10.3354/cr01160.
Margulis, S. A., Cortés, G., Girotto, M., and Durand, M. (2016). A Landsat-era Sierra Nevada snow reanalysis (1985--2015). *J. Hydrometeorol.* 17, 1203–1221.
Marlier, M. E., Xiao, M., Engel, R., Livneh, B., Abatzoglou, J. T., and Lettenmaier, D. P. (2017). The 2015 drought in Washington State: A harbinger of things to come? *Environ. Res. Lett.* doi:10.1088/1748-9326/aa8fde.
Marshall, A. G., Scaife, A. A., and Ineson, S. (2009). Enhanced Seasonal Prediction of European Winter Warming following Volcanic Eruptions. *J. Clim.* 22, 6168–6180. doi:10.1175/2009JCLI3145.1.
Marshall, G. J., Thompson, D. W. J., and van den Broeke, M. R. (2017). The Signature of Southern Hemisphere Atmospheric Circulation Patterns in Antarctic Precipitation. *Geophys. Res. Lett.* 44, 11,580-11,589. doi:10.1002/2017GL075998.
Marshall, J., Donohoe, A., Ferreira, D., and McGee, D. (2014). The ocean's role in setting the mean position of the Inter-Tropical Convergence Zone. *Clim. Dyn.* doi:10.1007/s00382-013-1767-z.
Martel, J.-L., Mailhot, A., Brissette, F., and Caya, D. (2018). Role of Natural Climate Variability in the Detection of Anthropogenic Climate Change Signal for Mean and Extreme Precipitation at Local and Regional Scales. *J. Clim.* 31, 4241–4263. doi:10.1175/JCLI-D-17-0282.1.
Martens, B., Waegeman, W., Dorigo, W. A., Verhoest, N. E. C., and Miralles, D. G. (2018). Terrestrial evaporation response to modes of climate variability. *npj Clim. Atmos. Sci.* 1, 43. doi:10.1038/s41612-018-0053-5.
Martin, E. R., Thorncroft, C., and Booth, B. B. B. (2014). The Multidecadal Atlantic SST—Sahel Rainfall Teleconnection in CMIP5 Simulations. *J. Clim.* 27, 784–806. doi:10.1175/JCLI-D-13-00242.1.
Martinez, J. A., and Dominguez, F. (2014). Sources of atmospheric moisture for the La Plata River Basin. *J. Clim.* 27, 6737–6753. doi:10.1175/JCLI-D-14-00022.1.
Martins, E. S. P. R., Coelho, C. A. S., Haarsma, R., Otto, F. E. L., King, A. D., van Oldenborgh, G., et al. (2018). A Multimethod Attribution Analysis of the Prolonged Northeast Brazil Hydrometeorological Drought (2012--16). *Bull. Am. Meteorol. Soc.* 99, S65--S69.
Marty, C., Tilg, A.-M., and Jonas, T. (2017a). Recent evidence of large-scale receding snow water equivalents in the European Alps. *J. Hydrometeorol.* 18, 1021–1031. doi:10.1175/JHM-D-16-0188.1.
Marty, C., Tilg, A. -m., and Jonas, T. (2017b). *Recent evidence of large scale receding snow water equivalents in the European Alps*, *J*. Hydrometeorology doi:http://dx.doi.org/10.1175/JHM-D-16-0188.s1.
Marvel, K., Biasutti, M., Bonfils, C., Taylor, K. E., Kushnir, Y., and Cook, B. I. (2017). Observed and projected changes to the precipitation annual cycle. *J. Clim.* doi:10.1175/JCLI-D-16-0572.1.
Marvel, K., Cook, B., Bonfils, C., Durack, P., Smerdon, J., and Williams, P. (2019). Evidence for human influence on twentieth century hydroclimate. *Nature* 1, 1.
Marzeion, B., Kaser, G., Maussion, F., and Champollion, N. (2018). Limited influence of climate change mitigation on short-term glacier mass loss. *Nat. Clim. Chang.*, 1–4. doi:10.1038/s41558-018-0093-1.
Masato, G., Hoskins, B. J., and Woollings, T. (2013). Winter and summer Northern Hemisphere blocking in CMIP5 models. *J. Clim.* 26, 7044–7059. Available at: https://doi.org/10.1175/JCLI-D-12-00466.1.
Masson-Delmotte, V., Schulz, M., Abe-Ouchi, A., Beer, J., Ganopolski, A., González Rouco, J. F., et al. (2013). "Information from Paleoclimate Archives," in *Climate Change 2013: The Physical Science Basis. Contribution of Working Group I to the Fifth Assessment Report of the Intergovernmental Panel on Climate Change*, eds. T. F. Stocker, D. Qin, G.-K. Plattner, M. Tignor, S. K. Allen, J. Boschung, et al. (Cambridge, United Kingdom and New York, NY, USA: Cambridge University Press), 383–464. doi:10.1017/CBO9781107415324.013.
Masson-Delmotte, V., Zhai, P., Pörtner, H.-O., Roberts, D., Skea, J., Shukla, P. R., et al. eds. (2018). "Summary for Policymakers.," in *Global Warming of 1.5°C. An IPCC Special Report on the impacts of global warming of 1.5°C above pre-industrial levels and related global greenhouse gas emission pathways, in the context of strengthening the global response to the threat of climate change*, (World Meteorological Organization, Geneva, Switzerland,), 32 pp. Available at: https://www.ipcc.ch/sr15/chapter/summary-for-policy-makers/.
Matsueda, M., and Endo, H. (2017). The robustness of future changes in Northern Hemisphere blocking: a large ensemble projection with multiple sea surface temperature patterns. *Geophys. Res. Lett.* 44, 5158–5166. Available at: https://doi.org/10.1002/2017GL073336.
Matthews, T., Murphy, C., Wilby, R. L., and Harrigan, S. (2016). A cyclone climatology of the British-Irish Isles 1871--2012. *Int. J. Climatol.* 36, 1299–1312.

Matti, B., Dahlke, H. E., Dieppois, B., Lawler, D. M., and Lyon, S. W. (2017). Flood seasonality across Scandinavia-Evidence of a shifting hydrograph? *Hydrol. Process.* 31, 4354–4370. doi:10.1002/hyp.11365.
Mattingly, K. S., Mote, T. L., and Fettweis, X. (2018). Atmospheric River Impacts on Greenland Ice Sheet Surface Mass Balance. *J. Geophys. Res. Atmos.* 123, 8538–8560. doi:10.1029/2018JD028714.
Maule, C. F., Mendlik, T., and Christensen, O. B. (2017). The effect of the pathway to a two degrees warmer world on the regional temperature change of Europe. *Clim. Serv.* 7, 3–11. doi:https://doi.org/10.1016/j.cliser.2016.07.002.
Mauritsen, T., Stevens, B., Roeckner, E., Crueger, T., Esch, M., Giorgetta, M., et al. (2012). Tuning the climate of a global model. *J. Adv. Model. Earth Syst.* 4, 1–18. doi:10.1029/2012MS000154.
McCabe, G. J., Wolock, D. M., Pederson, G. T., Woodhouse, C. A., and McAfee, S. (2017). Evidence that recent warming is reducing upper Colorado river flows. *Earth Interact.* doi:10.1175/EI-D-17-0007.1.
McColl, K. A., Alemohammad, S. H., Akbar, R., Konings, A. G., Yueh, S., and Entekhabi, D. (2017). The global distribution and dynamics of surface soil moisture. *Nat. Geosci.* 10, 100–104. doi:10.1038/ngeo2868.
McGee, D., Donohoe, A., Marshall, J., and Ferreira, D. (2014a). Changes in ITCZ location and cross-equatorial heat transport at the Last Glacial Maximum, Heinrich Stadial 1, and the mid-Holocene. *Earth Planet. Sci. Lett.* doi:10.1016/j.epsl.2013.12.043.
McGee, D., Donohoe, A., Marshall, J., and Ferreira, D. (2014b). Changes in ITCZ location and cross-equatorial heat transport at the Last Glacial Maximum, Heinrich Stadial 1, and the mid-Holocene. *Earth Planet. Sci. Lett.* doi:10.1016/j.epsl.2013.12.043.
McGraw, M. C., Barnes, E. A., and Deser, C. (2016). Reconciling the observed and modeled Southern Hemisphere circulation response to volcanic eruptions. *Geophys. Res. Lett.* 43, 7259–7266. doi:10.1002/2016GL069835.
McGregor, S., Timmermann, A., Stuecker, M. F., England, M. H., Merrifield, M., Jin, F. -f., et al. (2014). Recent Walker circulation strengthening and Pacific cooling amplified by Atlantic warming. *Nat* 4, 888–892. doi:10.1038/nclimate2330.
McInerney, D., and Moyer, E. (2012). Direct and disequilibrium effects on precipitation in transient climates. *Atmos. Chem. Phys. Discuss.* 12, 19649–19681. doi:10.5194/acpd-12-19649-2012.
McManus, J. F., Francois, R., Gherardl, J. M., Kelgwin, L., and Drown-Leger, S. (2004). Collapse and rapid resumption of Atlantic meridional circulation linked to deglacial climate changes. *Nature*. doi:10.1038/nature02494.
Mearns, L. O., Sain, S., Leung, L. R., Bukovsky, M. S., McGinnis, S., Biner, S., et al. (2013). Climate change projections of the North American Regional Climate Change Assessment Program (NARCCAP). *Clim. Change* 120, 965–975. doi:10.1007/s10584-013-0831-3.
Medlyn, B. E., Zaehle, S., De Kauwe, M. G., Walker, A. P., Dietze, M. C., Hanson, P. J., et al. (2015). Using ecosystem experiments to improve vegetation models. *Nat. Clim. Chang.* 5, 528–534. doi:10.1038/nclimate2621.
Meehl, G. A., Hu, A., Santer, B. D., and Xie, S.-P. (2016). Contribution of the Interdecadal Pacific Oscillation to twentieth-century global surface temperature trends. *Nat. Clim. Chang.* 6, 1005–1008. doi:10.1038/nclimate3107.
Meehl, G. A., Tebaldi, C., Teng, H., and Peterson, T. C. (2007). Current and future U.S. weather extremes and El Niño. *Geophys. Res. Lett.* 34, L20704. doi:10.1029/2007GL031027.
Meixner, T., Manning, A. H., Stonestrom, D. A., Allen, D. M., Ajami, H., Blasch, K. W., et al. (2016a). Implications of projected climate change for groundwater recharge in the western United States. *J. Hydrol.* 534, 124–138. doi:10.1016/j.jhydrol.2015.12.027.
Meixner, T., Manning, A. H., Stonestrom, D. A., Allen, D. M., Ajami, H., Blasch, K. W., et al. (2016b). Implications of projected climate change for groundwater recharge in the western United States. *J. Hydrol.* 534, 124–138. doi:10.1016/j.jhydrol.2015.12.027.
Meixner, T., Manning, A. H., Stonestrom, D. A., Allen, D. M., Ajami, H., Blasch, K. W., et al. (2016c). Implications of projected climate change for groundwater recharge in the western United States. *J. Hydrol.* doi:10.1016/j.jhydrol.2015.12.027.
Mekonnen, M. M., and Hoekstra, A. Y. (2016). Four billion people facing severe water scarcity. *Sci. Adv.* 2, DOI: 10.1126/sciadv.1500323.
Meng, Q., Latif, M., Park, W., Keenlyside, N. S., Semenov, V. A., and Martin, T. (2011). Twentieth century Walker Circulation change: data analysis and model experiments, Clim. *Dyn., DOI* 10, 1047–1048.
Merlis, T. M. (2015). Direct weakening of tropical circulations from masked CO 2 radiative forcing . *Proc. Natl. Acad. Sci.* doi:10.1073/pnas.1508268112.
Merrifield, M. A. (2011). A shift in western tropical Pacific sea level trends during the 1990s. *J. Clim.* 24, 4126–4138. doi:10.1175/2011JCLI3932.1.
Metcalfe, S. E., Barron, J. A., and Davies, S. J. (2015). The Holocene history of the North American Monsoon: "known knowns" and "known unknowns" in understanding its spatial and temporal complexity. *Quat. Sci. Rev.* 120, 1–27. doi:10.1016/j.quascirev.2015.04.004.
Meyer, J. D. D., and Jin, J. (2017). The response of future projections of the North American monsoon when combining dynamical downscaling and bias correction of CCSM4 output. *Clim. Dyn.* doi:10.1007/s00382-016-3352-8.
Michael, V., and Richard, A. W. (2002). Global climatic impacts of a collapse of the Atlantic thermohaline circulation.

Clim. Change 54, 251.
Michaelis, A. C., Willison, J., Lackmann, G. M., and Robinson, W. A. (2017). Changes in Winter North Atlantic Extratropical Cyclones in High-Resolution Regional Pseudo–Global Warming Simulations. *J. Clim.* 30, 6905–6925. doi:10.1175/JCLI-D-16-0697.1.
Milillo, P., Rignot, E., Rizzoli, P., Scheuchl, B., Mouginot, J., Bueso-Bello, J., et al. (2019). Heterogeneous retreat and ice melt of Thwaites Glacier, West Antarctica. *Sci. Adv.* 5, eaau3433. doi:10.1126/sciadv.aau3433.
Miller, P. W., Kumar, A., Mote, T. L., Moraes, F. D. S., and Mishra, D. R. (2019). Persistent Hydrological Consequences of Hurricane Maria in Puerto Rico. *Geophys. Res. Lett.* doi:10.1029/2018GL081591.
Milly, P. C. D., and Dunne, K. A. (2016). Potential evapotranspiration and continental drying. *Nat. Clim. Chang.* 6, 946–949. doi:10.1038/nclimate3046.
Milner, A. M., Khamis, K., Battin, T. J., Brittain, J. E., Barrand, N. E., Füreder, L., et al. (2017). Glacier shrinkage driving global changes in downstream systems. *Proc. Natl. Acad. Sci.* 114, 9770 LP-9778. doi:10.1073/pnas.1619807114.
Min, S.-K., Zhang, X., Zwiers, F. W., and Hegerl, G. C. (2011). Human contribution to more-intense precipitation extremes. *Nature* 470, 378–381. doi:10.1038/nature09763.
Miralles, D. G., Jiménez, C., Jung, M., Michel, D., Ershadi, A., Mccabe, M. F., et al. (2016). The WACMOS-ET project - Part 2: Evaluation of global terrestrial evaporation data sets. *Hydrol. Earth Syst. Sci.* 20, 823–842. doi:10.5194/hess-20-823-2016.
Miralles, D. G., van den Berg, M. J., Gash, J. H., Parinussa, R. M., de Jeu, R. A. M., Beck, H. E., et al. (2014). El Niño–La Niña cycle and recent trends in continental evaporation. *Nat. Clim. Chang.* 4, 122–126. doi:10.1038/nclimate2068.
Mishra, V., Smoliak, B. V., Lettenmaier, D. P., and Wallace, J. M. (2012). A prominent pattern of year-to-year variability in Indian Summer Monsoon Rainfall. *Proc. Natl. Acad. Sci.* 109, 7213–7217. doi:10.1073/pnas.1119150109.
Mo, K. C., and Schemm, J. E. (2008). Relationships between ENSO and drought over the southeastern United States. *Geophys. Res. Lett.* 35, L15701. doi:10.1029/2008GL034656.
Mohtadi, M., Oppo, D. W., Steinke, S., Stuut, J. -b. W., Pol-Holz, R. De, Hebbeln, D., et al. (2011). Glacial to Holocene swings of the Australian-Indonesian monsoon. *Nat. Geosci.* 4, 540–544. doi:10.1038/ngeo1209.
Mohtadi, M., Prange, M., and Steinke, S. (2016). Palaeoclimatic insights into forcing and response of monsoon rainfall. *Nature*. doi:10.1038/nature17450.
Molina, R. D., Salazar, J. F., Martínez, J. A., Villegas, J. C., and Arias, P. A. (2019). Forest-induced exponential growth of precipitation along climatological wind streamlines over the Amazon. *J. Geophys. Res. Atmos.*, 1–22.
Molnar, P., Fatichi, S., Gaál, L., Szolgay, J., and Burlando, P. (2015). Storm type effects on super Clausius-Clapeyron scaling of intense rainstorm properties with air temperature. *Hydrol. Earth Syst. Sci.* 19, 1753–1766. doi:10.5194/hess-19-1753-2015.
Monerie, P.-A., Robson, J., Dong, B., Hodson, D. L. R., and Klingaman, N. P. (2019a). Effect of the Atlantic Multidecadal Variability on the Global Monsoon. *Geophys. Res. Lett.* 46, 1765–1775. doi:10.1029/2018GL080903.
Monerie, P.-A., Robson, J., Dong, B., Hodson, D. L. R., and Klingaman, N. P. (2019b). Effect of the Atlantic Multidecadal Variability on the Global Monsoon. *Geophys. Res. Lett.* 46, 1765–1775. doi:10.1029/2018GL080903.
Moon, H., Guillod, B. P., Gudmundsson, L., and Seneviratne, S. I. (2019). Soil moisture effects on afternoon precipitation occurrence in current climate models. *Geophys. Res. Lett.* doi:10.1029/2018GL080879.
Moore, G. W. K., Renfrew, I. A., and Pickart, R. S. (2013). Multidecadal Mobility of the North Atlantic Oscillation. *J. Clim.* 26, 2453–2466. doi:10.1175/JCLI-D-12-00023.1.
Morales, M. S., Christie, D. A., Villalba, R., Argollo, J., Pacajes, J., Silva, J. S., et al. (2012). Precipitation changes in the South American Altiplano since 1300 AD reconstructed by tree-rings. *Clim. Past* 8, 653–666.
Moseley, C., Hohenegger, C., Berg, P., and Haerter, J. O. (2016). Intensification of convective extremes driven by cloud-cloud interaction. *Nat. Geosci.* 9, 748–752. doi:10.1038/ngeo2789.
Moss, R. H., Edmonds, J. A., Hibbard, K. A., Manning, M. R., Rose, S. K., Van Vuuren, D. P., et al. (2010). The next generation of scenarios for climate change research and assessment. *Nature*. doi:10.1038/nature08823.
Mote, P. W., Li, S., Lettenmaier, D. P., Xiao, M., and Engel, R. (2018). Dramatic declines in snowpack in the western US. *Npj Clim. Atmos. Sci.* 1, 2.
Mote, P. W., Rupp, D. E., Li, S., Sharp, D. J., Otto, F., Uhe, P. F., et al. (2016). Perspectives on the causes of exceptionally low 2015 snowpack in the western United States. *Geophys. Res. Lett.* doi:10.1002/2016GL069965.
Muchan, K., Lewis, M., Hannaford, J., and Parry, S. (2015). The winter storms of 2013/2014 in the UK: hydrological responses and impacts. *Weather* 70, 55–61. doi:10.1002/wea.2469.
Mueller, B., and Zhang, X. (2016). Causes of drying trends in northern hemispheric land areas in reconstructed soil moisture data. *Clim. Change* 134, 255–267. doi:10.1007/s10584-015-1499-7.

Muis, S., Verlaan, M., Winsemius, H. C., Aerts, J. C. J. H., and Ward, P. J. (2016). A global reanalysis of storm surges and extreme sea levels. *Nat. Commun.* 7, 11969. Available at: https://doi.org/10.1038/ncomms11969.
Mujumdar, M., Sooraj, K. P., Krishnan, R., Preethi, B., Joshi, M. K., Varikoden, H., et al. (2017). Anomalous convective activity over sub-tropical east Pacific during 2015 and associated boreal summer monsoon teleconnections. *Clim. Dyn.* 48, 4081–4091. doi:10.1007/s00382-016-3321-2.
Muller, C., and Bony, S. (2015). What favors convective aggregation and why? *Geophys. Res. Lett.* 42, 5626–5634. doi:10.1002/2015GL064260.
Muller, C. J., and O'Gorman, P. A. (2011). An energetic perspective on the regional response of precipitation to climate change. *Nat. Clim. Chang.* 1, 266–271. doi:10.1038/nclimate1169.
Müller, W. A., and Roeckner, E. (2008). ENSO teleconnections in projections of future climate in ECHAM5/MPI-OM. *Clim. Dyn.* 31, 533–549. doi:10.1007/s00382-007-0357-3.
Mundhenk, B. D., Barnes, E. A., Maloney, E. D., and Baggett, C. F. (2018). Skillful empirical subseasonal prediction of landfalling atmospheric river activity using the Madden–Julian oscillation and quasi-biennial oscillation. *npj Clim. Atmos. Sci.* 1, 20177. doi:10.1038/s41612-017-0008-2.
Murphy, L. N., Bellomo, K., Cane, M., and Clement, A. (2017). The role of historical forcings in simulating the observed Atlantic multidecadal oscillation. *Geophys. Res. Lett.* 44, 2472–2480. doi:10.1002/2016GL071337.
Murray-Tortarolo, G., Jaramillo, V. J., Maass, M., Friedlingstein, P., and Sitch, S. (2017). The decreasing range between dry- and wet-season precipitation over land and its effect on vegetation primary productivity. *PLoS One* 12, e0190304. doi:10.1371/journal.pone.0190304.
Musselman, K. N., Lehner, F., Ikeda, K., Clark, M. P., Prein, A. F., Liu, C., et al. (2018). Projected increases and shifts in rain-on-snow flood risk over western North America. *Nat. Clim. Chang.* 8, 808–812. doi:10.1038/s41558-018-0236-4.
Myhre, G., Forster, P. M., Samset, B. H., Hodnebrog, Ø., Sillmann, J., Aalbergsjø, S. G., et al. (2017). PDRMIP: A Precipitation Driver and Response Model Intercomparison Project—Protocol and Preliminary Results. *Bull. Am. Meteorol. Soc.* 98, 1185–1198. doi:10.1175/BAMS-D-16-0019.1.
Myhre, G., Samset, B. H., Hodnebrog, O., Andrews, T., Boucher, O., Faluvegi, G., et al. (2018). Sensible heat has significantly affected the global hydrological cycle over the historical period. *Nat. Commun.* 9. doi:10.1038/s41467-018-04307-4.
Nakazawa, T. (1986). Intraseasonal Variations of OLR in the Tropics During the FGGE Year. *J. Meteorol. Soc. Japan. Ser. II* 64, 17–34. doi:10.2151/jmsj1965.64.1_17.
Nash, D. (2017). *Changes in Precipitation Over Southern Africa During Recent Centuries*. Oxford University Press doi:10.1093/acrefore/9780190228620.013.539.
Neelin, J. D., Sahany, S., Stechmann, S. N., and Bernstein, D. N. (2017). Global warming precipitation accumulation increases above the current-climate cutoff scale. *Proc. Natl. Acad. Sci.* 114, 1258–1263. doi:10.1073/pnas.1615333114.
Neiman, P. J., Ralph, F. M., Wick, G. A., Lundquist, J. D., and Dettinger, M. D. (2008). Meteorological characteristics and overland precipitation impacts of atmospheric rivers affecting the West Coast of North America based on eight years of SSM/I satellite observations. J. *Hydrometeor.,* 9, 22–47. doi:10.1175/2007JHM855.1.
Neu, U., Akperov, M. G., Bellenbaum, N., Benestad, R., Blender, R., Caballero, R., et al. (2013). Imilast: A community effort to intercompare extratropical cyclone detection and tracking algorithms. *Bull. Am. Meteorol. Soc.* doi:10.1175/BAMS-D-11-00154.1.
Neumann, R. B., Moorberg, C. J., Lundquist, J. D., Turner, J. C., Waldrop, M. P., McFarland, J. W., et al. (2019). Warming Effects of Spring Rainfall Increase Methane Emissions From Thawing Permafrost. *Geophys. Res. Lett.* doi:10.1029/2018gl081274.
Neupane, N., and Cook, K. H. (2013). A nonlinear response of sahel rainfall to atlantic warming. *J. Clim.* 26, 7080–7096. doi:10.1175/JCLI-D-12-00475.1.
Neves, M. C., Jerez, S., and Trigo, R. M. (2019). The response of piezometric levels in Portugal to NAO, EA, and SCAND climate patterns. *J. Hydrol.* 568, 1105–1117. doi:10.1016/j.jhydrol.2018.11.054.
Nguyen, H., Evans, A., Lucas, C., Smith, I., and Timbal, B. (2013). The Hadley Circulation in Reanalyses: Climatology, Variability, and Change. *J. Clim.* 26, 3357–3376. doi:10.1175/JCLI-D-12-00224.1.
Nguyen, H., Hendon, H. H., Lim, E. P., Boschat, G., Maloney, E., and Timbal, B. (2018a). Variability of the extent of the Hadley circulation in the southern hemisphere: a regional perspective. *Clim. Dyn.* 50, 129–142. doi:10.1007/s00382-017-3592-2.
Nguyen, H., Hendon, H. H., Lim, E. P., Boschat, G., Maloney, E., and Timbal, B. (2018b). Variability of the extent of the Hadley circulation in the southern hemisphere: a regional perspective. *Clim. Dyn.* 50, 129–142. doi:10.1007/s00382-017-3592-2.
Nguyen, H., Lucas, C., Evans, A., Timbal, B., and Hanson, L. (2015). Expansion of the Southern Hemisphere Hadley Cell in Response to Greenhouse Gas Forcing. *J. Clim.* 28, 8067–8077. doi:10.1175/JCLI-D-15-0139.1.
Nguyen, P., Thorstensen, A., Sorooshian, S., Hsu, K., AghaKouchak, A., Ashouri, H., et al. (2017). Global precipitation

trends across spatial scales using satellite observations. *Bull. Am. Meteorol. Soc.* doi:10.1175/BAMS-D-17-0065.1.
Ni, S., Chen, J., Wilson, C. R., Li, J., Hu, X., and Fu, R. (2018). Global Terrestrial Water Storage Changes and Connections to ENSO Events. *Surv. Geophys.* 39, 1–22. doi:10.1007/s10712-017-9421-7.
Nicholls, R. J., and Cazenave, A. (2010). Sea-Level Rise and Its Impact on Coastal Zones. *Science (80-.).* 328, 1517 LP-1520. doi:10.1126/science.1185782.
Nicholson, S. (2000). Land surface processes and Sahel climate. *Rev. Geophys.* 38, 117–139. doi:10.1029/1999RG900014.
Nicholson, S. (2005). On the question of the "recovery" of the rains in the West African Sahel. *J. Arid Environ.* 63, 615–641.
Nicholson, S. E. (2013). The West African Sahel: A Review of Recent Studies on the Rainfall Regime and Its Interannual Variability. *ISRN Meteorol.* 2013, 1–32. doi:10.1155/2013/453521.
Nicholson, S. E. (2017). Climate and climatic variability of rainfall over eastern Africa. *Rev. Geophys.* 55, 590–635. doi:10.1002/2016RG000544.
Nick, F. M., Vieli, A., Andersen, M. L., Joughin, I., Payne, A., Edwards, T. L., et al. (2013). Future sea-level rise from Greenland�s main outlet glaciers in a warming climate. *Nature* 497, 235.
Nie, J., Sobel, A. H., Shaevitz, D. A., and Wang, S. (2018). Dynamic amplification of extreme precipitation sensitivity. *Proc. Natl. Acad. Sci.*, 201800357. doi:10.1073/pnas.1800357115.
Niemeier, U., Schmidt, H., Alterskjær, K., and Kristjánsson, J. E. (2013). Solar irradiance reduction via climate engineering: Impact of different techniques on the energy balance and the hydrological cycle. *J. Geophys. Res. Atmos.* 118, 11905–11917. doi:10.1002/2013JD020445.
Niranjan Kumar, K., Rajeevan, M., Pai, D. S., Srivastava, A. K., and Preethi, B. (2013). On the observed variability of monsoon droughts over India. *Weather Clim. Extrem.* 1, 42–50. doi:10.1016/j.wace.2013.07.006.
Nobre, C. A., Sampaio, G., Borma, L. S., Castilla-Rubio, J. C., Silva, J. S., and Cardoso, M. (2016). Land-use and climate change risks in the Amazon and the need of a novel sustainable development paradigm. *Proc. Natl. Acad. Sci.* 113, 10759–10768. doi:10.1073/pnas.1605516113.
Norris, J. R., Allen, R. J., Evan, A. T., Zelinka, M. D., O'Dell, C. W., and Klein, S. A. (2016). Evidence for climate change in the satellite cloud record. *Nature* 536, 72–75. doi:10.1038/nature18273.
Novello, V. F., Cruz, F. W., Vuille, M., Stríkis, N. M., Edwards, R. L., Cheng, H., et al. (2017). A high-resolution history of the South American Monsoon from Last Glacial Maximum to the Holocene. *Sci. Rep.* 7, 1–8. doi:10.1038/srep44267.
Novello, V. F., Vuille, M., Cruz, F. W., Stríkis, N. M., de Paula, M. S., Edwards, R. L., et al. (2016). Centennial-scale solar forcing of the South American Monsoon System recorded in stalagmites. *Sci. Rep.* 6, 1–8. doi:10.1038/srep24762.
Nur'utami, M. N., and Hidayat, R. (2016). Influences of IOD and ENSO to Indonesian Rainfall Variability: Role of Atmosphere-ocean Interaction in the Indo-pacific Sector. *Procedia Environ. Sci.* 33, 196–203. doi:10.1016/j.proenv.2016.03.070.
O'Gorman, P. A. (2014a). Contrasting responses of mean and extreme snowfall to climate change. *Nature* 512, 416–418. doi:10.1038/nature13625.
O'Gorman, P. A. (2014b). Contrasting responses of mean and extreme snowfall to climate change. *Nature* 512, 416–418. doi:10.1038/nature13625.
O'Gorman, P. A. (2015). Precipitation Extremes Under Climate Change. *Curr. Clim. Chang. Reports* 1, 49–59. doi:10.1007/s40641-015-0009-3.
O'Gorman, P. A., Allan, R. P., Byrne, M. P., and Previdi, M. (2012). Energetic Constraints on Precipitation Under Climate Change. *Surv. Geophys.* 33, 585–608. doi:10.1007/s10712-011-9159-6.
O'Gorman, P. A., and Dwyer, J. G. (2018). Using Machine Learning to Parameterize Moist Convection: Potential for Modeling of Climate, Climate Change, and Extreme Events. *J. Adv. Model. Earth Syst.* doi:10.1029/2018MS001351.
O'Gorman, P. A., and Schneider, T. (2009). The physical basis for increases in precipitation extremes in simulations of 21st-century climate change. *Proc. Natl. Acad. Sci.* 106, 14773–14777. doi:10.1073/pnas.0907610106.
O'Gorman, P. A., and Singh, M. S. (2013). Vertical structure of warming consistent with an upward shift in the middle and upper troposphere. *Geophys. Res. Lett.* doi:10.1002/grl.50328.
O'Reilly, C. H., Woollings, T., and Zanna, L. (2017). The Dynamical Influence of the Atlantic Multidecadal Oscillation on Continental Climate. *J. Clim.* 30, 7213–7230. doi:10.1175/JCLI-D-16-0345.1.
Oki, T., and Kanae, S. (2006). Global Hydrological Cycles and World Water Resources. *Science (80-.).* 313, 1068 LP-1072. doi:10.1126/science.1128845.
Okkonen, J., and Kløve, B. (2011). A sequential modelling approach to assess groundwater-surface water resources in a snow dominated region of Finland. *J. Hydrol.* 411, 91–107.
Okumura, Y. M., DiNezio, P., and Deser, C. (2017). Evolving Impacts of Multiyear La Niña Events on Atmospheric

Circulation and U.S. Drought. *Geophys. Res. Lett.* 44, 11,614-11,623. doi:10.1002/2017GL075034.
Oliver, E. C. J., and Thompson, K. R. (2012). A Reconstruction of Madden–Julian Oscillation Variability from 1905 to 2008. *J. Clim.* 25, 1996–2019. doi:10.1175/JCLI-D-11-00154.1.
Oltmanns, M., Straneo, F., and Tedesco, M. (2018). Increased Greenland melt triggered by large-scale, year-round precipitation events. *Cryosph. Discuss.* 13, 1–18. doi:10.5194/tc-2018-243.
on Wetlands, R. C. (2018). *Global Wetland Outlook: State of the World's Wetlands and their Services to People*. Gland, Switzerland: Ramsar Convention Secretariat.
Ordoñez, P., Nieto, R., Gimeno, L., Ribera, P., Gallego, D., Ochoa-Moya, C. A., et al. (2019). Climatological moisture sources for the Western North American Monsoon through a Lagrangian approach: their influence on precipitation intensity. *Earth Syst. Dyn.* 10, 59–72. doi:10.5194/esd-10-59-2019.
Orlanski, I. (2013). What Controls Recent Changes in the Circulation of the Southern Hemisphere : Polar Stratospheric or Equatorial Surface Temperatures ? *Atmos. Clim. Sci.* 2013, 497–509.
Osborn, T. J., Wallace, C. J., Harris, I. C., and Melvin, T. M. (2016). Pattern scaling using ClimGen: monthly-resolution future climate scenarios including changes in the variability of precipitation. *Clim. Change*. doi:10.1007/s10584-015-1509-9.
Ose, T. (2019). Characteristics of future changes in summertime East Asian monthly precipitation in MRI-AGCM global warming experiments. *J. Meteorol. Soc. Japan* 97. Available at: https://doi.org/10.2151/jmsj.2019-018.
Oshima, K., and Yamazaki, K. (2017). Atmospheric hydrological cycles in the Arctic and Antarctic during the past four decades. *Czech Polar Reports* 7, 169–180. doi:10.5817/CPR2017-2-17.
Otkin, J. A., Anderson, M. C., Hain, C., Svoboda, M., Johnson, D., Mueller, R., et al. (2016). Assessing the evolution of soil moisture and vegetation conditions during the 2012 United States flash drought. *Agric. For. Meteorol.* doi:10.1016/j.agrformet.2015.12.065.
Otkin, J. A., Svoboda, M., Hunt, E. D., Ford, T. W., Anderson, M. C., Hain, C., et al. (2018). Flash droughts: A review and assessment of the challenges imposed by rapid-onset droughts in the United States. *Bull. Am. Meteorol. Soc.* doi:10.1175/BAMS-D-17-0149.1.
Otterå, O. H., Bentsen, M., Drange, H., and Suo, L. (2010). External forcing as a metronome for Atlantic multidecadal variability. *Nat. Geosci.* 3, 688–694. doi:10.1038/ngeo955.
Otto-Bliesner, B. L., Brady, E. C., Fasullo, J., Jahn, A., Landrum, L., Stevenson, S., et al. (2016). Climate Variability and Change since 850 CE: An Ensemble Approach with the Community Earth System Model. *Bull. Am. Meteorol. Soc.* 97, 735–754. doi:10.1175/BAMS-D-14-00233.1.
Otto-Bliesner, B. L., Russell, J. M., Clark, P. U., Liu, Z., Overpeck, J. T., Konecky, B., et al. (2014). Coherent changes of southeastern equatorial and northern African rainfall during the last deglaciation. *Science (80-.).* 346, 1223–1227. doi:10.1126/science.1259531.
Otto, F. E. L., Wolski, P., Lehner, F., Tebaldi, C., van Oldenborgh, G. J., Hogesteeger, S., et al. (2018). Anthropogenic influence on the drivers of the Western Cape drought 2015–2017. *Environ. Res. Lett.* 13, 124010. doi:10.1088/1748-9326/aae9f9.
Oueslati, B., and Bellon, G. (2015). The double ITCZ bias in CMIP5 models: interaction between SST, large-scale circulation and precipitation. *Clim. Dyn.* 44, 585–607. doi:10.1007/s00382-015-2468-6.
Oueslati, B., Bony, S., Risi, C., and Dufresne, J. L. (2016). Interpreting the inter-model spread in regional precipitation projections in the tropics: role of surface evaporation and cloud radiative effects. *Clim. Dyn.* 47, 2801–2815. doi:10.1007/s00382-016-2998-6.
Overland, J. E., Dethloff, K., Francis, J. A., Hall, R. J., Hanna, E., Kim, S.-J., et al. (2016). Nonlinear response of mid-latitude weather to the changing Arctic. *Nat. Clim. Chang.* 6, 992–999. doi:10.1038/nclimate3121.
Overland, J., Francis, J. A., Hall, R., Hanna, E., Kim, S.-J., and Vihma, T. (2015). The melting Arctic and midlatitude weather patterns: Are they connected? *J. Clim.* 28, 7917–7932. doi:10.1175/jcli-d-14-00822.1.
Overpeck, J. T. (2013). Climate science: The challenge of hot drought. *Nature* 503, 350–351.
Oyama, M. D., and Nobre, C. A. (2003). A new climate-vegetation equilibrium state for Tropical South America. *Geophys. Res. Lett.* doi:10.1029/2003GL018600.
Paegle, J. N., Byerle, L. A., and Mo, K. C. (2000). Intraseasonal Modulation of South American Summer Precipitation. *Mon. Weather Rev.* 128, 837–850. doi:10.1175/1520-0493(2000)128<0837:IMOSAS>2.0.CO;2.
PAGES Hydro2K Consortium (2017). Comparing proxy and model estimates of hydroclimate variability and change over the Common Era. *Clim. Past* 13, 1851–1900. doi:10.5194/cp-13-1851-2017.
Paltan, H., Waliser, D., Lim, W. H., Guan, B., Yamazaki, D., Pant, R., et al. (2017). Global Floods and Water Availability Driven by Atmospheric Rivers. *Geophys. Res. Lett.* 44, 10,387-10,395. doi:10.1002/2017GL074882.
Pan, S., Tian, H., Dangal, S. R. S., Yang, Q., Yang, J., Lu, C., et al. (2015). Responses of global terrestrial evapotranspiration to climate change and increasing atmospheric CO2in the 21st century. *Earth's Futur.* doi:10.1002/2014EF000263.
Pan, X., Chin, M., Ichoku, C. M., and Field, R. D. (2018). Connecting Indonesian Fires and Drought With the Type of El Niño and Phase of the Indian Ocean Dipole During 1979-2016. *J. Geophys. Res.*

*Atmos.*doi:10.1029/2018JD028402.
Panthou, G., Lebel, T., Vischel, T., Quantin, G., Sane, Y., Ba, A., et al. (2018). Rainfall intensification in tropical semi-arid regions: the Sahelian case. *Environ. Res. Lett.* 13, 064013. doi:10.1088/1748-9326/aac334.
Panthou, G., Vischel, T., and Lebel, T. (2014). Recent trends in the regime of extreme rainfall in the Central Sahel. *Int. J. Climatol.* 34, 3998–4006. doi:10.1002/joc.3984.
Park, J., Bader, J., and Matei, D. (2016). Anthropogenic Mediterranean warming essential driver for present and future Sahel rainfall. *Nat. Clim. Chang.* 6, 941–945. doi:10.1038/nclimate3065.
Parsons, L. A., Coats, S., and Overpeck, J. T. (2018). The continuum of drought in southwestern North America. *J. Clim.* 31, 8627–8643.
Parsons, L. A., Loope, G. R., Overpeck, J. T., Ault, T. R., Stouffer, R., and Cole, J. E. (2017). Temperature and Precipitation Variance in CMIP5 Simulations and Paleoclimate Records of the Last Millennium. *J. Clim.* 30, 8885–8912. doi:10.1175/JCLI-D-16-0863.1.
Parsons, L. A., Yin, J., Overpeck, J. T., Stouffer, R. J., and Malyshev, S. (2014). Influence of the atlantic meridional overturning circulation on the monsoon rainfall and carbon balance of the American tropics. *Geophys. Res. Lett.* doi:10.1002/2013GL058454.
Parsons, S., Renwick, J. A., and McDonald, A. J. (2016). An assessment of future Southern Hemisphere blocking using CMIP5 projections from four GCMs. *J. Clim.* 29, 7599–7611. doi:doi:10.1175/JCLI-D-15-0754.1.
Pascale, S., Boos, W. R., Bordoni, S., Delworth, T. L., Kapnick, S. B., Murakami, H., et al. (2017). Weakening of the North American monsoon with global warming. *Nat. Clim. Chang.* 7, 806–812. doi:10.1038/nclimate3412.
Pascale, S., Lucarini, V., Feng, X., Porporato, A., and ul Hasson, S. (2016). Projected changes of rainfall seasonality and dry spells in a high greenhouse gas emissions scenario. *Clim. Dyn.* doi:10.1007/s00382-015-2648-4.
Pathirana, A., Denekew, H. B., Veerbeek, W., Zevenbergen, C., and Banda, A. T. (2014). Impact of urban growth-driven landuse change on microclimate and extreme precipitation - A sensitivity study. *Atmos. Res.* doi:10.1016/j.atmosres.2013.10.005.
Paul, S., Ghosh, S., Oglesby, R., Pathak, A., Chandrasekharan, A., and Ramsankaran, R. (2016). Weakening of Indian Summer Monsoon Rainfall due to Changes in Land Use Land Cover. *Sci. Rep.* 6, 32177. doi:10.1038/srep32177.
Pausata, F. S. R., Messori, G., and Zhang, Q. (2016). Impacts of dust reduction on the northware expansion of the African monsoon during the Green Sahara period. *Earth Planet. Sci. Lett.* 434, 298–307.
Payne, A. E., and Magnusdottir, G. (2015). An evaluation of atmospheric rivers over the North Pacific in CMIP5 and their response to warming under RCP 8.5. *J. Geophys. Res.* 120, 11173–11190.
Pechlivanidis, I. G., Arheimer, B., Donnelly, C., Hundecha, Y., Huang, S., Aich, V., et al. (2017). Analysis of hydrological extremes at different hydro-climatic regimes under present and future conditions. *Clim. Change* 141, 467–481. doi:10.1007/s10584-016-1723-0.
Pederson, N., Hessl, A. E., Baatarbileg, N., Anchukaitis, K. J., and Di Cosmo, N. (2014). Pluvials, droughts, the Mongol Empire, and modern Mongolia. *Proc. Natl. Acad. Sci.* doi:10.1073/pnas.1318677111.
Pedron, I. T., Silva Dias, M. A. F., de Paula Dias, S., Carvalho, L. M. V., and Freitas, E. D. (2017). Trends and variability in extremes of precipitation in Curitiba - Southern Brazil. *Int. J. Climatol.* 37, 1250–1264. doi:10.1002/joc.4773.
Peings, Y., and Magnusdottir, G. (2014). Response of the wintertime northern hemisphere atmospheric circulation to current and projected arctic sea ice decline: A numerical study with CAM5. *J. Clim.* 27, 244–264. doi:10.1175/JCLI-D-13-00272.1.
Peings, Y., Simpkins, G., and Magnusdottir, G. (2016). Multidecadal fluctuations of the North Atlantic Ocean and feedback on the winter climate in CMIP5 control simulations. *J. Geophys. Res. Atmos.* 121, 2571–2592. doi:10.1002/2015JD024107.
Pekel, J. -f., Cottam, A., Gorelick, N., and Belward, A. S. (2016). High-resolution mapping of global surface water and its long-term changes. *Nature* 540, 418–422.
Pendergrass, A. G. (2018). What precipitation is extreme? *Science (80-.).* 360, 1072–1073. doi:10.1126/science.aat1871.
Pendergrass, A. G., and Hartmann, D. L. (2014a). The Atmospheric Energy Constraint on Global-Mean Precipitation Change. *J. Clim.* 27, 757–768. doi:10.1175/JCLI-D-13-00163.1.
Pendergrass, A. G., and Hartmann, D. L. (2014b). Two modes of change of the distribution of rain. *J. Clim.* 27, 8357–8371. doi:10.1175/JCLI-D-14-00182.1.
Pendergrass, A. G., Knutti, R., Lehner, F., Deser, C., and Sanderson, B. M. (2017). Precipitation variability increases in a warmer climate. *Sci. Rep.* 7, 1–9. doi:10.1038/s41598-017-17966-y.
Pendergrass, A. G., Lehner, F., Sanderson, B. M., and Xu, Y. (2015). Does extreme precipitation intensity depend on the emissions scenario? *Geophys. Res. Lett.* 42, 8767–8774. doi:10.1002/2015GL065854.
Pendergrass, A. G., Reed, K. A., and Medeiros, B. (2016). The link between extreme precipitation and convective organization in a warming climate: Global radiative-convective equilibrium simulations. *Geophys. Res. Lett.* 43, 11,445-11,452. doi:10.1002/2016GL071285.

Pepler, A., S., J. F., and Alexander, L. V (2017). Australian east coast mid-latitude cyclones in the 20th Century Reanalysis ensemble. *Int. J. Clim.* 37, 2187–2192. doi:10.1002/joc.4812.
Persad, G. G., Ming, Y., Shen, Z., and Ramaswamy, V. (2018). Spatially similar surface energy flux perturbations due to greenhouse gases and aerosols. *Nat. Commun.* 9, 3247. doi:10.1038/s41467-018-05735-y.
Pervez, M. S., and Henebry, G. M. (2015). Spatial and seasonal responses of precipitation in the Ganges and Brahmaputra river basins to ENSO and Indian Ocean dipole modes: implications for flooding and drought. *Nat. Hazards Earth Syst. Sci.* 15, 147–162. doi:10.5194/nhess-15-147-2015.
Peters, W., van der Velde, I. R., van Schaik, E., Miller, J. B., Ciais, P., Duarte, H. F., et al. (2018a). Increased water-use efficiency and reduced CO_2 uptake by plants during droughts at a continental scale. *Nat. Geosci.*, 11–16. doi:10.1038/s41561-018-0212-7.
Peters, W., van der Velde, I. R., van Schaik, E., Miller, J. B., Ciais, P., Duarte, H. F., et al. (2018b). Increased water-use efficiency and reduced CO_2uptake by plants during droughts at a continental scale. *Nat. Geosci.* 11, 744–748. doi:10.1038/s41561-018-0212-7.
Peterson, L. C., Haug, G. H., Hughen, K. A., and Rohl, U. (2000). Rapid changes in the hydrologic cycle of the tropical Atlantic during the last glacial. *Science (80-.).* doi:10.1126/science.290.5498.1947.
Petrie, M. D., Collins, S. L., Gutzler, D. S., and Moore, D. M. (2014). Regional trends and local variability in monsoon precipitation in the northern Chihuahuan Desert, USA. *J. Arid Environ.* 103, 63–70. doi:10.1016/j.jaridenv.2014.01.005.
Peyron, O., Jolly, D., Braconnot, P., Bonnefille, R., Guiot, J., Wirrmann, D., et al. (2006). Quantitative reconstructions of annual rainfall in Africa 6000 years ago: Model-data comparison. *J. Geophys. Res. Atmos.* 111.
Pfahl, S., O'Gorman, P. A., and Fischer, E. M. (2017). Understanding the regional pattern of projected future changes in extreme precipitation. *Nat. Clim. Chang.* 7, 423–427. doi:10.1038/nclimate3287.
Pfahl, S., Schwierz, C., Croci-Maspoli, M., Grams, C. M., and Wernli, H. (2015). Importance of latent heat release in ascending air streams for atmospheric blocking. *Nat. Geosci.* 8, 610–614. Available at: https://doi.org/10.1038/NGEO2487.
Phibbs, S., and Toumi, R. (2016). The dependence of precipitation and its footprint on atmospheric temperature in idealized extratropical cyclones. *J. Geophys. Res.* 121, 8743–8754. doi:10.1002/2015JD024286.
Philip, S., Kew, S. F., van Oldenborgh, G. J., Otto, F., O'Keefe, S., Haustein, K., et al. (2018). Attribution analysis of the Ethiopian drought of 2015. *J. Clim.* doi:10.1175/JCLI-D-17-0274.1.
Phillips, T. J., Bonfils, C. J. W., and Zhang, C. (2019). Model consensus projections of US regional hydroclimates under greenhouse warming. *Environ. Res. Lett.* 14, 014005. doi:10.1088/1748-9326/aaf03d.
Phillips, T. J., Klein, S. A., Ma, H. -y., Tang, Q., Xie, S., Williams, I. N., et al. (2017). Using ARM observations to evaluate climate model simulations of land-atmosphere coupling on the U.S. *South. Gt. Plains, J. Geophys. Res. Atmos.* 122, 11. Available at: https://doi.org/10.1002/2017JD027141.
Pierce, D. W., Barnett, T. P., Hidalgo, H. G., Das, T., Bonfils, C., Santer, B. D., et al. (2008). Attribution of declining Western U.S. Snowpack to human effects. *J. Clim.* doi:10.1175/2008JCLI2405.1.
Pinto, O., Pinto, I. R. C. A., and Ferro, M. A. S. (2013). A study of the long-term variability of thunderstorm days in southeast Brazil. *J. Geophys. Res. Atmos.* 118, 5231–5246. doi:10.1002/jgrd.50282.
Pires, G. F., and Costa, M. H. (2013). Deforestation causes different subregional effects on the Amazon bioclimatic equilibrium. *Geophys. Res. Lett.* 40, 3618–3623. doi:10.1002/grl.50570.
Pithan, F., Shepherd, T. G., Zappa, G., and Sandu, I. (2016). Climate model biases in jet streams, blocking and storm tracks resulting from missing orographic drag. *Geophys. Res. Lett.* 43, 7231–7240. doi:10.1002/2016GL069551.
Plazzotta, M., Séférian, R., Douville, H., Kravitz, B., and Tjiputra, J. (2018). Land Surface Cooling Induced by Sulfate Geoengineering Constrained by Major Volcanic Eruptions. *Geophys. Res. Lett.* 45, 5663–5671. doi:10.1029/2018GL077583.
Plesca, E., Buehler, S. A., and Grützun, V. (2018). The fast response of the tropical circulation to CO_2 forcing. *J. Clim.*, JCLI-D-18-0086.1. doi:10.1175/JCLI-D-18-0086.1.
Pohl, B., and Matthews, A. J. (2007). Observed Changes in the Lifetime and Amplitude of the Madden–Julian Oscillation Associated with Interannual ENSO Sea Surface Temperature Anomalies. *J. Clim.* 20, 2659–2674. doi:10.1175/JCLI4230.1.
Pokhrel, Y. N., Felfelani, F., Shin, S., Yamada, T., and Satoh, Y. (2017). Modeling large-scale human alteration of land surface hydrology and climate. *Geosci. Lett.* 4, 10. Available at: https://doi.org/10.1186/s40562-017-0076-5.
Pokhrel, Y. N., Hanasaki, N., Wada, Y., and Kim, H. (2016). Recent progresses in incorporating human land–water management into global land surface models toward their integration into Earth system models. *WIREs Water* 3, 548–574. doi:10.1002/wat2.1150.
Pokhrel, Y. N., Koirala, S., Yeh, P. J. -f., Hanasaki, N., Longuevergne, L., Kanae, S., et al. (2015). Incorporation of groundwater pumping in a global Land Surface Model with the representation of human impacts. *Water Resour. Res.* 51, 78. doi:10.1002/2014WR015602.
Polade, S. D., Gershunov, A., Cayan, D. R., Dettinger, M. D., and Pierce, D. W. (2017). Precipitation in a warming

world: Assessing projected hydro-climate changes in California and other Mediterranean climate regions. *Sci. Rep.* 7, 10783. doi:10.1038/s41598-017-11285-y.
Polade, S. D., Pierce, D. W., Cayan, D. R., Gershunov, A., and Dettinger, M. D. (2014). The key role of dry days in changing regional climate and precipitation regimes. *Sci. Rep.* 4, 1–8. doi:10.1038/srep04364.
Policelli, F., Slayback, D., Brakenridge, B., Nigro, J., Hubbard, A., and Zaitchik B. ... & Jung, H. (2017). "The NASA global flood mapping system," in (Remote Sensing of Hydrological Extremes), 47–63.
Polson, D., Bollasina, M., Hegerl, G. C., and Wilcox, L. J. (2014). Decreased monsoon precipitation in the Northern Hemisphere due to anthropogenic aerosols. *Geophys. Res. Lett.* 41, 6023–6029. doi:10.1002/2014GL060811.
Polson, D., and Hegerl, G. C. (2017). Strengthening contrast between precipitation in tropical wet and dry regions. *Geophys. Res. Lett.* 44, 365–373. doi:10.1002/2016GL071194.
Polvani, L., and Bellomo, K. (2019). The Key Role of Ozone-Depleting Substances in Weakening the Walker Circulation in the Second Half of the Twentieth Century, J. *Climate* 32, 1411–1418.
Polyak, V. J., Rasmussen, J. B. T., and Asmerom, Y. (2004). Prolonged wet period in the southwestern United States through the Younger Dryas. *Geology*. doi:10.1130/G19957.1.
Popp, M., and Silvers, L. G. (2017). Double and single ITCZs with and without clouds. *J. Clim.* doi:10.1175/JCLI-D-17-0062.1.
Portmann, F. T., Döll, P., Eisner, S., and Flörke, M. (2013). Impact of climate change on renewable groundwater resources: assessing the benefits of avoided greenhouse gas emissions using selected CMIP5 climate projections. *Environ. Res. Lett.* 8, 024023. doi:10.1088/1748-9326/8/2/024023.
Pottapinjara, V., Girishkumar, M. S., Ravichandran, M., and Murtugudde, R. (2014). Influence of the Atlantic zonal mode on monsoon depressions in the Bay of Bengal during boreal summer. *J. Geophys. Res. Atmos.* 119, 6456–6469. doi:10.1002/2014JD021494.
Pottapinjara, V., Girishkumar, M. S., Sivareddy, S., Ravichandran, M., and Murtugudde, R. (2016). Relation between the upper ocean heat content in the equatorial Atlantic during boreal spring and the Indian monsoon rainfall during June-September. *Int. J. Climatol.* 36, 2469–2480. doi:10.1002/joc.4506.
Potter, S. F., Dawson, E. J., and Frierson, D. M. W. (2017). Southern African orography impacts on low clouds and the Atlantic ITCZ in a coupled model. *Geophys. Res. Lett.* 44, 3283–3289. doi:10.1002/2017GL073098.
Power, S., Delage, F., Chung, C., Kociuba, G., and Keay, K. (2013). Robust twenty-first-century projections of El Niño and related precipitation variability. *Nature* 502, 541–545. doi:10.1038/nature12580.
Power, S., and Kociuba, G. (2011). What caused the observed twentieth century weakening of the Walker circulation? *J. Clim.* 24, 6501–6514. doi:10.1175/2011JCLI4101.1.
Prado, L. F., Wainer, I., and Chiessi, C. M. (2013a). Mid-Holocene PMIP3/CMIP5 model results: Intercomparison for the South American Monsoon System. *Holocene* 23, 1915–1920. doi:10.1177/0959683613505336.
Prado, L. F., Wainer, I., Chiessi, C. M., Ledru, M.-P., and Turcq, B. (2013b). A mid-Holocene climate reconstruction for eastern South America. *Clim. Past* 9, 2117–2133. doi:10.5194/cp-9-2117-2013.
Prasanna, V. (2018). Statistical bias correction method applied on CMIP5 datasets over the Indian region during the summer monsoon season for climate change applications. *Theor. Appl. Climatol.* 131, 471–488. doi:10.1007/s00704-016-1974-8.
Preethi, B., Mujumdar, M., Kripalani, R. H., Prabhu, A., and Krishnan, R. (2017). Recent trends and tele-connections among South and East Asian summer monsoons in a warming environment. *Clim. Dyn.* 48, 2489–2505. doi:10.1007/s00382-016-3218-0.
Prein, A. F., Rasmussen, R. M., Ikeda, K., Liu, C., Clark, M. P., and Holland, G. J. (2017). The future intensification of hourly precipitation extremes. *Nat. Clim. Chang.* 7, 48–52. doi:10.1038/nclimate3168.
Prentice, I. C., Liang, X., Medlyn, B. E., and Wang, Y.-P. (2015). Reliable, robust and realistic: the three R's of next-generation land-surface modelling. *Atmos. Chem. Phys.* 15, 5987–6005. doi:10.5194/acp-15-5987-2015.
Prigent, C., Lettenmaier, D. P., Aires, F., and Papa, F. (2016). "Toward a high-resolution monitoring of continental surface water extent and dynamics, at global scale: from GIEMS (Global Inundation Extent from Multi-Satellites) to SWOT (Surface Water Ocean Topography)," in, eds. R. Sensing and W. R. S. I. Publishing, 149–165.
Pritchard, M. S., and Yang, D. (2016). Response of the Superparameterized Madden–Julian Oscillation to Extreme Climate and Basic-State Variation Challenges a Moisture Mode View. *J. Clim.* 29, 4995–5008. doi:10.1175/JCLI-D-15-0790.1.
Prospero, J. M., Ginoux, P., Torres, O., Nicholson, S. E., and Gill, T. E. (2002). Environmental characterization of global sources of atmospheric soil dust identified with the Nimbus 7 Total Ozone Mapping Spectrometer (TOMS) absorbing aerosol product. *Rev. Geophys.* doi:10.1029/2000RG000095.
Qian, C., and Zhou, T. (2014). Multidecadal Variability of North China Aridity and Its Relationship to PDO during 1900–2010. *J. Clim.* 27, 1210–1222. doi:10.1175/JCLI-D-13-00235.1.
Qian, Y., Gong, D., Fan, J., Leung, L. R., Bennartz, R., Chen, D., et al. (2009). Heavy pollution suppresses light rain in China: Observations and modeling. *J. Geophys. Res.* 114, D00K02. doi:10.1029/2008JD011575.
Qin, Y., and Lin, Y. (2018). Alleviated Double ITCZ Problem in the NCAR CESM1: A New Cloud Scheme and the

Working Mechanisms. *J. Adv. Model. Earth Syst.* 10, 2318–2332. doi:10.1029/2018MS001343.

Qiu, B., Guo, W., Xue, Y., and Dai, Q. (2016). Journal of Geophysical Research : Atmospheres. 145–163. doi:10.1002/2016JD025328.

Qu, Y., Chen, B., Ming, J., Lynn, B. H., and Yang, M.-J. (2017). Aerosol Impacts on the Structure, Intensity, and Precipitation of the Landfalling Typhoon Saomai (2006). *J. Geophys. Res. Atmos.* 122, 11,825-11,842. doi:10.1002/2017JD027151.

Rach, O., Kahmen, A., Brauer, A., and Sachse, D. (2017). A dual-biomarker approach for quantification of changes in relative humidity from sedimentary lipid D/H ratios. *Clim. Past*. doi:10.5194/cp-13-741-2017.

Rachmayani, R., Prange, M., and Schulz, M. (2016). Intra-interglacial climate variability: model simulations of Marine Isotope Stages 1, 5, 11, 13, and 15. *Clim. Past* 12, 677–695. doi:10.5194/cp-12-677-2016.

Radić, V., Bliss, A., Beedlow, A. C., Hock, R., Miles, E., and Cogley, J. G. (2014). Regional and global projections of twenty-first century glacier mass changes in response to climate scenarios from global climate models. *Clim. Dyn.* doi:10.1007/s00382-013-1719-7.

Rahmstorf, S. (1995). Bifurcations of the Atlantic thermohaline circulation in response to changes in the hydrological cycle. *Nature*. doi:10.1038/378145a0.

Rahmstorf, S., Box, J. E., Feulner, G., Mann, M. E., Robinson, A., Rutherford, S., et al. (2015). Exceptional twentieth-century slowdown in Atlantic Ocean overturning circulation. *Nat. Clim. Chang.* doi:10.1038/nclimate2554.

Raible, C. C., Messmer, M., Lehner, F., Stocker, T. F., and Blender, R. (2018). Extratropical cyclone statistics during the last millennium and the 21st century. *Clim. Past* 14, 1499–1514. doi:10.5194/cp-14-1499-2018.

Rajendran, K., Kitoh, A., Srinivasan, J., Mizuta, R., and Krishnan, R. (2012). Monsoon circulation interaction with Western Ghats orography under changing climate: Projection by a 20-km mesh AGCM. *Theor. Appl. Climatol.* doi:10.1007/s00704-012-0690-2.

Ralph, F. M., and Dettinger, M. D. (2011). Storms, floods, and the science of atmospheric rivers. *Eos, Trans. Am. Geophys. Union* 92, 265–266.

Ralph, F. M., Dettinger, M. D., Cairns, M. M., Galarneau, T. J., and Eylander, J. (2018). Defining “atmospheric river”: How the Glossary of Meteorology helped resolve a debate. *Bull. Am. Meteorol. Soc.* 99, 837–839.

Ralph, F. M., Neiman, P. J., and Wick, G. A. (2004). Satellite and CALJET aircraft observations of atmospheric rivers over the eastern North Pacific Ocean during the winter of 1997/98. Mon. *Wea* 132, 1721–1745. doi:10.1175/1520-0493(2004)132<1721:SACAOO>2.0.CO;2.

Ralph, F. M., Prather, K. A., Cayan, D., Spackman, J. R., Demott, P., Dettinger, M., et al. (2016). Calwater field studies designed to quantify the roles of atmospheric rivers and aerosols in modulating U.S. West Coast Precipitation in a changing climate. *Bull. Am. Meteorol. Soc.* doi:10.1175/BAMS-D-14-00043.1.

Ramanathan, V., and Carmichael, G. (2008). Global and regional climate changes due to black carbon. *Nat. Geosci.* 1, 221–227. doi:10.1038/ngeo156.

Ramarao, M. V. S., Krishnan, R., Sanjay, J., and Sabin, T. P. (2015). Understanding land surface response to changing South Asian monsoon in a warming climate. *Earth Syst. Dyn.* 6. doi:10.5194/esd-6-569-2015.

Ramarao, M. V. S., Sanjay, J., Krishnan, R., Mujumdar, M., Bazaz, A., and Revi, A. (2018). On observed aridity changes over the semiarid regions of India in a warming climate. *Theor. Appl. Climatol.* doi:10.1007/s00704-018-2513-6.

Ramos, A. M., Tomé, R., Trigo, R. M., Liberato, M. L. R., and Pinto, J. G. (2016). Projected changes in atmospheric rivers affecting Europe in CMIP5 models. *Geophys. Res. Lett.* 43, 9315–9323. doi:10.1002/2016GL070634.

Ramsar Convention on Wetlands, R. C. on (2018). *Global Wetland Outlook: State of the World’s Wetlands and their Services to People*. Gland, Switzerland: Ramsar Convention Secretariat.

Raoult, N. M., Jupp, T. E., Cox, P. M., and Luke, C. M. (2016). Land-surface parameter optimisation using data assimilation techniques: the adJULES system V1.0. *Geosci. Model Dev.* 9, 2833–2852. Available at: https://doi.org/10.5194/gmd-9-2833-2016.

Reason, C. J. C., Allan, R. J., Lindesay, J. A., and Ansell, T. J. (2000). ENSO and climatic signals across the Indian Ocean Basin in the global context: part I, interannual composite patterns. *Int. J. Climatol.* 20, 1285–1327. doi:10.1002/1097-0088(200009)20:11<1285::AID-JOC536>3.0.CO;2-R.

Reimi, M. A., and Marcantonio, F. (2016). Constraints on the magnitude of the deglacial migration of the ITCZ in the Central Equatorial Pacific Ocean. *Earth Planet. Sci. Lett.* doi:10.1016/j.epsl.2016.07.058.

Reintges, A., Martin, T., Latif, M., and Keenlyside, N. S. (2017). Uncertainty in twenty-first century projections of the Atlantic Meridional Overturning Circulation in CMIP3 and CMIP5 models. *Clim. Dyn.* doi:10.1007/s00382-016-3180-x.

Renssen, H., Goosse, H., Roche, D. M., and Seppä, H. (2018). The global hydroclimate response during the Younger Dryas event. *Quat. Sci. Rev.* doi:10.1016/j.quascirev.2018.05.033.

Rhein, M., Rintoul, S. R., Aoki, S., Campos, E., Chambers, D., Feely, R. A., et al. (2013). “Observations: Ocean,” in *Climate Change 2013: The Physical Science Basis. Contribution of Working Group I to the Fifth Assessment Report of the Intergovernmental Panel on Climate Change*, eds. T. F. Stocker, D. Qin, G.-K. Plattner, M. Tignor,

S. K. Allen, J. Boschung, et al. (Cambridge, United Kingdom and New York, NY, USA: Cambridge University Press), 255–316. doi:10.1017/CBO9781107415324.010.

Rhoades, A. M., Jones, A. D., and Ullrich, P. A. (2018). The Changing Character of the California Sierra Nevada as a Natural Reservoir. *Geophys. Res. Lett.* 45, 8–13,13,19. doi:10.1029/2018GL080308.

Riahi, K., van Vuuren, D. P., Kriegler, E., Edmonds, J., O'Neill, B. C., Fujimori, S., et al. (2017). The Shared Socioeconomic Pathways and their energy, land use, and greenhouse gas emissions implications: An overview. *Glob. Environ. Chang.* 42, 153–168. doi:10.1016/j.gloenvcha.2016.05.009.

Richardson, T. B., Forster, P., Andrews, T., Boucher, O., Faluvegi, G., Fläschner, D., et al. (2018a). Drivers of precipitation change: An energetic understanding. *J. Clim.* 31, 9641–9657. doi:10.1175/JCLI-D-17-0240.1.

Richardson, T. B., Forster, P. M., Andrews, T., Boucher, O., Faluvegi, G., Fläschner, D., et al. (2018b). Carbon Dioxide Physiological Forcing Dominates Projected Eastern Amazonian Drying. *Geophys. Res. Lett.* doi:10.1002/2017GL076520.

Richardson, T. B., Forster, P. M., Andrews, T., and Parker, D. J. (2016). Understanding the Rapid Precipitation Response to CO 2 and Aerosol Forcing on a Regional Scale*. *J. Clim.* 29, 583–594. doi:10.1175/JCLI-D-15-0174.1.

Richter, I., and Xie, S.-P. (2008). Muted precipitation increase in global warming simulations: A surface evaporation perspective. *J. Geophys. Res.* 113, D24118. doi:10.1029/2008JD010561.

Ridley, H. E., Asmerom, Y., Baldini, J. U. L. L., Breitenbach, S. F. M. M., Aquino, V. V., Prufer, K. M., et al. (2015). Aerosol forcing of the position of the intertropical convergence zone since ad 1550. *Nat. Geosci.* 8, 195–200. doi:10.1038/ngeo2353.

Rind, D., Schmidt, G. A., Jonas, J., Miller, R., Nazarenko, L., Kelly, M., et al. (2018). Multicentury Instability of the Atlantic Meridional Circulation in Rapid Warming Simulations With GISS ModelE2. *J. Geophys. Res. Atmos.* doi:10.1029/2017JD027149.

Risbey, J. S., Pook, M. J., McIntosh, P. C., Wheeler, M. C., and Hendon, H. H. (2009). On the Remote Drivers of Rainfall Variability in Australia. *Mon. Weather Rev.* 137, 3233–3253. doi:10.1175/2009MWR2861.1.

Risser, M. D., and Wehner, M. F. (2017). Attributable human-induced changes in the likelihood and magnitude of the observed extreme precipitation during Hurricane Harvey. *Geophys. Res* 44, 412–457. doi:10.1002/2017GL075888.

Rivera, J. A., Araneo, D. C., Penalba, O. C., and Villalba, R. (2018). Regional aspects of streamflow droughts in the Andean rivers of Patagonia, Argentina. Links with large-scale climatic oscillations. *Hydrol. Res.* 49, 134–149. doi:10.2166/nh.2017.207.

Roberts, M. J., Vidale, P. L., Mizielinski, M. S., Demory, M. E., Schiemann, R., Strachan, J., et al. (2015). Tropical cyclones in the UPSCALE ensemble of high-resolution global climate models. *J. Clim.* 28, 574–596. doi:10.1175/JCLI-D-14-00131.1.

Roberts, M. J., Vidale, P. L., Senior, C., Hewitt, H. T., Bates, C., Berthou, S., et al. (2018). The benefits of global high-resolution for climate simulation: process-understanding and the enabling of stakeholder decisions at the regional scale. *Bull. Am. Meteorol. Soc.*, BAMS-D-15-00320.1. doi:10.1175/BAMS-D-15-00320.1.

Robertson, A. W., Moron, V., Qian, J.-H., Chang, C.-P., Tangang, F., Aldrian, E., et al. (2011). "The Maritime Continent Monsoon," in, 85–98. doi:10.1142/9789814343411_0006.

Robertson, F. R., Bosilovich, M. G., and Roberts, J. B. (2016). Reconciling land--ocean moisture transport variability in reanalyses with P- ET in observationally driven land surface models. *J. Clim.* 29, 8625–8646.

Robertson, F. R., Bosilovich, M. G., Roberts, J. B., Reichle, R. H., Adler, R., Ricciardulli, L., et al. (2014). Consistency of estimated global water cycle variations over the satellite era. *J. Clim.* 27, 6135–6154.

Robeson, S. M. (2015). Revisiting the recent California drought as an extreme value. *Geophys. Res. Lett.* 42, 6771–6779.

Robock, A., and Liu, Y. (1994). The Volcanic Signal in Goddard Institute for Space Studies Three-Dimensional Model Simulations. *J. Clim.* 7, 44–55. doi:10.1175/1520-0442(1994)007<0044:TVSIGI>2.0.CO;2.

Robock, A., Oman, L., and Stenchikov, G. L. (2008). Regional climate responses to geoengineering with tropical and Arctic SO<inf>2</inf> injections. *J. Geophys. Res. Atmos.* doi:10.1029/2008JD010050.

Rodell, M., Beaudoing, H. K., L'Ecuyer, T. S., Olson, W. S., Famiglietti, J. S., Houser, P. R., et al. (2015). The observed state of the water cycle in the early twenty-first century. *J. Clim.* 28, 8289–8318. doi:10.1175/JCLI-D-14-00555.1.

Rodell, M., Famiglietti, J. S., Wiese, D. N., Reager, J. T., Beaudoing, H. K., Landerer, F. W., et al. (2018). Emerging trends in global freshwater availability. *Nature* 557, 651–659. doi:10.1038/s41586-018-0123-1.

Rodell, M., Houser, P. R., Jambor, U., Gottschalck, J., Mitchell, K., Meng, C. J., et al. (2004). The Global Land Data Assimilation System. *Bull. Am. Meteorol. Soc.* doi:10.1175/BAMS-85-3-381.

Rodell, M., Velicogna, I., and Famiglietti, J. S. (2009). Satellite-based estimates of groundwater depletion in India. *Nature* 460, 999–1002. doi:10.1038/nature08238.

Roderick, M. L., Sun, F., Lim, W. H., and Farquhar, G. D. (2014). A general framework for understanding the response

of the water cycle to global warming over land and ocean. *Hydrol. Earth Syst. Sci.* 18, 1575–1589. doi:10.5194/hess-18-1575-2014.
Roderick, T. P., Wasko, C., and Sharma, A. (2019). Atmospheric moisture measurements explain increases in tropical rainfall extremes. *Geophys. Res. Lett.* doi:10.1029/2018GL080833.
Rodríguez-Fonseca, B., Mohino, E., Mechoso, C. R., Caminade, C., Biasutti, M., Gaetani, M., et al. (2015a). Variability and predictability of west African droughts: A review on the role of sea surface temperature anomalies. *J. Clim.* 28, 4034–4060. doi:10.1175/JCLI-D-14-00130.1.
Rodríguez-Fonseca, B., Mohino, E., Mechoso, C. R., Caminade, C., Biasutti, M., Gaetani, M., et al. (2015b). Variability and Predictability of West African Droughts: A Review on the Role of Sea Surface Temperature Anomalies. *J. Clim.* 28, 4034–4060. doi:10.1175/JCLI-D-14-00130.1.
Roehrig, R., Bouniol, D., Guichard, F., Hourdin, F., and Redelsperger, J. L. (2013). The present and future of the west african monsoon: A process-oriented assessment of cmip5 simulations along the amma transect. *J. Clim.* 26, 6471–6505.
Rogers, A., Medlyn, B. E., Dukes, J. S., Bonan, G., Caemmerer, S., Dietze, M. C., et al. Niinemets, Ü. , Prentice, I. C., Serbin, S. P., Sitch, S. , Way, D. A. and Zaehle, S. (2017), A roadmap for improving the representation of photosynthesis in Earth system models. *New Phytol.* 213, 22–42. doi:10.1111/nph.14283.
Rojas, M., Arias, P. A., Flores-Aqueveque, V., Seth, A., and Vuille, M. (2016). The South American monsoon variability over the last millennium in climate models. *Clim. Past* 12, 1681–1691. doi:10.5194/cp-12-1681-2016.
Romps, D. M. (2016). Clausius–Clapeyron Scaling of CAPE from Analytical Solutions to RCE. *J. Atmos. Sci.* doi:10.1175/jas-d-15-0327.1.
Ropelewski, C. F., and Halpert, M. S. (1989). Precipitation Patterns Associated with the High Index Phase of the Southern Oscillation. *J. Clim.* 2, 268–284. doi:10.1175/1520-0442(1989)002<0268:PPAWTH>2.0.CO;2.
Roscoe, H. K., and Haigh, J. D. (2007). Influences of ozone depletion, the solar cycle and the QBO on the Southern Annular Mode. *Q. J. R. Meteorol. Soc.* 133, 1855–1864. doi:10.1002/qj.153.
Rosenfeld, D., Andreae, M. O., Asmi, A., Chin, M., de Leeuw, G., Donovan, D. P., et al. (2014). Global observations of aerosol-cloud-precipitation-climate interactions. *Rev. Geophys.* 52, 750–808. doi:10.1002/2013RG000441.
Rosenfeld, D., Clavner, M., and Nirel, R. (2011). Pollution and dust aerosols modulating tropical cyclones intensities. *Atmos. Res.* 102. doi:10.1016/j.atmosres.2011.06.006.
Rosenfeld, D., Lohmann, U., Raga, G. B., O'dowd, C. D., Kulmala, M., Fuzzi, S., et al. (2008a). Flood or drought: How do aerosols affect precipitation? *Science (80-.).* 321, 1309–1313.
Rosenfeld, D., Rudich, Y., and Lahav, R. (2002). Desert dust suppressing precipitation: A possible desertification feedback loop. *Proc. Natl. Acad. Sci.* doi:10.1073/pnas.101122798.
Rosenfeld, D., Woodley, W. L., Khain, A., Cotton, W. R., Carrió, G., Ginis, I., et al. (2012). Aerosol effects on microstructure and intensity of tropical cyclones. *Bull. Am. Meteorol. Soc.* 93. doi:10.1175/BAMS-D-11-00147.1.
Rosenfeld, D., Woodley, W. L., Lerner, A., Kelman, G., and Lindsey, D. T. (2008b). Satellite detection of severe convective storms by their retrieved vertical profiles of cloud particle effective radius and thermodynamic phase. *J. Geophys. Res. Atmos.* 113. doi:10.1029/2007JD008600.
Rosenfeld, D., Zheng, Y., Hashimshoni, E., Pöhlker, M. L., Jefferson, A., Pöhlker, C., et al. (2016). Satellite retrieval of cloud condensation nuclei concentrations by using clouds as CCN chambers. *Proc. Natl. Acad. Sci. U. S. A.* 113, 5828–34. doi:10.1073/pnas.1514044113.
Rotstayn, L. D., and co-authors (2007). Have Australian rainfall and cloudiness increased due to the remote effects of Asian anthropogenic aerosols? *J. Geophys. Res.* 112. doi:10.1029/2006JD007712.
Rotstayn, L. D., Collier, M. A., Chrastansky, A., Jeffrey, S. J., and Luo, J. J. (2013). Projected effects of declining aerosols in RCP4.5: Unmasking global warming? *Atmos. Chem. Phys.* doi:10.5194/acp-13-10883-2013.
Rotstayn, L. D., Collier, M. A., and Luo, J. -j. (2015). Effects of declining aerosols on projections of zonally averaged tropical precipitation. *Environ. Res. Lett.* 10. doi:10.1088/1748-9326/10/4/044018.
Rotstayn, L. D., Jeffrey, S. J., Collier, M. A., Dravitzki, S. M., Hirst, A. C., Syktus, J. I., et al. (2012). Aerosol- and greenhouse gas-induced changes in summer rainfall and circulation in the Australasian region: a study using single-forcing climate simulations. *Atmos. Chem. Phys.* 12, 6377–6404. doi:10.5194/acp-12-6377-2012.
Rotstayn, L. D., and Lohmann, U. (2002). Tropical Rainfall Trends and the Indirect Aerosol Effect. *J. Clim.* 15, 2103–2116. doi:10.1175/1520-0442(2002)015<2103:TRTATI>2.0.CO;2.
Roundy, J. K., and Santanello, J. A. (2017). Utility of Satellite Remote Sensing for Land–Atmosphere Coupling and Drought Metrics. *J. Hydrometeorol.* 18, 863. Available at: https://doi.org/10.1175/JHM-D-16-0171.1.
Routson, C., McKay, N., Kaufman, D., Erb, M. P., Goosse, H., Shuman, B., et al. (2019). Mid-latitude net precipitation decreased with Arctic warming during the Holocene. *Nature* 568, in press. doi:10.1038/s41586-019-1060-3.
Rowell, D. P., and Chadwick, R. (2018). Causes of the Uncertainty in Projections of Tropical Terrestrial Rainfall Change: East Africa. *J. Clim.* 31, 5977–5995. doi:10.1175/JCLI-D-17-0830.1.
Roxy, M. K., Ghosh, S., Pathak, A., Athulya, R., Mujumdar, M., Murtugudde, R., et al. (2017). A threefold rise in widespread extreme rain events over central India. *Nat. Commun.* 8. doi:10.1038/s41467-017-00744-9.

Roxy, M. K., Ritika, K., Terray, P., Murtugudde, R., Ashok, K., and Goswami, B. N. (2015). Drying of Indian subcontinent by rapid Indian ocean warming and a weakening land-sea thermal gradient. *Nat. Commun.* 6, 1–10. doi:10.1038/ncomms8423.

Roy, I., Tedeschi, R. G., and Collins, M. (2019). ENSO teleconnections to the Indian summer monsoon under changing climate. *Int. J. Climatol.* doi:10.1002/joc.5999.

Ruosteenoja, K., Markkanen, T., Venäläinen, A., Räisänen, P., and Peltola, H. (2018). Seasonal soil moisture and drought occurrence in Europe in CMIP5 projections for the 21st century. *Clim. Dyn.* 50, 1177–1192. doi:10.1007/s00382-017-3671-4.

Rupp, D. E., Abatzoglou, J. T., Hegewisch, K. C., and Mote, P. W. (2013). Evaluation of CMIP5 20th century climate simulations for the Pacific Northwest USA. *J. Geophys. Res. Atmos.* 118, 10884–10906. doi:10.1002/jgrd.50843.

Ruprich-Robert, Y., Msadek, R., Castruccio, F., Yeager, S., Delworth, T., and Danabasoglu, G. (2017). Assessing the Climate Impacts of the Observed Atlantic Multidecadal Variability Using the GFDL CM2.1 and NCAR CESM1 Global Coupled Models. *J. Clim.* 30, 2785–2810. doi:10.1175/JCLI-D-16-0127.1.

Sabin et al (2013). High resolution simulation of the South Asian monsoon using a variable resolution global climate model.

Saha, A., Ghosh, S., Sahana, A. S., and Rao, E. P. (2014). Failure of CMIP5 climate models in simulating post-1950 decreasing trend of Indian monsoon. *Geophys. Res. Lett.* 41, 7323–7330. doi:10.1002/2014GL061573.

Saji, N., and Yamagata, T. (2003). Possible impacts of Indian Ocean Dipole mode events on global climate. *Clim. Res.* 25, 151–169. doi:10.3354/cr025151.

Sakschewski, B., von Bloh, W., Boit, A., Poorter, L., Peña-Claros, M., Heinke, J., et al. (2016). Resilience of Amazon forests emerges from plant trait diversity. *Nat. Clim. Chang.* 6, 1032 EP-. Available at: http://dx.doi.org/10.1038/nclimate3109.

Salazar, J. F., Villegas, J. C., Rendón, A. M., Rodríguez, E., Hoyos, I., Mercado-Bettín, D., et al. (2018). Scaling properties reveal regulation of river flows in the Amazon through a "forest reservoir." *Hydrol. Earth Syst. Sci.* 22, 1735–1748. doi:10.5194/hess-22-1735-2018.

Salih, A. A. ., Zhang, Q., and Tjernström, M. (2015). Lagrangian tracing of Sahelian Sudan moisture sources. *J. Geophys. Res. Atmos.* 120, 6793–6808. doi:10.1002/2015JD023238.Received.

Salzmann, M. (2016). Global warming without global mean precipitation increase'. *Sci. Adv.* 2, e1501572--e1501572. doi:10.1126/sciadv.1501572.

Salzmann, M., and Cherian, R. (2015). On the enhancement of the Indian summer monsoon drying by Pacific multidecadal variability during the latter half of the twentieth century. *J. Geophys. Res. Atmos.* 120, 9103–9118. doi:10.1002/2015JD023313.

Samaniego, L., Kumar, R., Breuer, L., Chamorro, A., Flörke, M., Pechlivanidis, I. G., et al. (2017). Propagation of forcing and model uncertainties on to hydrological drought characteristics in a multi-model century-long experiment in large river basins. *Clim. Change* 141, 435–449. doi:10.1007/s10584-016-1778-y.

Sampson, C. C., Smith, A. M., Bates, P. D., Neal, J. C., Alfieri, L., and Freer, J. E. (2015). A high-resolution global flood hazard model. Water resources research. 51, 7358–7381.

Samset, B. H., Myhre, G., Forster, P. M., Hodnebrog, Andrews, T., Faluvegi, G., et al. (2016). Fast and slow precipitation responses to individual climate forcers: A PDRMIP multimodel study. *Geophys. Res. Lett.* 43, 2782–2791. doi:10.1002/2016GL068064.

Samset, B. H., Myhre, G., Forster, P. M., Hodnebrog, Ø., Andrews, T., Boucher, O., et al. (2017). Weak hydrological sensitivity to temperature change over land, independent of climate forcing. *npj Clim. Atmos. Sci.* 1, 3. doi:10.1038/s41612-017-0005-5.

Samset, B. H., Sand, M., Smith, C. J., Bauer, S. E., Forster, P. M., Fuglestvedt, J. S., et al. (2018). Climate Impacts From a Removal of Anthropogenic Aerosol Emissions. *Geophys. Res. Lett.* 45, 1020–1029. doi:10.1002/2017GL076079.

Sánchez, E., Solman, S., Remedio, A. R. C., Berbery, H., Samuelsson, P., Da Rocha, R. P., et al. (2015). Regional climate modelling in CLARIS-LPB: a concerted approach towards twentyfirst century projections of regional temperature and precipitation over South America. *Clim. Dyn.* 45, 2193–2212. doi:10.1007/s00382-014-2466-0.

Sandeep, S., and Ajayamohan, R. S. (2015). Poleward shift in Indian summer monsoon low level jetstream under global warming. *Clim. Dyn.* 45, 337–351. doi:10.1007/s00382-014-2261-y.

Sandeep, S., and Ajayamohan, R. S. (2018). Modulation of Winter Precipitation Dynamics Over the Arabian Gulf by ENSO. *J. Geophys. Res. Atmos.* 123, 198–210. doi:10.1002/2017JD027263.

Sandeep, S., Ajayamohan, R. S., Boos, W. R., Sabin, T. P., and Praveen, V. (2018). Decline and poleward shift in Indian summer monsoon synoptic activity in a warming climate. *Proc. Natl. Acad. Sci.* 115, 2681–2686. doi:10.1073/pnas.1709031115.

Sanderson, B. M., Wehner, M., and Knutti, R. (2017). Skill and independence weighting for multi-model assessments. *Geosci. Model Dev.* 10, 2379–2395. doi:10.5194/gmd-10-2379-2017.

Sandvik, M. I., Sorteberg, A., and Rasmussen, R. (2018). Sensitivity of historical orographically enhanced extreme

precipitation events to idealized temperature perturbations. *Clim. Dyn.* 50, 143–157. doi:10.1007/s00382-017-3593-1.
Sanogo, S., Fink, A. H., Omotosho, J. A., Ba, A., Redl, R., and Ermert, V. (2015a). Spatio-temporal characteristics of the recent rainfall recovery in West Africa. *Int. J. Climatol.* 35, 4589–4605. doi:10.1002/joc.4309.
Sanogo, S., Fink, A. H., Omotosho, J. A., Ba, A., Redl, R., and Ermert, V. (2015b). Spatio-temporal characteristics of the recent rainfall recovery in West Africa. *Int. J. Climatol.* 35, 4589–4605. doi:10.1002/joc.4309.
Santanello, J. A., Dirmeyer, P. A., Ferguson, C. R., Findell, K. L., Tawfik, A. B., Berg, A., et al. (2018). Land–Atmosphere Interactions: The LoCo Perspective. *Bull. Am. Meteorol. Soc.* 99, 1253. Available at: https://doi.org/10.1175/BAMS-D-17-0001.1.
Santer, B. D., and Wigley, T. M. L. (1990). Regional validation of means, variances, and spatial patterns in general circulation model control runs. *J. Geophys. Res.* 95, 829–850. doi:10.1029/JD095iD01p00829.
Sarangi, C., Tripathi, S. N., Qian, Y., Kumar, S., and Ruby Leung, L. (2018). Aerosol and Urban Land Use Effect on Rainfall Around Cities in Indo-Gangetic Basin From Observations and Cloud Resolving Model Simulations. *J. Geophys. Res. Atmos.* 123, 3645–3667. doi:10.1002/2017JD028004.
Sarojini, B. B., Stott, P. A., and Black, E. (2016). Detection and attribution of human influence on regional precipitation. *Nat. Clim. Chang.* 6, 669–675. doi:10.1038/nclimate2976.
Saunois, M., Bousquet, P., Poulter, B., Peregon, A., Ciais, P., and Canadell, J. G. ... & Janssens-Maenhout, G. (2016). *Glob. methane Budg.* 8, 697–751.
Scanlon, B. R., Döll, P., Longuevergne, L., Reedy, R. C., Müller Schmied, H., Wada, Y., et al. (2018). Global models underestimate large decadal declining and rising water storage trends relative to GRACE satellite data. *Proc. Natl. Acad. Sci.* doi:10.1073/pnas.1704665115.
Scanlon, B. R., Faunt, C. C., Longuevergne, L., Reedy, R. C., Alley, W. M., McGuire, V. L., et al. (2012). Groundwater depletion and sustainability of irrigation in the US High Plains and Central Valley. *Proc. Natl. Acad. Sci. U. S. A.* 109, 9320–5. doi:10.1073/pnas.1200311109.
Schaller, N., Cermak, J., Wild, M., and Knutti, R. (2013). The sensitivity of the modeled energy budget and hydrological cycle to CO2 and solar forcing. *Earth Syst. Dyn.* doi:10.5194/esd-4-253-2013.
Scheff, J., and Frierson, D. M. W. (2012). Robust future precipitation declines in CMIP5 largely reflect the poleward expansion of model subtropical dry zones. *Geophys. Res. Lett.* 39. doi:10.1029/2012GL052910.
Scheff, J., and Frierson, D. M. W. (2014). Scaling potential evapotranspiration with greenhouse warming. *J. Clim.* 27, 1539–1558. doi:10.1175/JCLI-D-13-00233.1.
Scheff, J., and Frierson, D. M. W. (2015). Terrestrial aridity and its response to greenhouse warming across CMIP5 climate models. *J. Clim.* 28, 5583–5600. doi:10.1175/JCLI-D-14-00480.1.
Scheff, J., Seager, R., Liu, H., and Coats, S. (2017). Are glacials dry? Consequences for paleoclimatology and for greenhouse warming. *J. Clim.* doi:10.1175/JCLI-D-16-0854.1.
Schepanski, K. (2018). Transport of mineral dust and its impact on climate. *Geosciences* 8, 151.
Schewe, J., Heinke, J., Gerten, D., Haddeland, I., Arnell, N. W., Clark, D. B., et al. (2014). Multimodel assessment of water scarcity under climate change. *Proc. Natl. Acad. Sci.* 111, 3245 LP-3250. doi:10.1073/pnas.1222460110.
Schleussner, C. F., Lissner, T. K., Fischer, E. M., Wohland, J., Perrette, M., Golly, A., et al. (2016). Differential climate impacts for policy-relevant limits to global warming: The case of 1.5 °c and 2 °c. *Earth Syst. Dyn.* 7, 327–351. doi:10.5194/esd-7-327-2016.
Schmid, P. E., and Niyogi, D. (2017). Modeling urban precipitation modification by spatially heterogeneous aerosols. *J. Appl. Meteorol. Climatol.* 56, 2141–2153. doi:10.1175/JAMC-D-16-0320.1.
Schmidt, G. A., Bader, D., Donner, L. J., Elsaesser, G. S., Golaz, J. C., Hannay, C., et al. (2017). Practice and philosophy of climate model tuning across six US modeling centers. *Geosci. Model Dev.* 10, 3207–3223. doi:10.5194/gmd-10-3207-2017.
Schmidt, G. A., Jungclaus, J. H., Ammann, C. M., Bard, E., Braconnot, P., Crowley, T. J., et al. (2011). Climate forcing reconstructions for use in PMIP simulations of the last millennium (v1.0). *Geosci. Model Dev.* 4, 33–45. doi:10.5194/gmd-4-33-2011.
Schmidt, G. A., Jungclaus, J. H., Ammann, C. M., Bard, E., Braconnot, P., Crowley, T. J., et al. (2012). Climate forcing reconstructions for use in PMIP simulations of the Last Millennium (v1.1). *Geosci. Model Dev.* 5, 185–191. doi:10.5194/gmd-5-185-2012.
Schneider, D. P., Ammann, C. M., Otto-Bliesner, B. L., and Kaufman, D. S. (2009). Climate response to large, high-latitude and low-latitude volcanic eruptions in the Community Climate System Model. *J. Geophys. Res.* 114, D15101. doi:10.1029/2008JD011222.
Schneider, T., Bischoff, T., and Haug, G. H. (2014). Migrations and dynamics of the intertropical convergence zone. *Nature*. doi:10.1038/nature13636.
Schubert, J. J., Stevens, B., and Crueger, T. (2013a). Madden-Julian oscillation as simulated by the MPI Earth System Model: Over the last and into the next millennium. *J. Adv. Model. Earth Syst.* 5, 71–84. doi:10.1029/2012MS000180.

Schubert, J. J., Stevens, B., and Crueger, T. (2013b). Madden-Julian oscillation as simulated by the MPI Earth System Model: Over the last and into the next millennium. *J. Adv. Model. Earth Syst.* 5, 71–84. doi:10.1029/2012MS000180.

Schubert, S. D., Stewart, R. E., Wang, H., Barlow, M., Berbery, E. H., Cai, W., et al. (2016). Global Meteorological Drought: A Synthesis of Current Understanding with a Focus on SST Drivers of Precipitation Deficits. *J. Clim.* 29, 3989–4019. doi:10.1175/JCLI-D-15-0452.1.

Schubert, S. D., Wang, H., Koster, R. D., Suarez, M. J., and Groisman, P. Y. (2014). Northern Eurasian heat waves and droughts. *J. Clim.* 27, 3169–3207. Available at: https://doi.org/10.1175/JCLI-D-13-00360.1.

Schwendike, J., Berry, G. J., Reeder, M. J., Jakob, C., Govekar, P., and Wardle, R. (2015). Trends in the local Hadley and local Walker circulations. *J. Geophys. Res.* 120, 7599–7618. doi:10.1002/2014JD022652.

Schwendike, J., Govekar, P., Reeder, M. J., Wardle, R., Berry, G. J., and Jakob, C. (2014). Local partitioning of the overturning circulation in the tropics and the connection to the Hadley and Walker circulations. *J. Geophys. Res.* 119, 1322–1339. doi:10.1002/2013JD020742.

Schwingshackl, C., Hirschi, M., and Seneviratne, S. I. (2018). A theoretical approach to assess soil moisture-climate coupling across CMIP5 and GLACE-CMIP5 experiments. *Earth Syst. Dyn.* 9, 1217–1234. doi:10.5194/esd-9-1217-2018.

Scoccimarro, E., Villarini, G., Vichi, M., Zampieri, M., Fogli, P. G., Bellucci, A., et al. (2015). Projected changes in intense precipitation over Europe at the daily and subdaily time scales. *J. Clim.* 28, 6193–6203. doi:10.1175/JCLI-D-14-00779.1.

Screen, J. A., Bracegirdle, T. J., and Simmonds, I. (2018). Polar Climate Change as Manifest in Atmospheric Circulation. *Curr. Clim. Chang. Reports* 4, 383–395. doi:10.1007/s40641-018-0111-4.

Screen, J. A., and Simmonds, I. (2013). Exploring links between Arctic amplification and mid-latitude weather. *Geophys. Res. Lett.* 40, 959–964. doi:10.1002/grl.50174.

Seager, R., Harnik, N., Kushnir, Y., Robinson, W., and Miller, J. (2003). Mechanisms of Hemispherically Symmetric Climate Variability*. *J. Clim.* 16, 2960–2978. doi:10.1175/1520-0442(2003)016<2960:MOHSCV>2.0.CO;2.

Seager, R., and Hoerling, M. (2014). Atmosphere and Ocean Origins of North American Droughts. *J. Clim.* 27, 4581–4606. doi:10.1175/JCLI-D-13-00329.1.

Seager, R., Hoerling, M., Schubert, S., Wang, H., Lyon, B., Kumar, A., et al. (2015). Causes of the 2011-14 California drought. *J. Clim.* doi:10.1175/JCLI-D-14-00860.1.

Seager, R., Kushnir, Y., Herweijer, C., Naik, N., and Velez, J. (2005). Modeling of tropical forcing of persistent droughts and pluvials over western North America: 1856-2000. *J. Clim.* doi:10.1175/JCLI3522.1.

Seager, R., Naik, N., and Vecchi, G. A. (2010). Thermodynamic and dynamic mechanisms for large-scale changes in the hydrological cycle in response to global warming. *J. Clim.* doi:10.1175/2010JCLI3655.1.

Seeley, J. T., and Romps, D. M. (2015). Why does tropical convective available potential energy (CAPE) increase with warming? *Geophys. Res. Lett.* doi:10.1002/2015GL066199.

Seiler, C., Hutjes, R. W. A., and Kabat, P. (2013). Climate variability and trends in bolivia. *J. Appl. Meteorol. Climatol.* 52, 130–146. doi:10.1175/JAMC-D-12-0105.1.

Semenov, V. A., and Latif, M. (2015). Nonlinear winter atmospheric circulation response to Arctic sea ice concentration anomalies for different periods during 1966-2012. *Environ. Res. Lett.* 10. doi:10.1088/1748-9326/10/5/054020.

Seneviratne, S. I., Nicholls, N., Easterling, D., Goodess, C. M., Kanae, S., Kossin, J., et al. (2012). “Changes in climate extremes and their impacts on the natural physical environment,” in *Managing the Risks of Extreme Events and Disasters to Advance Climate Change Adaptation. A Special Report of Working Groups I and II of the Intergovernmental Panel on Climate Change (IPCC)*, eds. C. B. Field, V. Barros, T. F. Stocker, D. Qin, D. J. Dokken, K. L. Ebi, et al. (Cambridge, UK, and New York, NY, USA: Cambridge University Press), 109–230.

Seneviratne, S. I., Wilhelm, M., Stanelle, T., Van Den Hurk, B., Hagemann, S., Berg, A., et al. (2013). Impact of soil moisture-climate feedbacks on CMIP5 projections: First results from the GLACE-CMIP5 experiment. *Geophys. Res. Lett.* 40, 5212–5217. doi:10.1002/grl.50956.

Seo, K. H., Frierson, D. M. W., and Son, J. H. (2014). A mechanism for future changes in Hadley circulation strength in CMIP5 climate change simulations. *Geophys. Res. Lett.* doi:10.1002/2014GL060868.

Serra, C., Mart\'\inez, M. D., Lana, X., and Burgueño, A. (2014). European dry spell regimes (1951--2000): clustering process and time trends. *Atmos. Res.* 144, 151–174.

Seth, A., Rojas, M., and Rauscher, S. A. (2010). CMIP3 projected changes in the annual cycle of the South American Monsoon. *Clim. Change* 98, 331–357. doi:10.1007/s10584-009-9736-6.

Seviour, W. J. M., Davis, S. M., Grise, K. M., and Waugh, D. W. (2018). Large Uncertainty in the Relative Rates of Dynamical and Hydrological Tropical Expansion. *Geophys. Res. Lett.* 45, 1106–1113. doi:10.1002/2017GL076335.

Sgubin, G., Swingedouw, D., Drijfhout, S., Mary, Y., and Bennabi, A. (2017). Abrupt cooling over the North Atlantic in modern climate models. *Nat. Commun.* doi:10.1038/ncomms14375.

Shakun, J. D., Burns, S. J., Fleitmann, D., Kramers, J., Matter, A., and Al-Subary, A. (2007). A high-resolution, absolute-dated deglacial speleothem record of Indian Ocean climate from Socotra Island, Yemen. *Earth Planet. Sci. Lett.* 259, 442–456. doi:10.1016/j.epsl.2007.05.004.

Shanahan, T. M., McKay, N. P., Hughen, K. A., Overpeck, J. T., Otto-Bliesner, B., Heil, C. W., et al. (2015). The time-transgressive termination of the African Humid Period. *Nat. Geosci.*

Shannon, S., Smith, R., Wiltshire, A., Payne, T., Huss, M., Betts, R., et al. (2019). Global glacier volume projections under high-end climate change scenarios. *Cryosphere* 13, 325–350. doi:10.5194/tc-13-325-2019.

Sharma, S., Blagrave, K., O'Reilly, C. M., Samantha, O., Ryan, B., Magee, M., et al. (2019). Widespread loss of lake ice around the Northern Hemisphere in a warming world. Submitted. *Nat. Clim. Chang.* doi:10.1038/s41558-018-0393-5.

Shaw, T. A., Baldwin, M., Barnes, E. A., Caballero, R., Garfinkel, C. I., Hwang, Y. T., et al. (2016). Storm track processes and the opposing influences of climate change. *Nat. Geosci.* 9, 656–664. doi:10.1038/ngeo2783.

Shaw, T. A., and Tan, Z. (2018). Testing latitudinally-dependent explanations of the circulation response to increased CO2 using aquaplanet models. *Geophys. Res. Lett.* doi:10.1029/2018GL078974.

Shaw, T. A., and Voigt, A. (2016). Land dominates the regional response to CO2 direct radiative forcing. *Geophys. Res. Lett.* 43, 11,383-11,391. doi:10.1002/2016GL071368.

Shepherd, T. G. (2014). Atmospheric circulation as a source of uncertainty in climate change projections. *Nat. Geosci.* 7, 703–708. doi:10.1038/ngeo2253.

Shepherd, T. G., Boyd, E., Calel, R. A., Chapman, S. C., Dessai, S., Dima-West, I. M., et al. (2018). Storylines: an alternative approach to representing uncertainty in physical aspects of climate change. *Clim. Change*. doi:10.1007/s10584-018-2317-9.

Sherwood, S. C., Bony, S., Boucher, O., Bretherton, C., Forster, P. M., Gregory, J. M., et al. (2015). Adjustments in the forcing-feedback framework for understanding climate change. *Bull. Am. Meteorol. Soc.* 96, 217–228. doi:10.1175/BAMS-D-13-00167.1.

Shi, G., Cai, W., Cowan, T., Ribbe, J., Rotstayn, L., and Dix, M. (2008). Variability and trend of north west Australia rainfall: observations and coupled climate modelling. *J. Clim.* 21, 2938–2959. doi:10.1175/2007JCLI1908.1.

Shige, S., Kida, S., Ashiwake, H., Kubota, T., and Aonashi, K. (2013). Improvement of TMI rain retrievals in mountainous areas. *J. Appl. Meteorol. Climatol.* 52, 242–254. Available at: https://doi.org/10.1175/JAMC-D-12-074.1.

Shige, S., Nakano, Y., Yamamoto, M. K., Shige, S., Nakano, Y., and Yamamoto, M. K. (2017). Role of orography, diurnal cycle, and intraseasonal oscillation in summer monsoon rainfall over Western Ghats and Myanmar coast. *J. Clim.* 30, 9365–9381. doi:10.1175/JCLI-D-16-0858.1.

Shige, S., Yamamoto, M. K., and Taniguchi, A. (2015). Improvement of TMI rain retrieval over the {I}ndian subcontinent. *Remote Sens. Terr. Water Cycle, Geophys. Monogr.* 206, 27–42. Available at: https://doi.org/10.1002/9781118872086.ch2.

Shiklomanov, I. A., and Sokolov, A. A. (1985). "Methodological basis of world water balance investigation and computation.," in *New Approaches in Water Balance Computations [Van der Beken, A. and A. Herrmann (Eds.)]*., 77–92.

Shindell, D., Kuylenstierna, J. C. I., Vignati, E., van Dingenen, R., Amann, M., Klimont, Z., et al. (2012). Simultaneously mitigating near-term climate change and improving human health and food security. *Science* 335, 183–9. doi:10.1126/science.1210026.

Shine, K. P., Allan, R. P., Collins, W. J., and Fuglestvedt, J. S. (2015). Metrics for linking emissions of gases and aerosols to global precipitation changes. *Earth Syst. Dyn.* 6, 525–540. doi:10.5194/esd-6-525-2015.

Shinozuka, Y., Clarke, A. D., Nenes, A., Jefferson, A., Wood, R., McNaughton, C. S., et al. (2015). The relationship between cloud condensation nuclei (CCN) concentration and light extinction of dried particles: indications of underlying aerosol processes and implications for satellite-based CCN estimates. *Atmos. Chem. Phys.* 15, 7585–7604. doi:10.5194/acp-15-7585-2015.

Shiogama, H., Hanasaki, N., Masutomi, Y., Nagashima, T., Ogura, T., Takahashi, K., et al. (2010). Emission scenario dependencies in climate change assessments of the hydrological cycle. *Clim. Change*. doi:10.1007/s10584-009-9765-1.

Shrestha, S., Hoang, N. A. T., Shrestha, P. K., and Bhatta, B. (2018). Climate change impact on groundwater recharge and suggested adaptation strategies for selected Asian cities. *APN Sci. Bull.* doi:10.30852/sb.2018.499.

Siew, J. H., Tangang, F. T., and Juneng, L. (2014). Evaluation of CMIP5 coupled atmosphere--ocean general circulation models and projection of the Southeast Asian winter monsoon in the 21st century, Int. *J. Clim.* 34, 2872–2884. doi:10.1002/joc.3880.

Sigmond, M., and Fyfe, J. C. (2016). Tropical Pacific impacts on cooling North American winters. *Nat. Clim. Chang.* 6, 970–974. doi:10.1038/nclimate3069.

Siler, N., Roe, G. H., and Armour, K. C. (2018a). Insights into the zonal-mean response of the hydrologic cycle to global warming from a diffusive energy balance model. *J. Clim.* 31, JCLI-D-18-0081.1. doi:10.1175/JCLI-D-18-

0081.1.
Siler, N., Roe, G. H., Armour, K. C., and Feldl, N. (2018b). Revisiting the surface-energy-flux perspective on the sensitivity of global precipitation to climate change. *Clim. Dyn.* doi:10.1007/s00382-018-4359-0.
Sillmann, J., Stjern, C. W., Myhre, G., and Forster, P. M. (2017). Slow and fast responses of mean and extreme precipitation to different forcing in CMIP5 simulations. *Geophys. Res. Lett.* 44, 6383–6390. doi:10.1002/2017GL073229.
Silvestri, G. E. (2003). Antarctic Oscillation signal on precipitation anomalies over southeastern South America. *Geophys. Res. Lett.* 30, 2115. doi:10.1029/2003GL018277.
Sime, L. C., Hopcroft, P. O., and Rhodes, R. H. (2019). Impact of abrupt sea ice loss on Greenland water isotopes during the last glacial period. 1–6. doi:10.1073/pnas.1807261116.
Simpson, I. R., Seager, R., Ting, M., and Shaw, T. A. (2016). Causes of change in Northern Hemisphere winter meridional winds and regional hydroclimate. *Nat. Clim. Chang.* 6, 65–70. doi:10.1038/nclimate2783.
Singarayer, J. S., Valdes, P. J., and Roberts, W. H. G. (2017). Ocean dominated expansion and contraction of the late Quaternary tropical rainbelt. *Sci. Rep.* 7. doi:10.1038/s41598-017-09816-8.
Singh, D., Ghosh, S., Roxy, M. K., and McDermid, S. (2019a). "{I}ndian summer monsoon: Extreme events, historical changes, and role of anthropogenic forcings," in *Interdisciplinary Reviews: Climate Change, 10(2), e571* Available at: https://doi.org/10.1002/wcc.571.
Singh, D., Ghosh, S., Roxy, M. K., and McDermid, S. (2019b). Indian summer monsoon: Extreme events, historical changes, and role of anthropogenic forcings. *Wiley Interdiscip. Rev. Clim. Chang.* 10, e571. doi:10.1002/wcc.571.
Singh, D., Tsiang, M., Rajaratnam, B., and Diffenbaugh, N. S. (2014). Observed changes in extreme wet and dry spells during the south Asian summer monsoon season. *Nat. Clim. Chang.* 4, 456–461. doi:10.1038/nclimate2208.
Singh, M. S., and O'Gorman, P. A. (2014). Influence of microphysics on the scaling of precipitation extremes with temperature. *Geophys. Res. Lett.* 41, 6037–6044. doi:10.1002/2014GL061222.
Sinha, A., Kathayat, G., Cheng, H., Breitenbach, S. F. M., Berkelhammer, M., Mudelsee, M., et al. (2015). monsoon rainfall over the last two millennia. *Nat. Commun.* 6, 1–8. doi:10.1038/ncomms7309.
Sippel, S., Zscheischler, J., Heimann, M., Lange, H., Mahecha, M. D., Jan Van Oldenborgh, G., et al. (2017). Have precipitation extremes and annual totals been increasing in the world's dry regions over the last 60 years? *Hydrol. Earth Syst. Sci.* 21, 441–458. doi:10.5194/hess-21-441-2017.
Siqueira, L., and Kirtman, B. P. (2016). Atlantic near-term climate variability and the role of a resolved Gulf Stream. *Geophys. Res. Lett.* 43, 3964–3972. doi:10.1002/2016GL068694.
Skansi, M. de los M., Brunet, M., Sigró, J., Aguilar, E., Arevalo Groening, J. A., Bentancur, O. J., et al. (2013). Warming and wetting signals emerging from analysis of changes in climate extreme indices over South America. *Glob. Planet. Change* 100, 295–307. doi:10.1016/j.gloplacha.2012.11.004.
Skinner, C. B., and Poulsen, C. J. (2016). The role of fall season tropical plumes in enhancing Saharan rainfall during the African Humid Period. *Geophys. Res. Lett.* doi:10.1002/2015GL066318.
Skliris, N., Marsh, R., Josey, S. A., Good, S. A., Liu, C., and Allan, R. P. (2014). Salinity changes in the World Ocean since 1950 in relation to changing surface freshwater fluxes. *Clim. Dyn.* 43, 709–736. doi:10.1007/s00382-014-2131-7.
Skliris, N., Zika, J. D., Nurser, G., Josey, S. A., and Marsh, R. (2016). Global water cycle amplifying at less than the Clausius-Clapeyron rate. *Sci. Rep.* 6. doi:10.1038/srep38752.
Slangen, A. B. A., Church, J. A., Agosta, C., Fettweis, X., Marzeion, B., and Richter, K. (2016). Anthropogenic forcing dominates global mean sea-level rise since 1970. *Nat. Clim. Chang.* 6, 701. Available at: https://doi.org/10.1038/nclimate2991.
Smeed, D. A., Josey, S. A., Beaulieu, C., Johns, W. E., Moat, B. I., Frajka-Williams, E., et al. (2018). The North Atlantic Ocean Is in a State of Reduced Overturning. *Geophys. Res. Lett.* doi:10.1002/2017GL076350.
Smith, I. N. (2004). An assessment of recent trends in Australian rainfall. *Aust. Meteorol. Mag.* 53, 163–173.
Smith, R. J., and Mayle, F. E. (2018). Impact of mid- to late Holocene precipitation changes on vegetation across lowland tropical South America: a paleo-data synthesis. *Quat. Res.* 89, 134–155. doi:https://doi.org/10.1017/qua.2017.89.
Smyth, J. E., Russotto, R. D., and Storelvmo, T. (2017). Thermodynamic and dynamic responses of the hydrological cycle to solar dimming. *Atmos. Chem. Phys.* 17, 6439–6453. doi:10.5194/acp-17-6439-2017.
Sniderman, J. M. K., Brown, J. R., Woodhead, J. D., King, A. D., Gillett, N. P., Tokarska, K. B., et al. (2019). Southern Hemisphere subtropical drying as a transient response to warming. *Nat. Clim. Chang.* doi:10.1038/s41558-019-0397-9.
Soares-Filho, B. S., Nepstad, D. C., Curran, L. M., Cerqueira, G. C., Garcia, R. A., Ramos, C. A., et al. (2006). Modelling conservation in the Amazon basin. *Nature*. doi:10.1038/nature04389.
Soden, B. J., Jackson, D. L., Ramaswamy, V., Schwarzkopf, M. D., and Huang, X. (2005). The Radiative Signature of Upper Tropospheric Moistening. *Science (80-.).* 310, 841. Available at: http://science.sciencemag.org/content/310/5749/841.abstract.

Sohn, B. J., and Park, S. -c. (2010). Strengthened tropical circulations in past three decades inferred from water vapor transport. *J. Geophys. Res* 115. Available at: https://doi.org/10.1029/2009JD013713.
Sohn, B. J., Ryu, G. -h., Song, H. -j., and Ou, M. -l. (2013a). Characteristic features of warm-type rain producing heavy rainfall over the Korean peninsula inferred from TRMM measurements. *Mon. Weather Rev.* 141, 3873–3888. Available at: https://doi.org/10.1175/MWR-D-13-00075.1.
Sohn, B. J., Yeh, S. W., Schmetz, J., and Song, H. J. (2013b). Observational evidences of Walker circulation change over the last 30 years contrasting with GCM results. *Clim. Dyn.* 40, 1721–1732. doi:10.1007/s00382-012-1484-z.
Solman, S. A., and Orlanski, I. (2014). Poleward Shift and Change of Frontal Activity in the Southern Hemisphere over the Last 40 Years. *J. Atmos. Sci.* 71, 539–552. doi:10.1175/JAS-D-13-0105.1.
Solman, S. A., and Orlanski, I. (2016). Climate change over the extratropical Southern Hemisphere: The tale from an ensemble of reanalysis datasets. *J. Clim.* 29, 1673–1687. doi:10.1175/JCLI-D-15-0588.1.
Solomon, S., Plattner, G. -k., Knutti, R., and Friedlingstein, P. (2009). Irreversible climate change due to carbon dioxide emissions. in *Proc. Natl* (Acad. Sci).
Song, F., Leung, L. R., Lu, J., and Dong, L. (2018). Seasonally dependent responses of subtropical highs and tropical rainfall to anthropogenic warming. *Nat. Clim. Chang.* 8, 787–792. doi:10.1038/s41558-018-0244-4.
Song, F., Zhou, T., and Qian, Y. (2014). Responses of East Asian summer monsoon to natural and anthropogenic forcings in the 17 latest CMIP5 models. *Geophys. Res. Lett.* 41, 596–603. doi:10.1002/2013GL058705.
Song, H., Ferguson, C. R., and Roundy, J. K. (2016). Land–Atmosphere Coupling at the Southern Great Plains Atmospheric Radiation Measurement (ARM) Field Site and Its Role in Anomalous Afternoon Peak Precipitation. *J. Hydrometeorol.* 17, 541. Available at: https://doi.org/10.1175/JHM-D-15-0045.1.
Sood, A., and Smakhtin, V. (2015). Global hydrological models: a review. *Hydrol. Sci. J.* 60, 549–565. doi:10.1080/02626667.2014.950580.
Sousa, P. M., Trigo, R. M., Barriopedro, D., Soares, P. M., Ramos, A. M., and Liberato, M. L. (2017). Responses of European precipitation distributions and regimes to different blocking locations. *Clim. Dyn.* 48, 1141–1160.
Sperber, K. R., Annamalai, H., Kang, I.-S., Kitoh, A., Moise, A., Turner, A., et al. (2013). The Asian summer monsoon: an intercomparison of CMIP5 vs. CMIP3 simulations of the late 20th century. *Clim. Dyn.* 41, 2711–2744. doi:10.1007/s00382-012-1607-6.
Spracklen, D. V., and Garcia-Carreras, L. (2015). The impact of Amazonian deforestation on Amazon basin rainfall. *Geophys. Res. Lett.* 42, 9546–9552. doi:10.1002/2015GL066063.
Spracklen, D. V, Arnold, S. R., and Taylor, C. M. (2012). Observations of increased tropical rainfall preceded by air passage over forests. *Nature* 489, 282–285. Available at: http://dx.doi.org/10.1038/nature11390.
Staal, A., Dekker, S. C., Hirota, M., and van Nes, E. H. (2015). Synergistic effects of drought and deforestation on the resilience of the south-eastern Amazon rainforest. *Ecol. Complex.* 22, 65–75. doi:10.1016/j.ecocom.2015.01.003.
Stager, J. C., Ryves, D. B., Chase, B. M., and Pausata, F. S. R. (2011). Catastrophic drought in the Afro-Asian monsoon region during Heinrich event 1. *Science (80-.).* 331, 1299–1302.
Staten, P. W., Lu, J., Grise, K. M., Davis, S. M., and Birner, T. (2018). Re-examining tropical expansion. *Nat. Clim. Chang.* 8, 768–775. doi:10.1038/s41558-018-0246-2.
Stephens, E., Day, J. J., Pappenberger, F., and Cloke, H. (2015a). Precipitation and floodiness. *Geophys. Res. Lett.* 42, 10316–10323. doi:10.1002/2015GL066779.
Stephens, G. L., Hakuba, M. Z., Webb, M. J., Lebsock, M., Yue, Q., Kahn, B. H., et al. (2018). Regional Intensification of the Tropical Hydrological Cycle During ENSO. *Geophys. Res. Lett.* 45, 4361–4370. doi:10.1029/2018GL077598.
Stephens, G. L., O'Brien, D., Webster, P. J., Pilewski, P., Kato, S., and Li, J. L. (2015b). The albedo of earth. *Rev. Geophys.* 53, 141–163. doi:10.1002/2014RG000449.
Stevens, B., and Feingold, G. (2009). Untangling aerosol effects on clouds and precipitation in a buffered system. *Nature* 461, 607. doi:10.1038/nature08281.
Stevenson, S., Overpeck, J. T., Fasullo, J., Coats, S., Parsons, L., Otto-Bliesner, B., et al. (2018). Climate Variability, Volcanic Forcing, and Last Millennium Hydroclimate Extremes. *J. Clim.* 31, 4309–4327. doi:10.1175/JCLI-D-17-0407.1.
Stevenson, S., Timmermann, A., Chikamoto, Y., Langford, S., and DiNezio, P. (2015). Stochastically Generated North American Megadroughts. *J. Clim.* 28, 1865–1880. doi:10.1175/JCLI-D-13-00689.1.
Stjern, C. W., Samset, B. H., Myhre, G., Forster, P. M., Hodnebrog, Ø., Andrews, T., et al. (2017). Rapid Adjustments Cause Weak Surface Temperature Response to Increased Black Carbon Concentrations. *J. Geophys. Res. Atmos.* 122, 11,462-11,481. doi:10.1002/2017JD027326.
Stocker, T. F., Qin, D., Plattner, G.-K., Alexander, L. V, Allen, S. K., Bindoff, N. L., et al. (2013). "Technical Summary," in *Climate Change 2013: The Physical Science Basis. Contribution of Working Group I to the Fifth Assessment Report of the Intergovernmental Panel on Climate Change*, eds. T. F. Stocker, D. Qin, G.-K. Plattner, M. Tignor, S. K. Allen, J. Boschung, et al. (Cambridge, United Kingdom and New York, NY, USA: Cambridge University Press), 33–115. doi:10.1017/CBO9781107415324.005.

Stommel, H. (1961). Thermohaline Convection with Two Stable Regimes of Flow. *Tellus* 13, 224–230. doi:10.3402/tellusa.v13i2.9491.
Stott, P. A., Christidis, N., Otto, F. E. L., Sun, Y., Vanderlinden, J. P., van Oldenborgh, G. J., et al. (2016). Attribution of extreme weather and climate-related events. *Wiley Interdiscip. Rev. Clim. Chang.* 7, 23–41. doi:10.1002/wcc.380.
Stouffer, R. ., Yin, J., Gregory, J. ., Dixon, K., and Spelman, M. (2006). Investigating the Causes of the Response of the Thermohaline Circulation to Past and. *J. Clim.* 19, 1365–1387. doi:10.1002/9781119115397.ch25.
Strachan, J., Vidale, P. L., Hodges, K., Roberts, M., and Demory, M. E. (2013). Investigating global tropical cyclone activity with a hierarchy of AGCMs: The role of model resolution. *J. Clim.* 26, 133–152. doi:10.1175/JCLI-D-12-00012.1.
Stríkis, N. M., Chiessi, C. M., Cruz, F. W., Vuille, M., Cheng, H., De Souza Barreto, E. A., et al. (2015). Timing and structure of Mega-SACZ events during Heinrich Stadial 1. *Geophys. Res. Lett.* doi:10.1002/2015GL064048.
Studholme, J., and Gulev, S. (2018). Concurrent changes to Hadley circulation and the meridional distribution of tropical cyclones. *J. Clim.* 31, 4367–4389.
Stuecker, M. F., Bitz, C. M., Armour, K. C., Proistosescu, C., Kang, S. M., Xie, S. P., et al. (2018). Polar amplification dominated by local forcing and feedbacks. *Nat. Clim. Chang.* 8, 1076–1081. doi:10.1038/s41558-018-0339-y.
Su, C. H., Ryu, D., Dorigo, W., Zwieback, S., Gruber, A., Albergel, C., et al. (2016). Homogeneity of a global multisatellite soil moisture climate data record. *Geophys. Res. Lett.* 43, 11,245-11,252. doi:10.1002/2016GL070458.
Su, H., Jiang, J. H., Neelin, J. D., Shen, T. J., Zhai, C., Yue, Q., et al. (2017). Tightening of tropical ascent and high clouds key to precipitation change in a warmer climate. *Nat. Commun.* 8, 15771. doi:10.1038/ncomms15771.
Su, H., Jiang, J. H., Zhai, C., Shen, T. J., Neelin, J. D., Stephens, G. L., et al. (2014). Weakening and strengthening structures in the Hadley Circulation change under global warming and implications for cloud response and climate sensitivity. *J. Geophys. Res.* doi:10.1002/2014JD021642.
Su, H., and Neelin, J. D. (2005). Dynamical mechanisms for African monsoon changes during the mid-Holocene. *J. Geophys. Res. D Atmos.* doi:10.1029/2005JD005806.
Su, H., Zhai, C., Jiang, J. H., Wu, L., Neelin, J. D., and Yung, Y. L. (2019). A dichotomy between model responses of tropical ascent and descent to surface warming. *npj Clim. Atmos. Sci.* 2, 8. doi:10.1038/s41612-019-0066-8.
Subramanian, A., Jochum, M., Miller, A. J., Neale, R., Seo, H., Waliser, D., et al. (2014). The MJO and global warming: a study in CCSM4. *Clim. Dyn.* 42, 2019–2031. doi:10.1007/s00382-013-1846-1.
Sudeepkumar, B. L., Babu, C. A., and Varikoden, H. (2018). Future projections of active-break spells of Indian summer monsoon in a climate change perspective. *Glob. Planet. Change* 161, 222–230. doi:10.1016/j.gloplacha.2017.12.020.
Sugi, M., and Yoshimura, J. (2004). A mechanism of tropical precipitation change due to CO2increase. *J. Clim.* 17, 238–243. doi:10.1175/1520-0442(2004)017<0238:AMOTPC>2.0.CO;2.
Sun, C., Liu, L., Li, L.-J., Wang, B., Zhang, C., Liu, Q., et al. (2018). Uncertainties in simulated El Niño-Southern Oscillation arising from internal climate variability. *Atmos. Sci. Lett.* 19, e805. doi:10.1002/asl.805.
Sun, Q., Miao, C., and Duan, Q. (2015). Comparative analysis of CMIP3 and CMIP5 global climate models for simulating the daily mean, maximum, and minimum temperatures and daily precipitation over China. *J. Geophys. Res. Atmos.* 120, 4806–4824. doi:10.1002/2014JD022994.
Sun, Y., Clemens, S. C., Morrill, C., Lin, X., Wang, X., and An, Z. (2012). Influence of Atlantic meridional overturning circulation on the East Asian winter monsoon. *Nat. Geosci.* 5, 46–49. doi:10.1038/ngeo1326.
Supari, Tangang, F., Salimun, E., Aldrian, E., Sopaheluwakan, A., and Juneng, L. (2018). ENSO modulation of seasonal rainfall and extremes in Indonesia. *Clim. Dyn.* 51, 2559–2580. doi:10.1007/s00382-017-4028-8.
Sutton, R. T. (2018). ESD Ideas: A simple proposal to improve the contribution of IPCC WGI to the assessment and communication of climate change risks. *Earth Syst. Dyn.* 9, 1155–1158. doi:10.5194/esd-9-1155-2018.
Swann, A. L. S. (2018). Plants and Drought in a Changing Climate. *Curr. Clim. Chang. Reports*. doi:10.1007/s40641-018-0097-y.
Swann, A. L. S., Hoffman, F. M., Koven, C. D., and Randerson, J. T. (2016). Plant responses to increasing CO2 reduce estimates of climate impacts on drought severity. *Proc. Natl. Acad. Sci.* 113, 10019–10024. doi:10.1073/pnas.1604581113.
Swapna, P., Krishnan, R., and Wallace, J. M. (2012). Indian Ocean and monsoon coupled interactions in a warming environment. *Clim. Dyn.* 42, 2439–2454. doi:10.1007/s00382-013-1787-8.
Swingedouw, D., Mignot, J., Ortega, P., Khodri, M., Menegoz, M., Cassou, C., et al. (2017). Impact of explosive volcanic eruptions on the main climate variability modes. *Glob. Planet. Change* 150, 24–45. doi:10.1016/j.gloplacha.2017.01.006.
Tague, C., and Grant, G. E. (2009). Groundwater dynamics mediate low-flow response to global warming in snow-dominated alpine regions. *Water Resour. Res.* 45.
Takacs, L. L., Suárez, M. J., and Todling, R. (2016). Maintaining atmospheric mass and water balance in reanalyses. *Q.*

J. R. Meteorol. Soc. 142, 1565–1573.
Takahashi, C., Sato, N., Seiki, A., Yoneyama, K., and Shirooka, R. (2011). Projected Future Change of MJO and its Extratropical Teleconnection in East Asia during the Northern Winter Simulated in IPCC AR4 Models. *SOLA* 7, 201–204. doi:10.2151/sola.2011-051.
Takahashi, C., and Watanabe, M. (2016). Pacific trade winds accelerated by aerosol forcing over the past two decades. *Nat. Clim. Chang.* 6, 768–772. doi:10.1038/nclimate2996.
Talib, J., Woolnough, S. J., Klingaman, N. P., and Holloway, C. E. (2018a). The Role of the Cloud Radiative Effect in the Sensitivity of the Intertropical Convergence Zone to Convective Mixing. *J. Clim.* 31, 6821–6838. doi:10.1175/JCLI-D-17-0794.1.
Talib, J., Woolnough, S. J., Klingaman, N. P., and Holloway, C. E. (2018b). The Role of the Cloud Radiative Effect in the Sensitivity of the Intertropical Convergence Zone to Convective Mixing. *J. Clim.* 31, 6821–6838. doi:10.1175/JCLI-D-17-0794.1.
Tan, J., Jakob, C., Rossow, W. B., and Tselioudis, G. (2015). Increases in tropical rainfall driven by changes in frequency of organized deep convection. *Nature* 519, 451–454. doi:10.1038/nature14339.
Tan, J., Oreopoulos, L., Jakob, C., and Jin, D. (2018). Evaluating rainfall errors in global climate models through cloud regimes. *Clim. Dyn.* 50, 3301–3314. doi:10.1007/s00382-017-3806-7.
Tan, X., and Gan, T. Y. (2015). Contribution of human and climate change impacts to changes in streamflow of Canada. *Sci. Rep.* 5. doi:10.1038/srep17767.
Tandon, N. F., Zhang, X., and Sobel, A. H. (2018). Understanding the Dynamics of Future Changes in Extreme Precipitation Intensity. *Geophys. Res. Lett.* 45, 2870–2878. doi:10.1002/2017GL076361.
Tang, J., Riley, W. J., and Niu, J. (2015). Incorporating root hydraulic redistribution in CLM4.5: Effects on predicted site and global evapotranspiration, soil moisture, and water storage. *J. Adv. Model. Earth Syst.* 7, 1828–1848. doi:10.1002/2015MS000484.
Tang, Q., Zhang, X., and Francis, J. A. (2014). Extreme summer weather in northern mid-latitudes linked to a vanishing cryosphere. *Nat. Clim. Chang.* 4, 45–50. doi:10.1038/nclimate2065.
Tang, T., Shindell, D., Samset, B. H., Boucher, O., Forster, P. M., Hodnebrog, Ø., et al. (2018). Dynamical response of Mediterranean precipitation to greenhouse gases and aerosols. *Atmos. Chem. Phys.* 18, 8439–8452. doi:10.5194/acp-18-8439-2018.
Taniguchi, A., Shige, S., Yamamoto, M. K., Mega, T., Kida, S., Kubota, T., et al. (2013). Improvement of high-resolution satellite rainfall product for Typhoon Morakot (2009) over Taiwan. *J. Hydrometeorol.* 14, 1859–1871. Available at: https://doi.org/10.1175/JHM-D-13-047.1.
Tao, L., Zhao, J., and Li, T. (2015). Trend analysis of tropical intraseasonal oscillations in the summer and winter during 1982-2009. *Int. J. Climatol.* 35, 3969–3978. doi:10.1002/joc.4258.
Tapiador, F. J., Behrangi, A., Haddad, Z. S., Katsanos, D., and de Castro, M. (2016). Disruptions in precipitation cycles: Attribution to anthropogenic forcing. *J. Geophys. Res.* doi:10.1002/2015JD023406.
Taschetto, A. S., and Ambrizzi, T. (2012). Can Indian Ocean SST anomalies influence South American rainfall? *Clim. Dyn.* 38, 1615–1628. doi:10.1007/s00382-011-1165-3.
Taschetto, A. S., and England, M. H. (2009). An analysis of late twentieth century trends in Australian rainfall. *Int. J. Climatol.* 29, 791–807. doi:10.1002/joc.1736.
Tawfik, A. B., Dirmeyer, P. A., and Santanello, A. (2015a). The heated condensation framework. *Part I Descr. South. Gt. Plains case study, J. Hydrometeorol.* 16, 1929. Available at: https://doi.org/10.1175/JHM-D-14-0117.1.
Tawfik, A. B., Dirmeyer, P. A., and Santanello, A. (2015b). The heated condensation framework. *Part II Climatol. Behav. Convect. Initiat. Land–atmosph. coupling over conterminous United States, J. Hydrometeorol.* 16, 1946. Available at: https://doi.org/10.1175/JHM-D-14-0118.1.
Taylor, C. M. (2015). Detecting soil moisture impacts on convective initiation in Europe. *Geophys. Res. Lett.* 42, 4631–4638. doi:10.1002/2015GL064030.
Taylor, C. M., Belusic, D., Guichard, F., Parker, D. J., Vischel, T., Bock, O., et al. (2017a). Frequency of extreme Sahelian storms tripled since 1982 in satellite observations. *Nature* 544, 475–478. doi:10.1038/nature22069.
Taylor, C. M., Belušić, D., Guichard, F., Parker, D. J., Vischel, T., Bock, O., et al. (2017b). Frequency of extreme Sahelian storms tripled since 1982 in satellite observations. *Nature* 544, 475–478. doi:10.1038/nature22069.
Taylor, C. M., Birch, C. E., Parker, D. J., Dixon, N., Guichard, F., Nikulin, G., et al. (2013a). Modeling soil moisture-precipitation feedback in the Sahel: Importance of spatial scale versus convective parameterization. *Geophys. Res. Lett.* 40, 6213–6218. doi:10.1002/2013GL058511.
Taylor, R. G., Scanlon, B., Döll, P., Rodell, M., Van Beek, R., Wada, Y., et al. (2013b). Ground water and climate change. *Nat. Clim. Chang.* 3, 322–329. doi:10.1038/nclimate1744.
Tebaldi, C., and Arblaster, J. M. (2014). Pattern scaling: Its strengths and limitations, and an update on the latest model simulations. *Clim. Change* 122, 459–471. doi:10.1007/s10584-013-1032-9.
Tegen, I., and Schepanski, K. (2018). Climate feedback on aerosol emission and atmospheric concentrations. *Curr. Clim. Chang. Reports* 4, 1–10.

Terray, L., Corre, L., Cravatte, S., Delcroix, T., Reverdin, G., Ribes, A., et al. (2012). Near-Surface Salinity as Nature's Rain Gauge to Detect Human Influence on the Tropical Water Cycle. *J. Clim.* 25, 958–977. doi:10.1175/JCLI-D-10-05025.1.
Terzago, S., Fratianni, S., and Cremonini, R. (2013). Winter precipitation in Western Italian Alps (1926–2010). *Meteorol. Atmos. Phys.* 119, 125–136. doi:10.1007/s00703-012-0231-7.
Thackeray, C. W., and Fletcher, C. G. (2016a). Snow albedo feedback. *Prog. Phys. Geogr.* 40, 392–408. doi:10.1177/0309133315620999.
Thackeray, C. W., and Fletcher, C. G. (2016b). Snow albedo feedback. *Prog. Phys. Geogr.* 40, 392–408. doi:10.1177/0309133315620999.
Thackeray, C. W., Fletcher, C. G., and Derksen, C. (2015). Quantifying the skill of CMIP5 models in simulating seasonal albedo and snow cover evolution. *J. Geophys. Res. Atmos.* 120, 5831–5849. doi:10.1002/2015JD023325.
Thackeray, C. W., Fletcher, C. G., Mudryk, L. R., and Derksen, C. (2016). Quantifying the uncertainty in historical and future simulations of Northern Hemisphere spring snow cover. *J. Clim.* 29, 8647–8663. doi:10.1175/JCLI-D-16-0341.1.
Thompson, D. W. J., Barnes, E. A., Deser, C., Foust, W. E., and Phillips, A. S. (2015). Quantifying the Role of Internal Climate Variability in Future Climate Trends. *J. Clim.* 28, 6443–6456. doi:10.1175/JCLI-D-14-00830.1.
Thornalley, D. J. R., Oppo, D. W., Ortega, P., Robson, J. I., Brierley, C. M., Davis, R., et al. (2018). Anomalously weak Labrador Sea convection and Atlantic overturning during the past 150 years. *Nature*. doi:10.1038/s41586-018-0007-4.
Thornton, J. A., Virts, K. S., Holzworth, R. H., and Mitchell, T. P. (2017). Lightning enhancement over major oceanic shipping lanes. *Geophys. Res. Lett.* 44, 9102–9111. doi:10.1002/2017GL074982.
Thorpe, L., and Andrews, T. (2014). The physical drivers of historical and 21st century global precipitation changes. *Environ. Res. Lett.* 9, 64024. doi:10.1088/1748-9326/9/6/064024.
Tian, D., Dong, W., Gong, D., Guo, Y., and Yang, S. (2017). Fast responses of climate system to carbon dioxide, aerosols and sulfate aerosols without the mediation of SST in the CMIP5. *Int. J. Climatol.* 37, 1156–1166. doi:10.1002/joc.4763.
Tian, F., Dong, B., Robson, J., and Sutton, R. (2018a). Forced decadal changes in the East Asian summer monsoon: the roles of greenhouse gases and anthropogenic aerosols. *Clim. Dyn.* 51, 3699–3715. doi:10.1007/s00382-018-4105-7.
Tian, Z., Li, T., and Jiang, D. (2018b). Strengthening and Westward Shift of the Tropical Pacific Walker Circulation during the Mid-Holocene: PMIP Simulation Results. *J. Clim.* 31, 2283–2298. doi:10.1175/JCLI-D-16-0744.1.
Tierney, J. E., and deMenocal, P. B. (2013). Abrupt shifts in Horn of Africa hydroclimate since the last glacial maximum. *Science (80-.).* 342. doi:10.1126/science.1240411.
Tierney, J. E., Pausata, F. S. R., and deMenocal, P. B. (2017). Rainfall regimes of the Green Sahara. *Sci. Adv.* 3. doi:10.1126/sciadv.1601503.
Tierney, J. E., Russell, J. M., Huang, Y., Sinninghe Damsté, J. S., Hopmans, E. C., and Cohen, A. S. (2008). Northern hemisphere controls on tropical southeast African climate during the past 60,000 years. *Science (80-.).* doi:10.1126/science.1160485.
Tierney, J. E., Ummenhofer, C. C., and DeMenocal, P. B. (2015). Past and future rainfall in the Horn of Africa. *Sci. Adv.* 1, e1500682--e1500682. doi:10.1126/sciadv.1500682.
Tilinina, N., Gulev, S. K., and Bromwich, D. (2014). New view of Arctic cyclone activity from the Arctic System reanalysis. *Geophys. Res Lett* 43. doi:10.1002/2013GL058924.
Tilinina, N., Gulev, S. K., Rudeva, I., and Koltermann, P. (2013). Comparing cyclone life cycle characteristics and their interannual variability in different reanalyses. *J. Clim.* doi:10.1175/JCLI-D-12-00777.1.
Tillman, F. D., Gangopadhyay, S., and Pruitt, T. (2017). Changes in Projected Spatial and Seasonal Groundwater Recharge in the Upper Colorado River Basin. *Groundwater*. doi:10.1111/gwat.12507.
Tilmes, S., Fasullo, J., Lamarque, J. F., Marsh, D. R., Mills, M., Alterskjær, K., et al. (2013). The hydrological impact of geoengineering in the Geoengineering Model Intercomparison Project (GeoMIP). *J. Geophys. Res. Atmos.* doi:10.1002/jgrd.50868.
Timmermann, A., Okumura, Y., An, S. I., Clement, A., Dong, B., Guilyardi, E., et al. (2007). The influence of a weakening of the Atlantic meridional overturning circulation on ENSO. *J. Clim.* doi:10.1175/JCLI4283.1.
Todd Alexander (2018). Diagnosing ENSO and Global Warming Tropical Precipitation Shifts Using Surface Relative Humidity and Temperature. 1413–1433. doi:10.1175/JCLI-D-17-0354.1.
Todd, M. C., Taylor, R. G., Osborne, T., Gosling, S. N., Arnell, N. W., and Kingston, D. (2010). Quantifying the impact of climate change on water resources at the basin scale on five continents – a unified approach. *Hydrol. Earth Syst. Sci. Discuss.* doi:10.5194/hessd-7-7485-2010.
Tokinaga, H., Xie, S. P., Deser, C., Kosaka, Y., and Okumura, Y. M. (2012). Slowdown of the Walker circulation driven by tropical Indo-Pacific warming. *Nature* 491, 439–443. doi:10.1038/nature11576.
Trancoso, R., Larsen, J. R., McVicar, T. R., Phinn, S. R., and McAlpine, C. A. (2017). CO2-vegetation feedbacks and

other climate changes implicated in reducing base flow. *Geophys. Res. Lett.* doi:10.1002/2017GL072759.
Trenberth, K. E. (1999). "Conceptual Framework for Changes of Extremes of the Hydrological Cycle With Climate Change BT - Weather and Climate Extremes: Changes, Variations and a Perspective from the Insurance Industry," in *Weather and Climate Extremes* (Springer), 327–339. doi:10.1007/978-94-015-9265-9_18.
Trenberth, K. E. (2011). Changes in precipitation with climate change. *Clim. Res.* 47, 123–138. doi:10.3354/cr00953.
Trenberth, K. E., Branstator, G. W., Karoly, D., Kumar, A., Lau, N.-C., and Ropelewski, C. (1998). Progress during TOGA in understanding and modeling global teleconnections associated with tropical sea surface temperatures. *J. Geophys. Res. Ocean.* doi:10.1029/97JC01444.
Trenberth, K. E., Cheng, L., Jacobs, P., Zhang, Y., and Fasullo, J. (2018). Hurricane Harvey links to ocean heat content and climate change adaptation. *Earth's Futur.* 2018.
Trenberth, K. E., and Dai, A. (2007). Effects of Mount Pinatubo volcanic eruption on the hydrological cycle as an analog of geoengineering. *Geophys. Res. Lett.* 34. doi:10.1029/2007GL030524.
Trenberth, K. E., Dai, A., Rasmussen, R. M., and Parsons, D. B. (2003). The changing character of precipitation. *Bull. Am. Meteorol. Soc.* 84, 1205–1217+1161. doi:10.1175/BAMS-84-9-1205.
Trenberth, K. E., Fasullo, J. T., and Mackaro, J. (2011). Atmospheric moisture transports from ocean to land and global energy flows in reanalyses. *J. Clim.* 24, 4907–4924. doi:10.1175/2011JCLI4171.1.
Trenberth, K. E., Fasullo, J. T., and Shepherd, T. G. (2015). Attribution of climate extreme events. *Nat. Clim. Chang.* doi:10.1038/nclimate2657.
Trenberth, K. E., Zhang, Y., and Gehne, M. (2017). Intermittency in Precipitation: Duration, Frequency, Intensity, and Amounts Using Hourly Data. *J. Hydrometeorol.* 18, 1393–1412. doi:10.1175/JHM-D-16-0263.1.
Tsanis, I., and Tapoglou, E. (2019). Winter North Atlantic Oscillation impact on European precipitation and drought under climate change. *Theor. Appl. Climatol.* 135, 323–330. doi:10.1007/s00704-018-2379-7.
Turner, A. G., and Annamalai, H. (2012). Climate change and the South Asian summer monsoon. *Nat. Clim. Chang.* 2, 587–595. doi:10.1038/nclimate1495.
Turner, A. G., and Hannachi, A. (2010). Is there regime behavior in monsoon convection in the late 20th century? *Geophys. Res. Lett.* 37, 1–5. doi:10.1029/2010GL044159.
Turner, A. J., Fiore, A. M., Horowitz, L. W., and Bauer, M. (2013). Summertime cyclones over the Great Lakes Storm Track from 1860--2100: variability, trends, and association with ozone pollution. *Atmos. Chem* 13, 565–578. doi:10.5194/acp-13-565-2013.
Turner, J., Phillips, T., Thamban, M., Rahaman, W., Marshall, G. J., Wille, J. D., et al. (2019). The Dominant Role of Extreme Precipitation Events in Antarctic Snowfall Variability. *Geophys. Res. Lett.* doi:10.1029/2018GL081517.
Udall, B., and Overpeck, J. (2017). The twenty-first century Colorado River hot drought and implications for the future. *Water Resour. Res.* doi:10.1002/2016WR019638.
Uhe, P., Philip, S., Kew, S., Shah, K., Kimutai, J., Mwangi, E., et al. (2018). Attributing drivers of the 2016 Kenyan drought. *Int. J. Climatol.* doi:10.1002/joc.5389.
Ukkola, A. M., Prentice, I. C., Keenan, T. F., Van Dijk, A. I. J. M., Viney, N. R., Myneni, R. B., et al. (2016). Reduced streamflow in water-stressed climates consistent with CO2 effects on vegetation. *Nat. Clim. Chang.* doi:10.1038/nclimate2831.
Ummenhofer, C. C., England, M. H., McIntosh, P. C., Meyers, G. A., Pook, M. J., Risbey, J. S., et al. (2009a). What causes southeast Australia's worst droughts? *Geophys. Res. Lett.* 36, L04706. doi:10.1029/2008GL036801.
Ummenhofer, C. C., Sen Gupta, A., England, M. H., and Reason, C. J. C. (2009b). Contributions of Indian Ocean Sea Surface Temperatures to Enhanced East African Rainfall. *J. Clim.* 22, 993–1013. doi:10.1175/2008JCLI2493.1.
Undorf, S., Bollasina, M. A., and Hegerl, G. C. (2018a). Impacts of the 1900--74 Increase in Anthropogenic Aerosol Emissions from North America and Europe on Eurasian Summer Climate. *J. Clim.* 31, 8381–8399.
Undorf, S., Polson, D., Bollasina, M. A., Ming, Y., Schurer, A., and Hegerl, G. C. (2018b). Detectable Impact of Local and Remote Anthropogenic Aerosols on the 20th Century Changes of West African and South Asian Monsoon Precipitation. *J. Geophys. Res. Atmos.* 123, 4871–4889. doi:10.1029/2017JD027711.
Urrutia-Jalabert, R., González, M. E., González-Reyes, Á., Lara, A., and Garreaud, R. (2018). Climate variability and forest fires in central and south-central Chile. *Ecosphere* 9, e02171. doi:10.1002/ecs2.2171.
Van Den Hurk, B., Kim, H., Krinner, G., Seneviratne, S. I., Derksen, C., Oki, T., et al. (2016). LS3MIP (v1.0) contribution to CMIP6: The Land Surface, Snow and Soil moisture Model Intercomparison Project - Aims, setup and expected outcome. *Geosci. Model Dev.* 9, 2809–2832. doi:10.5194/gmd-9-2809-2016.
Van Der Ent, R. J., Keys, P. W., and Savenije, H. H. G. (2014). Contrasting roles of interception and transpiration in the hydrological cycle – Part 2 : Moisture recycling. *Earth Syst. Dyn.* 5, 471–489. doi:10.5194/esd-5-471-2014.
van der Ent, R. J., and Savenije, H. H. G. (2013). Oceanic sources of continental precipitation and the correlation with sea surface temperature. *Water Resour. Res.* 49, 3993–4004. doi:10.1002/wrcr.20296.
Van Loon, A. F., Gleeson, T., Clark, J., Van Dijk, A. I. J. M., Stahl, K., Hannaford, J., et al. (2016). Drought in the Anthropocene. *Nat. Geosci.* 9, 89.
Van Nes, E. H., and Scheffer, M. (2005). Implications of spatial heterogeneity for catastrophic regime shifts in

ecosystems. *Ecology* 86, 1797–1807. doi:10.1890/04-0550.
van Niekerk, A., Scinocca, J. F., and Shepherd, T. G. (2017). The Modulation of Stationary Waves, and Their Response to Climate Change, by Parameterized Orographic Drag. *J. Atmos. Sci.* 74, 2557–2574. doi:10.1175/JAS-D-17-0085.1.
Van Oldenborgh, G. J., van der Wiel, K., Sebastian, A., Singh, R., Arrighi, J., Otto, F., et al. (2017). Attribution of extreme rainfall from Hurricane Harvey, August 2017. *Environ. Res* 12, 12400.
Vanniere, B., Demory, M.-E., Vidale, P. L., Schiemann, R., Roberts, M. J., Roberts, C., et al. (2018). Multi-model evaluation of the sensitivity of the global energy budget and hydrological cycle to resolution. *Clim. Dyn. print*. doi:10.1007/s00382-018-4547-y.
Varble, A. (2018). Erroneous attribution of deep convective invigoration to aerosol concentration. *J. Atmos. Sci* 75, 1351–1368.
Varino, F., Arbogast, P., Joly, B., Riviere, G., Fandeur, M., Bovy, H., et al. (2019). Northern Hemisphere extratropical winter cyclones variability over the 20th century derived from ERA-20C reanalysis. *Clim. Dyn.* 52, 1027–1048.
Vazifehkhah, S., and Kahya, E. (2018). Hydrological drought associations with extreme phases of the North Atlantic and Arctic Oscillations over Turkey and northern Iran. *Int. J. Climatol.* 38, 4459–4475. doi:10.1002/joc.5680.
Vázquez, M., Nieto, R., Drumond, A., and Gimeno, L. (2018). Moisture transport from the arctic: A characterization from a lagrangian perspective. *Geogr. Res. Lett.* 44, 659–673. doi:10.18172/cig.3477.
Vecchi, G. A., and Soden, B. J. (2007). Global warming and the weakening of the tropical circulation. *J. Clim.* doi:10.1175/JCLI4258.1.
Vecchi, G. A., Soden, B. J., Wittenberg, A. T., Held, I. M., Leetmaa, A., and Harrison, M. J. (2006). Weakening of tropical Pacific atmospheric circulation due to anthropogenic forcing. *Nature* 441, 73–76. doi:10.1038/nature04744.
Vega, I., Gallego, D., Ribera, P., de Paula Gómez-Delgado, F., García-Herrera, R., and Peña-Ortiz, C. (2018). Reconstructing the Western North Pacific Summer Monsoon since the Late Nineteenth Century. *J. Clim.* 31, 355–368. doi:10.1175/JCLI-D-17-0336.1.
Velasco, E. M., Gurdak, J. J., Dickinson, J. E., Ferré, T. P. A., and Corona, C. R. (2017a). Interannual to multidecadal climate forcings on groundwater resources of the U.S. West Coast. *J. Hydrol. Reg. Stud.* 11, 250–265. doi:10.1016/j.ejrh.2015.11.018.
Velasco, E. M., Gurdak, J. J., Dickinson, J. E., Ferré, T. P. A., and Corona, C. R. (2017b). Interannual to multidecadal climate forcings on groundwater resources of the U.S. West Coast. *J. Hydrol. Reg. Stud.* 11, 250–265. doi:10.1016/j.ejrh.2015.11.018.
Veldkamp, T. I. E., Zhao, F., Ward, P. J., de Moel, H., Aerts, J. C. J. H., Schmied, H. M., et al. (2018). Human impact parameterizations in global hydrological models improve estimates of monthly discharges and hydrological extremes: a multi-model validation study. *Environ. Res. Lett.* 13, 055008. doi:10.1088/1748-9326/aab96f.
Vera, C., and Diaz, L. B. (2015). Anthropogenic influence on summer precipitation trends over South America in CMIP5 models. *Int. J. Climatol.* 35, 3172–3177.
Vera, C. S., and Osman, M. (2018). Activity of the Southern Annular Mode during 2015-2016 El Niño event and its impact on Southern Hemisphere climate anomalies. *Int. J. Climatol.* 38, e1288–e1295. doi:10.1002/joc.5419.
Vergnes, J.-P., Decharme, B., and Habets, F. (2014). Introduction of groundwater capillary rises using subgrid spatial variability of topography into the ISBA land surface model. *J. Geophys. Res. Atmos.* 119, 11,065-11,086. doi:10.1002/2014JD021573.
Verseghy, D. L., and MacKay, M. D. (2017). Offline Implementation and Evaluation of the Canadian Small Lake Model with the Canadian Land Surface Scheme over Western Canada. *J. Hydrometeorol.* 18, 1563. Available at: https://doi.org/10.1175/JHM-D-16-0272.1.
Vihma, T. (2014). Effects of Arctic Sea Ice Decline on Weather and Climate: A Review. *Surv. Geophys.* 35, 1175–1214. doi:10.1007/s10712-014-9284-0.
Vilasa, L., Miralles, D. G., de Jeu, R. A. M., and Dolman, A. J. (2017). Global soil moisture bimodality in satellite observations and climate models. *J. Geophys. Res. Atmos.* 122, 4299–4311. doi:10.1002/2016JD026099.
Villafuerte, M. Q., and Matsumoto, J. (2015). Significant Influences of Global Mean Temperature and ENSO on Extreme Rainfall in Southeast Asia. *J. Clim.* 28, 1905–1919. doi:10.1175/JCLI-D-14-00531.1.
Vitart, F. (2014). Evolution of ECMWF sub-seasonal forecast skill scores. *Q. J. R. Meteorol. Soc.* 140, 1889–1899. doi:10.1002/qj.2256.
Vitart, F. (2017). Madden-Julian Oscillation prediction and teleconnections in the S2S database. *Q. J. R. Meteorol. Soc.* 143, 2210–2220. doi:10.1002/qj.3079.
Vitart, F., and Robertson, A. W. (2018). The sub-seasonal to seasonal prediction project (S2S) and the prediction of extreme events. *npj Clim. Atmos. Sci.* 1, 3. doi:10.1038/s41612-018-0013-0.
Vittal, H., Ghosh, S., Karmakar, S., Pathak, A., and Murtugudde, R. (2016). Lack of Dependence of Indian Summer Monsoon Rainfall Extremes on Temperature: An Observational Evidence. *Sci. Rep.* 6. doi:10.1038/srep31039.
Vizy, E. K., and Cook, K. H. (2016). Understanding long-term (1982–2013) multi-decadal change in the equatorial and

subtropical South Atlantic climate. *Clim. Dyn.* 46, 2087–2113. doi:10.1007/s00382-015-2691-1.

Vizy, E. K., Cook, K. H., Vizy, E. K., and Cook, K. H. (2017). Seasonality of the Observed Amplified Sahara Warming Trend and Implications for Sahel Rainfall. *J. Clim.* 30, 3073–3094. doi:10.1175/JCLI-D-16-0687.1.

Voelker, S. L., Stambaugh, M. C., Guyette, R. P., Feng, X., Grimley, D. A., Leavitt, S. W., et al. (2015). Deglacial hydroclimate of midcontinental North America. *Quat. Res. (United States)*. doi:10.1016/j.yqres.2015.01.001.

Vogel, M. M., Orth, R., Cheruy, F., Hagemann, S., Lorenz, R., van den Hurk, B. J. J. M., et al. (2017). Regional amplification of projected changes in extreme temperatures strongly controlled by soil moisture-temperature feedbacks. *Geophys. Res. Lett.* 44, 1511–1519. doi:10.1002/2016GL071235.

Voss, K. A., Famiglietti, J. S., Lo, M., de Linage, C., Rodell, M., and Swenson, S. C. (2013). Groundwater depletion in the Middle East from GRACE with implications for transboundary water management in the Tigris-Euphrates-Western Iran region. *Water Resour. Res.* 49, 904–914. doi:10.1002/wrcr.20078.

Vuille, M., Burns, S. J., Taylor, B. L., Cruz, F. W., Bird, B. W., Abbott, M. B., et al. (2012). A review of the South American monsoon history as recorded in stable isotopic proxies over the past two millennia. *Clim. Past* 8, 1309–1321. doi:10.5194/cp-8-1309-2012.

Wada, Y., and Bierkens, M. F. P. (2014). Sustainability of global water use: Past reconstruction and future projections. *Environ. Res. Lett.* 9, 104003. doi:10.1088/1748-9326/9/10/104003.

Wada, Y., Van Beek, L. P. H., Van Kempen, C. M., Reckman, J. W. T. M., Vasak, S., and Bierkens, M. F. P. (2010). Global depletion of groundwater resources. *Geophys. Res. Lett.* 37, 1–5. doi:10.1029/2010GL044571.

Wagner, J. D. M., Cole, J. E., Beck, J. W., Patchett, P. J., Henderson, G. M., and Barnett, H. R. (2010). Moisture variability in the southwestern United States linked to abrupt glacial climate change. *Nat. Geosci.* doi:10.1038/ngeo707.

Waliser, D. E., Gautier, C., Waliser, D. E., and Gautier, C. (1993). A Satellite-derived Climatology of the ITCZ. *J. Clim.* 6, 2162–2174. doi:10.1175/1520-0442(1993)006<2162:ASDCOT>2.0.CO;2.

Waliser, D., and Guan, B. (2017). Extreme winds and precipitation during landfall of atmospheric rivers. *Nat. Geosci.* 10, 179–183. doi:10.1038/ngeo2894.

Walker, G. T. (1925). Correlation in seasonal variations of weather: A further study of world weather. *Mon. Weather Rev.* 53, 252–254. doi:10.1175/1520-0493(1925)53<252:CISVOW>2.0.CO;2.

Walsh, K. J. E., Camargo, S. J., Vecchi, G. A., Daloz, A. S., Elsner, J., Emanuel, K., et al. (2015). Hurricanes and climate: The U.S. Clivar working group on hurricanes. *Bull. Am. Meteorol. Soc.* 96, 997–1017. doi:10.1175/BAMS-D-13-00242.1.

Walsh, K. J. E., McBride, J. L., Klotzbach, P. J., Balachandran, S., Camargo, S. J., Holland, G., et al. (2016). Tropical cyclones and climate change. *Wiley Interdiscip. Rev. Clim. Chang.* 7, 65–89. doi:10.1002/wcc.371.

Walvoord, M. A., and Kurylyk, B. L. (2016). Hydrologic Impacts of Thawing Permafrost—A Review. *Vadose Zo. J.* 15, 0. doi:10.2136/vzj2016.01.0010.

Wang-Erlandsson, L., van der Ent, R. J., Gordon, L. J., and Savenije, H. H. G. (2014). Contrasting roles of interception and transpiration in the hydrological cycle – Part 1 : Temporal characteristics over land. *Earth Syst. Dyn.* 5, 441–469. doi:10.5194/esd-5-441-2014.

Wang, B., and Ding, Q. (2006). Changes in global monsoon precipitation over the past 56 years. *Geophys. Res. Lett.* 33.

Wang, B., Li, J., Cane, M. A., Liu, J., Webster, P. J., Xiang, B., et al. (2018a). Toward Predicting Changes in the Land Monsoon Rainfall a Decade in Advance. *J. Clim.* 31, 2699–2714. doi:10.1175/JCLI-D-17-0521.1.

Wang, B., and LinHo (2002). Rainy Season of the Asian–Pacific Summer Monsoon*. *J. Clim.* 15, 386–398. doi:10.1175/1520-0442(2002)015<0386:RSOTAP>2.0.CO;2.

Wang, B., Liu, J., Kim, H.-J., Webster, P. J., and Yim, S.-Y. (2012). Recent change of the global monsoon precipitation (1979–2008). *Clim. Dyn.* 39, 1123–1135. doi:10.1007/s00382-011-1266-z.

Wang, B., Liu, J., Kim, H.-J., Webster, P. J., Yim, S.-Y., and Xiang, B. (2013a). Northern Hemisphere summer monsoon intensified by mega-El Nino/southern oscillation and Atlantic multidecadal oscillation. *Proc. Natl. Acad. Sci.* 110, 5347–5352. doi:10.1073/pnas.1219405110.

Wang, B., Wu, R., and Lau, K.-M. (2001). Interannual Variability of the Asian Summer Monsoon: Contrasts between the Indian and the Western North Pacific–East Asian Monsoons*. *J. Clim.* 14, 4073–4090. doi:10.1175/1520-0442(2001)014<4073:IVOTAS>2.0.CO;2.

Wang, B., Xiang, B., Li, J., Webster, P. J., Rajeevan, M. N., Liu, J., et al. (2015). Rethinking Indian monsoon rainfall prediction in the context of recent global warming. *Nat. Commun.* 6, 7154. doi:10.1038/ncomms8154.

Wang, C., and Wang, X. (2013). Classifying El Niño Modoki I and II by Different Impacts on Rainfall in Southern China and Typhoon Tracks. *J. Clim.* 26, 1322–1338. doi:10.1175/JCLI-D-12-00107.1.

Wang, G., Wang, D., Trenberth, K. E., Erfanian, A., Yu, M., Bosilovich, M. G., et al. (2017a). The peak structure and future changes of the relationships between extreme precipitation and temperature. *Nat. Clim. Chang.* 7, 268–274. doi:10.1038/nclimate3239.

Wang, J., Kim, H.-M., and Chang, E. K. M. (2017b). Changes in Northern Hemisphere Winter Storm Tracks under the Background of Arctic Amplification. *J. Clim.* 30, 3705–3724. doi:10.1175/JCLI-D-16-0650.1.

Wang, L., Cole, J. N. S., Bartlett, P., Verseghy, D., Derksen, C., Brown, R., et al. (2016a). Journal of Geophysical Research : Atmospheres for snow-covered forests in CMIP5 models. 1104–1119. doi:10.1002/2015JD023824.Received.

Wang, L., Kushner, P. J., and Waugh, D. W. (2013b). Southern hemisphere stationary wave response to changes of ozone and greenhouse gases. *J. Clim.* 26, 10205–10217. doi:10.1175/JCLI-D-13-00160.1.

Wang, L., and Yu, J.-Y. (2018). A Recent Shift in the Monsoon Centers Associated with the Tropospheric Biennial Oscillation. *J. Clim.* 31, 325–340. doi:10.1175/JCLI-D-17-0349.1.

Wang, P. X., Wang, B., Cheng, H., Fasullo, J., Guo, Z. T., Kiefer, T., et al. (2017c). The global monsoon across time scales: Mechanisms and outstanding issues. *Earth-Science Rev.* doi:10.1016/j.earscirev.2017.07.006.

Wang, Q., Wang, Z., and Zhang, H. (2017d). Impact of anthropogenic aerosols from global, East Asian, and non-East Asian sources on East Asian summer monsoon system. *Atmos. Res.* 183, 224–236. doi:10.1016/j.atmosres.2016.08.023.

Wang, S. S. -y., Zhao, L., Yoon, J. -h., Klotzbach, P., and Gillies, R. R. (2018b). Quantitative attribution of climate effects on Hurricane Harvey's extreme rainfall in Texas. *Environ. Res* 13.

Wang, T., Wang, H. J., Otterå, O. H., Gao, Y. Q., Suo, L. L., Furevik, T., et al. (2013c). Anthropogenic agent implicated as a prime driver of shift in precipitation in eastern China in the late 1970s. *Atmos. Chem. Phys.* 13, 12433–12450. doi:10.5194/acp-13-12433-2013.

Wang, W., Lee, X., Xiao, W., Liu, S., Schultz, N., Wang, Y., et al. (2018c). Global lake evaporation accelerated by changes in surface energy allocation in a warmer climate. *Nat. Geosci.* 11, 410–414. doi:10.1038/s41561-018-0114-8.

Wang, X. L., Feng, Y., Chan, R., and Isaac, V. (2016b). Inter-comparison of extra-tropical cyclone activity in nine reanalysis datasets. *Atmos. Res.* doi:10.1016/j.atmosres.2016.06.010.

Wang, X. L., Feng, Y., Compo, G. P., Swail, V. R., Zwiers, F. W., Allan, R. J., et al. (2013d). Trends and low frequency variability of extra-tropical cyclone activity in the ensemble of twentieth century reanalysis. *Clim. Dyn.* 40, 2775–2800. doi:10.1007/s00382-012-1450-9.

Wang, Y., Khalizov, A., Levy, M., and Zhang, R. (2013e). New Directions: Light absorbing aerosols and their atmospheric impacts. *Atmos. Environ.* 81, 713–715. doi:10.1016/J.ATMOSENV.2013.09.034.

Wang, Y., Lee, K.-H., Lin, Y., Levy, M., and Zhang, R. (2014). Distinct effects of anthropogenic aerosols on tropical cyclones. *Nat. Clim. Chang.* 4, 368–373. doi:10.1038/nclimate2144.

Wang, Z., Lin, L., Yang, M., Xu, Y., and Li, J. (2017e). Disentangling fast and slow responses of the East Asian summer monsoon to reflecting and absorbing aerosol forcings. *Atmos. Chem. Phys.* 17, 11075–11088.

Wang, Z., Yang, S., Lau, N.-C., and Duan, A. (2018d). Teleconnection between Summer NAO and East China Rainfall Variations: A Bridge Effect of the Tibetan Plateau. *J. Clim.* 31, 6433–6444. doi:10.1175/JCLI-D-17-0413.1.

Warner, M. D., and Mass, C. F. (2017). Changes in the Climatology, Structure, and Seasonality of Northeast Pacific Atmospheric Rivers in CMIP5 Climate Simulations. *J. Hydrometeorol.* doi:10.1175/jhm-d-16-0200.1.

Warner, M. D., Mass, C. F., and Salathé, E. P. (2015). Changes in Winter Atmospheric Rivers along the North {A}merican West Coast in CMIP5 Climate Models. *J. Hydrometeorol.* 16, 118–128.

Wasko, C., Parinussa, R. M., and Sharma, A. (2016a). A quasi-global assessment of changes in remotely sensed rainfall extremes with temperature. *Geophys. Res. Lett.* 43, 12,659-12,668. doi:10.1002/2016GL071354.

Wasko, C., and Sharma, A. (2015). Steeper temporal distribution of rain intensity at higher temperatures within Australian storms. *Nat. Geosci.* 8, 527–529. doi:10.1038/ngeo2456.

Wasko, C., Sharma, A., and Westra, S. (2016b). Reduced spatial extent of extreme storms at higher temperatures. *Geophys. Res. Lett.* 43, 4026–4032. doi:10.1002/2016GL068509.

Watanabe, M., Kamae, Y., Shiogama, H., DeAngelis, A. M., and Suzuki, K. (2018). Low clouds link equilibrium climate sensitivity to hydrological sensitivity. *Nat. Clim. Chang.*, 1. doi:10.1038/s41558-018-0272-0.

Weaver, A. J., Sedláček, J., Eby, M., Alexander, K., Crespin, E., Fichefet, T., et al. (2012). Stability of the Atlantic meridional overturning circulation: A model intercomparison. *Geophys. Res. Lett.* doi:10.1029/2012GL053763.

Webb, M. J., Lock, A. P., and Lambert, F. H. (2018). Interactions between hydrological sensitivity, radiative cooling, stability, and low-level cloud amount feedback. *J. Clim.* 31, 1833–1850. doi:10.1175/JCLI-D-16-0895.1.

Webb, N. P., and Pierre, C. (2018). Quantifying anthropogenic dust emissions. *Earth's Futur.* 6, 286–295.

Weiss, J. L., Castro, C. L., and Overpeck, J. T. (2009). Distinguishing pronounced droughts in the southwestern United States: seasonality and effects of warmer temperatures. *J. Clim.* 22, 5918–5932.

Weiss, M., Miller, P. A., van den Hurk, B. J. J. M., van Noije, T., Ştefănescu, S., Haarsma, R., et al. (2014). Contribution of dynamic vegetation phenology to decadal climate predictability. *J. Clim.* 27, 8563–8577. doi:10.1175/JCLI-D-13-00684.1.

Weller, E., and Cai, W. (2013). Realism of the Indian Ocean Dipole in CMIP5 Models: The Implications for Climate Projections. *J. Clim.* 26, 6649–6659. doi:10.1175/JCLI-D-12-00807.1.

Weller, E., Jakob, C., and Reeder, M. J. (2017). Projected Response of Low-Level Convergence and Associated Precipitation to Greenhouse Warming. *Geophys. Res. Lett.* 44, 10,682-10,690. doi:10.1002/2017GL075489.

Wen, C., Chang, P., and Saravanan, R. (2011). Effect of Atlantic meridional overturning circulation on tropical atlantic variability: A regional coupled model study. *J. Clim.* doi:10.1175/2011JCLI3845.1.
Wen, N., Liu, Z., and Li, L. (2018). Direct ENSO impact on East Asian summer precipitation in the developing summer. *Clim. Dyn.* doi:10.1007/s00382-018-4545-0.
Weng, H., Behera, S. K., and Yamagata, T. (2009). Anomalous winter climate conditions in the Pacific rim during recent El Niño Modoki and El Niño events. *Clim. Dyn.* 32, 663–674. doi:10.1007/s00382-008-0394-6.
Wentz, F. J., Ricciardulli, L., Hilburn, K., and Mears, C. (2007). How Much More Rain Will Global Warming Bring? *Science (80-.).* 317, 233–235. doi:10.1126/science.1140746.
Wester, P., Mishra, A., Mukherji, A., and Shrestha, A. B. (2019). *The Hindu Kush Himalaya Assessment*. International Publishing: Springer doi:10.1007/978-3-319-92288-1.
Westervelt, D. M., Conley, A. J., Fiore, A. M., Lamarque, J.-F., Shindell, D. T., Previdi, M., et al. (2018). Connecting regional aerosol emissions reductions to local and remote precipitation responses. *Atmos. Chem. Phys.* 18, 12461–12475.
Westervelt, D. M., Horowitz, L. W., Naik, V., Golaz, J. C., and Mauzerall, D. L. (2015). Radiative forcing and climate response to projected 21st century aerosol decreases. *Atmos. Chem. Phys.* doi:10.5194/acp-15-12681-2015.
Westra, S., Alexander, L. V., and Zwiers, F. W. (2013). Global increasing trends in annual maximum daily precipitation. *J. Clim.* doi:10.1175/JCLI-D-12-00502.1.
Westra, S., Fowler, H. J., Evans, J. P., Alexander, L. V., Berg, P., Johnson, F., et al. (2014). Future changes to the intensity and frequency of short-duration extreme rainfall. *Rev. Geophys.* 52, 522–555. doi:10.1002/2014RG000464.
Widlansky, M. J., Annamalai, H., Gingerich, S. B., Storlazzi, C. D., Marra, J. J., Hodges, K. I., et al. (2019). Tropical Cyclone Projections: Changing Climate Threats for Pacific Island Defense Installations. *Weather. Clim. Soc.* 11, 3–15. doi:10.1175/WCAS-D-17-0112.1.
Wilcox, C., Puckridge, M., Schuyler, Q. A., Townsend, K., and Hardesty, B. D. (2018). A quantitative analysis linking sea turtle mortality and plastic debris ingestion. *Sci. Reports 2018 81* 8, 12536. doi:10.1038/s41598-018-30038-z.
Wilcox, L. J., Dong, B., Sutton, R. T., and Highwood, E. J. (2015). The 2014 Hot, Dry Summer in Northeast Asia. *Bull. Am. Meteorol. Soc.* 96, S105–S110. doi:10.1175/BAMS-D-15-00123.1.
Wild, M. (2012). Enlightening Global Dimming and Brightening. *Bull. Am. Meteorol. Soc.* 93, 27–37. doi:10.1175/BAMS-D-11-00074.1.
Wilhite, D. A. (2000). Chapter I Drought as a Natural Hazard: Concepts and Definitions. *Drought A Glob. Assess.* doi:10.1177/0956247807076912.
Wilhite, D. A., and Glantz, M. H. (1985). Understanding: The drought phenomenon: The role of definitions. *Water Int.* doi:10.1080/02508068508686328.
Willett, K. M., Dunn, R. J. H., Thorne, P. W., Bell, S., De Podesta, M., Parker, D. E., et al. (2014). HadISDH land surface multi-variable humidity and temperature record for climate monitoring. *Clim. Past* 10, 1983–2006. doi:10.5194/cp-10-1983-2014.
Williams, A. P., Seager, R., Abatzoglou, J. T., Cook, B. I., Smerdon, J. E., and Cook, E. R. (2015). Contribution of anthropogenic warming to California drought during 2012-2014. *Geophys. Res. Lett.* doi:10.1002/2015GL064924.
Willison, J., Robinson, W. A., and Lackmann, G. M. (2015). North Atlantic Storm-Track Sensitivity to Warming Increases with Model Resolution. *J. Clim.* 28, 4513–4524. doi:10.1175/JCLI-D-14-00715.1.
Wills, R. C., Byrne, M. P., and Schneider, T. (2016a). Thermodynamic and dynamic controls on changes in the zonally anomalous hydrological cycle. *Geophys. Res. Lett.* 43, 4640–4649. doi:10.1002/2016GL068418.
Wills, R. C., Byrne, M. P., and Schneider, T. (2016b). Thermodynamic and dynamic controls on changes in the zonally anomalous hydrological cycle. *Geophys. Res. Lett.* 43, 4640–4649. doi:10.1002/2016GL068418.
Wills, R. C., and Schneider, T. (2016). How stationary eddies shape changes in the hydrological cycle: Zonally asymmetric experiments in an idealized GCM. *J. Clim.* 29, 3161–3179. doi:10.1175/JCLI-D-15-0781.1.
Wing, A. A., Emanuel, K., Holloway, C. E., and Muller, C. (2017). Convective Self-Aggregation in Numerical Simulations: A Review. *Surv. Geophys.* 38, 1173–1197. doi:10.1007/s10712-017-9408-4.
Wise, E. K., and Dannenberg, M. P. (2017). Reconstructed storm tracks reveal three centuries of changing moisture delivery to North America. *Sci. Adv* 2017, 3.
Wodzicki, K. R., and Rapp, A. D. (2016). Long-term characterization of the Pacific ITCZ using TRMM, GPCP, and ERA-Interim. *J. Geophys. Res. Atmos.* 121, 3153–3170. doi:10.1002/2015JD024458.
Woldemeskel, F., and Sharma, A. (2016). Should flood regimes change in a warming climate? The role of antecedent moisture conditions. *Geophys. Res. Lett.* 43, 7556–7563. doi:10.1002/2016GL069448.
Wolding, B. O., Maloney, E. D., Henderson, S., and Branson, M. (2017). Climate change and the Madden-Julian Oscillation: A vertically resolved weak temperature gradient analysis. *J. Adv. Model. Earth Syst.* 9, 307–331. doi:10.1002/2016MS000843.
Woodhouse, C. A., Pederson, G. T., Morino, K., McAfee, S. A., and McCabe, G. J. (2016). Increasing influence of air

temperature on upper Colorado River streamflow. *Geophys. Res. Lett.* doi:10.1002/2015GL067613.
Woollings, T., Barriopedro, D., Methven, J., Son, S. W., Martius, O., Harvey, B., et al. (2018a). Blocking and its Response to Climate Change. *Curr. Clim. Chang. Reports* 4, 287–300. doi:10.1007/s40641-018-0108-z.
Woollings, T., Barriopedro, D., Methven, J., Son, S. W., Martius, O., Harvey, B., et al. (2018b). Blocking and its Response to Climate Change. *Curr. Clim. Chang. Reports* 4, 287–300. doi:10.1007/s40641-018-0108-z.
Woolway, R. I., and Merchant, C. J. (2019). Worldwide alteration of lake mixing regimes in response to climate change. *Nat. Geosci. 2019* 12. doi:10.1038/s41561-019-0322-x.
Wooster, M. J., Perry, G. L. W., and Zoumas, A. (2012). Fire, drought and El Niño relationships on Borneo (Southeast Asia) in the pre-MODIS era (1980–2000). *Biogeosciences* 9, 317–340. doi:10.5194/bg-9-317-2012.
Wortham, B. E., Wong, C. I., Silva, L. C. R., McGee, D., Montañez, I. P., Rasbury, T. E., et al. (2017). Assessing response of local moisture conditions in central Brazil to variability in regional monsoon intensity using speleothem 87 Sr/ 86 Sr values. *Earth Planet. Sci. Lett.* 463, 310–322. doi:10.1016/j.epsl.2017.01.034.
Wright, J. S., Fu, R., Worden, J. R., Chakraborty, S., Clinton, N. E., Risi, C., et al. (2017). Rainforest-initiated wet season onset over the southern Amazon. *Proc. Natl. Acad. Sci.* 114, 8481–8486. doi:10.1073/pnas.1621516114.
Wu, P., Christidis, N., and Stott, P. (2013). Anthropogenic impact on Earth's hydrological cycle. *Nat. Clim. Chang.* 3, 807–810. doi:10.1038/nclimate1932.
Wu, P., Wood, R., Ridley, J., and Lowe, J. (2010). Temporary acceleration of the hydrological cycle in response to a CO 2 rampdown. *Geophys. Res* 37. doi:10.1029/2010GL043730.
Wu, X., Che, T., Li, X., Wang, N., and Yang, X. (2018a). Slower snowmelt in spring along with climate warming across the Northern Hemisphere. *Geophys. Res. Lett.* doi:10.1029/2018GL079511.
Wu, X., Che, T., Li, X., Wang, N., and Yang, X. (2018b). Slower snowmelt in spring along with climate warming across the Northern Hemisphere. *Geophys. Res. Lett.* 45, 12,331-12,339. doi:10.1029/2018GL079511.
Wurtzel, J. B., Abram, N. J., Lewis, S. C., Bajo, P., Hellstrom, J. C., Troitzsch, U., et al. (2018). Tropical Indo-Pacific hydroclimate response to North Atlantic forcing during the last deglaciation as recorded by a speleothem from Sumatra, Indonesia. *Earth Planet. Sci. Lett.* doi:10.1016/j.epsl.2018.04.001.
Xia, Y., and Huang, Y. (2017). Differential Radiative Heating Drives Tropical Atmospheric Circulation Weakening. *Geophys. Res. Lett.* 44, 10,592-10,600. doi:10.1002/2017GL075678.
Xiang, B., Zhao, M., Held, I. M., and Golaz, J. C. (2017). Predicting the severity of spurious "double ITCZ" problem in CMIP5 coupled models from AMIP simulations. *Geophys. Res. Lett.* 44, 1520–1527. doi:10.1002/2016GL071992.
Xiao, M., Udall, B., and Lettenmaier, D. P. (2018). On the Causes of Declining Colorado River Streamflows. *Water Resour. Res.* doi:10.1029/2018WR023153.
Xiao, M., Zhang, Q., and Singh, V. P. (2015). Influences of ENSO, NAO, IOD and PDO on seasonal precipitation regimes in the Yangtze River basin, China. *Int. J. Climatol.* 35, 3556–3567. doi:10.1002/joc.4228.
Xie, S.-P., Deser, C., Vecchi, G. A., Collins, M., Delworth, T. L., Hall, A., et al. (2015). Towards predictive understanding of regional climate change. *Nat. Clim. Chang.* 5, 921–930. doi:10.1038/nclimate2689.
Xie, S.-P., Lu, B., and Xiang, B. (2013). Similar spatial patterns of climate responses to aerosol and greenhouse gas changes. *Nat. Geosci.* 6, 828–832. doi:10.1038/ngeo1931.
Xie, S. P., Deser, C., Vecchi, G. A., Ma, J., Teng, H., and Wittenberg, A. T. (2010). Global warming pattern formation: Sea surface temperature and rainfall. *J. Clim.* 23, 966–986. doi:10.1175/2009JCLI3329.1.
Xie, X., Wang, H., Liu, X., Li, J., Wang, Z., and Liu, Y. (2016). Distinct effects of anthropogenic aerosols on the East Asian summermonsoon between multidecadal strong and weakmonsoon stages. *J. Geophys. Res.* 121, 7026–7040. doi:10.1002/2015JD024228.
Xu, L., and Yu, J.-Y. (2018). An ENSO-induced aerosol dipole in the west-central Pacific and its potential feedback to ENSO evolution. *Clim. Dyn.*, 1–11. doi:10.1007/s00382-018-4435-5.
Xu, S., and Huang, F. (2015). Impacts of the two types of El Niño on Pacific tropical cyclone activity. *J. Ocean Univ. China* 14, 191–198. doi:10.1007/s11802-015-2421-7.
Xu, T., Valocchi, A. J., Ye, M., Liang, F., and Lin, Y.-F. (2017a). Bayesian calibration of groundwater models with input data uncertainty. *Water Resour. Res.* 53, 3224–3245. doi:10.1002/2016WR019512.
Xu, T., Valocchi, A. J., Ye, M., Liang, F., and Lin, Y.-F. (2017b). Bayesian calibration of groundwater models with input data uncertainty. *Water Resour. Res.* 53, 3224–3245. doi:10.1002/2016WR019512.
Xu, Y., and Hu, A. (2018). How Would the Twenty-First-Century Warming Influence Pacific Decadal Variability and Its Connection to North American Rainfall: Assessment Based on a Revised Procedure for the IPO/PDO. *J. Clim.* 31, 1547–1563. doi:10.1175/JCLI-D-17-0319.1.
Yadav, R. K. (2017). On the relationship between east equatorial Atlantic SST and ISM through Eurasian wave. *Clim. Dyn.* 48, 281–295. doi:10.1007/s00382-016-3074-y.
Yamamoto, A., and Palter, J. B. (2016). The absence of an Atlantic imprint on the multidecadal variability of wintertime European temperature. *Nat. Commun.* 7, 10930. doi:10.1038/ncomms10930.
Yang, B., Qian, Y., Lin, G., Leung, L. R., Rasch, P. J., Zhang, G. J., et al. (2013). Uncertainty quantification and

parameter tuning in the cam5 zhang-mcfarlane convection scheme and impact of improved convection on the global circulation and climate. *J. Geophys. Res. Atmos.* 118, 395–415. doi:10.1029/2012JD018213.
Yang, H., Zhou, F., Piao, S., Huang, M., Chen, A., Ciais, P., et al. (2017). Regional patterns of future runoff changes from Earth system models constrained by observation. *Geophys. Res. Lett.* 44, 5540–5549. doi:10.1002/2017GL073454.
Yang, K., Wang, C., and Li, S. (2018a). Improved Simulation of Frozen-Thawing Process in Land Surface Model (CLM4.5). *J. Geophys. Res. Atmos.* 123, 2017JD028260. doi:10.1029/2017JD028260.
Yang, K., Zhu, L., Chen, Y., Zhao, L., Qin, J., Lu, H., et al. (2016). Land surface model calibration through microwave data assimilation for improving soil moisture simulations. *J. Hydrol.* 533, 266. Available at: https://doi.org/10.1016/J.JHYDROL.2015.12.018.
Yang, S., Ding, Z., Feng, S., Jiang, W., Huang, X., and Guo, L. (2018b). A strengthened East Asian Summer Monsoon during Pliocene warmth: Evidence from 'red clay' sediments at Pianguan, northern China. *J. Asian Earth Sci.* 155, 124–133. doi:10.1016/j.jseaes.2017.10.020.
Yang, S., Li, Z., Yu, J.-Y., Hu, X., Dong, W., and He, S. (2018c). El Niño–Southern Oscillation and its impact in the changing climate. *Natl. Sci. Rev.* 5, 840–857. doi:10.1093/nsr/nwy046.
Yang, Y., and Roderick, M. L. (2019). Radiation, surface temperature and evaporation over wet surfaces. *Q. J. R. Meteorol. Soc.* doi:10.1002/qj.3481.
Yang, Y., Roderick, M. L., Zhang, S., McVicar, T. R., and Donohue, R. J. (2018d). Hydrologic implications of vegetation response to elevated CO2 in climate projections. *Nat. Clim. Chang.* 9, 44–48. doi:10.1038/s41558-018-0361-0.
Yang, Y., Zhang, S., McVicar, T. R., Beck, H. E., Zhang, Y., and Liu, B. (2018e). Disconnection Between Trends of Atmospheric Drying and Continental Runoff. *Water Resour. Res.*, 1–14. doi:10.1029/2018WR022593.
Yarosh, E. S., Ropelewski, C. F., and Berbery, E. H. (1999). *Biases of the observed atmospheric water budgets over the central United States*. JGR Atmosphere.
Yeager, S. G., Danabasoglu, G., Rosenbloom, N. A., Strand, W., Bates, S. C., Meehl, G. A., et al. (2018). Predicting Near-Term Changes in the Earth System: A Large Ensemble of Initialized Decadal Prediction Simulations Using the Community Earth System Model. *Bull. Am. Meteorol. Soc.* 99, 1867–1886. doi:10.1175/BAMS-D-17-0098.1.
Yeh, S.-W., Cai, W., Min, S.-K., McPhaden, M. J., Dommenget, D., Dewitte, B., et al. (2018). ENSO Atmospheric Teleconnections and Their Response to Greenhouse Gas Forcing. *Rev. Geophys.* 56, 185–206. doi:10.1002/2017RG000568.
Yettella, V., and Kay, J. E. (2017). How will precipitation change in extratropical cyclones as the planet warms? Insights from a large initial condition climate model ensemble. *Clim. Dyn.* doi:10.1007/s00382-016-3410-2.
Yin, J., Gentine, P., Zhou, S., Sullivan, S. C., Wang, R., Zhang, Y., et al. (2018). Large increase in global storm runoff extremes driven by climate and anthropogenic changes. *Nat. Commun.* 9, 4389. doi:10.1038/s41467-018-06765-2.
Yin, L., Fu, R., Zhang, Y.-F., Arias, P. ., Fernando, D. N., Li, W., et al. (2014a). What controls the interannual variation of the wetseason onsets over the Amazon? *J. Geophys. Res. Atmos.* 119, 2314–2328.
Yin, L., Fu, R., Zhang, Y.-F., Arias, P. . P. A., Fernando, D. N., Li, W., et al. (2014b). What controls the interannual variation of the wetseason onsets over the Amazon? *J. Geophys. Res. Atmos.* 119, 2314–2328.
Ying, J., Huang, P., Lian, T., and Chen, D. (2019). Intermodel Uncertainty in the Change of ENSO's Amplitude under Global Warming: Role of the Response of Atmospheric Circulation to SST Anomalies. *J. Clim.* 32, 369–383. doi:10.1175/JCLI-D-18-0456.1.
Yoden, S., Otsuka, S., Trilaksono, N. J., and Hadi, T. W. (2017). "Recent progress in research on the Maritime Continent Monsoon," in *The Global Monsoon System: World Scientific Series on Asia-Pacific Weather and Climate*, eds. C. P. Chaing and others C. P. Chaing al (H., A. Moise, P. Liang and L. Hanson (2013) The response of summer monsoon onset/retreat in Sumatra--Java and tropical Australia region to global warming in CMIP3 models, Climate Dynamics, 40, 377--399: Zhang), 63–77. doi:10.1007/s00382-012-1389-x.
Yoo, C., Feldstein, S., and Lee, S. (2011). The impact of the Madden-Julian Oscillation trend on the Arctic amplification of surface air temperature during the 1979-2008 boreal winter. *Geophys. Res. Lett.* 38, n/a-n/a. doi:10.1029/2011GL049881.
Yu, J.-Y., and Zou, Y. (2013). The enhanced drying effect of Central-Pacific El Niño on US winter. *Environ. Res. Lett.* 8, 014019. doi:10.1088/1748-9326/8/1/014019.
Yu, K., D'Odorico, P., Bhattachan, A., Okin, G. S., and Evan, A. T. (2015). Dust-rainfall feedback in West African Sahel. *Geophys. Res. Lett.* 42, 7563–7571.
Yu, R., and Zhou, T. (2007). Seasonality and Three-Dimensional Structure of Interdecadal Change in the East Asian Monsoon. *J. Clim.* 20, 5344–5355. doi:10.1175/2007JCLI1559.1.
Yu, T., Guo, P., Cheng, J., Hu, A., Lin, P., and Yu, Y. (2018). Reduced connection between the East Asian Summer Monsoon and Southern Hemisphere Circulation on interannual timescales under intense global warming. *Clim. Dyn.* doi:10.1007/s00382-018-4121-7.
Yuan, C., and Yamagata, T. (2015). Impacts of IOD, ENSO and ENSO Modoki on the Australian Winter Wheat Yields

in Recent Decades. *Sci. Rep.* 5, 17252. doi:10.1038/srep17252.
Yuan, S., and Quiring, S. M. (2017). Evaluation of soil moisture in CMIP5 simulations over the contiguous United States using in situ and satellite observations. *Hydrol. Earth Syst. Sci.* 21, 2203–2218. doi:10.5194/hess-21-2203-2017.
Yuan, X., and Zhu, E. (2018). A First Look at Decadal Hydrological Predictability by Land Surface Ensemble Simulations. *Geophys. Res. Lett.* 45, 2362–2369. doi:10.1002/2018GL077211.
Yue, C., Ciais, P., Luyssaert, S., Li, W., McGrath, M. J., Chang, J., et al. (2018). Representing anthropogenic gross land use change, wood harvest, and forest age dynamics in a global vegetation model ORCHIDEE-MICT v8.4.2. *Geosci. Model Dev.* 11, 409–428. Available at: https://doi.org/10.5194/gmd-11-409-2018.
Yun, K.-S., and Timmermann, A. (2018). Decadal Monsoon-ENSO Relationships Reexamined. *Geophys. Res. Lett.* 45, 2014–2021. doi:10.1002/2017GL076912.
Zambri, B., LeGrande, A. N., Robock, A., and Slawinska, J. (2017). Northern Hemisphere winter warming and summer monsoon reduction after volcanic eruptions over the last millennium. *J. Geophys. Res.* 122, 7971–7989. doi:10.1002/2017JD026728.
Zanardo, S., Nicotina, L., Hilberts, A. G. J., and Jewson, S. P. (2019). Modulation of economic losses from European floods by the North Atlantic Oscillation. *Geophys. Res. Lett.* doi:10.1029/2019GL081956.
Zanchettin, D., Khodri, M., Timmreck, C., Toohey, M., Schmidt, A., Gerber, E. P., et al. (2016). The Model Intercomparison Project on the climatic response to Volcanic forcing (VolMIP): Experimental design and forcing input data for CMIP6. *Geosci. Model Dev.* 9, 2701–2719. doi:10.5194/gmd-9-2701-2016.
Zappa, G., Hawcroft, M. K., Shaffrey, L., Black, E., and Brayshaw, D. J. (2015). Extratropical cyclones and the projected decline of winter Mediterranean precipitation in the CMIP5 models. *Clim. Dyn.* doi:10.1007/s00382-014-2426-8.
Zappa, G., Masato, G., Shaffrey, L., Woollings, T., and Hodges, K. (2014a). Linking Northern Hemisphere blocking and storm track biases in the CMIP5 climate models. *Geophys. Res. Lett.* 41, 135–139. doi:10.1002/2013GL058480.
Zappa, G., Shaffrey, L., and Hodges, K. (2013). The ability of CMIP5 models to simulate North Atlantic extratropical cyclones. *J. Clim.* doi:10.1175/JCLI-D-12-00501.1.
Zappa, G., Shaffrey, L., and Hodges, K. (2014b). Can Polar Lows be Objectively Identified and Tracked in the ECMWF Operational Analysis and the ERA-Interim Reanalysis? *Mon. Weather Rev.* 142, 2596–2608. doi:10.1175/MWR-D-14-00064.1.
Zappa, G., and Shepherd, T. G. (2017a). Storylines of atmospheric circulation change for European regional climate impact assessment. *J. Clim.* 30, 6561–6577. doi:10.1175/JCLI-D-16-0807.1.
Zappa, G., and Shepherd, T. G. (2017b). Storylines of atmospheric circulation change for European regional climate impact assessment. *J. Clim.* 30, 6561–6577. doi:10.1175/JCLI-D-16-0807.1.
Zarzycki, C. M. (2018). Projecting Changes in Societally Impactful Northeastern U.S. Snowstorms. *Geophys. Res. Lett.* doi:10.1029/2018GL079820.
Zaveri, E., Grogan, D. S., Fisher-Vanden, K., Frolking, S., Lammers, R. B., Wrenn, D. H., et al. (2016). Invisible water, visible impact: groundwater use and Indian agriculture under climate change. *Environ. Res. Lett.* 11, 084005. doi:10.1088/1748-9326/11/8/084005.
Zemp, D. C., Schleussner, C. F., Barbosa, H. M. J., Hirota, M., Montade, V., Sampaio, G., et al. (2017). Self-amplified Amazon forest loss due to vegetation-atmosphere feedbacks. *Nat. Commun.* doi:10.1038/ncomms14681.
Zeng, N., Neelin, J. D., Lau, K. M., and Tucker, C. J. (1999). Enhancement of interdecadal climate variability in the Sahel by vegetation interaction. *Science (80-.).* 286, 1537–1540. doi:10.1126/science.286.5444.1537.
Zeng, R., and Cai, X. (2016). Climatic and terrestrial storage control on evapotranspiration temporal variability: Analysis of river basins around the world. *Geophys. Res. Lett.* 43, 185–195.
Zeng, X., Broxton, P., and Dawson, N. (2018a). Snowpack Change From 1982 to 2016 Over Conterminous United States. *Geophys. Res. Lett.* doi:10.1029/2018gl079621.
Zeng, Z., Peng, L., and Piao, S. (2018b). Response of terrestrial evapotranspiration to Earth's greening. *Curr. Opin. Environ. Sustain.* doi:10.1016/j.cosust.2018.03.001.
Zeng, Z., Piao, S., Li, L. Z. X., Wang, T., Ciais, P., Lian, X., et al. (2018c). Impact of Earth greening on the terrestrial water cycle. *J. Clim.* 31, 2633–2650. doi:10.1175/JCLI-D-17-0236.1.
Zeng, Z., Wang, T., Zhou, F., Ciais, P., Mao, J., Shi, X., et al. (2014). worldwide analysis of spatiotemporal changes in water balance based evapotranspiration from 1982 to 2009. *J Geophys Res D Atmos* 119, 1186–1202.
Zhai, P., Zhang, X., Wan, H., Pan, X., Zhai, P., Zhang, X., et al. (2005). Trends in Total Precipitation and Frequency of Daily Precipitation Extremes over China. *J. Clim.* 18, 1096–1108. doi:10.1175/JCLI-3318.1.
Zhan, S., Song, C., Wang, J., Sheng, Y., and Quan, J. (2019). *No Title*. A global assessment of terrestrial evapotranspiration increase due to surface water area change. Earth's Future.
Zhang, E., Sun, W., Chang, J., Ning, D., and Shulmeister, J. (2018a). Variations of the Indian summer monsoon over the last 30 000 years inferred from a pyrogenic carbon record from south-west China. *J. Quat. Sci.* 33, 131–138.

doi:10.1002/jqs.3008.
Zhang, G. J., Wu, X., Zeng, X., and Mitovski, T. (2016a). Estimation of convective entrainment properties from a cloud resolving model simulation during twp-ice. *Clim. Dyn.* 47, 2177–2192.
Zhang, H., and Delworth, T. L. (2018). Robustness of anthropogenically forced decadal precipitation changes projected for the 21st century. *Nat. Commun.* 9, 1150. doi:10.1038/s41467-018-03611-3.
Zhang, H., Dong, G., Moise, A., Colman, R., Hanson, L., and Ye, H. (2016b). Uncertainty in CMIP5 model-projected changes in the onset/retreat of the Australian summer monsoon. *Clim. Dyn.* 46, 2371–2389. doi:10.1007/s00382-015-2107-x.
Zhang, H., and Moise, A. (2016). "The Australian summer monsoon in current and future climate," in *The Monsoons and Climate Change*, eds. C. Jones and L. Carvalho (Berlin: Springer, , doi.org/10.1007/978-3-319-21650-8_5), 67–120.
Zhang, H., Moise, A., Liang, P., and Hanson, L. (2013a). The response of summer monsoon onset/retreat in Sumatra-Java and tropical Australia region to global warming in CMIP3 models. *Clim. Dyn.* 40, 377–399. doi:10.1007/s00382-012-1389-x.
Zhang, K., Kimball, J. S., Nemani, R. R., Running, S. W., Hong, Y., Gourley, J. J., et al. (2015a). Vegetation Greening and Climate Change Promote Multidecadal Rises of Global Land Evapotranspiration. *Sci. Rep.* doi:10.1038/srep15956.
Zhang, L., and Li, T. (2017). Relative roles of differential SST warming, uniform SST warming and land surface warming in determining the Walker circulation changes under global warming. *Clim. Dyn.* doi:10.1007/s00382-016-3123-6.
Zhang, L., Wu, P., and Zhou, T. (2017a). Aerosol forcing of extreme summer drought over North China. *Environ. Res. Lett.* 12, 034020. doi:10.1088/1748-9326/aa5fb3.
Zhang, L., Wu, P., Zhou, T., Roberts, M. J., and Schiemann, R. (2016c). Added value of high resolution models in simulating global precipitation characteristics. *Atmos. Sci. Lett.* 17, 646–657. doi:10.1002/asl.715.
Zhang, L., Zhou, T., Klingaman, N. P., Wu, P., and Roberts, M. (2018b). Effect of Horizontal Resolution on the Representation of the Global Monsoon Annual Cycle in AGCMs. *Adv. Atmos. Sci.* 35, 1003–1020. doi:10.1007/s00376-018-7273-9.
Zhang, Q., Fan, K., Singh, V. P., Song, C., Xu, C.-Y., and Sun, P. (2019a). Is Himalayan-Tibetan Plateau "drying"? Historical estimations and future trends of surface soil moisture. *Sci. Total Environ.* 658, 374–384. doi:S0048969718350721.
Zhang, Q., Fan, K., Singh, V. P., Song, C., Xu, C., and Sun, P. (2019b). Is Himalayan-Tibetan Plateau ``drying''? *Hist. Estim. Futur. trends Surf. soil moisture* 658, 374–384. doi:S0048969718350721.
Zhang, R., and Delworth, T. L. (2005). Simulated Tropical Response to a Substantial Weakening of the Atlantic Thermohaline Circulation. *J. Clim.* 18, 1853–1860. doi:10.1175/JCLI3460.1.
Zhang, R., Wang, X., and Wang, C. (2018c). On the Simulations of Global Oceanic Latent Heat Flux in the CMIP5 Multimodel Ensemble. *J. Clim.* 31, 7111–7128. doi:10.1175/JCLI-D-17-0713.1.
Zhang, W., Brandt, M., Guichard, F., Tian, Q., and Fensholt, R. (2017b). Using long-term daily satellite based rainfall data (1983–2015) to analyze spatio-temporal changes in the sahelian rainfall regime. *J. Hydrol.* 550, 427–440. doi:10.1016/J.JHYDROL.2017.05.033.
Zhang, W., Brandt, M., Tong, X., Tian, Q., and Fensholt, R. (2018d). Impacts of the seasonal distribution of rainfall on vegetation productivity across the Sahel. *Biogeosciences* 15, 319–330. doi:10.5194/bg-15-319-2018.
Zhang, W., and Luo, M. (2016). A possible linkage of the western North Pacific summer monsoon with the North Pacific Gyre Oscillation. *Atmos. Sci. Lett.* 17, 437–445. doi:10.1002/asl.676.
Zhang, X., He, J., Zhang, J., Polyakov, I., Gerdes, R., Inoue, J., et al. (2013b). Enhanced poleward moisture transport and amplified northern high-latitude wetting trend. *Nat. Clim. Chang.* 3, 47–51. doi:10.1038/nclimate1631.
Zhang, X., and Tang, Q. (2014). Runoff sensitivity to global mean temperature change in the CMIP5 Models. *Geophys. Res. …*, 5492–5498. doi:10.1002/2014GL060382.Received.
Zhang, X., Tang, Q., Liu, X., Leng, G., and Di, C. (2018e). Nonlinearity of Runoff Response to Global Mean Temperature Change Over Major Global River Basins. *Geophys. Res. Lett.* 45, 6109–6116. doi:10.1029/2018GL078646.
Zhang, X., Zwiers, F. W., Li, G., Wan, H., and Cannon, A. J. (2017c). Complexity in estimating past and future extreme short-duration rainfall. *Nat. Geosci.* 10, 255–259. doi:10.1038/ngeo2911.
Zhang, Y., Peña-Arancibia, J. L., McVicar, T. R., Chiew, F. H. S., Vaze, J., Liu, C., et al. (2016d). Multi-decadal trends in global terrestrial evapotranspiration and its components. *Sci. Rep.* 6, 1–12. doi:10.1038/srep19124.
Zhang, Z., Chao, B. F., Chen, J., and Wilson, C. R. (2015b). Terrestrial water storage anomalies of Yangtze River Basin droughts observed by GRACE and connections with ENSO. *Glob. Planet. Change* 126, 35–45. doi:10.1016/j.gloplacha.2015.01.002.
Zhang, Z., Ralph, F. M., and Zheng, M. (2018f). The Relationship between Extratropical Cyclone Strength and Atmospheric River Intensity and Position. *Geophys. Res. Lett.* 46, 1814–1823. doi:10.1029/2018gl079071.

Zhao, C., Lin, Y., Wu, F., Wang, Y., Li, Z., Rosenfeld, D., et al. (2018a). Enlarging rainfall area of tropical cyclones by atmospheric aerosols. *Geophys. Res. Lett.* doi:10.1029/2018GL079427.

Zhao, M., Golaz, J.-C., Held, I. M., Guo, H., Balaji, V., Benson, R., et al. (2018b). The GFDL Global Atmosphere and Land Model AM4.0/LM4.0: 2. Model Description, Sensitivity Studies, and Tuning Strategies. *J. Adv. Model. Earth Syst.* 10, 735–769. doi:10.1002/2017MS001209.

Zheng, X.-T., Hui, C., and Yeh, S.-W. (2018). Response of ENSO amplitude to global warming in CESM large ensemble: uncertainty due to internal variability. *Clim. Dyn.* 50, 4019–4035. doi:10.1007/s00382-017-3859-7.

Zheng, X.-T., Xie, S.-P., Lv, L.-H., and Zhou, Z.-Q. (2016). Intermodel Uncertainty in ENSO Amplitude Change Tied to Pacific Ocean Warming Pattern. *J. Clim.* 29, 7265–7279. doi:10.1175/JCLI-D-16-0039.1.

Zhisheng, A., Guoxiong, W., Jianping, L., Youbin, S., Yimin, L., Weijian, Z., et al. (2015). Global Monsoon Dynamics and Climate Change. *Annu. Rev. Earth Planet. Sci.* 43, 29–77. doi:https://doi.org/10.1146/annurev-earth-060313-054623.

Zhou, T., Chen, X., Wu, B., Guo, Z., Sun, Y., Zou, L., et al. (2017). A Robustness Analysis of CMIP5 Models over the East Asia-Western North Pacific Domain. 3, 773–778. doi:10.1016/J.ENG.2017.05.018.

Zhou, T., Turner, A., Kinter, J., Wang, B., Qian, Y., Chen, X., et al. (2016). Overview of the Global Monsoons Model Inter-comparison Project (GMMIP). *Geosci. Model Dev. Discuss.*, 1–25. doi:10.5194/gmd-2016-69.

Zhou, T., Yu, R., Li, H., and Wang, B. (2008). Ocean Forcing to Changes in Global Monsoon Precipitation over the Recent Half-Century. *J. Clim.* 21, 3833–3852. doi:10.1175/2008JCLI2067.1.

Zhou, Y., and Lau, W. K. M. (2017). The relationships between the trends of mean and extreme precipitation. *Int. J. Climatol.* 37, 3883–3894. doi:10.1002/joc.4962.

Zhou, Y. P., Xu, K.-M., Sud, Y. C., and Betts, A. K. (2011). Recent trends of the tropical hydrological cycle inferred from Global Precipitation Climatology Project and International Satellite Cloud Climatology Project data. *J. Geophys. Res.* 116, D09101. doi:10.1029/2010JD015197.

Zhu, Y., and Newell, R. E. (1998). A proposed algorithm for moisture fluxes from atmospheric rivers. Mon. *Wea* 126, 725–735. doi:10.1175/1520-0493(1998)126<0725:APAFMF>2.0.CO;2.

Zhu, Z., Piao, S., Myneni, R. B., Huang, M., Zeng, Z., and Canadell, J. G. C. C. (2016). Greening of the Earth and its drivers. *Nat Clim Chang.* 6, 791–795.

Zickfeld, K., Arora, V. K., and Gillett, N. P. (2012). Is the climate response to CO2 emissions path dependent? *Geophys. Res. Lett.* 39, n/a-n/a. doi:10.1029/2011GL050205.

Zickfeld, K., Knopf, B., Petoukhov, V., and Schellnhuber, H. J. (2005). Is the Indian summer monsoon stable against global change? *Geophys. Res. Lett.* 32. doi:10.1029/2005GL022771.

Zickfeld, K., MacDougall, A. H., and Matthews, H. D. (2016). On the proportionality between global temperature change and cumulative CO2 emissions during periods of net negative CO2 emissions. *Environ. Res. Lett.* 11, 055006. doi:10.1088/1748-9326/11/5/055006.

Zika, J. D., Skliris, N., Blaker, A. T., Marsh, R., Nurser, A. J. G., and Josey, S. A. (2018). Improved estimates of water cycle change from ocean salinity: The key role of ocean warming. *Environ. Res. Lett.* 13. doi:10.1088/1748-9326/aace42.

Zolina, O., Simmer, C., Belyaev, K., Gulev, S. K., and Koltermann, P. (2013). Changes in the duration of European wet and dry spells during the last 60 years. *J. Clim.* doi:10.1175/JCLI-D-11-00498.1.

Zolina, O., Simmer, C., Kapala, A., Shabanov, P., Becker, P., MäcHel, H., et al. (2014). Precipitation variability and extremes in Central Europe: New View from STAMMEX Results. *Bull. Am. Meteorol. Soc.* 95, 995–1002. doi:10.1175/BAMS-D-12-00134.1.

Zou, Y., Wang, Y., Ke, Z., Tian, H., Yang, J., and Liu, Y. (2019). Development of a REgion-specific ecosystem feedback fire (RESFire) model in the Community Earth System Model. *J. Adv. Model. Earth Syst.* 11. Available at: https://doi.org/10.1029/2018MS001368.

Figures

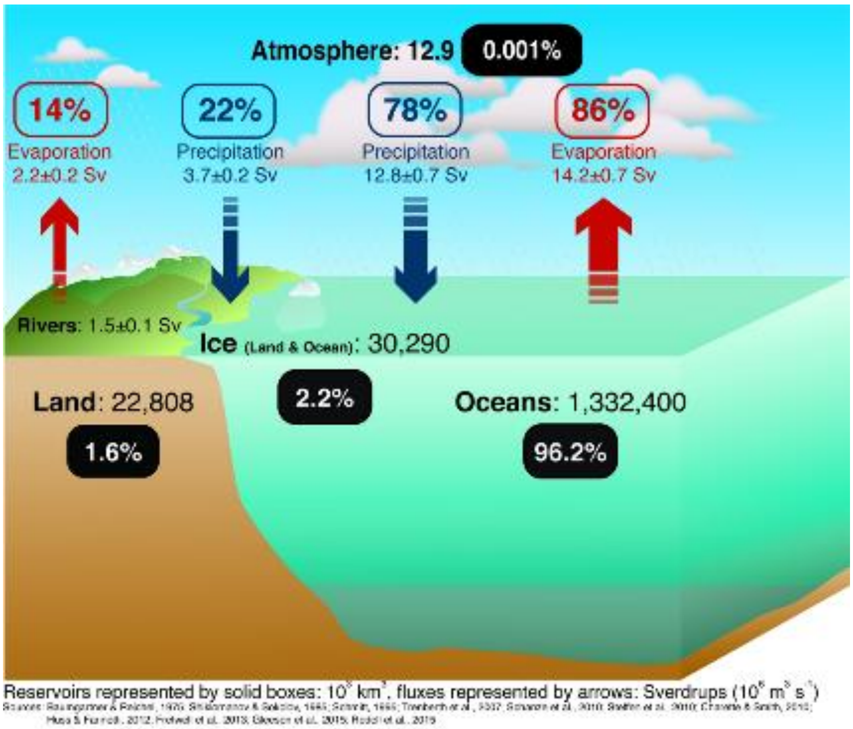

Figure 8.1: Components of the global water cycle. The ocean is the Earth's primary water reservoir (96.2%), with remaining water stored as ice (2.2%) or on land (1.6%). Approximately 86% of surface water fluxes occurring over the ocean, with the remaining 14% generated over land. Reservoirs represented by solid boxes: 103 km3, fluxes represented by arrows: Sverdrups (106 m3 s–1). Source: Durack (2015).

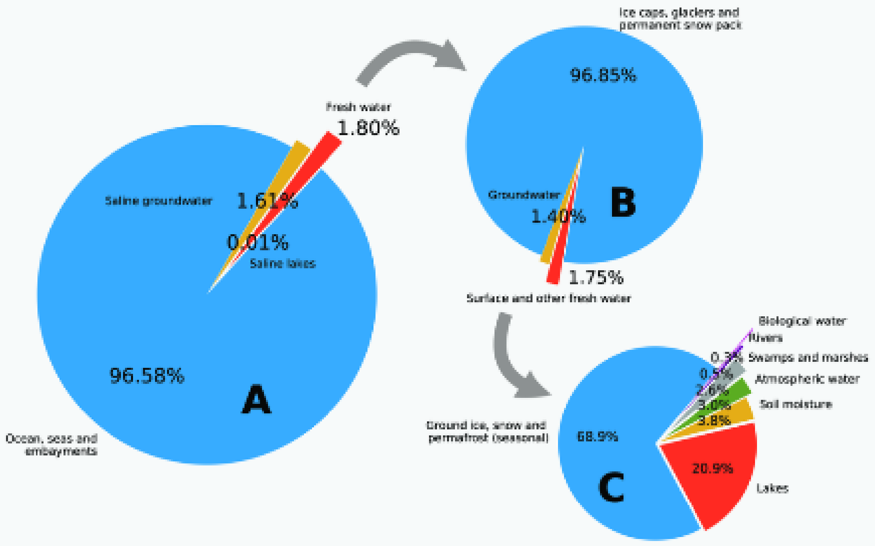

Figure 8.2: Distribution of the Earth's water (hydrosphere). The global ocean is the primary water reservoir and the ultimate source of all terrestrial water (A, Left). Ice caps, glaciers and permanent snow comprise the largest freshwater stores (B, top right), and seasonal ice, snow and permafrost along with freshwater lakes comprise the largest surface and other fresh water storages that are available for human use (C, bottom left). Reproduced and updated from Shiklomanov and Sokolov (1985); Charette and Smith (2010); and Gleeson et al., (2015).

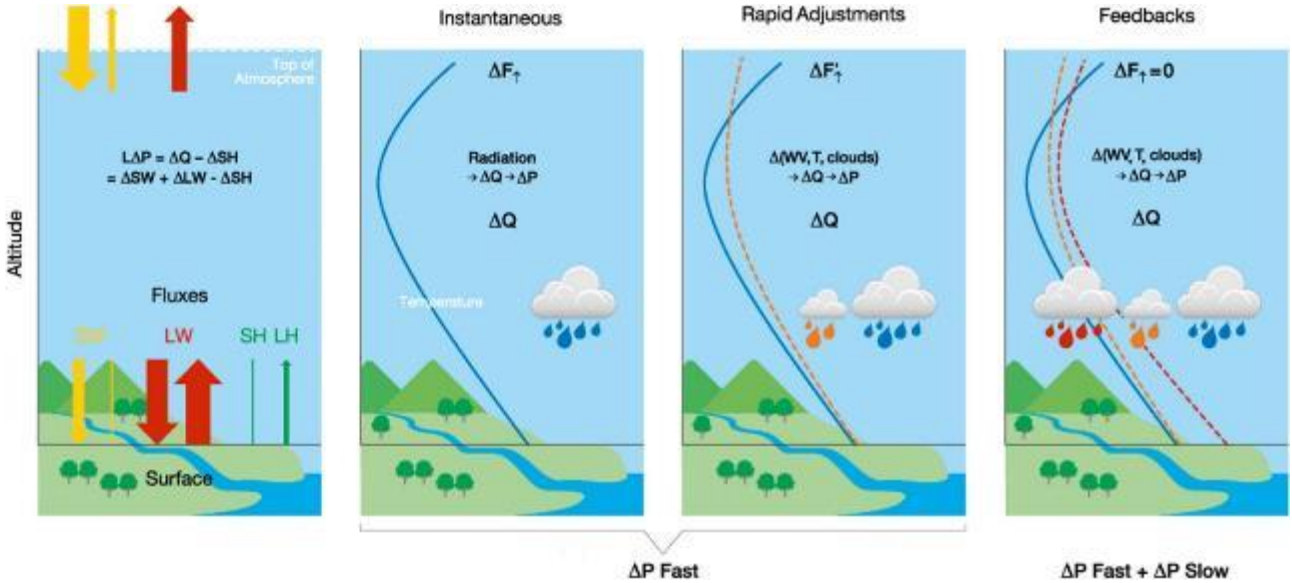

Figure 8.3: **(TO BE ADAPTED/SIMPLIFIED)** Schematic diagram of the energy fluxes and fast and slow precipitation change (ΔP) processes. (left) At the TOA, in the atmosphere, and at the surface, the energy budget is nearly in balance on a global scale. Changes in the atmospheric radiative cooling ΔQ can be caused by changes in absorption of shortwave radiation (SW) or changes in absorption/emission of longwave radiation (LW) or both. Here, LH = LΔP is the latent heat and SH is the sensible heat. (left center) An external driver of climate change alters the radiative fluxes at the top of the atmosphere and this may alter the atmospheric absorption. (right center) The instantaneous change through radiation may further alter the atmospheric temperature, water vapor, and clouds, through rapid adjustments. These rapid adjustments may lead to decreases or increases in clouds and water vapor, and they can vary through the atmosphere. The instantaneous radiative perturbation and rapid adjustments change precipitation on a fast time scale (from days to a few years). (right) Climate feedback processes through changes in the surface temperature further alter the atmospheric absorption, which occurs on a long time scale (decades). Net radiative fluxes at the TOA are given as F, water vapor as WV, temperature as T, and latent heat of vaporization as L. In the left center and right panels, the blue curve indicates the unperturbed state, the orange curve represents the rapid adjustments, and the red curve represents the effects of both fast and slow adjustments.**https://journals.ametsoc.org/doi/10.1175/BAMS-D-16-0019.1#**

Alternative idea:

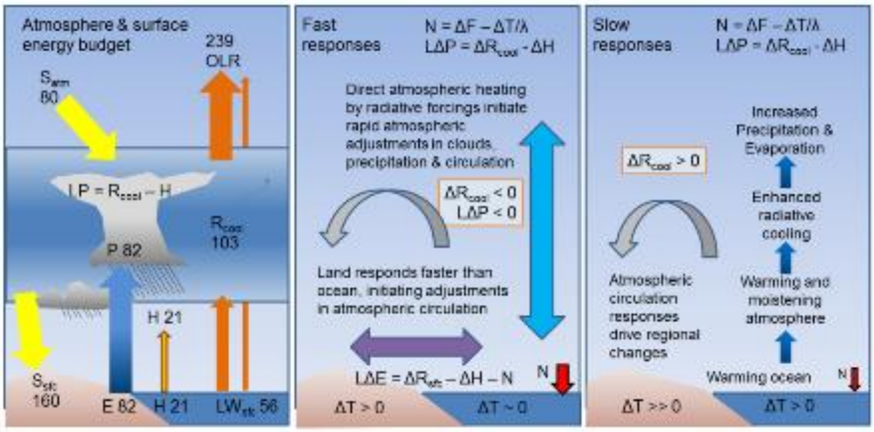

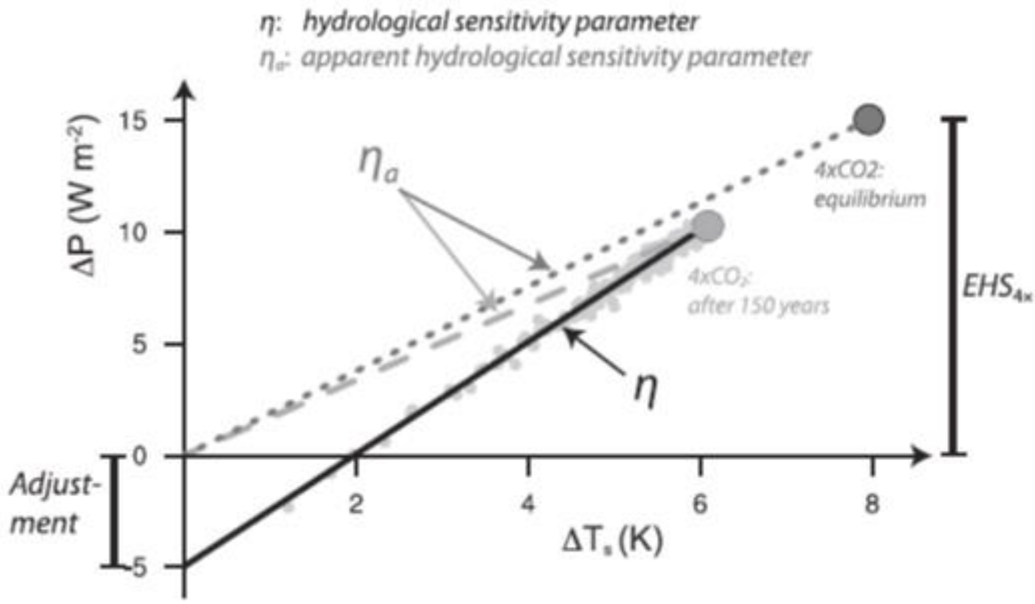

Figure 8.4: Precipitation change with surface temperature change for abrupt4xCO2 experiment with the IPSL-CM5A LR model. The hydrological sensitivity parameter η is the slope of the global-mean precipitation response with respect to surface temperature change when explicitly taking into account the rapid "adjustment" of precipitation due to forcing agents. The apparent hydrological sensitivity parameter η_a is given by the slope of global time-mean responses without accounting for rapid precipitation adjustments. The equilibrium precipitation change due to a quadrupling of CO2 is denoted as equilibrium hydrological sensitivity at 4 × CO2 (EHS4×). Small circles signify annual global means, and large circles the endpoint and equilibrium mean. [Fläschneret al (2016) J. Climhttps://journals.ametsoc.org/doi/10.1175/JCLI-D-15-0351.1 – to updated with CMIP6 data]

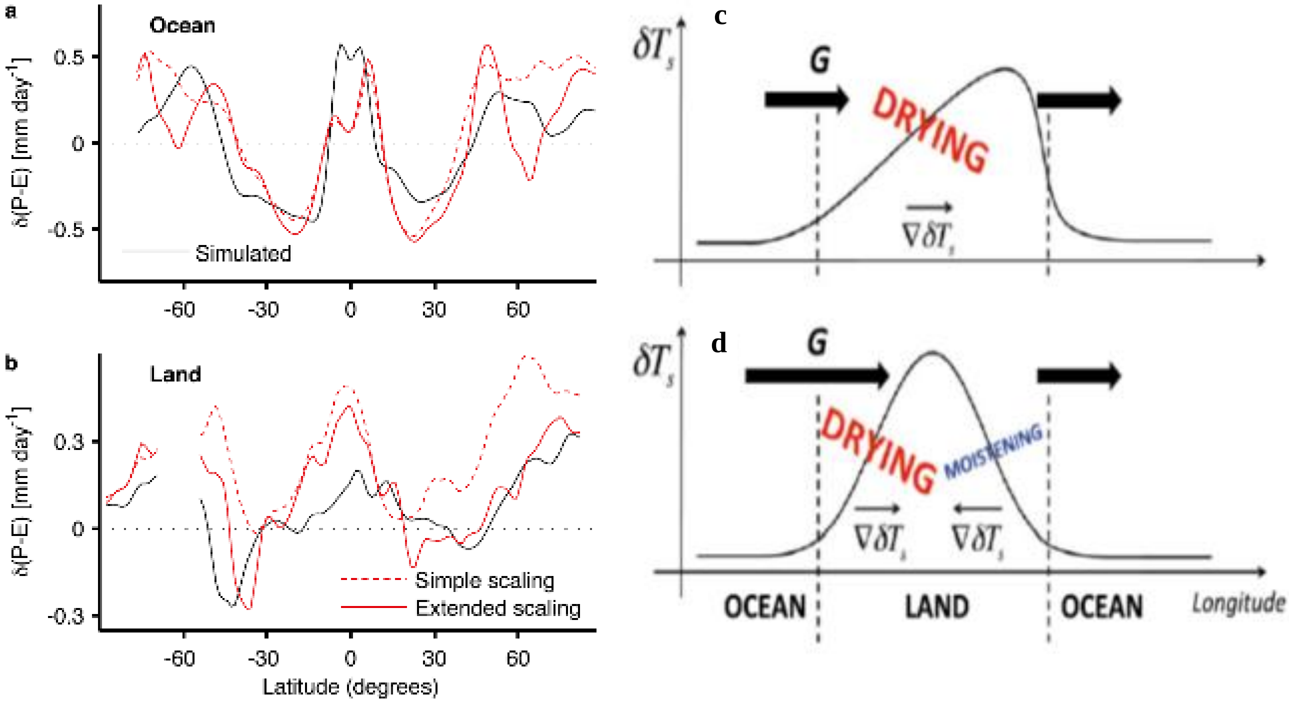

Figure 8.5: Multimodel-mean changes in zonal-mean P − E over (a) oceans and (b) land. Black lines show the simulated changes. Red dashed lines show a simple scaling in which P-E scales with the Clausius Clapeyron equation while the solid red line shows an extended scaling accounting for changes in relative humidity and spatial gradients in temperature and moisture and more realistically captures subtropical decline in P-E over land depicted by coupled climate models. The effect of land-ocean warming contrasts (c-d) can further drive continental drying through altered moisture fluxes driven by (c) asymmetric warming and (b) enhanced land warming. The heavy black arrows represent the modified moisture flux G in the base climate and the curves are idealized profiles of surface air temperature change verses longitude. [Figure 3 and 8 from Byrne and O'Gorman (2015) J. Climhttps://journals.ametsoc.org/doi/full/10.1175/JCLI-D-15-0369.1 to be updated with CMIP6]

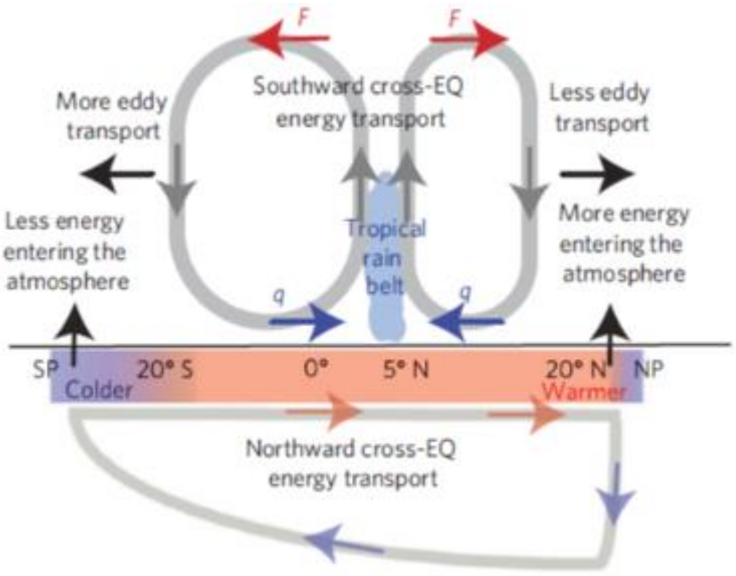

Figure 8.6: Schematic of the role of the oceanic overturning circulation in forcing the Northern Hemisphere maximum of tropical precipitation.Heat is released from the ocean to the atmosphere in the Northern Hemisphere owing to cross-equatorial ocean heat transport (7.2). The atmosphere responds through eddy energy transports in the extratropics and a cross-equatorial Hadley circulation, which fluxes energy from the Northern Hemisphere to the Southern Hemisphere. The moisture transport by the Hadley circulation is in the opposite direction as the energy transport, so tropical precipitation moves northwards. SP, South Pole; NP, North Pole; cross-EQ, cross-equatorial; q, moisture transport; F, energy transport. [From Frierson et al (2013) Nature Geosci. https://www.nature.com/articles/ngeo1987 (Figure 3)]

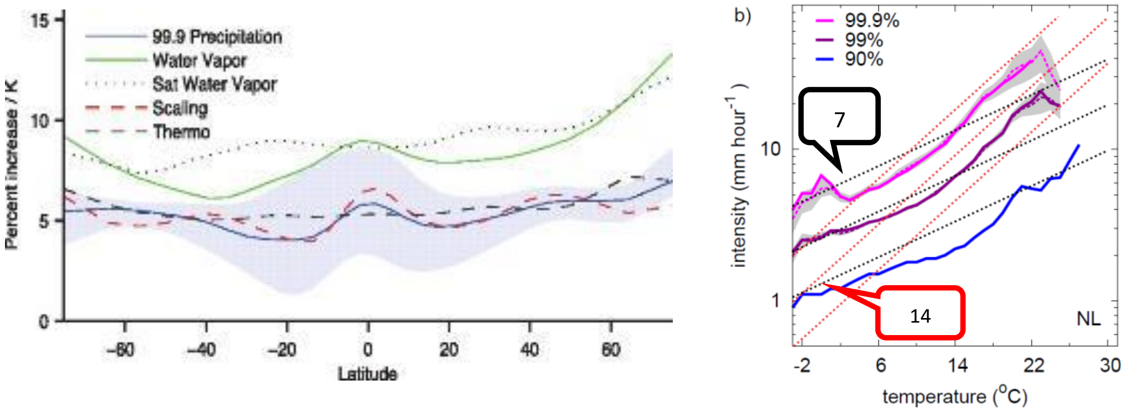

Figure 8.7: (a)Fractional changes relative to the 20th century (multi-model median, see (O'Gorman and Schneider, 2009)in the 99.9th percentile of daily precipitation (blue), zonally averaged atmospheric water vapor content (green), saturation water vapor content of the troposphere (black dotted), a simple scalings accounting for thermodynamic and dynamic changes (red dashed) and a thermodynamic-only scaling (black dashed). Water vapour increases slighty less than expected from thermodynamics due to reduced relative humidity, particularly in the subtropics, while increases are larger than at surface levels as saturation specific humidity increases at a greater rate with temperature for higher, colder regions of the atmosphere. The precipitation scaling is closely related to but slightly less than thermodynamic changes near the surface due to dynamical changes(b) Observed scaling of the 90th, 99th and 99.9th percentile of hourly rainfall with daily mean surface temperature for the Netherlands (grey shading denotes the 98% uncertainty range) with the super-Clausius Clapeyron (14%/K) and Clausius Clapeyron (7%/K) scalings denoted. [Or use Figure 2 from O'Gorman 2015 Curr. Clim. Change. Rep. (Can this be updated to CMIP6?) http://link.springer.com/article/10.1007%2Fs40641-015-0009-3 and Lenderink et al. (2011) HESShttps://www.hydrol-earth-syst-sci.net/15/3033/2011/ (Fig. 1)]

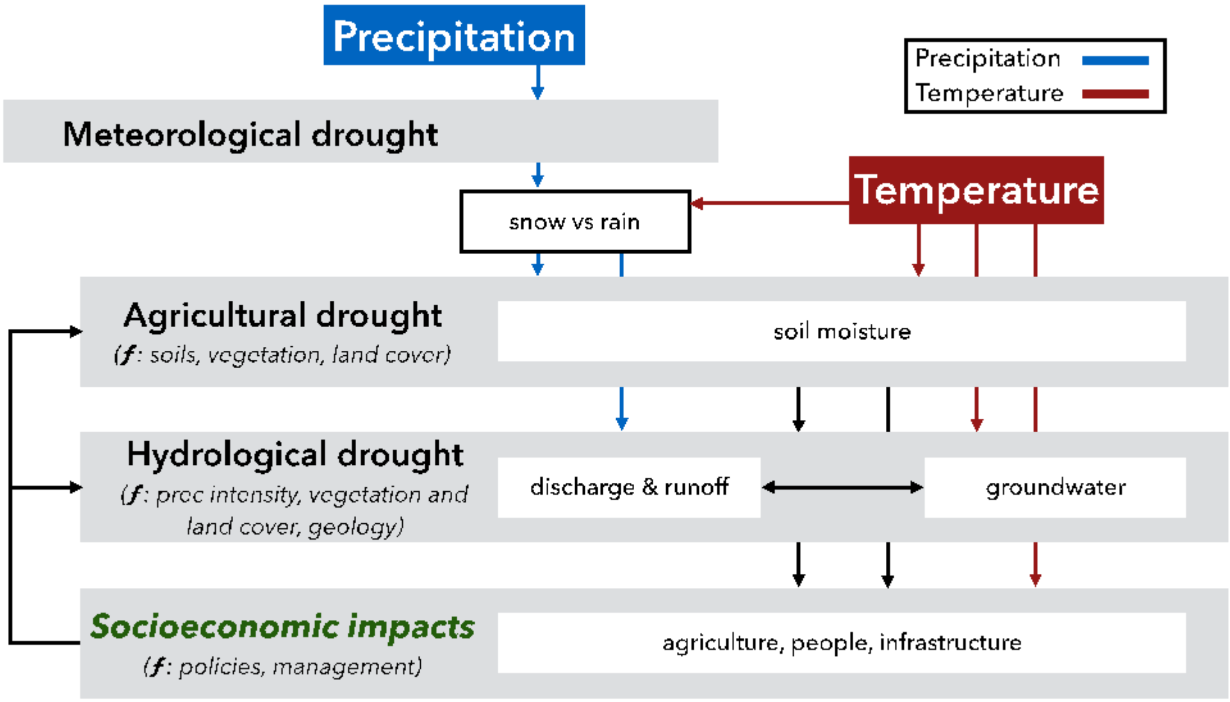

Figure 8.8: Definitions of drought and the role of precipitation, temperature, soil and groundwater storage, and anthropogenic influences. From Cook, Mankin&Anchukaitis, 2018.

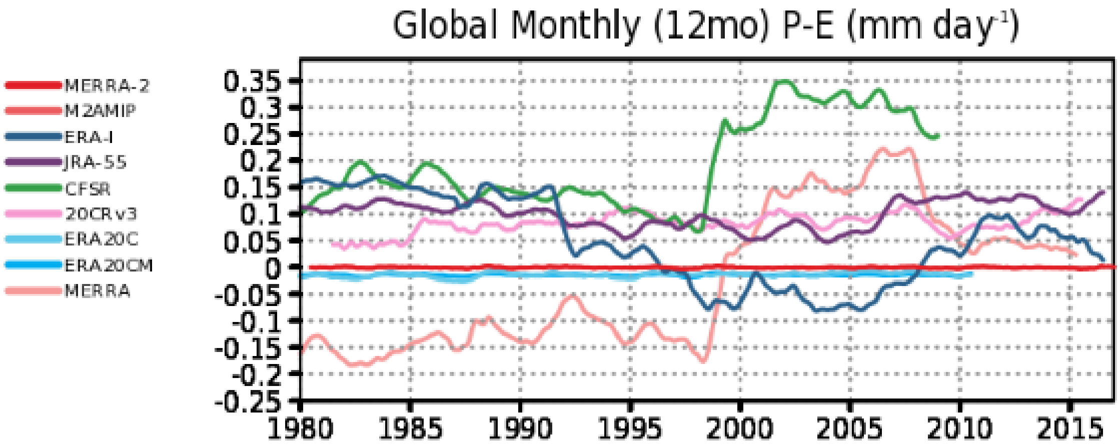

Figure 8.9: Intercomparison of global (P-E) from various reanalyses over the satellite data period (monthly means, with a 12 month running mean). Updated from (Bosilovich et al., 2017). CFSR, ERA-I, JRA-55, MERRA and MERRA-2 are satellite data reanalyses, ERA20C and 20CRv3 use reduced observing systems. ERA20CM and M2AMIP are atmospheric model ensemble simulations.

(a)

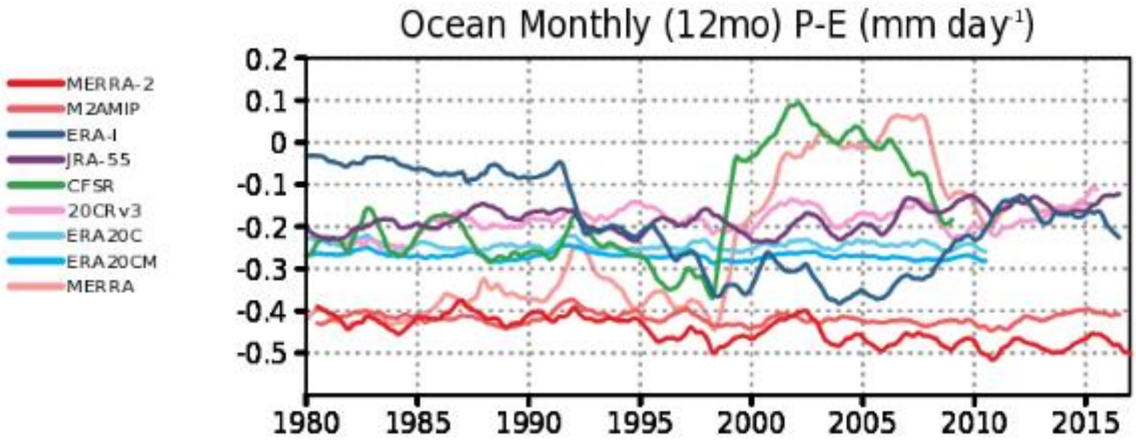

(b)

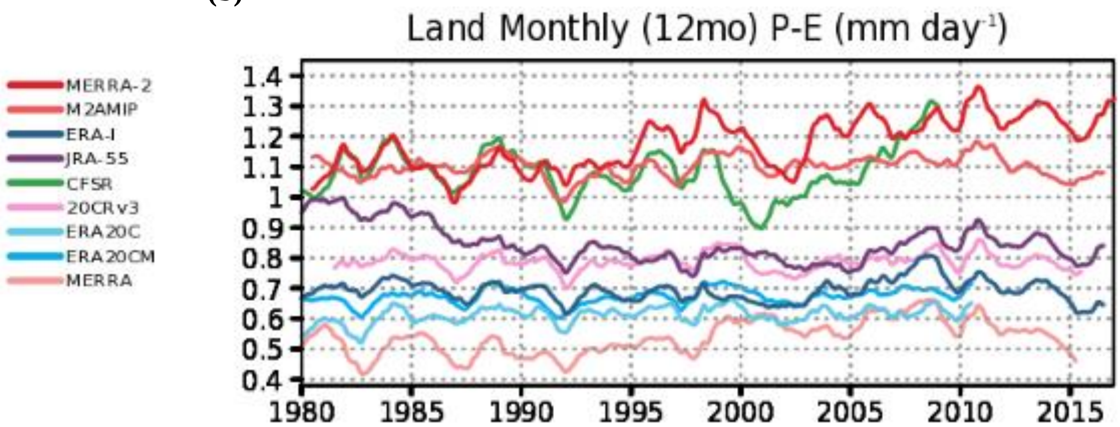

Figure 8.10: As in Fig.8.10, except for P-E over (a) Global oceans (b) Global land

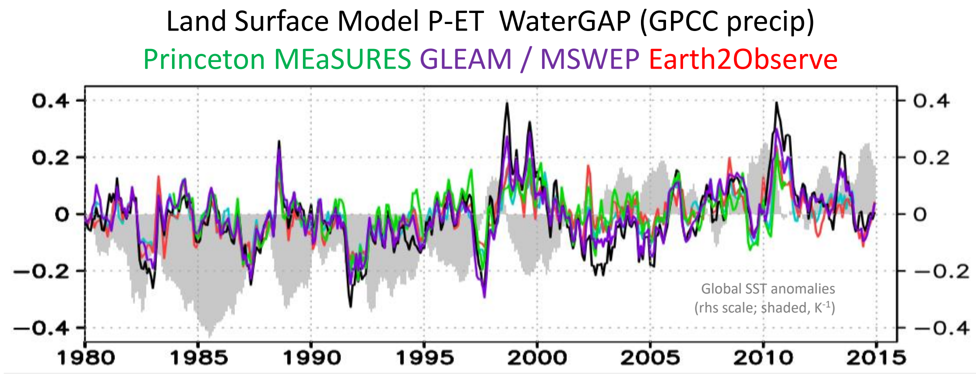

Figure 8.11: P-E land surface anomalies (base climate 1990-2010) from land surface models for the area between 60N and 60S (including 3 month running mean). Updated from Robertson et al., (2016). Units are kg m^{-2}.

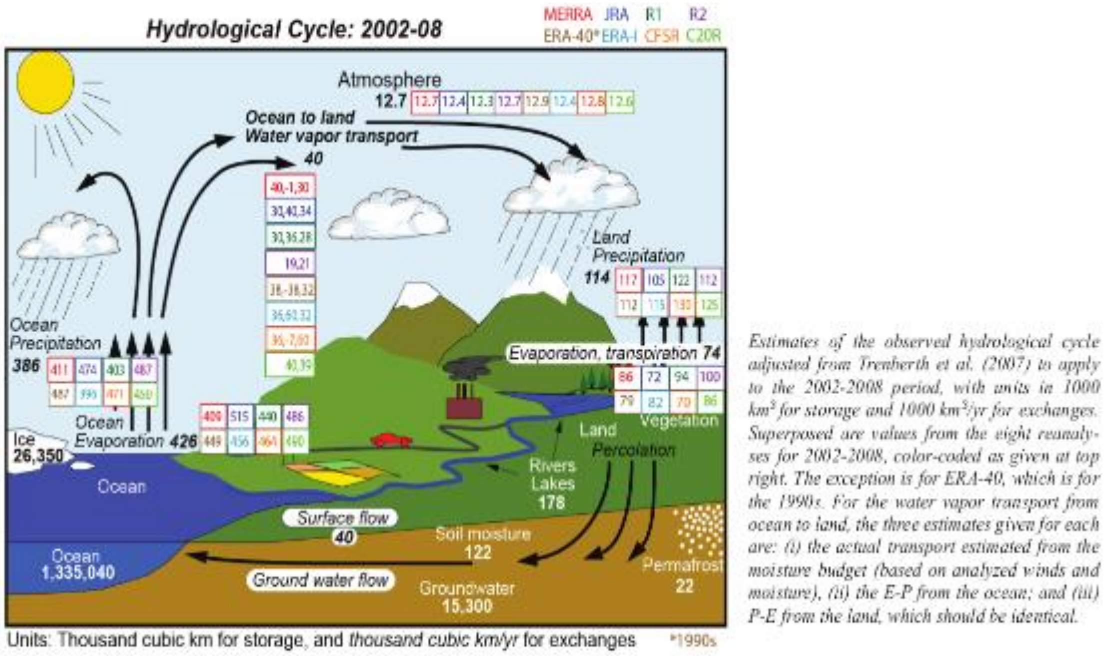

Figure 8.12: Water cycle fluxes and reservoirs originally published by (Trenberth et al., 2011) and a placeholder for an updated analysis of the reanalysis data.

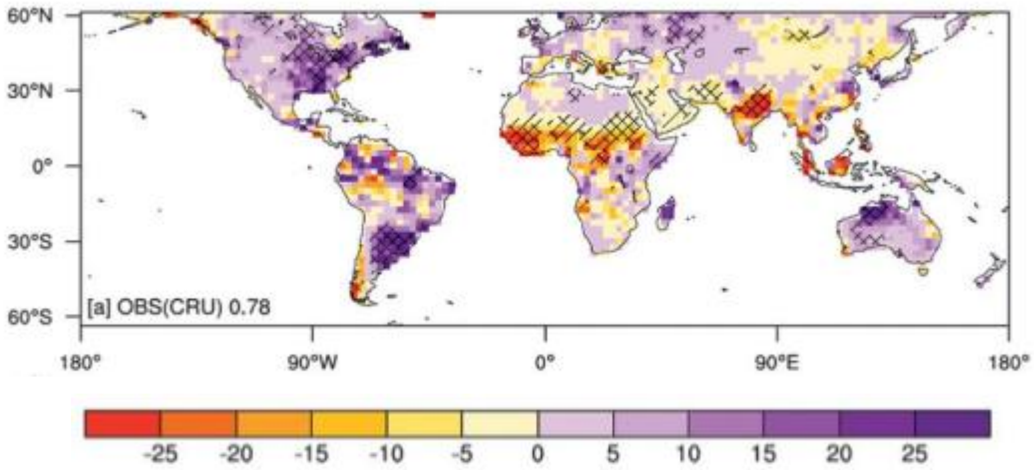

Figure 8.13: Linear trends in annual precipitation, using CRU precipitation data, 1930-2004. From (Kumar et al., 2013).

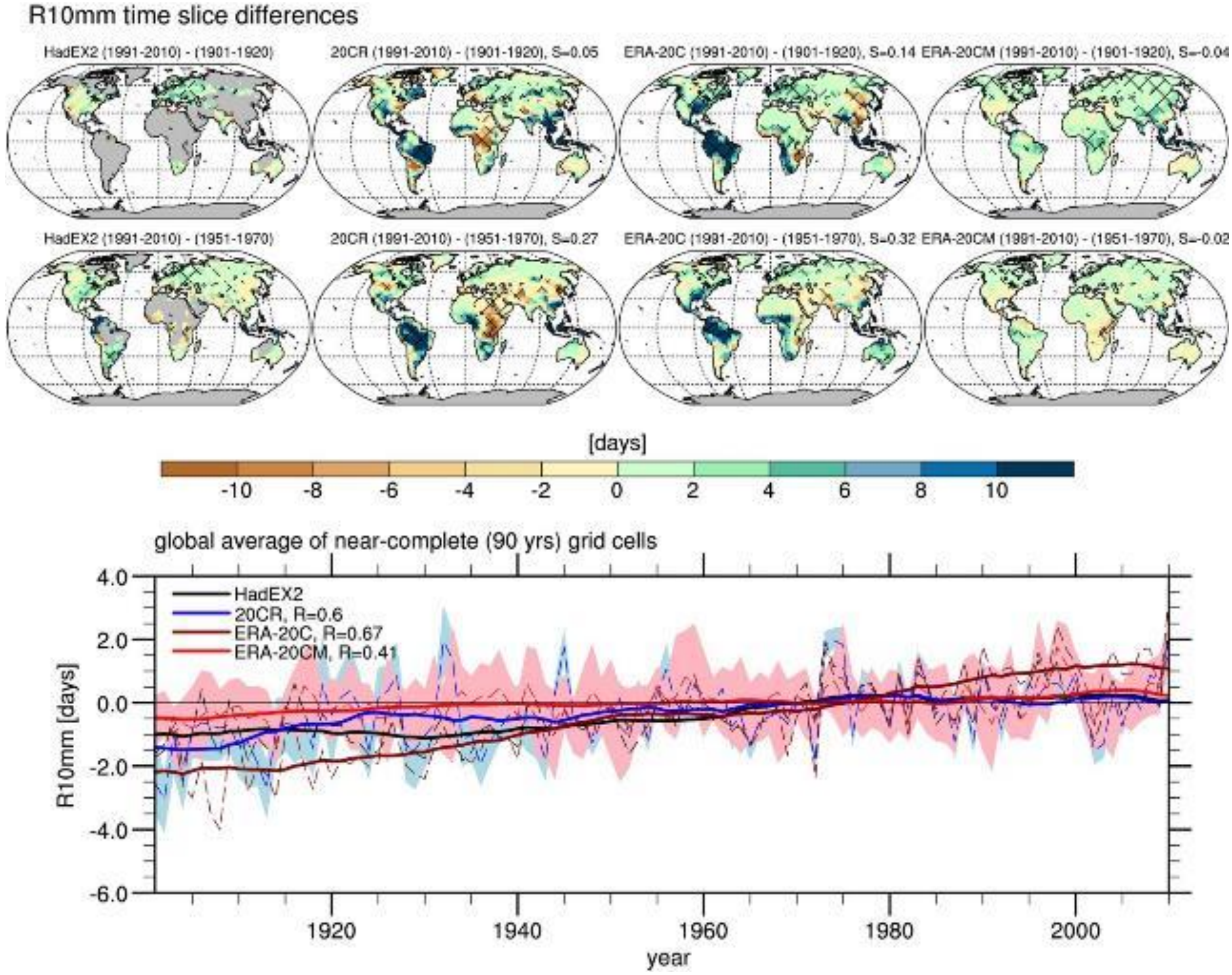

Figure 8.14: Regional and global changes in heavy precipitation days (R10mm). From (Donat et al., 2016a).

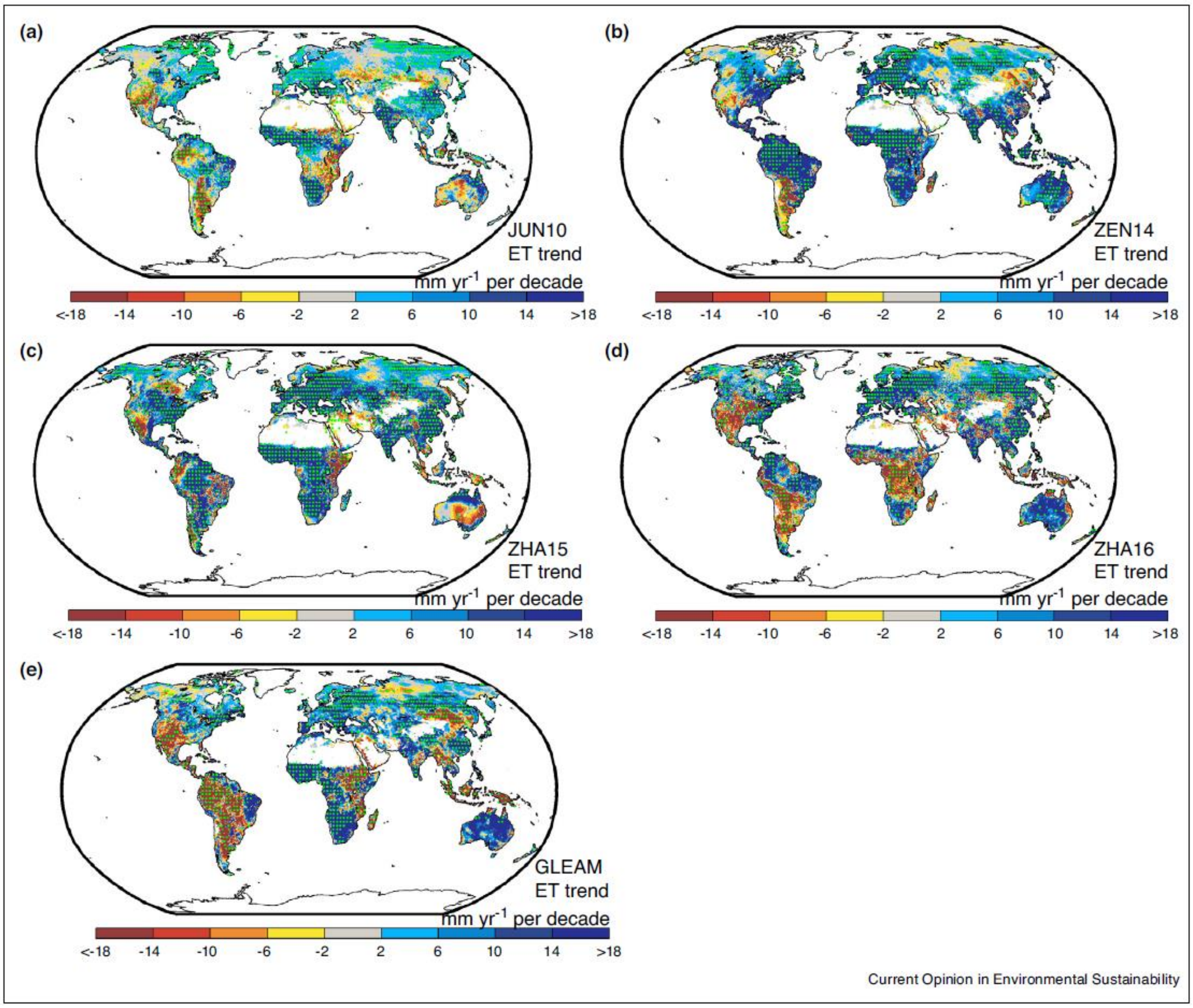

Figure 8.15: Linear trends in total annual terrestrial evapotranspiration. From (Zeng et al., 2018b)..

Figure 8.16: The Muir Glacier, Alaska photographed in August 1941 (a) by William O Field and in August 2004 from the same vantage point (b) by Bruce F. Molnia of U.S. Geological Survey (taken from Barry and Gan, 2011).

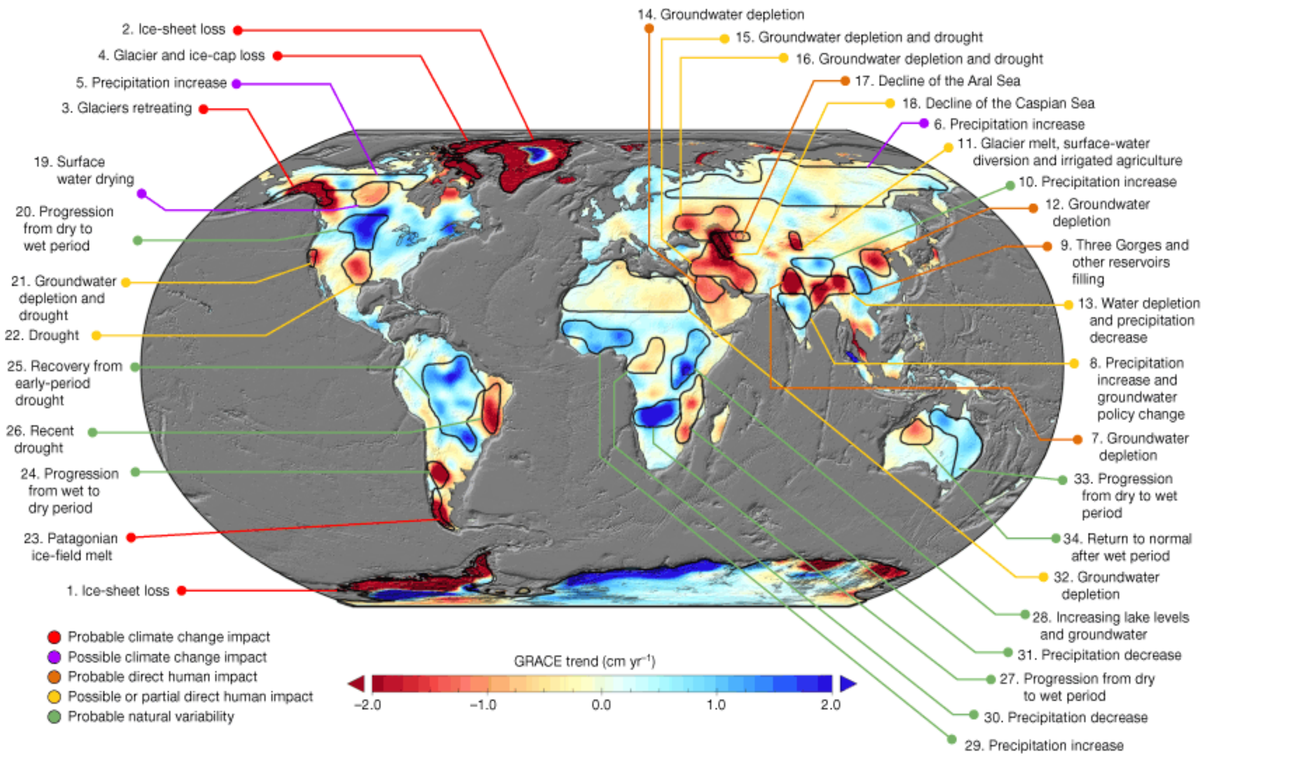

Figure 8.17: Trends in TWS (in centimetres per year) obtained on the basis of GRACE observations from April 2002 to March 2016. The cause of the trend in each outlined study region is briefly explained and colour-coded by category. The trend map was smoothed with a 150-km-radius Gaussian filter for the purpose of visualization; however, all calculations were performed at the native 3° resolution of the data product. Figure from Rodell et al. (2018).

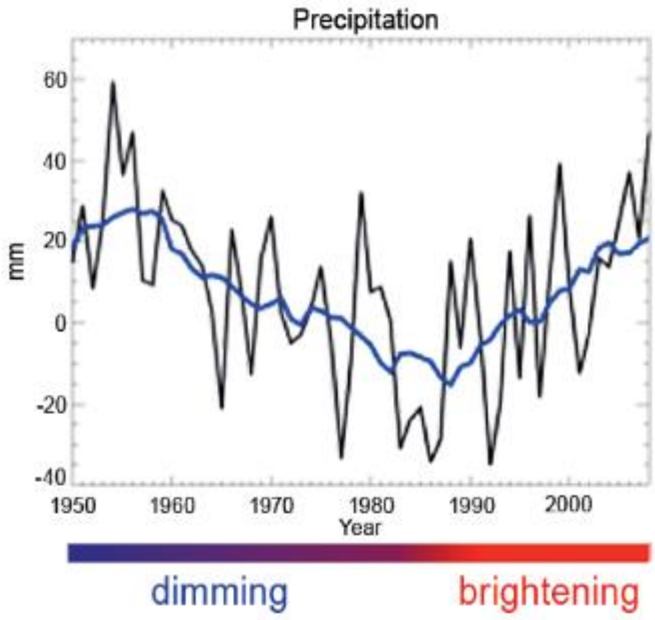

Figure 8.18: Global dimming and brightening, from(Wild, 2012).

Figure 8.19: Placeholder for Bonfils et al. 2019 - Formal pattern-based D&A for meridional shift in the ITCZ

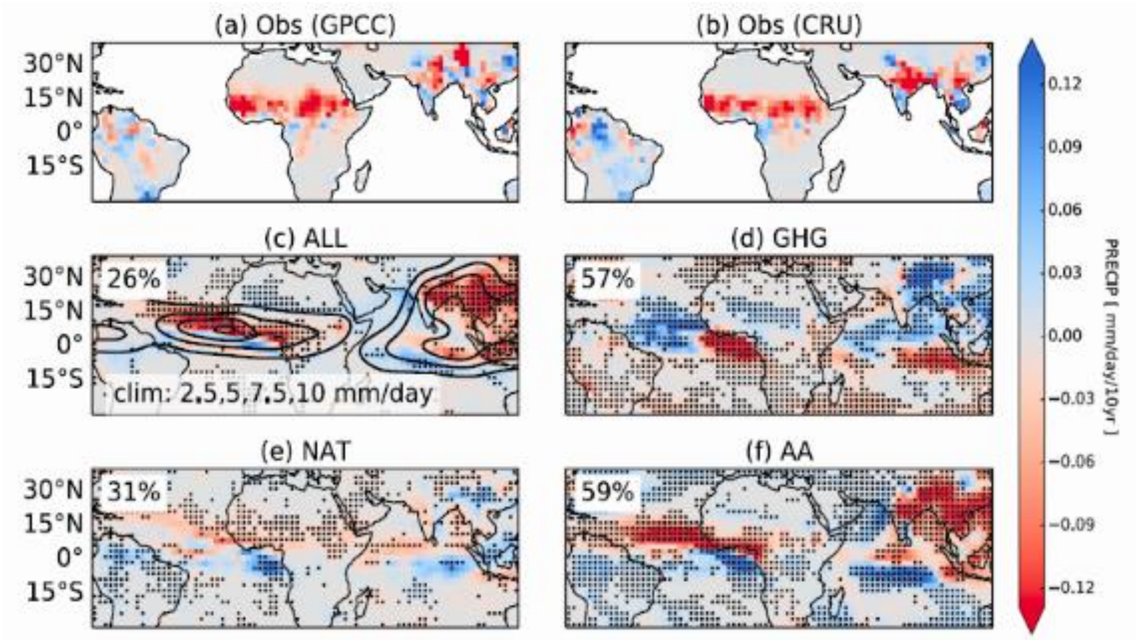

Figure 8.20: Excerpt from Fig. 1 of (Undorf et al., 2018).

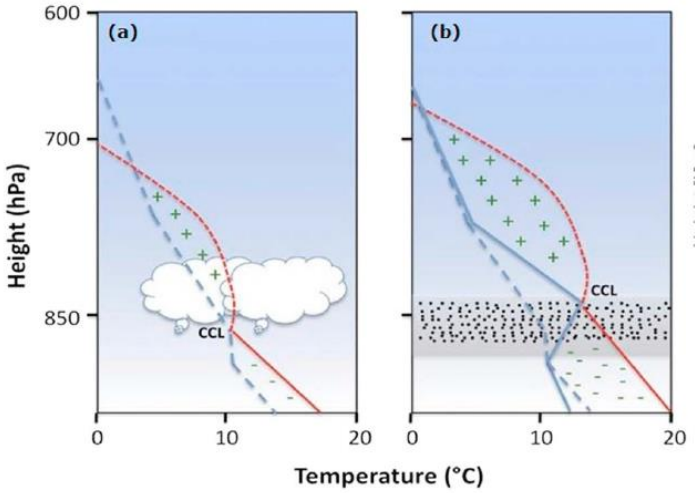

Figure 8.21: Redistribution of surface and low tropospheric heating due to aerosol absorption of solar radiation. The broken blue line represents the temperature in clean atmosphere. The solid blue line shows low level cooling and mid-level warming due to air pollution, which inhibits cloud formation, but increasing the conditional instability. This leads to suppression of small clouds and light precipitation while enhancing deep clouds with heavy precipitation. From (Wang et al., 2013).

.

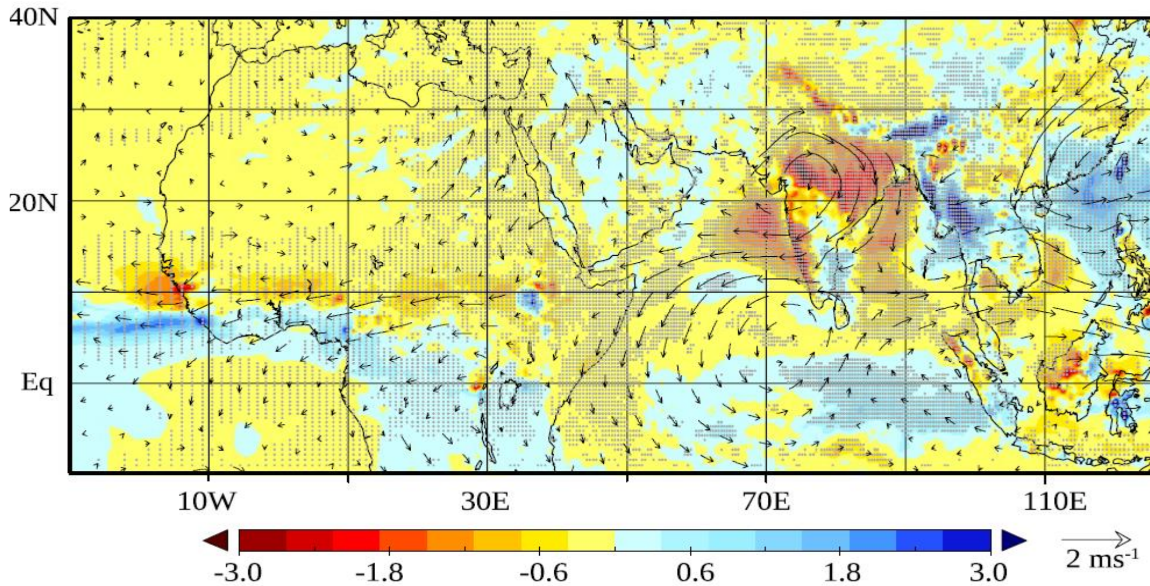

Figure 8.22: Attributing the monsoon weakening to anthropogenic influence Map showing the difference in June–September mean precipitation (mm day^{-1}) and 850 hPa winds (vectors; ms^{-1}) between the HIST1 and HISTNAT1 simulations for the period (1951–2005). *Grey dots* correspond to mean precipitation differences (HIST1 minus HISTNAT1) which exceed 95 % confidence level based on a two-tailed student's t-test Krishnan et al., (2016).

Figure 8.23: Placeholder for D & A of changes in the global and regional monsoon precipitation based on CMIP6

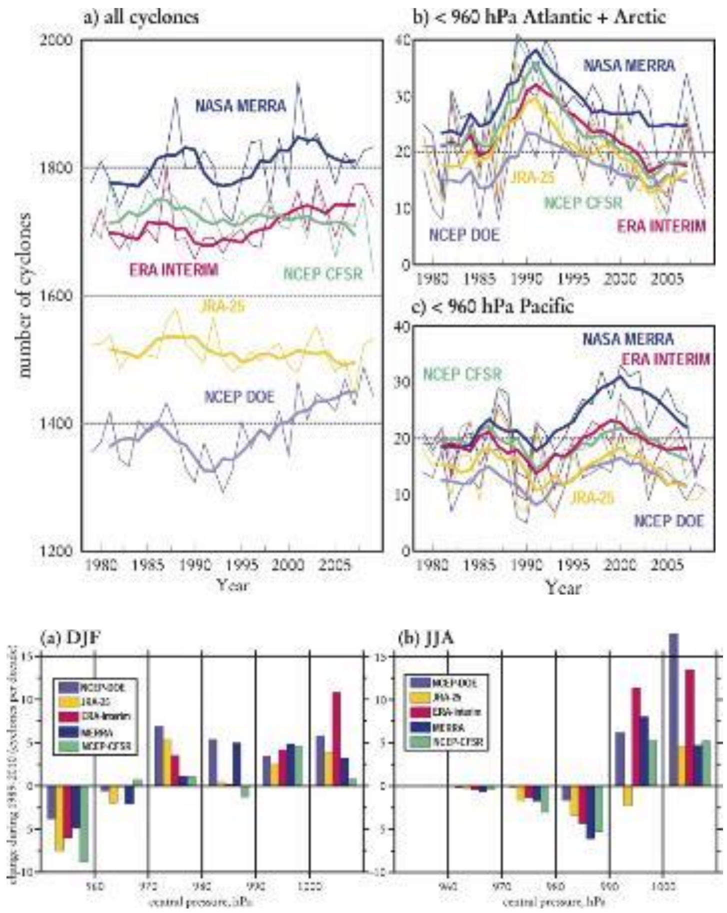

Figure 8.24: Left - time series of (a) the total annual number of cyclones over the NH and (b),(c) the number of very deep (<960 hPa) cyclones over the North Atlantic and North Pacific, respectively. Thin lines correspond to interannual values and thick lines show 5-yr running means. Right - changes in the number of cyclones of different intensities during the 32-yr period (1979–2010) for (a) DJF and (b) JJA in different reanalyses(Tilinina et al., 2013).

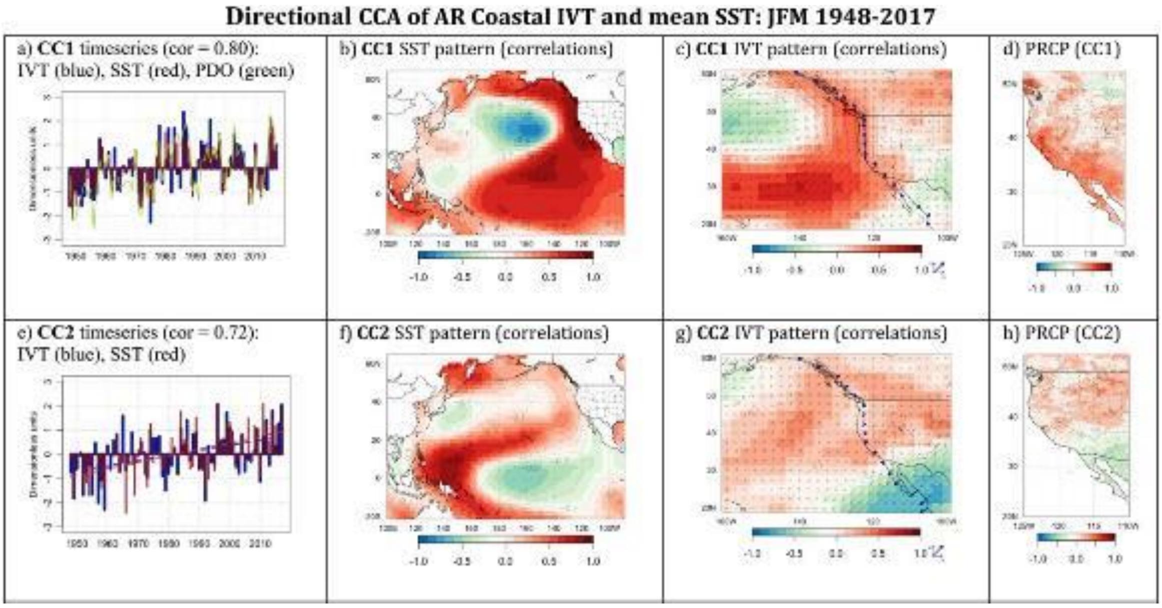

Figure 8.25: Excerpts from Gershunov et al. 2017 (Panels e-h of Figure 3 (top) and e-h of Figure S10 (bottom) in). Results of directional Canonical Correlation Analysis (CCA) applied to Pacific SST and AR IVT landfalling upon the North American West Coast during January – March. Second leading canonical correlates (time series, panel a) and their associated spatial patterns expressed as correlations between the time series and their respective fields of variables: SST (b) during the January – March, JFM, season and seasonally summed AR-associated IVT (c). Correlations between the IVT time series (a, blue bars) and AR-associated precipitation (d). The bottom row shows the second leading coupled mode (e-h) of an analogous CCA applied to Pacific SST and TOTAL IVT while the bottom row shows the third leading mode (i-l). The analysis was done on AR-related vector IVT confined to the coastal zone grid cells and expressed as correlations with the entire domain of AR-related IVT, both u and v components (arrows) and magnitude (colors), while the coastal grids that comprised the analysis domain are marked with thick arrows (c, g, k). Maximum possible arrow length is sqrt(2), shown to the right of the color scale, corresponding to unit (r=1) u and v components. AR-associated JFM precipitation (PRCP) correlated with the corresponding modal IVT time series shown in panels (d, h, l). Note that PRCP data span a shorter period (1950-2013) compared to SST and IVT data (1948-2017). The least squares-fitted trends on panel (e) are significant with p-values < 0.0005.

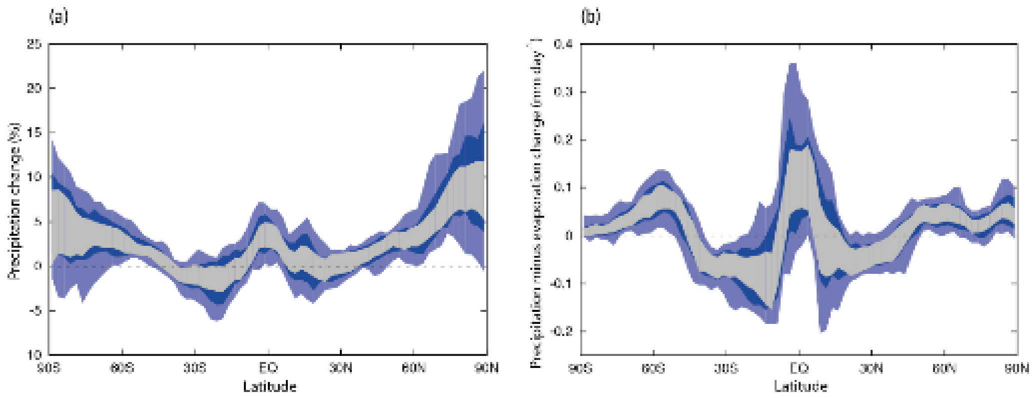

Figure 8.26: AR5 Fig. 11.13 CMIP5 multi-model projections of changes in annual and zonal mean (a) precipitation (%) and (b) precipitation minus evaporation (mm day^{-1}) for the period 2016–2035 relative to 1986–2005 under RCP4.5. The light blue denotes the 5 to 95% range, the dark blue the 17 to 83% range of model spread. The grey indicates the 1s range of natural variability derived from the pre-industrial control runs. **Need an updated AR6 version of this figure.**

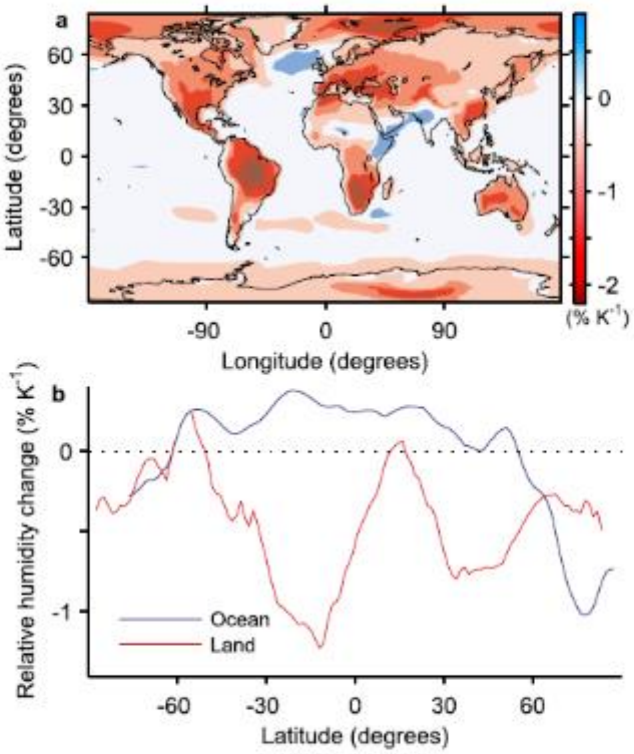

Figure 8.27: Changes in surface-air relative humidity from (Byrne and O'Gorman 2016). To be updated or duplicated with CMIP6 model outputs when available.

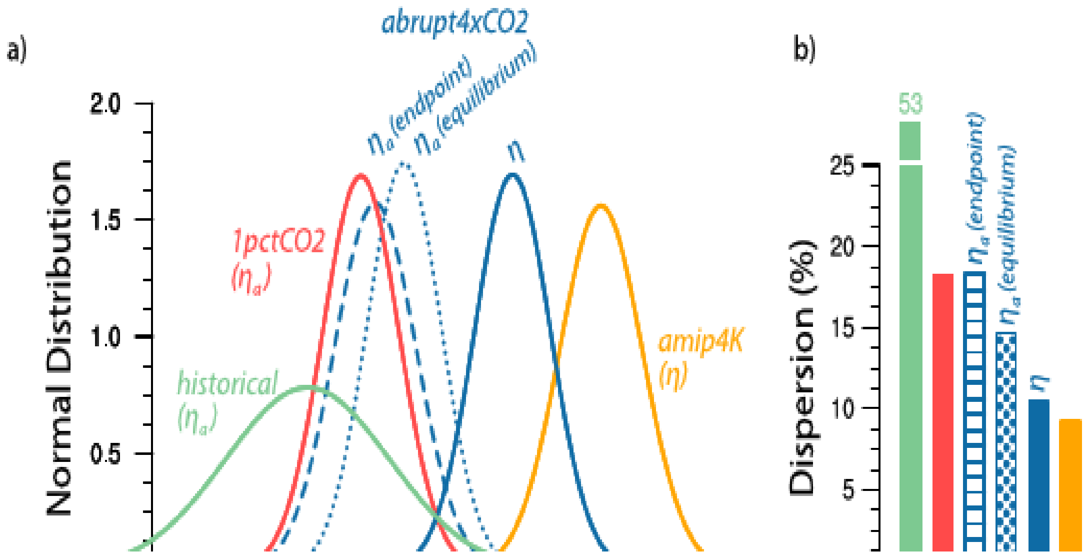

Figure 8.28: Hydrological sensitivity in CMIP5 from (Fläschner, Mauritsen, and Stevens 2016).

Figure 8.49:

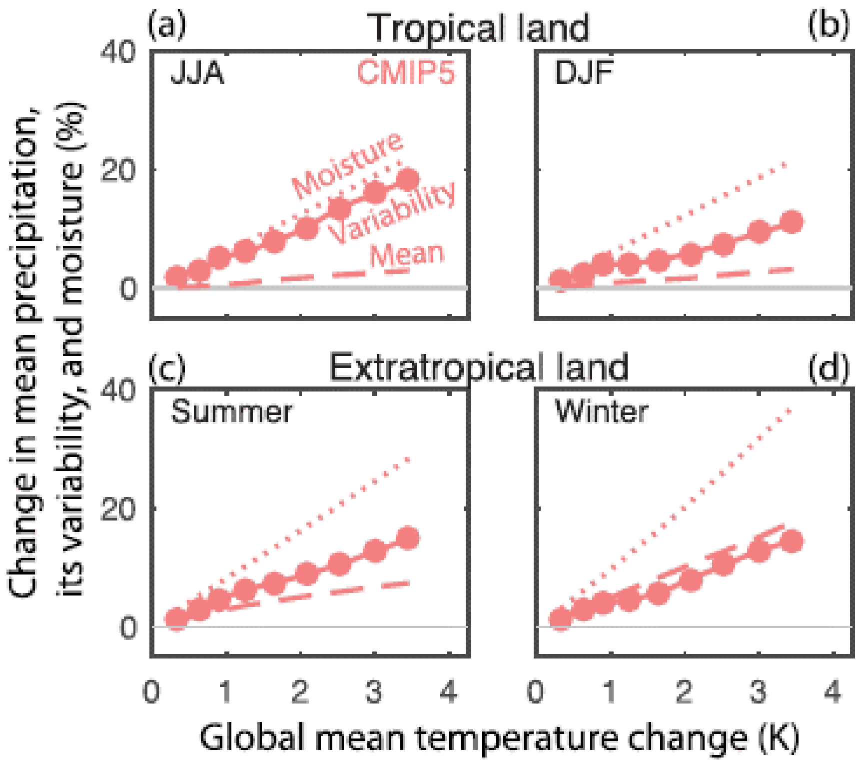

Figure 8.29: Rate of change of moisture mean and variability with temperature from (Pendergrass et al. 2017). To be updated with CMIP6 model outputs (using another colour) when available.

[CMIP6 ET]

Figure 8.30: CMIP6 global map of change in ET.

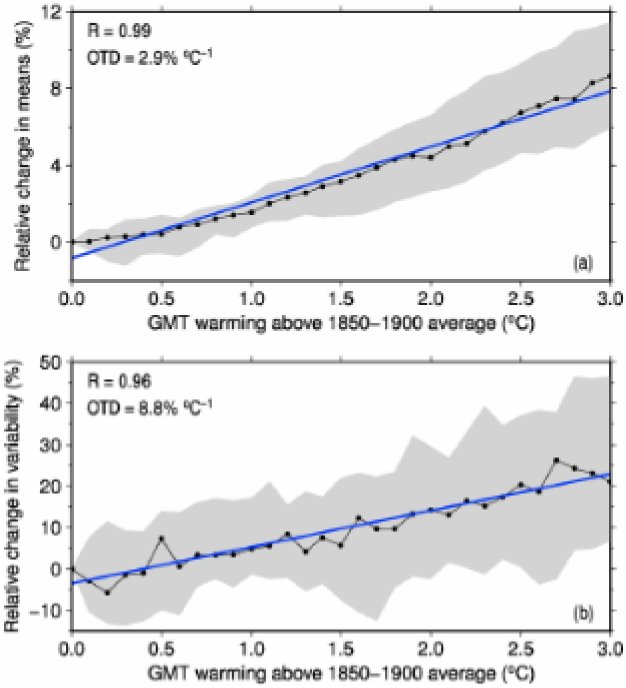

Figure 8.31: Relative changes in global mean runoff from (Zhang et al. 2018). To be updated or duplicated with CMIP6 model outputs when available. Also add relative changes in precipitation and evapotranspiration?

[CMIP6 Soil Moisture]

Figure 8.32: CMIP6 global map of change in soil moisture.

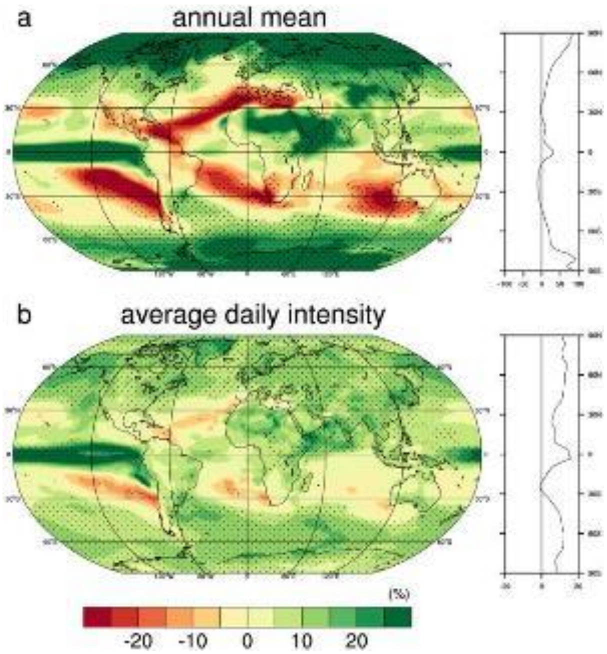

Figure 8.33: CMIP5 multi-model ensemble average percent change in (a) annual mean precipitation; (b) precipitation intensity during precipitating days. Stippling indicates areas where at least 70% of the models agree on the sign of the change.[Fig. 3 from Polade et al. 2014]

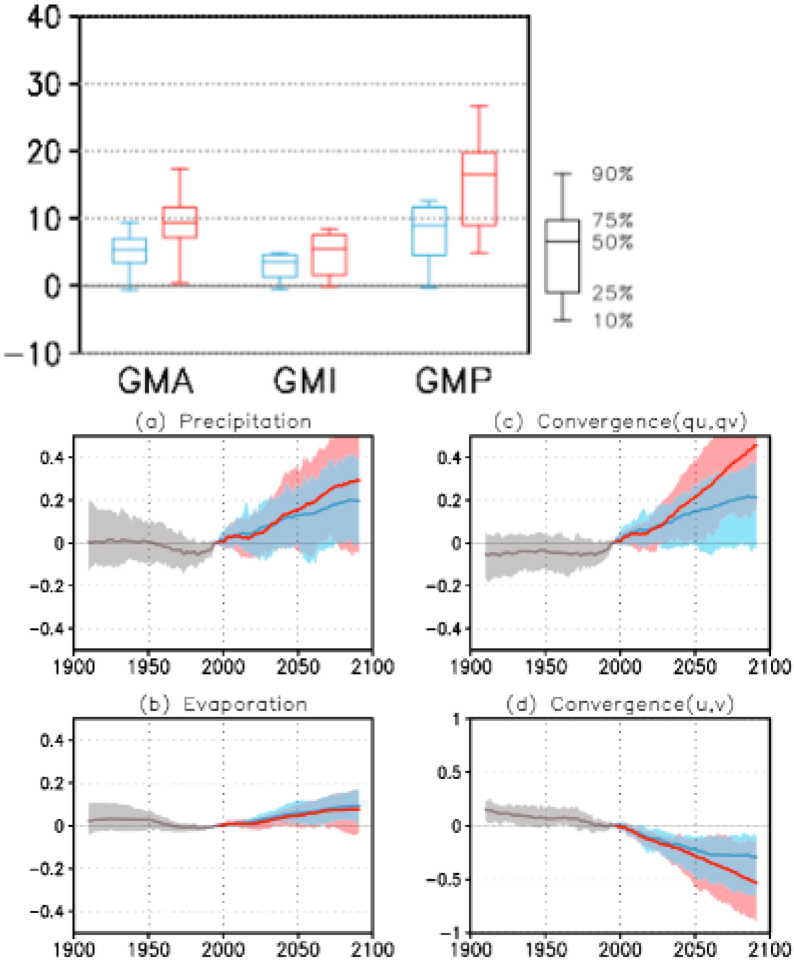

Figure 8.34: Fig3 and Fig 10 from(Kitoh et al. 2013)

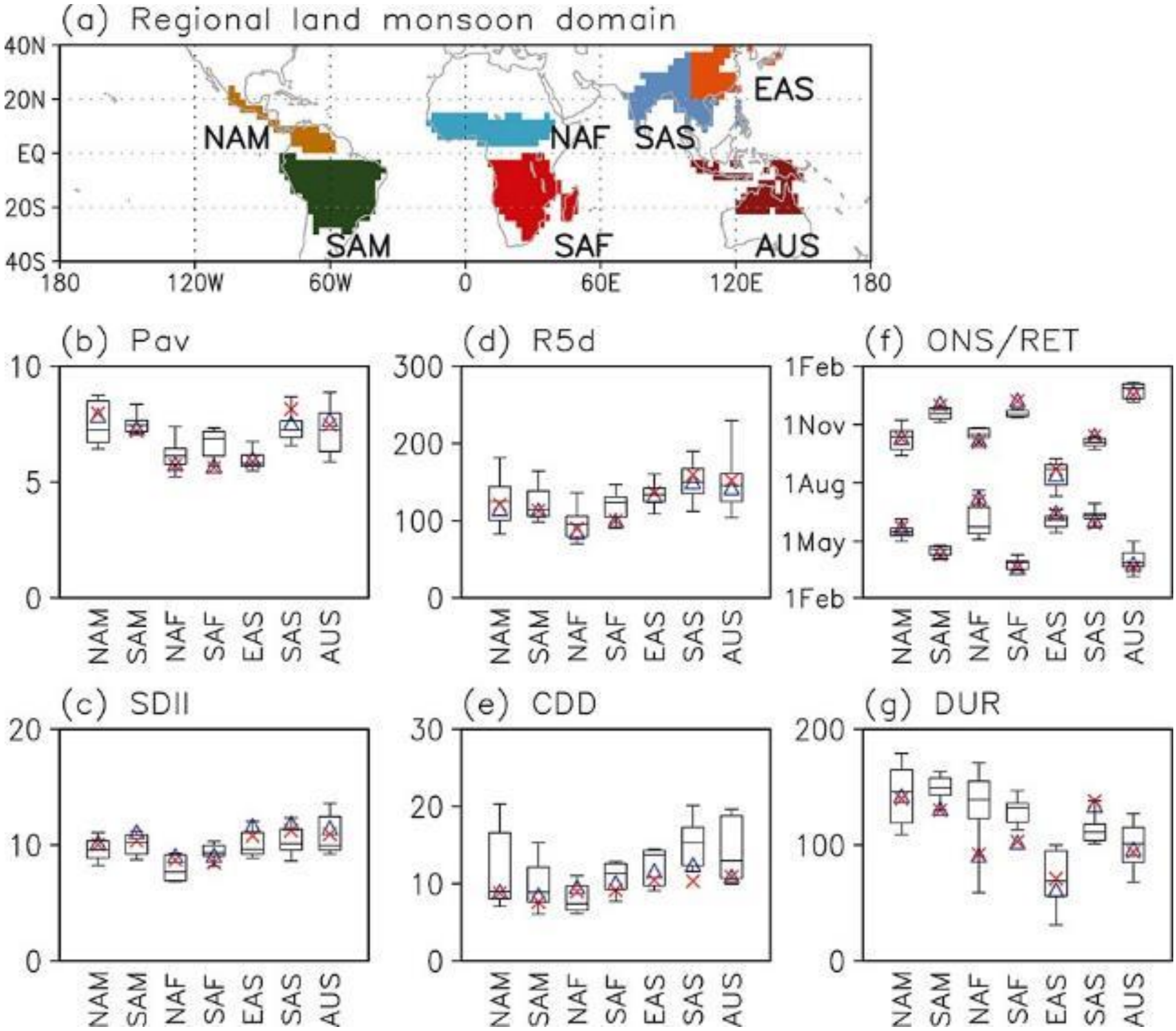

Figure 8.35: Fig 5 from(Kitoh et al. 2013) – probably better for a box dedicated to Monsoons ("How will monsoons change in a changing climate?" or something similar)

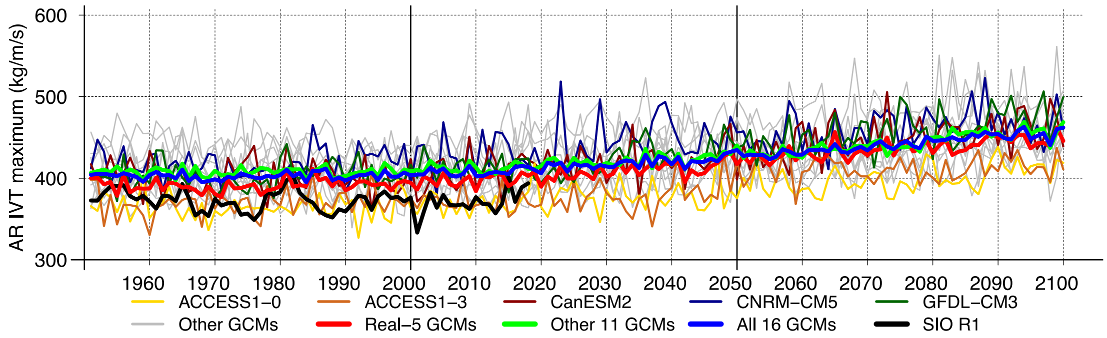

Figure 8.36: From (Gershunov et al., 2019).Annual average maximum IVT for AR events landfalling upon the West Coast of North America [20-60°N] in historical (1951-2005, left) and projected (2006-2100, right) epochs. Real-5 GCMs are plotted in thin colored lines, while other GCMs are outlined in gray. Thick curves represent the ensemble averages of the Real-5 GCMs (red), the other 11 GCMs (green), and the full ensemble of 16 GCMs (blue). The thick black curve shows the observed (SIO-R1) variability.

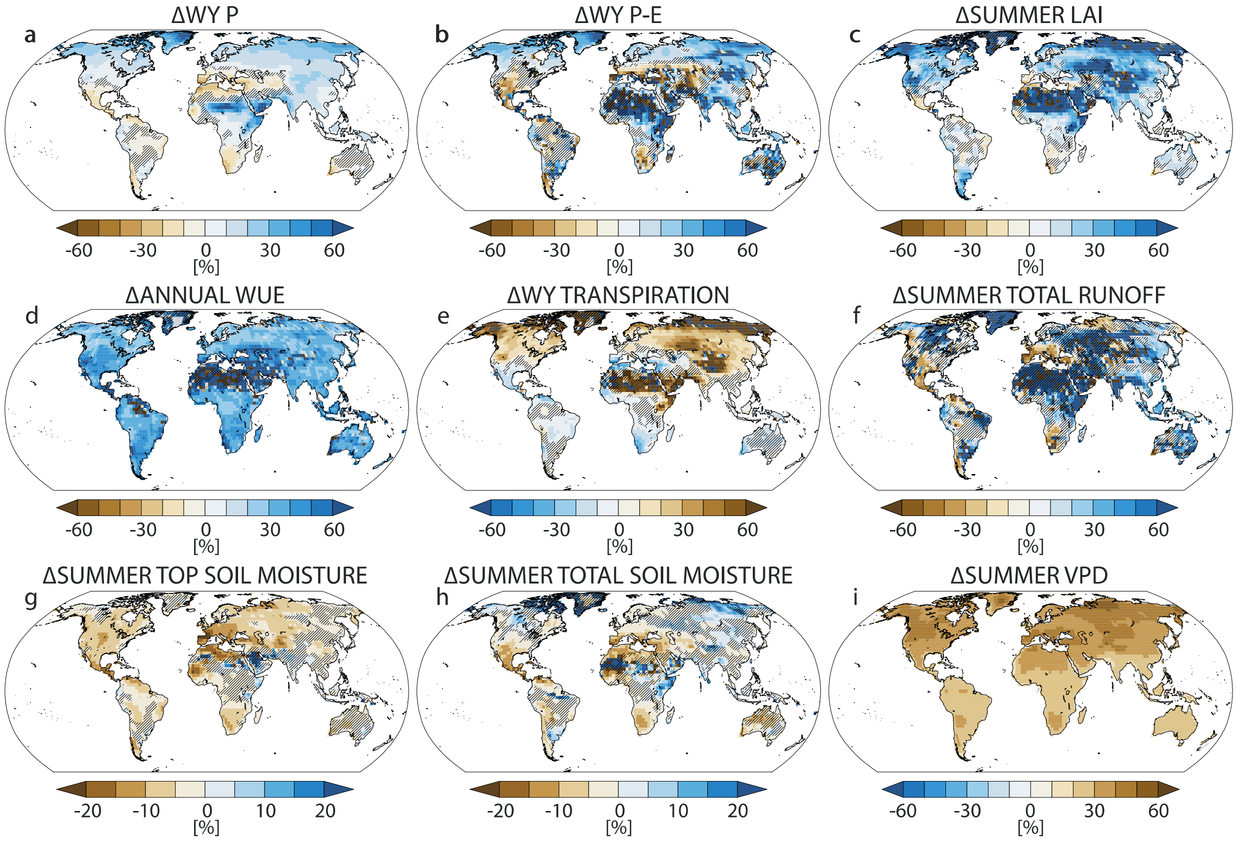

Figure 8.37: End-of-century changes in hydroclimate variables from 17 models in the CMIP5 archive (2070-2099 minus 1976-2005) in (a) water-year (WY; October--September in the Northern Hemisphere and July-June in the Southern Hemisphere) precipitation (P), (b) WY precipitation minus evapotranspiration (P-E), (c) summer (June-July-August in the Northern Hemisphere; December-January-February in the Southern Hemisphere) leaf area index (LAI), (d) annual plant water use efficiency (WUE), (e) WY transpiration, (f) summer total runoff, (g) summer near surface soil moisture (~0.1m), (h) summer full-column soil moisture (note depth varies by model), (i) summer vapor pressure deficit (VPD) all in percent (%). In all panels, drying tendencies are indicated in brown, wetting tendencies in blue (note the reverse color scales in (e) and (i)). Ensemble agreement is based on a pooled model-year K-S test (95%), with the additional requirement that at least two-thirds of models agree with the direction of ensemble mean change. Hatched areas are insignificant. From (B. I. Cook, Mankin, and Anchukaitis 2018).

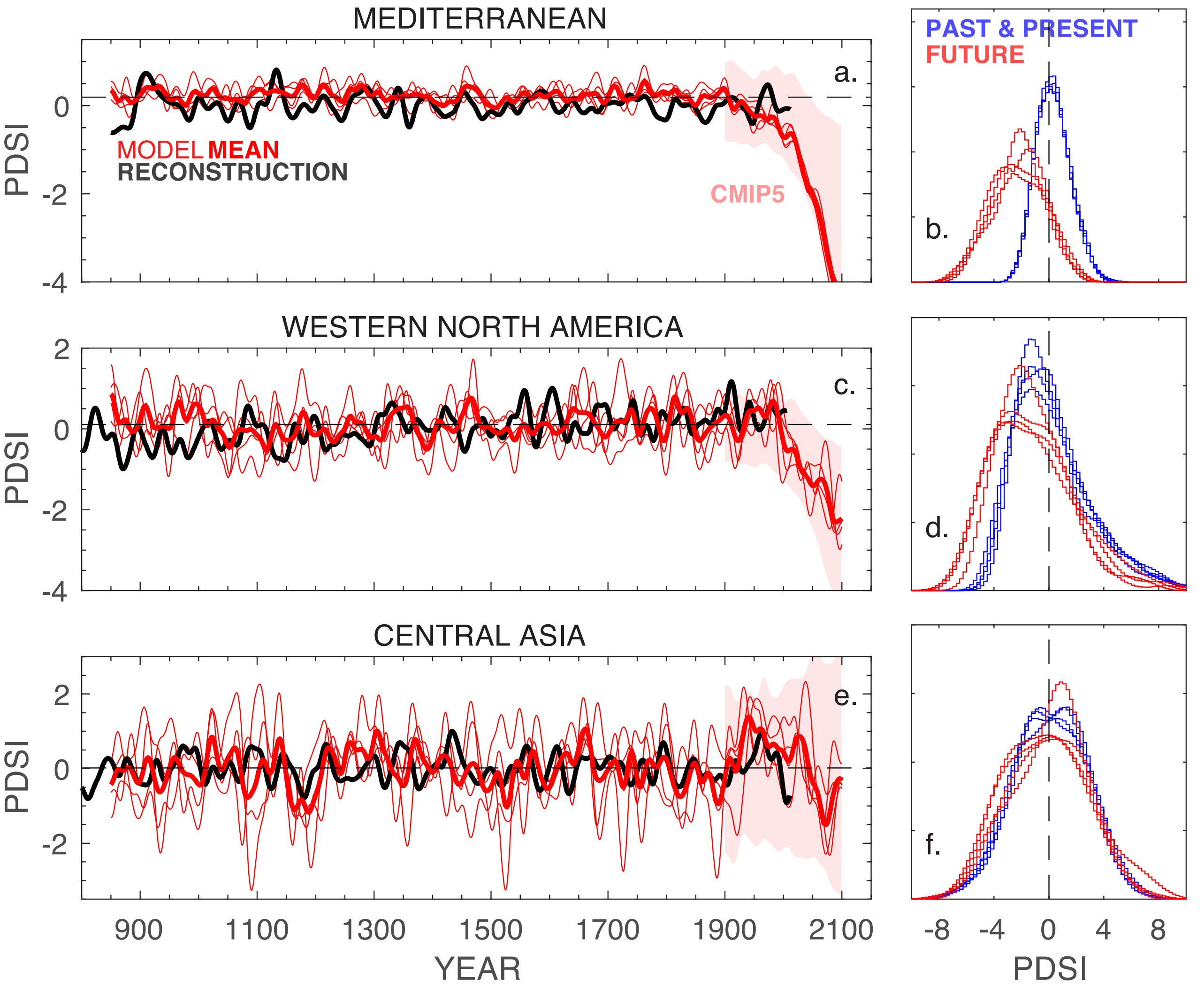

Figure 8.38: Past-to-future drought variability in paleoclimate reconstructions and models for regions of (a,b) the Mediterranean (10W-45E, 30N-47N); (c,d) western North America (124W--117W, 32N-38N), and (e,f) central Asia (99E-107E, 47N-49N). Long tree-ring reconstructed Palmer Drought Severity Index (PDSI) series (black line) for the (a) Mediterranean (E. R. Cook et al. 2015; B. I. Cook et al. 2016), (b) California and Nevada (E. R. Cook et al. 2010; Griffin and Anchukaitis 2014) and (c) Mongolia (Pederson et al. 2014; Hessl et al. 2018) plotted in comparison to the past-to-future fully-forced simulations from the NCAR CESM Last Millennium (red line) (Otto-Bliesner et al. 2016) for the same region. The pink envelope represents the range of historical and future PDSI simulations from CMIP5 for the same regions (B. I. Cook et al. 2014) (b,d,f: The distribution of annual PDSI values from the paleoclimate and historical period (850 to 2005 CE) and future (2006 to 2100 CE) from the long past-to-future CESM simulations.

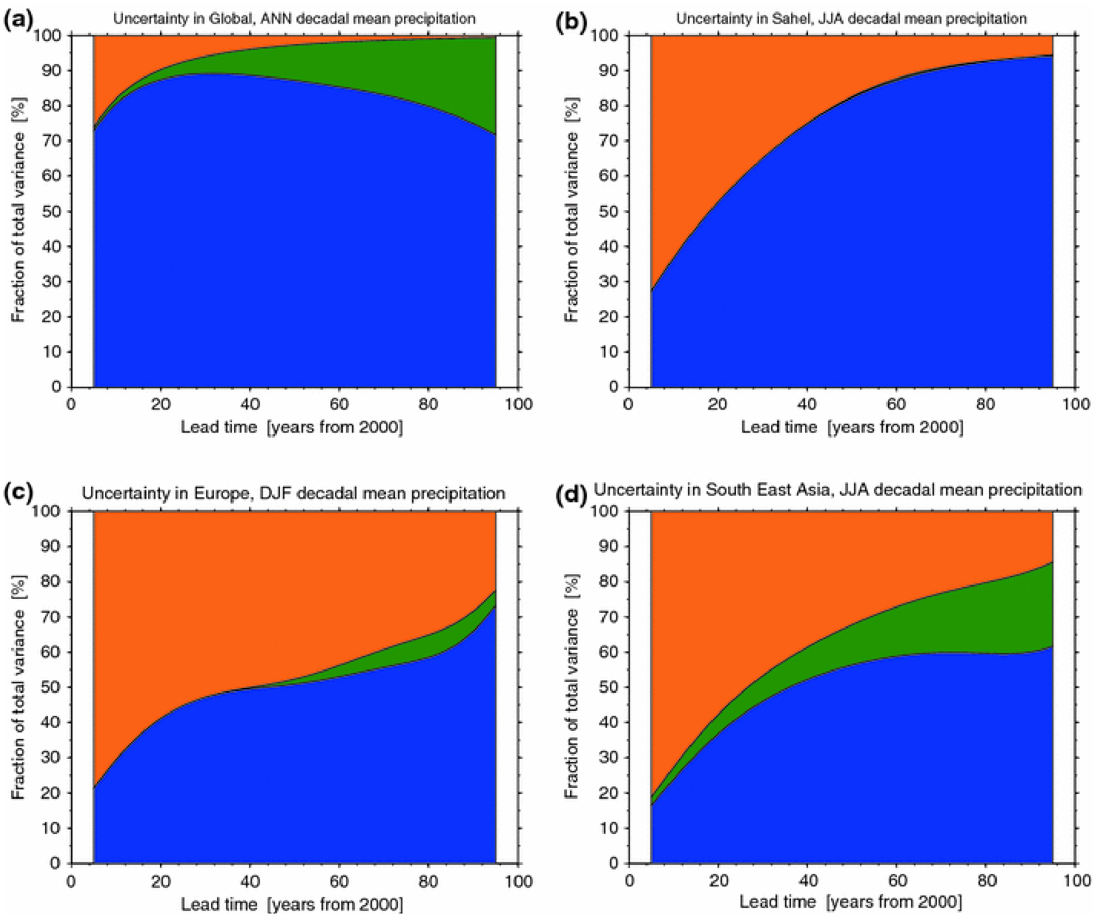

Figure 8.39: Fraction of total variance in decadal mean precipitation projections explained by internal variability (orange), model uncertainty (blue) and scenario uncertainty (green), for (a) global, annual mean, (b) Sahel JJA mean, (c) European DJF mean, and (d) South East Asian JJA mean. All calculations are based on CMIP3 models and SRES scenarios (*Hawkins and Sutton, 2011*). Partly replicated with CMIP5 models and RCP scenarios (Fig. 11.8 dealing with both T and P) in AR5 WGI. To be replicated with CMIP6 models and SSP scenarios.

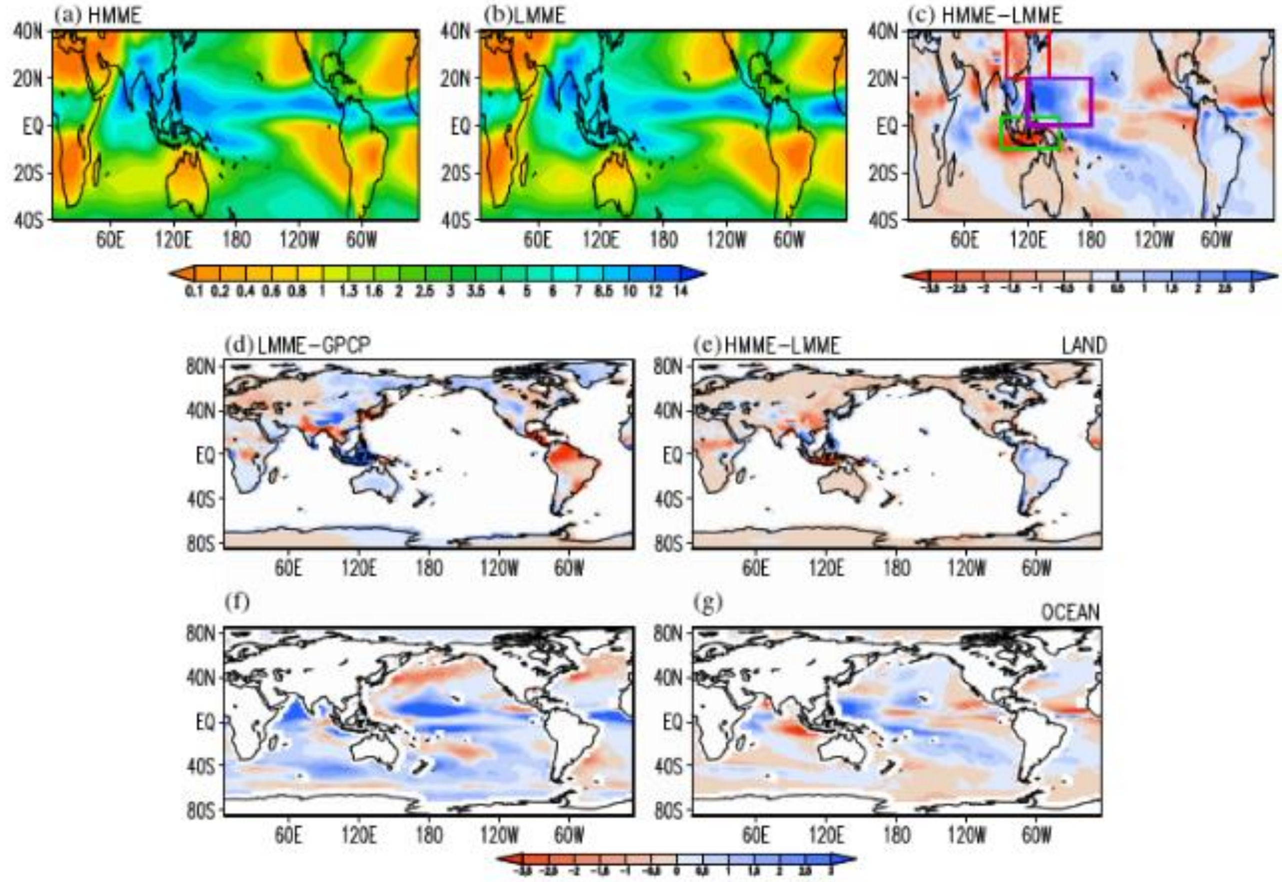

Figure 8.40: The 27-year mean precipitation in the high-resolution multi-model ensemble (HMME) (a), low-resolution multi-model ensemble (LMME) (b), and the differences between HMME and LMME (c), LMME and GPCP (d, f) and HMME and LMME (e, g). (unit: mm/day). The d, e, f, and g indicate the differences over continent and ocean, respectively. Calculations are based on the outputs of the top-six and bottom-six horizontal resolution models among 23 CMIP5 models (*Huang et al., 2018*). All model outputs as well as the GPCP observed climatology have been regridded onto a common 128xG4 regular grid. Similar maps to be replicated with CMIP6 models, paying attention to focus on pairs of simulations differing only by their resolution (in order to avoid mixing structural uncertainties with the influence of model resolution), and possibly distinguishing a third category of 'very-high' resolution models from HighResMIP. Stippling should be added to highlight statistical significance.

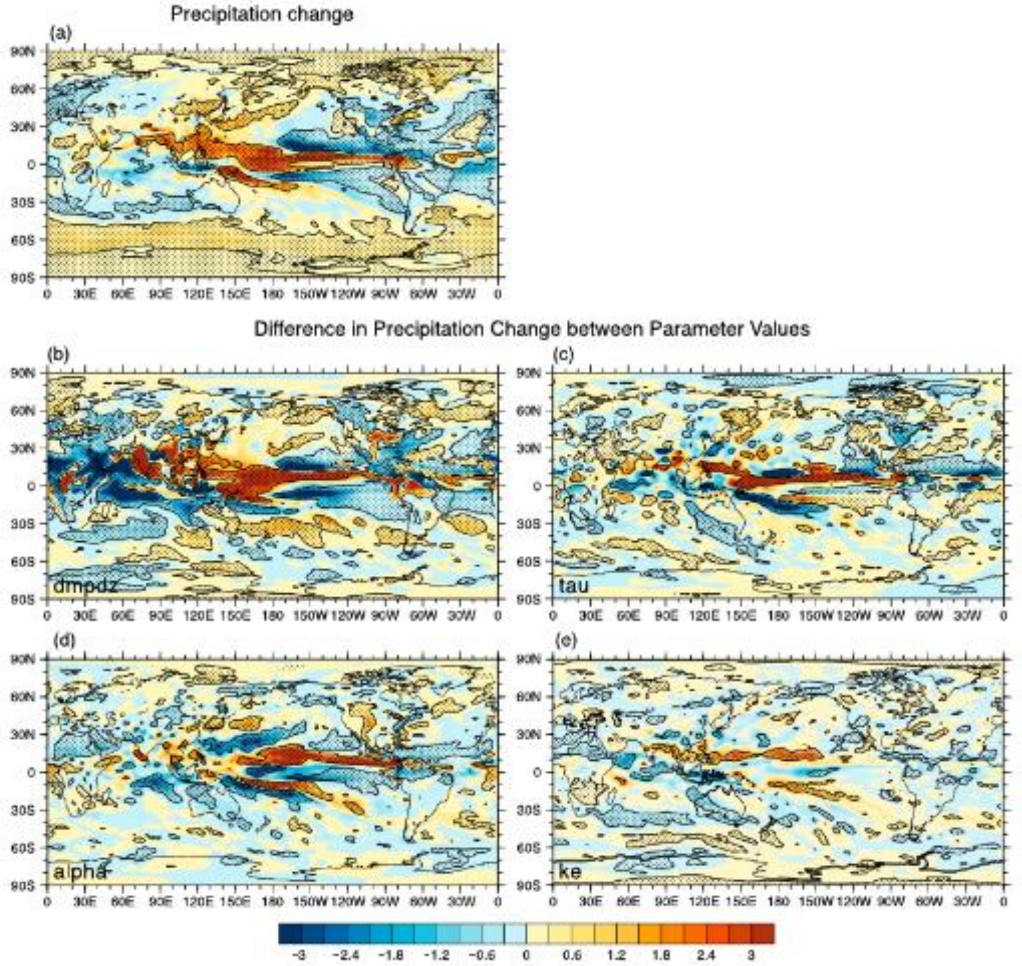

Figure 8.41: (a) Precipitation (mm/d) change for 2081–2100 relative to the 1986–2005 base period under the RCP8.5 global warming scenario for CESM1 standard values for JJA. Differences in projected JJA precipitation change (mm/d) under global warming (2081–2100 relative to the 1986–2005 base period) for simulations done with different parameter values. Differences are across the feasible range for four parameters in the deep convection scheme: (b) entrainment; (c) deep convective adjustment time; (d) downdraft fraction; (e) evaporation efficiency. Stippled areas pass a t test at the 95% level. (*Bernstein and Neelin, 2016*).

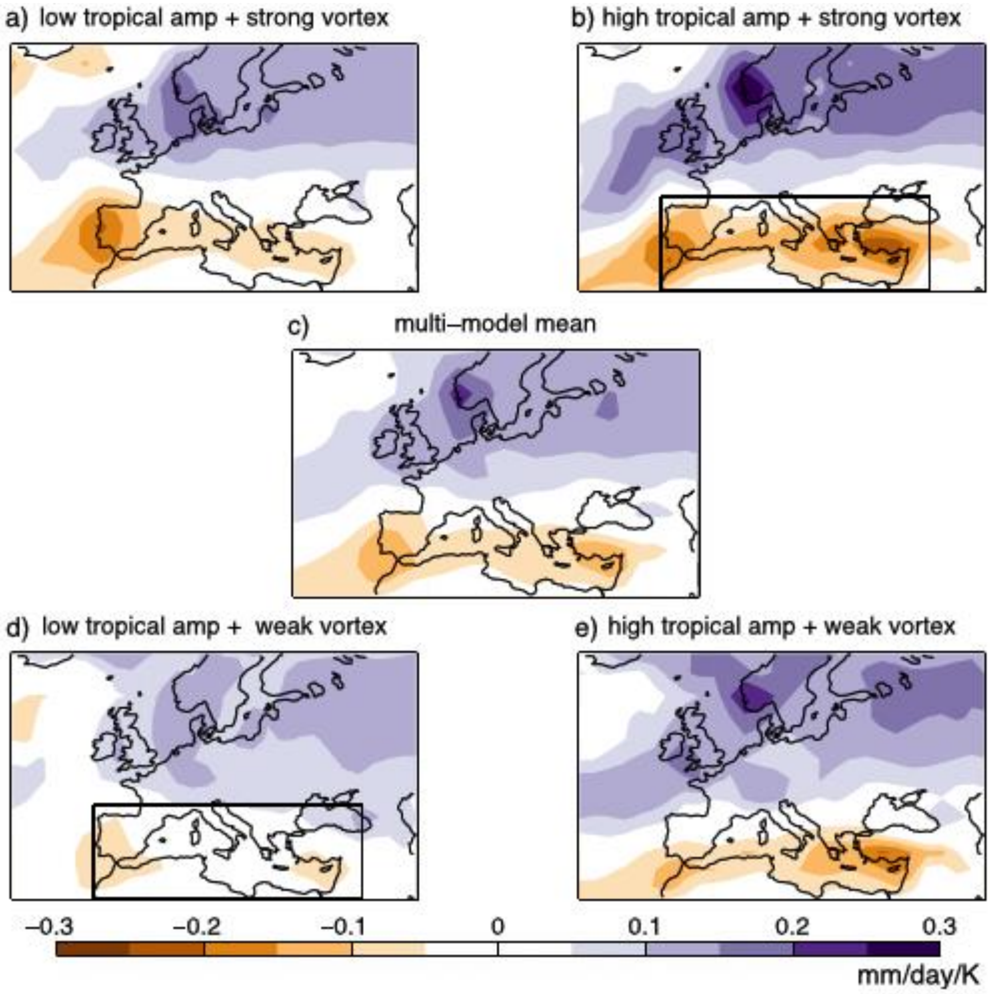

Figure 8.42: Cold season Mediterranean precipitation response per degree of global warming (mm day-1 K-1) according to (a),(b),(d),(e) four plausible storylines of climate change that are conditioned on the tropical amplification and stratospheric vortex responses. The storylines have been selected to be of particular relevance for Mediterranean precipitation change. The storylines in (a) and (b) are characterized by a stronger stratospheric vortex, while those in (d) and (e) have a weaker vortex; also, the storylines in (b) and (e) are characterized by higher tropical amplification of global warming, while those in (a) and (d) have lower tropical amplification. (c) The multimodel mean response scaled by global warming. (Fig. 8 from Zappa and Sheperd, 2017) [Check whether it is not used in Chapter 10 and could be updated with CMIP6 models]

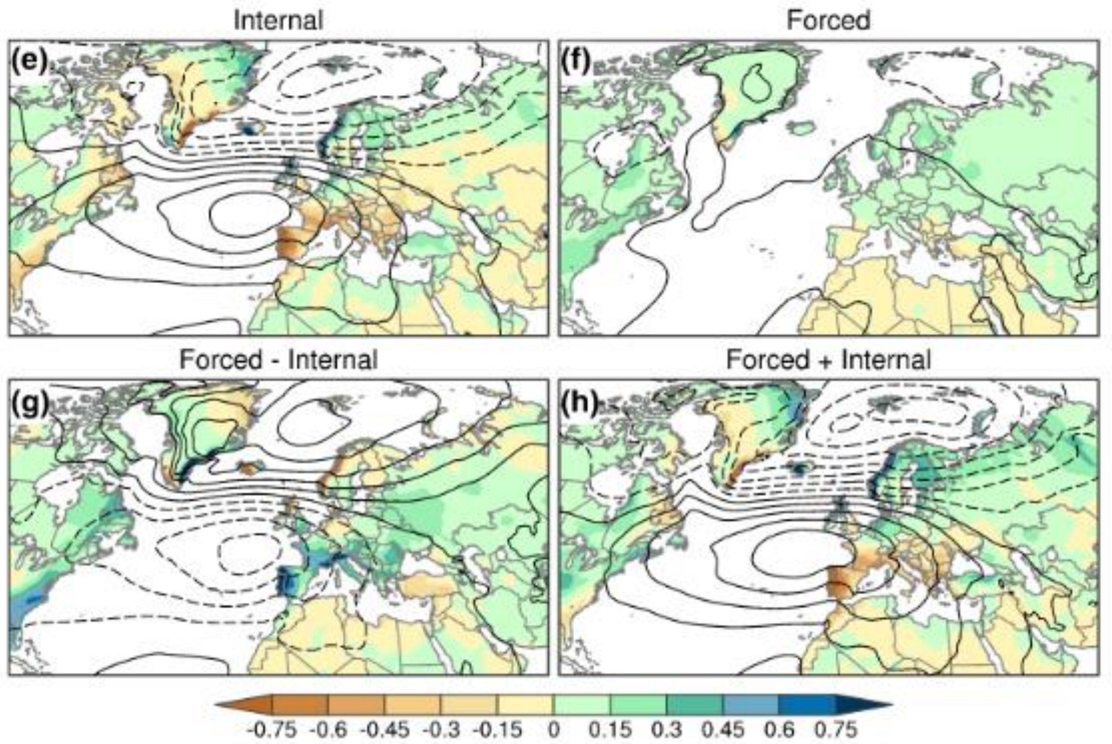

Figure 8.43: Impact of the NAO on future 30-year climate trends (2016–2045). (e) Regressions of winter SLP and precipitation trends upon the normalized leading PC of winter SLP trends in the CESM1 Large Ensemble, multiplied by two to correspond to a two standard deviation anomaly of the PC; (f) CESM1 ensemble-mean winter SLP and precipitation trends; (g) f − e; (h) f + e. Precipitation in color shading (mm/day per 30 years) and SLP in contours (interval = 1 hPa per 30 years with negative values dashed) (*Deser et al. 2017*). Possibly duplicated using other large Initial Condition Ensembles

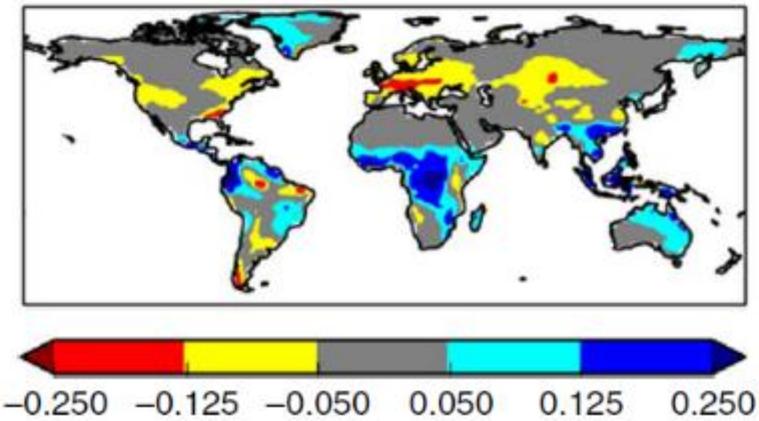

Figure 8.44: Ensemble mean precipitation differences (in mm per day) between the second 2K minus the first 2K global warming under RCP8.5 mitigation conditions. Calculations are based on a subset of 25 CMIP5 models (*Good et al., 2016*). Could be duplicated with CMIP6 models under the same mitigation scenario or using the abrupt2xCO2 and abrupt4xCO2 simulations, and possibly showing not only precipitation but also evapotranspiration and runoff (or even soil moisture).

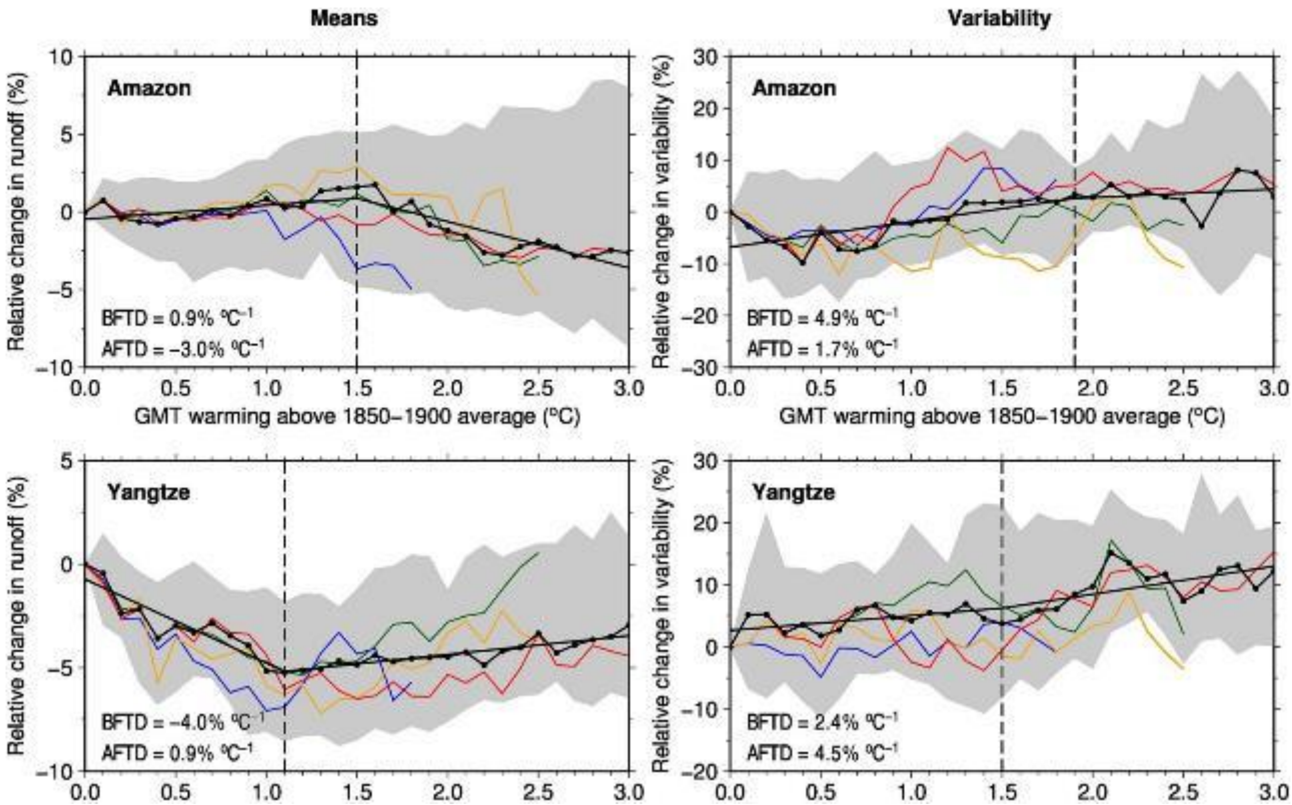

Figure 8.45: Relative changes (%) in basin-averaged annual mean runoff estimated as the multi-model ensemble mean averaged across a subset of CMIP5 models and across all RCPs over two representative river basins: Amazon (top panel) and Yangtze (bottom penel) rivers. The dashed line indicates the critical global mean temperature (GMT) warming at which a turning point is identified in the projected runoff. BFTD indicates the magnitude of trend before TP; AFTD indicates the magnitude of trend after TP; OTD indicates the magnitude of overall trend. The shaded area indicates the interquartile range of the ensemble values across all RCPs. Only the warming levels with more than 10 models available are shown for each RCP scenario. To be replaced or duplicated with CMIP6 models/scenarios. [RCP2.6 : Blue, RCP4.5 : Green, RCP6.0 : Yellow, RCP8.5 : Red, All RCPs : Black]

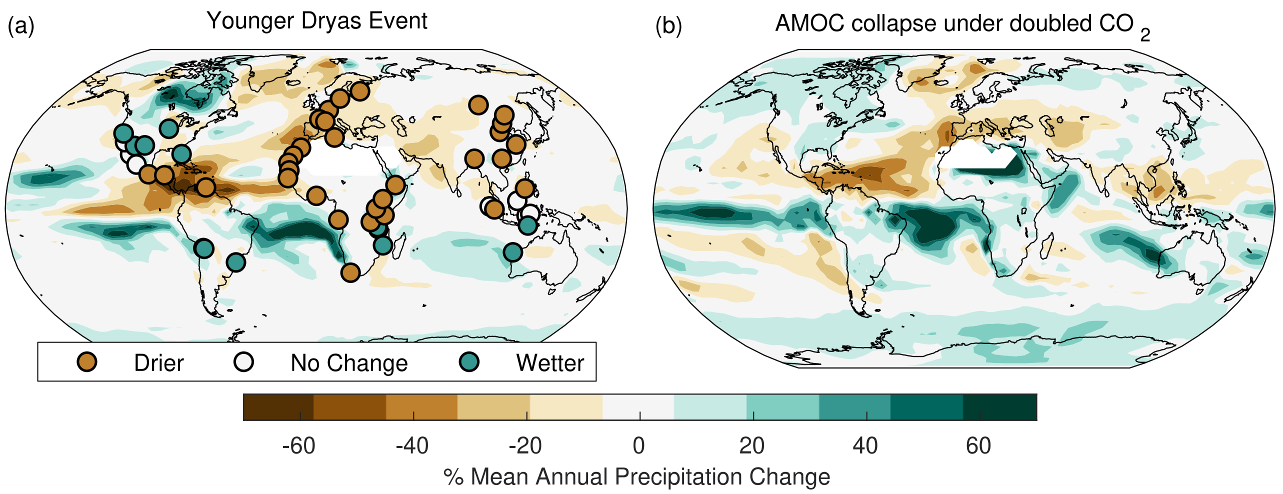

Figure 8.46: (a) Model simulation of precipitation response to the Younger Dryas event, relative to the preceding warm Bølling-Allerød period (base colors, from the TraCE paleoclimate simulation of (Liu et al. 2009)), with paleoclimate proxy evidence superimposed on top (dots, see Technical Annex II). (b) Model simulation of precipitation response to an abrupt collapse in AMOC under a doubling of CO_2 (after (Liu et al. 2017)). Regions with rainfall rates below 20 mm/year are masked.

Figure 8.47: Examples of abrupt changes in plant cover, precipitation, aridification in future model projection scenarios from CMIP6 [*TBD, if these occur*].

Figure 8.48: Abrupt snowpack/SWE changes for select regions (Sierra Nevada, Andes, Himalaya?) for the CMIP6 high-emissions scenario [*TBD, if these occur*].

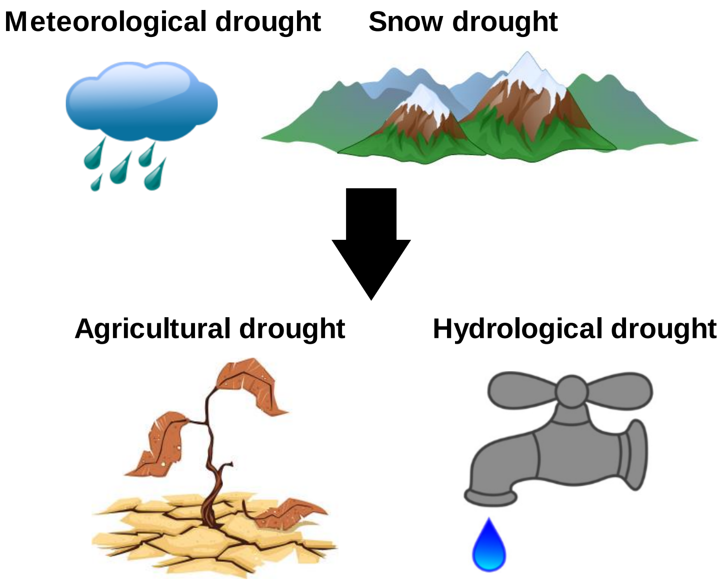

FAQ 8.3, Figure 1: Clip-art style illustration of types of droughts.

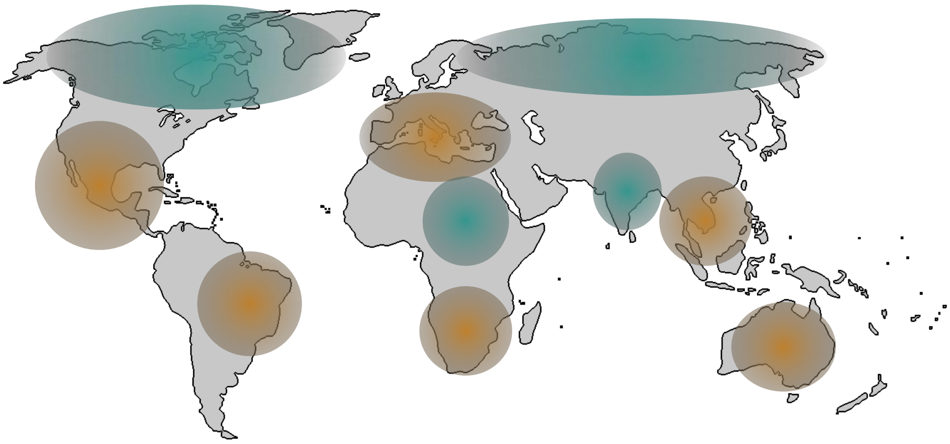

FAQ 8.3, Figure 2: Global map with regions expected to experience more or less drought labeled in brown (more) and blue-green (less) (use colors from precipitation diverging palette). Recommend contour-hugging shading; mock up below is just for the general idea. Would need to ensure accuracy w/r/t both CMIP5 and CMIP6 results.